WORLD GEOTHERMAL CONGRESS – WGC 2010

BALI, 24-29 April, 2010

SHORT COURSE 1 (SC1)

DRILLING, COMPLETION AND TESTING OF GEOTHERMAL WELLS

LECTURE NOTES

Convener: Pierre Ungemach

Co-convener: Miklos Antics

Lecturers: Miklos Antics, Peter Eric Danielsen, Hagen Hole and Pierre Ungemach

CONTENTS

DAY 2 : SUNDAY, 25 APRIL 2010. MORNING SESSION.

Lecturers: Miklos Antics, Hagen Hole, Pierre Ungemach

08:30 – 10:00 Miscellaneous, drilling/completion related, issues

- Production/injection equipment
- Well monitoring, maintenance and workover
- Geothermal district heating & cooling. Typical well designs and drilling/completion programs
- Corrosion scaling abatement
- Water injection
- Risk mitigation. Quantifying risk in geothermal development. The high and low enthalpy cases

10:00 – 10:30 Break

Lecturer: Pierre Ungemach

10:30 – 11:00 Geothermal well logging. An overview

- Objectives
- Tool descriptions
- Field applications

Lecturer: Peter Eric Danielsen

11:00 – 12:00 Geothermal well testing. Part 1

- Objectives
- Technology
- Safety measures

12:00 – 13:30 Lunch

DAY 2 : SUNDAY, 25 APRIL 2010. AFTERNOON SESSION.

Lecturer: Peter Eric Danielsen

13:30 – 14:30 Geothermal well testing. Part 2

- Well test interpretation

14:30 – 15:00 Break

Lecturer: Peter Eric Danielsen

15:00 – 16:00 Geothermal well testing. Part 3

- Case studies

16:00 – 17:00 Round table. FAQ session. Questionnaire

17:00 – 17:15 Short course closure. Presenting the certificates of attendance

PROGRAMME

DAY 1 : SATURDAY, 24 APRIL 2010. MORNING SESSION.

Lecturer: Pierre Ungemach

08:30 – 08:45 Keynotes
- Introduction to the course
- Background and scope
- Presentation of the lecturers

08:45 – 10:00 An introduction to geothermal systems
- Geothermal environments
- Reservoir physics. An overview
- Physical and thermodynamic properties
- Resource/reserve classifications
- The EGS issue

10:00 – 10:30 Break

Lecturer: Miklos Antics

10:30 – 12:00 Insight into wellbore mass and heat transfers
- Mass transfer. Single phase flow
- Mass transfer. Two phase flow
- Mass transfer. The single phase liquid case

12:00 – 13:30 Lunch

DAY 1 : SATURDAY, 24 APRIL 2010. AFTERNOON SESSION.

Lecturer: Hagen Hole

13:30 – 15:00 Drilling and completion of geothermal wells. Part 1
- An introduction to geothermal well drilling practices
- Geothermal well design. Casing and wellhead
- Directional drilling

15:00 – 15:30 Break

15:30 – 17:00 Drilling and completion of geothermal wells. Part 2
- Drilling fluids
- Cementing
- Drilling service contracts and risk analysis

Drilling, Completion and Testing of Geothermal Wells

Section 1. Keynotes

Introduction to the Course
Background and Scope
Presentation of the Lecturers

Pierre Ungemach

GPC INSTRUMENTATION PROCESS, Roissy-en-France, France

1 Introduction to the course

The course material addresses the core of the geothermal resource reclamation process, deemed vital for the success of any geothermal development venture. As a matter of fact, geothermal well drilling, completion and testing achieve, downstream of prior surface and subsurface geological, hydrologeological, geochemical and geophysical investigations, a direct assessment of reservoir properties and well performance. As evidenced by the surface reconnaissance to reservoir management chain displayed in fig. 1, sound design and operation of these crucial segments are likely to produce a relevant conceptual model, indeed a key prerequesite to sustainable reservoir management issues.Main Heading

2 Background and scope

Two thirds of the course material are dedicated to drilling/completion and well testing operations, with special emphasis placed on high enthalpy sources, a distinctive attribute when compared to current oil and gas drilling/completion and testing practice. Actually, the latter addresses dominantly low to medium temperature fluids and sedimentary rock environments as opposed to high temperature, thermochemically sensitive, fluid and rock prevailing volcano-tectonic settings. Although much is to be shared between hydrocarbon and geothermal *modus operandi*, a statement particularly pertinent with respect to low enthalpy geothermal engineering, in no way can the transfer be regarded as a straight forward process, as highlighted by the following course headlines.

Drilling / completion

Introduction to geothermal well drilling practice
Geothermal well design
Directional drilling
Drilling fluids
Cementing
Drilling service contracts and risk analysis

Well testing

Objectives, technology, safety regulations
Interpretation
Case studies (single phase (liquid, steam), two phase)

In parallel to the foregoing, additional clues will be provided to SC attendees regarding geothermal systems, wellbore heat and mass transfers, corrosion/scaling, water injection, well logging, risk mitigation, low enthalpy drilling/completion/production and, last but not least, EGS issues.

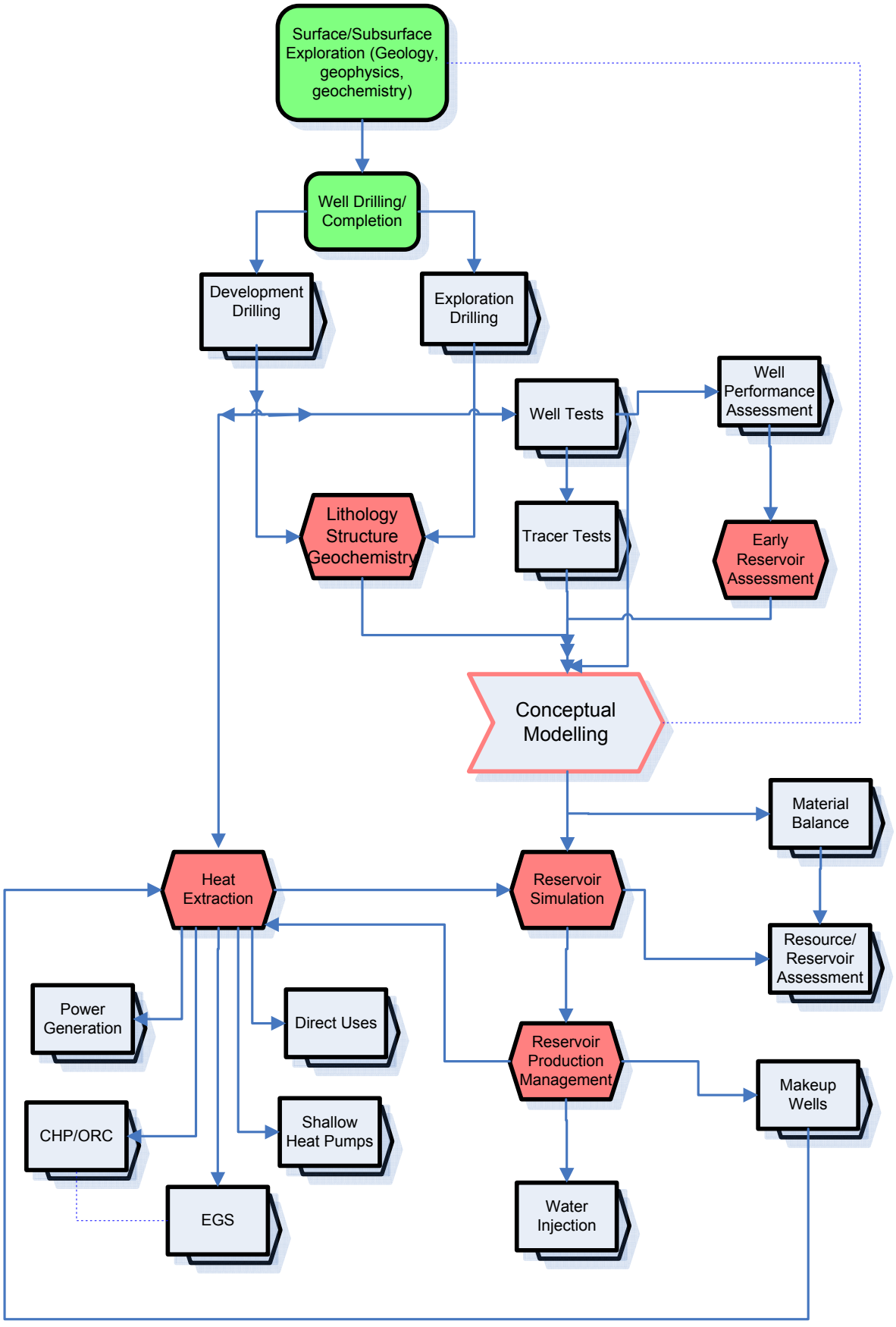

Figure 1: From Surface Reconnaissance to Reservoir Management

3 Presentation of the lecturers

Biography resumes may be found in Appendix

Miklos Antics, presently Managing Director of GPC IP, is a graduate and post graduate reservoir engineer of the Ploïesti (Romania) School of Petrol. Holds a PHD in well testing, multiphase flow and reservoir simulation. Miklos Antics has gained a wide experience in resevoir engineering, simulation, well testing/logging and drilling/production in teaching, field practice and operation management areas. He served as Secretary of the Romanian Geothermal Association and is currently secretary of EGEC (European Geothermal Energy Council), member of the IGA BoD, Chairman of the Programme and Planning Committee, and Vice-President of the IGA European Branch Forum. He authored/co-authored over 35 technical papers and four textbooks.

Peter Danielsen, presently deputy manager of the Technical Department of the Iceland Geosurvey (ISOR), in charge of high temperature logging nationwide. Holds a Masters degree in hard rock geology. His rewarding experience in geophysical logging and well testing, in both high and low enthalpy environments, could be valued abroad via consulting and expertise in Norway, Denmark, Germany and East Africa. Peter Danielsen is currently acting Chairman of the Safety Committee in ISOR, preparing, documenting and implementing OSH standards he is registered as an expert in geothermal issues in the "Great Danish Encyclopedia" project.

Hagen Hole, currently Managing Director/Principal Consultant at Geo Consultants New Zealand Ltd (GCNZL), is a renowned international geothermal and drilling consultant. With a mechanical engineering background he got involved in geothermal matters under an Auckland University fellowship in geothermal two-phase flow and has since then accumulated a 32 years experience in geothermal development projects, mainly focused on drilling design and operation. His worldwide record includes drilling and well testing management in Indonesia (Kamojang) for GENZL, exploration drilling technical management for UNDP in Ethiopa (Aluto-Langano), Senior Drilling Engineer, Supervisor and Manager in Kenya (Olkaria/Eburru World Bank funded project), Indonesia (Ulumbi-western Flores-project), West Indies (Saint Lucia-Sulphur Springs/Soufriere, UN Revolving Fund), Mexico (Los Humeros, Tres Virgines, Commission Federal de Electricidad), Azores (Sao Miguel, Sogeo), Japan (Nigorikawa, Hokkaido, Sumikawa-Honshu, Japan Metals & Chemicals) among other undertakings. Hagen Hole has developed a somewhat unique expertise in aerated ("balanced") drilling he could exercise in Japan, New Zealand, Germany, Philippines, Indonesia, Kenya, Mexico and Iceland. Hagen Hole has given lectures as guest speaker at the Auckland University, the UN University Geothermal Training Programme in Reykjavik, Iceland, the UNIDO Geothermal School in Trieste, Italy and Petroleum Engineering School in Dubrovnik, Croatia. Member of SPE, IGA, NZ Geothermal Association and Geothermal Resources Council and Iceland Deep Drilling Project.

Pierre Ungemach, presently Chairman of GPC IP, a geothermal engineering and service company he founded in 1989. Holds Masters degrees in Physics and Applied Maths and a post graduate degree in Geophysical Engineering. His wide professional experience covers the areas of physics of the Earth interior, geophysical prospecting, reservoir engineering and simulation, well testing and log analysis, geothermal engineering and servicing. Pierre Ungemach served successively, among other appointments, as ground water consultant (Ital Consult, Italy), research engineer (French School of Mines, French Geological Survey, BRGM), R&D Programme Manager in geothermal energy(European Commission, DGXII). Served two terms (1995-2001) as IGA BoD member. Currently Board member of the IGA European Branch Forum and of EGEC (European Geothermal Energy Council) and member of the GRC (Geothermal Resources council). Authored and co-authored over seventy technical/scientific papers, including six books and conference proceedings. Holds six patents in drilling/completion and production processes.

APPENDIX

RESUMES
- Miklos Antics
- Peter Eric Danielsen
- Hagen Hole
- Pierre Ungemach

CURRICULUM VITAE

Miklos ANTICS. (Romania/France). Graduated and post graduated in Petroleum Engineering from the Ploiesti (Romania) School of Petrol. Attended in 1992 a one year course at the Geothermal Institute in New Zealand in geothermal reservoir engineering and computer simulation, where he specialised in geothermal well testing and two phase flow modelling. Ph.D. thesis on geothermal well testing and reservoir simulation. Served five years as well testing/logging engineer in the Oradea based FORADEX Inc. staff. During 1995-2003 was with GEOFLUID S.A. (a French-Romanian geothermal consulting company he co-founded in 1995), where he implemented well testing and geothermal and petroleum reservoir simulation codes, which were successfully applied to the simulation of the Oradea geothermal reservoir in the framework of the feasibility strategy of development of the city district heating network. Technical Manager of Geoproduction Consultants (GPC) France, during 2003-2006. Currently Managing Director of GPC Instrumentation Process (GPC IP) and Associate Professor at the Faculty of Energy Engineering and the International Geothermal Training Centre of the University of Oradea, Romania. Former secretary of the Romanian Geothermal Association. Secretary of the Board of EGEC (European Geothermal Council) since 2003. Member of the Board of Directors of the International Geothermal Association (IGA), Chairman of the Programme and Planning Committee. Vice-President of the IGA European Branch Forum. Lectured on Geothermal Reservoir Simulation and Sustainable development of geothermal resources at several ISS summer schools and seminars. Member of the IGA available lecturers roster. Authored and co-authored over 35 technical papers (English and Romanian) and four textbooks.

CURRICULUM VITAE

Name/Country **Peter E. Danielsen, Iceland**
Year of Birth **1968**

Resume

Presently Assistant Head of the Technical Department at Iceland GeoSurvey with a Masters degree in Hard Rock Geology, managing High Temperature logging nationwide. Part of a team designing logging trucks for both Low and High Temperature applications. Team leader for design / re-design of logging equipment for special case scenarios. Extensive experience in geophysical logging and well testing, at Low and High Temperature conditions, and subsequent interpretation and consulting.
Acting Chairman of the Safety Committee at Iceland GeoSurvey. In charge of preparing, documenting and implementing OSH standards.
Further experience counts geophysical exploration for metals in Norway. TEM soundings throughout Denmark locating groundwater reservoirs. Interpretation on oil well reports to establish possible geothermal potential in the Rhine Graben, Germany. Improvement of the Aegir Ridge bathymetric map based on multibeam echosounder data. Seismic soundings and interpretation to establish foundation depth for an Aluminum smelter at Reyðarfjörður, East-Iceland.
Registered as an expert on geothermal issues at the “Great Danish Encyclopedia” project (www.denstoredanske.dk).

CURRICULUM VITAE

Hagen HOLE:

With a mechanical engineering background, Hagen commenced his involvement in the geothermal industry carrying out research on geothermal two phase fluid flow, under a New Zealand Energy Research and Development Fellowship at the University of Auckland, and has since accumulated some 32 years specialist experience in geothermal development projects, and in particular geothermal drilling.

In 1978 he joined Geothermal Energy New Zealand Ltd. (GENZL) and acted as Measurements Engineer, and then Steamfield Manager with responsibilities for direction and management of the drilling and well testing of the production drilling phase of the Kamojang Geothermal Project for the New Zealand Government funded Kamojang Geothermal Development Project in Indonesia. In 1980 Hagen was appointed as UNDP Chief Technical Advisor for the Aluto - Langano exploration drilling programme in Lakes district of Ethiopia which he fulfilled until the completion of the project in 1985.

From late 1985 to 1991, he then filled the position of Senior Drilling Engineer for the World Bank funded, Olkaria development project and the Eburru exploration project in the Rift Valley of Kenya.

Between April 1991 and March 1997 Hagen was the sole manager for the Ulumbu Mini Geothermal Power Project, in western Flores, Indonesia. In addition, he was Supervisor for the United Nations Revolving Fund for Natural Resources Exploration, on the St Lucia Geothermal Development Project at Sulphur Springs / Soufriere, St Lucia; Aerated drilling assistance and training to Commision Federal de Electricad at the Los Humeros and Tres Virgenes Fields in Mexico; drilling supervision services at the Darajat Geothermal Field, Indonesia for Amoseas Indonesia Inc.; Consulting supervisor for drilling and well testing operations on the Island of Sao Miguel, Azores; for The Consorcio Geotermico de Sao Miguel; Consulting services for aerated drilling operations at the Nigorikawa geothermal field, Hokkaido, and at the Sumikawa geothermal Field, Honshu, Japan; for Japan Metals and Chemicals, Japan.

Between March 1997 and October 2000 Hagen acted as Steamfield Services Manager / Principal Consultant, PB Power – GENZL Division, and was involved in the implementation of the OrPower 4 development of the West Olkaria Field in Kenya; the Oserian Development Company mini geothermal power plant and greenhouse heating system, Olkaria Kenya; Rural electrification pre-feasibility studies for development of Mini geothermal power plants at Hu'u in Sumbawa, and Sukoria in Flores, Indonesia; and Wayang Windu Geothermal Project, central Java, Indonesia.

In October 2000, Hagen resigned from PB Power – GENZL and formed Geothermal Consultants New Zealand Ltd. (GCNZL) From this time to the present he has continued consultancy work specialising in geothermal drilling and related activities in many countries around the world, including Germany, Mexico, Kenya, Iran, New Zealand, Indonesia, Philippines, Iceland, and United Arab Emirates

Responsibilities have included the management and technical specification of all phases of projects from site selection and preparation, design and specification of wells, procurement of materials and drilling services, supervision of drilling activities, well testing and preparation of a Feasibility Study reports.
In addition, Hagen has been integrally involved in the development of aerated drilling systems, and has also participated as a guest lecturer for the Auckland University Geothermal Institute Diploma course, the United Nations University, Geothermal Training Programme, Reykjavik, Iceland; Petroleum Engineering Summer School, Dubrovnic, Croatia; UNIDO-ICS, Geothermal Training Programmes, Trieste, Italy.

CURRICULUM VITAE

Pierre UNGEMACH. Presently chairman/CEO of GPC IP a geothermal engineering and service company he created in 1989. Master degrees in Physics and Applied Mathematics. Post graduate degree in geophysical engineering. Wide experience in Physics of the Earth Interior, geophysical prospecting, reservoir engineering and simulation, well testing and log analysis, geothermal engineering and servicing.

Served successively as member of academic staff (University of Strasbourg), ground water consultant (Italconsult, Roma), research engineer (French School of Mines, BRGM), project/region manager (Middle East, BRGM), reservoir simulation expert (BRGM), R&D programme manager in geothermal energy (European Commission, DG XII), geothermal manager (Geophase/Geotherma, Geoservices group).

Sixty two technical/scientific papers including six books and conference proceedings published to date. Holder of six patents in drilling/completion and production processes.

Served two terms (1995-2001) as member of the Board of Directors of the International Geothermal Association (IGA). Presently member of the board of IGA European Branch (IGA EB) and of the European Geothermal Energy Council (EGEC). Reviewer of Geothermics (Elsevier Publishing).

Drilling, Completion and Testing of Geothermal Wells

Section 2. An Introduction to Geothermal Systems

1. GEOTHERMAL ENVIRONMENTS

Pierre Ungemach

GPC INSTRUMENTATION PROCESS, Roissy-en-France, France

1 GEOTHERMAL ENVIRONMENTS

Terrestrial heat and geothermal environments are dictated by Earth's (inner) structure and the lithospheric plate boundaries and tectonic processes illustrated in fig. 1 to 3 respectively.

The geothermal heat flow is a planetary concept applied to planet Earth with heat flowing outwards from the Earth interior. Its losses amount to ca 42 TW (i.e. # 0.08 W/m^2 less than 10^{-4} of total solar irradiation) of which 20% are supplied by planetary accretion and meteorite impact and 80% by radioactive decay of Uranium, Thorium and Potassium isotopes within the crust and mantle, distributed as shown in table 1. From the difference between the total terrestrial heat losses and radiogenic replenishment (# 32 TW) can be inferred the cooling rate of the Earth, which actually is very slow (ca one degree in 10 million years). The heat flow density q is derived from the Fourier law of heat conduction

$$q(w/m^2) = \lambda(w/mK)\frac{\partial\theta}{\partial z}(K/m) \qquad (1)$$

with:

λ= thermal conductivity

$\frac{\partial\theta}{\partial z}$ = i = geothermal gradient

Assuming a uniform granite rock mass (λ # 3.0 W/mK) and an average 0.02 K/m gradient the heat flow density would be equal to 0.06 W/m^2 a figure actually close to the continental average bearing in mind that the ocean average value is nearing 0.100 W/m^2.

Assuming a reference average surface temperature of 15 °C, the total thermal energy of the Earth would amount to ca 12.6 10^{24} MJ of which # 5.4 10^{21} MJ emanating from the Crust [Armstead, 1983, quoted by Dickson and Fanelli, 2004], indeed a huge potential (twice the total human energy consumption). However, its exploitation, presently restricted to continental areas and by conventional extraction technologies is limited to those settings meeting the four prerequisites required to structure a geothermal reservoir (see sketch in fig. 4).

- a heat source which may be a magma body or simply hot rocks at depth;
- sealing/trapping bed rocks and cap rocks in which only conductive heat transfer occurs as opposed to the confined reservoir where convection (advection) is the prevailing transfer mode;
- porous and permeable rocks (of matrix or fractured types) constituting the reservoir material proper;
- last but not least, a heat carrier fluid, either hot water or steam (single phase) or both (two phase).

Such areas, eligible to commercial exploitation, can be identified in zones selected thanks to the geodynamic guidelines provided by the Global Plate Tectonics model of the lithosphere illustrating the impact of the Earth "thermal engine", driven by upper mantle convection, quoted by Dickson and Fanelli [2004].

Table 1: Radiogenic heat features from U, Th and K isothopes

Isotope	Heat release [W/kg isotope]	Half-life [years]	Mean mantle concentration [kg isotope/kg mantle]	Heat release [W/kg mantle]
^{238}U	9.46 × 10-5	4.47 × 109	30.8 × 10-9	2.91 × 10-12
^{235}U	5.69 × 10-4	7.04 × 108	0.22 × 10-9	1.25 × 10-13
^{232}Th	2.64 × 10-5	1.40 × 1010	124 × 10-9	3.27 × 10-12
^{40}K	2.92 × 10-5	1.25 × 109	36.9 × 10-9	1.08 × 10-12

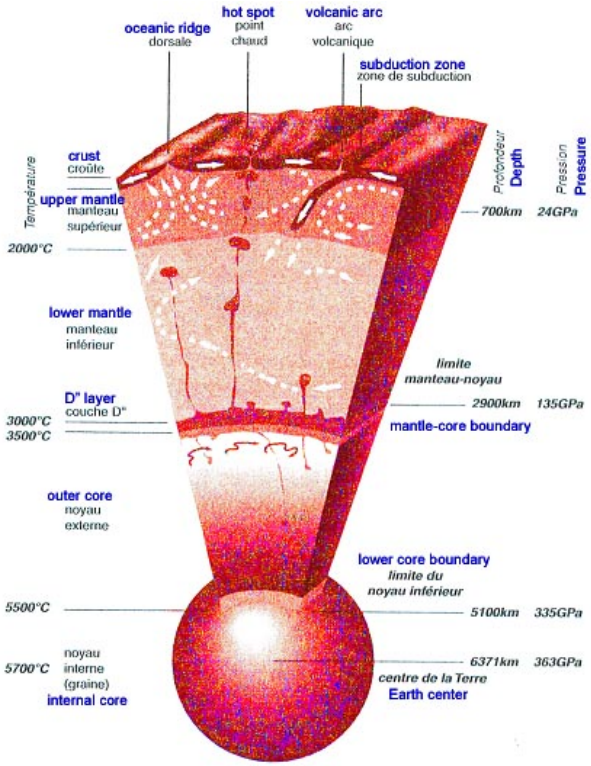

Figure 1: Structure of the Earth interior [V. Courtillot, 2009]

Figure 2: Lithospheric plate boundaries [Geothermal Education Office, CA, USA]

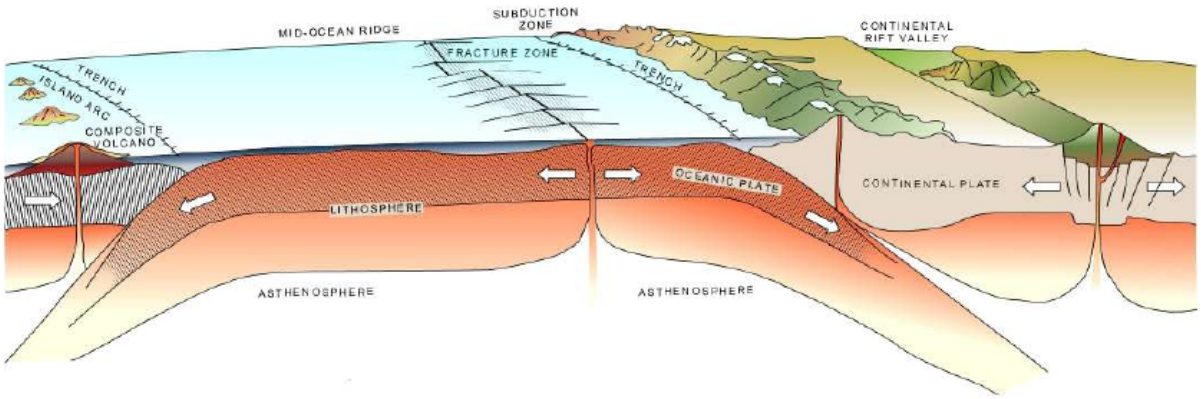

Figure 3: Plate tectonics process schematics [Dickson and Fanelli, 2004]

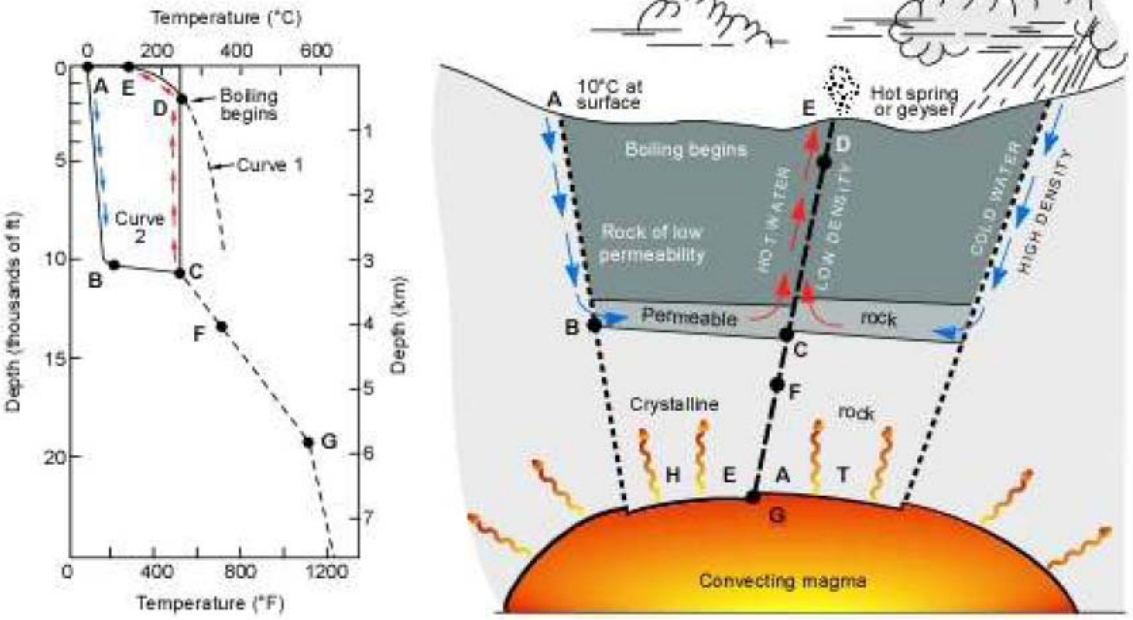

Boiling curve temperature vs depth profile

Reservoir model showing fluid circulation patterns

Figure 4: Geothermal system sketch [White, 1973, quoted by Dickson and Fanelli, 2004]

As fas as Europe is concerned, it exhibits a variety of geothermal resource settings, displayed in fig. 5, which address distinctive geodynamic environments namely:

- Large sedimentary units subdivided into (i) intracratonic (Paris – Hampshire, Aquitaine, Tajo, Castillan, Rhone – Languedoc, West Yorkshire – Netherland, North German, Danish, Warsaw, Thracean), (ii) orogenic belt (Pyrenean, Ebro, Caltanisetta, Alpine, Po Valley, Appenninic, Carpathian) foredeep, and (iii) marginal/back arc basins (Pannonian, Transylvanian, Aegean) hosting, generally multiple, aquifer systems with normal, low and high geothermal gradients respectively, favouring direct uses, among which geothermal district heating (GDH) holds a prevailing share.
- Tertiary-quaternary continental rifts (Rhine Graben, Limagne, Rhone – Bresse, Campidano, Pantelleria) eligible to medium enthalpy/CHP prospects and, ultimately, to EGS developments of which two are online (Soultz, Landau) and one (Basel) temporarily abandoned.

- Orogenic folded belts and foreland platforms, often associated with deep faulted – upwelling hydrothermalism and medium enthalpy reservoirs.
- Crystalline massifs (Iberic Meseta, Armorican, Central France, Bohemian, Rhodope) with hot springs and hydrothermal faulted systems.
- Recent "in plate" Pliocene/quaternary volcanism (Catalunya, Puy Chain, Effel, Campidano, Susaki), regarded as candidate medium enthalpy, if not EGS, projects.
- Last but not least, active subduction, volcanic island arcs (Aeolian, Aegean), active magmatic (Tuscany) and recent/active "pull a part" extensional horst and graben structures (Anatolian coastline), the field of excellence of present and future high enthalpy geopower

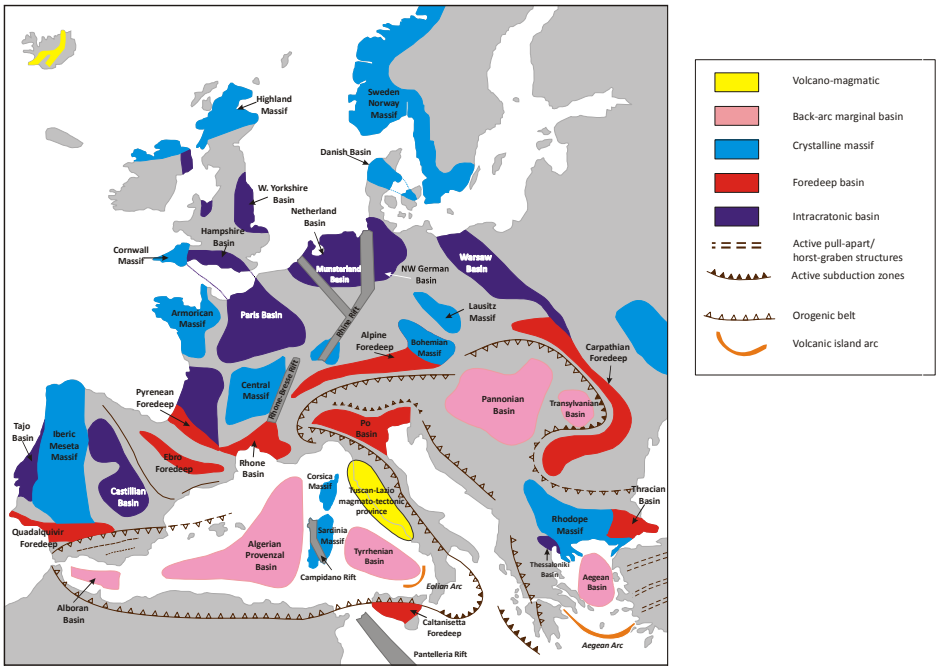

Figure 5: European geodynamic settings [C. Sommaruga, 1981]

REFERENCES

Armstead, H.C.H. (1983). Geothermal Energy. E&F.N.Spon, London.

Courtillot, V. (2009). Nouveau Voyage au Centre de la Terre. Odile Jacob Ed., Paris.

Dickson, M.H. and Fanelli, M. (2004). What is Geothermal Energy? Int. Geoth. Ass. (IGA).

Mufler, P. and Cataldi, R. (1978). Methods for Regional Assessment of Geothermal Resources, *Geothermics*, **7**, 53-89.

Sommaruga, C. (1981). Personal communication.

White, D.E., Muffler, L.J.P. and Truesdell, A.A. (1971). Vapor Dominated Hydrothermal Systems Compared with Hot Water Systems, *Economic Geology*, **66**, 75-97.

White, D.E.. (1981). Characteristics of Geothermal Resources. In: Kruger, P. and Otte, C., eds, Geothermal Energy, Stanford University Press, Stanford, Ca, 69-94.

2. RESERVOIR PHYSICS. AN OVERVIEW

Pierre Ungemach
GPC INSTRUMENTATION PROCESS, Roissy-en-France, France

1 RESERVOIR PHYSICS. AN OVERVIEW

A hydrothermal system meeting the four reservoir prerequisites stated previously will host hot fluids, whose physics and chemistry are governed by heat and mass transfer processes and chemical thermodynamics.

Heat flow, the source of geothermal energy, is governed by the Fourier law of heat conduction, which relates heat flow density to the temperature gradient via the heat conduction coefficient of the rock mass. Similarily, in a porous rock, the soaking fluid(s) will flow at a rate given by the Darcy law relating the pressure gradient (diminished, in the vertical direction, by gravity) to velocities via the rock permeability divided by the fluid dynamic viscosity. Note here that the Darcy law applies separately to each fluid phase (liquid, vapour) by applying a relative permeability criterion, in which phase relative permeability is expressed as a function of liquid saturation.

Note also that capillary effects are usually neglected in practical reservoir simulation studies. Finally, mass flows of the fluid constituants, such as dissolved salts and non condensable gases (principally CO_2) soluble in water and also in the gaseous phase, will take place according to the Fick law of molecular diffusion, which relates the mass fraction gradient to mass fluxes via a combination of a diffusivity factor, porosity and porous medium tortuosities [Pruess, 2002].

Natural heat convection will occur in the form of convective rolls [Combarnuous, 1975] as a result of fluid density changes (buoyancy) at depth and upward heating from bed rocks.

Forced convection will take place in presence of sources and sinks and become clearly the driving mass and heat transport mechanism, creating, when amplified by commercial exploitation, an imbalance in the natural field recharge vs well discharge budget, between renewability and exhaustion, a mining issue at the center of the sustainability debate [Ungemach, 2007, Sanyal, 2005, Rybach, 1999].

Before moving to the derivation of the mass and energy conservation equations, worth mentioning, with respect to the *in situ* fluid states, are the physical properties of the main geothermal fluid, i.e. water under its two, liquid and gaseous, states illustrated in fig. 1 to 3.

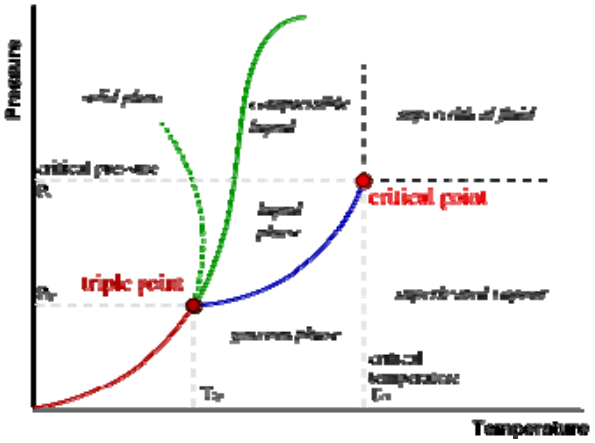

Figure 1: Phase diagram for pure water.

Fig. 1 evidences, in the pressure vs temperature diagram, the phases of pure water and the transition from liquid to vapour across the saturation curve. The latter, also called boiling curve, is displayed in more detail in fig. 2 for pure water and brines up to 25% (mass) equivalent salinity. Fig. 3 synthesises, in a form more appropriate for thermodynamic calculations, the water phases and transitions (liquid/two phase/vapor), the pressure vs enthalpy relationship [Mollier diagram] for pure water together with iso density, temperature and steam quality (mass fraction) contours.

With reference to the saturation curve (thick blue line in fig. 3) (i) compressed water reservoirs require pressures (at reservoir temperature) higher than saturation pressure; (ii) two phase reservoirs pressures equal to saturation pressure, and (iii) superheated steam pressures lower than saturation pressures. Note that "dry steam" systems (of the Larderello, Geysers, Matsukawa type) exhibit reservoir pressures and temperatures close to those corresponding to the maximum enthalpy of water (marked B in fig. 3), i.e. 2803 kJ/kg, 240 °C, 33.47 bar. Above the critical point (C on fig. 3) the state of the supercritical fluid is neither water nor steam but that of a "dense" fluid [Economides, 1987]. Economides [1987] stresses the existence of a fourth fluid state in geothermal systems, that of adsorbed water, studied by Hsieh and Ramey [1983] which could account for as much as 20 times the mass of water present in a superheated reservoir.

From the Mollier diagram (fig. 3) and steam tables can be derived the energy contents of the host rock and soaking fluid, with respect to three fluid states, single state liquid (compressed water), single phase vapour (super heated steam) and two phase (liquid flashed to vapour) respectively.

Based on the equations summarised in Appendix, and applied to a 250 °C reservoir, a 15% porosity, 40/34 bar initial and final pressures and a 50 MWe rated/30 year operated geopower plant results of the exercise listed in table 1 lead to the following conclusions.

(i) Most of the energy is stored in the rock, neither in the water nor in the steam;
(ii) The energy of the steam is less than that of the water, its higher enthalpy being more than counterbalanced by its lower density;
(iii) The reservoir volumes required to sustain the target 50 MWe plant stand almost identical for single phase (liquid, vapour) states but significantly lower for a two phase state (liquid moving to vapour) owing to the expansion of denser compressed water to lighter flashed superheated steam.

Table 1: Energy densities and volume requirements to sustain a 50 MWe rated geoelectric plant over 30 years for various high enthalpy reservoir settings (initial temperature 250 °C; initial/final pressures 40/34 bars; reservoir porosity 15%).

ITEM	Single phase liquid (compressed water)	Two phase liquid/vapor	Single phase vapor (superheated steam)
Total reservoir (rock + density) energy density (kJ/m^3)	25,170	145,086	23,089
Volume required to sustain a 50 MWe 30 yrs plant life (10^9 m^3)	8,844	1,534	9,641

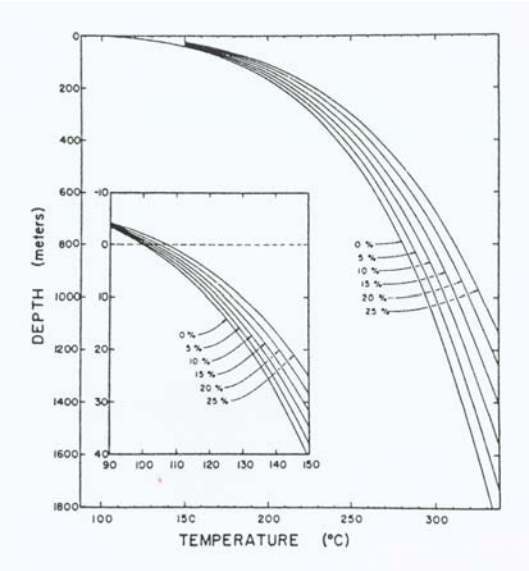

Figure 2: Boiling curves for pure water and brines.

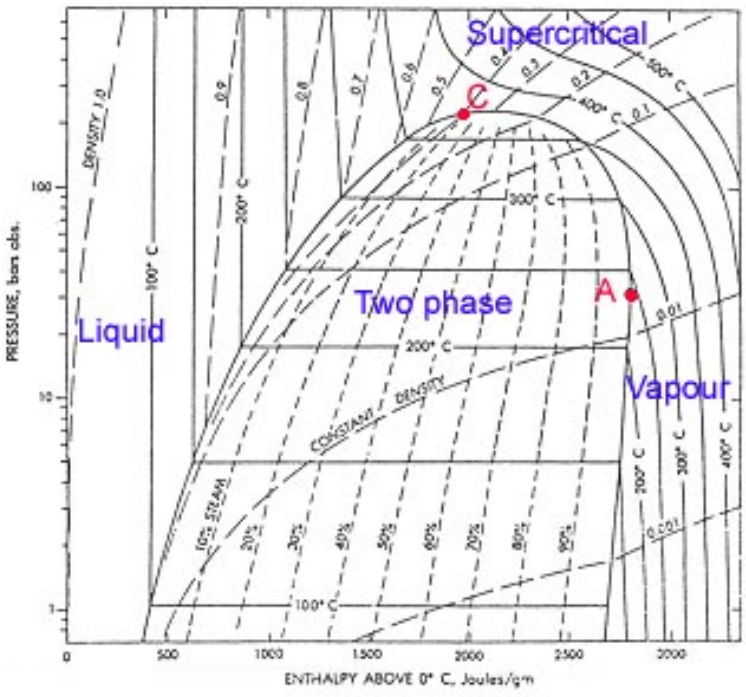

A: maximum enthalpy (2803 kJ/kg, 240 °C, 33.47 bar)
C: critical point (374.1 °C, 224 . 91 bar)

Figure 3: Pressure-enthalpy diagram for pure water [Mollier].

The quantification of the mass and energy balances follows the rationale summarised below.

If A, Q and q refer to unit (mass, energy) contents, fluxes and sources (sinks) respectively and m and e subscripts to mass and energy fields, mass and energy conservation equations (assuming for energy conservation that advection is the driving transport mechanism) can be expressed as follows (O'Sullivan, 1987, Bodvarsson, 1986):

Mass conservation

$$\frac{\partial A_m}{\partial_t} + \nabla Q_m + q_m = 0 \qquad (2)$$

with:

$A_m = (\rho_v S_v + \rho_l S_l)$ unit mass

$Q_m = (\rho_v V_v + \rho_l V_l)$ unit flux (3)

$\rho, V, S =$ density, velocity, saturation index

$l, v =$ liquid, vapor subscripts

Energy conservation

$$\frac{\partial A_e}{\partial_t} + \nabla Q_e + q_e = 0 \qquad (4)$$

with:

$A_e = (1-\phi)\rho_r u_r + \phi(\rho_v u_v S_v + \rho_l u_l S_l)$

$Q_e = \rho_v h_v v_v + \rho_l h_l v_l - \lambda \nabla \theta$ (5)

u, h = specific internal energy and enthalpy

$\lambda =$ thermal conductivity

$\theta =$ temperature

Combination of the conservation of momentum $[\nabla(\rho v) = 0]$ and of the Darcy law, dynamic equation, relating flow velocities to pressures, applied to liquid and vapor phases, i.e:

$$V_v = -k \frac{k_{rv}}{\mu_v}(\nabla_p - \rho_v g) \qquad (6)$$

$$V_l = -k \frac{k_{rl}}{\mu_l}(\nabla_p - \rho_l g) \qquad (7)$$

with:

k = intrinsec permeability

k_r = intrinsec relative phase permeability

p = pressure (8)

g = gravity

μ = dynamic viscosity

leads to the following, fully developed, pair of simultaneous partial differential equations (PDE):

$$\nabla[k \frac{k_{rv}}{\mu_v}(\nabla p - \rho_v g) + k \frac{k_{rl}}{\mu_l}(\nabla p - \rho_l g)] = \frac{\partial A_m}{\partial t} + q_m \qquad (9)$$

$$\nabla[h_v k \frac{k_{rv}}{\mu_v}(\nabla p - \rho_v g) + h_l k \frac{k_{rl}}{\mu_l}(\nabla p - \rho_l g)] = \frac{\partial A_e}{\partial t} + q_e \qquad (10)$$

To the foregoing ought to be added the equations of state expressing the temperature and pressure dependance of thermo-hydrodynamic rock and soaking fluid characteristics, namely, densities, viscosities, thermal conductivities and heat capacities.

Note that, for a low enthalpy, single phase liquid, geothermal source, the mass and heat transfer PDEs reduce to:

$$\nabla[\frac{k}{\mu}\nabla(p+\rho gz)] = \phi c_t \frac{\partial p}{\partial t} + q \qquad (11)$$

$$\nabla(\lambda\nabla\theta) - \gamma_f(\phi U\nabla\theta) = \gamma_t \frac{\partial\theta}{\partial t} \qquad (12)$$

with:

U = flow velocity

z = vertical coordinate

c_t = total (rock + fluid) compressibility

γ_t = reservoir heat capacity = $\phi\gamma_f + (1-\phi)\gamma_r$

f, r = fluid and rock subscripts

Equations of state

$$\rho = \rho(p,\theta)$$

$$\mu = \mu(p,\theta) \qquad (13)$$

$$\lambda = \lambda(p,\theta)$$

$$\gamma = \gamma(p,\theta)$$

These simultaneous sets of PDEs, coupled with their equations of state and relevant boundary and initial conditionss are non linear as a result of temperature dependant velocity fields and fluid states.

They are solved by means of numerical modelling techniques and reservoir simulation algorithms discussed by Pruess & O'Sullivan [2006].

1.1 Material balance approach

The method, popularised by petroleum reservoir engineers, has been extensively used in lumped parameter modelling as a geothermal reservoir evaluation tool.

It assumes that the reservoir behaves as a single, averaging, entity in response to (inner) field production/injection and (outer) peripheral water influx [Gundmundsson, 1988].

Hence, the material balance can be written under a simplified form:

$$W(t) = Wo - Wp + Wi + Wr \qquad (14)$$

where W stands for masses and subscripts o, p, i and r for initial in place, production, injection and recharge fluid masses respectively.

Assuming further, that (i) neither water influx nor injection occurs, and (ii) withdrawn fluid mass Wp can be related to pressure drawdown Δp as:

$$\Delta p = Wp/(\phi V\rho c_f) \qquad (15)$$

where Φ, V, ρ and c_f refer to porosity, reservoir volume, fluid density and compressibility respectively. Note incidentally that heated fluid compressibility may increase by several orders of magnitude from liquid water, to steam and two phase mixtures.

(15) is a straight line, Wp vs Δp plot, assuming a constant $1/\phi V\rho c_f$ slope, an assumption no longer valid for superheated steam reservoirs owing to a strongly pressure dependant compressibility coefficient. The pseudo-reduced natural gas pressure function p/Z (Z = gas deviation factor) is used instead and plotted against the cumulative steam production, an approach pioneered and successfully verified by Whiting and Ramey [1969] and Ramey [1970], the latter on the Geysers field, and illustrated in fig. 4, which yields, by extrapolating to zero pressure the straight line plot, the initial steam in place mass Wo.

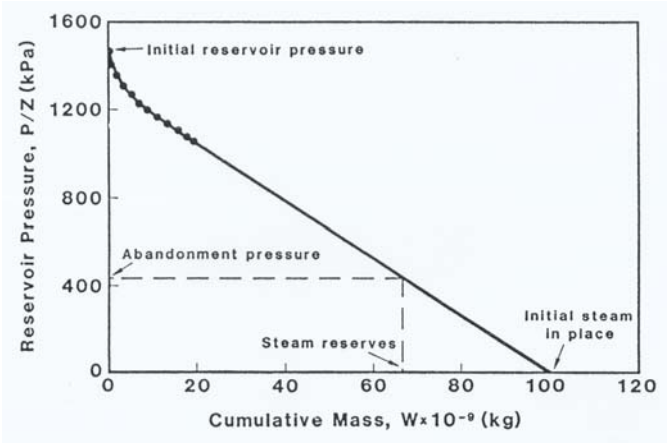

Figure 4: Pressure depletion vs cumulative mass production superheated steam reservoir [Gudmundsson, 1988].

Economides [1987] has refined the approach, by extending to two phase (water/steam) geothermal reservoirs the methodology applied by Havlena and Odeh [1963] to a variety of field settings addressing undersaturated, gas cap and solution gas drive, hydrocarbon reservoirs. Accordingly, the volumetric balance may be expressed as follows (compaction effects negligible):

Withdrawal = Liquid water expansion + Steam cap expansion + Desorbed water expansion.

leading ultimately to the following equation:

$$W_i(E_l + mE_g) = F \tag{16}$$

where:

$$F = W_p[x\upsilon_g + (1-x)\upsilon_l] - Ah_v\rho_r M(x_i - x)\upsilon_g \tag{17}$$

$$E_l = (\upsilon_l - \upsilon_{li}) + (\upsilon_{\lg} - \upsilon_{\lg i}) \tag{18}$$

$$E_g = (\upsilon_g - \upsilon_{gi}) - \rho_r M(x_i - x)\upsilon_g\upsilon_i \tag{19}$$

with:

A = area

M = molecular weight

x = absorbed water (kg mole/kg rock)

x = liquid mole fraction (steam quality)

m = slope of pression vs log time semi-log plot

Wi = initial steam in place

Wp = cumulative production

υ = specific volume

h_v = vapor zone thickness

i, g, l = initial, gas and liquid subscripts

Note that, for a single phase liquid reservoir, equation (16) reduces to:

$$E_l W_i = F \qquad (20)$$

In spite of these somewhat esoteric formalism and nomenclature, equation (16) matches a straightline (F/E_l) vs (E_g/E_l) plot whose slope (mWi) and origin ordinate (Wi) deliver the initial steam in place.

The exercise had been earlier applied by Economides and Miller [1984] to the vapour dominated material balance case, accounting for the water absorption/desorbption phenomenology whose importance and magnitude had been demonstrated by previous experimental works [Hsieh, 1980].

Again, the result, approximated as:

$$W_p = \frac{M\sigma}{p*}(p_i - p)m_r \qquad (21)$$

with:

m_r = rock mass

p* = vapor pressure

is the equation of a straight line when cumulative production is plotted against pressure, providing the initial steam in place when extrapolated to the p = 0 axis.

Nevertheless, in spite of the advent of modern, powerful, distributed parameter reservoir simulation techniques, lumped parameter methods should not be necessarily regarded obsolete and overlooked. Actually, the approximation of uniform reservoir properties and behaviour is often verified given the generally high performance of commercially developed fields which tends to mask the impact of local reservoir heterogeneities and singularities.

The method can still be valuably implemented as a preliminary global approach, an exercise exemplified by a recent work by Sanyal [2005], elaborating on sustainable exploitation issues further to a worldwide compilation of major liquid dominated geothermal reservoirs.

From a material balance, approximated as:

$$m - m_{sr} = -S(\frac{dp}{dt}) + m_r \qquad (22)$$

with:

m = mass depletion rate

m_{sr} = steady-state component of, exploitation free, natural state reservoir recharge

m_r = pressure dependant, exploitation induced, reservoir recharge (r = recharge coefficient, Δp = pressure draw down)

S = global (rock + fluid) reservoir elastic storage coefficient

the following pressure response may be derived:

$$\Delta p = -(\frac{m - m_{sr}}{r})[1 - l^{-\frac{r}{s}t}] \qquad (23)$$

1.2 Reservoir simulation

Geothermal reservoir simulation aims basically at solving by numercial techniques the set of simultaneous PDEs and related equations of state and boundary/initial conditions governing the mass and heat transfers in the reservoir in view of (i) checking the consistency of the conceptual model, (ii) assessing reservoir structure, resource status, flow patterns and discharge/recharge mechanisms, and

(iii) last but not least, optimising field development in a, preferably, sustainable reservoir management perspective.

Accordingly, it has become, over the past decade, a standard widely used reservoir evaluation tool, whose methodology conforms to the interactive sequence sketched in fig.5 flow chart.

It should be readily stressed here that the elaboration of a relevant conceptual model of the reservoir is, whatever the degree of sophistication of the applied – deterministic vs. probabilistic, forward or inversion – modelling techniques, of utmost importance in securing further simulation and assessment stages.

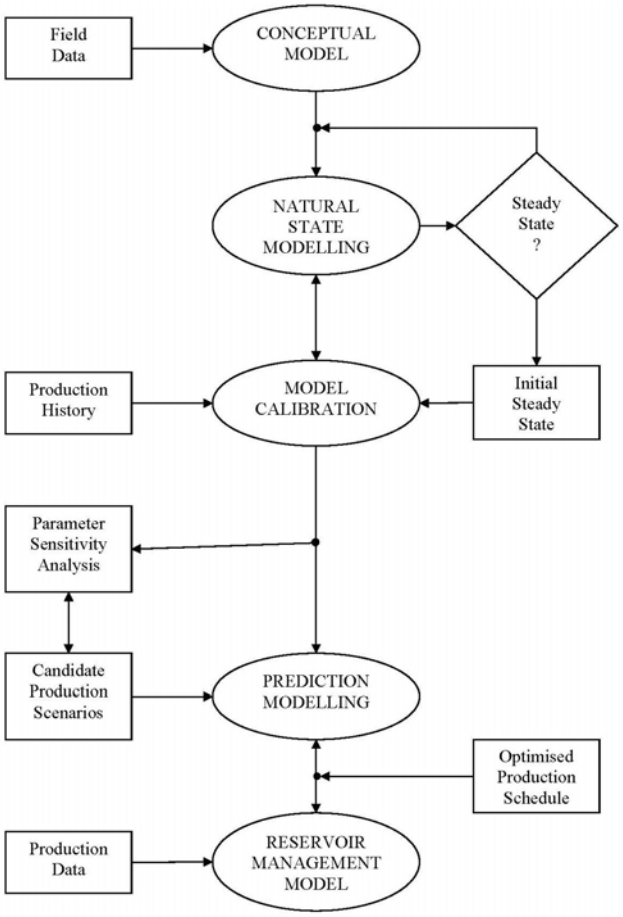

Figure 5: Simulation methodology.

Hence, a reliable interpretation of all field data collected from surface/subsurface geological, hydrogeological, geophysical, geochemical surveys, drilling/logging/testing, tracer tests and their integration into a comprehensive conceptual model, imaging reservoir structure and extent, major flow paths, intake/outflow zones and temperature patterns, is a major concern for the reservoir engineer.

Natural state modelling and model calibration phases come next. Natural state modelling often requires repeated simulation runs over long periods, several thousands years or more, until the system reaches steady state (see simulation flow chart in fig. 5). The next step consists of matching model temperature and flow outputs against measured data according to the modelling methodology summarised in fig. 6.

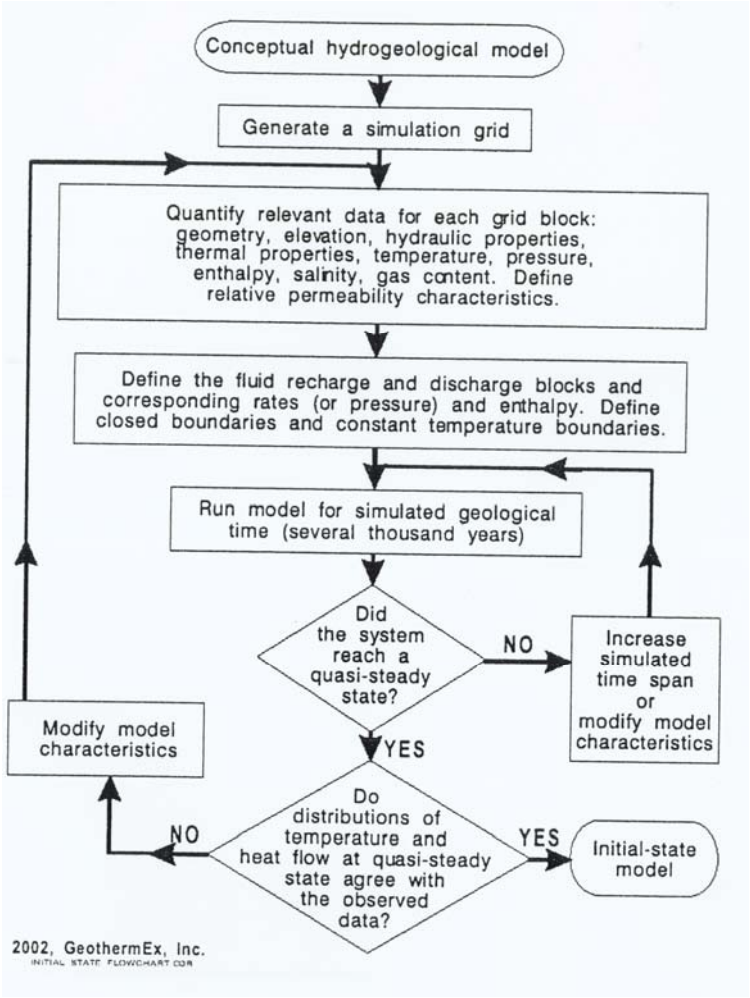

Figure 6: Natural state modelling flowchart [Sanyal, 2002].

Interpolation of measured field data (temperature, pressure, enthalpies) and parameters (permeability, porosity, …) is generally performed by means of statistical [Kriging] methods available from routine computer software.

Model calibration is a similar, history matching, trial and error process, carried out under transient conditions provided by well (production, pressure, enthalpy, non condensable gas contents, …) exploitation records. It enables to assess the most consistent field parameter distribution according to a best fit criterion between computed and recorded well data. The latter suggests parameter inversion techniques, widely applied in geophysical data processing, based on minimising of differences between computed vs observed field patterns be implemented instead of the current, somewhat tedious, forward (direct) trial and error parameter adjustment practice. As a matter of fact, most geothermal modellists have resisted so far this appealing trend preferring to rely on physically dependable conceptual and natural state models. They should not be blamed for that.

APPENDIX

Rock and fluid energy densities and energy outputs (source: Ungemach et al, 2007)

Energy densities

- *Rock*

$$E_r = (I - \phi)\rho_r c_r (\theta_o - \theta_f) \quad (1)$$

with:

ϕ = porosity

ρ_r = rock density (kg/m^3)

c_r = rock specific heat (kJ/kg °K)

θ_o = initial rock temperature (°C, °K)

θ_f = final rock temperature (°C, °K)

- *Fluid*
  - Single phase liquid (compressed water)

$$E_w = \phi\left[\frac{h_w(p_i,\theta_i)}{\nu_w(\theta_i)} - \frac{h_w(p_f,\theta_f)}{\nu_w(\theta_f)}\right] = \phi\left(\frac{h_{wi}}{\nu_{wi}} - \frac{h_{wf}}{\nu_{wf}}\right) \quad (2)$$

with:

h_{wi}, h_{wf} = liquid (water) enthalpies at initial and final reservoir conditions (kJ/kg)

ν_{wi}, ν_{wf} = liquid (water) specific volume at initial and final reservoir conditions (m^3/kg)

p_i, p_f = fluid (water) pressure at initial and final reservoir conditions (Pa)

  - Two phase (liquid water/steam)

$$E_{2\varphi} = E_{wi} - E_{sf} = \phi\left(\frac{h_{wi}}{\nu_{wi}} - \frac{h_{sf}}{\nu_{sf}}\right) \quad (3)$$

with:

h_{sf} = saturated steam enthalpy at final state

ν_{wf} = saturated steam specific volume at final state

  - Single phase vapor (superheated steam)

$$E_s = \phi\left[\frac{h_s(p_i,\theta_i)}{\nu_s(\theta_i)} - \frac{h_s(p_f,\theta_f)}{\nu_s(\theta_f)}\right] = \phi\left(\frac{h_{si}}{\nu_{si}} - \frac{h_{sf}}{\nu_{sf}}\right) \quad (4)$$

with:

h_{si}, h_{sf} = superheated steam enthalpies at initial and final reservoir conditions

ν_{si}, ν_{sf} = superheated steam specific volumes at initial and final reservoir conditions

p_i, p_f = superheated steam pressures at initial and final reservoir conditions (Pa)

- *Total reservoir energy densities*
  - Single phase liquid

$$E_{wt} = E_w + E_r$$

  - Two phase

$$E_{2\varphi t} = E_{2\varphi} + E_r$$

(5)

  - Single phase vapor

$$E_{st} = E_{st} + E_r$$

- *Reservoir volumes required to sustain geoelectric power plant life*

$$W_{el} = P_{el}\Delta t \quad (6)$$

$$W_{th} = W_{el}/\eta$$

with:

W_{el} = electrical energy (kWhe)

P_{el} = installed electrical power (kWe)

Δt = plant life (hrs)

W_{th} = thermal energy (kWh$_{th}$)

η = conversion efficiency

- *Volume requirements*
  - Single phase liquid

$$V_w = W_{th}/E_{wt}$$

  - Two phase

$$V_{2\varphi} = W_{th}/E_{2\varphi t} \quad (7)$$

  - Single phase vapor

$$V_s = W_{th}/E_{st}$$

Energy outputs

- *Superheated steam (reserver and turbine inlet)*

$$W_s = \phi\, h_s/\nu_s \quad (8)$$

with:

W_s = recoverable energy per unit reservoir volume (kJ/m^3)

h_s = steam enthalpy at reservoir conditions

ν_s = steam specific volume at reservoir conditions

- *Compressed water (reservoir)/two phase (separator outlet)*

$$W_l = \phi\, x\, h_l \nu_l \quad (9)$$

with:

W_l = recoverable energy per unit reservoir volume (kJ/m^3)

x = steam quality = $\dfrac{h_l - h_w}{h_s - h_w}$

h_l = compressed liquid enthalpy at reservoir conditions

h_w = water enthalpy at turbine inlet pressure

h_s = separated (flashed) steam at turbine inlet pressure

ν_l = water specific volume at reservoir conditions

Geothermal reservoir heat and power assessments. Summary sheet

DEFINITIONS

- Heat in place HIP
  $HIP = \gamma_t * Ah(\theta_i - \theta_0)$
- Recoverable heat RCH
  $RCH = \eta\gamma_t * Ah(\theta_i - \theta_r) = r * HIP$
- Heat recovery factor r
  $r = RCH / HIP = \eta(\theta_i - \theta_r)/(\theta_i - \theta_0)$
- Efficiency of the heat extraction scheme η
  $\eta = (q/Ah) * (\gamma_w/\gamma_t) * t^*$
- EGS power (W) and energy supply (E)
  $W = \eta' q' \gamma_w (\theta_i - \theta_c)/3600$
  $E = W * t'^*$

NOMENCLATURE

A = area (m^2)

h = effective thickness (m)

q, q' = flowrates (m^3/h)

r = recovery factor

t^*, t'^* = system life (hrs)

$\gamma_t = \phi\gamma_w + (1-\phi)\gamma_r$ = total (fluid + rock) heat capacity (kJm^{-3}K^{-1})

γ_t, γ_r = rock and water heat capacities (kJm^{-3}K^{-1})

$\theta_i, \theta_0, \theta_r, \theta_c$ = reservoir, mean ground, rejection and condensing temperatures (°K)

η, η' = efficiencies

REFERENCES

Bodvarsson, G.S. (1988). Numerical Modelling of Geothermal Systems with Applications to Krafla, Iceland, and Olkaria, Kenya. *Geothermal Reservoir Engineering (Okadan, E. ed.),* Kluwer Academic Press Publ., Dordrecht, 297-316.

Combarnous, M. and Bories, S. (1975). Hydrothermal Convection in Saturated Porous Media. *Advances in Hydroscience*, Academic Press, vol. 10, 231.

Economides, M. and Miller, F.G. (1984). Geothermal Reservoir Evaluation Considering Fluid Absorption and Composition. *Paper SPE12740*, California Regional Meeting of SPE.

Economides, M. (1987). Engineering Evaluation of Geothermal Reservoirs. *Applied Geothermics (Economides, M. and Ungemach, P. eds)*. John Wiley & Sons, 91-109.

Economides, M. (1987). Physical and Thermodynamic Properties of Geothermal Systems. *Applied Geothermics (Economides, M. and Ungemach, P. eds).* John Wiley & Sons, 19-34.

Gudmundsson, J.S. (1988). Material Balance of Geothermal Reservoirs. *Geothermal Reservoir Engineering (Okadan, E. ed)*, Kluwer Academic Press Publ., Dordrecht, 143-156.

Havlena, D. and Odelh, A.S. (1963). The Material Balance as an Equation of a Straight Line. *J. Pet. Tech*., August, 896-900.

Hsieh, C.H. and Ramey, H.J. (1983). Vapour Pressure Lowering in Geothermal Systems. *Soc. Pet. Eng. J*., February 1983, 157-167.

Pruess, K. (2002). Mathematical Modelling of Fluid Flow and Heat Transfer in Geothermal Systems. An Introduction in Five Lectures. United Nations University, Geothermal Training Program, rev, Report 3, Reykjavik, Iceland, Oct. 2002.

O'Sullivan, M.J. (1987). Geothermal Reservoir Simulation. *Applied Geothermics (Economides, M. and Ungemach, P. eds).* John Wiley & Sons, 111-124.

Sanyal, S.K. (2005). Sustainability and Renewability of Geothermal Power Capacity. *Proc., World Geothermal Congress 2005 (WGC 2005)*, Antalya, Turkey, April 24-29, 2005.

Ungemach, P., Papachristou, M., Antics, M. (2007). Renewability vd Sustainability. A Reservoir Management Approach. *Proc., European Geothermal Energy Congress 2007*, Unterhaching, Germany, 30 May – 1 June, 2007.

Whiting, R.L. and Ramey, H.J., Jr. (1969). Application of Material Energy Balance to Geothermal Steam Production. *J. Pet. Tech*., July 1969, 893-900.

Drilling, Completion and Testing of Geothermal Wells

Section 2: An Introduction to Geothermal Systems

3. PHYSICAL AND THERMAL PROPERTIES

Pierre Ungemach

GPC INSTRUMENTATION PROCESS, Roissy-en-France, France

1 FLUID THERMAL PROPERTIES

1.1 Vapour pressure

Within the 150-315 °C temperature range vapour pressure may be written, in consistent units [Whiting and Ramey, 1969]:

$$\log p(bar) = -\frac{2026.86}{\theta(K)} + 5.47 \qquad (1)$$

1.2 Specific volume (two phase mixture)

$$v = xv_g + (1-x)v_l \qquad (2)$$

where

x = steam fraction = mass of steam / total mass (3)

v_g, v_l = specific volumes of gaseous (steam) and liquid (water) phases given by the steam tables.

Specific enthalpy (two phase mixture)

$$h = xh_g + (1-x)h_l \qquad (4)$$

where h_g, h_l are the gas and liquid specific enthalpies respectively listed in the steam tables.

1.3 Specific latent heat of vaporisation

It is by definition the difference between the vapour and liquid specific heats and can be approximated as [Farouq Ali, 1970]:

h_{sl} (kJ/kg) = 2424 p (bar) $e^{-0.08774}$ (5)

1.4 Density

Density of aqueous saline solutions (i.e. geothermal brines) expressed against pressure, temperature and salinity can be derived from the monogram attached in fig. 1.

Otherwise density would be easily calculated for pure water as a reciprocal of the specific volumes listed in the steam tables.

Economides [1979] has proposed the following correlation for vapour density:

ρ_v (kg/m^3) # 0.203 + 0.493 p (bar) (6)

1.5 Viscosity

The dynamic viscosity of a fluid as a function of temperature, pressure and salinity can be estimated from the chestnut curves shown in fig. 2.

Farouq Ali [1970] has approximated the steam dynamic viscosity through the following equation:

$$\mu(cp) = 8.802*10^{-3} + 3.2827*10^{-5}\theta(°C) + 2.153*10^{-8}\theta^3(°C)$$
$$-\rho(kg/m^3)[1.858*10^{-4} - 5.9*10^{-7}\theta(°C)] \qquad (7)$$

1.6 Thermal conductivity

Thermal conductivities of pure water within the (1-220) bar/(125-373) °C pressure/temperature range issued by authorised sources, namely Sprang, 2000 (table 1), Perry's Chemical Handbook, 1999, (table 2) and IAPWS, 2008, (table3), the latter along the saturation line, are given in Appendix. It may be noticed small changes from one source to another whose impact on heat transfer calculations should be regarded as minimum. Thermal conductivity plots against varying pressures and temperatures, based on Sprang, figures are displayed in fig. 3, which evidences the sharp induced by liquid to vapour phase changes.

1.7 Heat capacity

Heat capacity is defined as the amount of heat required to raise the temperature of a body by one degree.

Heat capacity being the product of fluid specific heat by density, its variations with temperature and pressure are easily derived from table 1 which lists specific heat and specific volume (the reciprocal of density) vs temperature and pressure figures.

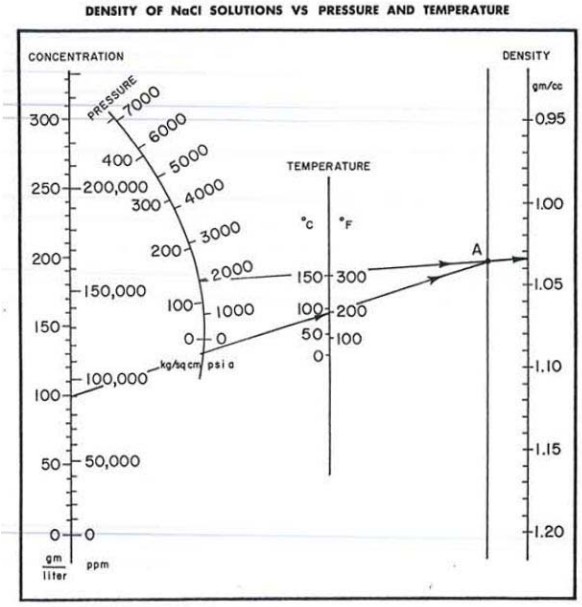

Figure 1: Density of saline brines vs pressure and temperature [Schlumberger, 1973]

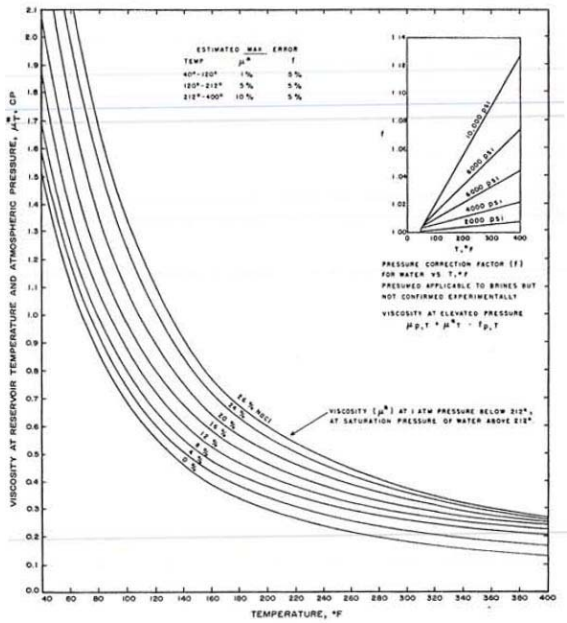

Figure 2: Water viscosity at various salinities and temperatures [Matthews and Russel, data of Chestnut].

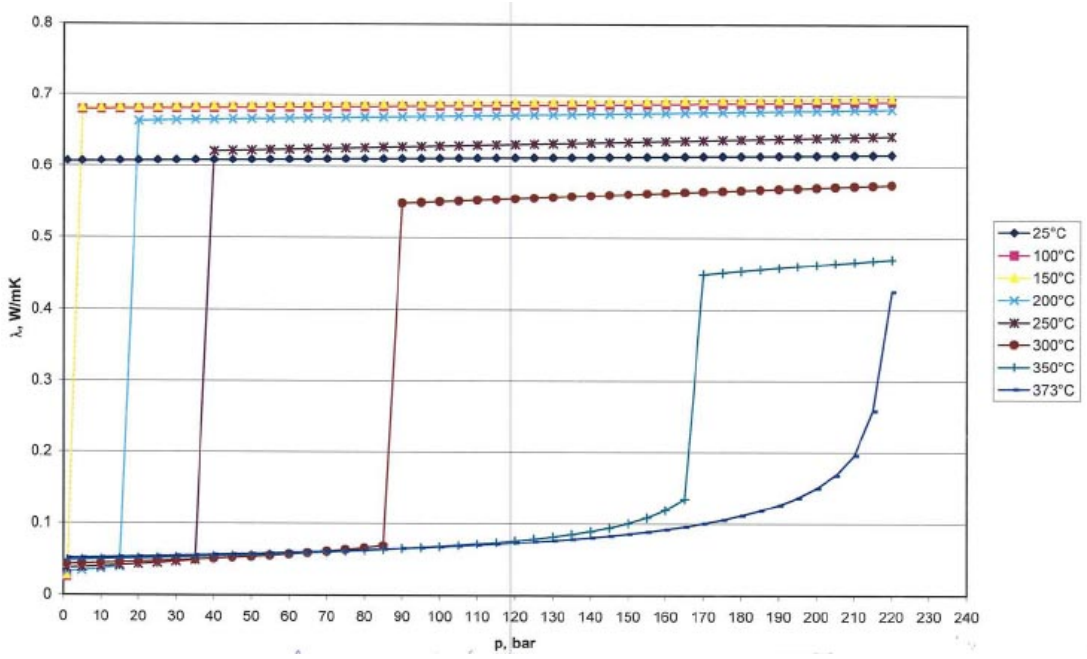

Figure 3: Thermal conductivity of pure water vs pressure and temperature [plotted from Sprang, 2000]

1.8 Gas deviation factor

The gas deviation factor Z [Standing-Katz, 1942] measures the deviation of a real gas from an ideal gas which can be written

$$pV = ZnRT \qquad (8)$$

which rearranged and simplified yields

$$Z = \frac{pV}{nRT} = \frac{pv_g M}{RT} \qquad (9)$$

where:

M: water molecular weight

R: gas constant

T: temperature

V: volume

v_g: specific volume

Fig. 4 shows the variation of the gas deviation factor against pressures and temperature.

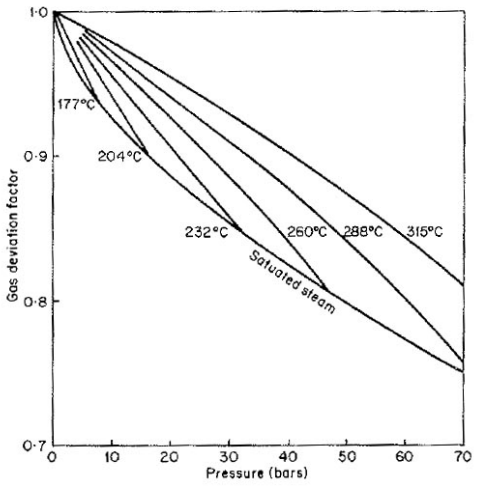

Figure 4: The gas deviation factor [Standing and Katz, 1942]

2 THERMAL PROPERTIES OF ROCKS

2.1 Thermal conductivity

This variable important in heat transfer process is abundantly documented in the works of Birch and Clark [1940], Somerton [1992] and Clauser and Huenges [1995] among other contributions. Variations of rock thermal conductivities with temperature may be significant as depicted in fig. 5 and 6 established for various, low permeability, rock types quartz, quartzitic sandstones and holocrystalline species. The trend is general a decline with increasing temperatures.

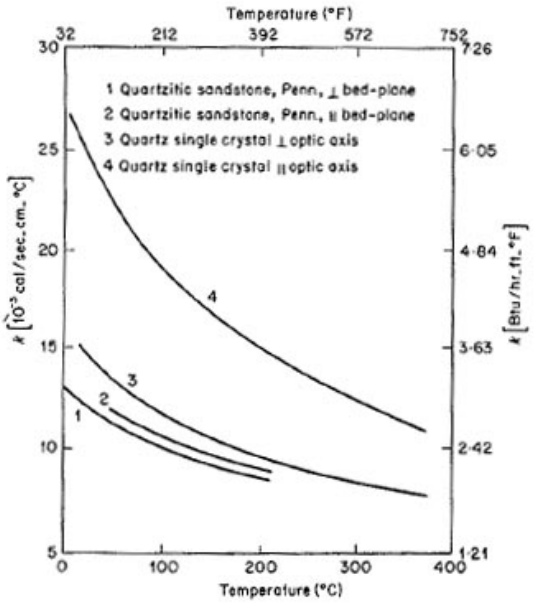

Figure 5: Thermal conductivity of quartz and quartzitic sandstone [Birch and Clark, 1940]

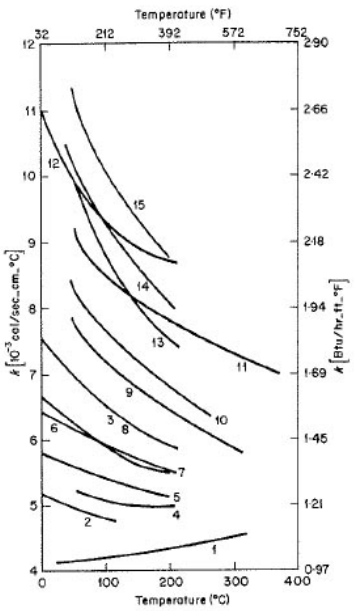

Figure 6: Thermal conductivity of holocrystalline rocks [Birch and Clark, 1940]

Clauser and Huenges [1995] quote the analysis of tabulated data compiled by Zoth and Hänel [1988] who suggested a reliationship of the form

$$\lambda(T) = A + \frac{B}{350 + T} \qquad (10)$$

Where λ and T are expressed in $Wm^{-1}K^{-1}$ and °C respectively and A and B are constants whose values for different rock types are listed in table 1.

Table 1: Constants A and B for various rock types [Zoth and Hänel, 1988]

Rock type	T (°C)	A	B
(1) rock salt	-20 – 40	-2.11	2960
(2) limestones	0 – 500	0.13	1073
(3) metamorphic rocks	0 – 1200	0.75	705
(4) acid rocks	0 – 1400	0.64	807
(5) basic rocks	50 – 1100	1.18	474
(6) ultra-basic rocks	20 – 1400	0.73	1293
(7) rock types (2)-(5)	0 – 800	0.70	770

The thermal properties of fluid saturated rocks have been investigated by Somerton [1992] who proposed the following empirical relationship:

$$\frac{\lambda_s}{\lambda_d} = \left[\frac{\lambda_f}{\lambda_d}\right]^{c\phi} \qquad (11)$$

Where λ is the rock thermal conductivity, with subscripts *s*, *d* and *f* referring to the saturated and dry rock and *f* to the soaking fluid respectively, ϕ the porosity and *c* a constant ranging between 0.9 and 1.3.

When there is more than one reservoir fluid, Economides [1987] proposes the following correlation:

$$\lambda_{(f1+f2)} - \lambda_{f1} = (\lambda_{f2} - \lambda_{f1})S_2^{0.5} \qquad (12)$$

where λ_{f1}, λ_{f2} and λ_{f1+f2} refer to the thermal conductivities of the rock saturated by fluids *f1*, *f2* only and both fluids *f1* and *f2* respectively and S_2 to the saturation of fluid *f2*. However equation (12) is modified in two-phase (water-steam) systems owing to boiling and phase change which lead to at least a two fold increase of thermal conductivities.

2.2 Heat capacity

Economides [1987] cites an empirical relationship provided by Martin and Dew [1964], which in consistent units yields:

$$Cp(kJ/kgK) = 2.326\frac{(T/K)2000}{10000} \qquad (13)$$

whenever the rock is an assemblage of different minerals the resulting heat capacity may be calculated from a weighted average of its constituents.

Somerton [1995] has compiled experimental heat capacity data as a function of temperature for different rocks, shown in fig. 7.

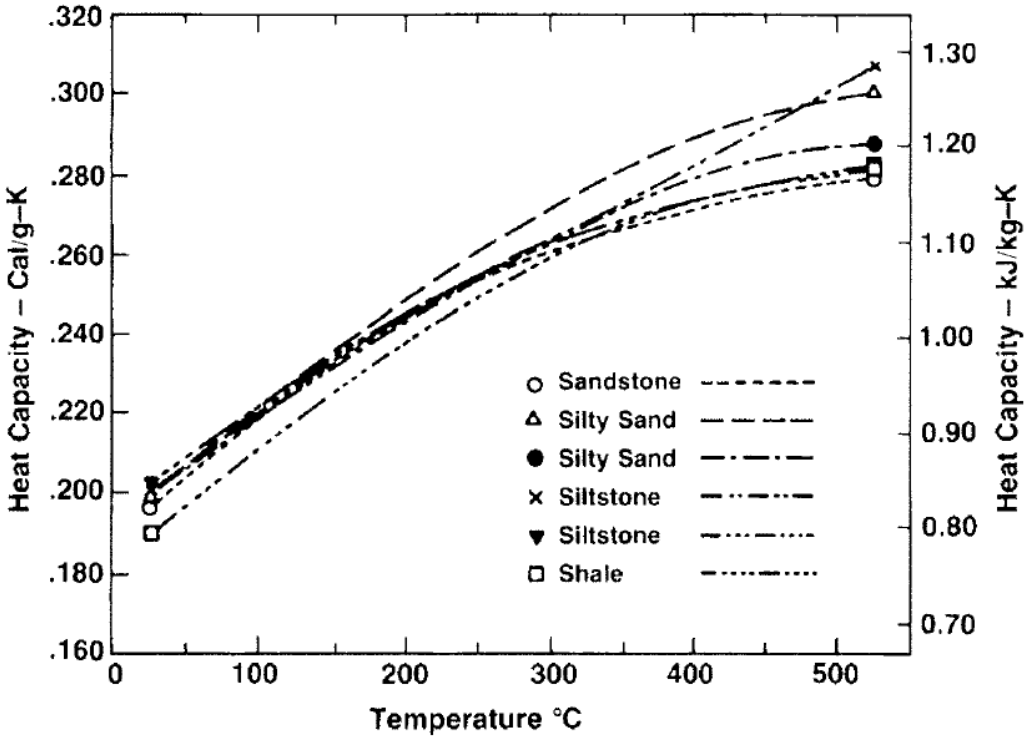

Figure 7: Experimental heat capacities for different rock types function of temperature [Somerton, 1995]

3 OTHER PHYSICAL CORRELATIONS

3.1 Compressibilities

Fluid compressibilities are generally expressed as:

$$\beta_T = -\frac{1}{V}\left(\frac{\partial V}{\partial p}\right)_T \qquad \text{isothermal compressibility} \qquad (14)$$

and

$$\beta_S = -\frac{1}{V}\left(\frac{\partial V}{\partial p}\right)_S \qquad \text{adiabiatic compressibility} \qquad (15)$$

Sveinsson et al [1988] suggest the latter be more appropriate to two phase steam water mixtures, which leads to a calculated adiabiatic (i.e. under isotropic conditions) compressibility be equal to:

$$\beta_h = \frac{c_{pl}\left[\alpha\rho_s + (1-\alpha)\rho_f\right](1/\rho_s - 1/\rho_l)}{h_{ls}(dp/dT)sat} \qquad (16)$$

where:

c_p = heat capacity at cost

h_{ls} = latent heat of vaporisation

ρ_l, ρ_s = lquid and steam densities

p = pressure

T = temperature

They further concluded heat compressibility could be correlated with sonic velocities via the steam/water mixture density.

For any real gas the compressibility factor is expressed as Z = actual volume/ideal volume and can be plotted against reduced pressure $p_r = p/p_c$ and temperature $T_r = T/T_c$, where subscript c refers to critical values, under the form displayed in fig. 8 graph.

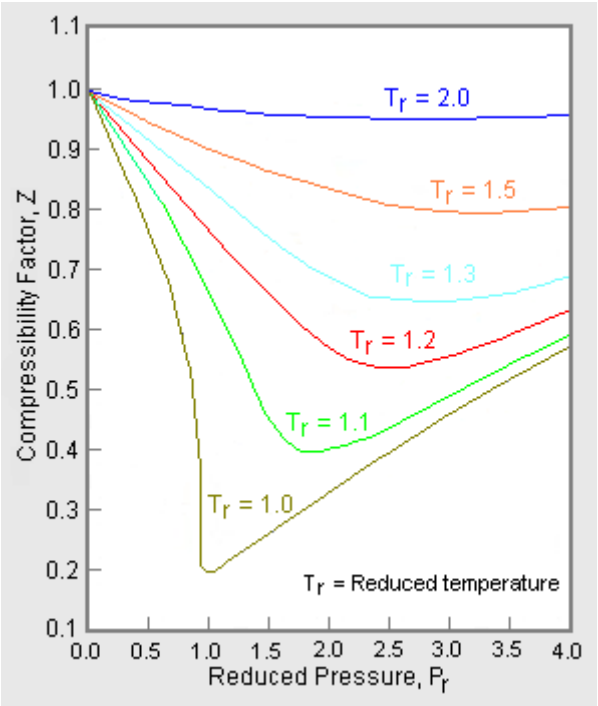

Figure 8: Example of a generalized compressibility factor graph

The compressibility of water as a function of temperature and brine salinity is estimated from fig. 9a (pure water), 9b (100,000 ppm NaCl) and 9c (200,000 ppm NaCl).

Practically the compressibility factores are derived from PVT analyses carried out on bottom hole fluid samples.

The compressibility c_w of an unsaturated water or brine including solution gases may be estimated from the correlation recommended by Long and Chierici [1961]

$$c_w = (c_w)_{0,n}[1 + 0.0088 * 10^{-Kn}(Rsw)] \qquad (17)$$

where:

$(c_w)_{0,n}$ = compressibility of the gas free brine containing *n* gram equivalents of dissolved solids

n = dissolved solids (ppm)/58,443: concentration of dissolved solids in gram-equivalent/liter

K = Sacenov's coefficient decreasing from 0.14 to 0.12 with increasing temperatures.

Rsw = gas solubility in pure water at the required pressure and temperature

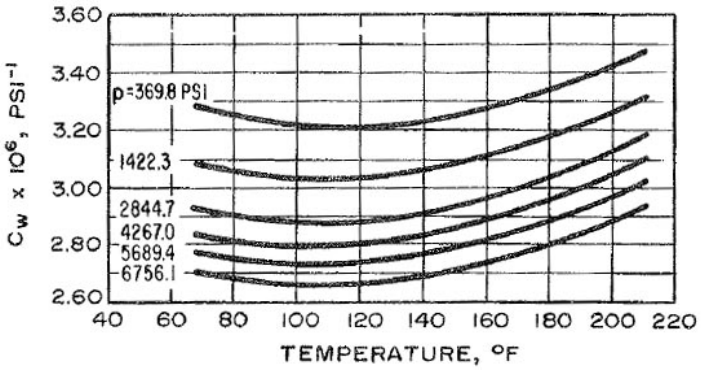

Figure 9a: Pure water

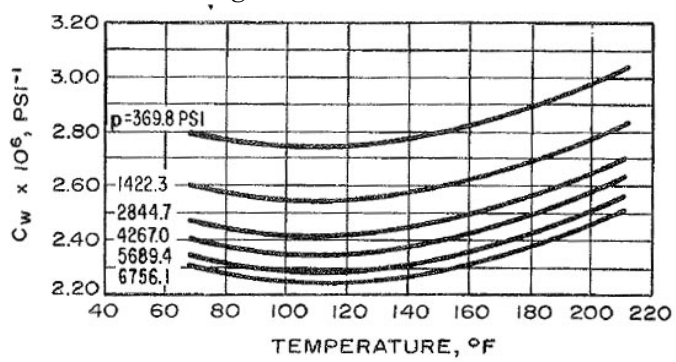

Figure 9b: 100,000 ppm NaCl

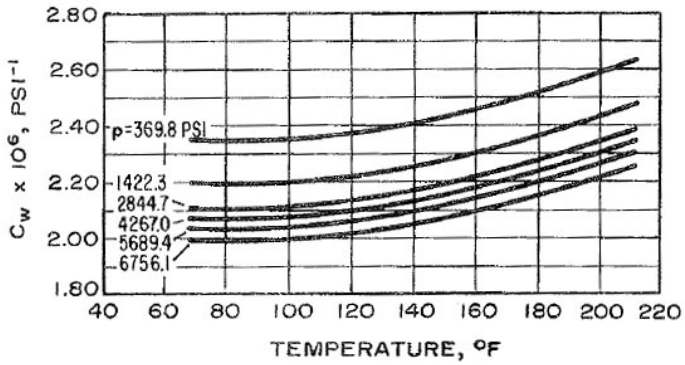

Figure 9c: 200,000 ppm NaCl

Figure 9: Average compressibility of water as a function of temperature for various brine contents [Long and Chierici]

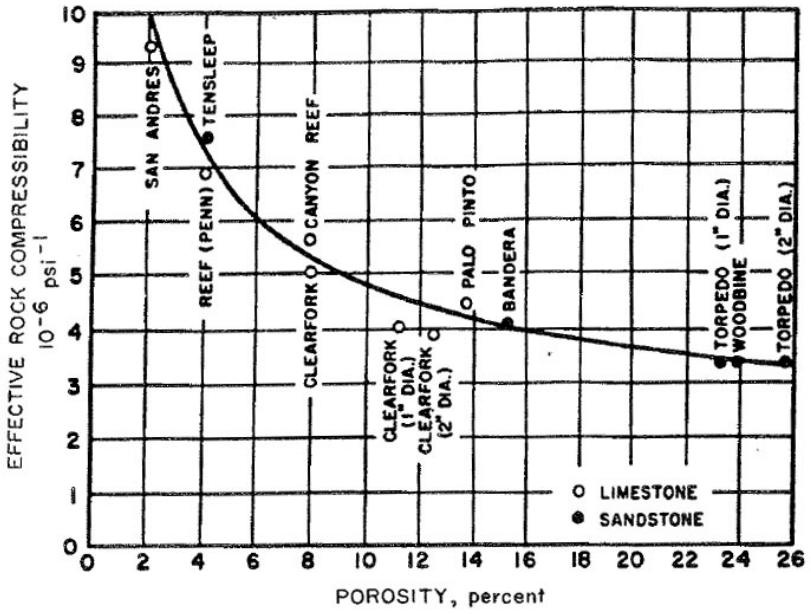

Figure 10: Effective formation (rock) compressibility [Hall, 1953]

There is evidence that rocks are poorly compressible compared to gases and even liquids. However rock compressibility may vary significantly with porosities a trend illustrated in fig. 10 which addresses limestone and sandstone rocks within the 2 to 26% porosity range (Hall, 1953).

3.2 Thermal expansion

The thermal expansion coefficient for water defined as:

$$\alpha(K^{-1}) = \frac{\Delta V}{Vo}\frac{I}{\Delta T} = -\frac{1}{\rho}\frac{\partial \rho}{\partial T} \qquad (18)$$

where:

ΔV = volume variation

Vo = initial volume

ΔT = temperature variation

ρ = density (kg/m^3)

Its variations with temperature are given in table 2.

Table 2: Thermal expansion of pure water as a function of temperature

Temperature (°C)	Expansion coefficient (10^{-4} K^{-1})	Temperature (°C)	Expansion coefficient (10^{-4} K^{-1})
5	1.6	100	7.52
10	0.88	120	8.60
20	2.07	140	9.75
30	3.03	180	12.33
40	3.85	200	13.92
50	4.57	220	15.97
60	5.23	240	18.62
80	6.43	260	22.1
90	6.65		

The thermal expansion of rocks is small compared to liquids. Its magnitude expressed in percent expansion of various rock forming minerals is shown in table 3 for temperatures varying from 20 °C to 600 °C by 100 °C to 200 °C increments.

Table 3: Thermal expansion of rock forming minerals relative to crystallographic axes [Clark, 1966]

Mineral	Axis	Percent expansion from 20 °C to:			
		100 °C	200 °C	400 °C	600 °C
Quartz	⊥c	0.14	0.30	0.73	1.75
	∥c	0.08	0.18	0.43	1.02
Orthoclase	∥a	0.05	0.14	0.48	0.90
	∥b	0.00	0.10	0.04	0.13
	⊥001	0.00	.005	.065	.155
Plagioclase	∥a	0.09	0.22	0.50	0.83
	⊥010	0.03	0.06	0.16	0.29
Calcite	⊥c	0.19	0.48	1.12	1.82
	∥c	-.04	-.10	-.18	-.22
Hornblende	⊥100	0.05	0.12	0.29	0.48
	∥b	0.06	0.17	0.39	0.64
	∥c	0.05	0.13	0.29	0.46

Thermal expansion (and contraction) of, dry or saturated, rocks under constant or varying confining stresses and pore fluid pressures have been further investigated by Somerton [1995].

3.3 Non condensable CO_2

CO_2 is by far the most commonly encountered non condensable gas (NCG) in geothermal systems. Soluble in water it is therefore present in both the liquid (solution gas) and vapour (free gas) phases. A part from the thermochemical shortcomings leading to carbonate scale deposition, a topic previously discussed in section 6.5, the presence of CO_2 in the geothermal steam causes an elevation of dew point pressures, penalising turbine efficiency and ultimately leading to abandon flash condensing cycles and move to atmospheric exhaust and back pressure flash instead.

The solubility of a gas into a liquid, in our case carbon dioxide (CO_2) vs liquid water (H_2O), is governed by the Henry's law which states that the concentration of a gas dissolved in a liquid is proportional to the partial pressure of the gas in equilibrium with the liquid, which can be written:

$$P = Khz \qquad (19)$$

Where *Kh* is the Henry's law coefficient, *z* the mole fraction of the gas in the solution and *P* the gas partial pressure.

Kh is strongly sensitive to temperature variations as shown by fig. 11 correlations, in close agreement with each other, particularly that from Battistelli et al [1987] which covers the whole 5 to 350 °C temperature range.

Economides [1987] and Economides and Miller [1986] calculates dew point pressure elevations in the CO_2 aqueous systems from Sutton's [1976] correlations relating equilibrium constants to temperature based on experimental data, depicted in fig. 12. dew point pressure equilibrium verifies the following equation:

$$\frac{z_{CO2}}{K_{CO2}} + \frac{z_{H2O}}{K_{H2O}} = 1 \qquad (20)$$

where *z* and *K* are the CO_2 and H_2O mole fractions and equilibrium constants respectively.

Furthermore it is assumed the equilibrium constant K_{H2O} may be approximated as:

$$K_{H2O} = Pv_{H2O} / P_{CO2+H2O} \qquad (21)$$

where Pv_{H2O} and $P_{CO2+H2O}$ are the vapour and total pressures respectively

combining equations (20) and (21) yelds:

$$P_{CO2+H2O} = 1/\left[\frac{z_{CO2}}{K_{CO2}P_{CO2+H2O}} + \frac{z_{H2O}}{Pv_{H2O}}\right] \qquad (22)$$

Finally, from reservoir temperatures, steam tables, Sutton's correlation and mole fraction the total system pressure may be derived from equation (22) and dew point pressure of the system calculated accordingly. The results of the exercise are summarised in fig. 13 plots of dew point pressure elevations as a function of temperature and CO_2 concentrations.

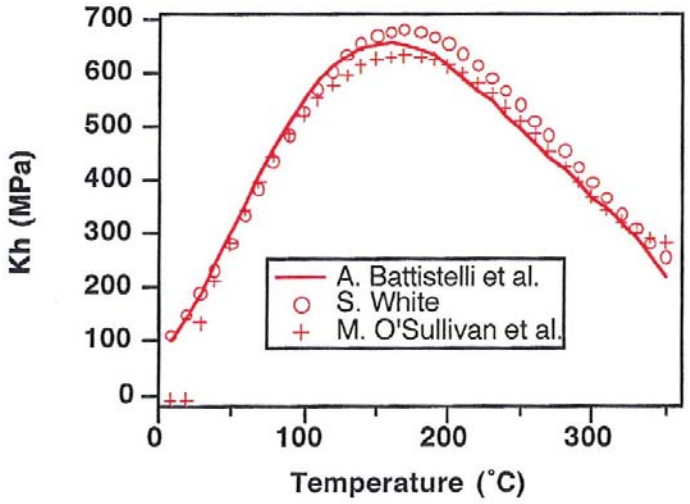

Figure 11: Henry's law coefficients for dissolution of CO_2 in water [Pruess, 1998]

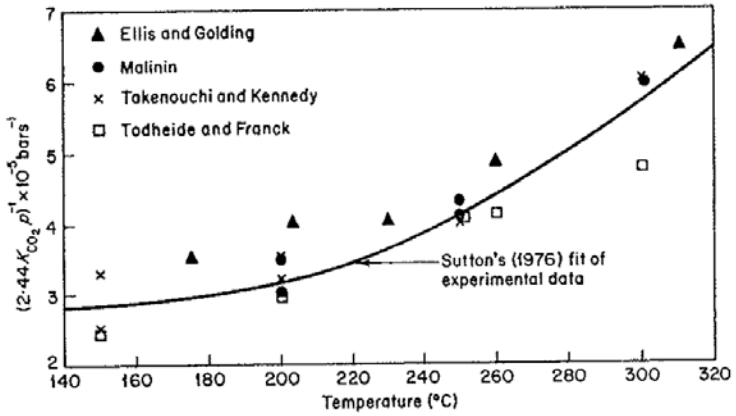

Figure 12: Equilibrium constant for the H_2O-CO_2 system [Sutton, 1976]

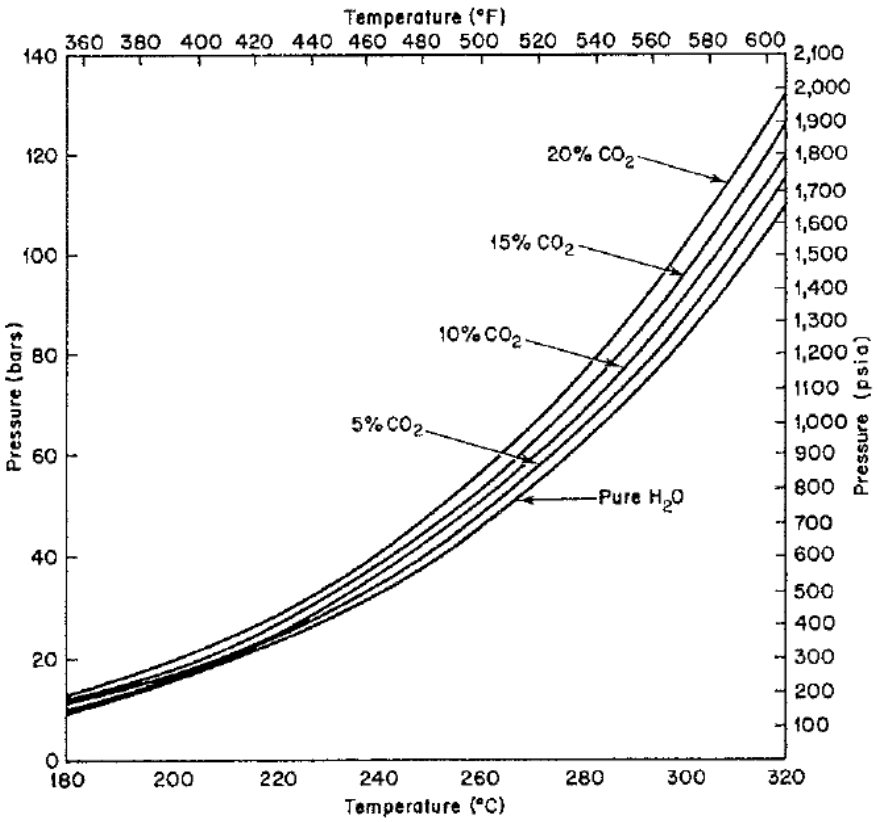

Figure 13: Dew point pressure elevation for the H_2O-CO_2 system [Economides and Miller, 1986]

APPENDIX

Thermal conductivity of water

T°C	25	50	75	100	125	150	175	200	225	250	275	300	325	350	373
P, bar | T, K	298.15	323.15	348.15	373.15	398.15	423.15	448.15	473.15	498.15	523.15	548.15	573.15	598.15	623.15	646.15
1	0.607195	0.643607	0.666804	0.025079	0.026868	0.028856	0.031004	0.033284	0.035679	0.038174	0.040759	0.043423	0.046161	0.048967	0.051603
5	0.607375	0.643792	0.667003	0.679316	0.683721	0.682057	0.033175	0.034933	0.036956	0.039182	0.04157	0.044091	0.046722	0.049448	0.052028
10	0.607601	0.644023	0.667252	0.679589	0.684024	0.682395	0.675377	0.037212	0.038674	0.040516	0.042632	0.044957	0.047446	0.050067	0.052575
15	0.607827	0.644254	0.667502	0.679862	0.684326	0.682733	0.675759	0.039805	0.040558	0.041944	0.043753	0.045864	0.048199	0.050708	0.053139
20	0.608054	0.644485	0.667751	0.680135	0.684628	0.683071	0.67614	0.663716	0.042645	0.043485	0.044942	0.046815	0.048984	0.051373	0.053721
25	0.60828	0.644717	0.668	0.680408	0.684931	0.683408	0.67652	0.664153	0.045003	0.04516	0.046209	0.047816	0.049803	0.052063	0.054324
30	0.608506	0.644948	0.668249	0.680681	0.685233	0.683745	0.676901	0.66459	0.646086	0.046998	0.047567	0.048873	0.05066	0.052781	0.054949
35	0.608733	0.64518	0.668498	0.680954	0.685535	0.684082	0.677281	0.665026	0.646603	0.049047	0.049031	0.049995	0.05156	0.05353	0.055598
40	0.608959	0.645411	0.668748	0.681227	0.685837	0.684419	0.67766	0.665461	0.647119	0.621217	0.050623	0.05119	0.052508	0.054312	0.056271
45	0.609186	0.645643	0.668997	0.681499	0.686138	0.684756	0.678039	0.665896	0.647634	0.621861	0.052372	0.052469	0.053508	0.05513	0.056972
50	0.609413	0.645875	0.669246	0.681772	0.68644	0.685092	0.678418	0.666329	0.648147	0.622501	0.054319	0.053848	0.054569	0.055989	0.057703
55	0.609639	0.646107	0.669495	0.682045	0.686742	0.685428	0.678796	0.666762	0.648659	0.623139	0.056528	0.055343	0.055697	0.056892	0.058465
60	0.609866	0.646338	0.669745	0.682318	0.687043	0.685764	0.679174	0.667195	0.649169	0.623774	0.588799	0.05698	0.056902	0.057843	0.059262
65	0.610093	0.64657	0.669994	0.68259	0.687344	0.6861	0.679552	0.667627	0.649678	0.624406	0.589643	0.05879	0.058195	0.058849	0.060097
70	0.61032	0.646802	0.670243	0.682863	0.687646	0.686436	0.679929	0.668058	0.650186	0.625036	0.590481	0.060817	0.059591	0.059915	0.060973
75	0.610547	0.647034	0.670492	0.683135	0.687947	0.686771	0.680306	0.668488	0.650692	0.625662	0.591314	0.06312	0.061108	0.061049	0.061894
80	0.610775	0.647266	0.670742	0.683408	0.688248	0.687106	0.680683	0.668918	0.651197	0.626286	0.59214	0.065794	0.062767	0.062259	0.062865
85	0.611002	0.647498	0.670991	0.68368	0.688549	0.687442	0.681059	0.669346	0.651701	0.626908	0.592961	0.069008	0.064595	0.063554	0.063889
90	0.611229	0.64773	0.67124	0.683952	0.68885	0.687776	0.681435	0.669775	0.652203	0.627526	0.593776	0.548388	0.066631	0.064948	0.064972
95	0.611456	0.647962	0.671489	0.684225	0.68915	0.688111	0.68181	0.670202	0.652705	0.628143	0.594586	0.549538	0.06892	0.066453	0.066121
100	0.611684	0.648195	0.671739	0.684497	0.689451	0.688445	0.682186	0.670629	0.653204	0.628756	0.595391	0.550675	0.07153	0.068088	0.067343
105	0.611911	0.648427	0.671988	0.684769	0.689751	0.68878	0.68256	0.671056	0.653703	0.629367	0.59619	0.5518	0.074556	0.069871	0.068645
110	0.612139	0.648659	0.672237	0.685041	0.690052	0.689114	0.682935	0.671482	0.6542	0.629976	0.596984	0.552914	0.078143	0.07183	0.070037
115	0.612367	0.648891	0.672486	0.685313	0.690352	0.689448	0.683309	0.671907	0.654697	0.630582	0.597773	0.554017	0.082541	0.073995	0.071529
120	0.612594	0.649124	0.672736	0.685585	0.690652	0.689781	0.683683	0.672331	0.655192	0.631186	0.598557	0.555108	0.088236	0.076408	0.073134
125	0.612822	0.649356	0.672985	0.685857	0.690952	0.690115	0.684056	0.672755	0.655685	0.631788	0.599336	0.556188	0.500701	0.079119	0.074867
130	0.61305	0.649588	0.673234	0.686129	0.691252	0.690448	0.684429	0.673178	0.656178	0.632387	0.600111	0.557258	0.502288	0.0822	0.076743
135	0.613277	0.649821	0.673483	0.686401	0.691552	0.690781	0.684802	0.673601	0.65667	0.632984	0.60088	0.558317	0.503849	0.085743	0.078784
140	0.613505	0.650053	0.673732	0.686672	0.691851	0.691114	0.685175	0.674023	0.65716	0.633578	0.601646	0.559366	0.505385	0.089876	0.081013
145	0.613733	0.650285	0.673981	0.686944	0.692151	0.691447	0.685547	0.674444	0.657649	0.63417	0.602406	0.560406	0.506897	0.09479	0.08346
150	0.613961	0.650518	0.67423	0.687216	0.69245	0.691779	0.685919	0.674865	0.658137	0.634761	0.603162	0.561436	0.508388	0.100792	0.086161
155	0.614189	0.65075	0.674479	0.687487	0.692749	0.692112	0.68629	0.675285	0.658624	0.635348	0.603914	0.562457	0.509858	0.108452	0.08916
160	0.614417	0.650983	0.674728	0.687759	0.693049	0.692444	0.686661	0.675705	0.65911	0.635934	0.604661	0.563468	0.511307	0.118933	0.092514
165	0.614645	0.651215	0.674977	0.68803	0.693348	0.692776	0.687032	0.676124	0.659595	0.636518	0.605404	0.564471	0.512737	0.134682	0.096293
170	0.614872	0.651448	0.675226	0.688301	0.693647	0.693107	0.687403	0.676543	0.660078	0.637099	0.606143	0.565465	0.514147	0.449634	0.100586
175	0.6151	0.65168	0.675475	0.688572	0.693945	0.693439	0.687773	0.676961	0.660561	0.637679	0.606878	0.56645	0.515539	0.452125	0.105509
180	0.615328	0.651913	0.675724	0.688844	0.694244	0.69377	0.688143	0.677378	0.661042	0.638256	0.607609	0.567428	0.516913	0.454521	0.111217
185	0.615556	0.652145	0.675973	0.689115	0.694543	0.694102	0.688513	0.677795	0.661523	0.638832	0.608336	0.568397	0.518269	0.45682	0.117932
190	0.615784	0.652378	0.676221	0.689386	0.694841	0.694433	0.688882	0.678211	0.662002	0.639405	0.609058	0.569359	0.519608	0.459028	0.126006
195	0.616012	0.65261	0.67647	0.689657	0.695139	0.694763	0.689251	0.678627	0.662481	0.639977	0.609777	0.570312	0.52093	0.461151	0.135999
200	0.61624	0.652843	0.676719	0.689927	0.695438	0.695094	0.68962	0.679042	0.662958	0.640546	0.610493	0.571259	0.522235	0.463199	0.14893
205	0.616468	0.653075	0.676968	0.690198	0.695736	0.695425	0.689988	0.679457	0.663435	0.641114	0.611204	0.572197	0.523524	0.46518	0.166942
210	0.616696	0.653308	0.677216	0.690469	0.696034	0.695755	0.690356	0.679871	0.66391	0.64168	0.611912	0.573129	0.524798	0.467104	0.195417
215	0.616924	0.65354	0.677465	0.690739	0.696331	0.696085	0.690724	0.680285	0.664385	0.642244	0.612616	0.574054	0.526057	0.468977	0.257776
220	0.617152	0.653773	0.677713	0.69101	0.696629	0.696415	0.691091	0.680698	0.664858	0.642806	0.613317	0.574971	0.527301	0.470807	0.426218

TABLE 2-356 Specific Heat and Other Thermophysical Properties of Water Substance*

Pressure, bar		Temperature, K														
		300	350	400	450	500	600	700	800	900	1000	1200	1400	1600	1800	2000
1	μ	8.57.–4	3.70.–4	1.32.–5	1.52.–5	1.73.–5	2.15.–5	2.57.–5	2.98.–5	3.39.–5	3.78.–5	4.48.–5	5.06.–5	5.65.–5	6.19.–5	6.70.–5
	c_p	4.18	4.19	1.99	1.97	1.98	2.02	2.09	2.15	2.22	2.29	2.43	2.58	2.73	3.02	3.79
	k	0.614	0.668	0.0268	0.0311	0.0358	0.0464	0.0581	0.0710	0.0843	0.0981	0.13	0.16	0.21	0.33	0.57
	Pr	5.81	2.32	0.980	0.967	0.955	0.936	0.920	0.906	0.891	0.881	0.83	0.80	0.75	0.57	0.45
5	μ	8.57.–4	3.70.–4	2.17.–4	1.49.–5	1.72.–5	2.15.–5	2.57.–5	2.98.–5	3.39.–5	3.78.–5	4.45.–5	5.06.–5	5.65.–5	6.19.–5	6.70.–5
	c_p	4.18	4.19	4.26	2.21	2.10	2.07	2.11	2.16	2.23	2.29	2.43	2.58	2.73	2.98	3.40
	k	0.614	0.668	0.689	0.0335	0.0369	0.0469	0.0585	0.0713	0.0846	0.0984	0.13	0.16	0.20	0.28	0.43
	Pr	5.82	2.32	1.34	0.983	0.973	0.947	0.925	0.907	0.892	0.881	0.83	0.81	0.77	0.65	0.53
10	μ	8.57.–4	3.70.–4	2.17.–4	1.51.–4	1.71.–5	2.15.–5	2.58.–5	2.99.–5	3.39.–5	3.78.–5	4.45.–5	5.06.–5	5.65.–5	6.19.–5	6.70.–5
	c_p	4.18	4.19	4.25	4.39	2.29	2.13	2.13	2.18	2.24	2.30	2.44	2.58	2.73	2.95	3.29
	k	0.615	0.668	0.689	0.677	0.0380	0.0474	0.0590	0.0717	0.0851	0.0988	0.13	0.16	0.20	0.26	0.39
	Pr	5.82	2.32	1.34	0.981	1.028	0.963	0.931	0.908	0.892	0.881	0.84	0.82	0.78	0.70	0.57
20	μ	8.56.–4	3.71.–4	2.18.–4	1.51.–4	1.68.–5	2.15.–5	2.59.–5	3.00.–5	3.40.–5	3.79.–5	4.46.–5	5.06.–5	5.65.–5	6.19.–5	6.70.–5
	c_p	4.17	4.19	4.25	4.39	2.84	2.26	2.19	2.21	2.26	2.32	2.45	2.59	2.73	2.92	3.21
	k	0.616	0.669	0.689	0.679	0.0402	0.0485	0.0599	0.0726	0.0859	0.0996	0.13	0.16	0.20	0.25	0.36
	Pr	5.80	2.32	1.34	0.979	1.19	0.999	0.946	0.912	0.893	0.881	0.84	0.82	0.79	0.72	0.60
40	μ	8.55.–4	3.71.–4	2.18.–4	1.52.–4	1.19.–4	2.15.–5	2.61.–5	3.02.–5	3.42.–5	3.80.–5	4.47.–5	5.07.–5	5.65.–5	6.19.–5	6.70.–5
	c_p	4.17	4.19	4.25	4.38	4.65	2.60	2.32	2.28	2.30	2.34	2.46	2.59	2.73	2.90	3.14
	k	0.617	0.671	0.690	0.680	0.644	0.516	0.0620	0.0744	0.0877	0.101	0.13	0.16	0.19	0.24	0.33
	Pr	5.78	2.31	1.34	0.977	0.862	1.08	0.975	0.924	0.895	0.881	0.84	0.82	0.80	0.73	0.63
60	μ	8.54.–4	3.72.–4	2.19.–4	1.53.–4	1.20.–4	2.14.–5	2.63.–5	3.04.–5	3.43.–5	3.82.–5	4.48.–5	5.07.–5	5.66.–5	6.19.–5	6.70.–5
	c_p	4.16	4.18	4.24	4.37	4.63	3.11	2.47	2.35	2.34	2.37	2.48	2.60	2.73	2.89	3.11
	k	0.619	0.672	0.692	0.682	0.646	0.0561	0.0645	0.0764	0.0895	0.103	0.13	0.16	0.19	0.24	0.32
	Pr	5.74	2.31	1.34	0.976	0.859	1.19	1.008	0.934	0.899	0.879	0.84	0.82	0.81	0.74	0.65
80	μ	8.53.–4	3.72.–4	2.19.–4	1.53.–4	1.20.–4	2.14.–5	2.66.–5	3.06.–5	3.45.–5	3.83.–5	4.48.–5	5.08.–5	5.66.–5	6.19.–5	6.70.–5
	c_p	4.16	4.18	4.24	4.36	4.62	3.88	2.65	2.43	2.39	2.40	2.49	2.61	2.73	2.88	3.09
	k	0.620	0.674	0.693	0.684	0.648	0.0628	0.0672	0.0785	0.0914	0.105	0.13	0.16	0.10	0.24	0.31
	Pr	5.72	2.31	1.34	0.975	0.856	1.33	1.046	0.946	0.902	0.877	0.84	0.83	0.81	0.74	0.66
100	μ	8.52.–4	3.73.–4	2.20.–4	1.53.–4	1.21.–4	2.14.–5	2.69.–5	3.08.–5	3.47.–5	3.85.–5	4.49.–5	5.08.–5	5.66.–5	6.19.–5	6.70.–5
	c_p	4.15	4.17	4.23	4.35	4.60	5.22	2.85	2.52	2.44	2.44	2.50	2.62	2.73	2.88	3.08
	k	0.622	0.675	0.694	0.685	0.651	0.0730	0.0704	0.0807	0.0934	0.107	0.13	0.16	0.19	0.24	0.31
	Pr	5.69	2.31	1.34	0.975	0.853	1.74	1.088	0.960	0.905	0.876	0.84	0.83	0.81	0.74	0.67
150	μ	8.51.–4	3.74.–4	2.22.–4	1.56.–4	1.22.–4	8.22.–5	2.72.–5	3.12.–5	3.51.–5	3.89.–5	4.52.–5	5.09.–5	5.67.–5	6.19.–5	6.70.–5
	c_p	4.14	4.16	4.22	4.34	4.54		3.55	2.74	2.57	2.53	2.54	2.65	2.75	2.88	3.06
	k	0.624	0.678	0.699	0.693	0.657	0.520	0.079	0.086	0.098	0.110	0.14	0.16	0.19	0.23	
	Pr	5.64	2.30	1.34	0.974	0.842		1.22	0.994	0.916	0.891	0.84	0.83	0.82	0.76	
200	μ	8.50.–4	3.75.–4	2.24.–4	1.57.–4	1.23.–4	8.32.–5	2.80.–5	3.17.–5	3.54.–5	3.93.–5	4.54.–5	5.11.–5	5.67.–5		
	c_p	4.12	4.15	4.21	4.32	4.51		4.67	3.04	2.71	2.62	2.57	2.67	2.76	2.88	3.05
	k	0.626	0.681	0.702	0.697	0.661	0.525	0.095	0.095	0.104	0.113	0.14	0.16	0.19		
	Pr	5.59	2.29	1.34	0.974	0.833		1.38	1.014	0.925	0.903	0.84	0.83	0.82		
250	μ	8.49.–4	3.76.–4	2.26.–4	1.59.–4	1.23.–4	8.41.–5	2.89.–5	3.24.–5	3.59.–5	3.98.–5	4.56.–5	5.12.–5	5.68.–5		
	c_p	4.12	4.14	4.20	4.30	4.49	5.90	6.16	3.40	2.86	2.71	2.61	2.69	2.77	2.89	3.04
	k	0.627	0.683	0.705	0.701	0.672	0.537	0.112	0.103	0.110	0.119	0.136	0.16			
	Pr	5.57	2.28	1.34	0.974	0.826	0.924	1.590	1.070	0.940	0.910	0.85	0.84			
300	μ	8.49.–4	3.77.–4	2.28.–4	1.60.–4	1.24.–4	8.50.–5	3.7.–5	3.4.–5	3.64.–5	4.02.–5	4.59.–5	5.14.–5	5.68.–5		
	c_p	4.10	4.13	4.19	4.29	4.44	5.60	10.20	3.82	3.03	2.81	2.65	2.72	2.78	2.90	3.04
	k	0.629	0.685	0.708	0.704	0.675	0.548	0.173	0.113	0.113	0.123	0.14				
	Pr	5.53	2.27	1.34	0.973	0.820	0.859	2.18	1.149	0.976	0.917	0.87				
400	μ	8.49.–4	3.80.–4	2.30.–4	1.62.–4	1.26.–4	8.64.–5	5.3.–5	3.6.–5	3.8.–5	4.1.–5	4.6.–5	5.17.–5			
	c_p	4.08	4.12	4.16	4.26	4.42	5.31	13.20	4.86	3.39	3.01	2.70	2.77	2.81	2.91	3.04
	k	0.631	0.689	0.714	0.710	0.676	0.567	0.327	0.145	0.129	0.134	0.15				
	Pr	5.49	2.26	1.34	0.971	0.817	0.799	2.14	1.207	0.999	0.926					
500	μ	8.50.–4	3.82.–4	2.31.–4	1.64.–4	1.28.–4	8.83.–5	5.8.–5	4.0.–5	4.0.–5	4.2.–5	4.7.–5				
	c_p	4.06	4.10	4.15	4.23	4.38	5.08	8.44	5.70	3.90	3.21	2.77	2.81	2.84	2.92	3.04
	k	0.634	0.695	0.719	0.717	0.693	0.583	0.378	0.186	0.147	0.145					
	Pr	5.44	2.25	1.33	0.971	0.814	0.773	1.30	1.225	1.061	0.932					

TABLE 2-356 Specific Heat and Other Thermophysical Properties of Water Substance (*Concluded*)

Pressure, bar		Temperature, K														
		300	350	400	450	500	600	700	800	900	1000	1200	1400	1600	1800	2000
600	μ	8.51.–4	3.85.–4	2.32.–4	1.66.–4	1.30.–4	9.17.–5	6.5.–5	4.4.–5	4.2.–5	4.4.–5					
	c_p	4.04	4.08	4.13	4.20	4.33	4.92	6.93	6.83	4.19	3.38	2.87	2.86	2.86	2.92	3.04
	k	0.639	0.699	0.725	0.725	0.700	0.597	0.420	0.239	0.170	0.159					
	Pr	5.38	2.24	1.32	0.970	0.812	0.755	1.073	1.175	1.035	0.935					
700	μ	8.52.–4	3.87.–4	2.33.–4	1.69.–4	1.33.–4	9.50.–5	6.9.–5	4.9.–5	4.5.–5	4.6.–5					
	c_p	4.01	4.07	4.12	4.17	4.29	4.78	6.12	6.26	4.62	3.59	2.94	2.91	2.88	2.93	3.05
	k	0.644	0.706	0.730	0.732	0.707	0.614	0.442	0.279	0.198	0.177					
	Pr	5.33	2.23	1.32	0.970	0.810	0.739	1.047	1.098	1.010	0.935					
800	μ	8.53.–4	3.90.–4	2.34.–4	1.72.–4	1.36.–4	9.82.–5	7.3.–5	5.4.–5	4.8.–5	4.8.–5					
	c_p	3.99	4.05	4.10	4.15	4.26	4.67	5.60	6.09	4.77	3.75	3.01	2.96	2.91	2.95	3.05
	k	0.648	0.709	0.735	0.736	0.714	0.625	0.478	0.320	0.228	0.193					
	Pr	5.28	2.23	1.31	0.970	0.808	0.725	0.855	1.028	1.003	0.933					
900	μ	8.54.–4	3.93.–4	2.35.–4	1.74.–4	1.38.–4	1.00.–4	7.6.–5	5.8.–5	5.1.–5	5.0.–5					
	c_p	3.98	4.03	4.08	4.13	4.23	4.57	5.29	5.86	4.85	3.86	3.08	3.00	2.94	2.97	3.06
	k	0.651	0.713	0.738	0.742	0.724	0.636	0.496	0.351	0.260	0.210					
	Pr	5.23	2.22	1.30	0.969	0.806	0.712	0.810	0.965	0.950	0.919					
1000	μ	8.56.–4	3.96.–4	2.36.–4	1.76.–4	1.40.–4	1.02.–4	7.9.–5	6.2.–5	5.4.–5	5.1.–5					
	c_p	3.97	4.02	4.06	4.11	4.20	4.47	5.08	5.51	4.88	3.96	3.16	3.05	2.97	2.98	3.07
	k	0.653	0.717	0.743	0.747	0.731	0.650	0.516	0.372	0.288	0.228					
	Pr	5.19	2.22	1.30	0.968	0.804	0.701	0.778	0.918	0.900	0.886					

*μ = viscosity, Ns/m^2; c_p = specific heat at constant pressure, kJ/(kg·K); k = thermal conductivity, W/(m·K); Pr = Prandtl number.

Table E.II. Values of the Thermal Conductivity of Ordinary Water Substance Obtained with the Aid of the Recommended Interpolating Equation for General and Scientific Use, Calculated along the Saturation Line

t °C	p MPa	λ' mW K^{-1} m^{-1}	λ'' mW K^{-1} m^{-1}
0.01	0.000 611 7	561.0	17.07
10	0.001 228	580.0	17.62
20	0.002 339	598.4	18.23
30	0.004 247	615.5	18.89
40	0.007 385	630.6	19.60
50	0.012 35	643.6	20.36
60	0.019 95	654.3	21.19
70	0.031 20	663.1	22.07
80	0.047 41	670.0	23.01
90	0.070 18	675.3	24.02
100	0.1014	679.1	25.10
110	0.1434	681.7	26.24
120	0.1987	683.2	27.47
130	0.2703	683.7	28.76
140	0.3615	683.3	30.14
150	0.4762	682.0	31.60
160	0.6182	680.0	33.13
170	0.7922	677.0	34.75
180	1.0028	673.3	36.45
190	1.255	668.8	38.24
200	1.555	663.3	40.11
210	1.908	657.0	42.09
220	2.320	649.7	44.17
230	2.797	641.3	46.38
240	3.347	631.8	48.73
250	3.976	621.2	51.27
260	4.692	609.2	54.04
270	5.503	595.9	57.12
280	6.417	581.1	60.62
290	7.442	565.0	64.72
300	8.588	547.4	69.67
310	9.865	528.8	75.86
320	11.284	509.2	83.94
330	12.858	489.1	95.00
340	14.601	468.6	111.0
350	16.529	447.4	136.1
360	18.666	425.8	181.8
370	21.044	425.1	324.5
371	21.297	438.5	368.1
372	21.554	467.5	439.1
373	21.814	548.2	592.2

Thermal conductivity of saturated steam as function of temperature

T°C	25	50	75	100	125	150	175	200	225	250	275	300	325	350	373
	298.15	323.15	348.15	373.15	398.15	423.15	448.15	473.15	498.15	523.15	548.15	573.15	598.15	623.15	646.15
	0.01855	0.020365	0.022531	0.025096	0.028106	0.031595	0.035587	0.040112	0.045255	0.051262	0.0588	0.069646	0.088906	0.135788	0.558284

Thermal conductivity of saturated steam as function of pressure

P, bar	
1	0.025052
5	0.031871
10	0.036428
15	0.039786
20	0.042573
25	0.045025
30	0.047263
35	0.049357
40	0.051357
45	0.053296
50	0.055203
55	0.0571
60	0.059006
65	0.060938
70	0.062913
75	0.064946
80	0.067054
85	0.06925
90	0.071552
95	0.073974
100	0.076534
105	0.079251
110	0.082144
115	0.085237
120	0.088557
125	0.092134
130	0.096004
135	0.100207
140	0.104789
145	0.109803
150	0.115303
155	0.121351
160	0.128009
165	0.135338
170	0.143931
175	0.153519
180	0.16451
185	0.177295
190	0.192461
195	0.210951
200	0.234408
205	0.266091
210	0.313861
215	0.405561
220	0.972242

REFERENCES

Batistelli, A.C., Calore, C. and Pruess, K. (1997). The Simulatore TOUGH2/EWASG for Modelling Geothermal Reservoirs with Brines and Non Condensable Gas, *Geothermics*, **26**, 437-464.

Birch, F. and Clark, H. (1940). The Thermal Conductivity of Rocks and its Dependance upon Temperature and Composition, Part I and II, Am. J. Science, 238, 529-558, 613-635.

Chestnut. Dynamic Viscosity vs Temperature Chart. Shell Development Unpublished doc., quoted by Matthews, C.S. and Russel, D.G.

Clark, S. Jr. (1966). Handbook of Physical Constants. Revised Edition. GSA Memoir 97, 459-482.

Clauser, C. and Huenges, E. (1995). Thermal Conductivity of Rocks and Minerals. Rocks Physics and Phase Relations (Ahrens, T.J. ed.). A Handbook of Physical Constants. AGV Reference Shelf, 3, 105-126.

Earlougher, R.C. Jr. (1977). Advances in Well Test Analysis. Henry L. Doherty Series. SPE. New York, Dallas.

Economides, M. (1979). Shut in and Flowing Bottom hole Pressure Calculation for Geothermal Steam Wells, *Proc. Fifth Stanford Workshop Geothermal Reservoir Engineering*, 139-152.

Economides, M. (1987). Physical and Thermodynamic Properties of Geothermal Systems. *Applied geothermics* (Economides, M. and Ungemach, P. eds), John Wiley & Sons, 19-34.

Economides, M. and Miller, F.G. (1986). Geothermal Reservoir Evaluation Considering Fluid Absorption and Composition, SPE Res. Eng., Vol. 1, 131-147.

Farouk Ali, S.M. (1970). Oil Recovery by Steam Injection, Producers Pub. Co., Bradford, Pensylvania.

Hall, H.N. (1953). Effective (rock) Compressibility. *Trans. AIME*, **198**, 309 (quoted by Matthews, C.S. and Russel, D.G.).

IAPWS. Int. Ass. Prop. Of Water and Steam.

Long, G. and Chierici, G. (1961). Salt Content Changes of Reservoir Brines, Pet. Eng., B-25 to B-31, quoted by Earlougher, R.C. Jr.

Martin, W.L. and Dew, J.N. (1964). How to Calculate Air Requirements for Forward combustion. *Pet. Eng*., Dec. 323-326.

Matthews C.S. and Russell D. G. (1967). Pressure Buildup and Flow Tests in Wells. SPE, 1967

Perry's Chemical Engineer's Handbook, Mc Graw Hill, 1999.

Pruess, K., Oldenburg, C. and Morides, G. (1999). TOUGH2, User's Guide, Version 2.0. Earth SC. Div., LBL Nat-Lab., University of California, Berkley, California.

Ramey, H.J. Jr., Brigham, W.E., Chen, H.K., Atkinson, P.G. and Arihara, N. (1974). Thermodynamic and Hydrodynamic properties of Hydrothermal Systems. *Proc. NSF Conf. on Utilisation of Volcano Energy*, Hilo, Hawaii, Feb. 4-8, 1974.

Somerton, W.H. (1992). Thermal Properties and Temperature Related Behaviour of Rock/Fluid Systems. *Petroleum Science*, **37**, Elsevier.

Spang, B. (2002). Excel Add-in for Properties of Water and Steam, Hamburg, Germany.

Standing, H.B. and Katz, D.L. (1942). Density of Natural Bases. *Trans. AIME*, **146**, 144.

Sutton, F.M. (1976). Pressure-temperature Curves for a Two Phase Mixture of Water and Carbone Dioxide. *New Zealand J. of Sci*., **19**, 297-301.

Sveinsson, S., Gudmondsson, J.S. and Jonsson, V (1988). Compressibility and Sonic Velocoity in Steam/Water Mixtures. *Proceedings Thirteenth Workshop on Geothermal Reservoir Engineering,* Stanford, University of Stanford, Ca, Jan. 19-21, 1988, 19-24.

Whitting, R.L. and Ramey, H.J., Jr. (1969). Application of Material and Energy Balances to Geothermal Steam Production, J. Pet. Tech., July, 893-900.

Zoth, G. and Hänel, R. (1988). Appendix, Handbook of Terrestrial Heat & Flow Density Determination (Hänel, R., Rybach, L. and Stegena, L. eds), 449-466, Kluwer, Dordrecht.

4. RESOURCE/RESERVE CLASSIFICATIONS

Pierre Ungemach
GPC INSTRUMENTATION PROCESS, Roissy-en-France, France

1 Resource/reserve classifications

There are various routes for characterising and assessing geothermal resources and reserves, depending on the definition and classification criteria. The most popular one applies a mining oriented volumetric evaluation standard. Others classify the resource according to its energy content (i.e. its enthalpy) or to its uses, either direct (non electric) or electric, with respect to source temperatures.

The former Mac Kelvey classification diagram has been modified by Cataldi and Mufler [1976] and structured as shown in fig. 1 according to the degrees of economic viability and geologic assurance of the resource. In brief, economic viability decreases with increasing depths and reliability depends on whether or not the resource has been identified (i.e. directly assessed or inferred), in which case it becomes a reserve ranking from proven to probable, or unidentified (i.e. hypothetical, speculative). Depth here is obviously a key factor governing exploitation economics. It is generally accepted that 3 to 3.5 km is an economic limit by current technological and energy pricing standards. As a matter of fact, over 90% of exploited geothermal deposits stands below this depth. However, the 5 km depth targeted by EGS projects (as in Soultz-sous-Forêts, the most advanced to date) evidence a trend towards deeper seated objectives, presently regarded as sub-economic but which may become economic in a foreseeable future.

This classification leads to the following concepts, accessible resource base or heat in place, recoverable heat, heat recovery factors/extraction efficiencies and power/energy outputs respectively which are summarised in table 1.

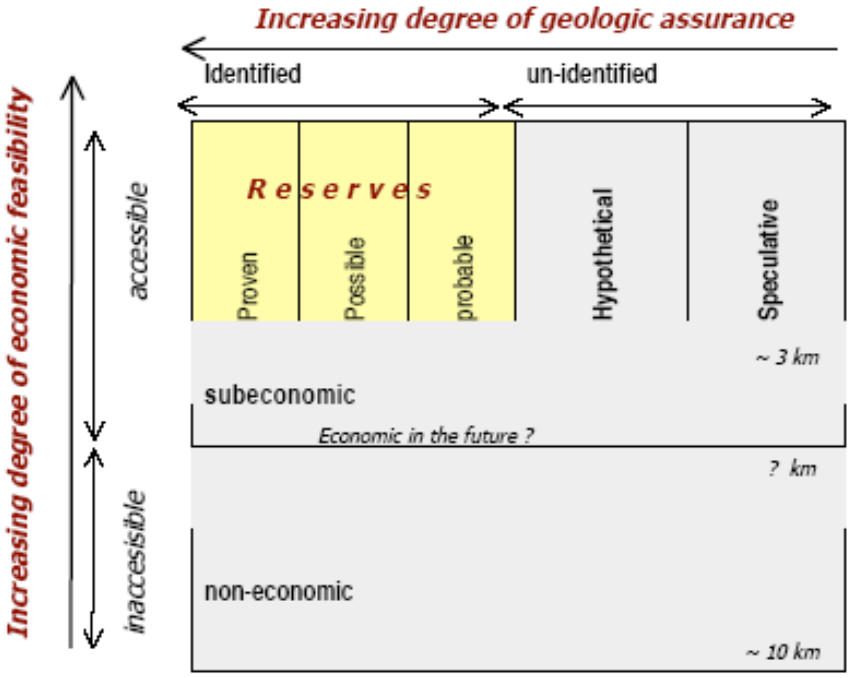

Figure 1: The Mac Kelvey Mineral Resource Classification Diagram [adapted by Mufler and Cataldi, 1978]

Table 1: Geothermal reservoir heat and power assessments. Summary Sheet.

The foregoing logically lead to the assessment of the geothermal development potential of any area of

DEFINITIONS

- Heat in place HIP
  $HIP = \gamma_t * Ah(\theta_i - \theta_0)$
- Recoverable heat RCH
  $RCH = \eta\gamma_t * Ah(\theta_i - \theta_r) = r * HIP$
- Heat recovery factor *r*
  $r = RCH / HIP = \eta(\theta_i - \theta_r)/(\theta_i - \theta_0)$
- Efficiency of the heat extraction scheme η
  $\eta = (q / Ah) * (\gamma_w / \gamma_t) * t^*$
- EGS power (*W*) and energy supply (*E*)
  $W = \eta' q' \gamma_w (\theta_i - \theta_c)/3600$
  $E = W * t'^*$

NOMENCLATURE

A = area (m^2)
h = effective thickness (m)
q, q' = flowrates (m^3/h)
r = recovery factor
t^*, t'^* = system life (hrs)
$\gamma_t = \phi\gamma_w + (1-\phi)\gamma_r$ = total (fluid + rock) heat capacity ($kJm^{-3}K^{-1}$)
γ_t, γ_r = rock and water heat capacities ($kJm^{-3}K^{-1}$)
$\theta_i, \theta_0, \theta_r, \theta_c$ = reservoir, mean ground, rejection and condensing temperatures (°K)
η, η' = efficiencies

interest, an exercise which has been applied by Ungemach et al (2008b) to the Madrid region. The area belongs to the Tajo sedimentary basin of which it occupies its uppermost northern part. The sedimentary cover, ca 3.6 km thick, includes several medium depth layers exhibiting aquifer properties and a main hot geothermal reservoir, a thick multilayered sequence of tertiary detritic, consolidated, sandstone overlying radiogenic granitic basement rocks. The area benefits from a reliable data base – a dense seismic line coverage and well control, the deepest one, drilled to a depth of 3,000 m, having hit a hot (#150°C) and tight (#10 milli darcy permeability) indurated sandstone.

The resource/reserve assessment rationale addressed:

(i) two selected areas, Grand Madrid (1,400 km^2) and NE Madrid(150 km^2), the latter matching the perimeter investigated by four(one hydrocarbon, three geothermal) deep exploration wells;

(ii) a 5,000 m depth, i.e. rock volumes amounting to 7,000(Grand Madrid) and 750 km^3(NE Madrid);

(iii) a multiple interbedded aquifer sequence, split into four resource classes and uses, namely shallow depth/ground source-groundwater heat pump(GSHP/GWHP), medium depth(heat pump assisted) and deep(heat exchange alone)/geothermal district heating and cooling(GDHC) systems, and, last but not least, frontier, ultra-deep, combined heat and power(CHP) engineered geothermal schemes (EGS);

(iv) a sustainable reservoir management approach, aimed at a 75 year reservoir thermal life via the heat extraction designs illustrated in fig. 2;

(v) the evaluation criteria practiced by the mineral and geothermal industry in assessing recoverable heat and power quantities which are summarised in table 1.

Period	1985-2010	2011-2035	2036-2060
Mining Scheme	doublet	triplet	doublet
Flow rate (m3/h)	170	130	120
Injection temp. (°C)	48	40	30
Recovery time (yrs) constant pressure closed reservoir	57500 230000	316000 558000	1158000 380000

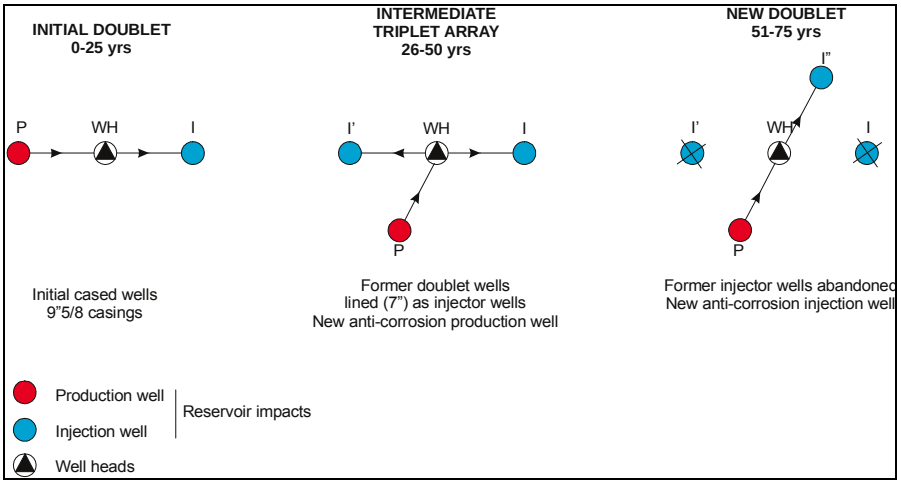

Figure 2: A 75 year sustainable geothermal district heating scenario, Paris basin, Dogger reservoir [Ungemach, 2007]

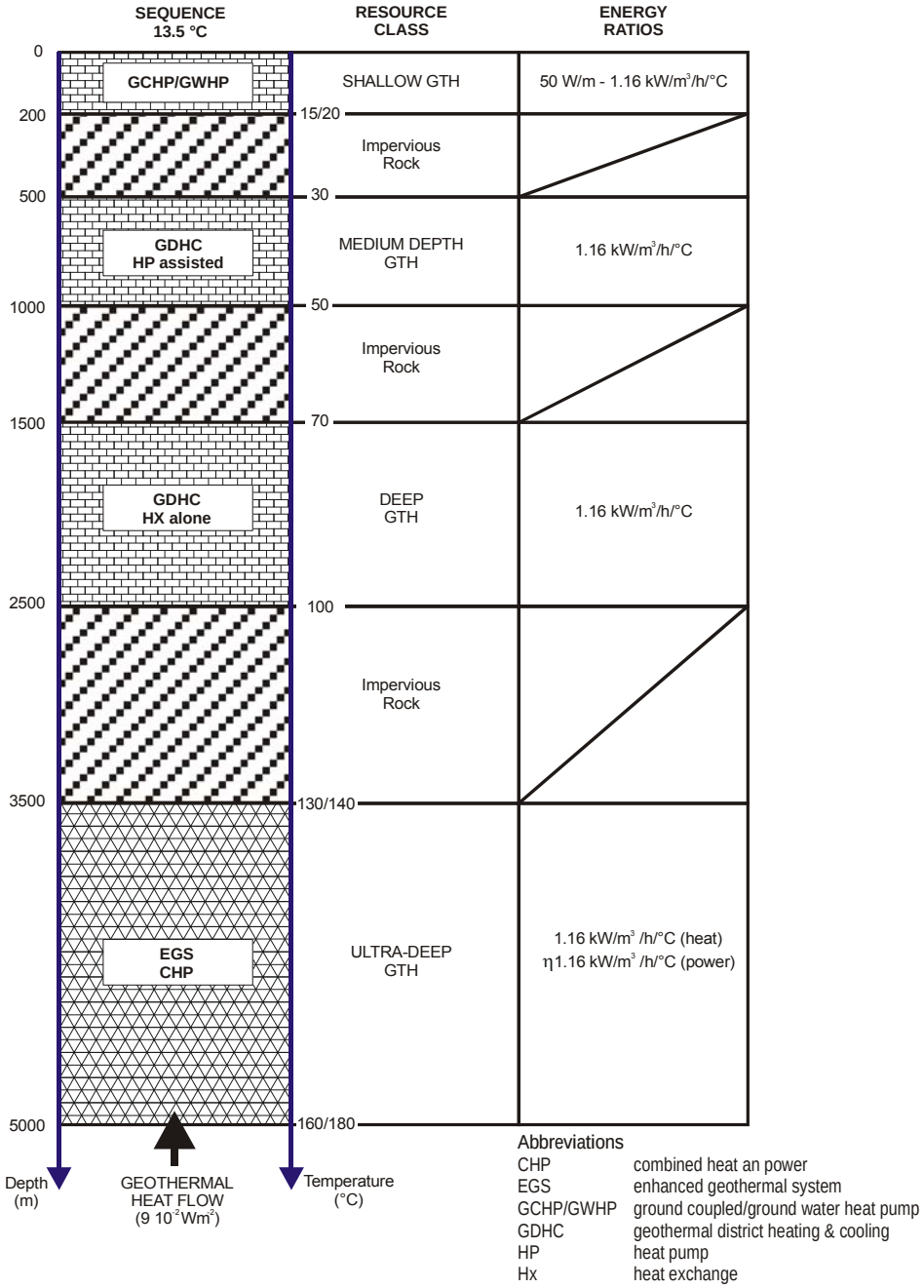

Figure 3: Resource classification vs. depth, temperature and aquifer occurrence [Ungemach et al, 2008]

Table 2: Summary of Resource/Reserve Assessments

ZONE	OVERALL (Grand Madrid)	SPECIFIC (NE Madrid)
AREA (km^2)	**1400**	**150**
HEAT IN PLACE (HIP) (10^{18} J)		
Shallow GTH	21	2.2
Medium depth GTH	18	3.9
Deep GTH	27	3.1
Ultra-deep GTH	115	13.1
TOTAL	**181 10^{18} J**	**22.3 10^{18} J**
RECOVERABLE HEAT (RCH) OVER 75 yrs		
Shallow GTH (BHE/GWD) (10^{18} J)	3.3/1	0.35/0.1
Medium depth GTH (10^{18} J)	6.3	1.4
Deep GTH (10^{18} J)	9.5	1.1
Ultra-deep GTH (10^{18} J)	5.8	0.7
TOTAL	**24.9/22.6 10^{18} J**	**3.6/3.3 10^{18} J**
EXPLOITABLE HEAT (AND POWER) OVER 75 yrs		
Shallow GHT (BHE/GWD) (10^{17} J)	0.36/0.07	0.04/0.007
Medium depth GTH (10^{17} J)	1.3	0.3
Deep GTH (10^{17} J)	4.4	1.1
Ultra-deep GTH CHP (10^{17} J)	1.2	0.3
TOTAL	**7.3/7 10^{17} J**	**1.7/1.7 10^{17} J**
HEAT RESUPPLY (10^{17} J)	**3.09**	**0.33**

The exercise, displayed in fig. 3 and table 2 summary sheet, leads to the overall projections listed herein after:

Item	Grand Madrid	NE Madrid
Heat in place (HIP) 1018 J	181	22
Recoverable heat (RCH) 75 yrs 1018 J	25	3.5
Exploitable heat(and power) (EXH) 75 yrs 1017 J	7.3	1.7
Heat resupply (assuming 90mWm-2 heat flow density) 1017 J	3.09	0.33
EXH/RCH ratio (%)	3	5

Noteworthy is that in this well documented, fast developing, area enjoying an optimum geoheat & cold resource to demand adequacy, only a few percents of the available geothermal heat is mined at a 75 year time scale.

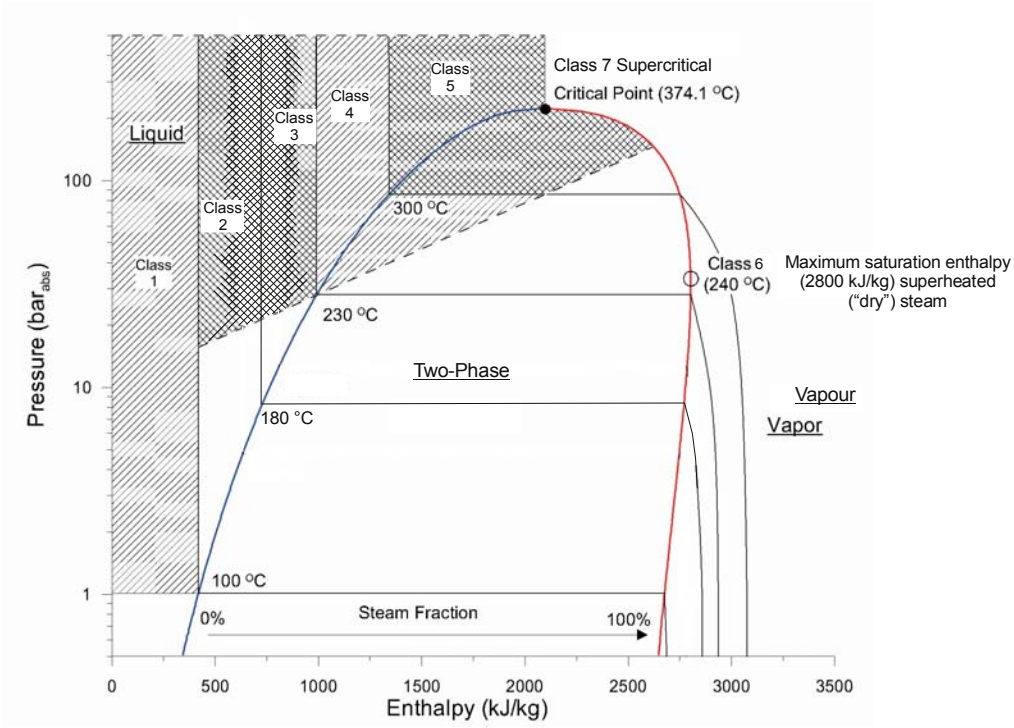

Pressure-Enthalpy-Temperature diagram for pure water

Figure 4: Classification of geothermal resources according to fluid enthalpies [Sanyal, 2005]

Subir Sanyal [2005] suggested an alternative classification, deemed more practical if not relevant in the context of the Western US states and its prevailing high enthalpy geoelectric potential, based on geothermal fluid enthalpies which can be visualised in the fig. 4 pressure-enthalpy diagram. Accordingly, seven classes have been distinguished respective to the saturation curve, namely:

Class 1	< 100 °C. Liquid water. Direct Uses.
Class 2	< 180 °C. Liquid water. Binary (ORC), and hybrid cycles single flash (back pressure, condensing, power generation).
Class 3	< 230 °C. Liquid water. Dual flash power generation.
Class 4	< 300 °C. Two phase water. Steam dual flash.
Class 5	> 300 °C (< 374 °C). Subcritical fluids. Two phase water/steam.
Class 6	Single phase superheated steam (close to maximum saturation enthalpy)
Class 7	> 374 °C. Supercritical (dense) fluids.

Subir Sanyal [2005] concluded that the US identified reserves, within the class 2 to 6 range, amounted to ca 29 000 MWe.

Note that this classification does not take into account EGS issues, not to mention the very low enthalpy shallow ground source/ground water heat pump systems, both ignored at this stage.

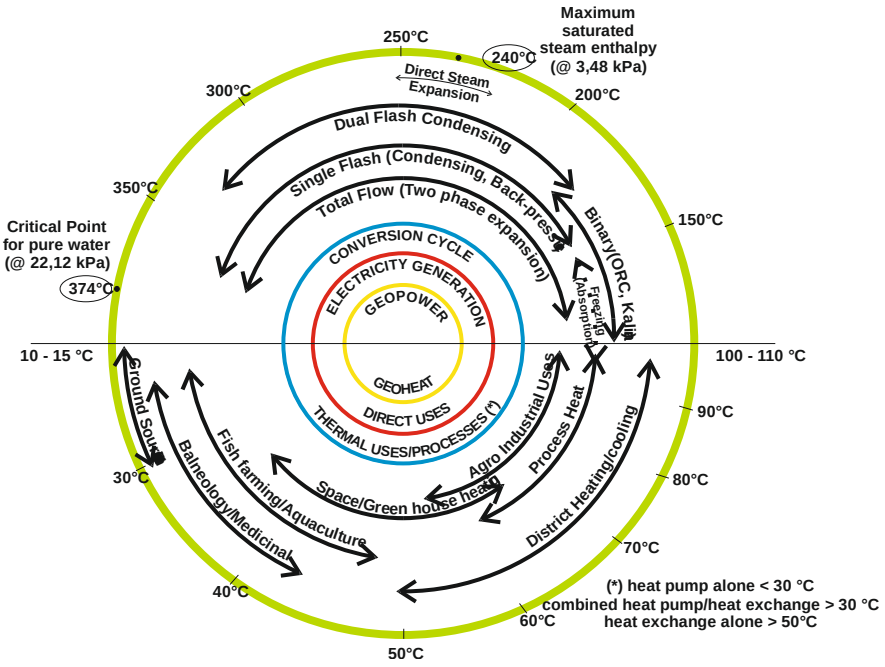

Figure 5: Geothermal Resource utilisation Diagram [Ungemach, 2007]

Finally, the geothermal utilisation spectrum displayed in the fig. 5 circular diagram may be contemplated while categorising geothermal resources.

As a result, the following classification could be adopted.

Very low temperature < 30 °C (Shallow geothermal, GSHP, ATES)	GEOHEAT < 100 °C	TOTAL
Low temperature < 50 °C (Medium/deep geothermal, GHX, GWHP)		
Medium temperature < 80 °C (Deep geothermal, GHX)		
High temperature < 100 °C (Deep geothermal, GHX, ORC)		
Very low temperature < 120 °C (Advanced binary Kalina Cycles, ORC)	GEOPOWER < 374 °C	
Low temperature < 150 °C (Binary ORC cycles, CHP)		
Medium temperature < 180 °C (Binary ORC, single flash back pressures, CHP)		
High temperature < 300 °C (Single flash, dual flash condensing, CHP)		
Very high temperature < 374 °C (Dual flash + ORC + CHP)		
Above critical point	SUPERCRITICAL > 374 °C	

ATES: aquifer thermal energy storage
CHP: combined heat and power
GHX: geothermal heat exchanger
GSHP: ground source heat pumps
GWHP: ground water heat pumps

Applications of the foregoing (options 1, volumetric method, and 3, resource utilisation classification) is illustrated in the reserve assessment exercise carried out North of Madrid by Ungemach et al [2008].

REFERENCES

Mufler, P. and Cataldi, R. (1978). Methods for Regional Assessment of Geothermal Resources. *Geothermics*, **7**, 53-89.

Sanyal, S.K. (2005). Classification of Geothermal Systems. A Possible Scheme. *Thirtieh Workshop on Geothermal Reservoir Engineering*, Stanford, CA, Jan. 31 – Feb. 2, 2005, 85-92.

Ungemach, P., Papachristou, M. and Antics, M. (2007). Renewability vs Sustainability. A Reservoir Management Approach. *Proc. European Geothermal Congress 2007*, Unterhaching, Germany, 30 May – 1 June, 2007.

Ungemach, P.; Hidalgo, R. and Antics, M. (2008). Geothermal Potential of the Madrid Area, A tentative Resource/Reserve Assessment. Geopower. Il Congreso de Energia Geotermica en la Edification y la Industria. Madrid, 13-16 Oct. 2008. *Conference Proceedings.* 83-96

Drilling, Completion and Testing of Geothermal Wells

Section 2. An Introduction to Geothermal Systems

5. THE EGS ISSUE

Pierre Ungemach

GPC INSTRUMENTATION PROCESS, Roissy-en-France, France

1 Introduction

Most of the geothermal resource base addresses the heat stored in deep seated, conductive/radiogenic dominated, tight sediments and hard crystalline basement rocks. The essence of EGS technology is the engineering of artificially created or/and enhanced geothermal reservoirs by stimulating these low permeability/low connectivity rock environments to recover a fraction of this vast dormant energy. It may therefore be regarded as the ultimate challenge of the geothermal community, bearing in mind that the recovery of say 1% of the heat stored within the 5 to 10 km depth over continental Europe, i.e. 10^{23} J (100,000 EJ) could cover European primary energy demand for centuries ahead.

The EGS route is a continuation of the former hot dry rock (HDR) concept of heat mining initiated in the 1970s. HDR raised considerable interest, since it suggested that man made geothermal systems could ultimately allow to extract terrestrial heat irrespective of the site specific limitations inherent to natural sources, that is, almost anywhere by-passing thus far the resource mining rationale. The idea got supported by early designs, which assumed deep seated rocks to conform to somewhat ideal elastic bodies, in which two wells, drilled sufficiently deep, would be connected via a large single penny shaped crack by hydraulic fracturing. This doublet system, in which injected cold water, once heated up, would be produced by thermosiphon (buoyant flow) could sustain a 50 MWt capacity over twenty years, provided the fractured heat exchange area be as large as 2 km^2.

Pilot field experiments, pioneered at Fenton Hill, USA (Los Alamos Labs) and Cornwall UK (Camborne School of Mines) led to more realistic views and designs. Both experienced the difficulty of achieving a multiple well to well connection by volumetric fracturing of a rock mass exhibiting two distinctive fractures (i) natural, pre-existing, fractures/joints, generally misaligned respective to the maximum horizontal *in situ* stress, and (ii) anisotropic *in situ* stress field and rock strenghts. Actually, fracture propagation is governed by shearing and self contained by in situ stresses.

Summing up, these field tests showed the difficulties of reconciling shear propagation of fractures with limited fluid losses and low resistance (hydraulic impedance) to flow of the connecting fracture network, highlighting the so-called HDR paradox.

Anyway, these projects ought to be regarded as large scale rock mechanics experiments, providing unvaluable scientific and engineering information with respect to basement rock mechanics, stimulation procedures and fracture mapping techniques.

They favoured the launching of several EGS projects ongoing in France, Germany, Switzerland, USA, Japan, Australia, of which the Soultz one, in Northern Alsace (Rhine Graben), has reached the more mature stage.

2 Objectives. Early Achievements

The primary objective of a commercial EGS plant is to sustain minimum 5-6 MW_e/10-15 MW_t installed capacities of power and heat, over a minimum 20 years lifetime, according to the specifications outlined in table 1.

A distinction ought to be made at this stage between the high grade and low grade EGS source settings, based on the connectivity concept displayed in fig. 1. High grade EGS would normally address tight sedimentary formations exhibiting some matrix (low permeability, in the milidarcy range) properties, generally overlying radiogenic granite basement rocks displaying no flow performance whatsoever, unless conductive fractures be accessed via stimulated flow paths.

These two settings coexist in the earlier assessed, non developed yet, North Madrid Tajo Basin location and the upper Rhine Graben continental rift where two such EGS undertakings have been completed at the Soultz and Landau sites.

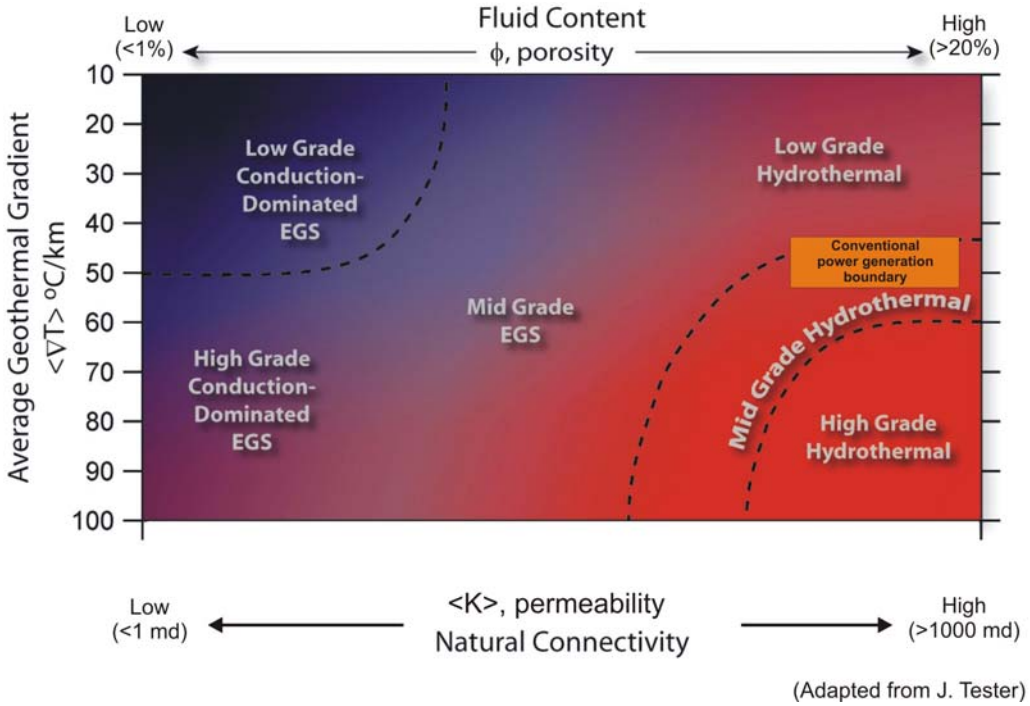

Figure 1: Geothermal continuum – The EGS issue

The Soultz EGS project is portrayed in fig. 2 artist view. It involves three wells, GPK1, GPK2 and GPK3, drilled at 5000 m depths and 200 °C bottomhole temperatures, in crystaline basement rocks underlying a, 1500 m thick, sedimentary cover (fig. 3). It is targeted at circulating, after due hydraulic stimulations, 100 kg/s of make up water via a single injector (GPK3) and dual producer (GPK1, GPK2) triplet well array, to drive a 6 MWe rated ORC turbine. A view of the circulation test facility is shown in fig. 4. Well tests demonstrated productivities below expectations, but encouraging in the sense further hydrofrac and mild acid treatments increased well performance that persisted long after, which was perceived as an evidence of self propping of active fractures. An intermediate, medium duration circulation test at ca 50 l/s, foreseen together with the installation of two downhole pump sets (1 lineshaft and one electrosubmersible – ESP), led to the implementation of a 1.5 MWe rated ORC plant connected to the grid on early April 2010.

Table 1: Man made/engineered geothermal reservoir issues [Ungemach, 2008a]

DRIVEN BY ECONOMICS: Target 5-6 MWe /module

LIFE OF THE SYSTEM:	~20 Years
TEMP/DEPTH OF THE WELLS:	~ 200°C
SEPARATION BETWEEN WELLS:	~600 m
PRODUCTION FLOW RATE:	~75 Kg/s
FLOW IMPEDANCE:	~ 0.1MPa/l/s
WATER LOSS:	~ 10% MAX
THERMAL DRAWDOWN	~ 10%
CONTACT SURFACE AREA:	~ 10 million m^2
RESERVOIR ROCK VOLUME	~ 300 million m^3
INTEREST RATE FOR THE CAPITAL:	~ 5%
SUPPORT :	No CO2 levy support etc

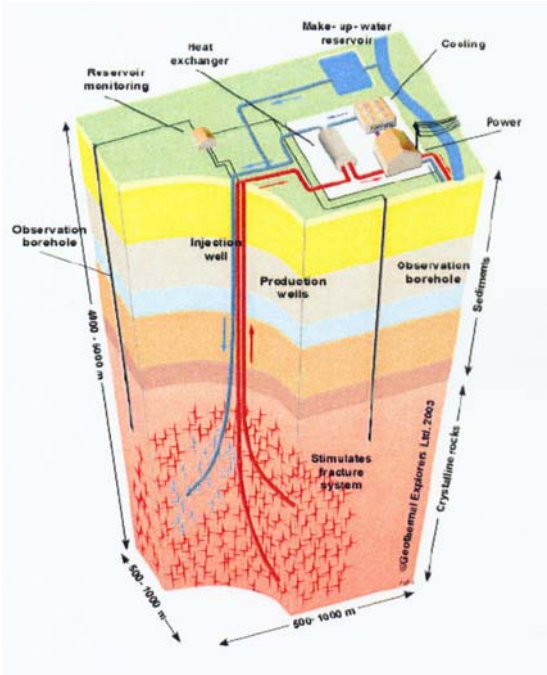

Figure 2: The Soultz EGS project. Artist view [ENGINE, 2006].

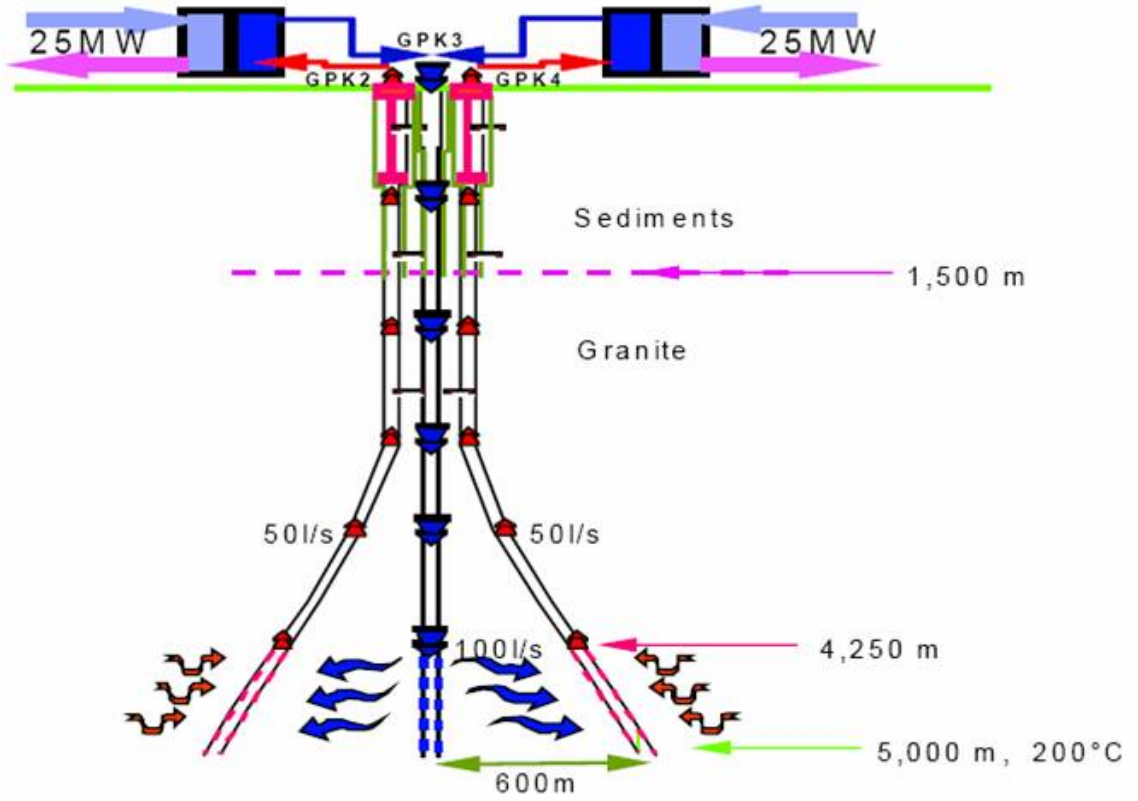

Figure 3: Soultz EGS project schematics [BRGM/ADEME 2004].

Figure 4: Soultz EGS project. Circulation test facility [ENGINE, 2006].

The project acted as a strong stimulus for advanced research in the fields of microseismic monitoring/prediction and interactive hydromechanical modelling of fracture propagation and associated, shear triggered, microseismic events [Kohl and Mégel, 2004, Bruel, 2004].

Future development of EGS prospects can be envisaged in selected areas exhibiting eligible tectonic and thermal attributes (see european EGS target resources mapped in fig. 5), provided the seismic risk be overcome and its impact mitigated.

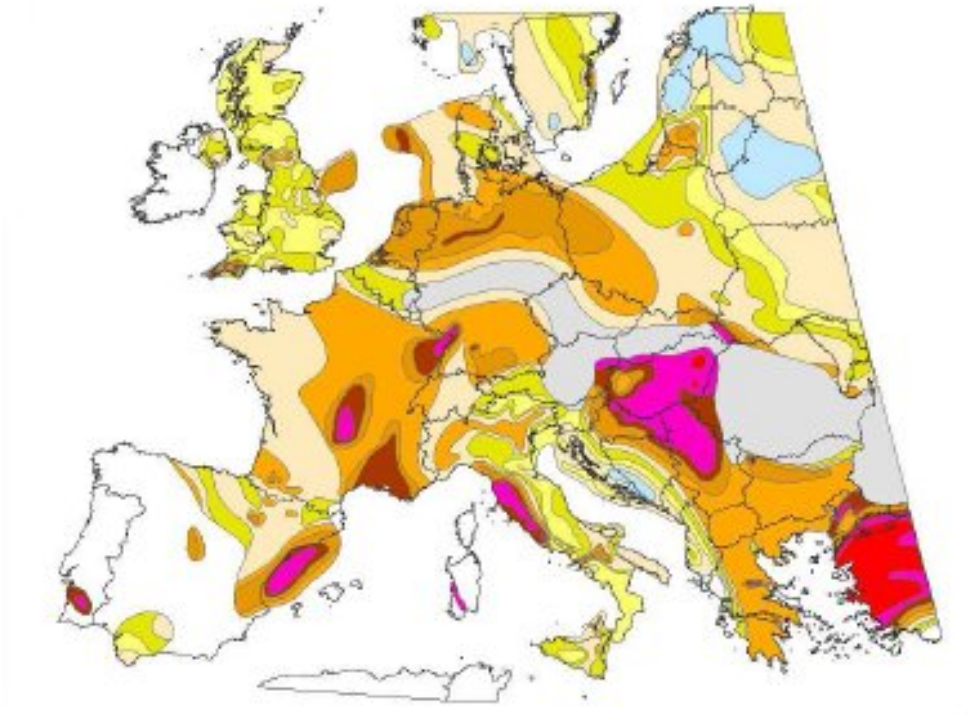

Figure 5: Eligible European EGS potential [Genter, BRGM, 2006].

The Landau site can be characterised as high grade EGS. Here, the second well of a planned CHP doublet scheme, initially dry, could be successfully stimulated thanks to fracturing techniques previously designed on the Soultz European EGS pilot test site, and the 5 MWe/10 MWt plant start up commercial operation. In Soultz, year 2008 concluded 22 years of a research stream materialised by the completion of a 5000 m deep well triplet array rooted in a crystalline basement and of a 1.5 MWe rated ORC plant, the first EGS ever achieved to date. Continuous plant operation and reservoir microseismic monitoring are required to analyse the long term behaviour of an engineered geothermal reservoir. The Soultz site is a prototype representative of low grade EGS, by far the most frequently encountered setting.

Still, although promising, the present outlook stands behind expectations as evidenced by table 2 targets vs. best so far accomplished records.

EGS performance may be upgraded by circulating working fluids other than water, such as CO_2, a topic investigated by Brown [2000] and Pruess [2007]. Owing to a higher mobility ratio, supercritical CO_2 could secure much higher flowrates and subsequent heat extraction, in spite of a lower heat capacity; contrasted production vs. injection well head pressures would elsewhere boost thermosiphon circulation (buoyant drive), possibly saving the operation of a submersible pump. Among the negative impacts are the faster cooling kinetics and more severe density segregation effects causing, if not carefully controlled at the production well, premature thermal breakthrough [Pruess, 2007]. Thermochemical interactions with respect to sensitive mineral species and related supersaturation/precipitation shortcomings studied by André et al [2007], in the framework of a CO_2 aquifer storage project, require in depth appraisals for candidate EGS rock petrographic settings. EGS/CO_2 can be turned into an advantage if combined to a carbon sequestration scheme (CCS), a synergy discussed by Pruess [2006], in which case, incidentally, fluid losses would be less a problem.

Present EGS know how and findings may be summarised as follows:

- fracture initiation and growth are governed by the natural fracture network and in situ stress field;
- low pressure shearing is the driving rock stimulation mechanism;
- low hydraulic impedance and large heat exchange areas, the so-called HDR paradox, are the key factors governing system efficiency;
- limited reservoir performance (≤2MWe capacity) recorded so far;
- system reliability merely site specific;
- social acceptance occasionally clouded by microseisms induced during hydraulic fracturing.

In this respect, the striking differences noticed between the Soultz (distensive graben stress field, sub-vertical fracture pattern, low pressure system) and the Australian Cooper Basin (compressive stress field, horizontal fracture propagation, overpressured reservoir) EGS sites ought to be mentioned, thus emphasising the need for widening the scope of EGS field assessments.

Ongoing and future research priorities should concentrate on:

- upgrading hydraulic conductivity/connectivity and relevant EGS reservoir performance;
- identifying active heat exchange area and stimulated rock volume respective to the in situ stress field;
- securing reservoir life and sustainability issues;
- last but not least, mastering induced seismicity according to stimulated reservoir growth, recorded natural background (micro)seismicity and (long) accumulated stress release

Table 2: EGS targets vs. achievements. 2008 status [Baria, 2008].

TOPIC	TARGETS	BEST SO FAR
System life	20 years	5 years Rosemanowes
Drilling cost	10m €for 6km well	5 m €for 5 km (GPK3)
Temperature	200°C+	270°C @ 2.2km Hijiori
Separation between wells	600m	600 m @ Soultz
Flow-rate	~ 75 l/s	26 l/s @ Soultz
Flow Impedance	0.1 MPa/l/s	0.29 @ Soultz
Water loss	10 %	0 % @ Soultz
Thermal drawdown	10 % after 20 years	
Contact surface area	10 million m2	
Reservoir rock volume	300 million m3	
Interest rate	~ 5%	

3 Induced Seismicity

A heightened awareness of the Public to geothermally induced seismic hazards focused essentially on the sole EGS and, occasionally, conventional water injection issues. Actually, many geothermal sites are located in seismically active areas, a fact which may introduce some confusion would the induced seismic impacts not be clearly identified and the risk assessed and mitigated accordingly.

The Rhine Graben is a geothermal province of known seismic activity. It hosts two EGS sites, the ongoing Soultz pilot plant operation and the Basel finally abandoned project. Earthquakes of magnitudes 5 and 6.4 have been recorded at Soultz [1970] and Basel [1456], the latter reported the worst damaging in Central Europe seismic history. Microseisms of magnitudes 2.9 (Soultz) and 3.4 (Basel) were recorded lately, further to hydraulic fracturing rock stimulation sequences, i.e. two to three orders of magnitude lower, but perceived and reported by the local population.

The Basel case, extensively described by Häring et al [2008], deserves a comment. After completing the first, 5,000 m deep, well, massive hydrofracturing was carried out over the lower 371 m openhole section. A 12,000 m^3 of water volume was injected during six days with flowrates and well head pressures peaking at 3300 l/min (# 200 m^3/h) and 296 bar respectively, accompanied by a quasi simultaneous microseismic activity of 185 events/h, maximum magnitudes nearing 3 (the maximum tolerance threshold borrowed to the Soultz microseismic monitoring), a response deemed unacceptable respective to the agreed protocol, which led the operator to reduce the injection rate and, due to a persistent microseismic activity, finally shut in and bleed off the well. A 3.4 magnitude event occurred before bleed off, then microseismicity decreased with well head pressures and venting. Surprisingly, three main aftershocks with magnitudes exceeding 3 occurred during the 56 days following well shut in/bleed off. The foregoing suggested a hydromechanical shearing process, triggering a cascading (in time and space) process in a very low permeability rock environment intersected by poorly conductive subvertical fracture zones [Häring et al, 2008].

These events, although non damaging to the nearby urbanised neighbourhood, were perceived emotionally (and negatively) by the population, actually highly sensitive to environmental hazards and disasters, and widely echoed by the media, resulted in the postponement "*sine die*" of the Basel EGS project.

The project outlook is however rewarding in the light of the following reccomendations:

(i) avoid the near vicinity of populated areas and districts while siting the well(s);
(ii) install and operate a thorough microseismic monitoring network and protocol aimed at reliably assessing the seismic signature and background noise prior to drilling, a

prerequisite particularly relevant in the Basel area subject to accumulated tectonic stresses at the Southern Rhine Graben edge, at the Jura/Bresse transition;

(iii) measure straight forwardly "*in situ*" stresses via standard packer hydrofrac tests;

(iv) carefully (re)design the rock stimulation strategy in order to secure a progressive build up of the EGS reservoir avoiding excessive and rapid volume/pressure increases and related poro-elastic stress accumulation/release, thus mitigating the seismic impact;

(v) thoroughly investigate the microseismic impact during "routine" plant operation in order to assess (and mitigate) the exploitation induced seismic risk if any;

(vi) last but not least, dedicate efforts to communicating with the public by clearly informing him on the real magnitude of geothermally induced seismic hazards.

Incidentally, several misleading "*a priori*" statements should be dissipated with respect to EGS seismic impacts.

EGS induced microseismic event signatures, in terms of epicentre depths and focal mechanisms, are often opposed to their natural earthquakes counterparts. As to epicentral depths there is evidence of a number of shallow natural earthquakes, at depths and magnitudes in the (2-4 km)/(4-5) ranges, recorded in the near Alpine and Jura regions [Deichmann, 2009]. Similar fault plane analysis may equally be applied as was the case in Basel [Deichmann et al, 2007].

The fact EGS induced seismicity may be turned into an asset owing to, deemed beneficial, release of long accumulated stresses, thus avoiding the advent of devastating earthquakes is illusory. Actually, there is at least a two orders of magnitude difference between EGS triggered and higher energy natural earthquakes

4 Conclusion

In conclusion, induced seismicity, a major contributor to fracture mapping and stimulated bulk volume estimates, may prove a sensitive issue regarding social acceptance whenever the magnitude of induced events exceeds the human detection threshold. Although the physical damages recorded in Basel were minimum, if not insignificant, they provoked public reactions echoed by the media and politicians. They caused the Basel EGS project to be stopped *sine die* after completion and stimulation of the first well, then definitely abandoned. Induced seismicity is a fatal issue during the build up of any EGS reservoir, which often happens to be hosted in seismically active tectonic environments. Therefore, accurate seismic monitoring/processing during all phases of a EGS project, along careful communication with the public are required to secure EGS present and future undertakings, a matter discussed by Rybach [2006].

REFERENCES

André, L., Andigane, P., Azaronal, M. and Menjoz, A. (2007): Numerical Modelling of Fluid-Rock Chemical Interactions at the Supercritical CO_2-Liquid Interface During CO_2 Injection Into a Carbonate Reservoir, the Dogger Aquifer (Paris Basin, France). *Energy Conversion & Management*, **48**, (2007), 1782-1797.

Baria, R. (2008): Global Perspective of engineering Geothermal Systems and how it can be brought to Market place in Europe. ENGINE. Final Conference, Vilnus, Lithuania 12-15 Feb. (2008).

Beaujard, C. and Bruel, D. (2005). Numerical Study of the Impact of Fluid Density on the Pressure Distribution and Stimulated Volume in the Soultz HDR Reservoir, *Geothermics*, **5-6**, 607-621.

Brown, D. W. (2000): A Hot Dry Rock Geothermal Energy Concept Utilising Supercritical CO_2 Instead of Water. *Proceedings Twenty-Fifth Workshop on Geothermal Reservoir Engineering*, Stanford University, Stanford, CA, Jan 24-26, 2000, Paper SGP-TR-165.

Deichmann, N., Ernst, J. and Wöhlbier, S. (2007). Data Analysis. In: Evaluation of the Induced Seismicity in Basel 2006/2007: Locations, Magnitudes, Focal Mechanisms, Statistical Forecasts and Earthquake Scenarios. Report of the Swiss Seismological Service to Geopower Basel AG, Basel, Switzerland, 152p, (2007).

Deichmann, N. (2009): Tremblements de Terre Exclus? (Are Earthquakes Excluded ?). Presentation given at the Roundtable on Deep Geothermal Energy Projects in Roman Switzerland, GREGE, Neuchatel, Switzerland, 11 June, (2009).

Gerard, A., Genter, A., Kohl, T., Lutz, P., Rose, P. and Rummel, F. (2006). The Deep EGS (Enhanced geothermal System) at Soultz-sous-Forêts (Alsace, France). *Geothermics*, **35**, issues 5-6 (Oct. – Dec. 2006), 473-483, (2006).

Häring, M.O., Schanz, U., Ladner, F. and Dyer, B.C. (2008): Characterisation of the Basel 1 Enhanced Geothermal Systems. *Geothermics*, **37**, 469-495, (2008).

MIT (2006): The future of Geotherml Energy. Impact of Enhanced Geothermal Systems (EGS) on the United Sates in the 21st Century, Mass. Inst. of Techn. Cambridge, MAS, (2006).

Pruess, K. (2006): Enhanced Geothermal Systems (EGS) Using CO_2 as working Fluid. A Novel Approach for Generating Renewable Energy with Simultaneous Sequestration of Carbon, *Geothermics*, **35**, 351-367, (2006).

Pruess, K. (2007): Enhanced Geothermal Systems (EGS): Comparing Water and CO_2 as Heat transmission Fluids. Lawrence Berkeley National Laboratory, Paper LBNL-63627, (2007).

Rybach, L. (2007). Induced Seismicity During EGS Operation. ENGINE. Enhanced Geothermal Innovative Network for Europe. Simulations of Reservoirs and Induced Seismicity. Workshop 3, Zürich, 29 June-01 July, 2006.

Ungemach, P. (2008): Sustainable Geothermal Development Technologies. European Insight. WIREC 2008, Washington DC, 5 March.

Drilling, Completion and Testing of Geothermal Wells

Short Course 1

3. INSIGHT INTO WELLBORE MASS AND HEAT TRANSFERS

Miklos ANTICS

GPC Instrumentation Process (GPC IP),Roissy-en-France, France

ABSTRACT

Production of geothermal fluids through wellbores is subject to complex phenomena such as mass and heat transfer. The present lecture notes aim at provinding the theoretical background for single and two phase mass transfer and for single phase heat transfer for the production and injection case. The development of governing equations of the above mentioned processes is presented. The lecture notes presented hereinafter use extensively the work presented by Hasan and Kabir in "Fluid flow and Heat Transfer in Welbores" [SPE 2002] and the lecture notes taken by the author at the Geothermal Institute, University of Auckland, New Zealand

INTRODUCTION

During production of a geothermal well fluid flow can be of different types. In order to optimise each flow process i.e. to achieve minimum pressure and heat losses in the wellbore it is necessary to understand and describe mathematically the processes involved. For example: after well completion the well is cooled by the circulation of drilling fluids; in the event of a blowout, due to the inflow from an over-pressured zone, transient two-phase flow may be encountered as the formation interacts with the wellbore prematurely. During production the geothermal fluid moves upward in the wellbore, the hot fluid begins exchanges heat with the surrounding formation resulting in coupled mass and heat transfer.

The objective is to make familiar the reader with the basics of single-phase flow, which forms the backbone for understanding the mechanics two-phase flow. Here, we attempted to capture some elements of fluid flow through conduits of various complexities, such as annulus and horizontal wells, and when fluid flow is accompanied by heat flow.

1 Single phase flow

from Hasan and Kabir, 2002

Fluid flow, in a variety of forms and complexities, is a basic entity that must be dealt with in the production of geothermal fluids. In its rudiments, single-phase water production/injection form the core of majority flow problems.

1.1 Mechanical Energy Balance.

A simple one-dimensional (ID) analysis of single-phase gas or liquid flow is best made with the aid of a schematic, as shown in Fig. 1.1. The channel, inclined at an arbitrary angle with the horizontal, shows upward flow of the fluid. For the present, we consider only the steady-state case and assume that pressure, at any point in the cross-sectional plane normal to flow, remains the same. With these simplifications, we derive the momentum balance equation.

Conservation of the Momentum

The sum of forces acting on the fluid element, shown in Fig. 1.1, equals the change of momentum of the fluid. The forces acting on the fluid element are those owing to pressure, p, friction, F, and gravity. Referring to the differential length, dz, of Fig. 1.1, we write $pA - (p + dp) - dF - A(dz)g\rho\sin\theta =$ change of momentum.

If the fluid mass flow rate is *w* and its velocity is *v*, then its momentum equals *wv*. For the general case of transient flow, when both flow rate and velocity change along the flow direction, fluid momentum change is given by (w+dw) (v+dv)-wv. Therefore,

$$pA - (p + dp)A - dF - A(dz)g\rho\sin\theta = (w + dw)(v + dv) - wv \quad (1.1)$$

Simplifying, we obtain:

$$- Adp - dF - A(dz)g\rho\sin\theta = wdv + vdw \quad (1.2)$$

Usually, the mass flow rate is invariant; that is, dw=0, leading to

$$- A dp - dF - A(dz)g\rho\sin\theta = w dv \cdot \quad (1.3)$$

Dividing both sides of Eq. 1.3 by Adz, we obtain:

$$-\left(\frac{dp}{dz}\right)+\left(\frac{dp}{dz}\right)_F - g\sin\theta - \frac{w}{A}\frac{dv}{dz} = 0 \quad (1.4)$$

$$\text{or } \left(\frac{dp}{dz}\right)=\left(\frac{dp}{dz}\right)_F +\left(\frac{dp}{dz}\right)_H +\left(\frac{dp}{dz}\right)_A \quad (1.5)$$

$$\text{where } \left(\frac{dp}{dz}\right)_H = g\rho\sin\theta \quad (1.6)$$

$$\text{and } -\left(\frac{dp}{dz}\right)_A = \frac{w}{A}\frac{dv}{dz} = g\rho\sin\theta \quad (1.7)$$

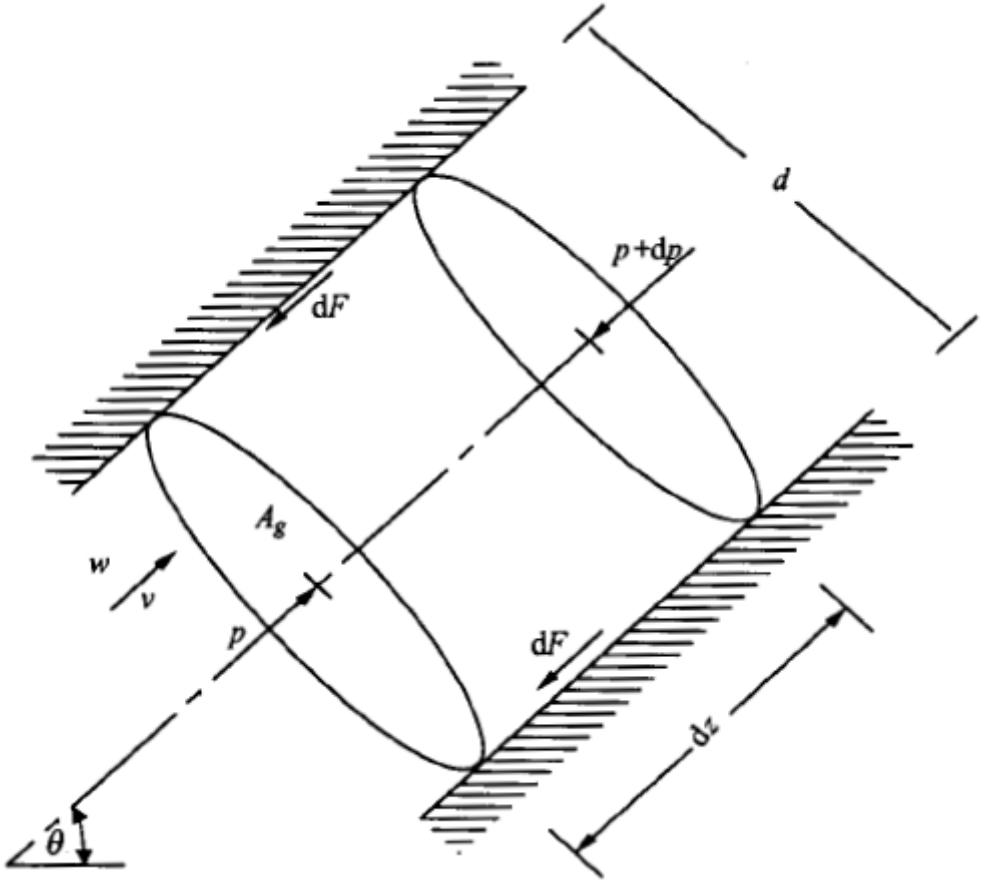

Figure 1.1: Momentum balance for a fluid element

Components of the Pressure Gradient

Equation 1.5 shows the total pressure gradient is the sum of the frictional gradient $(dp/dz)_F$ the hydrostatic gradient $(dp/dz)_H$ and the accelerational gradient $(dp/dz)_A$. Of these three terms, perhaps the static gradient is the easiest to estimate because it only requires knowledge of the fluid density and well-deviation angle. Because gas density depends on pressure, the static term will vary along the well for gas wells. Usually such variation is small, and relatively simple equations of state can be used to account for it. To some extent, even for single-phase oil production, oil-density variation with well depth, owing to temperature and dissolved gases, must be taken into account. The same comments

apply to the estimation procedure for the kinetic head (Eq. 1.7). For incompressible flow in a straight pipe with no change in cross-sectional area (gases at very high pressures and liquids), the change in fluid velocity with axial distance (dv/dz) is generally negligible. However, for gases at moderate and low pressures, and especially at high velocities, the kinetic energy loss can be a significant portion of the total pressure loss and must be accounted for properly. Computational complications that arise for gas flow have led to a number of correlations for calculating pressure drop in a wellbore. We recommend the widely used [Cullender and Smith[1]]method for computing pressure drop in a gas well.

The frictional pressure gradient is generally represented by:

$$\left(\frac{dp}{dz}\right)_F = -\frac{fv^2\rho}{2g_c d} \qquad (1.8)$$

where the Moody friction factor f, depends on the turbulence of the fluid and also on the pipe roughness. This friction factor is usually expressed as function of Reynolds number:

$$Re = \frac{dv\rho}{\mu} \qquad (1.9)$$

and roughness factor ε / d. The chart for friction factor as a function of Reynolds number with pipe roughness as a parameter is shown in Fig. 1.2; whereas, Fig. 1.3 presents the chart for estimating relative roughness. Note, k/d represents the relative roughness or ε / d in both figures, and in Fig. 1.3, the units of measure for pipe diameter (d) are in. Figure 1.2 is the Moody friction factor chart.

At low-Reynolds numbers (R<2,100), the flowing fluid elements do not interact with each other, and the flow is called laminar. For laminar flow in either rough or smooth pipes, friction factor is inversely related to Reynolds number:

$$f = \frac{64}{Re} = \frac{64dv\rho}{\mu} \qquad (1.10)$$

when Re<2100.

At high-Reynolds numbers (Re>4000), the flow is turbulent. During turbulent flow, the friction factor depends on both the Reynolds number and pipe roughness. For smooth pipes, such as plastic pipes and tubulars coated with PVC lining, friction factor can be estimated reliably from the Blassius equation,

$$f = 0.32(Re)^{-0.25} \qquad (1.11)$$

when Re>4000

For very high Reynolds numbers (Re>50,000), Eq. is slightly modified as f =0.184 (Re>50,000) Eq. 1.11 is slightly modified as:

$$f = 0.184(Re)^{-0.2} \qquad (1.11)$$

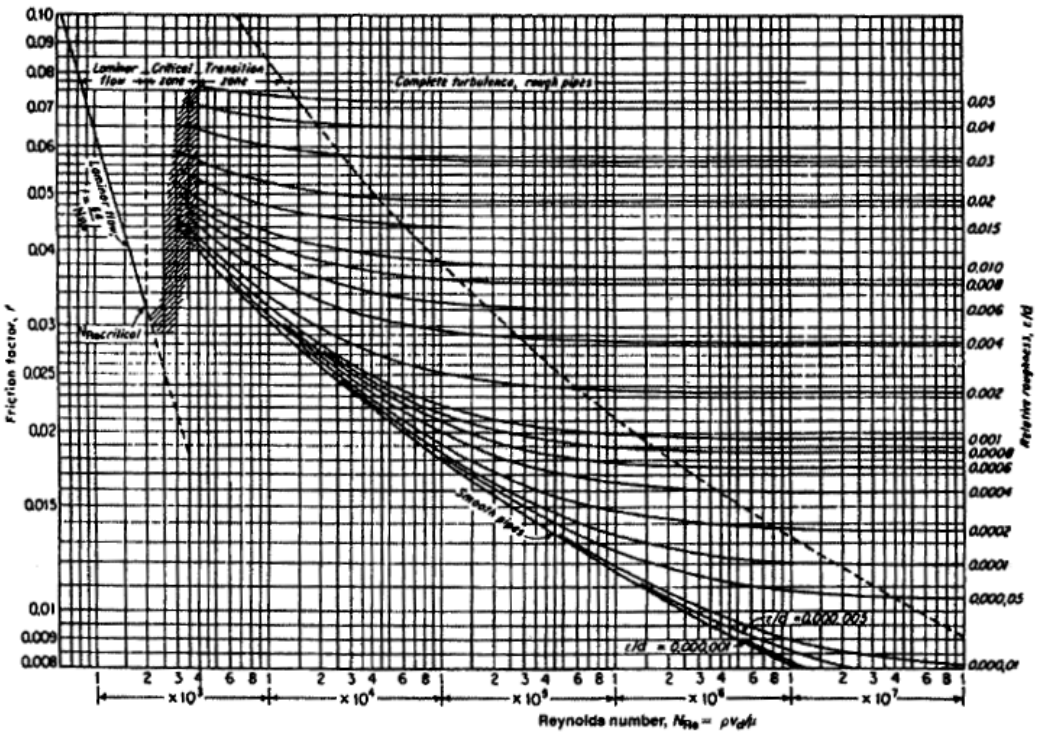

Figure 1.2: Moody friction factor chart for turbulent flow

Eq. 1.11, of course, is invalid for rough pipes. Although a chart is useful for all types of pipe roughness, chart reading is tedious and is not easily amenable to computer calculations. A number of equations, relating friction factor to Reynolds number and pipe roughness, has been proposed over the years and are in fair agreement with the original friction-factor charts. We recommend the following expression proposed by Chen, which yields Fanning friction factor and is given by:

$$f = \frac{1}{\left[4\log\left(\frac{\varepsilon}{3.7065\,d}\right) - \frac{5.0452}{Re}\log\Lambda\right]^2} \qquad (1.12)$$

where ε is the pipe roughness, and the dimensionless parameter, Λ, is given by:

$$\Lambda = \frac{\left(\frac{\varepsilon}{d}\right)^{1.1098}}{2.8257} + \left(\frac{7.149}{Re}\right)^{0.8981} \qquad (1.13)$$

The Fanning friction factor is one-fourth of the Moody friction factor. Unlike many other expressions, which require iterative solutions for friction factor, Eq. 1.12 is explicit and, therefore, computationally efficient.

The evaluation of various terms in Eq. 1.12 is relatively easier for flow of single-phase fluids, even for gases, than for two-phase mixtures. In the latter case, estimating the average density and friction factor can be challenging because these are complex functions of fluid properties and flow conditions. Chap. 2 discusses various approaches taken to• evaluate these entities in two-phase flow.

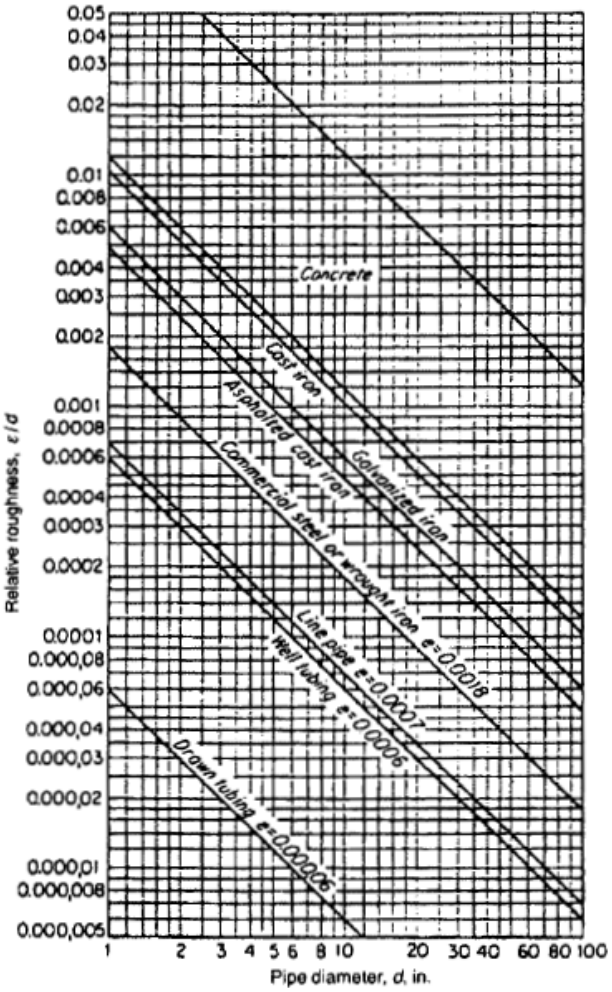

Figure 1.3: Relative roughness of pipes [ASME]

1.2 Flow in Nonisothermal Systems

Fluid temperature in the wellbore often varies significantly with depth, and sometimes with time. Many of the fluid properties that influence pressure drop, such as density and viscosity, are greatly influenced by the fluid temperature. Therefore, we cannot overemphasize the importance of accurate fluid temperature estimation as a function of well depth and production or injection time. This calculation can be done by a proper energy balance on the fluid-wellbore system, as shown in Chap. 3. For single-phase flow, the expression for fluid temperature, T_f, simplifies to

$$T_f = T_{ei} + \left[1 - e^{-zL_R}\right] g_G \sin\theta \qquad (1.14)$$

where the parameter, L_R, which is a function of wellbore heattransfer coefficient U_{to} and formation heat conductivity k_e, is defined by

$$L_R = \frac{2\pi}{c_p w}\left[\frac{r_{t0} U_{t0} k_e}{k_e + (r_{t0} U_{t0} T_D)}\right] \qquad (1.15)$$

In Eq. 1.15, T_D represents dimensionless temperature, which is a function of dimensionless time, $t_D = k_e c_e t / \rho_e r_{wb}^2$.

$$T_D = \ln\left[e^{-0.3t_D} + \left(1.5 - 0.3719 e^{-t_D}\right)\sqrt{t_D}\right]$$

1.3 Flow in Annulus

Although flow through a tubing string is the most common configuration, many completions dictate modelling for flow up the tubing-casing annulus. The presence of two walls makes flow through an annulus different from that through ordinary circular strings. The classical work of Bird et al.4 shows Eq. 1.8 is also applicable for such geometry, although the correlation for friction factor must be modified to reflect greater wall shear. For laminar flow in a concentric annulus, the Moody friction is given by:

$$f_{CA} = \frac{64}{Re}\frac{(1-K)^2}{\left\{\frac{1-K^4}{1-K^2} - \frac{1-K^2}{\ln\left(\frac{1}{K}\right)}\right\}} \tag{1.17}$$

where K is the diameter ration d_t/d_c. Following studies of Gunn and Darling and Caetano et al., we recommend expressing turbulent flow in a concentric annulus as:

$$\frac{1}{\left\{f_{CA}\left(\frac{F_p}{F_{CA}}\right)^{0.45\exp\left[-\left(\frac{Re-3000}{10^6}\right)\right]}\right\}^{0.5}} = 4\log\left[Re\left\{f_{CA}\left(\frac{F_p}{F_{CA}}\right)^{0.45\exp\left\{-\left(\frac{Re-3000}{10^6}\right)\right\}}\right\}^{0.5}\right] - 0.4 \tag{1.18}$$

where F_p is the laminar flow friction factor geometry parameter and F_{CA} is the ratio of friction factor for the annulus to that of a circular channel with the same d_c. Thus, from Eq. 1.18, F_p, for a concentric annulus, is given by:

$$F_p = \frac{(1-K)^2}{\left\{\frac{1-K^4}{1-K^2} - \frac{1-K^2}{\ln\left(\frac{1}{K}\right)}\right\}} \tag{1.19}$$

For eccentric annuli, eccentricity (E) is defined as:

$$E = \frac{D}{(d_c - d_t)} \tag{1.20}$$

where D is the distance between the pipe centers. The values of F_p, as a function of K and E, are shown in Fig. 1.4. For an eccentric annulus, the friction factor equation is similar to that of Eq. 1.18,

$$f_{ECA} = \frac{4}{Re}\frac{4(1-K^2)(1-K^2)}{\xi \sinh^4 \eta_0} \tag{1.21}$$

where η_0 and ξ incorporate the effect of eccentricity factor E. A complete treatment of flow through eccentric annuli is beyond the scope of this text; for further details, the reader is referred to the work of Caetano et al..

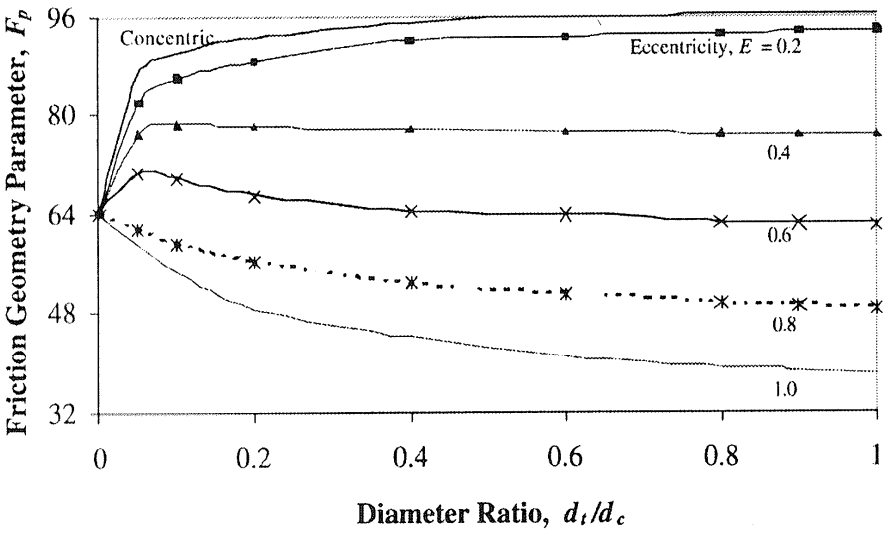

Figure 1.4: Friction geometry parameter for concentric and eccentric annuli.

1.4 Flow in Horizontal Wells

The recent interest in horizontal wells stems from significant increases in productivity and ultimate recovery in certain cases. Initial efforts' to couple the wellbore with reservoir using analytic approaches considered frictional effects only. In other words, fluid ingress along the well length leading to momentum and related effects was ignored in those formulations. Estimating pressure drop in horizontal wells presents a number of difficulties. First, pipe-surface roughness is a difficult entity to discern because of perforations along the well length in a cased boreho1e. Because most completions occur openhole, complexity increases significantly to ascribe a friction factor for an ill-defined surface-that is, the formation. The second factor revolves around fluid influx or changes in momentum that occur along the well length. Recent experimental studies- in perforated horizontal pipes, allowing fluid ingress along the well length, led to the development of several friction-factor correlations. Of these, the results of Ouyang et al. 10 and Yuan et al. are noteworthy. Ouyang et al. presented the following Moody friction-factor correlations for laminar and turbulent flows, respectively:

$$f = \frac{64}{Re}\left(1 + 0.04304\,Re_w^{0.6142}\right) \qquad (1.22)$$

$$\text{and } f = f_0\left(1 - 0.0153\,Re_w^{0.3978}\right) \qquad (1.23)$$

where f_o is the no-wall-flow friction factor, which can be estimated from Eq. 1.12. Note, Re_w represents the wall Reynolds number, which is based on the pipe ID and equivalent inflow velocity per unit wellbore length.

A somewhat different approach led Yuan et al. to obtain the following expression for the total or apparent friction factor, f_T (Moody friction factor), for fluid ingress along the borehole.

$$f_r = a\,Re^{-b} + C_n\,2d\varphi\frac{q_i}{q_a} \qquad (1.24)$$

$$\text{where } a = 102109.5\varphi - 3.25\frac{q_i}{q_a} - 8.87\times10^{-4}\varphi^2 + 5.37\times10^{-2}\varphi - 0.075 \qquad (1.25)$$

and

$$b = \left(-1.24\times10^{5}\,\varphi^{-3.075} + 42.4\right)\left(\frac{q_i}{q_a}\right)^2 + 1.577\times10^{3}\,\varphi^{-2.63}\,\frac{q_i}{q_a} - 5\times10^{-4}\,\varphi^{2} + 2.31\times10^{-2}\,\varphi + 0.085 \tag{1.26}$$

(q_i/q_a)<0:02, C_n=2.3, and for (q_i/q_a)>0.02, C_n is given by:

$$C_n = 4.25\left(\frac{q_i}{q_a}\right)^{-0.099} \tag{1.27}$$

Experiences show that pressure drop in horizontal wells becomes important in high-transmissivity reservoirs, where the pressure drop in the wellbore becomes comparable to that in the formation. When the wellbore pressure drop becomes important, in most cases, the frictional component becomes the dominant mechanism.

2 Two phase flow

from Geothermal Production Technology, lecture notes, Geothermal Institute, University of Auckland

2.1 Introduction

The characterization of flow (i.e., its pressure, temperature, enthalpy, flow pattern, etc.) at a point in a geothermal well is important Measurement of downhole conditions particularly at high mass flow rates, is difficult mainly because of an inability to keep a downhole gauge at a fixed position during discharge.

The capability of predicting flowing pressures-in a well producing steam-water mixtures is therefore desirable. Such well bore simulations have several potential applications. The estimation of the flashing zone is important particularly where the brine is expected to deposit calcium carbonate in the casing, the prediction of an output curve from one or two measurements where long term discharge is restricted due to environmental constraints or cost, the determination of procedures for starting or stimulating a well using say a gas lift, when combined with a reservoir simulator, prediction of the long term production of a system. are some of the applications that a reliable simulator could be used for.

Over the past years a number of simulations have been developed using a variety of correlations and including effects for gas and solids in the brine, bore heat transfer and reservoir drawdown. All claim to have accuracy for the range and wells tested. However none to date have proved to be completely universal mainly because the researchers have not had access to a wide range data. Measurements in wells are limited to low mass flow rates and well enthalpies, gas content, solids content, etc., vary over a very wide range.

The discussion in these notes is limited to three simulators, one a simple first order type of solution which can easily be programmed on a small programmable calculator or a manual operation using graphs and a hand calculator; the second and third are more sophisticated programs which illustrate to a second order what is possible to build into a simulator.

2.2 Vertical Two Phase Flow

It is recognised that in geothermal wells producing from a hot water reservoir the flow of fluid starts downhole where the temperature is lower than the saturation temperature corresponding to the local pressure, that is the fluid flows in a single phase. Two phase flow begins at a level where the two temperatures, fluid temperature and saturation temperature became equal; the liquid then flashes to vapour. As the fluid rises in the well, it continues to flash as the pressure falls. This pressure drop is the result of friction, gravitational and accelerational effects. That is, beyond the flash horizon the fluid exists as a mixture of liquid and vapour continually increasing in quality as it rises to the surface. It is also generally recognised that the flow pattern changes in a specific sequence as it approaches the surface. These flow patterns or flow regimes are subjective and are used by researchers to specify

differing sets of controlling equations. In vertical flow the sequence of flow patterns is as follows; bubble, slug, froth, annular mist. Not all patterns will necessarily appear in every well, for example the fluid may pass through bubble and reach the surface as a slug flow. The surface flow regime is a function of a number of variables including the geometry of the well, the mass flow and the initial condition of the fluid. also, that the 'froth' regime is often described as churn or transition flow. Figure 2.1.

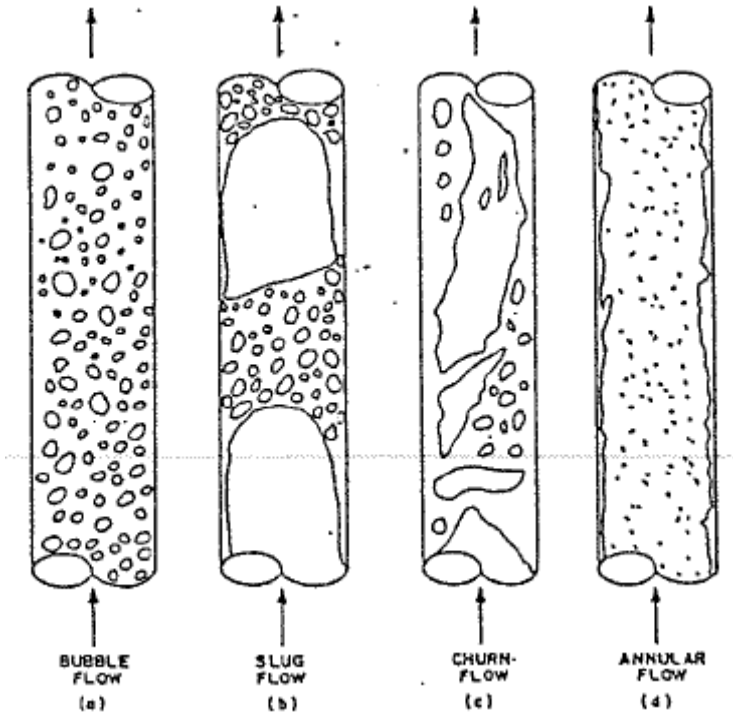

Figure 2.1: Flow Regimes Vertical Flow

2.3 Basic Equations and Methods

The calculation of pressure and temperature profiles along wells producing from water dominated systems calls for the evaluation of a number of effects.

1. Phase change and mass transfer between phases.
2. Flow regime change.
3. Two phase pressure drop.
4. Heat loss (or gain) to surrounding formations.

All these effects are inter-related. The pressure drop calculation requires that steam quality and flow regime need to be known at each point along the well and the phase change cannot be evaluated unless the enthalpy and pressure of the fluid are known and this in turn requires that the heat loss to the surrounding formations can be calculated.

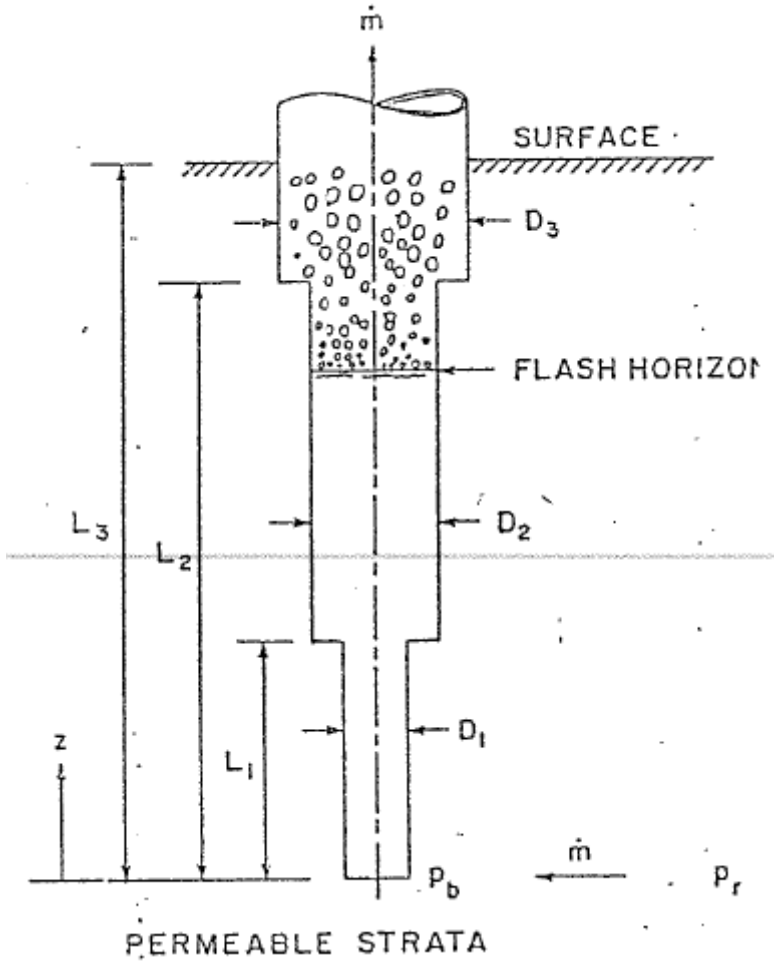

Figure 2.2: Schematics of flow in a geothermal well

The system (Fig. 2.2) can be considered to be divided into two parts:

a) the flow string through which the fluid flows from the reservoir to the surface,

b) the formation around the well bore where heat is transferred. Many of the earlier models and indeed some of the recent models ignore heat transfer effects.

Conservation of momentum gives the total pressure gradient $\left(\frac{dp}{dz}\right)$ as made up of three component gradients friction, acceleration, gravity:

$$\frac{dp}{dz} = \left(\frac{dp}{dz}\right)_F + \left(\frac{dp}{dz}\right)_A + \left(\frac{dp}{dz}\right)_G \qquad (2.1)$$

which terms of the respective variables:

$$\frac{dp}{dz} = \frac{P}{A}\tau_w + \frac{W}{A}\frac{dv}{dz} + \rho_m g\cos\theta \qquad (2.2)$$

Energy equation:

$$\frac{dq_e}{dz} = w\frac{d}{dz}\left(h + \frac{v^2}{2} + gz\right) \qquad (2.3)$$

and continuity

$$w = \rho_m v A \qquad (2.4)$$

Solutions of these equations depend upon the detail of analysis. For example, if bore heat transfer is assumed negligible then equation 3 is simplified giving a solution.

Property equations have to be formulated and it is then a question as to whether allowance should be made for gas and salt in the geofluid, both affect the properties; enthalpy, density, viscosity, etc.

Another approach is to ignore flow regimes and use an overall correlation for pressure drop. This is the technique employed by Hagedom and Brown [1965]. This method is particularly useful both because it is relatively simple and also that the pressures are calculated down the well starting from wellhead conditions. With an output curve it is then possible to calculate downhole conditions.

However some of the more useful programmes Ortiz-Raminez [1983] allow the calculation to proceed either up or down the well. If the calculation is to start from the bottom of the well it is necessary to have as data, not only the reservoir formation pressure but also a drawdown coefficient or productivity index.

k has been generally assumed that the pressure drop between reservoir and well (drawdown) is a linear function of the flow rate i.e. $p_d = p_r - k_d w$

or $\Delta p_d = k_d w$ where k_d is a constant of proportionality for a particular well. At high mass flow rates this assumption may be invalid. An increase of k_d acts like a decrease of the bottomhole pressure which lowers the flashing level. Ortiz-Ramirez [1983] uses the inverse of the drawdown equation called the productivity index (PI). The determination of PI or k_d is by using a long term shut in pressure and a measured flowing pressure corresponding to a mass flow or using a simulator to calculate the flowing pressure from a known well head measurement

An alternative approach an overall correlation calculate, in a stepwise manner, the flow conditions of velocity, density holdup, etc., through the well and to utilize correlations or theory to identify flow regime boundaries and then use a set of equations appropriate to the flow regime to obtain pressure drop. An example of this technique is that due to Bilicki et al. [1981]. Criteria are established for a particular flow pattern which are identified by limits indicating a transition from one to the other flow regime.

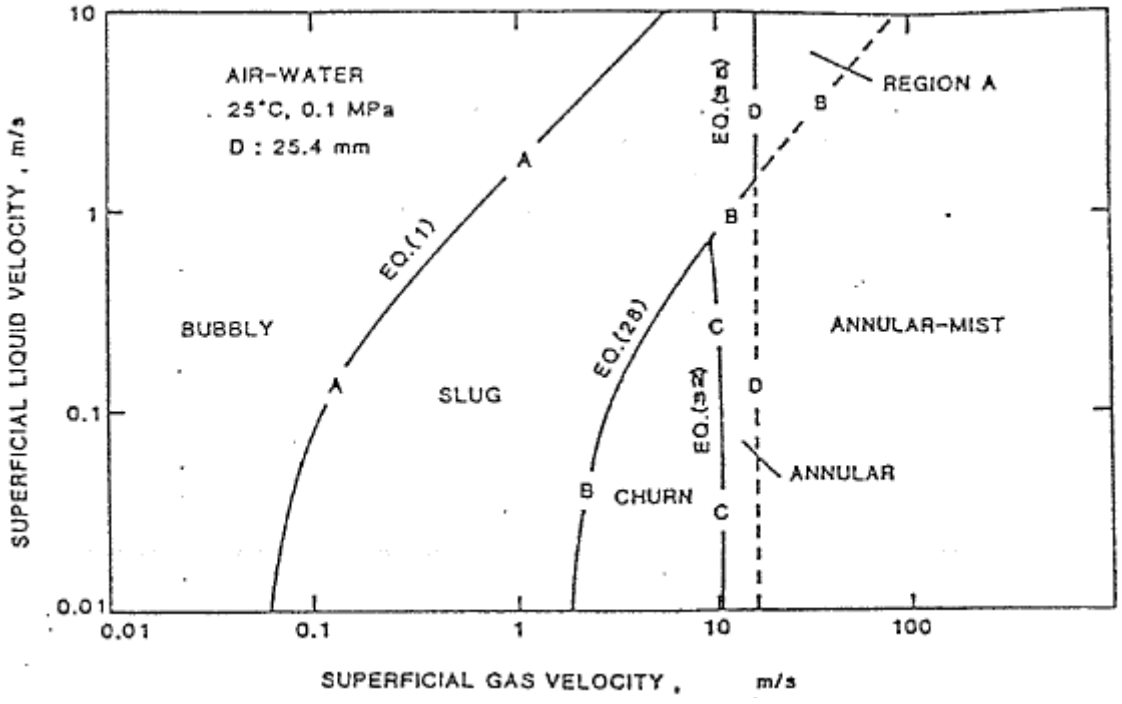

Figure 2.3: Flow-regime map based on transition criteria

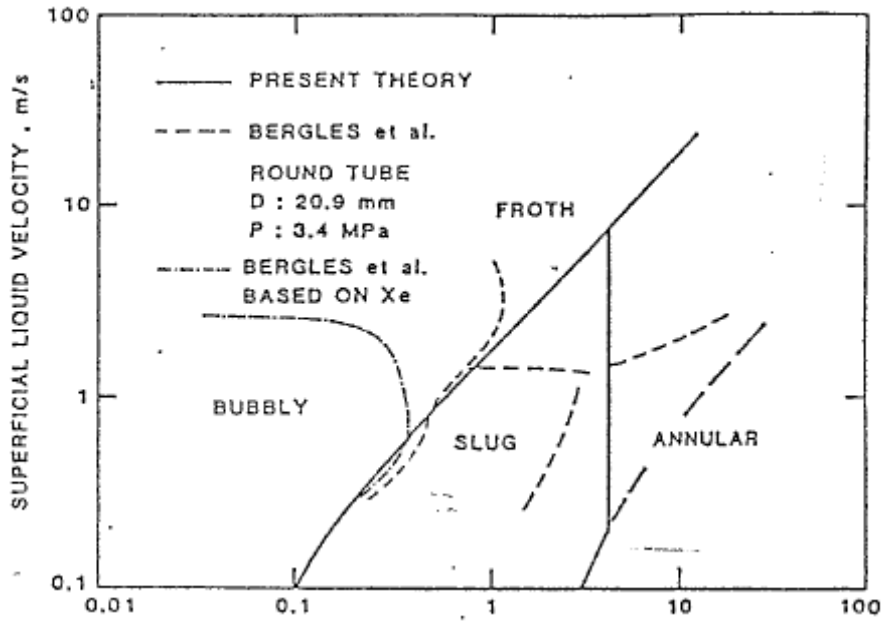

Figure 2.4: Comparison of the flow regime in terms of superficial velocities for steam-water flow at 3.4 MPa in a 20.9 mm ID tube.

Other authors use flow pattern maps (Fig. 2.3, 2.4) to identify flow regime changes whilst Orkiszewski introduces a liquid and a gas number, calculated values of which establish the transition criteria. This latter method is that used bv Ortiz-Raminez 1983 (Table 2.1).

Table 2.1 Transition criteria [Orkiszevski, 1967]

Limits	Flow regime
$\frac{q_g}{q_t} < (L)_B$	**Bubble**
$\frac{q_g}{q_t} > (L)_B, v_{gD} < (L)_S$	**Slug**
$(L)_M > v_g > (L)_S$	**Transition**
$v_{gD} > (L)_M$	**Mist**

The variables above are defined as:

$$v_{gD} = \frac{\left(\frac{\rho_L}{g\sigma}\right)^{1/4}}{A_p}$$

$$(L)_B = 1.071 - \left(\frac{0.2218 v_t^2}{dh}\right) \text{ with the limit } (L) \geq 0.13$$

$$(L)_S = 50 + 36 v_{gD} \frac{q_L}{q_g}$$

$$(L)_M = 75 + 84\left(v_g \frac{q_L}{q_g}\right)^{0.75}$$

where:

V_{gD} = dimensionless gas velocity

V_t = total fluid velocity (q_t/A_p), ft/sec

ρ_L =liquid density, lb/cu ft,

σ = liquid surface tension, lb/sec

Once the flow regime is determined mean densities (ρ_m) and shear stress (σ_w) etc., can be determined from another set of correlations. Different authors have their own preferences for correlations.

One feature that many of the simulators omit is recognition that the flow will 'choke'. That is, a critical flow condition exists analogous to that in single phase flow where sonic velocity at a point is obtained and the mass flow reaches a maximum. Bilicki et al. (1981) demonstrate that the critical mass flux $\psi_c = -\left(\frac{dp}{dz}\right)_S$ where the partial derivative can be expanded using thermodynamic identities and theorems. In the Bilicki et al. (1981) calculation method the criteria for choking is applied to determine where in the well choking will occur. In any flow up a vertical adiabatic pipe of constant cross sectional area choking can only occur at the end of the pipe. If the calculations indicate a choking condition at an elevation below the surface then the flow conditions are not physically realizable i.e. the assumed mass flow rate is too large for given cnditions.

If heat transfer between the formation and the well bore is to be accounted for, the Ramey (1962) solution is often used.

$$q = \frac{UA_n\left(\overline{T} - T_r\right)}{Wf(t)} \qquad (2.5)$$

where U is overall heat exchange coefficient evaluated as a function of production time. For wells with high flow rates where the convection heat transfer is predominant, the time function cancels out in equation (2.5). The simulator of Ortiz-Ramirez (1983) allows for bore heat transfer.

2.4 Calculation methods

2.4.1 Hagedorn & Brown [1965] – modified-

The version discussed here calculates the flowing down hole pressures starting from the surface conditions (well head). The assumptions are:

1) inflow at bottom of well only

2) an adiabatic flow- no heat losses

3) fluid is pure water - no gas or dissolved solids.

Rearrangement of equation 2.2, using finite differences to replace the differentials and using the single phase friction formulation of Darcy gives:

$$\Delta P = \lambda \frac{\Delta Z}{D} \frac{1}{2} \overline{\rho}_m \overline{v}_m^2 + \overline{\rho}_m \overline{v}_m \left(\overline{v}_2 - \overline{v}_1\right) + \overline{\rho}_m g \Delta z$$

where λ = friction factor

$\overline{\rho}_m$ = two phase mean density over increment ΔZ

$\overline{v}_m$ = mean two phase velocity over increment ΔZ

$$\text{or } \Delta Z = \frac{\frac{\Delta p}{\overline{\rho}_m} - \overline{v}_m \Delta \overline{v}}{\left(\frac{\lambda}{2D}\right)\overline{v}_m^2 + g} \tag{2.6}$$

$$\overline{\rho}_m \text{ is given by } \overline{\rho}_{TP} = \overline{\rho}_f H_L + \overline{\rho}_g \left(1 - H_L\right) \tag{2.7}$$

where H_L = liquid hold up

The assumption is made that over the finite interval the mixture of liquid and gas is treated as a homogeneous mixture and the Reynolds number can be written as:

$$Re_{TP} = \frac{\overline{\rho}_m \overline{v}_m D}{\overline{\mu}_m} \tag{2.8}$$

$$\text{where } \overline{v}_{TP} \text{ is defined as: } \overline{v}_{TP} = \frac{w}{\overline{\rho}_{TP} A} \tag{2.9}$$

The mixture viscosity $\overline{\mu}_{TP}$ is given by $\overline{\mu}_{TP} = \overline{\mu}_F^{H_L} \mu_g^{(1-H_L)}$

The Moody diagram or characteristic equation e.g. Churchill equation is used to determine λ.

In order to determine $\overline{\rho}_m, \overline{\mu}_m$ etc., estimation of hold up is necessary. Hagedorn & Brown (1965) present an empirical correlation for liquid hold up based on experiments on flowing pressure gradients in a 500 m experimental oil/gas well. The liquid hold up was not measured but was calculated to satisfy the total pressure drop measured after friction and acceleration effects had been determined. The calculated hold up were then correlated with flow rate pipe diameter and fluid properties. It was found that hold up is related to four dimensionless groups:

$$\text{Liquid velocity number } N_{LV} = \overline{v}_{sf}\left(\frac{\overline{\rho}_f}{g\sigma}\right)^{1/4} \tag{2.10}$$

$$\text{Gas velocity number } N_{GV} = \overline{v}_{sg}\left(\frac{\rho_f}{g\sigma}\right)^{1/4} \tag{2.11}$$

$$\text{Pipe diameter number } N_D = d\left(\frac{\rho_f g}{\sigma}\right)^{1/2} \tag{2.12}$$

$$\text{Liquid viscosity number } N_L = \mu_f\left(\frac{g}{\rho_f \sigma^3}\right)^{1/4} \tag{2.13}$$

These correlations are produced graphically in Hagedorn & Brown [1965] paper. For use in a computer curve fits have been produced as follows:

Secondary correction factor:

$$\psi = 0.5 + 30B + 454 \times 10^{-10} B^{-4.22} - 2.148 \times 10^{8} B^{6.785} \tag{2.14}$$

where $B = \frac{N_{GV} N_L^{0.38}}{N_D^{2.14}}$

Viscosity number coefficient

$$CNL = \frac{N_L + 0.058}{26} - 3.646 \times 10^{-8} (N_L)^{-1.379} - 390.625 (N_L)^{8}$$

Holdup correlation:

$$\frac{H_L}{\psi} = 22.348 E^{0482} - 5.103 \times 10^{5} E^{2.336} + 1.9 \times 10^{10} E^{4.355} - 10^{-7} E^{-1} + 0.05$$

$$\text{where } E = \left(\frac{N_{LV}}{N_{GV}^{0575}} \right) \left(\frac{p}{p_a} \right)^{0.1} \left(\frac{C_{NL}}{N_D} \right)$$

The method which is easily done by hand using a calculator, steam tables and curves rather than the equations above is:

1) Input well head conditions, calculate fluid properties at the well head.

2) Calculate superficial steam and water velocities then N_{LV}, N_{GV}, N_D and N_L

3) Using curves or curve fits above calculate hold up then two phase density and viscosity

4) Return to Step 1 add a pressure increment to the well head condition and repeat as far as Step 3.

5) Take the arithmetic mean of the two phase density ($\overline{\rho}_m$) viscosity ($\overline{\mu}_m$) and velocity across the increment and calculate the change of velocity $\Delta v = \overline{v}_2 - \overline{v}_1$

6) Calculate the two phase Reynolds number and using an appropriate roughness (typical values; Casing 4.57 x 10^{-} m, liner 1.37 x 10^{-}) determine

7) Calculate from equation 6.

8) Go back to Step 1 add a further pressure movement and repeat until bottom is reached or a change in diameter

9) At a change in diameter the calculation starts again with conditions at the transition. The above method has been used extensively and gives a reasonable fit to selected data. That is low mass flow rates, no gas, no dissolved solids and no heat transfer. If flow regimes are required the method outlined in Orkiszewski [1967] or a flow pattern map such as Fig. 2.3, Mishima [1984] can be used.

2.4.2 Bilicki Z. et al [1981]

In this model the void fraction is adjusted to the flow pattern, the programme keeping track of the changes in flow structure.

The following assumptions are made:

1) The flow is steady and one dimensional.

2) The liquid is in thermodynamic equilibrium with the vapour.

3) Above the flashing level the flow becomes two phase and the sequence of flow regimes is:

(a) bubble (b) slug (c) froth (d) annular mist

4) Each transition is described by a characteristic criterion.

5) The void fraction for each structure is described by a specific correlation.

6) The shear stress at the wall is described by Petrick's method i.e:

$$\tau_w = \frac{1}{2} f \frac{\psi^2}{\rho_f} \left(\frac{1-u}{1-\phi} \right)^2 \qquad (2.15)$$

$$f = 0.08 \left(\frac{\psi' D}{\mu_f} \right)^{-0.25}$$

$$\psi' = \psi \frac{1-\psi}{1-\phi}$$

here f = friction factor in a pipe of diameter D

ϕ = void factor

ψ = mass flux $\frac{w}{A}$

y = quality defined by the energy equation

7) The wall of the well is impermeable above the flashing level, the perforations end below this level.
8) The pressure drop between the reservoir and well (drawdown) is a linear function of the flow rate with a constant factor of proportionality i.e. $\Delta p_d = k_a w$, where k_d is a constant for each well but differs from well to well.

9) The void fraction varies along the channel and is a smooth function of Z.

The transition criteria are defined in Bilicki et al. [1981] and are formulated by consideration of bubble formation, bubble dynamics and the theory of surface waves.

Having established transition criteria, void fractions are calculated from a series of correlations taken from the literature. The calculation then proceeds from the well bottom by assuming a drawdown pressure loss and working up through the well in finite steps using property correlations to determine the pressure at a new height and testing the local conditions against the flow regime criteria.

The basic working equations are given in Bilicki [1981] but are essentially developments of those discussed earlier, equations 2.2, 2.3 and 2.4. When choking is approached the rates of change of the thermodynamic properties with respect to Z tend to infinity, so, within the programme small steps in Z are taken and two tests are applied a) whether flow is choked b) whether the surface has been reached. Only if the answer to both is negative does the programme proceed to the next step.

The input data required is mass flow rate, static reservoir pressure, reservoir temperature, depth at bottom and diameter of smallest casing, (up to a 4 casing string can be handled), reservoir drawdown coefficient, brine concentration, calculation step size.

The output gives pressure at well bottom, the pressure, quality, void fraction and depth for each flow pattern transition, the conditions at the well head.

2.4.3 Mechanistic method [Ansari, 1990]

from Antics, 1995

Flow Pattern Prediction

The basic work on mechanistic modelling flow of pattern transitions for upward flow was presented by Taitel et al. They identified four distinct flow patterns, and formulated and evaluated the transition boundaries among them. The four flow patterns are bubble flow, slug flow, churn flow and annular flow, as shown in Fig. 2.5.

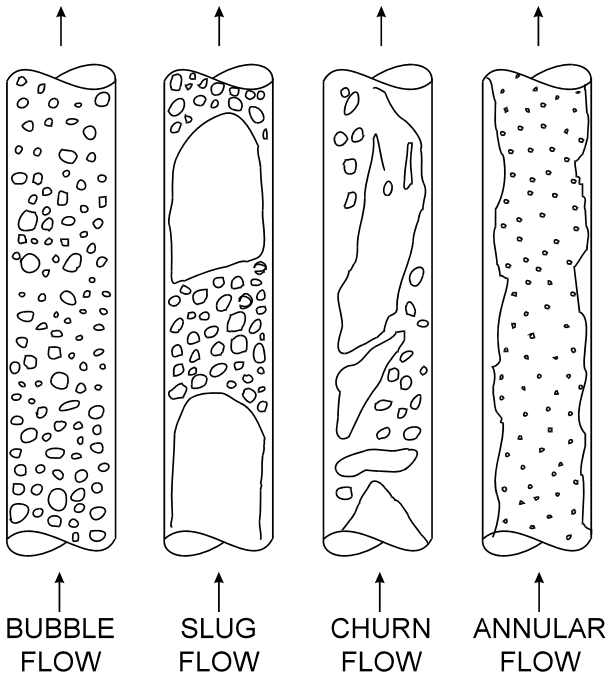

Figure 2.5: Flow patterns in upward two phase flow [Ansari et al. 1990]

In low temperature geothermal wells, due to the low gas water ratio, annular flow seldom occurs. Therefore in this study annular flow pressure drop calculations are not presented.

Bubble-Slug Transition: The minimum diameter at which bubble flow occurs is given by Taitel et al. as,

$$D = 19.01\left[\frac{(\rho_L - \rho_G)\sigma}{\rho_L^2 g}\right]^{1/2} \qquad (2.16)$$

For pipe sizes larger than this, the basic transition mechanism for bubble to slug flow is coalescence of small gas bubbles into large Taylor bubbles. Experimentally this was found at a void fraction of approximately 0.25. Using this value of void fraction, the transition can be expressed in terms of superficial and slip velocities as,

$$V_{SG} = 0.25\, v_s + 0.333\, V_{SL} \qquad (2.17)$$

where v_S is the slip or bubble rise velocity given by Harmathy as,

$$v_s = 1.53\left[\frac{g\sigma(\rho_L - \rho_G)}{\rho_L^2}\right]^{1/4} \qquad (2.18)$$

This is shown as transition A in Fig. 2.6.

At high liquid rates, turbulent forces break down large gas bubbles into small ones, even at void fractions greater than 0.25. This yields the transition to dispersed bubble flow given by Barnea et al. as,

$$(V_{SL} + V_{SG})^{2(3-n)/5} = 0.725 + 4.15\left(\frac{V_{SG}}{V_{SG} + V_{SL}}\right)^{0.5} \qquad (2.19)$$

This is shown as transition B in Fig. 2.6.

At high gas velocities this transition is governed by the maximum packing of bubbles to give coalescence. This occurs at a void fraction of 0.52, giving the transition for no-slip dispersed bubble flow as,

$$V_{SG} = 1.08\, V_{SL} \tag{2.20}$$

This is shown as transition C in Fig. 2.6.

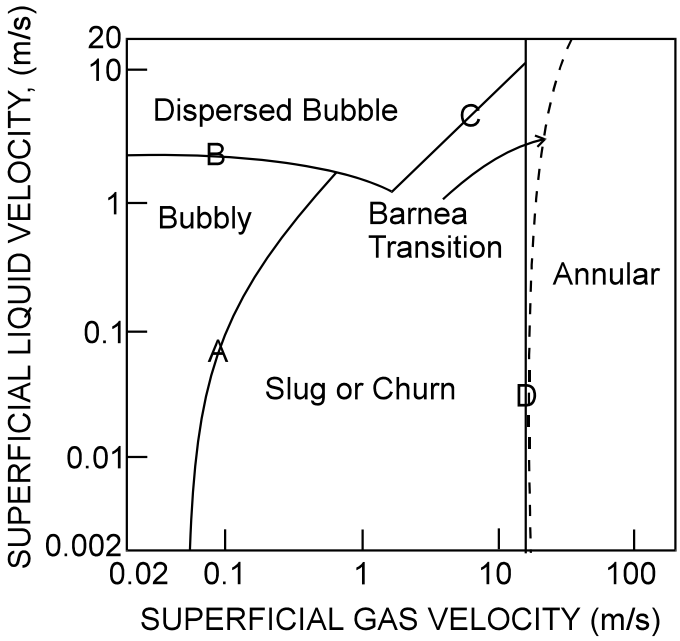

Figure 2.6: Typical flow pattern map for wellbores [Ansari et al. 1990]

Pressure Drop Calculations

Following the prediction of flow patterns, the next step is to calculate the pressure drop for two phase flow based on the physical models developed for the flow behaviour for each of the flow patterns.

Bubble Flow Model

The bubble flow model is based on the work by Caetano for flow in an annulus. The two bubble flow regimes, bubbly flow and dispersed bubble flow are considered separately in developing the model for the bubble flow pattern.

Due to the uniform distribution of gas bubbles in the liquid, and no slippage between the two phases, dispersed bubble flow can be approximated as a pseudo single phase. Due to this simplification, the two phase parameters can be expressed as,

$$\rho_{TP} = \rho_L \lambda_L + \rho_G (1 - \lambda_L) \tag{2.21}$$

$$\mu_{TP} = \mu_L \lambda_L + \mu_G (1 - \lambda_L) \tag{2.22}$$

$$v_{TP} = v_M = v_{SL} + v_{SG} \tag{2.23}$$

where,

$$\lambda_L = \frac{v_{SL}}{(v_{SL} + v_{SG})} \tag{2.24}$$

For bubbly flow, the slippage is considered by taking into account the bubble rise velocity relative to the mixture velocity. By assuming a turbulent velocity profile for the mixture with the rising bubble concentrated more at the centre than along the wall of the pipe, the slip velocity can be expressed as,

$$v_S = v_G - 1.2v_M \tag{2.25}$$

An expression for the bubble rise velocity was given by Harmathy. To account for the effect of bubble swarm, this expression was modified by Zuber and Hench as follows,

$$v_s = 1.53\left[\frac{g\sigma(\rho_L - \rho_G)}{\rho_L^2}\right]^{1/4} H_L^{n'} \tag{2.26}$$

where the value of n' varies from one study to another. Ansari et al. took a value of 0.1 for n' in order to give the best results. Thus, Eq. 10 yields,

$$1.53\left[\frac{g\sigma(\rho_L - \rho_G)}{\rho_L^2}\right]^{1/4} H_L^{0.1} = \frac{v_{SG}}{1 - H_L} - 1.2v_M \tag{2.27}$$

This gives an implicit equation for the actual hold-up for bubbly flow. The two phase parameters can now be calculated from,

$$\rho_{TP} = \rho_L H_L + \rho_G(1 - H_L) \tag{2.28}$$

$$\mu_{TP} = \mu_L H_L + \mu_G(1 - H_L) \tag{2.29}$$

The two phase pressure gradient is comprised of three components:

$$\left(\frac{dp}{dL}\right)_t = \left(\frac{dp}{dL}\right)_e + \left(\frac{dp}{dL}\right)_f + \left(\frac{dp}{dL}\right)_a \tag{2.30}$$

The elevation pressure gradient is given by,

$$\left(\frac{dp}{dL}\right)_e = \rho_{TP}\, g \sin\theta \tag{2.31}$$

The friction component is given by,

$$\left(\frac{dp}{dL}\right)_f = \frac{f_{TP}\rho_{TP}v_{TP}^2}{2\,D} \tag{2.32}$$

The explicit expression given by Zigrang and Sylvester can be use to define f_{TP} as,

$$\frac{1}{\sqrt{f_{TP}}} = -2\log\left[\frac{(\varepsilon/D}{3.7} - \frac{5.02}{Re_{TP}}\log\left(\frac{(\varepsilon/D}{3.7} + \frac{13.0}{Re_{TP}}\right)\right] \tag{2.33}$$

where,

$$Re_{TP} = \frac{\rho_{TP}v_{TP}D}{\mu_{TP}} \tag{2.34}$$

The acceleration pressure gradient is negligible compared to the other pressure gradients.

Slug Flow Model

The first thorough physical model for slug flow was developed by Fernandes et al. A simplified version of this model was presented by Sylvester. The basic simplification made was the use of a correlation for slug and void fraction. An important assumption of fully developed slug flow was used by these models. The concept of developing flow was introduced by McQuillan and Whalley during their study of flow pattern transitions. Due to the basic difference in the geometry of the flow, fully developed and developing flow are treated separately in the model.

For a fully developed slug unit, as shown in Fig. 2.5(a), the overall gas and liquid mass balances, respectively, give,

$$v_{SG} = \beta\, v_{GTB}(1 - H_{LTB}) + (1-\beta)v_{GLS}(1 - H_{LLS}) \qquad (2.35)$$

$$v_{SL} = (1-\beta)v_{LLS}H_{LLS} - \beta v_{LTB}H_{LTB} \qquad (2.36)$$

where,

$$\beta = \frac{L_{TB}}{L_{SU}} \qquad (2.37)$$

Mass balances for liquid and gas from liquid slug to Taylor bubble, respectively, give,

$$\left(v_{TB} - v_{LLS}\right)H_{LLS} = \left[v_{TB} - \left(-v_{LTB}\right)\right]H_{LTB} \qquad (2.38)$$

$$\left(v_{TB} - v_{GLS}\right)\left(1 - H_{LLS}\right) = \left(v_{TB} - v_{GTB}\right)\left(1 - H_{LTB}\right) \qquad (2.39)$$

The Taylor bubble rise velocity is equal to the centreline velocity plus the Taylor bubble rise velocity in a stagnant liquid column, i.e.,

$$v_{TB} = 1.2\, v_M + 0.35\left[\frac{gD\left(\rho_L - \rho_G\right)}{\rho_L}\right]^{1/2} \qquad (2.40)$$

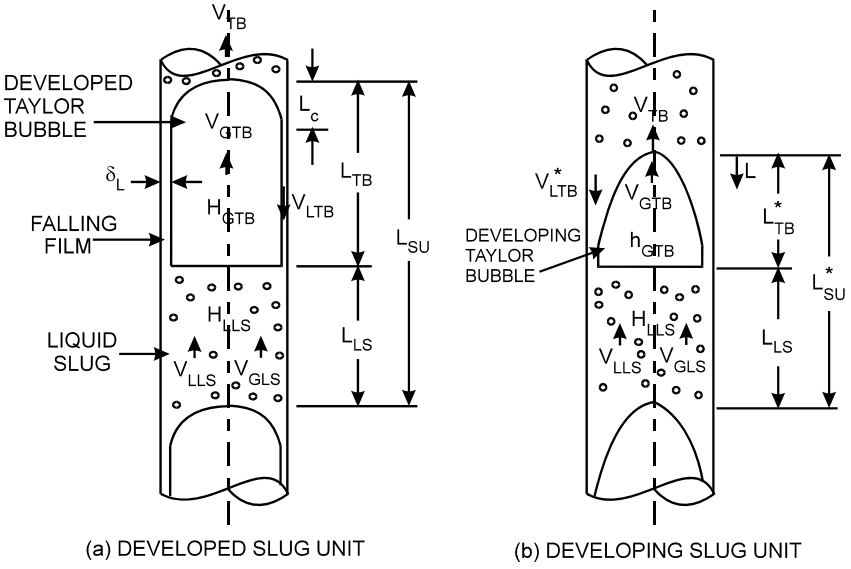

Figure 2.7. Schematic diagram of slug flow [Ansari et al. 1990]

Similarly, the velocity of the gas bubbles in the liquid slug is,

$$v_{GLS} = 1.2 v_M + 1.53 \left[\frac{g\sigma(\rho_L - \rho_G)}{\rho_L^2} \right]^{1/4} H_L^{0.1} \qquad (2.41)$$

where the second term on the right hand side represents the bubble rise velocity as defined earlier in Eq. (11).

The velocity v_{LTB} of the falling film can be correlated with the film thickness δ_L using Brotz expression,

$$v_{LTB} = \sqrt{196.7\, g\, \delta_L} \qquad (2.42)$$

where δ_L is the constant film thickness for developing flow, and can be expressed in terms of Taylor bubble void fraction to give,

$$v_{LTB} = 9.916 \left[g\, D \left(1 - \sqrt{H_{GTB}} \right) \right]^{1/2} \qquad (2.43)$$

The liquid slug void fraction can be obtained by the correlation developed by Sylvester from Fernandes et al. and Schmidt data,

$$H_{GLS} = \frac{v_{SG}}{0.425 + 2.65\, v_M} \qquad (2.44)$$

Equations 20-21, 23-26, 28-29 can be solved iterativelly to obtain all eight unknowns that define the developed slug model.

To model developing slug flow, as shown in Fig. 2.7(b) it is necessary to determine the existence of such flow. This requires calculating and comparing the cap length with the total length of a developed Taylor bubble. The expression for the cap length, as developed by McQuillan and Whalley, is given as,

$$L_c = \frac{1}{2g} \left[v_{TB} + \frac{v_{NGTB}}{H_{NLTB}} (1 - H_{NLTB}) - \frac{v_M}{H_{NLTB}} \right]^2 \qquad (2.45)$$

where v_{NGTB} and H_{NLTB} are calculated at the terminal film thickness δ_N (called Nusselt film thickness) given by,

$$\delta_N = \left[\frac{3}{4} D \frac{v_{NLTB} \mu_L (1 - H_{NLTB})}{g(\rho_L - \rho_G)} \right]^{1/3} \qquad (2.46)$$

The geometry of the film flow gives H_{NLTB} in terms of δ_N as,

$$H_{NLTB} = 1 - \left(1 - \frac{2\, \delta_N}{D} \right)^2 \qquad (2.47)$$

To determine v_{NGTB}, the net flowrate at δ_N can be used to obtain,

$$v_{NGTB} = v_{TB} - (v_{TB} - v_{GLS}) \frac{(1 - H_{LLS})}{(1 - H_{NLTB})} \qquad (2.48)$$

The length of the liquid slug can be calculated empirically from,

$$L_{LS} = C'D \tag{2.49}$$

where C' was found by Duckler et al. to vary from 16 to 45. It is taken 30 for the present study. This gives the length of the Taylor bubble as,

$$L_{TB} = \frac{L_{LS}}{(1-\beta)}\beta \tag{2.50}$$

From the comparison of L_c and L_{TB}, if $L_c > L_{TB}$, the flow is developing slug flow. this require new values for L_{TB*} and, H_{LTB*} and v_{LTB*} calculated earlier for developed flow.

For L_{TB*}, Taylor bubble volume can be used,

$$V_{GTB} = \int_0^{L_{TB}^{\bullet}} A_{TB}^{\bullet}(L)\, dL \tag{2.51}$$

where $A_{TB}^{\bullet}(L)$ can be expressed in terms of local hold-up $h_{LTB}(L)$, which in turn can be expressed in terms of velocities by using Eq. (20). This gives,

$$A_{TB}^{\bullet}(L) = \left[1 - \frac{(v_{TB} - v_{LLS})H_{LLS}}{\sqrt{2gL}}\right]A \tag{2.52}$$

The volume $v_{GTB}^{\bullet}(L)$ can be expressed in term of flow geometry as,

$$V_{GTB}^{\bullet} = V_{SU}^{\bullet} - V_{LS} \tag{2.53a}$$

or

$$V_{GTB}^{\bullet} = v_{SG}\, A\left(\frac{L_{TB}^{\bullet} + L_{LS}}{v_{TB}}\right) - v_{GLS}\, A\left(1 - H_{LLS}\right)\frac{L_{LS}}{v_{TB}} \tag{2.53b}$$

Substitution of Eqs. (2.52) and (2.53) into Eq. (2.51) gives:

$$v_{SG}\frac{\left(L_{TB}^{\bullet} + L_{LS}\right)}{v_{TB}} - v_{GLS}\left(1 - H_{LLS}\right)\frac{L_{LS}}{V_{TB}} = \int_0^{L_{LTB}^{\bullet}}\left[1 - \frac{\left(v_{TB} - v_{LLS}\right)H_{LLS}}{\sqrt{2gL}}\right]dL$$

Equation (2.52) can be integrated and then simplified to give,

$$L_{TB}^{\bullet 2} + \left[\frac{-2ab - 4c^2}{a^2}\right]L_{TB}^{\bullet 2} + \frac{b^2}{a^2} = 0 \tag{2.54}$$

where

$$a = 1 - \frac{v_{SG}}{v_{TB}} \tag{2.55}$$

$$b = \frac{v_{SG} - v_{GLS}\left(1 - H_{LLS}\right)}{v_{TB}}L_{LS} \tag{2.56}$$

$$c = \frac{v_{TB} - v_{GLS}}{\sqrt{2g}}H_{LLS} \tag{2.57}$$

After calculating $L^{\bullet}_{TB}$, the other local parameters can be calculated from,

$$v^{\bullet}_{LTB}(L) = \sqrt{2gL} - v_{TB} \tag{2.58}$$

$$h^{\bullet}_{LTB}(L) = \frac{(v_{TB} - v_{LLS})H_{LLS}}{\sqrt{2gL}} \tag{2.59}$$

In calculating pressure gradients, the effect of varying film thickness is considered and the effect of friction along Taylor bubble is neglected.

For developed flow, the elevation component occurring across a slug unit is given by,

$$\left(\frac{dp}{dL}\right)_e = \left[(1-\beta)\,\rho_{LS} + \beta\,\rho_G\right] g \sin\theta \tag{2.60}$$

where

$$\rho_{LS} = \rho_L H_{LLS} + \rho_G(1 - H_{LLS}) \tag{2.61}$$

The elevation component for developing slug flow is given by,

$$\left(\frac{dp}{dL}\right)_e = \left[(1-\beta^{\bullet})\,\rho_{LS} + \beta^{\bullet}\,\rho_{TBA}\right] g \sin\theta \tag{2.62}$$

where ρ_{TBA} is based on average void fraction in the Taylor bubble section with varying film thickness. It is given by,

$$\rho_{TBA} = \rho_L H_{LTBA} + \rho_G(1 - H_{LTBA}) \tag{2.63}$$

where H_{LTBA} is obtained by integrating Eq.43 and dividing by $L^{\bullet}_{TB}$ giving,

$$H_{LTBA}(L) = \frac{2(v_{TB} - v_{LLS})H_{LLS}}{\sqrt{2gL^{\bullet}_{TB}}} \tag{2.64}$$

The friction component is the same for both the developed and developing slug flow as it occurs only across the liquid slug. This is given as,

$$\left(\frac{dp}{dL}\right)_f = \frac{f_{LS}\rho_{LS}v_M^2}{2\,D}(1-\beta) \tag{2.65}$$

where f_{LS} can be calculated by using,

$$Re_{TP} = \frac{\rho_{LS}v_M D}{\mu_{LS}} \tag{2.66}$$

For stable slug flow, the acceleration component of pressure gradient can be neglected.

For the model presented above was designed a computer code (wellbore simulator) that takes into account all the discussed parameters. The schematic flowchart of the computer code developed for the wellbore simulator is presented in Fig. 2.8.

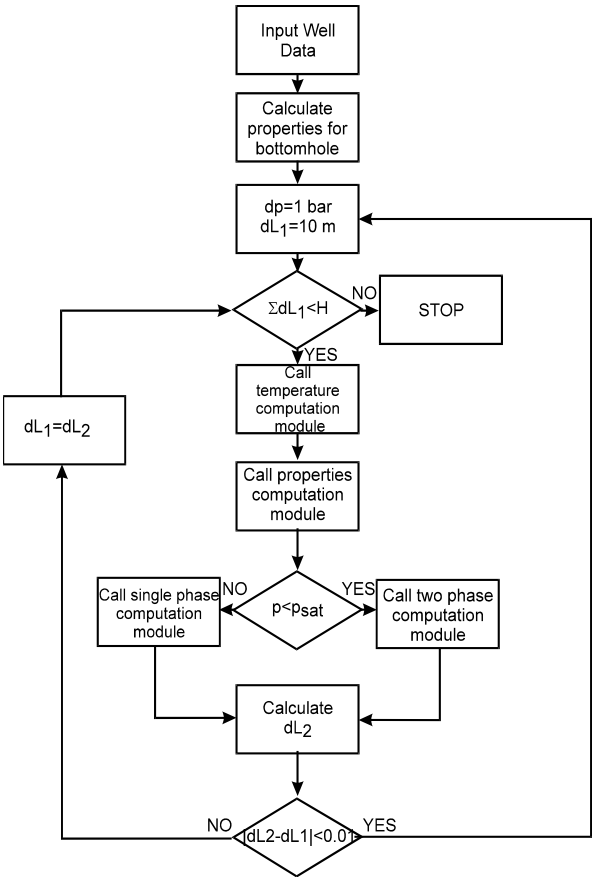

Figure 2.8: Schematic flowchart of the wellbore simulator code

3 Wellbore heat transfer

from Hasan and Kabir, 2002

3.1 Introduction

Fluid production or fluid injection inevitably involves significant heat exchange between the wellbore fluid and its surroundings. During production, the hot fluid continues to lose heat to the increasingly cold surroundings, as it ascends the borehole. In contrast, the injected fluid may either gain (cold water) or lose (steam or hot water) heat upon descent.

The heat-transfer process just described impacts fluid properties and, in turn, the dynamics of fluid flow. Consequently, the coupled nature of momentum and energy transport may require simultaneous solutions for both processes. While steady-state flow modelling is adequate for designing tubular hardware en route to optimal wellhead production, transient-pressure testing may demand rigorous treatment of the coupled and transient nature of momentum, fluid, and heat flows. Similar treatment may be required when shut-in passes are made during production logging runs.

The temperature difference between the wellbore fluid and the formation causes transfer of heat from the fluid to its surroundings. As Fig. 3.1 shows, the temperature difference increases with decreasing depth, causing greater heat transfer and lower fluid temperature as the fluid rises up the wellbore. At any given depth, the formation temperature will vary with radial distance from the well. The near-well bore formation temperature also varies somewhat with production or injection time. Therefore, heat loss from the producing fluid decreases with time. Fig. 3.1 also depicts the increase in the injected fluid temperature with well depth.

The importance of various aspects of heat transfer between a wellbore fluid and the formation has generated rich literature on the subject. For instance, the usefulness of measuring wellbore fluid temperature was pointed out as early as 1937 by Schlumberger et al.[1] Perhaps the earliest application of the heat-transfer principle was the use of temperature logs for estimating water and gas injection profiles in the However, a lack of complete understanding of physics of heat flow led to a few

problems in the field in the early days. Thermal stress failure of casings in steam-injection wells is a case in point.

A theoretical model for estimating fluid temperature as a function of well depth and production or injection time was first presented by Ramey. Ramey's pioneering work spawned a number of applications. Some of these applications include heat loss estimation in steam injection and geothermal wells, production log interpretation, and estimation of fluid circulation temperature and static formation temperature.

Although Ramey's method gave us a much needed impetus for further development, the method does have a few limitations. For example, the effects of kinetic energy and friction are neglected, and flow of only a single-phase fluid can be handled. Equally important, Ramey suggested the well radius to be vanishingly small in most cases; that is, the line-source well. This assumption can prove untenable in many instances. However, the work of Carslaw and Jaeger may be adapted to remove the restrictive line-source approximation. Methods have also been proposed to handle two-phase flow,- thereby removing the other assumption. The work of Hasan and Kabir shows how both assumptions can be removed for the general case of steady-state, wellbore two-phase flow.

In the following sections, we first model the formation temperature distribution. We then present the energy balance for the well bore fluid as it exchanges heat with the surrounding earth. In Sec. 3.4, we develop expressions for wellbore fluid temperature for both production and injection wells. Our development closely follows the work of Hasan and Kabir.

3.2 Formation Temperature Distribution

3.2.1 Diffusivity Equation

During production, the hot wellbore fluid provides a source of heat to the formation while, during fluid injection, the wellbore acts as a heat sink. To model heat flow and the resulting temperature distribu¬tion in such systems, we treat the formation as a homoge neous solid. Assuming symmetry around the well simplifies the three-dimensional (3D) problem into a two-dimensional (2D) problem. In addition, heat diffusion in the vertical direction may be ignored, owing to small vertical temperature gradients. Neglecting vertical heat flow reduces the sys¬tem to a one-dimensional (ID) heat-diffusion problem. This approach, adapted by Hasan and Kabir and others, introduces very little error and allows an analytical solution for the problem. The analytic approach is often preferred to the alternative numerical solutions, which may prove tedious and time consuming.

An energy balance on the formation then leads to the partial-differential equation, derived in cylindrical coordinates, for the variation of formation temperature with radial distance from the well and production time,

$$\frac{\partial^2 T_e}{\partial r^2} + \frac{1}{r}\frac{\partial T_e}{\partial r} = \frac{c_e \rho_e}{k_e}\frac{\partial T_e}{\partial t} \qquad (3.1)$$

In Eq. 5.1, Tis the formation temperature at an arbitrary depth at time, t, and distance, r, measured from the center of the wellbore. Heat capacity, density-and thermal conductivity of formation are given by c_e, ρ_e and k_e, respectively. The thermal diffusivity equation is analogous to that used in pres¬sure diffusion while solving pressure-transient problems.

The three boundary conditions needed for the solution of Eq. 3.1 can be obtained from the examination of the physical system. Fig. 3.2 is a schematic of the temperature distribution in the formation around a producing well at a given depth. At very early times, the formation temperature retains its initial value (T_{ei}) except near the wellbore, as shown by the inner curve. Thus, initially (t=0), we assume equals T_{ei} everywhere in the formation. As time increases, heat, transferred from the warm wellbore fluid, will raise the formation temperature in its vicinity. The formation temperature profile at such a time will look somewhat like the middle curve shown in Fig. 3.2. However, at the

outer boundary, formation temperature does not change with radial distance; that is, the slope is zero, or =0.

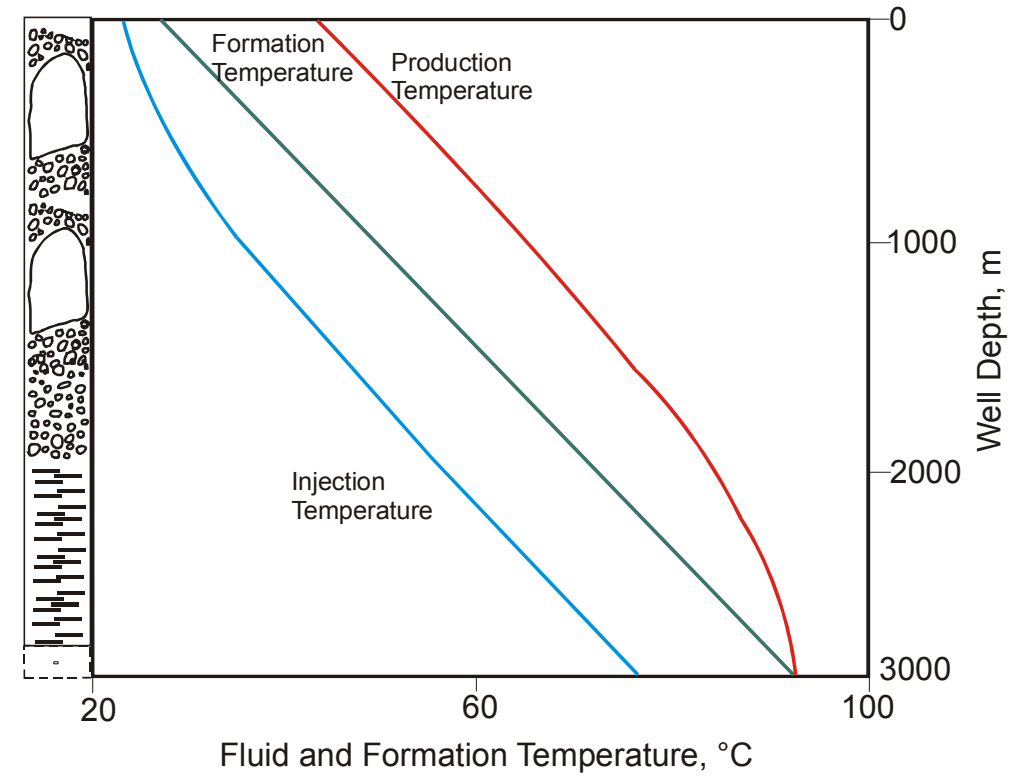

Figure 3.1: Fluid and formation temperature profiles during production and injection

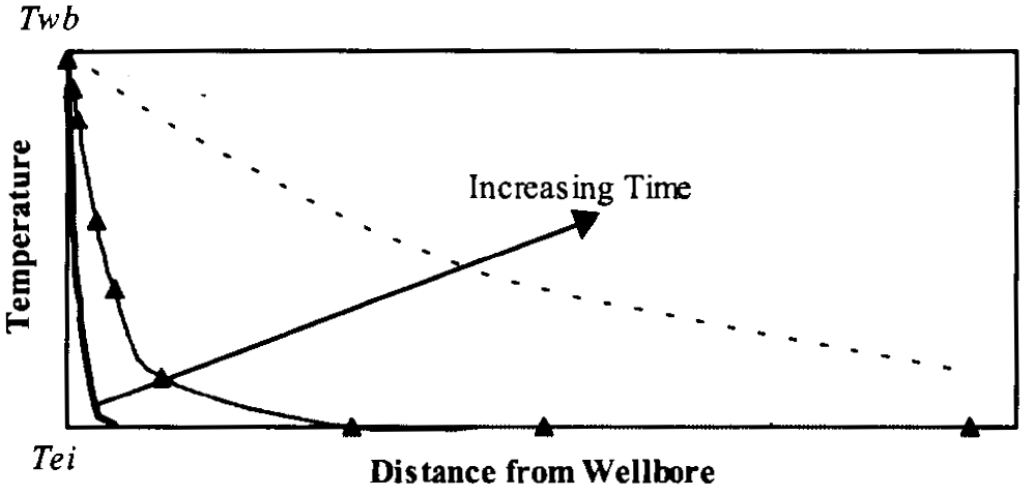

Figure 3.2: Schematic of formation temperature profile at a given depth around the wellbore

Finally, the heat flow rate at the wellbore/formation interface is governed by Fourier's law of heat conduction. Therefore, one can write the three boundary conditions,

$$\lim_{t\to 0} T_e = T_{ei} \qquad (3.2)$$

$$Q = 2\pi k_e \left. \frac{r\partial T_e}{\partial r} \right|_{r=r_{wb}} \qquad (3.3)$$

$$\text{and } \lim_{r\to\infty}\frac{\partial T_e}{\partial r}=0 \qquad (3.4)$$

In Eq. 3.3, Q is the heat flow rate from the formation to the well per unit length of the well, and r_{wb} is the outer radius of the wellbore.

As production continues, heat transfer from the wellbore causes a gradual rise in the temperature of the surrounding formation, which, in turn, causes a slow decrease in the rate of heat flow. Ameen used the superposition principle to account for changing heat flux using a numerical approach. His solution showed that the assumption of constant heat flux introduced very little inaccuracy.

3.2.2 Solution of Diffusivity Equation

Eq. 5.1 is generally solved in terms of dimensionless variables r_D (dimensionless radial distance=r/r_{wb}) and t_D (dimensionless time=$k_e t/\rho_e c_e r_{wb}^2$). Hasan and Kabir solved the resulting equation with the Laplace transform, following the approach suggested by van Everdingen and Hurst for a similar set of equations used for pressure transients. They presented the expression for formation temperature as a function of radial distance and time. For estimating flowing fluid temperature, the formation temperature and its spatial derivative at the wellbore/formation interface (r_D=1) are needed. We can write the expression for the temperature at the wellbore/formation interface as:

$$T_{wb}=T_{ei}+\frac{Q}{\pi^2 k_e}I \qquad (3.5)$$

$$\text{where } I=\int_0^\infty \frac{1-e^{-u^2 t_D}}{u^2}\,\frac{Y_1(u)J_0(u)-J_1(u)Y_0(u)}{J_1^2(u)+Y_1^2(u)}\,du \qquad (3.6)$$

Analogous to the dimensionless pressure, p_D, used in pressure transient analysis, we define dimensionless temperature, T_D, as:

$$T_D=\frac{2\pi k_e}{Q}\left(T_{wb}-T_{ei}\right) \qquad (3.7)$$

Thus, T_D =-2l/ π. Note that T_D is always positive and that it represents heat flow from the formation towards a well. For the more usual case of fluid production, T_{wb} is greater than T_{ei} causing the computed value of Q to be negative, meaning that the wellbore fluid loses heat to its surroundings.

Computations using Eqs. 3.5 through 3.7 require tedious evaluation of an integral involving modified Bessel functions of zero and first orders over the limits of zero and infinity. Hasan and Kabir found the following algebraic expressions for dimensionless temperature, T_D, in terms of dimensionless time, t_D, to represent the solutions quite accurately,

$$T_D=\left[0.4063+\frac{1}{2}\ln t_D\right]\left[1+\frac{0.6}{t_D}\right] \text{ if } t_D>1.5 \qquad (3.8)$$

$$\text{and } T_D=1.1281\sqrt{t_D}\left(1-0.3\sqrt{t_D}\right) \text{ if } t_D\le 1.5 \qquad (3.9)$$

The above expressions for TD are discontinuous at t_D= 1.5. The continuous expression for T_D may be more suitable in some applications and is written as:

$$T_D=\ln\left[e^{-0.2t_D}+\left(1.5-0.3719e^{-t_D}\right)\sqrt{t_D}\right] \qquad (3.10)$$

At large times, both Eqs. 5.8 and 5.10 reduce to the expression:

$$T_D=0.4063+\frac{1}{2}\ln t_D \qquad (3.11)$$

The log-linear representation of T_D, given by Eq. 3.11, was first used by Ramey and Edwardson et al. and is valid for wells of small diameters. Therefore, the expressions proposed by Hasan and Kabir and Ramey are equivalent at late times, although significant differences may occur at early times.

Eq. 3.7 is a convenient expression that relates heat flow to the temperature-difference driving force, (T_{wb}-T_{ei}), and allows heat-transfer computation with Eqs. 3.8 through 3.11. However, the temperature at the wellbore/formation interface, T_{wb} ' is unknown and must be replaced by the wellbore fluid temperature. This substitution of T_{wb} by T_f is accomplished by using an energy balance for the wellbore fluid.

3.3 Energy Balance for Wellbore Fluid

Temperature difference between the wellbore fluid and the surrounding formation results in energy exchange. An energy balance for the fluid may be performed following any standard text on thermodynamics. Ramey made an energy balance for the fluid by assuming single-phase flow. A general energy balance for either a single or two-phase system is presented here.

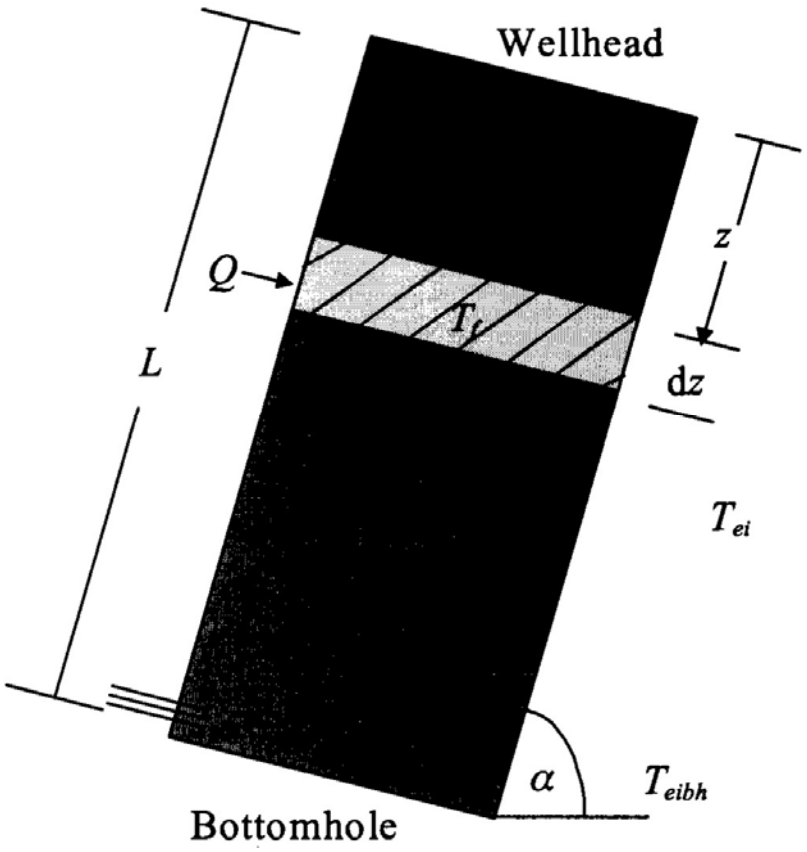

Figure 3.3: Energy balance for wellbore fluid

Fig. 3.3 shows a production system using single tubing, inclined at an angle, to the horizontal. Consider a control volume of length dz at a distance Z from the wellhead in this system, where the distance coordinate, z, is positive in the downward direction. The amount of heat enters the element at (z+dz) by convection, while conduction from the formation adds Q to the element.

Similarly, heat leaves the element at Z by convection. Adding potential and kinetic energies to the heat energy of the fluid, we obtain

$$wH\big|_{z+dz} + \frac{(z+dz)wg\sin\alpha}{Jg_c} + \frac{wv^2\big|_{z+dz}}{2Jg_c} + Qdz = wH\big|_z + \frac{zwg\sin\alpha}{Jg_c} + \frac{wv^2\big|_z}{2Jg_c} \qquad (3.12)$$

During injection, every term except Q in Eq. 3.12 changes sign. We can generalize the energy balance equation for both production and injection systems as:

$$\frac{dH}{dz}+\frac{g\sin\alpha}{Jg_c}+\frac{v}{Jg_c}\frac{dv}{dz}=\mp\frac{Q}{w} \qquad (3.13)$$

where the negative sign on the right side applies to production and the positive sign to injection. In Eq. 3.13, g_c and J. represent appropriate conversion factors. For a fluid undergoing no phase change, that is, when heat effects owing to evaporation/condensation, solution and mixing are negligible; enthalpy is a function of pressure and temperature and is given by:

$$dH=\left(\frac{\partial H}{\partial T_p}\right)dT+\left(\frac{\partial H}{\partial p}\right)_T dp=c_p dT-C_j c_p dp \qquad (3.14)$$

wltere C_j represents the Joule-Thompson coefficient and c_p is the mean heat capacity of the fluid at constant pressure. Note that because of significant evaporation/condensation during steam injection, Eq. 3.14, is inapplicable. Using Eq. 5.14, we can write the expression for the wellbore fluid temperature as a function of depth as:

$$\frac{dT_f}{dz}=C_j\frac{dp}{dz}+\frac{1}{c_p}\left[\mp\frac{Q}{w}-\frac{g\sin\alpha}{Jg_c}\frac{dv}{dz}\right] \qquad (3.15)$$

Combining Eqs. 3.16 and 3.18 and eliminating T_{wb}, one cqn arrive at an expression for T_f. However, to eliminate T_{wb} from the resultant expression, one must use the overall heat transfer coefficient for the wellbore.

3.3.1 Overall-Heat-Transfer Coefficient for Wellbores.

Radial heat transfer occurs between the well bore fluid and the earth, overcoming resistances offered by the tubing wall, tubing insulation, tubing-casing annulus, casing wall, and cement, as shown in Fig. 5.4. These resistances are in series, and except for the annulus, the only energy transport mechanism is conductive heat transfer. At steady state, the rate of heat flow, through a wellbore per unit length of the well, Q, can be expressed as:

$$Q=-2\pi r_{t0}U_{t0}\left(T_f-T_{wb}\right) \qquad (3.16)$$

In Eq. 5.16, U_{to} is defined as the overall-heat-transfer coefficient, based on the tubing outside surface area, 27frro , and the temperature difference between the wellbore fluid and wellbore/formation interface, (Tr Twb)' Thus, the overall-heat transfer coefficient for a given well is a very important parameter. When heat transfer occurs at steady state, heat, flowing through each of the elements (see Fig. 3.4), must be the same. Steady-state heat transfer allows us to derive the expression for the overall-heat-transfer coefficient,'

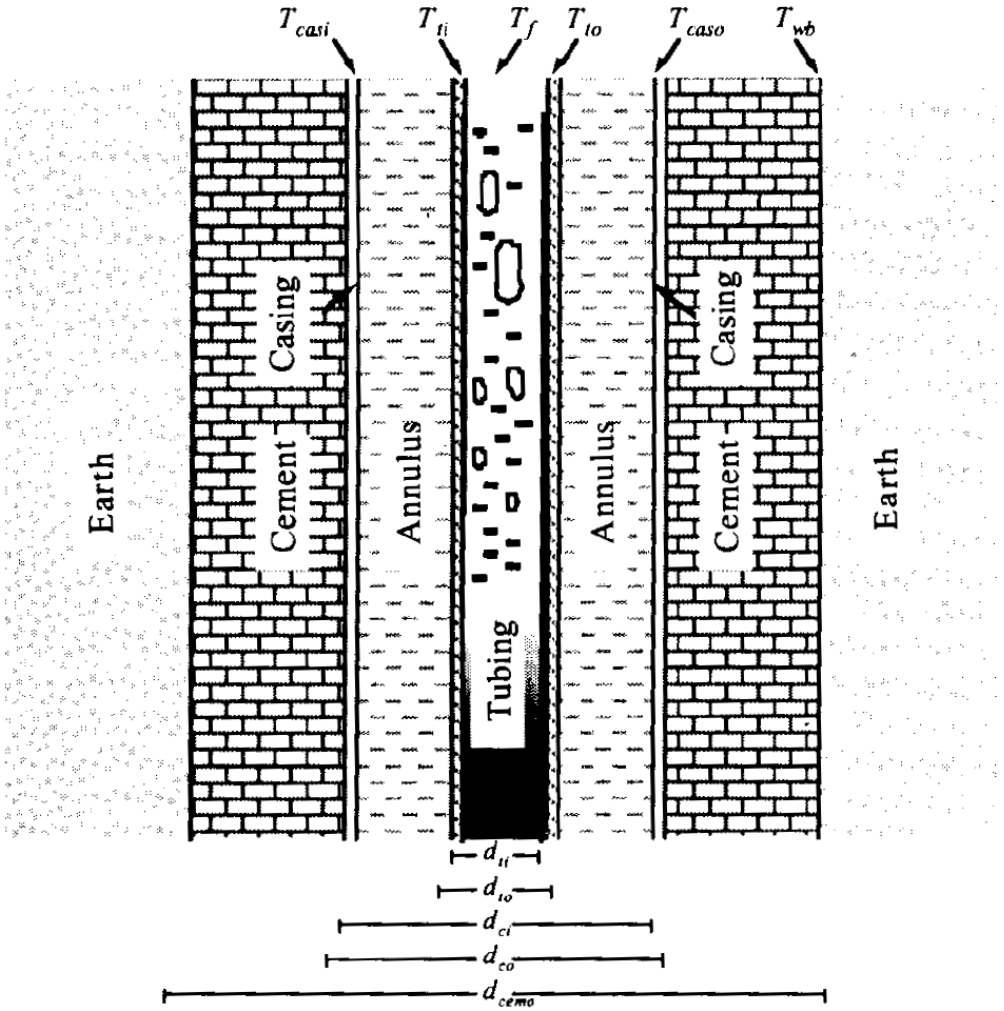

Figure 3.4: Resistance to heat flow in a wellbore

$$\frac{1}{U} = \frac{r_{t0}}{r_{ti} h_{t0}} + \frac{r_{t0} \ln\left(\frac{r_{ins}}{r_{t0}}\right)}{k_{ins}} + \frac{r_{t0}}{r_{ins}(h_c + h_r)} + \frac{r_{t0} \ln\left(\frac{r_{c0}}{r_{ci}}\right)}{k_c} + \frac{r_{t0} \ln\left(\frac{r_{wb}}{r_{co}}\right)}{k_{cem}} \qquad (3.17)$$

Most of the terms in Eq. 5.17 are easily computed. However, the resistance to heat transfer, offered by the annulus, represented by the fourth term in Eq. 3.17, is somewhat difficult to estimate. In case of steam injection or geothermal production, the large temperature difference between the tubing and annular fluids may cause both radiation and natural convection.

3.3.2 Heat Loss to the Formation

We may rewrite the expression for T_D (Eq. 3.7) in heat transfer from the formation to the wellbore/formation interface as:

$$Q \equiv -\frac{2\pi k_e}{T_D}(T_{wb} - T_{ei}) \qquad (3.18)$$

Combining Eqs. 5.16 and 5.18 and eliminating T_{wb} we obtain:

$$Q \equiv -L_R w c_p (T_f - T_{ei}) = -\frac{w c_p}{A}(T_f - T_{ei}) \qquad (3.19)$$

where L_R is the relaxation parameter defined as:

$$L_R = \frac{2\pi}{c_p w}\left[\frac{r_{t0}U_{t0}k_e}{k_e + (r_{t0}U_{t0}T_D)}\right] \quad (3.20)$$

Note that the relaxation parameter, L_R , is inverse of the parameter, A, which is defined by Ramey as:

$$A \equiv \frac{c_p w}{2\pi}\left[\frac{k_e + (r_{t0}U_{t0}T_D)}{r_{t0}U_{t0}k_e}\right] \quad (3.21)$$

3.3.3 Relaxation Parameter, L_R (1/A).

Eq. 3.19 shows that the heat loss (or gain) by the fluid in the wellbore to the formation is directly proportional to (T_f-T_{ei}) and the parameter, L_R. Thus, L_R may be viewed as a type of overall-heat-transfer coefficient for the formation/wellbore system having the units of 1/length, m^-. Note that the expression for L_R, contains thermal properties of both the formation and wellbore. It also includes the dimensionless temperature function, T_D, which varies with time. However, T_D is a weak function of time, especially that at late times. Therefore, constant L_R assumption works well in most practical applications.

The overall-heat-transfer coefficient for the wellbore system may vary with well depth because of the changing well configuration. In addition, as Eq. 3.17 suggests, natural convection in the annulus can contribute significantly to the value of U. Temperature difference, driving natural convection, varies with well depth, causing L_R to be a function of depth. However, variation of L_R with depth is usually small and generally neglected because U_{t0} appears both in the numerator and the denominator of Eq. 3.20. The assumption of constant L_R has important consequences for the solution of the differential equation representing wellbore fluid temperature, which is discussed in Sec. 3.4.

3.3.4 Wellbore Fluid Temperature

We relate fluid temperature to well depth by substituting the expression for heat loss to the formation, Q, (Eq. 3.19) into the energy balance equation (Eq. 3.15).

$$\frac{dT_f}{dz} = \pm(T_f - T_{ei})L_R - \frac{g\sin\alpha}{c_p J g_c} - \frac{v}{c_p J g_c}\frac{dv}{dz} + C_j\frac{dp}{dz} \quad (3.22)$$

where the + sign applies to production, and the - sign applies to injection. We assume that the undisturbed formation temperature, T_{ei}, varies linearly with depth. Therefore, one can write an expression for T_{ei} for a deviated well of length, L, as:

$$T_{ei} = T_{eibh} - (L - z)g_G \sin\alpha \quad (3.23)$$

where g_G represents the geothermal gradient in terms of vertical depth, and T_{eibh} is the static earth temperature at the bottomhole. Note that z is positive in the downward direction. Even when the earth temperature is not linear with depth, it .may be reasonably well represented by a few linear equations. Eq. 3.22 may be written as:

$$\frac{dT_f}{dz} = \pm L_R(T_f - T_{ei}) - \frac{g\sin\alpha}{c_p J g_c} + \phi \quad (3.24)$$

$$\text{where } \phi = -\frac{v}{c_p J g_c}\frac{dv}{dz} + C_j\frac{dp}{dz} \quad (3.25)$$

As expected, Eq. 3.24 shows that the change in fluid temperature with depth depends on the difference in temperature between the wellbore fluid and the surrounding formation. During production when $T_f > T_{ei}$, the fluid temperature decreases as the fluid moves up (Δz negative) the wellbore.

3.3.5 Producing fluid temperature.

Single phase liquid flow

Liquids, being essentially incompressible, allow a number of simplifications to Eq. 3.24 for single-phase oil or water flow. For example, fluid velocity change with depth, (dv/dz), becomes negligible. In addition, because liquid density variation with pressure is usually very small, one can write:

$$dH = dE + d(pV) = cdT + Vdp \tag{3.26}$$

$$\text{and } Cj \equiv \frac{1}{c_p}\left[\frac{\partial H}{\partial p}\right]_T = \frac{V}{c_p} = \frac{1}{\rho c_p} \tag{3.27}$$

Therefore for liquids:

$$\phi \equiv -\frac{v}{c_p J g_c}\frac{dv}{dz} + C_j\frac{dp}{dz} = \frac{1}{c_p \rho}\frac{dp}{dz} \tag{3.28}$$

However, for single-phase liquid flow, the static head loss nearly equals the total pressure gradient. In other words, $dp/dz \cong \rho(g/g_c)\sin\alpha$. Therefore, Eq. 3.24 reduces to:

$$\frac{dT_f}{dz} = L_R\left(T_f - T_{ei}\right) = L_R T_f - T_{eibh} + (L-z)g_G \sin\alpha \tag{3.29}$$

We can also arrive at Eq. 5.34 by noting that, for liquids, the energy balance (Eq. 3.13) may be simplified to: $c_p dT/dz = -Q/w = (T_f - T_{ei})L_R$. If the relaxation length, L_R, is assumed invariant with well depth, Eq. 3.29 becomes a simple first-order linear differential equation, which can be solved with the integrating factor method. The solution is:

$$T_f = T_{ei} + \left(\frac{g_G \sin\alpha}{L_R}\right) + ICe^{(z-l)L_R} \tag{3.30}$$

where IC, representing the integration constant, is evaluated by noting that, at the bottomhole (z=L), the fluid temperature is equal to the formation temperature (T_f=T_{eibh}). Therefore:

$$T_f = T_{ei} + \frac{g_G \sin\alpha\left(1 - e^{(z-L)L_R}\right)}{L_R} = T_{eibh} - g_G \sin\alpha\left[(L-z) - \frac{\left(1 - e^{(z-L)L_R}\right)}{L_R}\right] \tag{3.31}$$

Eq. 3.31 shows that the fluid temperature decreases exponentially from the bottomhole (z=L) to the wellhead. It also shows that while the temperature of the fluid and the formation are the same at the bottomhole, the fluid temperature is higher than the formation temperature at any other location in the well. The difference in temperature between the wellbore fluid and the formation gradually increases as the fluid ascends the well. For deep wells, (z-L)L_R might become a large negative number leading to the expression for the temperature difference between the wellbore fluid and the formation, written as:

$$Tf - Tei = \frac{g_G \sin\alpha}{L_R} \tag{3.32}$$

Eqs. 3.31 and 3.32 show that for very deep wells, the temperature difference (T_f-T_{ei}) might asymptotically approach a constant value. The magnitude of this temperature difference depends on the value of L_R. Thus, if the asymptotic approach holds, temperature logs may be used to estimate the value of L_R. When the thermal properties needed to calculate L_R (Eq. 3.21) are available, one may use temperature logs to calculate flow rates from various producing zones, as was proposed by Curtis and Witterholt. This estimation is possible because L_R is inversely proportional to the mass flow rate. However, various assumptions, inherent in this approach, often render such estimates very approximate.

3.3.6 Fluid Temperature in Injection Wells

Injection wells are common in geothermal operations. The differential equation describing flowing fluid temperature in wellbores, Eq. 3.24 with the negative sign, is valid for injection wells without evaporation/condensation. Eq. 3.24 is integrated for an injection well with the wellhead fluid, T_{fwh} ' and surface earth temperatures, T_e, are used as boundary conditions to yield:

$$T_f = T_{ei} - \frac{1 - e^{(z-L)L_R}}{L_R}\left[g_G \sin\alpha + \frac{\phi \sin\alpha}{c_p J g_c}\right] + e^{-\frac{z}{L_R}}\left(T_{fwh} - T_{es}\right) \qquad (3.33)$$

3.3.7 Variable geothermal gradient

Sometimes, one may encounter geologic formations with different heat-transfer characteristics, leading to a variable geothermal gradient. In such a case, Eq. 5.29 may be integrated by dividing the well into a number of intervals, with constant geothermal gradients being applied to each interval. The fluid temperature calculated at the end of the interval, is used as the entrance fluid temperature for the interval above or beneath it. Therefore, production from a formation with two values of geothermal gradient, g_{G1} and g_{G2} the expression for fluid temperature at the bottom interval is still given by Eq. 3.24, while that for the upper interval is given by:

$$T_f = T_{ei} + \frac{1 - e^{(z-L)L_R}}{L_R}\left[g_{G2} \sin\alpha + \phi - \frac{g \sin\alpha}{c_p J g_c}\right] + e^{(z-L_R)L_R}\left(T_{f1} - T_{ei1}\right) \qquad (3.34)$$

where T_{fl} and T_{eil} represent fluid and earth temperatures at the interface of the two intervals. The procedure, of course, can be extended to an infinite number of intervals.

NOMENCLATURE

Mass transfer

a = parameter defineed by Eq. 1.25, dimensionless
A = cross-sectional area for fluid flow, §12
A_g, A_l = cross-sectional area available for gas or liquid to flow, §12
b = parameter defined by Eq. 1.26, dimensionless
c_e = heat capacity of earth or formation, (J/kgK))
c_p = heat capacity of fluid, (J/kgK)
C_n = parameter defined by Eq. 1.27, dimensionless
d = pipe or well diameter, m.
d_e, d_t = casing or tubing diameter, m.
D = distance between pipe centres m Eq. 1.20, m
E = eccentricity factor, dimensionless
f = friction factor, dimensionless
fa = no-wall friction factor, dimensionless
f_{CA} = friction factor of concentric annulus, dimensionless
f_{ECA} = friction factor of eccentric annulus, dimensionless
m = apparent friction factor, dimensionless
F = force, N
F_p = friction geometry parameter, dimensionless
g = acceleration due to gravity, m/sec
g_e = conversion factor,
g_G = geothermal gradient, °C/m
H = fluid enthalpy, J/kg
k = formation permeability, D

k_e = earth conductivity, W/mK
K = diameter ratio of annulus to tubing, dimensionless
L_R = relaxation distance parameter, m-
p = pressure, Pa
(dp/dz) = pressure gradient, Pa/m
$(dp/dz)_A$ = accelerational (kinetic) pressure gradient, Pa/m
$(dp/dz)_F$ = frictional pressure gradient, Pa/m
$(dp/dz)_H$ = static pressure gradient, Pa/m
q_a = average flow rate over incremental length, m/hr
q_i = influx rate from each perforation m/hr
r_{wb} = wellbore radius, m
r_{to} = outside tubing radius, *ft*
Re = Reynolds number, dimensionless
Re_g,Re_L = Reynolds number for the gas or liquid phase dimensionless
Re_m = Reynolds number for the mixture, dimensionless
Re_w = wall Reynolds number, dimensionless
t = producing, injecting, or circulation) time, hr
t_D = dimensionless time
T_{ei}, T_e= formation temperature at initial condition or at any radial distance, °C
T_D = dimensionless temperature
T_f = fluid temperature, °C
T_{Wb} = wellbore fluid temperature, °C
U = overall heat transfer coefficient, W/mK
v = fluid velocity, m/s
w = mass flow rate of fluid, kg/s
Z = any vertical well depth, m
Z = gas-law deviation factor, dimensionless
α = wellbore inclination with horizontal, deg
Λ= parameter given by Eq. 1.13, dimensionless
μ= *oil viscosity, Ns/m*
ε = *pipe roughness factor, m*
ϕ = *parameter used in Eq. 1.21*
ρ = density, kg/m
η = *parameter used in Eq. 1.21*

Subscripts

c = casing

e = earth or formation

t = tubing

to = tubing outside

wb = wellbore

Heat transfer

A = inverse relaxation distance parameter, m
c_a = heat capacity °C annular fluid, J/(kg K)
c_e = formation heat capacity, J/(kgK)
c_p = heat capacity, J/(kg-°C)
c_{pa}, c_{pt} = heat capacity of annular or tubing fluid, J/(kg K)
c_{pm} = heat capacity of wellbore fluid mixture, J/(kg K)
c_t = total system compressibility, 1/Pa
C_J = Joule-Thomson coefficient, K/Pa
d = pipe or well diameter, m
d_c, d_t = casing or tubing diameter, m
E= internal energy, J/kg
f= friction factor, dimensionless
f_c= film friction factor for the gas core in annular flow, dimensionless
f_g = gas in-situ volume fraction (void fraction), dimensionless
F = force, N
g = acceleration owing to gravity, m/sec2
g_e = conversion factor
g_G = geothermal gradient, °C/m
Gr = Grashof number dimensionless
h = formation thickness, m
h_a, h_t = convective heat-transfer coefficient for annular or tubing fluid, W/(m K)
h_e = convective heat-transfer coefficient, W/(m K)
H = fluid enthalpy, J/kg
I = integral defined by Eq. 5.6, dimensionless
J_0, J_1 = Bessel functions of the first kind of order zero and one, dimensionless
k_a = conductivity of annular fluid, W/(m K)
k_e = conductivity of casing material, W/(m K)
k_{cem} = conductivity °C cement, J/(hr-m-°C)
k = conductivity °C earth or formation, W/(m K)
KU_{sg} = Kutadelaze number, dimensionless
L = total measured well depth, m
L_R = relaxation distance parameter, 11m
m = mass of fluid in a control volume, kg
M = mass of mud per unit well depth, kg/m
N_f = inverse viscosity number, dimensionless
Nu = Nusselt number, dimensionless
P = pressure, Pa
P_D = dimensionless pressure
P_{wf} = flowing bottomhole pressure, Pa
Pr = Prandtl number, dimensionless
q = fluid flow rate at standard conditions, m/s
q_{wh} = wellhead rate, m/s
Q =heat transfer rate per unit length of wellbore, W/(m K)
r_w = wellbore radius, m
r_D = dimensionless radial distance, dimensionless
R = universal gas constant
Re =Reynolds number, dimensionless
Re_m = Reynolds number for the mixture, dimensionless
Re_g, Re_L = Reynolds number for the gas or liquid phase, dimensionless
Rs =solution gas/liquid ratio, Nm/m
t = production or injection time, hr
t_e = effective superposition time, hr
t_D = dimensionless time

Δt = shut-in time, hr
T =temperature, °C
T_a, T_t = temperature °C annulus or tubing fluid, °C
T_{ai} , T_t; = inlet-temperature °C annular or tubing fluid, °C
T_e;, T_e = formation temperature at initial condition or at any radial distance, °C
T_{eibh}, T_{ew} = static formation temperature at the bottomhole or wellhead, °C
T_f = fluid temperature, °C
T_{wb} = temperature at wellbore/formation interface, °C
T_{ws}, T_{wso} = temperature, initial temperature, °C
T_D = dimensionless temperature
U = overall-heat-transfer coefficient, W/(m K)
v = fluid velocity, m/sec
w = mass flow rate of fluid, kg/hr
x = gas mass fraction in tubing fluid mixture, dimensionless
Y_o, Y_1 = Bessel function of the second kind of order zero and one
z = variable well depth from surface, m
α = wellbore inclination with horizontal, degrees
α' = heat diffusivity °C formation, m/s
β = fluid thermal expansion coefficient, 1/°C
μ = viscosity, Ns/m
ρ = density, kg/m
ρ_c, ρ_e = core fluid or earth (formation) density, kg/m3
ρ_g, ρ_L = gas or liquid phase density, kg/m3
σ = surface tension, kg/s

Subscripts

a = annulus

C = casing

cem = cement

ins = insulation

g = gas

L = liquid

t = tubing

ta = tubing to annulus for heat-transfer coefficient

ti = tubing inside

to = tubing outside

w = water

wb = wellbore

4 REFERENCES

Alves, LN., Alhanati, F.J.S., and Shoham, 0., 1992: "A Unified Model for Predicting Flowing Temperature Distribution in Wellbores and Pipelines," *SPEPE* (November 1992) 363.

Ameen, M.M., 1992: *Unified Model for Two-Phase Flow and Heat Transfer in Wellbores,* MS thesis, U. of North Dakota, Grand Forkes, North Dakota

Antics, M., 1995: Modelling Two Phase Flow in Low Temperature Geothermal Wells, Proceedings of WGC1995, Florence, Italy

Asheim, H., Kolnes, J., and Oudeman, P., 1992: "A Flow Resistance Correlation for Completed Wellbore," *J. Pet. Eng. Sci. (1992)* 8,97.

Bilicki Z, Kestin J, Michalides E E (1981). Flow in geothermal wells Part m. Calculation model for a self flowing well. Brown University Div of Eng Report Geoflo/5.

Bird, J.M., 1954: "Interpretation of Temperature Logs in Water-and Gas-Injection Wells and Gas-Producing Wells," *Drill. & Prod. Prac.* 187.

Bird, R.B., Stewart, W.E., and Lightfoot, E.N., 1973: *Transport Phenomena,* John Wiley and Sons, New York City.

Caetano, E.E, Shoham, 0., and Brill, I.P., 1992: "Upward Vertical Two-Phase Flow Through an Annulus, Part I: Single-Phase Friction Factor, Taylor Bubble Rise Velocity and Flow Pattern Prediction," *J. Energy Res. Tech.* (March 1992) **114,** 1.

Carslaw, H.S. and Jaeger, J.c., 1959: *Conduction of Heat in Solids,* Oxford U. Press, London

Chen, N.H., 1979: "An Explicit Equation for Friction Factor in Pipe," *lnd. Eng. Chem., Fundamentals* 18, No, 3, 296.

Cullender, M.H. and Smith, R.v., 1956: "Practical Solution of Gas Flow Equations for Wells and Pipelines With Large Temperature Gradients," *Trans.,* AIME 207.

Curtis, M.R. and Witterholt, EJ., 1973: "Use of the Temperature Log for Determining Flow Rates in Producing Wells," paper SPE 4637 presented at the 1973 SPE Annual Fall Meeting, Las Vegas, Nevada, 1-3 October.

Dikken, BJ., 1990: "Pressure Drop in Horizontal Wells and Its Effect on Production Performance," *JPT(November* 1990) 1426.

Dropkin, D. and Sommerscales, E., 1965: "Heat Transfer by Natural Convection in Liquids Confined by Two Parallel Plates Inclined at Various Angels with respect to the Horizontal," 1. *Heat Transfer, Trans.* ASME, Series C (February 1965) 87, 77.

Edwardson, MJ. *et al,* 1962.*:* "Calculation of Formation Temperature Disturbances Caused by Mud Circulation," *1PT* (April 1962) *416; Trans.,* AIME, 225.

Fishenden, M. and Saunders, O.A., 1950: *An Introduction to Heat Transfer,* first edition, Oxford U. Press, London 103.

Gebhart, B, 1971.: *Heat Transfer,* second edition, McGraw-Hill Book Co. Inc., New York City 272.

Geothermal Institute, 1992: Geothermal Production Technology, Lecture notes, 86.103, 65-73.

Gunn, *D.I.* and Darling, C.w.w., 1963: "Fluid Flow and Energy Losses in Non Circular Conduits," *Trans. Inst. Chem. Eng.* 41, 163.

Hagedorn A R, Brown K E, 1965: Experimental study of pressure gradients occurring during continuous two phase flow in small diameter vertical conduits. J Pet Tech April pp. 475-484.

Hasan, A. R., Kabir, C.S., 2002: Fluid flow and Heat Transfer in Wellbores, *SPE 2002*

Hasan, A.R. and Kabir, C.S., 1994: "Aspects of Heat Transfer During Two-phase Flow in Wellbores," *SPEPF* (August) 211.

Lesem, LB. *et al.*, 1957*:* "A Method of Calculating the Distribution of Temperature in Flowing Gas Wells," *Trans.,* AIME 210, 169.

Mishima K, Ishii M 1984: Flow Regime Transition criteria for upward two phase flow in vertical tubes. Int J Heat Mass Transfer

Moody, L.E, 1944: "Friction Factors for Pipe Flow," *Trans.,* ASME 66, No. 8,671.

Novy, R.A., 1995: "Pressure Drops in Horizontal Wells: When Can They be Ignored?," *SPERE* (February 1995) 29.

Orkiszewski J, 1967: Predicting two phase pressure drops in vertical pipes. J Pet Tech June 829-838 Trans AIME 240

Ortiz-Romirez, 1983: Two Phase Flow in geothermal wells: Development and uses of a computer code. Stanford Geothermal program Report SGP-TR-66 June.

Ouyang, L-B., Arbabi, S., and Aziz, K., 1998: "A Single-Phase Wellbore Flow Model for Horizontal, Vertical, and Slanted Wells," *SPEJ* (June 1998) 124.

Ramey, H.J., Jr., 1962: "Wellbore Heat Transmission," *1PT* (April 1962) 427; *Trans.,* AIME, 225.

Romero, J. and Touboul, E., 1998: "Temperature Prediction for Deepwater Wells: A Field Validated Methodology," paper SPE 49056 presented at the 1998 SPE Annual Technical Conference and Exhibition, New Orleans, 27-30 September.

Sagar, R.K., Dotty, D.R., and Schmidt, Z., 1991: "Predicting Temperature Profiles in a Flowing Well," *SPEPE* (November 1991) 441.

Satter, A., 1965: "Heat Losses of Steam Down a Wellbore," *JPT* (July 1965) 845.

Schlumberger, M., Doll, H.G, and Perebinossoff, AA, 1937: "Temperature Measurements in Oil Wells," *Inst. Pet. Technologists* (January 1937) 23, 159.

Shiu, K.c. and Beggs, H.D., 1980: "Predicting Temperatures in Flowing Oil Wells," 1. *Energy Resources Tech.* (March 1980) 1.

van Everdingen, A.F. and Hurst, w., 1949: "The Application of the Laplace Transformation to Flow Problems in Reservoirs," *Trans.,* AIME (1949) 186,305.

Willhite, GP., 1967: "Overall Heat Transfer Coefficients in Steam and Hot Water Injection Wells," *1PT* (May 1967) 607.

Yuan, H.J., Sarica, c., and Brill, J.P., 1999: "Effect of Perforation Density on Single-Phase Liquid Flow Behavior in Horizontal Wells," *SPEPF* (August 1999) 203.

GEOTHERMAL DEEP WELL DRILLING PRACTICES

- AN INTRODUCTION

Hagen Hole
Geothermal Consultants NZ Ltd., Birkenhead, Auckland, New Zealand.

ABSTRACT

An introduction to Geothermal Deep Well Drilling. The formation and reservoir conditions that characterise geothermal systems (typically higher enthalpy) require the adoption of drilling practices that differ from those utilised in conventional oil, gas, and water well drilling operations. Temperature, Geology, and Geochemistry are the principal areas of difference. This paper outlines typical geothermal drilling conditions, and the drilling practices that have been developed to optimise the drilling processes in these conditions.

Keywords: geothermal, drilling,

INTRODUCTION

Although heat from geothermal sources has been used by mankind from the earliest days – for cooking and bathing, for instance - it's major development has taken place during the past 30 years. This has occurred in parallel with the significant advances made in deep drilling practices, and it's importance has risen dramatically during the last few years as the price of petroleum has soared, and awareness of the importance of 'renewable energy' has developed.

The equipment and techniques used in the drilling of geothermal wells have many similarities with those used in exploring and exploiting petroleum reservoirs. However, the elevated temperatures encountered; the often highly fractured, faulted, and permeable volcanic and sedimentary rocks which must be drilled; and the geothermal fluids which may contain varying concentrations of dissolved solids and gases have required the introduction of specialised drilling practices and techniques.

Temperature

The temperature of the earth's crust increases gradually with depth with a thermal gradient that usually ranges from 5° to 70° per kilometre. In anomalous regions, the local heat flux and geothermal gradients may be significantly higher than these average figures. Such anomalous zones are typically associated with edges of the continental plates where weakness in the earth's crust allow magma to approach the surface, and are associated with geologically recent volcanism and earthquakes. It is in such settings that the majority of geothermal resources are found and that the majority of geothermal wells have been drilled.

While a few wells have been drilled into temperature conditions that approach the critical point of water (374°C) and a number of fields produce dry and superheated steam, the majority of higher enthalpy resources are two phase – either vapour or water dominated, with temperature and pressure conditions controlled by the saturated steam / water relationship – 'boiling point for depth'.

For design purposes, where downhole pressures and temperatures are not known, 'boiling point for depth' (BPD) conditions are assumed from ground level as indicated in Figure 1.0.

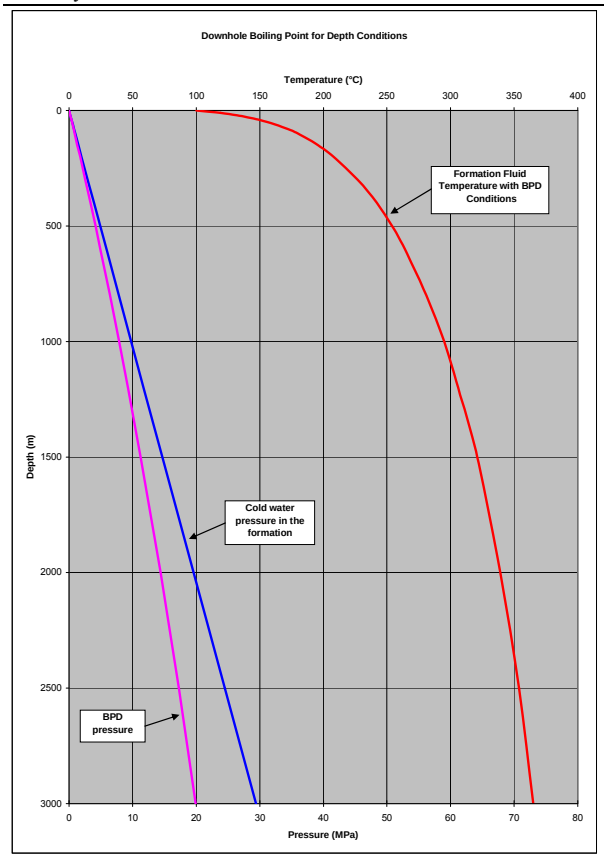

Figure 1.0 – Downhole fluid conditions - BPD.

Saturated steam has a maximum enthalpy at 235°C and consequently many geothermal fields are found to exist at temperatures approximating this value (dissolved solids and gases change this value somewhat).

Such elevated formation temperatures reduce drill bit and drilling jar performance and often precludes the use of mud motors and directional MWD instrumentation equipment; it adversely effects drilling fluid and cementing slurry properties; and reduces the performance of blow out prevention equipment. In addition it significantly increases the potential for reservoir fluid flashing to steam resulting in flowback or blowout from shallow depths.

The well, the downhole well components and the near well formations are subject to large temperature changes both during the drilling process and at the completion of drilling. The circulation or injection of large volumes of drilling fluid cools the well and the near well formation, but as soon as fluid circulation is ceased, rapid re-heating occurs. These large temperature differentials require special precautions to be taken:-

- to avoid entrapment of liquids between casing strings – which can exert extreme pressure when heated resulting in collapsed casing.
- to ensure casing grade and weight, and connection type is adequate for the extreme compressive forces caused by thermal expansion.
- to ensure the casings are completely cemented such that thermal stress are uniformly distributed.
- to ensure casing cement slurry is designed to allow for adequate setting times and to prevent thermal degradation.

Geology

Geothermal fields occur in a wide variety of geological environments and rock types. The hot water geothermal fields about the Pacific basin are predominantly rhyolitic or andesitic volcanism, whereas the widespread hydrothermal activity in Iceland occurs in extensively fractured and predominantly basaltic rocks. In contrast the Larderello steam fields in Italy are in a region of metamorphic rocks, and the Geysers steamfield in California is largely in fractured greywacke.

The one common denominator of all of these fields is the highly permeable, fractured and faulted nature of the formations in which the reservoirs reside. This high permeability being one of the fundamental and requisite components for any geothermal system to exist.

Typically, the permeable nature of the formations is not limited to the geothermal reservoir structure alone, but occurs in much of the shallower and overlying material as well.

In addition, a characteristic of most of these geothermal systems is that the static reservoir fluid pressures are less than those exerted by a column of cold water from the surface – the systems are "under-pressured". The high temperatures of the systems result in reservoir fluid densities which are less than that of cold water, and the majority of geothermal systems are located in mountainous and elevated situations – resulting in static water levels often hundreds of metres below the surface.

Drilling into and through these permeable and "under-pressured" zones is characterised by frequent and most often total loss of drilling fluid circulation.

Particularly in the volcanic geothermal systems, many of the shallow formations comprise low bulk density materials such as ashes, tuffs and

breccias, which as well as being permeable, are often unconsolidated and friable, and exhibit a low fracture gradient, and thus provide low resistance to blowouts.

Geochemistry

Geothermal fluids contain varying concentrations of dissolved solids and gases. The dissolved solids and gases often provide highly acidic and corrosive fluids and may induce scaling during well operations. Dissolved gases are normally dominated by CO_2 but can also contain significant quantities of H_2S, both of which can provide a high risk to personnel and induce failure in drilling tools, casings and wellhead equipment.

The presence of these dissolved solids and gases in the formation and reservoir fluids imposes specific design constraints on casing materials, wellhead equipment and casing cement slurry designs.

Drilling Practices:

In general, the drilling processes and equipment utilised to drill deep geothermal wells are substantially similar to those developed for petroleum and water well rotary drilling. However, the downhole conditions experienced in geothermal systems, as described above, require some significantly different practices to be adopted. Some of these differences are outlined below.

Well design

The thermal efficiency of converting geothermal steam/water to electricity is not particularly high (±20%), therefore large mass flows and therefore volume flowrates are required, particularly in vapour dominated systems. These large volume flowrate requirements necessitate large diameter production casings and liners.

Typically a 'standard' sized well will utilize standard API 9 5/8" diameter casing as production casing and either 7" or 7 5/8" diameter slotted liner in an 8½" diameter open hole section.

A "Large" diameter well will typically utilise standard API $13^3/_8$" diameter casing as the production casing, with either $9^5/_8$" or 10¾" diameter slotted liner in a 12¼" diameter open hole.

Casing sizes utilised for the Anchor, Intermediate, Surface and Conductor casings will be determined by geological and thermal conditions.

Figure 2 illustrates schematically the casing strings and liner of a typical geothermal well.

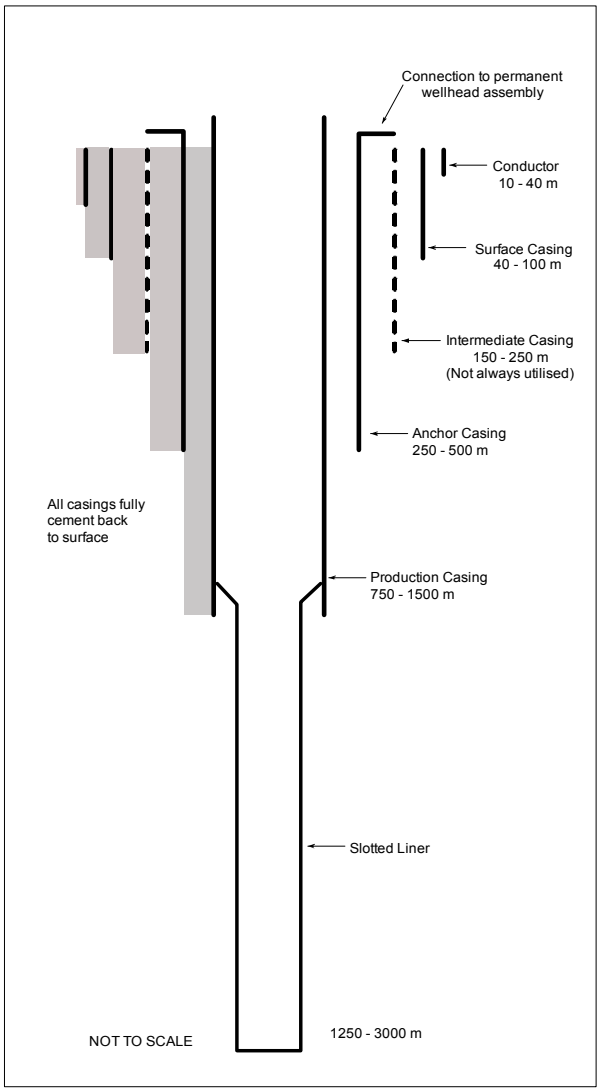

Figure 2. Casing strings and liner for typical well.

Casing Depths

The depths of all cemented casing strings and liners is determined such that the casings can safely contain all well conditions resulting from surface operations and from the characteristics of the formations and fluids encountered as drilling proceeds.

Casing shoe depths are determined by analysis of data from adjacent wells which will include rock characteristics, temperatures, fluid types and compositions and pressures. In particular fracture gradient data gathered from nearby wells. At any time the depth of open hole below a particular

casing shoe should be limited to avoid exposure of the formations immediately below the casing to pressures which could exceed the fracture gradient at that depth and hence lead to a blowout. It is usual to assume worst case scenario's such as exposing the previous casing shoe to the saturation steam pressure at the total drilled depth of that section. Figure 3 illustrates how the shoe depths may be chosen using a somewhat simplistic and theoretical model with boiling point for depth fluid pressure condition from a nominal water level at 200 m depth; and a uniform formation fracture gradient from the surface to the total depth of 2400 m.

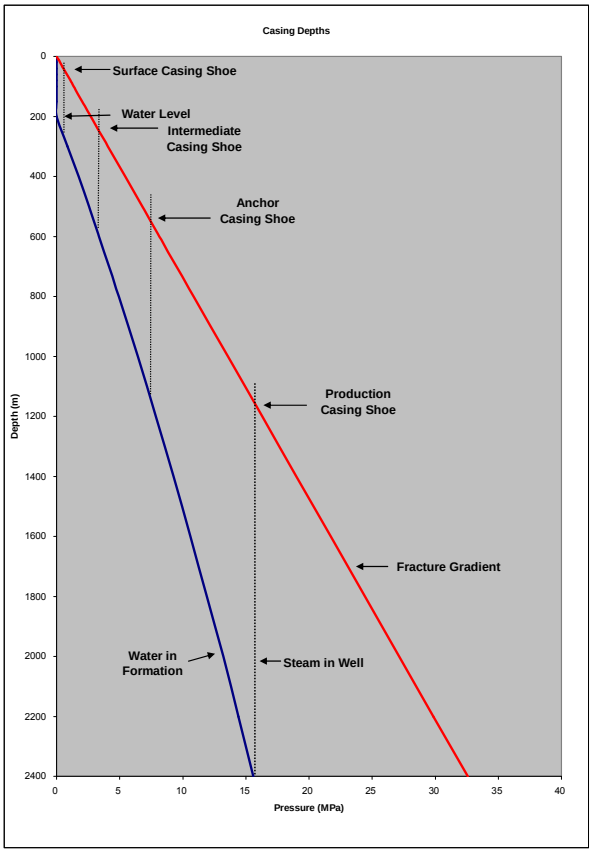

Figure 3. Casing Shoe Depths

This simplistic model suggests that the production casing shoe would need to be set no shallower than 1100m; the anchor casing shoe at approximately 550 m; an intermediate casing set at 250 m depth; and a surface casing set at around 40 m depth.
It is likely that with real data that this casing programme would be somewhat simplified, the production and other casings shoes somewhat shallower, and the intermediate casing eliminated.

Casing Diameters

Casing diameters will be dictated by the desired open hole production diameter – typically either 8½" or 12¼". Slotted or perforated liners run into these open hole sections should be the largest diameter that will allow clear running – there is an obvious advantage to utilise 'extreme line' casing connections from a diameter point of view, however this is often offset by reduced connection strength of this type of casing connection.

Casing internal diameters should not be less than 50 mm larger than the outside diameter of connection collars and accessories, to allow satisfactory cementing.

A typical well design would include:-

- Conductor:– 30" set at a depth of 24 metres, either driven or drilled and set with a piling augur.
- Surface Casing:- 20" casing set in 26" diameter hole drilled to 80 metres depth.
- Anchor Casing:- 13 3/8"casing set in a 17½" hole drilled to 270 metres depth.
- Production Casing:- 9 5/8" casing set in a 12¼" hole drilled to 800 metres depth.
- Open Hole – 7" perforated liner set in 8½" hole drilled to 2400 m –Total Depth.

Casing materials

Steel casing selected from the petroleum industry standard API Spec. 5CT or 5L.
In general the lowest tensile strength steel grades are utilised to minimise the possibilities of failure by hydrogen embrittlement or by sulphide stress corrosion. The preferred API steels are: Spec 5CT Grades H-40, J-55 and K-55, C-75 and L-80; Spec 5L grades A, B and X42.
In cases where special conditions are encountered, such as severely corrosive fluids, use of other specialised materials may be warranted.

Casing Connections

The compressive stress imposed on a casing strings undergoing heating after well completion is extreme. As an example, an 800 metre length of casing undergoing heating from the cement setup temperature of around 60°C to the final formation temperature of 210°C (a change of 150°C), would freely expand 1.44 m. If uniformly constrained over the full length, the compressive strength induced would be 360 MPa; the minimum yield strength of Grade K-55 casing steel is 379 MPa. As this illustrates, axial strength is critical and it is therefore important that the casing connection exhibits a compressive (and tensile) strength at least equivalent to that of the casing body.

It is usual that a square section thread form is chosen, and this is typically the API Buttress threaded connection.

Cementation of Casings

Unlike oil and gas wells, all of the casings down to the reservoir are usually run back to the surface, and are fully cemented back to the surface. The high thermal stresses imposed on the casings demand uniform cementation over the full casing length, such that the stress is distributed over the length of the casing as uniformly as is possible and such that stress concentration is avoided.

The objective of any casing cementing programme is to ensure that the total length of annulus (both casing to open hole annulus, and casing to casing annulus) is completely filled with sound cement that can withstand long term exposure to geothermal fluids and temperatures.

Of course, as suggested above, the permeable and under-pressured nature of the formations into which these casings are being cemented means that circulating a high density cement slurry with S.G.'s ranging from 1.7 to 1.9, inevitably result in loss of circulation during the cementing procedure.

The traditional method of mitigating this problem was to attempt to seal all permeability with cement plugs as drilling proceeded, however, this is usually an extremely time consuming process, and more often than not, circulation is still lost during the casing cementing process.

Many approaches to overcome this problem have been tried, and include:-

- Low density cement slurry additives – pozzalan, perlite, spherical hollow silicate balls
- Sodium silicate based sealing preflush
- Foamed cement
- Stage cementing
- Tie back casing strings – the casing is run and cemented in two separate operations.

Many of these options were tried but generally none have proven totally successful nor economic.

To date, in the experience of the author, the most successful procedure has been to utilise the most simple high density cement slurry blend, and to concentrate on the techniques of placing the cement such that a full return to the surface without fluid inclusions can be achieved. This nearly always involves a primary cement job carried out through the casing, and in the event of a poor or no return and immediate annulus flushing procedure, which is then followed by an initial backfill cement job through the casing to casing annulus, with sometimes repeated top-up cement jobs. Particular care must be taken to avoid entrapment of any water within the casing to casing annulus.

Perforated and Slotted Liner

Unlike the cemented casings discussed above, it is usual to run a liner within the production section of the well. This liner is usually perforated or slotted, typically, with the perforation or slots making up around 6% of the pipe surface area. As it is extremely difficult to determine exactly where the permeable zones within the production section lie, it is usual that the entire liner is made up of perforated pipe.

The liner is not cemented, but either hung from within the previous cemented production casing, or simply sat upon the bottom of the hole with the top of the liner some 20 to 40 metres inside the cemented production casing shoe, leaving the top of the liner free to move with expansion and contraction.

Drilling Rig and Associated Equipment

The drilling rig and associated equipment are typically the same as is utilised for oil and gas well drilling, however a few special provision are required.

- Because of the large diameter holes and casings utilised in the surface and intermediate (if used) casing strings, it is important that the rotary table is as large as practicable – typically a 27½" diameter rotary table is utilised, and even 37½" is sometimes seen.
- Again, due to the large hole diameters drilled in the upper sections, large diameter Blow Out Preventers (BOP's) are required, however only moderate pressure rated units are necessary – a typical set of BOP stacks would include:-

  - 30" (or 29½") 500/1000 psi annular diverter and associated large diameter hydraulically controlled diversion valve.

  - 21¼" 2000 psi BOP stack including blind and pipe ram BOP's and an annular BOP.

  - $13^{5}/_{8}$" 3000 psi BOP stack including blind and pipe ram BOP's and an annular BOP.

(comparatively – oil and gas rigs would usually have 5000 psi and 10000 psi rated BOP's)

For aerated drilling 21¼" and $13^5/_8$" rotating heads and a $13^5/_8$" 'Banjo box' is required.

- The use of a 'choke manifold' is not mandatory in geothermal operations, usually an inner and outer choke valve is sufficient.
- As the BOP stacks are relatively large and occupy a significant height above the ground level (in particular if aerated drilling is to be used) it is necessary that rigs are equipped with an 'extra' height sub structure – a clear height of at least 6 metres is necessary.
- All of the elastomeric parts of the BOP's must be high temperature rated.
- It is preferable, although not mandatory, that rigs are fitted with top drive units – allowing for drilling with a double or triple stand of drill pipe; for easy connection and circulation while tripping the drill string in or out of the hole; and for back reaming.
- Rig mud pumps – (usually tri-plex) must be capable of pumping 2000 to 3000 lpm on a continuous basis. Pressure rating is not as important as pumped volume, pumps must be fitted with large diameter liners (usually 7" diameter).
- Rig mud pumps must be piped to the rig such that fluid can be pumped to both the rig standpipe and to the kill line (annulus) at the same time. It is important that the pump sizes or quantity of pumps is such that sufficient fluid can be pumped for drilling purposes, while a secondary volume – say 1000 lpm can be simultaneously pumped to the kill line.
- The drilling fluid circulating system requires a fluid cooling unit – often a forced draft direct contact cooling tower, or chilling unit.
- Drilling water supply must be capable of providing a continuous supply of at least 2000 lpm and preferable 3000 lpm - backup pumps and often dual pipelines are utilised.
- Drillpipe should be lower tensile strength material to avoid hydrogen embrittlement and sulphide stress corrosion – usually API Grade E or G105. Drillpipe is now usually supplied with a plastic internal lining, it is important that this lining has a high temperature rating.
- A high temperature rated float valve, (non return valve), is always fitted immediately above the drill bit in the drill string to prevent backflow into the drill string which often results in blocking of the drill bit jets.
- Drill bits – usually tri-cone drill bits are utilised however the elastomeric parts of the bearing seals and the lubrication chamber pressure compensation diaphragm are particularly heat sensitive. It is important that while tripping the drill string into the hole, that the bit is periodically cooled by circulating through the drill string.
- PDC – polycrystalline diamond compact drill bits are now being used more often - initially they were found to be totally unsuitable for hard fractured rock drilling – improvements in materials are now making this type of bit a real option. With no moving parts, bearings and seals they are essentially impervious to temperature.
- Drilling tools – the high downhole temperatures limit use of mud motors and MWD instrumentation tools to the upper cooler sections of the hole.

Drilling Fluids

The upper sections of a well are usually drilled with simple water based bentonite mud treated with caustic soda to maintain pH. As drilling proceeds and temperatures increase, the viscosity of the mud is controlled with the addition of simple dispersants. If permeability is encountered above the production casing shoe depth, attempts will be made to seal these losses with 'Loss of Circulation Materials' (LCM), and cement plugs. If the losses cannot be controlled easily, then the drilling fluid is switched to either water 'blind' – that is drilling with water with no circulation back to the surface, or to aerated water.

Once the production casing shoe has been run and cemented, and drilling into the production part of the well commences, mud is no longer use as drilling fluid as it has the potential to irreparably damage the permeability and thus the production potential of the well.

Once permeability is encountered in the production section of a geothermal well, drilling was traditionally continued with water, 'blind' – with no return of the drilling fluid to the surface. The drill cuttings are washed into the formation, and periodic 'sweeps' with either mud or polymer assists in keeping the hole cleared of cuttings.

While this method alleviates the impractical and uneconomic loss of large volumes of mud, and the associated mud damage to the formation, the build up of cuttings within the hole often results in stuck drill strings, and the washing of cuttings into the formation causes damage to the permeability, although not on the same scale as bentonite mud.

Aerated water is now more commonly utilised for drilling this section of the well. To enable circulation of drilling fluids to be continued despite the presence of permeability and 'under pressured' reservoir conditions, the density of the drilling fluid must be reduced. The addition air to the circulating water allows a 'balanced' downhole pressure condition to be established, and the return and circulation of the drilling water and cuttings back to the surface.

Well Control

Perhaps one of the most crucial differences between geothermal and oil and gas drilling operations is the nature of the formation fluids and how they can be controlled.

A geothermal well has the potential of being filled with a column of water at boiling point – even the slightest reduction in pressure on that column can cause part of, or the entire column to boil and flash to steam. This process can occur almost instantaneously. The potential for 'steam kick' is always there and requires special drilling crew training and attention.

Whilst the likelihood of a well kicking at any time is real, the method of controlling such a kick is simple and effective. Steam is condensable, so by simply shutting in the BOP's and pumping cold water into the well – both down the drilling and down the annulus, the well can be quickly controlled. The pressures involved are not high, as they are controlled by the steam / water saturation conditions.

During such a 'steam kick' it is normal that some volume of non-condensable gas (predominantly CO_2) will be evolved. After the steam fraction has been quenched and cooled, it is usual that this usually small volume of non-condensable gas be bled from the well through the choke line. Some H_2S gas may be present, usually in small quantities, so precautions are required.

Running the Open-Hole Liner

One of the final tasks in completing the drilling of a geothermal well is the running and landing of the perforated or slotted liner. At this stage the drilling operations have been completed and hopefully permeability and a productive resource has been encountered. This operation is potentially critical as while a string of perforated or slotted liner (casing) is through the BOP stack, the functionality of the BOP stack is disabled. It is critical that a significant volume of quenching water is pumped to the well prior to and throughout the entire process.

In the event that a kick occurs in this condition, there are only two options available. A capped blank joint of pipe must be readily available so that it may be screwed in and run into the BOP stack so the well may be closed and then quenched. The alternative is that the liner is released and dropped through the BOP stack allowing it to then be closed and the well then quenched. Neither option a very satisfactory situation – it is crucial that a full understanding of the behaviour of the reservoir and the necessary quench volumes that are required to maintain the well in a fully controlled state.

The reliability of the water supply system for this process is of paramount importance.

Conclusion

The processes of drilling geothermal wells is very similar to those developed by the oil and gas and water well drilling industries, however the nature of a geothermal reservoir system; the temperature; the geology and the geochemistry require that some quite different practices be followed if the drilling process and the resulting well are to be successful.

References

Hole, H.M., 1996. "Seminar on geothermal Drilling Engineering – March 1996, Jakarta, Indonesia", Seminar Text, Geothermal Energy New Zealand Limited, Auckland, New Zealand.

Gabolde, G., Nguyen, J.P, 1999. "Drilling Data Handbook – Seventh Edition". Institut Francais du Pétrole Publications.

NZS 2403:1991, "Code of Practice for Deep Geothermal Wells" Standards Association of New Zealand.

GEOTHERMAL WELL DESIGN – CASING AND WELLHEAD

Hagen Hole
Geothermal Consultants NZ Ltd., Birkenhead, Auckland, New Zealand.

ABSTRACT

The Geothermal well design process includes consideration of the objectives and purpose of the well, the subsurface conditions likely to be encountered during the drilling process, and the identification of required equipment, materials, and drilling procedures needed to ensure a satisfactory well completion and an acceptable well life.

The design steps which are necessary to drill and complete a deep geothermal well safely are:

- Subsurface rock and fluid conditions.
- Depths of casings and well completion.
- Casing specification and cementing materials and programmes
- Wellhead specification
- Drilling fluids, drill string assemblies
- The necessary drilling tools and equipment.

Perhaps the most critical aspects of these design steps is the selection of casings, casing specification, casing shoe depths, and how the well is completed. This paper reviews the casing and wellhead specification process.

Keywords: geothermal, well design, casing design and specification.

INTRODUCTION

The choice of casing depths and specification of the materials weights and connections is vital to the success and safety of the well drilling process and to the integrity and life of the well.
The casing design and specification process includes reviewing the required services of the casings, determination of the setting depths and checking possible failure modes.

Casing Services

What is the purpose of the casing?
The reasons for including casing strings and liners include:-

- Prevention of loose formation material from collapsing into and blocking the hole.
- Provision of anchorage or support for drilling and the final wellhead.
- Containment of well fluids and pressures.
- Prevention of ingress or loss of fluid into or from the well, and "communication" or leakage of fluids between different aquifers.
- To counter losses of drilling fluid circulation during drilling.
- Protection of the well and formation against erosion, corrosion, fracturing and breakdown.

In general, the shallower and outer casing strings are necessary for the drilling operations, while the inner strings are required for production purposes. The drilling process follows a sequence of drilling to a certain depth, running and cementing a casing string, establishing a wellhead (drilling or final), which allows the drilling of the next smaller diameter section to proceed. As a minimum two, but usually more, completely cemented, concentrically located, steel casing strings are obligatory both from a technical and legal sense for a geothermal well.

Casing strings and liner for a typical geothermal is illustrated below in Figure 1.

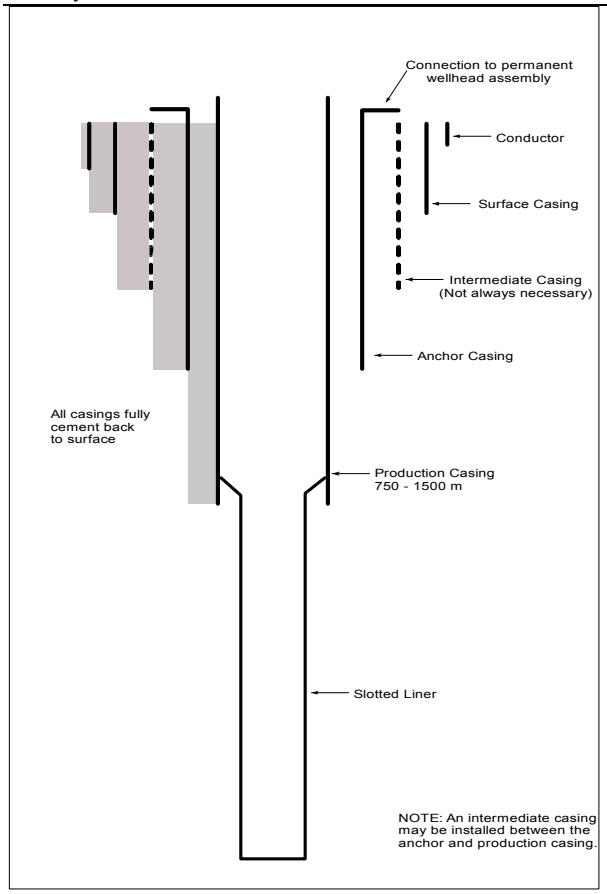

Figure 1. Casing strings and Liner for Typical Geothermal Well.

Casing Setting Depths

The casing setting depths for a typical geothermal well will be chosen from the following information and expectation related to the following aspects:

- Surface or Conductor Casings Strings –
  These are the largest casings which are set at a shallow depth and are employed to prevent loose near-surface material collapsing into the hole. They are also utilised to support the initial drilling wellhead, and to contain the circulating drilling fluid. The setting depth of the casing shoe will be estimated from geological deduction, but may be altered to reflect conditions found during the course of drilling, and may have to contain hot fluid under pressure if there is a thermal zone close to the surface.

- Anchor or Intermediate Casing Strings –
  These casings are intermediate in diameter and in setting depth which are set to support successive wellheads (usually including the permanent wellhead) and to contain drilling and formation fluids of relatively high temperature and pressure. Setting depths will be chosen from expected formation rock and fluid conditions to provide adequate permanent anchorage and additional security against drilling problems including blowouts.

- Production Casing –
  This casing is smaller in diameter and set at greater depth than previous casings, and is used primarily to convey steam and water to the surface, but it is also important in facilitating drilling to total depth and to prevent unwanted leakage of fluids into or out of different aquifers. The depth of this string should be chosen first, on the basis of the expected depths and temperatures of fluids to be included and excluded from production.

In the situation of appraisal or production drilling, the experience of earlier drilling and well testing in the area is the most useful guide in selecting casing depths. However, when drilling a first well in a new area, reasonable assumptions must be made as to the possible rock and fluid conditions to be expected down to the total drilled depth. These will be deduced from consideration of surface scientific surveys possibly supplemented by the results of drilling a shallow investigation hole at the site. In the absence of a clear understanding from the scientific data, it is frequently assumed that the reservoir fluid can be approximated to a column of water at boiling temperature throughout its depth – 'Boiling Point for depth (BPD). If the ground water level is known, the depth should be taken from below that datum.

In a hot water or two phase field with boiling conditions as assumed above, it is possible (although unlikely) at any stage of the drilling for the well to be filled with a column of steam at a temperature and saturation pressure corresponding closely to formation conditions at hole bottom, or at the level of greatest permeability. As this pressure is more than that of the formation fluid, there is a tendency for steam to escape into upper permeable formations, and in weak geological conditions blow out at the surface. Upper casing depths should beset to seal off possible leakage paths to the surface and to limit the well fluid pressure at the shoe to that imposed by the overburden pressure, or by the fracture gradient of the materials if this is known.

The competence of the rock and the incidence of drilling circulation fluid losses are likely to govern casings depths, and thus the number of casing strings needed to allow the target depth to be reached most economically.

This 'competence of the rock' can only be derived from experience as suggested above, but usually falls somewhere between a theoretically derived fracture gradient and a theoretical overburden pressure.

Figure 2 below illustrates a theoretically based casing shoe depth selection procedure.

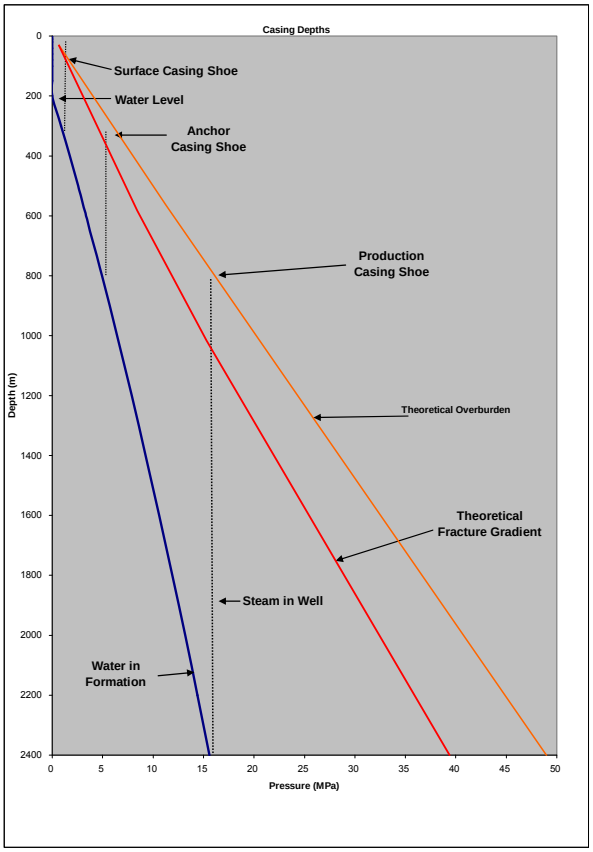

Figure 2. Example of Theoretical Casing Depth Selection.

This theoretical situation would require the production casing shoe being set at a depth of 800 m depth; the anchor casing shoe being set at 300 m depth; and the surface casing shoe being set at around 60 m depth.

Casing Diameters

The diameters of the various strings of casing in any well are chosen after consideration of the following aspects:-

- Sufficient cross-sectional area to convey the expected / desired flow of fluid;
- Sufficient annular clearances to run and cement concentric casing strings;
- The use of casing sizes which are standard manufactured products which are readily available and match the handling tools usually held by drilling contractors.

Due to the manner in which different pipe thicknesses are manufactured, tubular sizes are identified by their outside diameters and in accordance with the API specifications.

Service Conditions and Failure Modes

Whereas deep petroleum drilling considers the most important parameters in casing design to be fluid pressure, casing weight, and tensile loading, in geothermal service generally the most severe service occurs as a result of high temperature loadings. The problem is compounded by facts that the service temperatures can seldom be predicted at all accurately; and that the various types of casing steel grades and casing connections are manufactured specifically for petroleum service rather than geothermal service.

The effects of elevated geothermal temperatures on well components include:-

- Change in length of unrestrained pipe – for example, 1.8 m expansion over a length of 1000 m with a temperature change of 150°C.
- Alternatively a compressive stress due to restrained (cemented) pipe – for the same temperature rise of 150°C the compressive stress will be 360 MPa (52,000 psi).
- Reduction in steel strength – 5% or more in casing tensile strength tests at 300°C, and 17% in wellhead equipment pressure ratings at 300°C under ANSI Standards.
- Destruction of material competence – particularly flexible seals.

While loading in a longitudinal direction induces secondary stressing in the circumference of a pipe, it is convenient to separate the primary modes of failure into axial and radial.

AXIAL STRESS CONDITIONS

Axial stressing occurs due to:-

- Casing self weight
- Temperature effects – expansion and contraction

- Restraint from the surrounding cement and/or and connection at the wellhead or downhole (such as a hanger).

The design checks for axial stress can be separated into two sets of conditions – before and after the casing is cemented.

Axial Loading before and during cementing

Until the annular cement sets around the casing the tensile force at any depth includes the weight of the casing in air less the buoyant effect of any fluid in the well.

Thus: $F_p = [L_z W_p – (L_z-L_w)A_p/n]g$

Where:

F_p = the tensile force at the surface from casing weight
L_z = depth of casing
W_p = unit weight of casing
L_w = depth of water level in well
A_p = cross sectional area of pipe
n = mean specific volume of hot fluid
g = acceleration due to gravity

The design tensile force shall allow for the dynamic loads imposed during the running of the casing, which will include the drag force of the casing against the side of the well, particularly in a deviated well. This dynamic loading must be limited by specifying the maximum hook load which may be applied.

In a deviated hole the maximum bending stress induced is:-

$F_b = EqD$

Where:

F_b = maximum stress due to bending
E = modulus of elasticity
q = curvature of deviated hole (° per 30 m)
D = pipe outside diameter

This stress is additional to that caused by casing weight, temperature change etc.

Where axial loadings before cementing can occur simultaneously they shall be added together and the resultant maximum axial load checked against the minimum tensile strength of the casing.
The design factor applied to this is 1.8.

Axial Loading After Cementing

The thermal stress built up can be calculated by imagining that the pipe expands (using the coefficient of thermal expansion and the estimated temperature difference), and is then forced back to its original length by axial compression (using the modulus of elasticity).

For the compressive stress quoted above:-

Unit extension = strain = coefficient x temp. change

$= (12 \times 10^{-6}) \times 150$
$= 1.8 \times 10^{-3}$

Stress = modulus x strain = $(200 \times 10^3) \times 1.8 \times 10^{-3}$

= 360 MPa

The total axial stress in a cemented string varies continuously with depth and also with the difference in temperature at any time between the neutral value (when the casing was fixed in position) and that at any time subsequently. It should also be noted that if the formation into which casing has been cemented moves differentially by faulting or subsidence, then this too induces further stresses. An additional complication is that when steel is loaded at high temperatures over a long period of time, stress relaxation will occur.

The compressive force due to temperature rise when the casing is constrained both longitudinally and laterally by cement is:-

$F_c = C_t (T_2 – T_1)A_p$

$Ct = Ea$ = 200 x 12 x10-6 = 2.4 MPa/°C

Where:

F_c = compressive force due to heating
C_t = thermal stress constant for casing steel
T_1 = neutral temperature (temp. at time cement set)
T_2 = maximum expected temperature
A_p = cross sectional area of pipe.
E = modulus of elasticity
a = coefficient of linear thermal expansion

The tensile loading as calculated for the pre-cementing axial loading remains in the casing after cement setup (ignoring stress relaxation with time), therefore the resultant axial force (F_r) on the casing after cement setup and heating will be:-

$$F_r = F_c - F_p$$

The design factor to be utilised will be

$$\frac{\text{minimum compressive strength}}{\text{resultant compressive force}}$$

where the minimum strength refers to the lesser of the pipe body or the connection. The design factor shall not be less than 1.2.

Many of the casing failures that occur are the result of rapid cooling of the well. After the well has been completed and has heated and perhaps has been in production for some time and if the well is re-entered for subsequent drilling activities; undergoes a series of pumping tests; or is used for reinjection, the temperature reduction when cool fluid is pumped from the surface into the well causes contraction of the steel with a resultant tensile force. This tensile force can exceed the original resultant axial force.
Casing failures can occur if the well is not cooled in accordance with a strict well quenching and cooling programme. A slow and gradual cooling process allows the stress to be uniformly distributed over the full length of casing is essential.

Tensile axial loading of the top section of casing, which anchors the wellhead against the lifting force applied by the fluid in the well is:-

$$F_w = (\pi/4) P_w d^2$$

where
F_w = lifting force due to wellhead pressure
P_w – maximum wellhead pressure
d = pipe inside diameter

The design factor for all axial tensile and compressive loading shall not be less than 1.2

Axial Loading with Buckling and Bending

The setting of un-cemented liners through the production section of a well presents a number of design problems. Liners are either hung in tension using a liner hanger from just above the production casing shoe, or more preferably sat on the bottom of the hole with the top of the liner sitting free inside the production casing shoe – in this case the liner is in compression.
The perforated liner in the production section of the well is not cemented and is therefore not radially supported or constrained. Liners in this situation is subject to axial self weight compression and helical buckling and therefore must be analysed for extreme fibre compressive stress.

$$f_c = L_z W_p g [(1/A_p) + (D e/2l_p)]$$

where:
f_c = total extreme fibre compressive stress due to axial and bending forces.
L_z = length of liner
W_p = nominal unit weight of casing
g = acceleration due to gravity
A_p = cross sectional area of pipe
D = pipe outside diameter
e= eccentricity (actual hole diameter minus D)
L_p = net moment of inertia of the pipe section, allowing for slotting or perforating.

While the hole is drilled with a drill bit of known diameter, the actual hole diameter is usually some greater – due reaming caused by stabiliser, hole erosion and in some formations washouts. An uncemented liner string supported at the hole bottom and subject to compressive self weight stressing, will bend helically, within the limits set by the hole wall. The ratio of the hole diameter to the pipe diameter (eccentricity), will determine the amount of bending and therefore the bending stresses.
The buckling analysis is sensitive to the eccentricity term. It is therefore necessary to analyses for a range of actual hole diameters from the bit diameter up to around 1.5 times the bit diameter, depending formation integrity.

The design factor is –

$$\frac{\text{minimum yield stress x } R_j}{\text{total compressive stress}}$$

where (R_j) – the connection joint efficiency does not exceed 1.0.

where (R_j) – the connection joint efficiency does exceed 1.0., the design factor is –

$$\frac{\text{minimum yield stress}}{\text{total compressive stress}}$$

and shall be not less than 1.2.

The ability of the casing string to resist the above loadings is governed by the steel grade (which prescribes its strength), the type of connections,

and the loading condition at the neutral temperature state. As high strength steels are susceptible to stress corrosion cracking in a geothermal (H_2S) environment, API Grade K-55 and L-80 grade steels are typically utilised.
The "round" (Vee) threaded couplings typically used in oil and gas wells, tend to jump threads under high compressive loads. Geothermal service requires a square thread form and/or shouldered connections to transfer the full axial loading of the pipe body. API buttress threads and various proprietary square threaded connections have been found to be suitable.

radial stress conditions

Radial (Hoop or circumferential) loadings are applied primarily by internal and/or external fluid pressures. The ability of tubulars to resist the resultant differential pressures are listed in the API Standards.
In particular consideration must be given to;-

- The differential pressures that occur before and during cementing operations
- Well fluid pressures in the static condition or when producing or reinjecting.

Internal Yield – Bursting

The casing design must ensure that adequate safety margins exist against internal yield or 'burst, resulting from high internal fluid pressure due to a range of situations that occur during and after the cementing of the casing.
The maximum differential burst pressures usually occur near the casing shoe or stage cementing collar ports and will apply when-

- The casing is filled with high density cement slurry
- The annulus is either completely filled with water back to the surface or partially filled with water as controlled by formation pressure.
- A restriction within the casing, such as a blocked float valve or a cementing plug which will hold the differential pressure.

This scenario is not a likely situation, but it is possible, and therefore must be taken as a worst case scenario.
The differential burst pressure in this case is:-

The hydrostatic pressure inside the casing at the casing shoe caused by the cement slurry plus any applied pumping pressure – minus the hydrostatic pressure in the annulus at the casing shoe caused by the head of water in the annulus.

$$P_i = [(L_f\ G_f + P_p) – (L_z\ G_z)]g$$

Where:

P_i = maximum differential internal pressure
L_f = height above casing shoe of cement column inside casing
G_f = cement slurry density (eg 1.87 kg/l)
P_p = applied pumping pressure
L_z = height above casing shoe of water column in annulus
G_z = mean density of water in annulus

The design factor is:-

$$\frac{\text{casing internal yield pressure}}{\text{differential burst pressure}}$$

and the design factor shall be not less than 1.5.

Once the cement has been successfully displaced to the annulus and the well completed, the maximum differential burst pressure will occur at the wellhead and will be as a result of the wellhead pressure.
The design factor will be:-

$$\frac{\text{casing internal yield pressure}}{\text{maximum wellhead pressure}}$$

and the design factor shall be not less than 1.8.

Typically the maximum wellhead pressure occurs when the well is left shut in and a cold gas cap develops within the casing depressing that static water level to the casing shoe.
In this case the casing internal yield pressure must be limited by the sulphide stress corrosion limit.

If the casing being considered is the Anchor casing, to which the wellhead is connected, biaxial stressing will apply – the combination of the radial burst stresses and the tensile stress caused by the lifting force of the wellhead pressure against the wellhead.
The combined effects of axial and radial tension is calculated by the expression:-

$$f_t = \sqrt{3/2}\ (P_w\ d)/(D-d)$$

Where:

f_t = maximum tensile stress
Pw = maximum wellhead pressure

D = casing outside diameter
d = casing inside diameter

The top section of the anchor casing – from surface to around 25 m depth, also requires design compliance with the ASME Boiler and Pressure Vessel Code

Collapse

The casing design shall ensure an adequate margin of safety against pipe collapse due to external pressure from entrapped liquid expansion, applied pressure during pumping, and/or static pressure from a dense liquid column such as cement slurry.

Typically, the maximum differential external pressure occurs at the completion of displacement of high density cement slurry from inside the casing to the annulus. At this time the annulus is totally filled with high density cement slurry, and the inside is filled with water.

The hydrostatic pressure outside the casing at the casing shoe caused by the cement slurry plus any applied pumping pressure (such as a cement squeeze pressure) – minus the hydrostatic pressure inside the casing at the casing shoe caused by the head of water in the casing.

$$p_z = [\ (L_z\ G_z + P_p) - (L_f\ G_f)\ ]g$$

Where:

P_z = maximum differential external pressure
L_f = height above casing shoe of water column inside casing
G_f = mean density of water column inside casing.
L_z = height above casing shoe of cement slurry column in annulus
G_z = density of cement slurry in annulus (eg 1.87 kg/l)
P_p = applied pumping pressure

The design factor is:-

$$\frac{\text{casing external collapse pressure}}{\text{net external pressure}}$$

and the design factor shall be not less than 1.2.

It is to be noted that the large diameter, relatively thin walled surface and intermediate casings are particularly susceptible to this mode of failure.

For example:- the standard $18^5/_8$" diameter 87.5 lb/ft, Grade K-55 casing has a collapse pressure rating of only 4.3 MPa. If the design factor of 1.2 is applied, the maximum allowable differential collapse pressure is 3.58 MPa.
This implies that the deepest this casing can be set and cemented with a standard SG 1.87 cement slurry totally displaced to the annulus is 420 m depth.

Thermal Expansion of Trapped Fluid

As the bulk modulus of thermal expansion of water is not constant, particularly at low temperatures and pressures, the effect of heating water in a wholly confined space is best calculated by reference to the steam table, using a constant specific volume. However, at temperatures above 100°C, the resultant pressure rise due to change in temperature approximates to 1.6 MPa/°C.

The rated collapse pressure of $9^5/_8$" 47 lb/ft Grade L-80 casing is 32.8 MPa. In the event that a volume of water was trapped between an outer casing and this $9^5/_8$" casing, the collapse pressure of the $9^5/_8$" casing would be reached with a temperature rise of less than 20.5°C, although a large volume of trapped water would be required to deform the pipe to failure.
As indicated previously, a temperature rise from a nominal neutral temperature of say 80°C to a formation temperature of 240°C is typical, and therefore the maximum pressure possible from the thermal expansion of a trapped volume of liquid between casings far exceeds the strengths of normal casings strings in either burst or collapse. Because it is important to retain the integrity of the production casing string, it is desirable that any failure should be designed to occur in the outer string. Therefore, for the final pair of cemented casings, the collapse resistance of the inner string should exceed the burst resistance of the outer string with a design factor of not less than 1.2, being the ratio of:-

$$\frac{\text{production casing collapse strength}}{\text{outer casing burst strength}}$$

The added resistance to 'burst' provided by the cement sheath is to a degree countered by the secondary stressing effects of the thermal axial

compression, which tends to reduce the resistance to burst and increase the resistance to collapse.
For the purposes of design calculations and in the interests of conservative design, this support provided by the cement sheath is ignored.

wellheads

The permanent wellhead components include:

- Casing Head Flange (CHF) usually, and preferably, attached to the top of the Anchor casing – but in some instances is attached directly to the top of the production casing. The casing head flange may incorporate side outlets to which side valve are attached.
- Double flanged Expansion / Adaptor spool. Side outlets may be incorporated in the expansion spool (as an alternative to those on the CHF).
- Master Valve

A typical wellhead assembly for a 'Standard' well completed with an 8½" diameter production hole section, $9^{5}/_{8}$" production casing and $13^{3}/_{8}$" anchor casing is illustrated schematically in Figure 3 below.

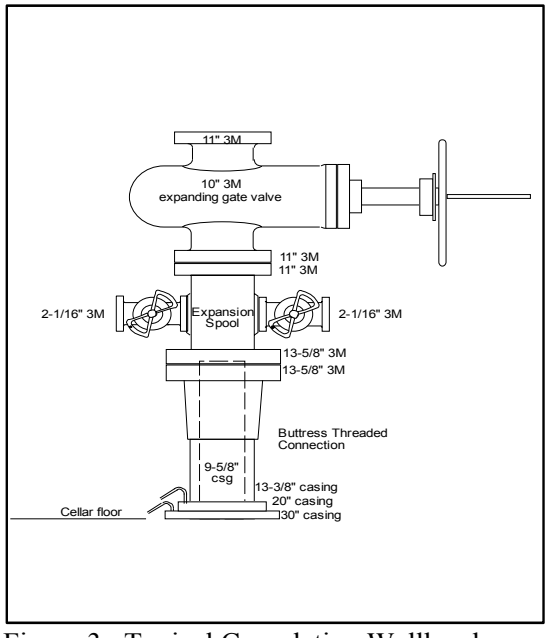

Figure 3. Typical Completion Wellhead.

In spite of the best efforts made in cementing the casing strings, there is usually some residual relative axial thermal expansion between casings at the surface. If the wellhead is mounted on the anchor casing (which is typical), the production casing movements relative to the anchor casing is accommodated below the master valve, within a double flanged spool such that interference with the base of the master valve is prevented.
The wellhead should be designed to comply with codes of practice for pressure vessels or boilers, and in accordance with API Spec. 6A – and most importantly, rated for the maximum pressure / temperature exposure possible at the surface under static or flowing conditions. The fluid at the wellhead may be water, saturated steam, superheated steam, cold gas, or mixtures of some of these fluids. Due to the column of fluid in the well, surface conditions cannot equate to downhole values, but in some circumstances can approach downhole conditions closely.

The pressure ratings are derated as temperature increases in accordance with ANSI B16.5 and API 6A.
The derated pressures are plotted against temperature in Figure 3.

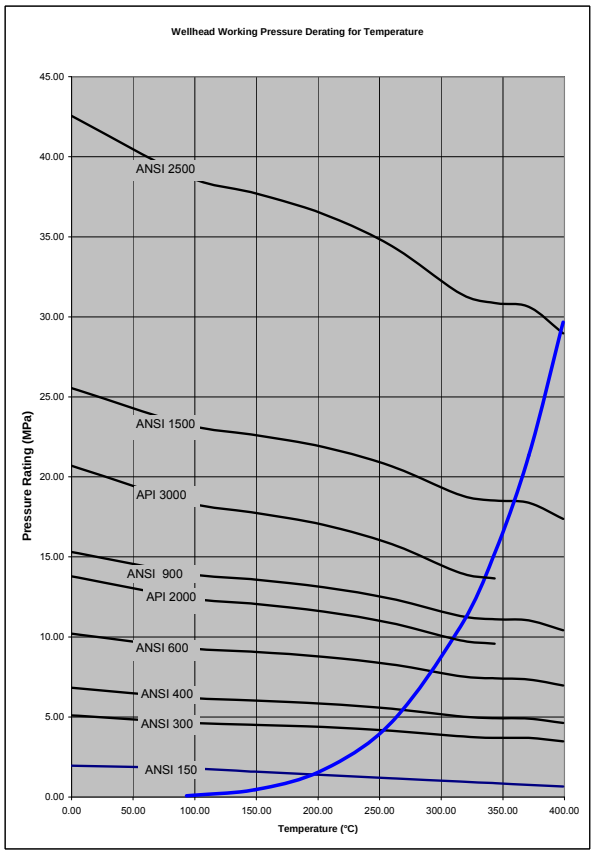

Figure 4. Wellhead Working Pressure Derated for Temperature.

References

Hole, H.M., 1996. "Seminar on Geothermal Drilling Engineering – March 1996, Jakarta, Indonesia", Seminar Text, Geothermal Energy New Zealand Limited, Auckland, New Zealand.

Gabolde, G., Nguyen, J.P, 1999. "Drilling Data Handbook – Seventh Edition". Institut Francais du Pétrole Publications.

NZS 2403:1991, "Code of Practice for Deep Geothermal Wells" Standards Association of New Zealand.

DIRECTIONAL DRILLING OF GEOTHERMAL WELLS

Hagen Hole
Geothermal Consultants NZ Ltd., Birkenhead, Auckland, New Zealand.

ABSTRACT

Directional drilling of geothermal wells has recently become more prevalent and popular. There are some significant advantages, including increased potential for encountering permeability and therefore production; greater flexibility in selecting well pad locations relative to the well target; and it introduces the possibility of drilling a number of wells from a single well pad.
The directional drilling technology available today from the oil industry provide an array of highly sophisticated equipment, instrumentation and techniques. However, the geothermal environment is generally too aggressive to allow the use of much of it.
The most successful directional wells are those with the most simple programme.
Directional drilling provides an option to drill a number of wells from one pad providing significant cost savings. The wellhead layout on a multi-well pad is predominantly dictated by the dimensions of the drilling rig.

Keywords: geothermal, drilling, directional drilling, multi-well drilling pad.

INTRODUCTION

"Directional Drilling" is the term given drilling of a well which is deviated from the vertical to a predetermined inclination and in a specified direction. This compares with the use of "deviated" which refers to a well that is drilled off-vertical in order to sidetrack or go around an obstacle in the well.
Directional wells may be drilled for the following reasons:

- Where the reservoir is covered by mountainous terrain, directional wells can access the resource from well sites located on the easier, foothill terrain.

- Where multi-well sites are constructed and a number of directional wells are drilled to access a large area of the resource from the single site.

- Where productivity is derived from vertical or near vertical fracturing, a directional well is more likely to intersect the fracture zone at the desired depth than is a vertical well.

- Where access to a critical section in another well is required – usually from which a blowout has occurred (i.e. relief well).

Where directional wells are drilled from a multi-well site, there are the following advantages:-

- Total site construction costs are reduced.
- Road construction costs are reduced.
- Water supply costs are reduced.
- Waste disposal ponds for drilling effluent can serve a number of wells.
- The cost of shifting the drilling rig and the time taken are both significantly reduced.
- When the wells are completed, the steam gathering pipe work costs are reduced.

The Directional Drilling Process

Having established the drilling target and the casing setting depths, the three dimensional geometric shape of the well needs to be determined. Typically this will be either a ‘J’ or an ‘S’ shaped well profile.

The more simple ‘J’ well shape is normally comprised of an initial vertical section to the ‘kick-off’ point (KOP); followed by a curve of constant radius determined by the "rate of build" to the end of build (EOB), following by a straight section hole at a constant angle from the vertical: (final drift angle), as is depicted in Figure 1.

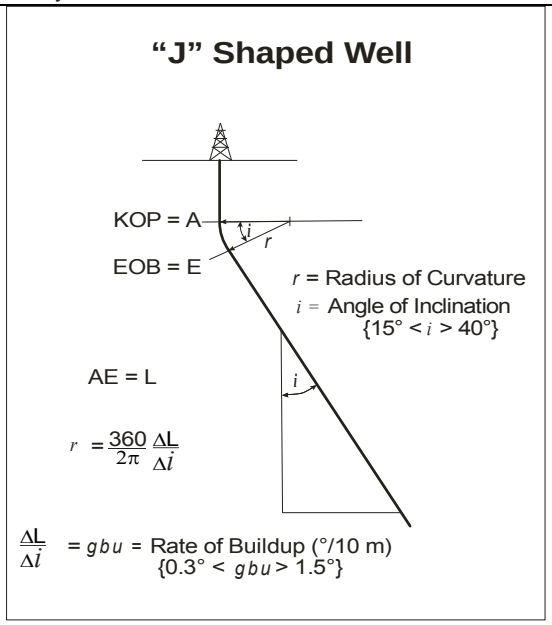

Figure 1. 'J' Shape Well

The 'S' well shape is normally comprised of an initial vertical section to the KOP; followed by a 'build section' with a curve of constant radius; following by a straight section hole at a constant angle from the vertical: (at the maximum drift angle); the drill bit is then allowed to fall (from the start of fall point (SOF) at a constant 'rate of fall' to the final drift angle, at the end of fall point (EOF); followed by a straight of hole with the drift angle being maintained at the final angle of inclination. Figure 2. depicts a typical 'S shaped' well.

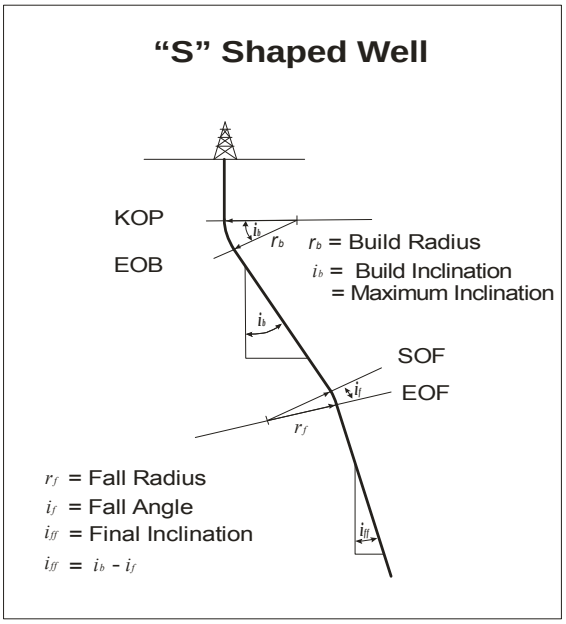

Figure 2. 'S' Shaped Well.

A planning well track profile, may be formulated utilising a relatively simplistic, top-down radius of curvature calculation sheet. Typically these calculation sheets are not target seeking – more sophisticated target seeking programs are utilised by Directional Drilling service companies.

Table 1. details a classic example of a simple "J" shaped well profile generated for Well MK-11 at the Mokai Geothermal Field, New Zealand.
The 13 3/8" anchor casing is set in a vertical hole at a depth of 258 m, and a 12¼" hole drilled vertically to 370 m. At this depth a mud motor is run in and the well 'kicked-off' with a rate of build of 2° per 30 m, with an azimuth of 110°. At a depth of 580 m MD (578 m VD), the mud motor assembly is pulled from the hole and a rotary build assembly run in. Drilling of the 12¼" hole continues to a measured depth of 765 m (751 m VD) where the maximum and final inclination of 26° is reached The 9 5/8" production casing is run in and set with the shoe at 760 m MD.
An 8½" "locked-up" rotary drilling assembly is run in and the well drilled to the final measured depth of 2400 m (2221 m VD).
The resulting target point has a lateral displacement (throw) of 806 m from the wellhead, in a direction of 110° (10° south of due East), with a final measure depth of 2400 m and a final vertical depth of 2221 m. The theoretical maximum dogleg being 2°per 30 m. The vertical section and plan of this well is depicted in Figures 3. and 4.

DIRECTIONAL SURVEY ANALYSIS

Radius of curvature method E&O E 30.00

FIELD **Mokai**
WELL No. **MK-11**
24-Nov-03
Units in METERS
Magnetic deviation -22.56 E
Azimuth True, Grid or Magnetic GRID

MEAS DEPTH (m)	DRIFT (°)	AZIM GRID (°)	VERT DEPTH (m)	COORD NORTH NZMG (m)	COORD EAST NZMG (m)	POLAR DIST (m.)	POLAR BEARING (°)	DOGLEG deg/30m
0								
0	0.00	110.00	0	6293151.07	2765363.94			
30	0.00	110.00	30	6293151.07	2765363.94	0.00	110.00	0.00
60	0.00	110.00	60	6293151.07	2765363.94	0.00	110.00	0.00
84.6	**0.00**	**110.00**	**85**	6293151.07	2765363.94	0.00	110.00	0.00
85.5	**0.00**	**110.00**	**86**	6293151.07	2765363.94	0.00	110.00	0.00
130	0.00	110.00	130	6293151.07	2765363.94	0.00	110.00	0.00
135	0.00	110.00	135	6293151.07	2765363.94	0.00	110.00	0.00
200	0.00	110.00	200	6293151.07	2765363.94	0.00	110.00	0.00
250	0.00	110.00	250	6293151.07	2765363.94	0.00	110.00	0.00
258	**0.00**	**110.00**	**258**	6293151.07	2765363.94	0.00	110.00	0.00
263	**0.00**	**110.00**	**263**	6293151.07	2765363.94	0.00	110.00	0.00
270	0.00	110.00	270	6293151.07	2765363.94	0.00	110.00	0.00
280	0.00	110.00	280	6293151.07	2765363.94	0.00	110.00	0.00
290	0.00	110.00	290	6293151.07	2765363.94	0.00	110.00	0.00
320	0.00	110.00	320	6293151.07	2765363.94	0.00	110.00	0.00
350	0.00	110.00	350	6293151.07	2765363.94	0.00	110.00	0.00
370	0.00	110.00	370	6293151.07	2765363.94	0.00	110.00	0.00
400	2.00	110.00	400	6293150.89	2765364.43	0.52	110.00	2.00
430	4.00	110.00	430	6293150.35	2765365.91	2.09	110.00	2.00
460	6.00	110.00	460	6293149.46	2765368.37	4.71	110.00	2.00
490	8.00	110.00	490	6293148.21	2765371.80	8.36	110.00	2.00
520	10.00	110.00	519	6293146.60	2765376.21	13.06	110.00	2.00
550	12.00	110.00	549	6293144.65	2765381.59	18.78	110.00	2.00
580	14.00	110.00	578	6293142.34	2765387.93	25.53	110.00	2.00
610	16.00	110.00	607	6293139.68	2765395.23	33.29	110.00	2.00
640	18.00	110.00	636	6293136.68	2765403.47	42.06	110.00	2.00
670	20.00	110.00	664	6293133.34	2765412.65	51.83	110.00	2.00
700	22.00	110.00	692	6293129.67	2765422.75	62.58	110.00	2.00
730	24.00	110.00	720	6293125.66	2765433.76	74.30	110.00	2.00
740	**24.67**	**110.00**	**729**	6293124.25	2765437.64	78.42	110.00	2.00
760	**26.00**	**110.00**	**747**	6293121.32	2765445.68	86.98	110.00	2.00
765	**26.00**	**110.00**	**751**	6293120.57	2765447.74	89.17	110.00	0.00
790	26.00	110.00	774	6293116.82	2765458.04	100.13	110.00	0.00
800	26.00	110.00	783	6293115.32	2765462.16	104.52	110.00	0.00
830	26.00	110.00	810	6293110.83	2765474.51	117.67	110.00	0.00
860	26.00	110.00	837	6293106.33	2765486.87	130.82	110.00	0.00
890	26.00	110.00	864	6293101.83	2765499.23	143.97	110.00	0.00
950	26.00	110.00	918	6293092.83	2765523.95	170.27	110.00	0.00
1000	26.00	110.00	962	6293085.34	2765544.54	192.19	110.00	0.00
1100	26.00	110.00	1052	6293070.34	2765585.74	236.03	110.00	0.00
1200	26.00	110.00	1142	6293055.35	2765626.93	279.86	110.00	0.00
1300	26.00	110.00	1232	6293040.36	2765668.12	323.70	110.00	0.00
1400	26.00	110.00	1322	6293025.36	2765709.32	367.54	110.00	0.00
1500	26.00	110.00	1412	6293010.37	2765750.51	411.37	110.00	0.00
1600	26.00	110.00	1502	6292995.38	2765791.70	455.21	110.00	0.00
1700	26.00	110.00	1592	6292980.39	2765832.90	499.05	110.00	0.00
1800	26.00	110.00	1681	6292965.39	2765874.09	542.89	110.00	0.00
1900	26.00	110.00	1771	6292950.40	2765915.28	586.72	110.00	0.00
2000	26.00	110.00	1861	6292935.41	2765956.48	630.56	110.00	0.00
2100	26.00	110.00	1951	6292920.41	2765997.67	674.40	110.00	0.00
2200	26.00	110.00	2041	6292905.42	2766038.86	718.23	110.00	0.00
2300	26.00	110.00	2131	6292890.43	2766080.06	762.07	110.00	0.00
2400	**26.00**	**110.00**	**2221**	6292875.43	2766121.25	805.91	110.00	0.00

Table 1. Mokai Well MK-11 Directional Drilling Profile

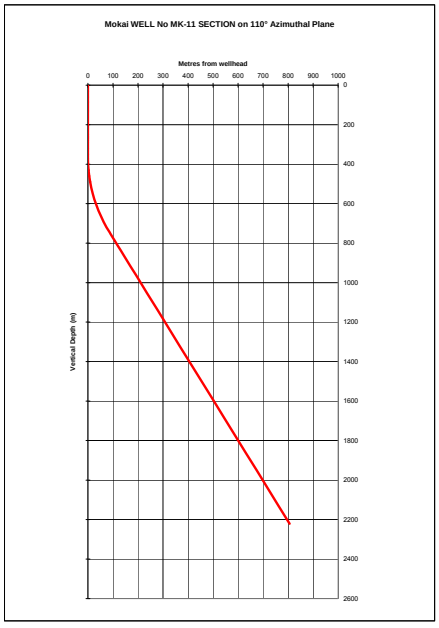

Figure 3. Well MK-11 Vertical Section

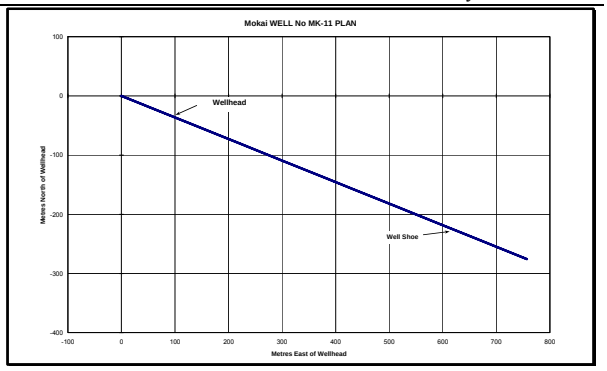

Figure 4. Well MK-11 Plan.

Table 2. details a more complex example of the "J" shaped well profile generated for Well MK-14 at the Mokai Geothermal Field. This well profile has a simple build in inclination, but adds a turn to the right just prior to the point where the maximum and final inclination is reached.

The 13 3/8" anchor casing is set in a vertical hole at a depth of 290 m. A 12¼" hole is then drilled vertically to 370 m, and the well kicked-off with a mud motor with a gentle rate of build of in inclination of 1.5° per 30 m and with the direction held constant at 30°.

At a depth of 570 m MD (568.99 m VD) the inclination is 10.0°, the tool face is adjusted and a turn to the right, at a turn rate of 3° per 30 m is initiated.

At a measured depth of 940 m MD (922.2 m VD) the final inclination of 21° is reach, and the turn to the right completed with an azimuth of 72°. The 9 5/8" production casing is set at this depth. The 8½" production hole is drilled with a fully 'locked up' rotary assembly to the final measured depth of 2400 m (2285 m VD).

The final target point has a lateral displacement of 637.6 m from the wellhead, and a final polar bearing of 67.7°. A maximum dogleg of 3.32° occurred at 760 m MD (752.5 m VD).

The vertical section and plan of this well are depicted in Figures 5. and 6.

DIRECTIONAL SURVEY ANALYSIS

Radius of curvature method E&O E 30.00

FIELD Mokai
WELL No. MK-14
18-Sep-06
Units in METERS
1.50 3.00 Magnetic deviation -22.56 E
Azimuth True, Grid or Magnetic GRID

MEAS DEPTH (m)	DRIFT (°)	AZIM GRID (°)	VERT DEPTH (m)	COORD NORTH NZMG (m)	COORD EAST NZMG (m)	POLAR DIST (m.)	POLAR BEARING (°)	DOGLEG deg/30m
0		30.00						
0	0.00	30.00	0.00	6293162.66	2765374.39			
30	0.00	30.00	30.00	6293162.66	2765374.39	0.00	30.00	0.00
60	0.00	30.00	60.00	6293162.66	2765374.39	0.00	30.00	0.00
85.0	**0.00**	**30.00**	**85.00**	6293162.66	2765374.39	0.00	30.00	0.00
130	0.00	30.00	130.00	6293162.66	2765374.39	0.00	30.00	0.00
135	0.00	30.00	135.00	6293162.66	2765374.39	0.00	30.00	0.00
200	0.00	30.00	200.00	6293162.66	2765374.39	0.00	30.00	0.00
250	0.00	30.00	250.00	6293162.66	2765374.39	0.00	30.00	0.00
258	0.00	30.00	258.00	6293162.66	2765374.39	0.00	30.00	0.00
263	0.00	30.00	263.00	6293162.66	2765374.39	0.00	30.00	0.00
270	0.00	30.00	270.00	6293162.66	2765374.39	0.00	30.00	0.00
280	0.00	30.00	280.00	6293162.66	2765374.39	0.00	30.00	0.00
290	**0.00**	**30.00**	**290.00**	6293162.66	2765374.39	0.00	30.00	0.00
320	0.00	30.00	320.00	6293162.66	2765374.39	0.00	30.00	0.00
350	0.00	30.00	350.00	6293162.66	2765374.39	0.00	30.00	0.00
370	0.00	30.00	370.00	6293162.66	2765374.39	0.00	30.00	0.00
390	1.00	30.00	390.00	6293162.81	2765374.48	0.17	30.00	1.50
420	2.50	30.00	419.98	6293163.60	2765374.94	1.09	30.00	1.50
450	4.00	30.00	449.94	6293165.07	2765375.79	2.79	30.00	1.50
480	5.50	30.00	479.83	6293167.22	2765377.03	5.28	30.00	1.50
510	7.00	30.00	509.65	6293170.05	2765378.66	8.54	30.00	1.50
540	8.50	30.00	539.38	6293173.56	2765380.68	12.59	30.00	1.50
570	10.00	30.00	568.99	6293177.73	2765383.09	17.41	30.00	1.50
600	11.50	33.00	598.46	6293182.50	2765386.02	23.00	30.36	1.60
630	13.00	36.00	627.77	6293187.75	2765389.62	29.35	31.26	1.63
660	14.50	39.00	656.91	6293193.40	2765393.96	36.45	32.48	1.66
690	16.00	42.00	685.86	6293199.40	2765399.09	44.28	33.90	1.69
720	17.50	45.00	714.58	6293205.67	2765405.04	52.82	35.47	1.73
750	19.00	48.00	743.07	6293212.14	2765411.85	62.07	37.13	1.77
760	19.50	51.00	752.51	6293214.28	2765414.36	65.29	37.75	3.32
780	19.17	54.00	771.39	6293218.31	2765419.61	71.71	39.09	1.57
810	18.91	57.00	799.75	6293223.85	2765427.67	81.15	41.05	1.01
840	18.93	60.00	828.12	6293228.94	2765435.97	90.47	42.89	0.97
870	19.25	63.00	856.47	6293233.62	2765444.59	99.82	44.69	1.03
900	19.83	66.00	884.75	6293237.94	2765453.64	109.31	46.47	1.16
920	20.42	69.00	903.53	6293240.57	2765460.00	115.76	47.70	1.78
940	**21.00**	**72.00**	922.23	6293242.93	2765466.67	122.31	48.98	1.82
945	**21.00**	**72.00**	926.90	6293243.48	2765468.37	123.96	49.30	0.00
970	21.00	72.00	950.24	6293246.25	2765476.89	132.27	50.80	0.00
1000	21.00	72.00	978.25	6293249.57	2765487.12	142.34	52.37	0.00
1100	21.00	72.00	1071.61	6293260.65	2765521.20	176.51	56.28	0.00
1200	21.00	72.00	1164.96	6293271.72	2765555.28	211.23	58.91	0.00
1300	21.00	72.00	1258.32	6293282.80	2765589.36	246.27	60.80	0.00
1400	21.00	72.00	1351.68	6293293.87	2765623.45	281.51	62.22	0.00
1500	21.00	72.00	1445.04	6293304.94	2765657.53	316.88	63.32	0.00
1600	21.00	72.00	1538.40	6293316.02	2765691.61	352.35	64.20	0.00
1700	21.00	72.00	1631.75	6293327.09	2765725.70	387.89	64.92	0.00
1800	21.00	72.00	1725.11	6293338.17	2765759.78	423.47	65.51	0.00
1900	21.00	72.00	1818.47	6293349.24	2765793.86	459.10	66.02	0.00
2000	21.00	72.00	1911.83	6293360.32	2765827.94	494.75	66.45	0.00
2100	21.00	72.00	2005.19	6293371.39	2765862.03	530.43	66.83	0.00
2200	21.00	72.00	2098.55	6293382.46	2765896.11	566.13	67.15	0.00
2300	21.00	72.00	2191.90	6293393.54	2765930.19	601.85	67.44	0.00
2400	**21.00**	**72.00**	**2285.26**	6293404.61	2765964.28	637.58	67.70	0.00

Table 2. Mokai Well MK-14 Directional Drilling Profile

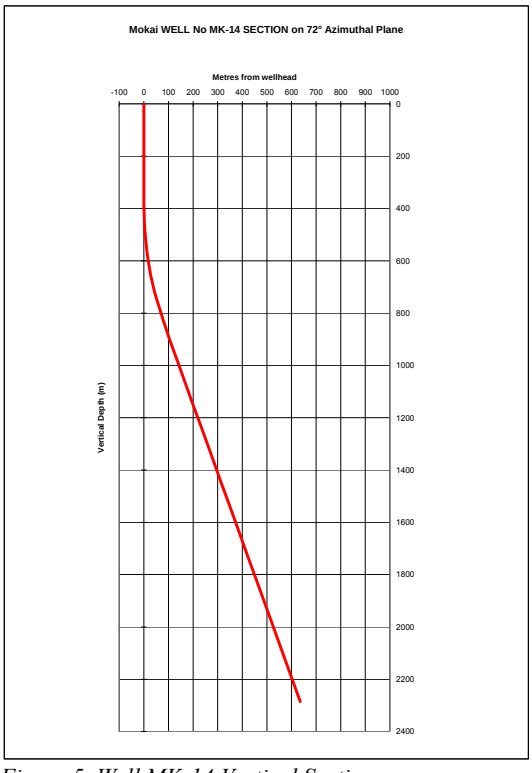

Figure 5. Well MK-14 Vertical Section

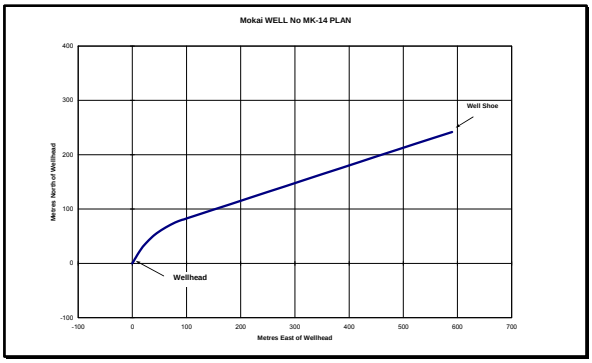

Figure 6. Well MK-14 Plan.

When these two wells were drilled the actual directional profile achieved in both wells was reasonable similar to the planned profile. However, the target depth of 2400 m measured depth was not reached in either, both being terminated at a little over 2200 m measured depth due to excessive torque and drag.

These results highlight the limitations the geothermal environment imposes upon directional drilling.

Limitations

Well design aspirations have to be tempered to what is realistically achievable. The directional drilling technology available from the drilling industry, far exceeds what is practicably useable in a geothermal environment. Simplicity of design, and of the equipment to be utilised are key to success.

- The majority of mud motors, MWD (Measure While Drilling), and downhole deviation instrumentation have operational temperature limitations of around 150°C. The KOP and initial build and directional drilling should be carried at depths where temperatures are not too high - < 150°C.
- The kick-off and the initial build and directional drilling is more efficient and more successful if carried out in a 'smaller' diameter hole – but the smallest diameter hole sections are deep and therefore hotter. Typically the KOP should be just below the anchor casing shoe (either 17½" or 12¼" hole section).
- Rate of build and rate of turn must be as low as possible – 1.5° to 3° per 30 m.
- A final drift angle in excess of 15° is desirable. Drift angles less than this may create difficulties in maintaining a constant direction (azimuth). Depending on the

formations being drilled, a final drift angle of 25° - 35° would be common.

These limitations generally require that a significant proportion of the directional drilling must be carried out with rotary bottom hole assemblies, and that directional measurements must be made using 'slickline' instruments – retrievable tools equipped with thermal protection, run and retrieved in the drillpipe on non-electrical wireline.
Rotary bottom hole assemblies and variation of the 'weight on the bit' (WOB) and the rotary speed (RPM), can be formatted to provide build, maintain a straight hole, or allow the inclination to fall. Rotary bottom hole assemblies provide little control over the hole direction (azimuth control).

Mud motors and MWD (Measure While Drilling) instrumentation can be utilised in the upper, lower temperature hole for the kick-off, to establish a smooth and regular build in inclination – usually to a round 10° to 20°; and to establish the desired direction (azimuth).
Beyond these depths it is advisable to utilise rotary bottom hole assemblies to continue the build, hold the current angle, or allow the inclination to fall.
Typical rotary assemblies to achieve these directional requirements are shown in Figures 7, 8, and 9.

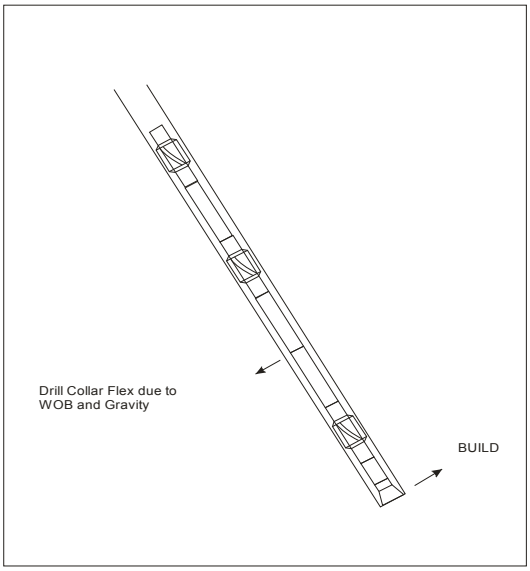

Figure 7. Typical Rotary Build Assembly

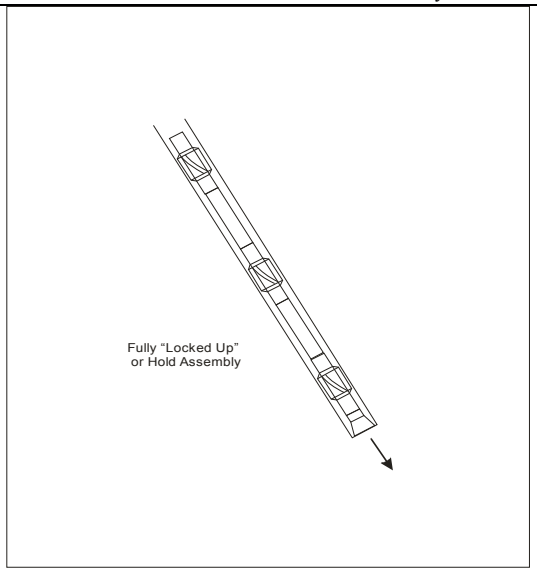

Figure 8. Typical Rotary "Hold" Assembly.

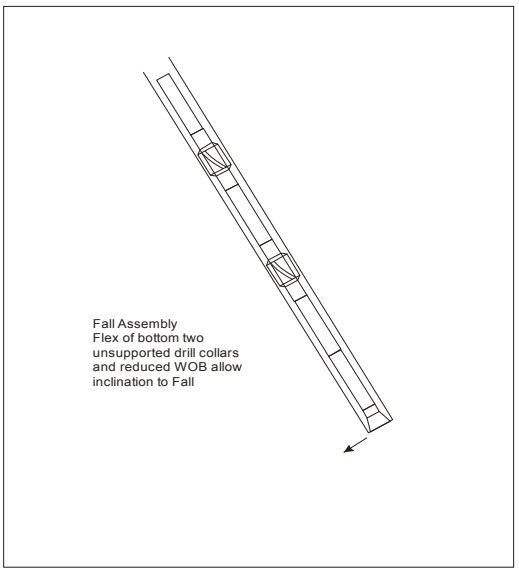

Figure 9. Typical Rotary Fall Assembly

Proximity of other wells

Where other vertical or directional wells are in the vicinity of a planned well, the new well track proximity to open hole section of other wells must be considered.
In the extreme, if the new well track being drilled passes close to an existing productive well, such that communication between the new well and the open hole section of the existing well is possible, the potential for a blowout in the new well exits.

Of less extreme concern is possibility of production interference between wells. If the spacing between two wells drawing from the same permeable horizon is insufficient, localised

drawdown can effect the productivity of both wells.

To avoid these possibilities it is desirable that the separation between the production casing shoes and the open production holes is maximised,
Typically the close approach of the production sections of any two wells should not be less than 200 m.

Multi- Well Pads

The ability to successfully drill directional geothermal wells has progressed to the obvious conclusion of drilling more than one well from the same drilling location. The economic savings accrue from:-

- reduced drilling pad civil construction costs – one slightly drilling pad with a slightly increased area can accommodate a number of wells. Only one access road requires construction, only one drilling effluent soak pit requires construction.
- Reduced rig moving costs – typically, the cost of moving a drilling rig from one location to another is in the order of US$500,000, taking a period of around two weeks; while a rig 'skid' from one well to the next on the same pad is generally carried out at the rig operating rate and can usually be achieved in a period of two days, at a cost in the order US$120,000.
- Reduced water supply system installation costs.
- Significantly reduced steam gathering pipework costs.

The disadvantages can be accommodated or easily mitigated.

- Live wellheads close to a drilling operation – an element of danger exists in that having completed a successful geothermal well, the rig is skidded only a distance of 5 to 10 metres from the now 'live' wellhead. There is a potential for damaging the live wellhead. This concern can be mitigated with the placement of a temporary protective cover over the 'live' wellhead.
- Drilling cutting soakage pits need to accommodate much greater quantities of cuttings and therefore need to be larger, and should be designed such that they can be emptied or at least partially emptied while in operation.

The well pad layout is generally dictated by the drilling rig being utilised to drill the wells, and by a rule of thumb minimum spacing of a least 5 m. such that the chance of collision in the initial vertical sections of the wells is minimised. Wellhead spacing must be such that when a well is completed, the rig can be 'skidded' or 'walked' off the well to the next wellhead, leaving the completed well accessible for completion tests, and even vertical discharge testing without significant interruption of drilling activities on the new well.
After completion of drilling of all of the wells on the well pad, there is always the possibility that workover activities may be required on any of the wells. The steam gathering pipework must be designed in such a manner that access to each wellhead is available without disconnection of adjacent wells.

An Example of a Multi-Well Pad – Mokai, New Zealand.

During the period October 2003 to June 2004 six (6) wells were drilled at the Mokai Geothermal Field. Wells MK-10 through MK-15 were drilled from a single wellpad designated MK-II, with Parker Drilling International Rig 188, a 2,700 HP, 1.2 million.lb, walking box base rig.
All six well were drilled directionally, with 9 5/8" production casing and 8½" diameter production hole sections.
Figure 10. is a map of the Mokai area with the well-tracks of the six production well-tracks overlaid The cased sections are indicated in grey, while the open productions are in white.

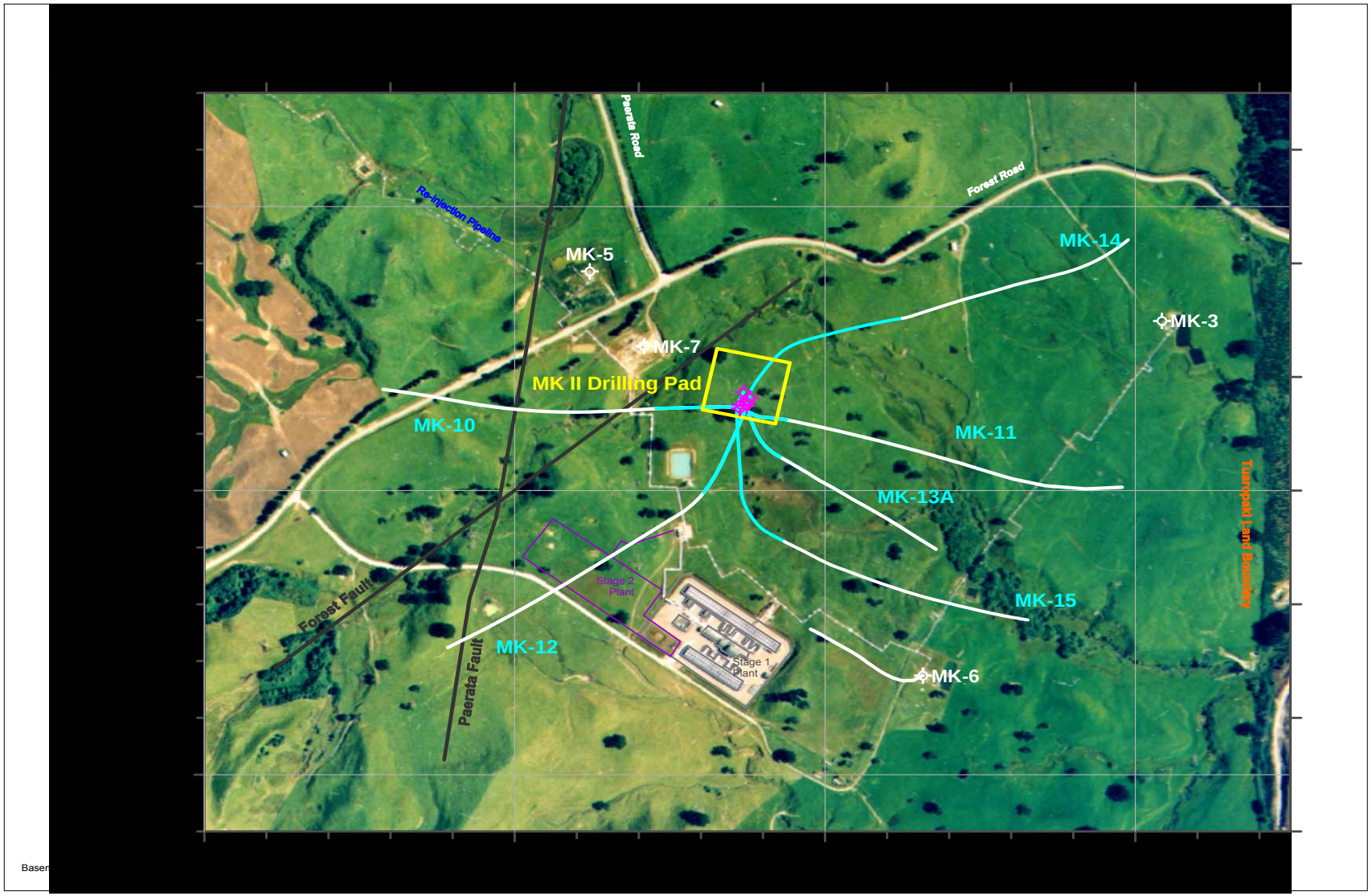

Figure 10. Mokai, Well Pad MK-II with Wells MK-10, MK-11, MK-12, MK-13, MK-14 and MK-15 as drilled Well Tracks (Cased sections indicated in grey/green; Production sections indicated in white).

The layout of the wellheads was dictated by the dimensions of the drilling rig sub-base, which was a hydraulically powered walking box base, allowing the rig to be easily walked backwards and forwards, and sideways in each direction. The box sub-base overall dimensions were 22m long by 9 metres wide, with 'hole centre' 10 m from the front toe and centred on the lateral dimension. These box base dimensions required that adjacent wells have at least a 6.0 m lateral spacing, and a 10 metre longitudinal spacing, relative to the rig sub-base.

Figure 11 is a plot of the wellhead locations on the MK-II drilling Pad.

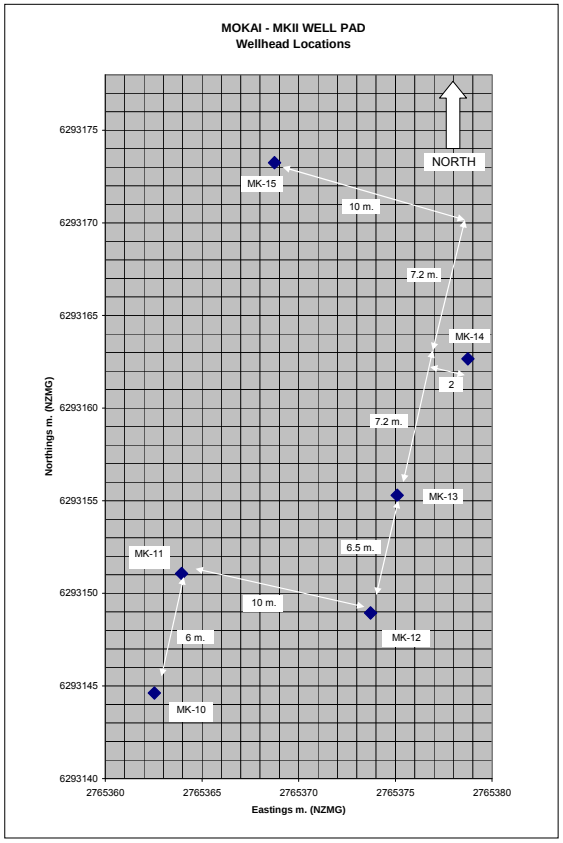

Figure 11. Wellhead locations on Mokai Well Pad MK-II

Drilling Cellar Options

One option which simplifies multi-well pad is to construct a single 'trough' type drilling cellar, approximately 2 metres deep with the wells spread in a single line along the trough. {Wayang Windu, Indonesia; Olkaria West, Kenya}. The wellhead and master valve being mounted such that the top of the master is just below ground level. This type of configuration allows a simple cover to be placed over the wellhead, eliminating interference to on-going drilling operations.

However, the concept of a relatively large and deep cellar has been 'de-popularised' by Health and Safety concerns relating to the possible accumulation of toxic gases.

More typically single cellars are constructed for each well, and the master-valve is mounted above ground level-requiring protective covers to put in place while on-going drilling operations continue.

Acknowledgements

I thank Tuaropaki Power Company, owners and operators of the Mokai Geothermal field, New Zealand, for the use of field data and information.

References

Hole, H M., 1996' "Seminar on Geothermal Drilling Engineering – Geothermal Energy New Zealand Ltd. Jakarta, Indonesia 4 – 8 March 1996", Seminar Handbook, Section III, pp 50 – 55.

Gabolde, G., Nguyen, J.P, 1999. "Drilling Data Handbook – Seventh Edition". Institut Francais du Pétrole Publications.

DRILLING FLUIDS FOR DRILLING OF GEOTHERMAL WELLS

Hagen Hole
Geothermal Consultants NZ Ltd., Birkenhead, Auckland, New Zealand.

ABSTRACT

Drilling fluids are required to remove cuttings from the well during drilling, to cool and lubricate the drill bit and drill string, to apply pressure to formation fluids to control flow into or out of the well, and to cool the formation, particularly prior to cementing casings. Various drilling fluids are selected according to reservoir pressures and temperatures and to the drilling techniques to be utilised. Drilling fluids normally used include water, water based bentonitic (or other) muds, aerated water, and stiff foam.
Because many geothermal reservoirs are set in interlayered volcanic and sedimentary rock and are normally associated with local and regional faulting, highly permeable features are common and cause major and frequent losses of drilling fluid circulation.

The utilisation of aerated fluids and the concept of 'balanced' downhole pressure conditions allows for full circulation of drilling fluids and drilling cuttings back to the surface while drilling through permeable formations, thus significantly reducing the risk of the drill string becoming stuck, of formation and wellbore skin damage, and for full geological control.

Keywords: geothermal, drilling fluids, aerated drilling

INTRODUCTION

The circulation of 'drilling fluid' is an integral part of rotary and percussion drilling, and depending on the fluid type can fulfil all or some of the following functions:-

- Removes cuttings from the bottom of the hole – at the bit face.
- Returns cuttings to the surface (circulating conditions).
- Holds cuttings in suspension when circulation is stopped.
- Releases cuttings from the drilling fluid at the surface.
- Cools and lubricates the drill bit.
- Lubricates the drill string.
- Cools the hole and prevent liquid in the well from boiling.
- Controls downhole pressure preventing the well from flowing.
- Carry weighting material to increase fluid density to prevent the well from flowing and possibly blowing out.
- Reduces losses of drilling fluid by forming an impermeable 'wall cake' or lining to the hole wall.
- Reduces the rate of breakdown of water sensitive formations.

These functions are those desirable in drilling fluids utilised in petroleum wells, some water wells, and in the upper parts of a geothermal well. However, not all of these properties are necessarily desirable in all sections of a geothermal well.

Drilling Fluid Properties

The primary function of a drilling fluid is to remove the drilling cuttings from the bottom of the hole and carry them to the surface.

Slip Velocity

The ability of a drilling fluid to entrap and carry granular particles from the drill bit face to the surface is dependent upon the annular velocity of the drilling fluid exceeding the 'slip velocity' of the cuttings particles in that drilling fluid.
In the context of drilling, this 'slip velocity' may be described as the upwards annular drilling fluid velocity required to impose an upwards drag force on a cuttings particle equal to the downward gravitational force on that particle. If the upwards drag force does not exceed the downwards gravitational force the cuttings particle will not be lifted.
The drag force on a cuttings particle is dependent upon the size, shape and density (or wetted surface area and mass) of the particles, the viscosity of the fluid, and the upwards vertical velocity component of the fluid.

The size, shape and density of the particles being drilled are related to the rock type, the drill bit type and how well cuttings are being cleared away from the bit (and not being reground). The rock density, and the size and shape of the cuttings being produced are parameters which are not easily controlled or changed, however the drilling fluid viscosity and the drilling fluid flow rate and therefore annular flow velocity can be controlled within certain limits.

Fluid Viscosity and Flow Velocity

Fluid viscosity and fluid flow velocity are inversely proportional with respect to 'Slip Velocity' of a particular particle – in other words, if the fluid viscosity is increased, a reduced fluid flow velocity will be required to maintain the same slip velocity for a particular particle.

However, there are practical limitations to the range of fluid viscosities and fluid annular velocities that can be utilised.

Higher viscosity drilling fluids impose higher drag forces upon entrained cuttings particles and therefore produce better hole cleaning – but, higher viscosity fluids also impose higher pressure losses and therefore require higher pumping pressures.

Higher annular velocities ensure the particle – fluid slip velocity is exceeded, but increase the risk of scouring unconsolidated formation from walls of the hole and also impose higher pressure losses and therefore require higher pumping pressures.

Thixotrophy and Gel Strength

The ability of a drilling fluid to hold cuttings in suspension during periods of no circulation, and of releasing the cuttings from suspension at the surface require a special property – Thixotrophy.

A Newtonian fluid such as water, oil, and glycerine, maintains a constant viscosity while stationary or while flowing – the fluid viscosity is independent of any applied sheers stress. The viscosities of Non-Newtonian fluids such as water based bentonite mud, some polymers and some cement slurries varies as a function of the applied sheer stress – this property is Thixotrophy. When the fluid is stationary the fluid builds gel strength and the viscosity increases; if the fluid is pumped and forced to flow, the viscosity reduces.

This thixotropic property is ideal for holding cuttings in suspension during period of no circulation, and for releasing cuttings when the fluid is subjected to high cheer stress, such as passing over a linear motion shale shaker.

In addition to this process of holding cuttings in suspension and releasing them at the shale shaker, this thixotropic property also allows a layer of gelled fluid to build on the hole wall, creating a protective and somewhat impermeable lining or 'wall cake' on the hole wall.

Water Based Bentonite Mud

The most commonly used geothermal drilling fluid that exhibits the properties described above is water based bentonite mud, which typically comprises bentonite, water and caustic soda. Other chemicals may be added to control the physical properties of the fluid as required by the downhole conditions, and these will include:-

- Thinners to control viscosity and gel strengths
- Fluid loss control agents to control the loss of water from the mud which in turn controls excessive build-up of wall cake.
- Weighting materials such as barite to increase mud density (rare in geothermal)
- Loss of Circulation Materials (LCM) to aid in reducing the loss of drilling fluid to the formation.
- Corrosion control additives may also be added to the mud.

The solid content of the mud is derived from bentonite, non-clay materials contained in the bentonite, weighting materials if utilised, and drilled cuttings particles which may include sand and clay minerals.

Solids other than bentonite or weighting materials generally have adverse effects on the drilling operations. Increased mud density can reduce penetration rates and cause circulation losses. Sands can increase wear on pumping equipment and downhole tools (stabilisers, reamers, bits), drill string and casing. Drilled clays can cause excessive viscosity build-up and, together with other drilled solids, can build up thick wall cakes in the hole and around stabilisers. It is therefore desirable to remove as many of the drilled solids from the drilling fluid as is possible.

As drilling proceeds and the formation temperatures increase with depth, the drilling fluid is inevitably heated. At elevated temperatures the gelling properties and viscosity of bentonite muds increase, and the mud begins to flocculate. Dispersant and deflocculating additives, and cooling the circulating fluid can assist in controlling this problem.

Over the past 10 years polymeric fluids have been developed and introduced into the drilling industry. Synthetic drilling polymers exhibit many of the same properties as water based bentonite and are now being utilised more frequently in geothermal drilling – however, polymeric drilling fluids are extremely expensive and are therefore used sparingly.

Underbalance and Overbalance

In a typical 'under-pressured' geothermal system, the pressure of the drilling fluid in the well exceeds the pressure of the fluids in the formation at the same depth. This is an "overbalanced" condition – the opposite condition or "underbalanced" conditions may occur when a total loss of circulation allows the liquid level in the annulus to move down the well, or when intentionally established using aerated drilling methods. Drilling in an underbalanced condition encourages inflow of formation fluids (gas, steam or hot water) and sloughing of formations. Unless controlled, kicks and stuck drill string can result. However, drilling with excessive overbalanced pressures can cause slow penetration rates, high loss of mud filtrate resulting in thick soft wall cake development and breakdown of the formation and subsequent loss of circulation.

Where conditions of a large overbalance pressure and a thick soft wall cake are present adjacent to the drill string (particularly non-stabilised and slick drill collars), the drilling tubulars can be forced into the wall cake by the overbalance pressure and cause the drill string to become securely stuck in the wall cake. This action, referred to as "differential sticking", is a frequent cause of stuck drill strings and is best avoided by using mud weights which give minimum water loss (to reduce the build up of wall cake) and low inactive solids content (to reduce the strength of the wall cake).

Loss of Circulation

The common denominator of all convective hydrothermal systems – the majority of all developed geothermal fields, is the highly permeable, fractured and faulted nature of the formations in which the geothermal reservoirs reside. This high permeability being one of the fundamental and requisite components for any geothermal system to exist.

Typically, the permeable nature of the formations is not limited to the geothermal reservoir structure alone, but often occurs in much of the shallower and overlying formations as well. This, coupled with the under-pressured nature of most geothermal systems, results in the partial or total loss of circulation of drilling fluid at some stage during the drilling of the well - in fact ultimately if circulation is not lost in an under-pressured system this is an indication that there is no permeability and therefore the well a 'dry well'.

The thixotropic and gelling nature of water based bentonite mud assists in the sealing of minor loss zones, and with the addition of loss circulation materials (LCM) many minor loss zones can be completely sealed. However, if major or total losses of circulation are encountered, and can't be sealed with LCM added to the mud, then it becomes impractical and uneconomic to continue drilling with mud. If high permeability and therefore significant or total losses of circulation are encountered within the upper cased sections of the well the use of water based bentonite mud and additives is normally ceased, and drilling is continued with water or with aerated water.

When drilling the production section of the well within the reservoir structure, the elevated temperatures and the targeted permeability render the properties of bentonite muds undesirable. The drilling of a geothermal well has as it's primary objective, drilling into, and preserving permeable formations within the reservoir structure, which will, after completion of drilling become the production zone of the well.

If bentonite mud is forced into the permeable structure of the reservoir, the gelling and sealing properties can cause permanent damage to the productivity of the zone. The high temperatures dehydrates and bakes the bentonite clay into a relatively inert and impermeable material. A process similar to baking clay into pottery.

It is therefore usual and accepted practice that this section of the well is drilled with water or aerated water.

Drilling with Water

Water as a drilling fluid was, in the past, used to continue drilling past an unsealable loss zone and for the final production section of a geothermal well. When drilling into a permeable 'under pressured' zones the drilling fluid circulation is lost, and the drilling fluid flows into the formation rather than returning to the surface.

The traditional method of dealing with this situation was to continue drilling 'blind' with water – the pumped water being totally lost to the formation with the drilling cuttings being washed

into the formation as well. The major problem with this method of drilling is that the cuttings rarely totally disappear into the formation. Stuck drill string due to a build up of cuttings in the hole, and well-bore skin damage being common occurrences.

The advantages using water as drilling fluid are:-

- As the water is not recirculated but is lost to the formation, the downhole temperature significantly lower, extending drill bit life and reducing the likelihood of a kick developing.
- As lower bottom hole circulating pressures are developed, penetration rates are higher.
- Because mud and thick wall cake ae not squeezed into permeable zones, reduced formation sealing and increased well productivity are achieved.
- Because a wall cake is not developed, differential sticking does not occur. Where a wall cake is present from earlier drilling, the lower downhole circulating pressures significantly reduces or eliminates the risk of differential sticking.

The disadvantages of using water as drilling fluid are:-

- A continuous large volume (~3500 lpm) supply of water to the drilling rig is required.
- As water has a low viscosity, is not thixotropic and cannot develop gel strength, slip velocities are higher requiring increased annular fluid velocities, and as soon as pumping to the drill string is stopped (e.g. to make a connection), any cuttings suspended in the annulus will start settling immediately, which increases the risk of stuck drill string.
- Cutting are not returned to the surface, but washed into the permeable zones.
- No geological data, as no return of cuttings to the surface.
- The loss of cuttings into the permeable zones may reduce permeability (not as much as mud).
- When pumping is stopped cuttings accumulated in permeable zones may flow back into the well increasing the risk of stuck drill string.
- Loss of large volumes of cold water to the formation can cause long recovery periods after drilling is completed before the well can be discharged.

Great care must be exercised when drilling with water to avoid becoming stuck with cuttings settling down the annulus.

Aerated Drilling

'Aerated Drilling' may be defined as the addition of compressed air to the drilling fluid circulating system to reduce the density of the fluid column in the wellbore annulus such that the hydrodynamic pressure within the wellbore annulus is 'balanced' with the formation pressure in the permeable 'loss zones' of a geothermal well.

Drilling Processes

The primary objective of utilising aerated drilling fluids is the ability to maintain drilling fluid circulation and therefore the clearance of cuttings from the hole as drilling proceeds into permeable and 'under pressured' zones.. This continuous clearance of cuttings from the hole significantly reduces the risk of the drill string getting stuck in the hole.

Aeration of the drilling fluid reduces the density of the fluid column and thus the hydraulic pressure exerted on the hole walls and the formation. As the introduced air is a compressible medium, the density of the column varies with depth – at the bottom of the hole where the hydrostatic pressure is greatest, the air component is highly compressed and therefore the density of the fluid is greatest; at the top of the hole, where the hydrostatic pressure is least, the air component is highly expanded and therefore the density of the fluid the least. The ratio of air to water pumped into the hole, and the back pressure applied to 'exhaust' or flowline from the well, allows the down-hole pressures in the hole to be 'balanced' with the formation pressure in the permeable zones, thus allowing for the return of the drilling fluids to the surface and therefore maintaining drilling fluid circulation. (In fact the term 'under-balanced' drilling as applied to this form of geothermal drilling is a misnomer).

Initially the technique was utilised only in the smaller diameter production hole section of a well, however, in some fields permeability is prevalent in the formations located above the production zone, and significant amounts of lost time can be incurred in attempting to plug and re-drill such

zones. Utilising aerated fluids to drill these zones has proven to be a highly successful solution.

Formation and The Resource

Perhaps the most important feature of aerated drilling is its effect on the productivity of the well. The removal of the drill cuttings from the well bore, rather than washing the cuttings into the permeable zones, reduces the potential of blocking up and in some cases sealing the permeability close to the wellbore – the effect called well-bore skin damage. A relatively small amount of interference to the flow from the formation into the well-bore, or skin damage, can have a significant effect on the productivity of the well.

Wells drilled with aerated fluids, and thus with full circulation and removal of drill cuttings show less skin damage than those drilled 'blind' with water.

In general terms, wells with the production zone drilled with aerated fluids demonstrate better productivity than those drilled blind with water, and significantly better productivity than those drilled with bentonite mud in the production zone.

A previous drilling campaign in Kenya allows for a direct comparison between a number wells drilled as immediate offsets, to similar depths in similar locations; the original set of wells were drilled blind with water(and in one case mud) and a more recent set drilled with aerated water. The productivity of the wells drilled with aerated fluids, on average is more than double that of the wells drilled without air.

Wells Drilled Blind with water		**Wells Drilled with Aerated Fluid**	
Well No.	**Output (MWt)**	**Well No.**	**Output (MWt)**
1	43.31	A-1	37.05
2	12.75	A-2	98.73
4	22.15	A-4	58.86
5(drilled with mud)	14.76	A-5	105.49
6	21.38		
		B-1	27.59
		B-3	36.26
		B-7	32.72
		B-9	67.63
Average	**22.87 MWt**		**58.04 MWt**

Table 1: Comparison of Thermal Outputs of wells drilled with and without Aerated Fluids at Olkaria – Kenya.

Cuttings Return

As indicated above, the primary objective of utilising aerated drilling fluids is the maintenance of drilling fluid circulation, the obvious corollary to this is the continued return of drilling cuttings back to the surface, and thus the ability to collect and analyse cuttings from the total drilled depth. While this is not always achieved for the entire drilled depth of wells drilled with aerated fluids, it is usual for circulation to be maintained for a significant proportion of the drilled depth.

Drilling Materials

A significant reduction in the consumption of bentonite drilling mud and treating chemicals, cement plugging materials, and bentonite and polymer 'sweep' materials can result from the use aerated water or mud.

In addition a major reduction in the quantities of water consumed occurs. Typically, approximately 2000 litres per minute will be 'lost to the formation' while drilling an 8½" hole 'blind with water'. Aeration of the fluid allows almost complete circulation and re-use of drilling water.

A Fishing Tool

Perhaps the most common reason for stuck drill-string is inadequate hole cleaning – the failure to remove cuttings from the annulus between the hole and the drill string. Often, the hole wall in the region of the loss zone acts as a filter, allowing fine cutting particles to be washed into the formation while larger particles accumulate in the annulus. Under these circumstances, if a new loss zone is encountered and all of the drilling fluid flows out of the bottom of the hole, these accumulated cuttings fall down around the bottom hole assembly and can result in stuck and lost drill strings. Aerated drilling prevents the accumulation of cuttings in the annulus and allows for circulation to be maintained even when new loss zones are encountered.

In the event that a significant loss zone is encountered and the pressure balance disrupted, circulation may be lost and in severe cases the drill string may become stuck; with adjustment of the air / water ratio it is usually possible to regain circulation, clear the annulus of cuttings and continue drilling with full returns of drill water cuttings to the surface.

The air compression equipment has on numerous occasions been utilised to pressurise the annulus around a stuck drill-string, such that the water

level in the annulus is significantly depressed. If the pressure in the annulus is then suddenly released the water in the annulus surges back up the hole, often washing cuttings or caved material packed around the drill string up the hole and thus freeing the stuck drill string.

Well Recovery

Wells drilled 'blind with water' usually experience a significant recovery heating period after completion of the well. The large volumes of water lost to the reservoir can take a long period to heat up. Aeration of the drilling fluid limits the loss of fluids to the formation and the cooling of the reservoir around the well. The temperature recovery of wells drilled with aerated fluids is significantly faster. Typically a well drilled with water 'blind' can take from 2 weeks to 3 months for full thermal recovery. Wells drilled with aerated fluids tend to recover in periods of 2 days to 2 weeks.

disadvantages

Whilst the aerated drilling technique provides many benefits, it also introduces some negative aspects.

Cost

The rental of aerated drilling equipment, the additional fuel consumed plus two operators imposes an additional operational daily cost against the well. Typically this additional cost will be in the order of US$150,000 to $250,000 per well, or if we assume a typical geothermal cost of US$3.5 million, the aerated drilling component of this cost will be in the order of ±6.0%.

Non-Productive Time Activities

Aerated drilling requires the utilisation of a number of non-return valves or 'string floats' to be placed in the drill string. Prior to any directional survey these floats must be removed from the drill string – this requirement imposes additional tripping time of approximately half an hour each time a survey is carried out.
However, when comparing 'non-productive' between aerated drilling and 'blind' drilling with water, the time lost when washing the hole to ensure cuttings are cleared when 'blind' drilling is comparable if not more than that lost retrieving float valves when aerated drilling.

Potential Dangers

Drilling with aerated fluids requires the drilling crew to deal with compressed air and with pressurised high temperature returned fluids at times, neither of which are a feature of 'blind' drilling with water. These factors are potentially dangerous to the drilling crew and require additional training, awareness and alertness. The author is not aware of any notifiable 'Lost Time Injuries' that have occurred as a direct result of using aerated drilling fluids since the technique was introduced in the early 1980's.

While drilling within a geothermal reservoir system under aerated 'balanced' conditions, the potential for the well to 'kick' is significantly higher than if being drilled with large volumes of cold water being 'lost' to the formation'. Well 'kicks' are a relatively common occurrence when drilling with aerated fluids, however the use of a throttle valve in the blooie line causes an increase in back-pressure when an increase in flow occurs, which tends to automatically control and subdue a 'kick'. The author is not aware of any uncontrolled blow-outs of geothermal wells that have results from the use of aerated fluids.

Drill Bit Life

Aerated drilling prevents the loss of drilling fluid to the formation and thus reduces the cooling of the formation and near well bore formation fluids. The drill bits and bottom hole assemblies used are therefore exposed to higher temperature fluids especially when tripping in, reducing bearing and seal life, and thus the bit life.
This reduced life is however, usually a time dependant factor, which, when drilling some formations is compensated by significantly increased rates of penetration. For example – the current aerated drilling operations in Iceland have seen average penetration rates of up to two time (2x) that previously achieved.

the process

As stated above, to maintain drilling fluid circulation while drilling permeable formations, the hydraulic (hydrostatic and hydrodynamic) pressure in the hole must be 'balanced' with the

formation pressure.. To balance the pressure in the hole with the formation pressure, the density of the fluid in the hole must be reduced. Figure 2. depicts some typical geothermal formation pressure regimes with respect to a cold hydrostatic column of water from the surface. A static water level of 400 metres has been assumed.

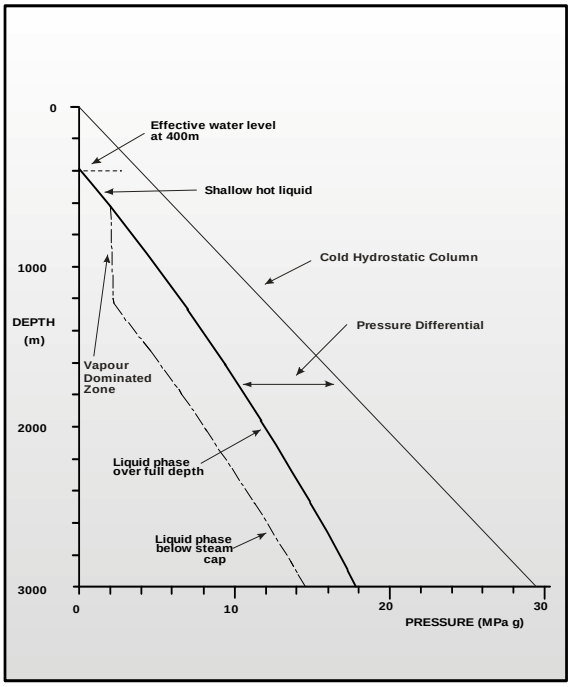

Figure. 2: Typical Formation Pressures

Figure 3. depicts typical pressures within a well with a range of drilling fluids with respect to a column of boiling water. The effective drilling fluid density can be varied in the approximate specific gravity range of 1.1 for un-aerated mud to 0.1 for air, by varying the ratio of air to liquid.

Fluid	Effective Specific Gravity
Water based bentonite Mud	1.1
Water	1.0
Oil Based muds	0.82
Aerated bentonite mud	0.4 – 1.1
Aerated water	0.3 – 1.0
Mist	0.05 – 0.4
Foam	0.05 - 0.25
Air	0.03 – 0.05

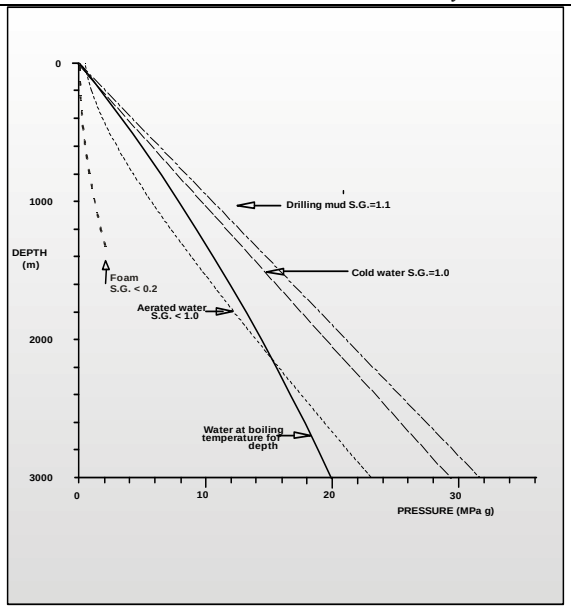

Figure 3. Typical Downhole Pressures

To 'balance' the downhole circulating fluid pressure with under-pressured formation conditions the density of the circulating fluid is reduced with the addition of air. The ratio of liquid to air, and the throttling of the circulating fluid outlet to produce a backpressure in the annulus are the variables which can be altered to provide the required pressure balance.

However, the addition of air into the drilling circulation system introduces a compressible component. The volume occupied by a unit mass of air at a particular depth in the hole is dependant on the fluid pressure at that depth. In other words the volume of a bubble of air at the bottom of the hole will be a small fraction of the volume occupied by the same bubble of air at the top of the hole. The density of the fluid column varies with depth and for simplicity purposes is described as a 'liquid volume fraction' (LVF).

A liquid volume fraction (LVF) of 1.0 = 100% liquid

A liquid volume fraction (LVF) of 0.0 - 100% air

So not only is the pressure regime within the hole altered, but circulating fluid volume, (the LVF) and therefore the fluid velocity varies with depth of the hole.

Table 2. indicates an output from the GENZL Aerated Drilling Computer Simulation Package, of a typical aerated downhole annular pressure profile with downhole pressure, differential pressure (the difference between the downhole

pressure and the formation pressure with a nominal static water level at 300 m depth), the flow velocity, and the Liquid volume fraction (LVF) indicated as a function of depth.
The simulation is of a well with production casing set at 700 m depth, and a 100 m bottom hole drilling assembly (drill collars) – hence the parameter changes at these depths.

Meas. Depth (m)	Vert. Depth (m)	Annular Pressure (Barg)	Diff. Press. (Barg)	Velocity (m/min)	LVF
Blooie Line	0.0	1.9	1	742.0	0.10
100.0	100.0	4.6	3.6	219.6	0.21
200.0	200.0	7.9	6.9	148.7	0.31
300.0	300.0	12.0	11.0	113.9	0.40
400.0	400.0	17.0	7.4	94.5	0.49
500.0	500.0	22.6	4.4	82.7	0.56
600.0	600.0	28.9	2.3	75.0	0.61
700.0	700.0	35.6	0.9	69.7	0.66
700.0	700.0	35.6	0.9	78.9	0.66
800.0	800.0	42.9	-0.1	74.6	0.70
900.0	900.0	50.4	-0.4	71.4	0.73
900.0	900.0	50.4	-0.4	101.7	0.73
1000.0	1000.0	58.7	0.0	98.0	0.76
Bottom Hole	1000.0	58.7	0.0	98.0	0.76

Table 2. Simulation of Aerated Downhole Conditions

Plots of the various parameters are indicated in Figures 4, 5, 6, and 7.

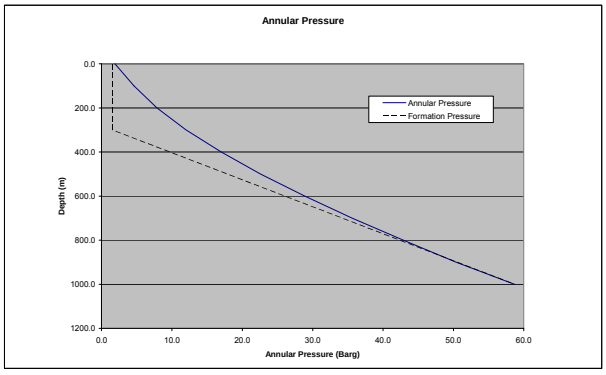

Figure 4. Annular Pressure and Formation Pressure V's Depth.

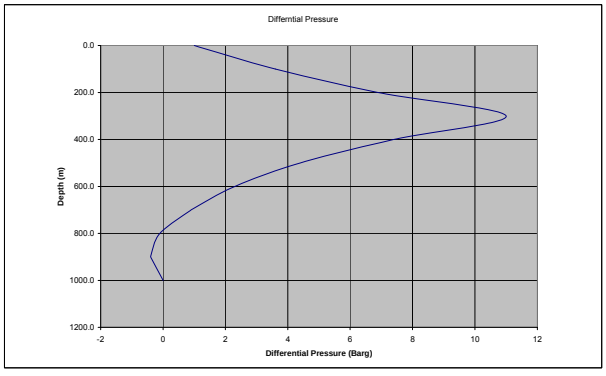

Figure 5. Differential Pressure V's Depth

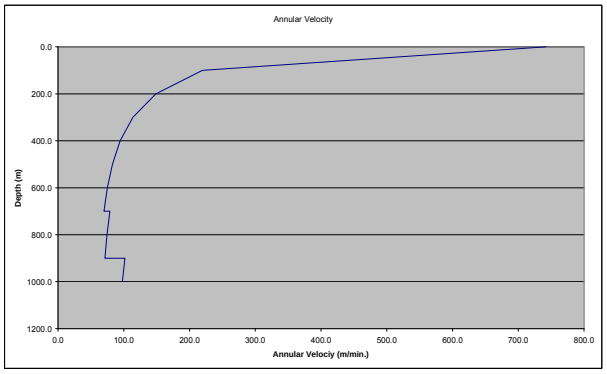

Figure 6. Annular Velocity V's Depth

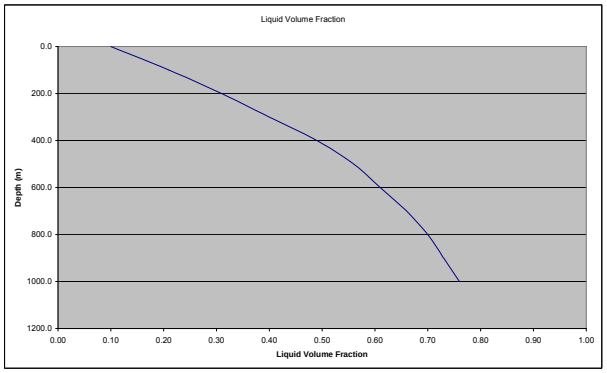

Figure 7. Liquid Volume Fraction V's depth

Perhaps the most critical point displayed by this data is that the fluid velocities around the drill bit and bottom hole assembly are very similar to the velocities that would occur without the addition of air. The volume of liquid to be pumped must be sufficient to provide lift to cuttings over the top of the bottom hole assembly, where the diameter of the drill string reduces from the drill collar diameter to the heavy weight drill pipe or drill pipe. Typically for water drilling, a minimum velocity of 45 to 55 metres per minute is required. The volume of air to be added to this liquid flow rate will be that required to reduce the density sufficiently to provide a balance, or a differential pressure of close to zero (0) at the permeable zone or zones.

Acknowledgements

Thanks are given to Mr. Lindsay Fooks, Geothermal Associates New Zealand Limited for his major efforts and inputs into developing and upgrading this component of Geothermal well drilling.

References

Hole, H.M, 1992. " The Use of Aerated Fluids for the Drilling of Geothermal Wells" Lecture notes, Geothermal Institute, University of Auckland, New Zealand.

Hole, H.M., 1996. "Seminar on geothermal Drilling Engineering – March 1996, Jakarta, Indonesia", Seminar Text, Geothermal Energy New Zealand Limited, Auckland, New Zealand.

International Association of Drilling Contractors, 2003. "Underbalanced Drilling Operations – HSE Planning Guidelines", International Association of Drilling Contractors, Houston Texas, USA.

Gabolde, G., Nguyen, J.P, 1999. "Drilling Data Handbook – Seventh Edition". Institut Francais du Pétrole Publications.

NZS 2403:1991, "Code of Practice for Deep Geothermal Wells" Standards Association of New Zealand.

GEOTHERMAL WELL CEMENTING

Hagen Hole
Geothermal Consultants NZ Ltd., Birkenhead, Auckland, New Zealand.

ABSTRACT

Perhaps the most critical component of the drilling process to the integrity and longevity of a Geothermal well is the cementation of the casings. The design of the cementing programme shall utilise materials and procedures which are most likely to ensure that the total length of both the cased annulus and the open hole annulus is completely filled with sound cement which will withstand long term exposure to geothermal fluids and temperature.
The cementing equipment, cementing materials, cement slurry designs and operational procedures are outlined and reviewed.

INTRODUCTION

Unlike oil and gas wells, the casings in Geothermal wells are all usually run back to the surface, and are fully cemented back to the surface. The high thermal stresses imposed on the casings demand uniform cementation over the full casing length, such that the stress is distributed over the length of the casing as uniformly as is possible and such that stress concentrations are avoided.

The objective of any casing cementing programme is to ensure that the total length of annulus (both casing to open hole annulus, and casing to casing annulus) is completely filled with sound cement that can withstand long term exposure to geothermal fluids and temperatures.

CEMENTING TECHNIQUES

The process of pumping cement to the annulus outside the casing being cemented may be carried out utilising one of three different techniques.

The traditional, and still often utilised technique of 'through the casing' cementing, involves pumping the cement slurry into the casing via at cementing head connected to the top of the casing; pumping a specific volume of cement slurry, then displacing the cement slurry from the casing into the annulus. Travelling plugs are utilised to separate the cement slurry from the fluid in the casing, and from the displacement fluid. The major disadvantage of this method is that usually the volume of the casing contents exceeds the annulus volume, and therefore a finite (calculated) cement slurry volume will be mixed and pumped, the top travelling plug released, and displacement commenced prior to any cement slurry reaching the annulus.

The 'Inner String' cementing technique requires a cementing string to be run inside the casing and 'stabbed' into a receptacle in the float collar, which is usually located at the top of the first or second joint of casing. The cement slurry is then pumped through the cementing string, through the 'shoe track' (the one or two joints of casing at the bottom of the casing string), and to the annulus directly. The small volume of the cementing string allows cement slurry to be mixed and pumped until good returns of cement slurry are returned to surface from the annulus. The volume to be mixed and pumped does not have to be finite. While this technique is more elegant with respect to mixing and pumping the cement slurry, the procedure requires that as soon as the casing has been run and the annulus circulated clear, the casing must be set in the rotary table and circulation ceased while the cementing 'inner' string is picked up and run into the hole. This is not usually a problem for shallow casings, but for the deeper production casings, the time required to pick up and run the cementing 'inner' string is such that, in wells with unconsolidated formations, the risk of the hole packing off against the casing, or the well kicking is high.

The third technique, 'reverse circulation', involves pumping the cement slurry directly to the annulus, with the displaced fluid being forced back through the casing shoe and through the casing to the surface. This technique is rarely utilised, as in the event of a loss of circulation there is no positive means of ensuring a cemented casing shoe.

Cementing Equipment

In Hole Equipment - Casing Accessories

When the casing is run into the hole it is fitted with a number of accessories specifically designed to enable the cementing procedure to be carried out.

- Casing Shoe (or Float Shoe) – is fitted to the bottom, or pin end of the first joint of casing, and is a heavy walled, rounded profile unit designed to guide the casing into the hole. It is fitted with a non-return valve which allows fluid (cement slurry) to flow from the casing into the well, but prevent flow from the well back into the casing. The internal structure is made from cement or some other easily drillable material.
- Float Collar - is fitted between either the first and second, or the second and third joint of casing and incorporates a non-return valve to ensure one way flow only from the casing out into the annulus.

  It is usual to utilise non-return, or float valves in both the shoe and the float collar for redundancy purposes.

  The float collar is also typically fitted with a 'stab in – latch down" receptacle to allow the "inner string" cementing process to be utilised which will be described below.
- Casing centralisers - are fitted periodically on the casing string to keep the casing concentric within the drilled hole.
- Travelling plugs – when utilising the 'through the casing' cementing process these plugs are utilised to separate the cement slurry from fluids in the well and from the displacement fluids.
- Cementing head – when utilising the 'through the casing' cementing process, the cementing head is attached to the top of the casing string and allows for connection of the cementing pipeline from the cement slurry mixing and pumping unit to the casing. The cementing head is usually designed to contain and release the travelling plugs.
- Tag-in adaptor and string centralisers – when utilising the 'inner string' cementing process, a tag in adaptor is fitted to the bottom of the cementing string (drillpipe) to allow the string to be 'stabbed in' to the 'stab-in – latch down' receptacle in the float collar.

Surface Equipment

It is usual that the cement mixing and pumping equipment are provided by a specialised oilfield cementing services contractor.

At significant contrast to the equipment utilised even 10 years ago, the equipment available from cementing services contractors today usually includes an automated computer controlled recirculating slurry mixing and pumping unit which can mix and pump uniform density slurries at rates of around 800 lpm at high pressures. These units are typically constructed with two independently powered triplex plunger type downhole pumps, and an independently powered recirculating mixing system with electronic density control.

Dry cement is typically stored in bulk pressure silos that allow pneumatic transfer of the dry cement to the mixing unit. Cement additive chemicals are either dry blended with the dry cement, or are added in liquid form to the mix water, which is delivered to the mixing unit automatically via the control system.

Cementing systems can mix and pump cement slurry volumes of up to 65,000 litres continuously within the allowable cement pumping time – sufficient for most geothermal well cement jobs.

CEMENTING MATERIALS

The petroleum industry has developed a wide range of highly sophisticated, and expensive materials specialised for the cementing of casings in oil and gas wells. Very few materials have been specifically developed for geothermal application, and many of the petroleum industry materials are inappropriate for geothermal environments.

Cement

During the 'early days' of geothermal well drilling, standard construction grade Portland cement was utilised, often successfully, for the cementing of casings. However, Portland cement, manufactured to API specification – typically API Class A or API Class G cements are now most commonly utilised. The quality control requirements of the API standards provides for cement slurries of highly reliable consistency.

Cement Blends

The high temperature environments of geothermal reservoir systems require blending of additional materials to ensure longevity of the cement used for cementing casings. API specifications recommend the blending of up to 40% by weight of cement (BWOC) of silica flour to prevent strength retrogression and increasing porosity as is seen with neat cement slurries exposed to elevated temperatures. However, work carried out by N. Milestone, Department of Scientific and Industrial Research, New Zealand, in the 80's showed that carbonation of the silica caused cement with higher concentrations of silica to rapidly develop high porosity. This work determined that the addition of between 15% to 20% of silica flour (BWOC) provided sufficient thermal stability but was not susceptible to attack by the CO_2 rich fluids commonly found in all geothermal systems.

More recently, the use of blast furnace slag with Class A Portland cement blended in the ratio of 30 : 70 has been found to provide a highly corrosion resistant cement, along with enhanced mixing and pumping properties.

This blend produces a slurry with more thixotropic properties, making it more suitable for use in permeable formations – a characteristic of nearly all geothermal systems. In addition the early and final compressive strengths of this blend are significantly higher than those of the standard API cements.

Additives

In addition to silica flour or blast furnace slag materials mentioned above, a selection of additives are included in the slurry blend.

- Retarders – when high bottom hole circulating temperatures are expected, a retarder is added to prevent set-up prior to completion of pumping of the slurry. Careful estimation and testing, where possible, of the maximum and minimum circulating temperatures is required such that the correct retarder and concentration is utilised to avoid flash setting, or very long setup times of the slurry in cooler sections of the well.
- Friction reducers – are added to the slurry to reduce slurry shear stress and hence pumping pressures.
- Fluid Loss control agents - the requirement to cement the total length of each casing in 'under pressured' reservoirs results in a tendency for the water fraction of the cement slurry being lost to the formation. This dehydration process can result in annular bridging with high water loss slurries. The addition of fluid loss agents binds the water fraction within the slurry, reducing this tendency.
- Free water additive – Wyoming bentonite and /or a specialised free water agent is added to the slurry to ensure no free water evolves during cement setup.
- Mica - Loss of circulation during the cementing process is a persistent problem. It is critically important that organic LCM materials, traditionally utilised in drilling mud formulations, is not used for cementing casings. Organic LCM materials may achieve the objective of sealing the permeable zones by accumulating and blocking the permeability, but after the well is completed and has heated up, this organic material will be carbonised, leaving high porosity within the loss zones providing a flow path for possibly corrosive formation fluids. The use of medium to finely ground mica flakes, which are completely inert and non-sensitive to temperature, dry blended into the cement has been found to be very effective.

Mix Water

It is important that the mix water to be used in the cement slurry is tested by the cement laboratory to ensure suitability. Water contaminated with geothermal brine fluids, or with dissolved organic materials can significantly alter the behaviour of the cement slurry, and the final properties of the cement.

CEMENTING PReparations

Slurry Design Laboratory Tests

Prior to drafting a cementing programme, including calculating cement slurry volumes and materials requirements, it is important that estimates of the bottom hole circulating and bottom hole static temperatures at the programmed casing depths are estimated on the basis of experience from adjacent wells or, if there are no nearby wells, on the basis of the scientific survey information of the field.

The cementing laboratory will carry out slurry design tests that will provide the best estimate for quantities of additives, slurry yield, mix water requirements, slurry gelling times and allowable pumping times.

Cementing Programme Preparation

Utilising the laboratory slurry design data, and the physical data of the casings in place, the new hole drilled, and casing to be cemented, a cementing programme detailing each step of the cementing procedure is prepared and issued. This programme will detail volumes of pre flush, scavenge slurry, main slurry, and displacement to be pumped, pumping rates and pressure limitations.

Hole and Casing Volume Calculations

It is usual to break the well volume calculations into a series of volume components:-

- Casing contents – the volume of fluid contained within the casing from the surface down to the float collar.
- Shoe track – the volume of fluid contained within the casing from the float collar down to the casing shoe.
- Rat hole – the new open hole volume from the depth of the casing shoe to the total drilled depth – typically a 'rat hole' of 2 to 3 metres is left from the depth of the bottom of the casing shoe to final drilled depth – this rat hole is left such that any cuttings or debris can settle on the hole bottom without interfering with the casing shoe.
- Casing to open hole annulus – the volume of the annulus between the new casing and the open hole from the casing shoe depth up to the previous casing shoe depth.
- Casing to casing annulus – the volume of the annulus between the new casing and the previous casing, from the previous casing shoe depth to the surface.

Excess Volume to be Pumped

The calculation of slurry volumes to be pumped must include allowances for displacement of contaminated slurry, over gauge hole and losses to the formation. It is usual that an excess of between 100% and 150% is applied to the rat hole volume plus the casing to open hole annulus volume.

Total Slurry Volume = Shoe track volume + (Rat hole volume + casing to open hole Volume) x (1 + 'excess') + casing to casing annulus volume.

Where 'excess' = 1.0 to 1.5 - depending on hole conditions.

CEMENTING PROCEDURES

Pre – Cementing

Prior to picking up the final joint of casing to run in, it is usual that a circulating swage and circulation hose is made up to the top of the joint of casing. When this joint is made up, circulation of fluids through the casing is commenced and the final joint washed down to the final setting depth. This procedure is carried out to ensure any settled cuttings or debris is washed away from the casing shoe as it is lowered toward the bottom of the hole, preventing possible blockage of the casing shoe port.

Circulation to Cool the Well

Once the casing is down to depth, pumping of fluid is continued to cool the hole down as much as is possible. This process may take a period of a few hours.
During this period the casing should reciprocated continuously.

Reduce Mud Gel Strength

It is usual that bentonite mud will have been used as drilling fluid to production casing shoe depth. Prior to cementing it is desirable that the mud viscosity and gel strength be reduced as much as is possible, and that wall cake that may have built up on the hole wall and casing be stripped away. The addition of mud thinners and deflocculants will aid in this process.
If the formations drilled have proven to be non-sensitive to water, and no swelling clays have been encountered, once the gel strength has been fully reduce, the mud is displace from the well, and water circulated in its place.
If water sensitive formations have been encountered then this step of displacing the mud to water is omitted.

Pressure Test

When the circulating fluid return temperatures have fully stabilised, indicating the well has been cooled, and the circulating drilling mud has been thinned or displaced from the hole with water, the drilling mud pumps are disconnected from the

casing, and the cementing unit line connected up and pressure tested.

Pre-Flush

A volume of water or proprietary pre-flush fluid is pumped to the casing. This pre-flush is typically just water, but may include mud stripping agents, or a sodium silicate based pre-flush fluid to aid in blocking permeable formation zones. Typically the volume of this pre-flush will be in the order of 5,000 litres.

Scavenge Slurry

Immediately after the pre-flush has been pumped, a bottom travelling plug will be released if the 'through the casing' cementing technique is being used. A volume of lightweight scavenge slurry is then pumped. This scavenge slurry typically has a specific gravity of around 1.2, and is pumped to scour any remaining mud and mud cake from the annulus. The dilute cement slurry rapidly flocculates any remaining mud allowing it to be easily washed with the scavenge slurry. Typically a volume 5,000 to 20,000 litres of scavenge slurry is pumped, depending the hole and casing sizes and depth, and on whether the mud has been previously displaced from the hole or not.

Main Slurry

After the scavenge slurry has been pumped, the slurry weight will be increased to the main slurry design weight which is typically a specific gravity of 1.87.

The main slurry is pumped at flow rates of around 800 litres per minute to ensure turbulent flow occurs within the annulus – this flow rate is also typically the practical maximum flow rate that most cement mixing and pumping units utilised on geothermal wells can operate at satisfactorily. During mixing and pumping of the main slurry, samples are periodically collected weighed and stored such that the slurry setup can be monitored.

Displacement

When the specified slurry volume has been pumped, the top travelling plug is released, and water or drilling mud pumped into the casing behind the travelling plug to push the cement slurry out of the casing and up into the annulus.

During displacement, and as long as returns of circulation are maintained, the returned fluid is carefully monitored and samples of returned cement slurry weighed and stored. While displacement proceeds, the casing continuously reciprocated until it begins to 'stick' (which usually occurs at some point during the displacement), reciprocation is stopped and the casing set to height.

Displacement is continued until the top travelling plug is 'bumped' onto the float collar.

Inner String Cementing

Exactly the same procedures, in principal, are followed if the inner string method is used. When the casing has been run in to depth, washed to bottom; the annulus circulated for a period, then the casing is set in the rig rotary table, and the inner cementing string picked up; run into the casing; and stabbed into the float collar receptacle. Circulation is then commenced through the cementing string, to cool the well, reduce the gel strength of the mud, displace the mud from the hole if appropriate and continue with the procedures as detailed above.

Annulus Squeeze

If displacement is completed with full returns, and the quality of the returned cement is good, the final procedure is to wait for a period of about 30 minutes for the cement to 'settle', and then to top up the annulus and apply a slight 'squeeze' to ensure cement is forced slightly into the formation and to ensure a good bond with the casing.

The cementing line is flushed to ensure only good quality cement is in the line, which is then connected up to one of the side outlets on the casing head – typically the 'kill line' outlet, the other 'Choke line' outlet is open and cement is pumped slowly until slurry flows from the open choke line valve indicating that the annulus has been 'topped up'. The choke line valve is then closed, and the annular BOP is 'soft closed' around the casing (with a lowered closing pressure to ensure the casing is not deformed by the annular BOP). Cement is then pumped very slowly until a pressure of around 0.35 MPa can be held. This 'squeeze' pressure is held for a period of 30 minutes, then released.

The cementing process is now complete and operations halted while the cement slurry sets up – waiting on cement (WOC).

Loss of Circulation

Of course, the permeable and under-pressured nature of the formations into which the casings of a geothermal well are being cemented means that circulating a high density cement slurry with specific gravities ranging from 1.7 to 1.9, inevitably result in loss of circulation during the cementing procedure.

The traditional method of mitigating this problem was to attempt to seal all permeability with cement plugs as drilling proceeded, however, this is usually an extremely time consuming process, and more often than not, circulation is still lost during the casing cementing process.

Many approaches to overcome this problem have been tried, and include:-

- Low density cement slurry additives – pozzalan, perlite, ceramic spheres
- Sodium silicate based sealing preflush
- Foamed cement
- Stage cementing
- Tie back casing strings – the casing is run and cemented in two separate operations.

Many of these options have been and are still being tried but generally none have proven totally successful nor economic.

To date, in the experience of the author, the most successful procedure has been to utilise the most simple high density cement slurry blend, and to concentrate on the techniques of placing the cement such that a full return to the surface without fluid inclusions can be achieved. This nearly always involves a primary cement job carried out through the casing, and in the event of a poor or no return and immediate annulus flushing procedure, which is then followed by an initial backfill cement job through the casing to casing annulus, with sometimes repeated top-up cement jobs. Particular care must be taken to avoid entrapment of any water within the casing to casing annulus.

Flushing the Annulus

In the event that while pumping the cement, or the displacement, returns to the surface stop partially or totally, this indicates that circulation has been lost. The cement slurry is flowing out into the formation rather than up the annulus. This is a very common occurrence when cementing casings in geothermal wells.

Pumping of the cement and displacement is continued, without stopping until the programmed cement slurry and displacement volumes have been pumped and the top travelling plug has been 'bumped'.

A line from the cementing unit is then immediately connected to the kill line outlet on the wellhead, and the annular BOP soft closed around the casing. Water is then immediately pumped to annulus to flush any cement that may have moved up into casing to casing annulus out. A volume of at least 1.5 times the casing to casing annulus volume is pumped. When pumping of the volume of flush water to the annulus by the cementing unit is complete, the rig pumps are then connected to the kill line valve, and water is pumped slowly and continuously to the ensure the flow path to the loss zone is maintained in an open condition. While the rig is pumping this water, the cementing unit prepares to pump the primary back fill cement slurry.

Primary Back Fill

As soon as pumping the annulus flush volume is completed, and the drilling rig pumps have taken over pumping top the annulus, a cement slurry of the same constituency as the main cement job, but without retarders, is mixed and made ready for pumping. When ready, pumping of water to the annulus by the rig is ceased, the cementing unit is reconnected to the kill line outlet. A volume of approximately the sum of the casing to casing annulus volume plus the open hole annulus volume is then pumped to the annulus. The density of this slurry is to be as for the main cement slurry – specific gravity of 1.87.

It is important that the entire programmed volume of this primary backfill is pumped, even if the annulus begins to build pressure – however, ensuring that the collapse pressure of the casing being cemented, and the burst pressure of the outer casing are not exceeded. Usually the annulus does not pressure up in this situation.

If, when the total programmed primary backfill volume has been pumped, the annulus remains pressured and the annulus is full of cement and remains so, then the procedure of applying a 'squeeze', as detailed above is carried out.

If on the other hand no pressure is evident and the annulus is not filled with cement, which is normally the case, the kill line valve is shut in; the cementing line disconnected; and the cementing unit and flow line flushed and cleaned up. All entries to the casing annulus must remain closed and absolutely no water is to be used near the wellhead to avoid any water entering the annulus.

The primary backfill cement is left for a period of 4 to 6 hours to begin setting up.

Top Up and Hesitation Cementing

After samples of the primary cement slurry indicate that the cement has gelled and begun setting up, the annulus is to be topped up and a squeeze applied.

When the top up cement slurry, (which is to be the same consistency as the main cement slurry, but without retarders), is ready to be pumped, the choke line valves are to be opened, the cementing

line flushed with good quality cement slurry, and then connected to the kill line valve. A volume of no more than 2500 litres of slurry is to be pumped. If returns are achieved then the 'Annulus Squeeze' procedure as detailed above is to be commenced. If no return is achieved when the 2500 litres has been pumped, the valves to the annulus are to be closed, the cement line broken off and the cementing unit cleaned up.

The top up cement is to be left to gel for a period of around 4 hours, and then this top up procedure repeated until a return to the surface is achieved.

Typically, returns are achieved on the first or second top up. The completion of the final top up and squeeze marks the completion of the casing cementing programme.

References

Hole, H.M., 1996. "Seminar on Geothermal Drilling Engineering – March 1996, Jakarta, Indonesia", Seminar Text, Geothermal Energy New Zealand Limited, Auckland, New Zealand.

Gabolde, G., Nguyen, J.P, 1999. "Drilling Data Handbook – Seventh Edition". Institut Francais du Pétrole Publications.

NZS 2403:1991, "Code of Practice for Deep Geothermal Wells" Standards Association of New Zealand.

GEOTHERMAL WELL DRILLING SERVICES CONTRACTS

Hagen Hole
Geothermal Consultants NZ Ltd., Birkenhead, Auckland, New Zealand.

ABSTRACT

The contract environments that are currently utilised by the geothermal well drilling industry range from unit time rate, unit metre rate, through to turnkey contracts. This paper reviews the associated benefits and drawbacks of these various contract formats.

Keywords: geothermal, drilling, drilling services contract.

INTRODUCTION

Iceland's current geothermal drilling operations are being executed under drilling service contract structures which are predominantly metre-rate and 'turnkey' in nature. This is in contrast to the contract environments currently adopted in recent New Zealand, Kenyan and Indonesian geothermal drilling operations which are predominantly 'unit time rate' contracts.

Components of a Geothermal Drilling Operation

Any geothermal drilling operation includes a wide range of activities and processes all of which must be provided and executed. These activities and processes will include, but not necessarily be limited to:-

- Reservoir engineering and well targeting
- Well design and specification
- Drilling materials specification and procurement
- Well pad, access road civil design and engineering
- Water supply design and engineering
- Civil construction supervision
- Well drilling engineering and supervision
- Provision of drilling rig and equipment
- Provision of drilling personnel
- Provision of top drive unit and personnel
- Provision of cementing equipment, personnel and services
- Provision of directional drilling equipment and personnel
- Provision of mud engineering personnel
- Provision of aerated drilling equipment and personnel
- Provision of mud logging / geology equipment and personnel
- Drilling tool rental
- Drillpipe inspection
- Drillpipe hard-banding
- Provision of well measurements equipment and personnel

These activities and processes may be provided to an Owner under a large number of totally separate and discrete service contracts, or conversely under one lead contract, or any mix between these two extremes.
An Owner who desires to drill a geothermal well, will have to decide on what contractual basis each and every one of these activities and process is to be provided. The level of control, responsibility and risk that the Owner wishes to take, will determine the mix between having many separate contracts or just one lead contract.

Geothermal Owner Risks

Owner risk could be defined as the 'potential cost to the Owner if the actual outcome of an operation does not match the planned and expected outcome'.

An Owner carrying out a geothermal drilling operation is faced with a number of risk components. Unlike a building or civil construction project, a drilling operation involves a significant 'unknown' factor.
A building or civil construction project is generally carried out on the basis of a 'blue-print' – a detailed plan of exactly how the construction process will occur and be completed. While the 'blue-print' can never totally eliminate all unknowns, the majority of the activities relate to 'visible' and tangible situations.
In comparison a drilling operation is based on a 'nominal' programme, which is based on 'best estimates' only, and deals with 'invisible' and 'interpreted' situations.

Responsibility, control and Risk

The 'scope of work' of a drilling services contract will define clearly the split of responsibility between the Owner and the Contractor.
For example, the contract may define that the Contractor is responsible for maintaining sufficient fuel on the rig site to ensure no interruption in the drilling activities. The contract may define that the cost of the fuel is carried directly by the Owner, or by the Contractor who shall be reimbursed with an appropriate mark-up. The responsibilities, as defined, place control of ordering and procurement of fuel with the Contractor. The Contractor carries the operational risk that in the event that he fails to maintain sufficient fuel on site and drilling operations are effected then he will be penalised accordingly – most likely he will not be paid for the period of lost time.
The Contractor will factor into his fee structure an amount to cover the possibility that he will be penalised at some stage.

Operational responsibility, control and risk are all interlinked. Operational responsibility implies operational control, but imposes operational risk, as depicted in Figure 1.

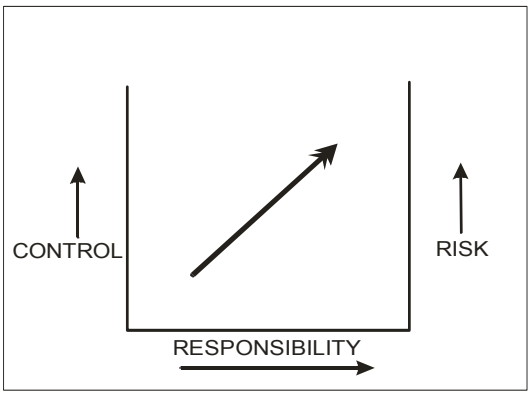

Figure 1. Responsibility, Control and Risk Matrix

An Owner who may decide to take technical and managerial responsibility, receives operational control but must accept the consequential risk.
This situation is implied when an Owner selects to enlist all, or a significant proportion, of the activities and process under separate and discrete contracts.

Typically an Owner may have within its own resources a geoscientific and engineering capability (or separately contracted these capabilities through a consultant). The reservoir engineering and well targeting; the well design, materials specification and procurement; the drilling pad and access road civil design and construction supervision; and finally the drilling engineering and drilling supervision, will all be provided by the Owner through his 'in-house' or consultant capabilities.
The drilling services contract in this scenario would typically be a simple unit day rate contract – the Owner is simply renting the drilling equipment and personnel required to operate it. The Owner is fully responsible for instructing the Contractor through each and every step of the operation, and has total control on how each step will be performed. The Owner carries all the operational responsibility, and of course all the operational risk. If there are some downhole problems and delays to progress, the Owner continues to pay the daily fee rate.

In contrast to this model, the Owner may decide that the operational responsibility and control should lie totally with the Contractor, a contractual model generally termed 'Turnkey'. In essence the scope of work given to the Contractor could be – "drill me a geothermal well in this particular place into this particular reservoir – come back and tell me when it is finished". The Owner may have no 'in-house' technical capability, and may not have the required managerial resources. The Contractor in this case, is totally responsible, has full control of how and when activities occur, and carries all of the operational risk.
The price the Contractor will charge the Owner will include an amount to cover the equipment rental and personnel, a management component, and an operational risk component – these management and risk components can be significant.

The Cost of Operational Risk

In comparing these two extreme contract models the costs of the equipment rental and personnel components should be the same.
The cost of the management component should be similar, either the Owner pays for his own resources or he contracts them in either through a consultant hired directly by the Owner, or through the Contractor.

It is the cost of the operational risk component that will be significantly different. In the case where the Owner takes full responsibility, he will incur costs associated with risk only in the event that a problem occurs. The Owner will pay for

additional rig time only in the event that there is a problem causing a delay.

In the Turnkey contractual model, the Contractor will have to assess the likelihood of problems occurring, and will build into his price a component to cover such an occurrence. Of course his objective will be that he will 'manage' the operation successfully and avoid problems, turning the operational risk component of the price into a pure profit component.

The difference to the Owner is that he will pay the operational risk component whether a problem occurs or not.

Downhole Risk

A significant sub-set of geothermal drilling operational risk is the downhole risk – the risk of losing drilling equipment down the hole, and the risk of losing the hole itself in part or in full. Typically, drilling contracts pass the downhole risk, in full, to the Owner. That is, any damage to or loss of equipment that occurs below ground level, and any damage to or loss of the hole itself is generally always to the full account of the Owner. The only exception will be when proven negligence by the Contractor can be shown to the cause of the loss.
In Turnkey type contracts there is often a proportional responsibility, where even though the Contractor has full responsibility and control of the operation, some proportion of the cost of covering the downhole loss or damage will be borne by the Owner.

Resource Risk

Perhaps the most significant Owner risk is the production (or reinjection) success of the completed well, generally termed the resource risk. This form of risk is obviously extreme in the case of exploration and green-field wells, and will be inversely proportional to quantity and quality of the geoscientific survey work carried out. The resource diminishes as understanding of the reservoir structure and the nature of the resource and formation increases. With each well drilled and completed comes a better understanding of the formations and the resource, resulting in the lowering the resource risk.

It is extremely uncommon that an Owner can pass the resource risk to others through a contract structure. One example where this can occur, is a steam production based drilling contract – where the Contractor is paid for drilling a well on the basis of the mass flow or the Megawatts of electricity produced from the completed well. This type of contract was used for a short period in New Zealand, but as far as the author is aware, with unsatisfactory results.

Consequential Risk

In the event that some significant drilling delay occurs or the productivity of a well or wells is not as expected, delays to commencement of planned generating may occur. The lost revenue, and possibly penalties for non-supply may be a result, and would fall into the category of a consequential loss. This type of loss is typically covered by insurance, but unless negligence can be proven, must be to the account of the Owner.

Financial Risk

The Owner of a geothermal drilling operation will usually be constrained to a financial budget of some form while executing the operation.
If an Owner desires full technical control of a drilling operation and accepts the associated responsibilities and risks, this normally leads to some form of a unit time rate contract, which will impose a financial risk with respect to the budget. By definition a unit time rate contract is unlikely to be completed 'on-budget', there is a chance that the well be completed 'under-budget', and there is a financial risk that the cost of completing the well will exceed the budget.
The only way an Owner can minimise the financial risk is by converting all or part of the drilling operation to a fixed or 'lump sum' contract. Any 'conversion' to a fixed fee, shifts responsibility and therefore control back to the Contractor and away from the Owner.

An Owner's Choice

The Owner of a geothermal drilling operation is faced with balancing the level of technical and managerial control of the drilling operation he desires, against the level of operational and financial risk he is willing to accept.

Observations

The trend observed recently in operations in New Zealand, Kenya and Indonesia, has been toward unit time rate contracting with owners demanding full technical and managerial control, with a willingness to accept the operational and financial risks.

The upswing in demand from the oil industry over the past five years has created a shortage of available drilling rigs and suitably qualified personnel, which has in turn hardened the market and reduced the willingness of drilling Contractors to accept risk unless significantly higher levels of compensation are offered.

As stated in the Introduction, this situation is in clear contrast to the current practice in Iceland, where it is evident that a unit metre rate contract structure that places significant operational risk with the Contractor is practiced and accepted by both Owners and Contractors.

The drilling Contractors that are, or were, operating in New Zealand, Kenya and Indonesia are without exception Contractors that operate predominantly in the Oil industry, with only relatively small involvement in the geothermal industry. It is evident that the reverse is the case for the Iceland based drilling Contractors.

References

Hole, H M., 2001, "Geothermal Drilling", Geothermal Institute, University of Auckland, Auckland New Zealand, Paper 665.620.

Drilling, Completion and Testing of Geothermal Wells

Section 6. Miscellaneous, Drilling/Completion Related, Issues

1. PRODUCTION/INJECTION EQUIPMENT

Pierre Ungemach, Miklos Antics

GPC INSTRUMENTATION PROCESS, Roissy-en-France, France

SUMMARY/ABSTRACT

This section addresses the equipments of the so-called geothermal loop which include (i) for high enthalpy systems, the steam-brine high and low pressure separators and the high and low pressure brine processing facilities required prior to injection, and (ii) for low enthalpy – mainly geothermal district heating (GDH) – systems, the submersible pump set, the injection pump, associated regulation/control (medium voltage transformer, variable speed drive, current filtering, etc…) electromechanical equipment, heat exchangers and brine treatment facilities (downhole chemical inhibition lines and filtering devices).

1 HIGH ENTHALPY SYSTEMS

A typical geothermal loop design is sketched in fig. 1 chain. It includes, downstream from the production, two phase flowing well head and upstream of the injection well head, the following units (i) a high pressure (HP) steam-brine separator, (ii) a HP scale handling equipment, (iii) a low pressure (LP) steam brine separator, and (iv) a LP brine processing facility [Cioppi, et al, 1982, Vetter and Kandarpa, 1982].

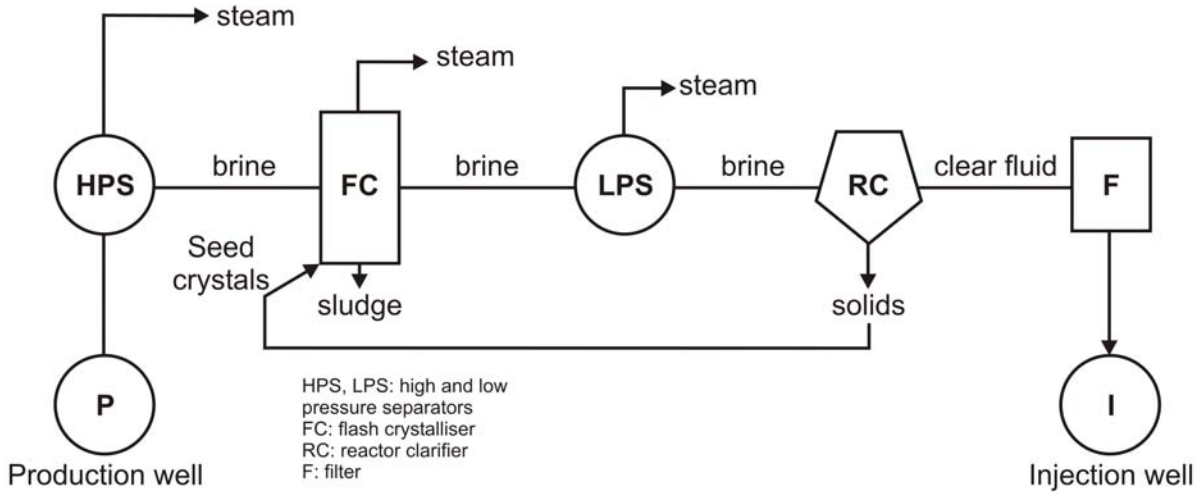

Figure 1: The steam brine separation and processing chain

1.1 Steam-brine separators

Quite often HP separators are of the vertical type and LP separators of the horizontal type.

Separators of the type (vertical) shown in fig. 2 and 3 act as cyclone separators at high flow rates and as gravity separators at low flow rates. They use the forced vortex principle, the fluid being introduced into the cylindric vessel via a streamline or tangential inlet.

Their height to diameter ratio varies between 5 and 7 and the separation efficiency stands higher to 99.9% which means that liquid carry over remains below 1 g per liter reservoir brine per liter of condensate.

Two basic designs are in use, either vertical or horizontal vessels, whose pros and cons, based on the Icelandic experience, discussed by Eliasson [2001] are summarised in table 1.

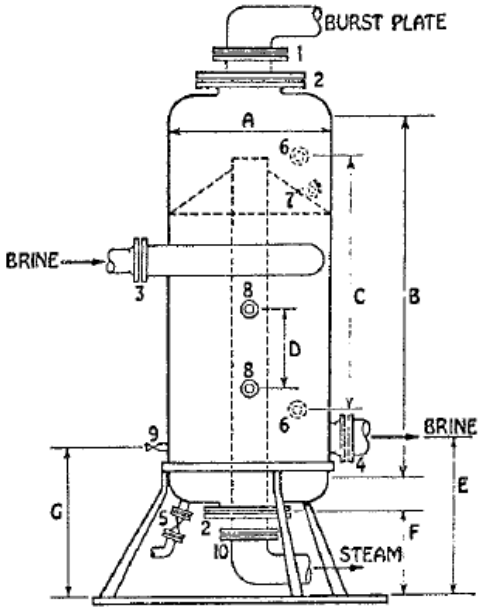

Figure 2: Separator (not to scale) [Cioppi et al, 1982]

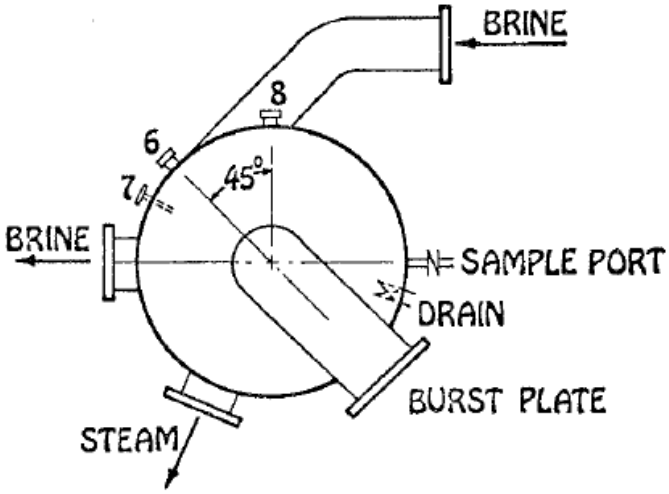

Figure 3: Separator (top view) [Cioppi et al, 1982]

Table 1: Summary of separator design features [Eliasson, 2001]

Type	Separation principle	Inlet	Discharge	Pros	Cons
Vertical	Centriful cyclone	Streamline	Radial	Sharper cut-off Cleaner stream wide pressure range Easy maintenance	Size limitations Height of construction
Horizontal	Gravity	Tangential	Tangential	Non contraining Larger throughput/unit	Lower steam quality (requires demisters) Greater maintenance

1.2 Flash crystallizers

The idea behind the flash crystallizing concept is not to avoid precipitation of solids, but to enhance it instead under controlled conditions in order to keep the flow facilities free of scale and precipitated solids in suspension.

A typical flash crystallizer concept is illustrated in fig. 4. The prime objective is to initiate the seeding process. Seed crystals obtained from the reactor-clarifier are forced into a pressure flash chamber which incidentally acts also as a separator. After removing the steam, precipitation will now take place in the brine seed mixture i.e. on the supplied seed crystals instead of equipment walls.

This design is very attractive to operators because of its basic simplicity. However, it presents a series of severe drawbacks with respect to environmental (silica disposal) considerations and mineral by product recovery which becomes economically unattractive (flotation processes).

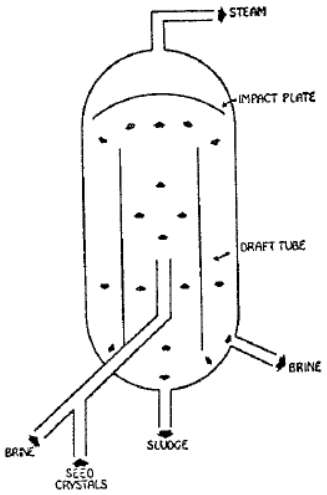

Figure 4: Flash crystallizer principle [Cioppi et al, 1982]

1.3 Brine processing (reactor clarificaction, filtration) facilities

Treatment of heat depleted brines is often overlooked in field development. It should be borne in mind that the brine exposed to atmospheric pressure conditions is still at its boiling point temperature and is supersaturated with respect to numerous (siliceous among others) species ("amorphous silica") providing the seed for relevant precipitations. This means that most of the suspended particles must be removed to decrease dramatically the degree of supersaturation and that, simultaneously, the temperature of the clear brine must remain as high as possible. Hence, the brine treatment facility must fulfil three prerequisites:

(i) seed and grow particles;

(ii) remove grown particles;

(iii) prevent excessive temperature drops and residence times between particle removal and reinjection of the heat depleted brine.

1.3.1 Reactor-clarification

Fig. 5 and 6 describe the basic principles involved in brine reactor-clarification. It should be mentioned it is a conventional technique in cleaning municipal and communal waste waters adapted to the specific conditions (high reactivity and supersaturation) of the geothermal industry.

The reactor clarification process described in fig. 5, is split into three components (fig. 6):

(i) reactor of "draft tube" (particle nucleation section);

(ii) fluidised bed (particle growth section), and

(iii) settling bed (clarification section).

Reactor zone

The reactor vessel (fig. 7) is assigned five functions:

(i) atmospheric flash chamber;

(ii) silencer (low noise steam stack);

(iii) steam cleaner (demister device);

(iv) inlet brine flow gauging, and

(v) first clarification stage.

Seeding within the reactor is initiated by high brine circulation velocity, enhanced by a ca 700 l/min rated pump, enhancing particle collisions. Accordingly, precipitation grows on the suspended particles rather than on vessel walls. Effects of residence times can be studied by adjusting the liquid level in the reactor.

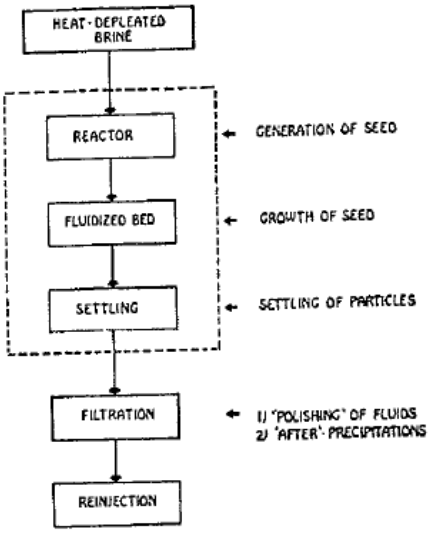

Figure 5: Principle of reactor-clarification [Cioppi et al, 1982]

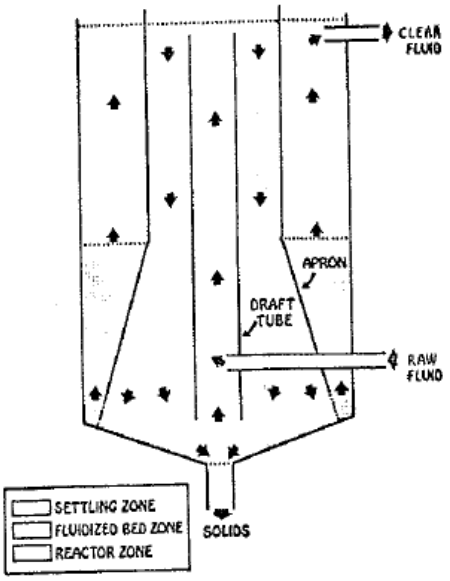

Figure 6: Principle of a geothermal reactor clarifier [Cioppi et al, 1982]

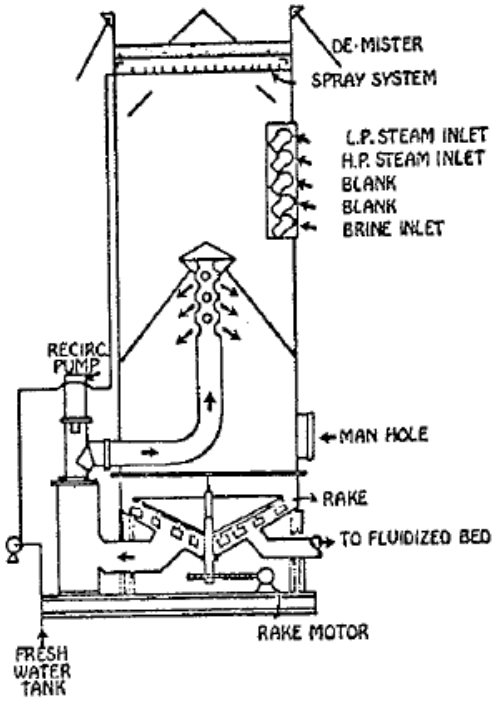

Figure 7: Reactor vessel [Cioppi et al, 1982]

Fluidised bed zone

The outlet brine from the reactor vessel is then transferred to fluidised bed tanks which are slowly recirculated in order to continue the crystallisation process initiated in the reactor. Here the objective is to grow particles and not to seed them. Their size should be such that they are able to settle within a short time in the downstream settling tanks. The effect of residence time on particle growth can be suitably studied in this system.

Settling bed zone

The settling bed system consists of four parallel tanks containing baffles, through which the brine containing the precipitate is forced. The flow is slow and linear to allow precipitates (sludge) to settle. Sludge volumes are monitored and, periodically vacuumed to avoid spillover into the filter tanks. Tank operation is controlled by temperatures rather than level measurements, because the self-floccing of suspended particles was found more sensitive to, even small, temperature changes than to flow variations.

1.3.2 Brine filtration

Filtration is operated by parallel mounted tanks filled with approximately four feet of graded filter media. The whole filter includes, from bottom to top, 3 gravel layers of decreasing grain size garnet gravel, fine garnet, sand and anthracite. Each tank is compartmented to reduce pump horsepower required for back washing whose frequency depends on solid concentrations, which in turn reduce filtering efficiency. Therefore, one tank is utilised as a spare that is back washed, while the others operate in filtering mode. Plugging by oxygen can be defeated by addition of oxygen scavengers (hydrazine).

2 LOW ENTHALPY SYSTEMS

Geothermal district heating (GDH) will be selected as a system representative of direct uses. Actually modern GDH undertakings may be regarded as technologically relevant, with respect to the geoheat utilisation spectrum.

2.1 GDH grid architecture

A typical design of a Paris Basin GDH grid is presented in fig. 8. It distinguishes two distinct systems, a subsurface system, the geothermal loop, which includes the mining production/injection infrastructures and a surface system, the distribution network supplying heat via substations and back-up/relief fossil fuel fired boilers, to end users. Both systems are interfaced by the geothermal heat exchanger.

The geothermal loop is based on the doublet concept of heat mining which combines a production well and an injection well pumping the heat depleted brine into the source reservoir.

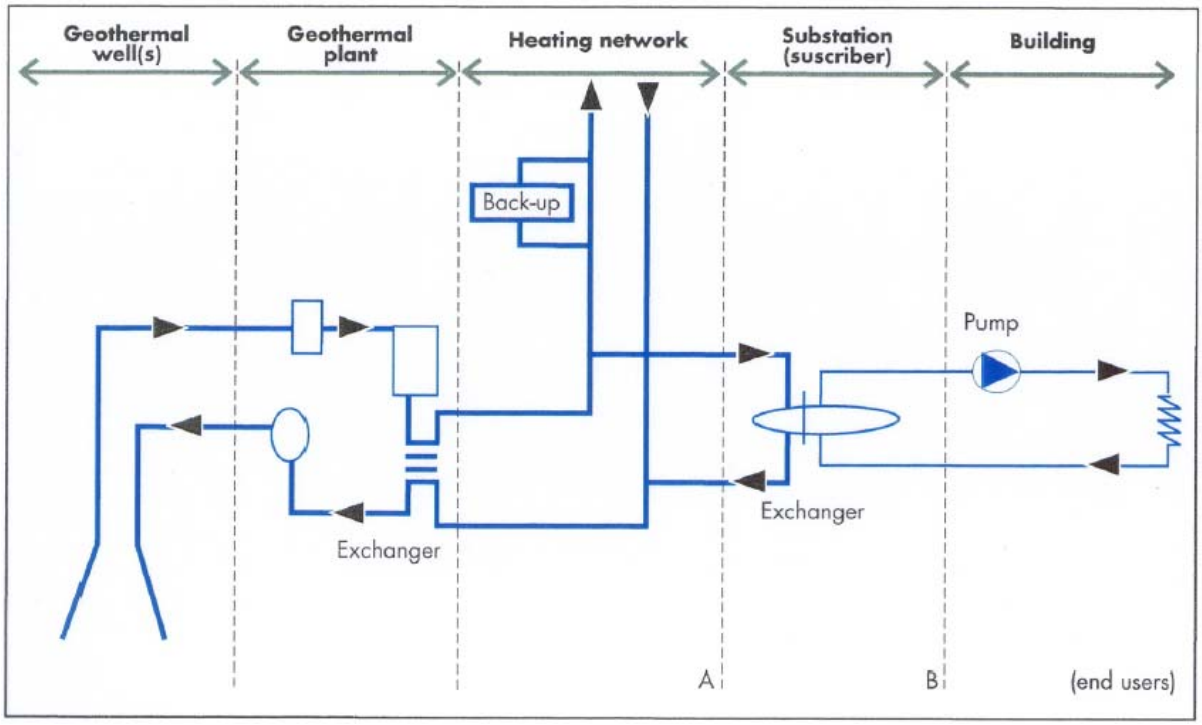

Figure 8: Geothermal district heating. Typical system design

2.2 Heat production

Various schemes, outlined in fig. 9, may be contemplated (i) a single well producing either in self flowing (SF) or artificial lift (AL) mode piped directly to the user and further wasted in the sewage system, which clearly addresses a fresh water resource, (ii) a single well producing a brine requiring a heat exchanger, the waste water being dumped into the sewage system, and (iii) the doublet scheme where the cooled brine is (re) injected into the geothermal reservoir.

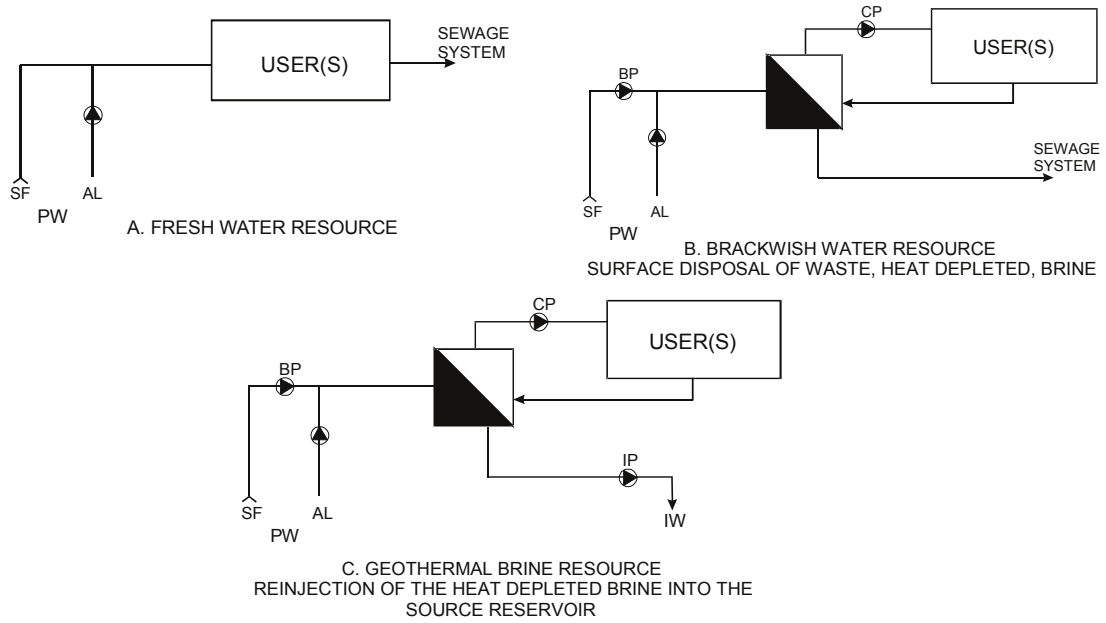

Figure 9: Space heating. Candidate heat extraction, waste heat disposal and injection schemes

2.2.1 Sustained production

The geothermal brine is pumped to surface at heat exchanger inlet via artificial lift (see fig. 10) calling for the three marketed pump sets, line shaft (LSP), electrosubmersible (ESP), and hydraulically driven turbine (HTP) described in fig. 11 alongside their figures of merit.

LSPs are extensively utilised in ground water supply for domestic (drinking, livestock) purposes. The downhole centrifugal pump is driven by a surface mounted motor via a lineshaft, either free or enclosed. The latter version has been developed for geothermal applications by Icelanders who designed a specific technology based on Teflon, abrasion resistant, bearings lubricated by the geothermal (instead of a makeup) fluid, which renders it compatible with high temperature (up to 160°C) service and environmentally friendly (no circulation of any exogenous makeup fluid whatsoever). LSPs are used in binary systems which structurally avoid in hole flashing.

One such unit is currently operating on the Soultz-sous-Forêts EGS pilot plant. Due to stringent shaft verticality constraints submersion depths should remain below 250 m, although greater depths have been reported.

ESPs are widely used in GDH systems as exemplified by Paris basin experience and performance records. Here, the induction, squirrel cage, motor is set in-hole which penalises to some extent motor efficiencies owing to obvious geometric limitations and subsequent elongated shapes. The motor and upward multi stage centrifugal pump are separated by a seal protector module. ESP are powered at generally medium voltages (maximum # 3 000 V) via transformers and coaxial and flat cables, the latter complying with the hole diameter restrictions. Recent ESP designs can cope with 160-170 °C downhole temperatures as recently demonstrated on the Soultz EGS plant site.

HTPs present the advantage of avoiding both in hole motors and shafts. A usually single stage centrifugal pump is driven by a high speed hydraulic turbine powered by a surface high pressure charge pump and an injection tubing. Pump intake and outlet are isolated by a sealing packer anchored below the pump/turbine assembly. The fluid is therefore produced in the casing energizing tubing annulus as shown in fig. 11c. Noteworthy is that the energizing fluid is provided by a fraction of the geothermal fluid diverted from the production line. Unfortunately, this appealing concept is mitigated by poor efficiencies as a result of an additional conversion item. Actually it hardly reaches 40% compared to 60-65% ESPs and LSPs conversion efficiencies.

Other, minor, pros and cons are listed in fig. 11 summary sheet. Important to note is that all artificial lift systems operate at variable speed, controlled by electronic frequency converters, to adjust to varying outdoor temperatures and heat demand of the grid.

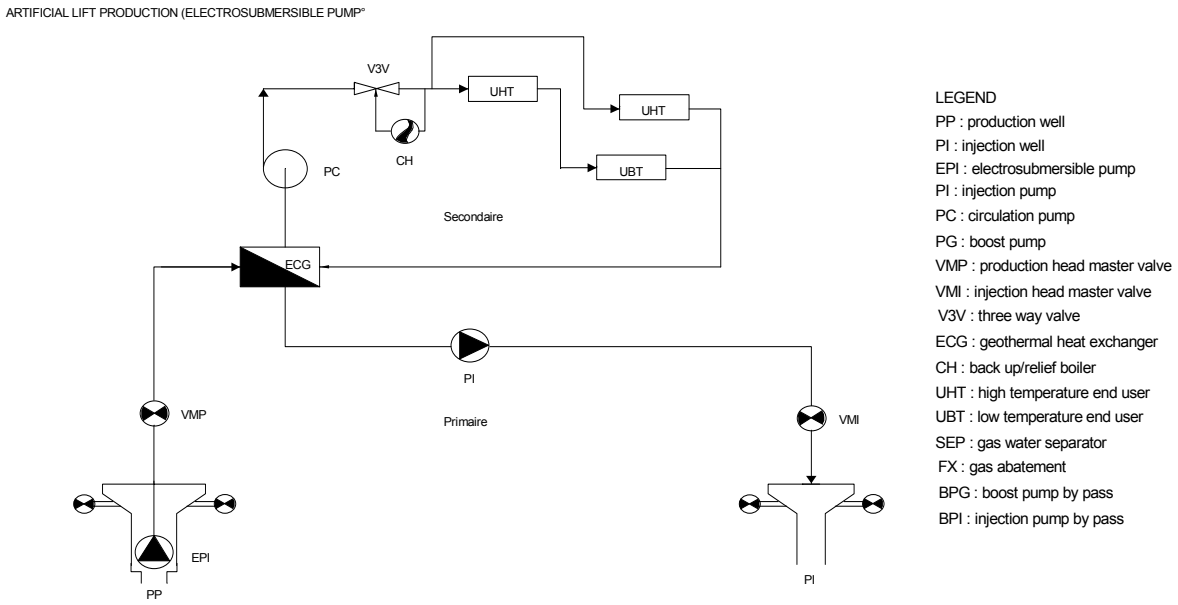

Figure 10: Geothermal loop. Sustained production mode

Figure 11: Artificial lift options. Downhole pump figures of merit [Ungemach, 2004]

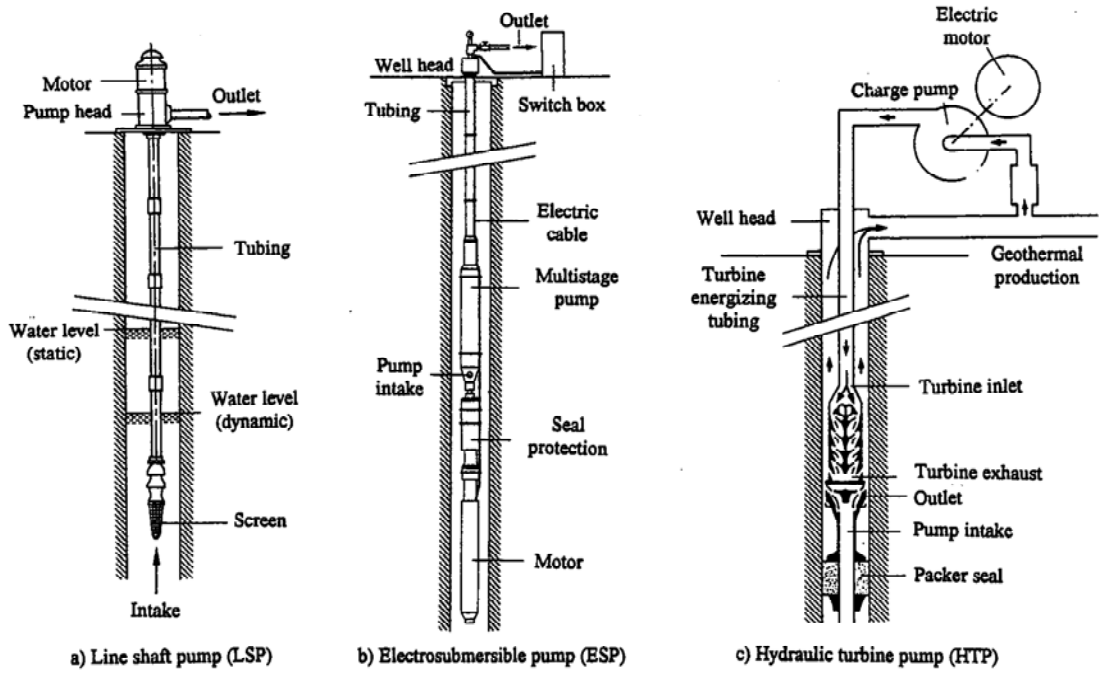

Figure 11: Artificial lift options. Downhole pump figures of merit [Ungemach, 2004]

Pump type	Pros	Cons
LSP	No electric parts in hole. Higher efficiency (surface motor). Long lifetime. Withstands high temperatures. Attractive costs.	Depths limited to 200 m. Delicate handling (installation/removal). Definition of enclosing tubing coating and bearing materials.
ESP	High submersion depths. Long lifetime. High flowrates in limited casing TD's (250 m3/hr in 9"5/8). Withstands high temperatures. Solution gas handling (in hole separator). Worldwide service factilities.	Lower efficiency. Electric insulation shortcomings. Higher costs.
HTP	Very long lifetime. No electric parts in hole. Withstands very high temperatures.	Low efficiency (additional energy conversion item). Large diameters (OD's) required. Packer anchoring problems. High costs. Limited manufacturing/service facilities.

2.2.2 Self flowing wells

Whenever authorised by overpressured well conditions, self flowing can substantiate high self flowing discharge rates at low well head pressures. This in turn requires (fig. 12) (i) a surface pump boosting well head pressure to heat exchanger inlet service pressure (generally close to 8-10 bars), and (ii) would well head flowing pressure fall below bubble point pressure, a solution gas separation/abatement outfit to cope with well head two phase (liquid and initially dissolved gas phase) flow and subsequent degassing. Fig. 13 depicts the designed solution gas separation/abatement line further portrayed in fig. 14 well head close up.

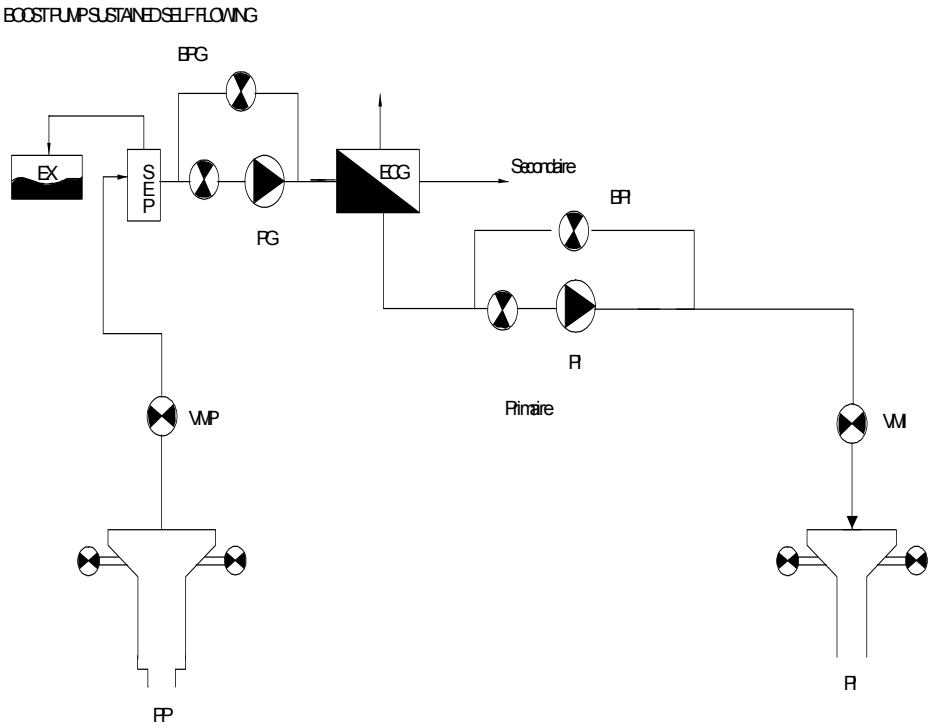

Figure 12: geothermal loop. Boost pump sustained self flowing mode

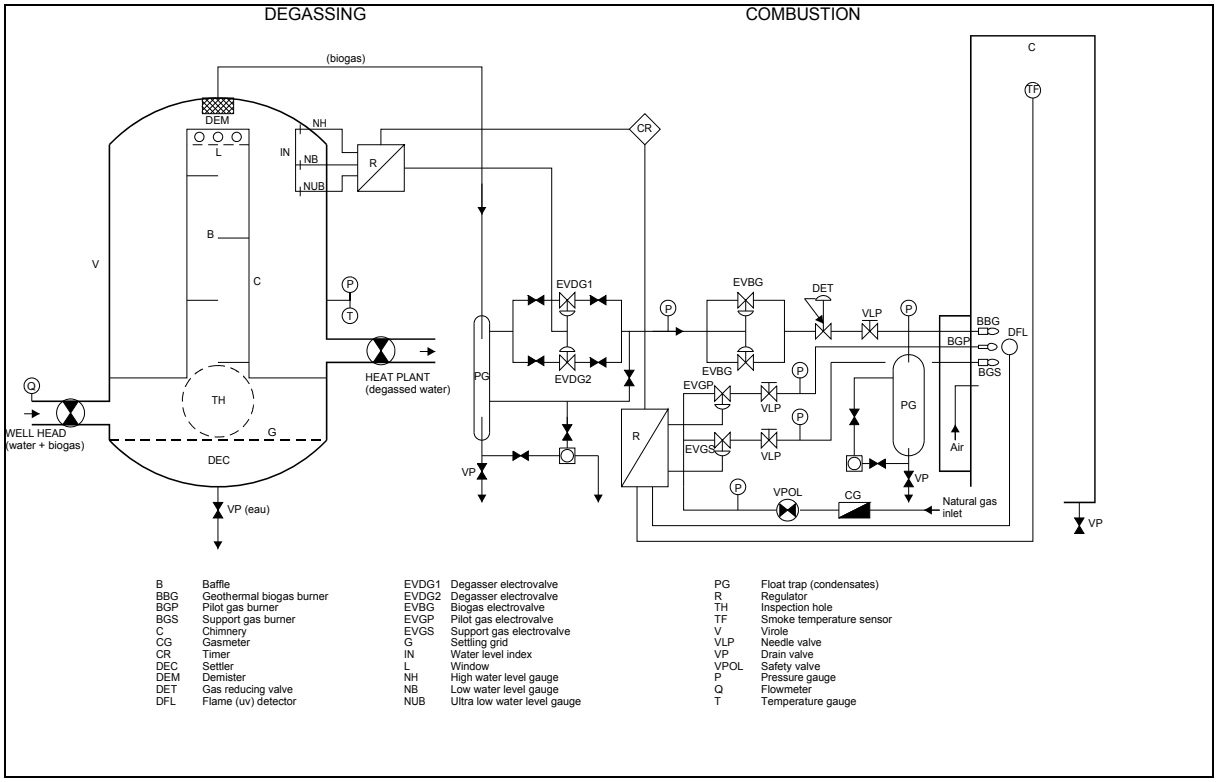

Figure 13:Geothermal biogas Degassing/Abatement line schematics [GPC]

Figure 14: Gas separation/abatement line [GPC]

2.3 Downhole chemical inhibition line

Most geothermal wells cope with thermochemically hostile fluid environments resulting, if not properly mitigated, in severe corrosion/scaling damage, a topic addressed in another section of the course.

The most reliable inhibition system implemented so far on Paris Basin GDH doublets consists of the AIT (Auxiliary Injection Tubing) coiled tubing type chemical injection line displayed in fig. 15. Such lines are compatible, depending on the encapsulated thermoplastics, with temperatures up to 190°C and with any artificial lift configuration.

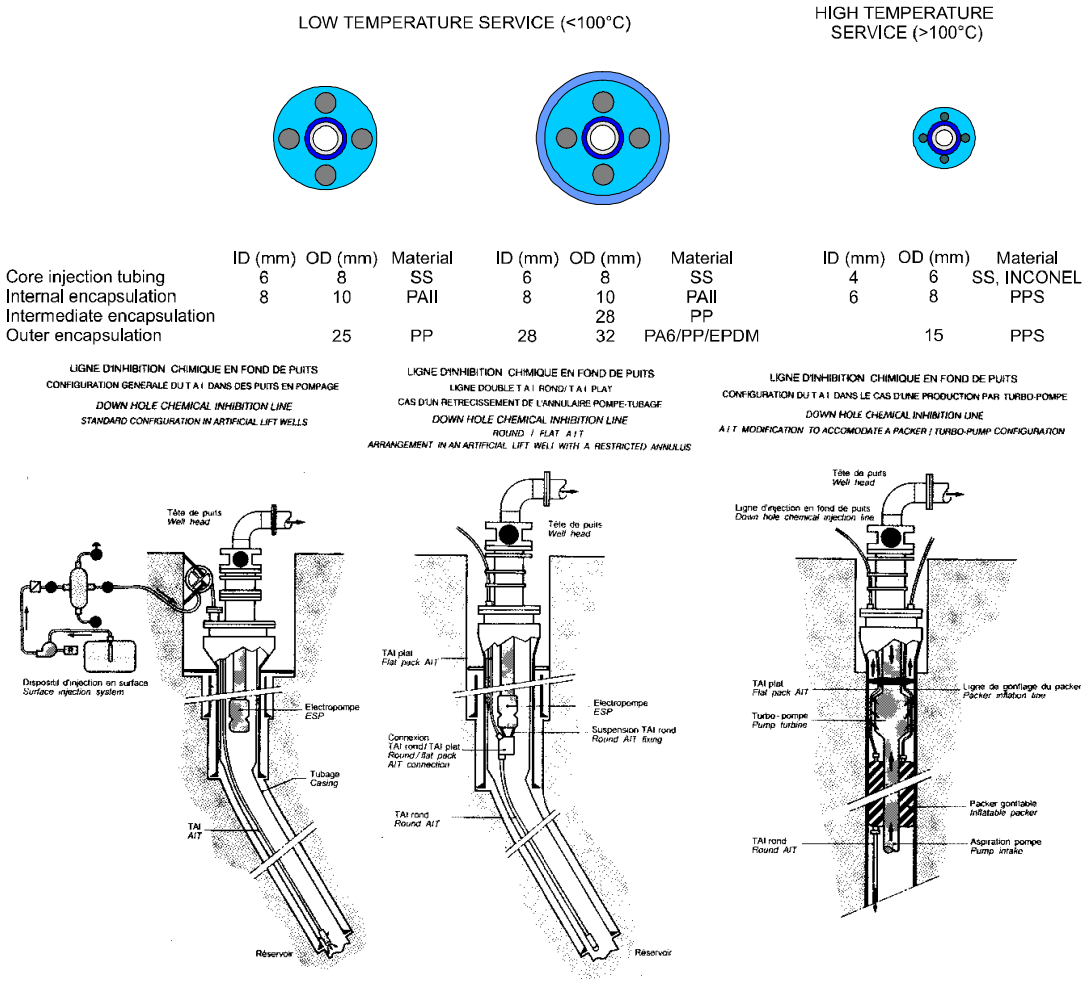

Figure 15: Downhole chemical inhibition. AIT lines [GPC]

2.4 Equipment reliability

Major geothermal loop equipment performances can be assessed through their lifetime records listed in table 2 which, in the case of the Paris Basin GDH systems, dates back to 30 years.

Table 2: Equipment performance and lifetime record [Ungemach, 2004]

ITEM	LIFE (yrs)
WELLS	20-25
XTREE VALVES	5
PRODUCTION PUMPS ESP HTP	 4-5 5-8
INJECTION PUMP *	10-15
PRODUCTION TUBING	6-8
DOWNHOLE CHEMICAL INJECTION LINE	5-8
PLATE HEAT EXCHANGER **	15-20
FREQUENCY CONVERTER *	15
SURFACE PIPING	15-20

* spare part replacement
** plate cleaning, joint replacement

REFERENCES

Cioppi, D., Quercia, F., Torre, G., Ungemach, P. And Vetter, O. (1982). A New Approach to Geothermal Production Testing. Recent Experiences in the USA and Italy. International Conference on Geothermal Energy, BHRA, Florence, Italy, May 11-14, 1982, paper D3, 235-252.

Vetter, O. and Kandarpa, V. (1982). Handling of Scale in Geothermal Operations. International Conference on Geothermal Energy, BHRA, Florence, Italy, May 11-14, 1982, paper 62, 355-372.

Ungemach, P. (2004). Carbonate Geothermal Reservoir Management in France. Int. Geoth. Days, IGD Poland 2004. Low Enth. Geoth. Resources Expl. and Development, Zakopane, 13-17 Sept. 2004.

2. WELL MONITORING, MAINTENANCE AND WORKOVER

Pierre Ungemach, Miklos Antics (*), Hagen Hole (**)

(*) GPC INSTRUMENTATION PROCESS, Roissy-en-France, France

(**) GCNZ, Aukland, New Zealand

SUMMARY/ABSTRACT

Well monitoring, maintenance and workover are vital post drilling, completion and testing phases. They aim at assessing fluid thermochemical behaviour, maintaining well integrities and ultimately secure reservoir longevity and sustainable system operation. This section will therefore focus on (i) high enthalpy (geopower) surface facilities designed to properly evaluate fluid scaling tendancies, clearly the main field development shortcoming, and (ii) maintenance and corrosion/scaling preventing policies implemented on a long exploited geothermal district heating scheme.

INTRODUCTION

As soon as wells have been completed, testing performed and hydrodynamic reservoir performance and well deliverants which assessed optimum system design and plant operation come into play.

With regard to high enthalpy, chiefly liquid dominated, reservoirs the crucial monitoring segment clearly addresses the assessment of fluid thermochemical properties and of its behaviour subject to various thermodynamic conditions and related, dominantly scaling, shortcomings which allow to select the adequate conversion cycle (single flash, dual flash, condency, back pressure atmospheric exhaust etc …) alongside fluid handling procedures.

Thermochemical damage can also affect direct use (geoheat) systems often facing sensitive fluid environments as exemplified by early Paris Basin GDH operations. As a result thorough monitoring and remedial protocols have been set up according to the mining and environmental regulation in force.

The foregoing are illustrated on two well documented sites dealing with (i) a high enthalpy fluid monitoring program, and (ii) a larger GDH system surveillance and maintenance policies.

1 HIGH ENTHALPY LIQUID DOMINATED SYSTEM

The integrated fluid processing facility being described in a previous section, we shall concentrate here on the fluid monitoring line and measurement procedures and devices. The general design of the line is shown in fig. 1 which consists briefly of three – two phase, steam, flashed brine – flow lines, a Russel James and two, pressurised and atmospheric, separators, associated brine (weir gauge) and steam (orifice meter) flow measurement devices and sampling ports controlled by appropriate valves and manifolds.

The gas/liquid, and simplified gas sampling facilities are presented in fig. 2 and 3 and the in line pH measurement outfit in fig. 4.

1.1 In-line sensors

1.1.1 Pressure measurements

Bourdon tubes are used for quick control and as a back-up devices for more accurate electronic transducers of the variable reluctance type. The flow interface at entry ports is handled via ball valves and cleaning rods.

1.1.2 Temperature measurements

They use bi-metallic thermometers in parallel with RTDs (resistance temperature devices) loosely inserted in thermo wells ports.

1.1.3 Flow rates

They are measured via four reliable gauging types, force meters, Pitot tubes, ultrasonic flow meters and orifice meters respectively.

1.1.4 pH meters

At high temperature the electrodes need to be restored, after short time exposure, by immersion into a cooling (ammonium fluoride solution) bath. The in line monitoring outfit is described in fig. 2

1.1.5 Corrosion measurements

Ultrasonic measurements controlling wall thicknesses can be utilised and combined with corrosion coupon, whenever corrosion metering devices fail.

1.1.6 Enthalpy measurement

Due to poorly reliable calorimetric methods, the Russel James lip pressure method for two phase flow is utilised instead, not to mention enthalpy derivation steam tables for separate water and steam phases

1.2 Sampling and chemical analyses

1.2.1 Sampling

Sampling deals only with single phase fluids at numerous locations, within the monitoring line. Assuming no unusual fluid behaviour occurs in the test unit, a minimum of 15 liquid and 12 gaseous samples should be collected on a daily basis at each location, to which must be added 9 samples of suspended particles at stations selected downstream from the brine treatment system. Scale samples are collected after shut-in i.e. after exposing the scale to atmosphere.

Liquids

Special care is required to overcome the problems caused when cooling thermodynamically unstable geothermal brines, mainly solid precipitations and gas redissolutions. Samples are therefore treated i.e. either acidized or/and diluted, the latter to prevent SiO_2 from precipitating. Conversely, precipitation is provoked to avoid gas evolution, particularly H_2S, during sampling. The equipment described in fig. 3 is used with $CdSO_4$ aqueous solution to trap such gases.

Gases

The system shown in fig. 4 is used to collect samples on the steam line. After cooling and condensing through a cooling coil the gas/condensate mixture is flowed into a separator and the liquid discharged in a graduated cylinder. The gas is bubbled through an inverted graduated cylinder, to determine the gas rate, then diverted into a gas trap. A special equipment is devised for CO_2 sampling.

Solids

Sampling of solids which can be formed as scale, sediments and suspended particles in liquid and gaseous phases poses *a priori* no problem. Suspended particle collection is performed at constant pressure filtration through Millipore filters (0.45 mm @ 2 bar).

1.2.2 Chemical analyses

Liquids

Raw acidified (RA) samples are screened for the presence of 36 components including metallous, silica, phosphorous by an ICAP (Inductively Coupled Argon Plasma) spectrometer. Raw unacidified samples are analysed for chloride by titrating using the mercuric nitrate method. pH recorded in the laboratory is compared to field measured values.

Cadmium sulphate treated samples are analysed for H_2S by Redox iodimetric titration. Samples treated by a NaOH absorption method are analysed for CO_2 by titrating for bicarbonate with a pH meter for end point determination. Filtered unacidified samples from which suspended solids have been removed are analysed by ICAP for Fe and SiO_2.

Gases

Gases are analysed by gas chromatography for carbon dioxide, nitrogen, argon, oxygen and methane.

Thermal conductivity and flame ionisation detectors are used for noncombustibles and methane respectively.

Solids

Analyses are handled here in a less methodical manner. Elemental analysis is conducted on a representative sample by energy dispersive X-ray microanalysis to detect in a semi quantitative way elements having an atomic number equal or greater than sodium. Whenever required solids are dissolved and solutions quantitatively analysed for their constituents.

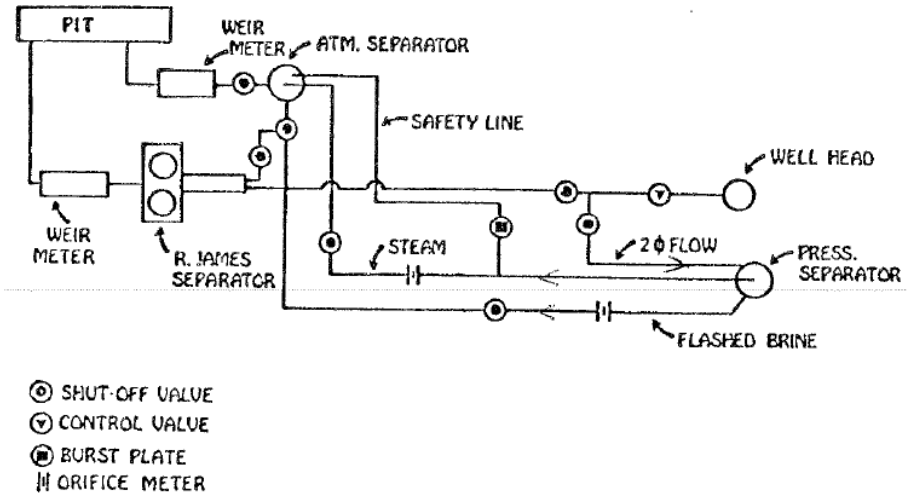

Figure 1: High enthalpy liquid dominated well. Testing/monitoring line [Cioppi et al, 1992]

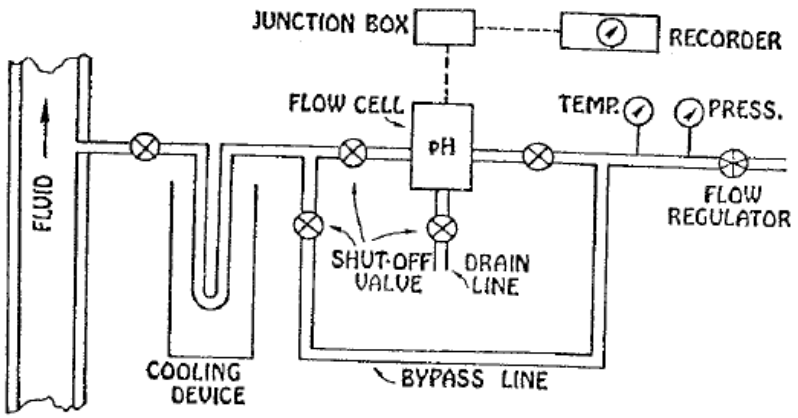

Figure 2: In-line pH monitoring [Cioppi et al, 1982]

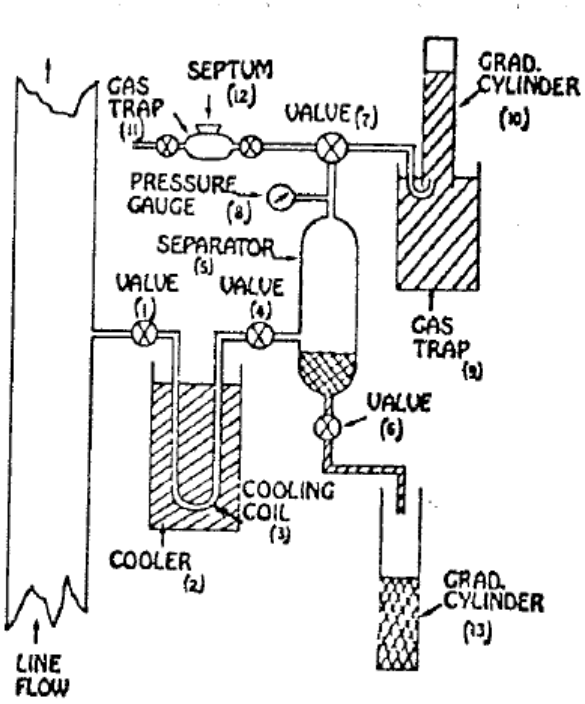

Figure 3: Gas and liquid sampling facility [Cioppi et al, 1982]

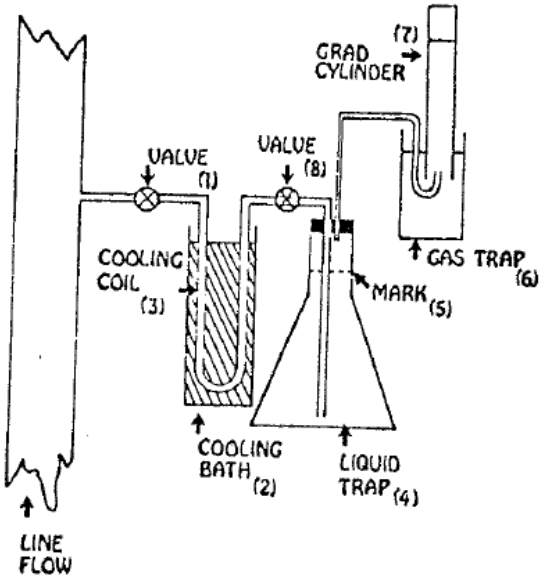

Figure 4: Simplified gas sampling kit [Vetter & Kandara, 1982]

It should be emphasized that the foregoing are likely to thoroughly assess reservoir production and (re)injection performance, contrary to the widely used sole Russel-James method which is structurally limited by the fact the geothermal fluid, flowing two phase at well head, undergoes flashing as the pressure of the flowing fluid decreases. As a result the method cannot provide (i) accurate measurements of two phase flowrates, (ii) sampling of the gaseous, steam and liquid phases at various thermodynamic conditions, and (iii) a sound evaluation of the thermochemical (i.e. scaling and corrosion) and mechanical (erosion, formation damage and well plugging) associated with the production and injection of geothermal brines.

2 LOW ENTHALPY GDH SYSTEMS

2.1 Operation and maintenance policy

Operation and maintenance of GDH systems include three main headings:

(i) monitoring and surveillance of heat production facilities;

(ii) well workover;

(iii) corrosion/scaling abatement, the latter exhaustively commented in a previous chapter.

2.2 Monitoring and surveillance of production facilities

According to the mining and environmental regulatory framework in force and to site specific amendments, monitoring and surveillance of the geothermal loop sketched in fig. 5 schematics comply with the following protocol :

2.2.1 Geothermal fluid:

- hydrochemistry (main anions/cations) and corrosion/scaling indicators : HS^-, $S2^-$, Fe^{2+}, Fe^{3+}, Ca^{2+}, HCO_3^-, etc …
- thermochemistry: PVT analysis (bubble point, gas/liquid ratio, dissolved gas phase),
- microbiology (sulphate reducing bacteria),
- suspended particle concentrations,
- corrosion monitoring (coupons, corrosion meters),

2.2.2 Loop parameters:

- well head pressures and temperatures,
- production well head dynamic water level,
- heat exchanger inlet/outlet temperatures,
- geothermal and heating grid flowrates,
- heat exchanger balance check,

2.2.3 Well deliverabilities:

- well head pressure/discharge (recharge) delivery curves (step drawdown/rise tests),

2.2.4 Pump and frequency converter characteristics:

- voltage, amperage, frequencies,
- powers,
- efficiencies,
- ESP insulation,

2.2.5 Inhibitor efficiencies:

- corrosion/scaling indicators control,
- inhibitor concentrations,
- filming (sorption/desorption) tests,

2.2.6 Inhibition equipment integrity:

- metering pump,
- regulation,
- downhole chemical injection line,

2.2.7 Wellhead, valves, spool, filter integrities,

2.2.8 Surface piping (ultrasonic) control,

2.2.9 Casing status:

periodical wireline logging (multifinger caliper, ultrasonic tools) inspection of production and injection casing integrities.

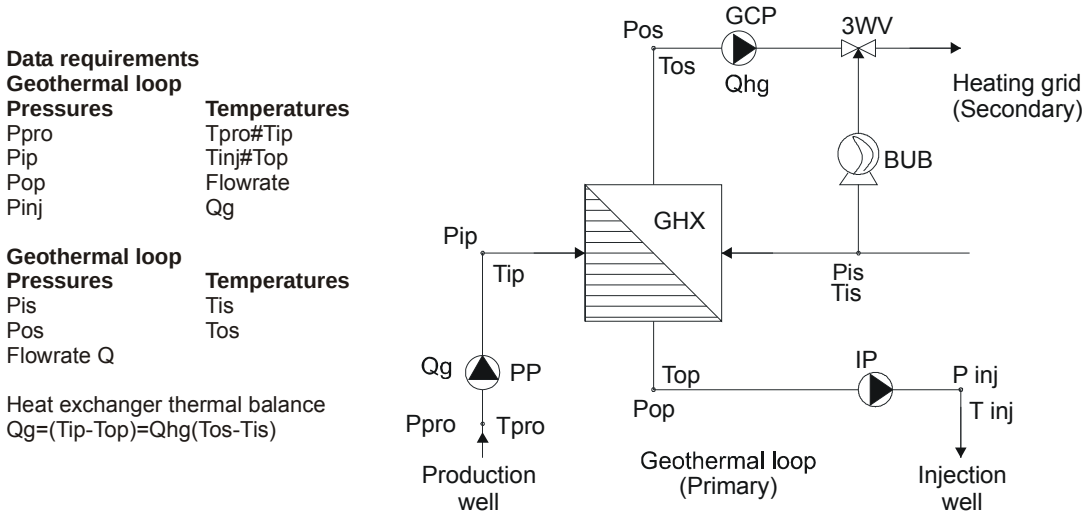

Figure 5: Geothermal loop parameters

Table 1 PVT Analysis of Bottom Hole and Surface Samples

	Sample n°				
	3	**4**	**5**	**6**	**7**
Depth (m bgl)	160	1.818	1.818	160	0
Pressure (kg/cm^2)	17	172	172	23	8.5
Temperature (°C)	62.2	64.2	64.2	60.2	63
Flowrate (m^3/hr)	158	46	46	46	125
Bubble point pressure (bars)	7.9	8.2	8.4	8.3	6.9
Gas liquid ratio GLR (vol/vol)	0.23	0.25	0.26	0.28	0.19
H_2S (% mol)	>1	>1	>1	>1	-
N_2 (% mol)	25.8	25.8	27.5	26.8	64.12
CO_2 (% mol)	51.09	52.3	51.18	52.7	1.07
CH_4 (% mol)	20.6	19.6	18.9	19.8	34.68
C_2H_6 (% mol)	1.49	1.50	1.40	1.70	0.13

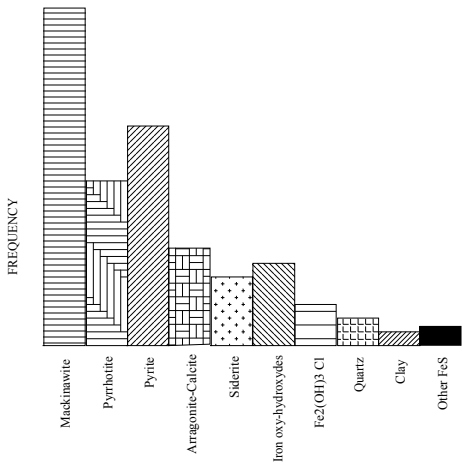

Figure 6: Frequency diagram of scale species sampled in damaged wells [IMRG]

2.3 Damage diagnosis

There is a wide spectrum of methods for identifying and evaluating thermochemically induced well damage, among which ought to be distinguished [Ungemach, 2004]:

2.3.1 Pressure/flow monitoring

It is a simple and obvious means of characterizing well impairment by losses in deliverability from nominal productivity/injectivity figures. These measurements can be usefully complemented by well testing and relevant pressure drawdown/rise and/or build up/ fall off analysis which will provide the bases for precise evolution of damage impact.

2.3.2 Direct damage assessment

It is performed via logging inspection based on multifinger caliper, ultrasonic or production tools. Casing calipers are reliable damage indicators which can achieve high resolution and accuracies thanks to 16 and even 40 simultaneously acquired radii values. Two way times from ultrasonic sources can also retrieve internal acoustic diameters, longer echos corresponding to wall piercing.

Tracer tests, easier and cheaper to operate than packer leak-off tests, have been successfully implemented in checking casing integrities [Ungemach et al, 2002].

Material balance calculations carried out on logs completed after restoration workovers allow for estimating damaging kinetics (i.e. corrosion or deposition rates).

2.3.3 Chemical control [Ungemach, 1997]

Analyses of liquid, gas and solid (suspended, deposited) samples enable to establish the fluid thermochemical profile and either validate or predict its corrosion/scaling tendancies.

Important in these respects are the PVT (table 1), the wet chemical (quantitative) and dry mineralogic (Xray diffractometry) (qualitative) analyses of water and scale samples collected at various in hole and surface localities. The example attached in table 1 demonstrates the poor reliability of the solution gas analysis carried out on the surface sample, even when collected at a pressure above bubble point.

Fig. 6, which accounts for numerous solid samples, exhibits the dominant share of unstable and porous iron sulphide crystal species such as mackinawite and pyrrhotite.

Thermodynamic modelling will be further applied to match actual data, predict future damaging trends and design adequate inhibition procedures.

2.4 Chemical inhibition of corrosion damage

Selected cases relevant to Paris basin low temperature geothermal wells are exemplified in fig. 7 to 11.

Fig. 7 illustrates the impact of a combined scale/corrosion inhibitor on both suspended particle numbers and sizes which trend towards a significant decrease. Average values, prior and further to chemical inhibition, stand at 23,000/2.3 µm and 15,000/1.3 µm respectively. It should be emphasized in this respect that this trend may be regarded as initiated prior to inhibition proper which suggests that, on this particular site, a self immunizing mechanism could have built up as a consequence of indurated deposits acting as a protective coating. Nevertherless further indications (material balances via direct logging assessments) proved the inhibition programme to yield quite satisfactory results, in terms of casing integrity among others.

On a nearby location, the outcome of specific agents could be appraised thanks to long lasting coupon monitoring time series. Fig. 8 clearly shows the modification of corrosion kinetics as a result of downhole chemical inhibition. Here, corrosion rates (in the sense of coupon weight losses) have been reduced from the initial 300 µm/yr figure to less than 100 µm/yr. Of interest to note, particularly at injector well head, is that this trend could be boosted via the injection of a combined corrosion/biocide formulation substituted to the former single anticorrosion agent.

Corrosion inhibition, in this geothermal context, is deemed efficient whenever total sulphides (i.e. sulphides proper + mercaptans) and iron (dissolved and total) concentrations exhibit sharp variations, i.e. increases and decreases respectively, as a consequence of inhibitor application. To simplify this means that the hydrophobic filming properties of the candidate agent keep acid gases (CO_2, H_2S) trapped in solution, thus preventing any interaction whatsoever with the casing metal lattice. This issue was clearly met on the example shown in fig. 9. Implementation of a corrosion inhibitor has caused sulphide contents to rise from 4 to 9 ppm and iron concentrations to drop from 2 to 0.2 ppm.

Checking filming/defilming (sorption/desorption) properties of corrosion inhibitors is another matter of concern. Those can be monitored via corrosion meters/recorders based on the polarization resistance principle in order to assess filming/defilming kinetics and related critical inhibitor doses and film remanence whenever injection ceases. These aspects are illustrate in fig. 10 and 11.

Preliminary investigations and simple thermochemical calculations can be exercised to design, and not a posteriori as often practiced by geothermal developers, adequate formulations. A typical scale assessment addressing a medium temperature carbonate field is summarized in table 2.

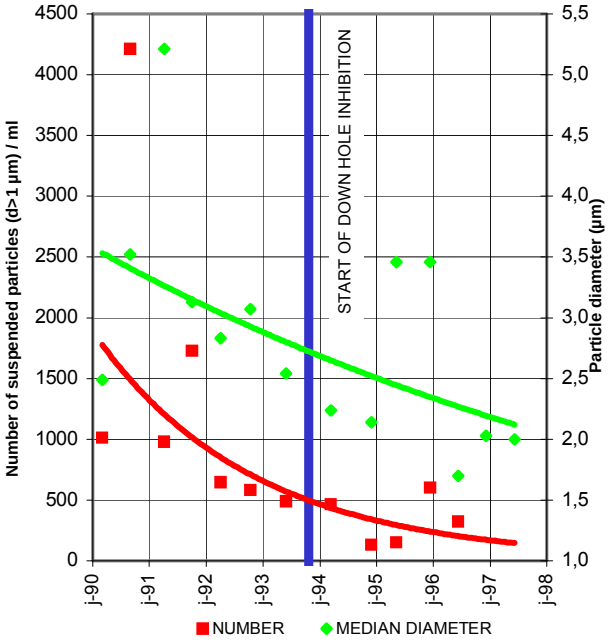

Figure 7: Suspended particiles monitoring. Geothermal doublet. Self-flowing well head

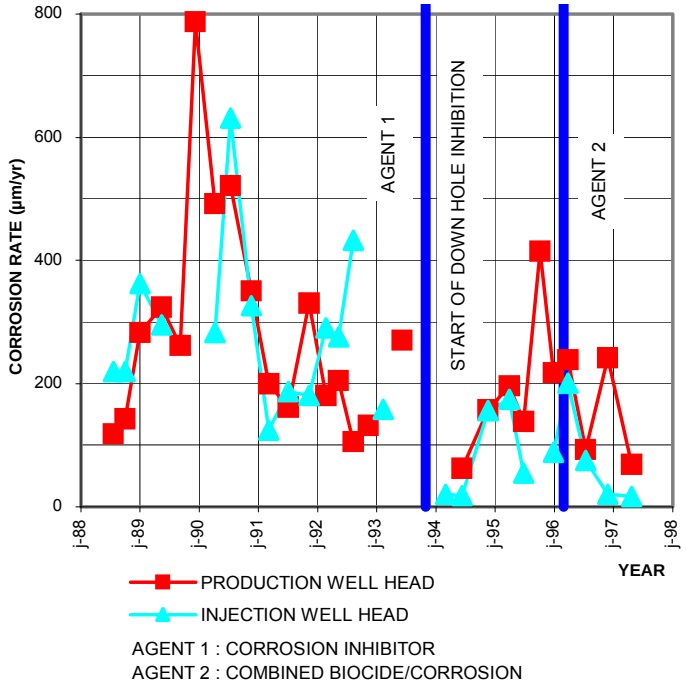

Figure 8: Corrosion rates measured on coupons. Self flowing production well

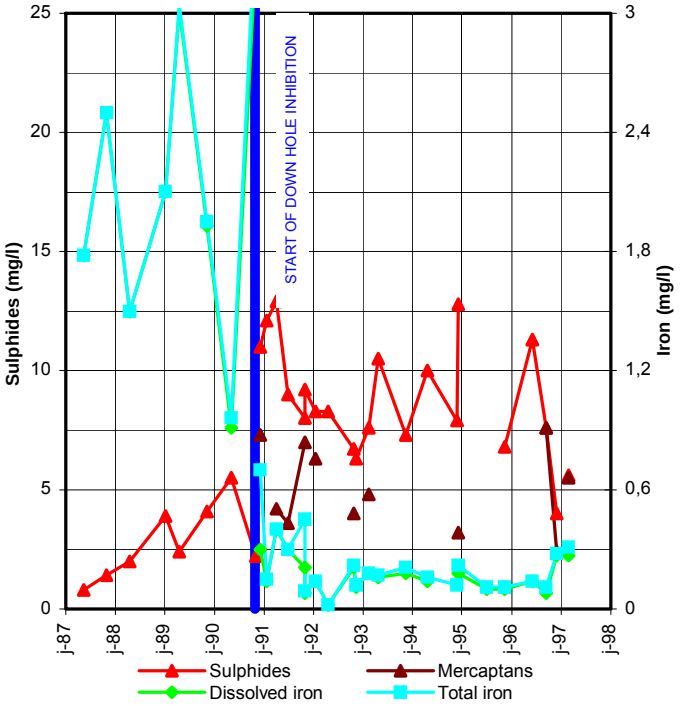

Figure 9: Chemical monitoring of corrosion indicators. Geothermal production well head

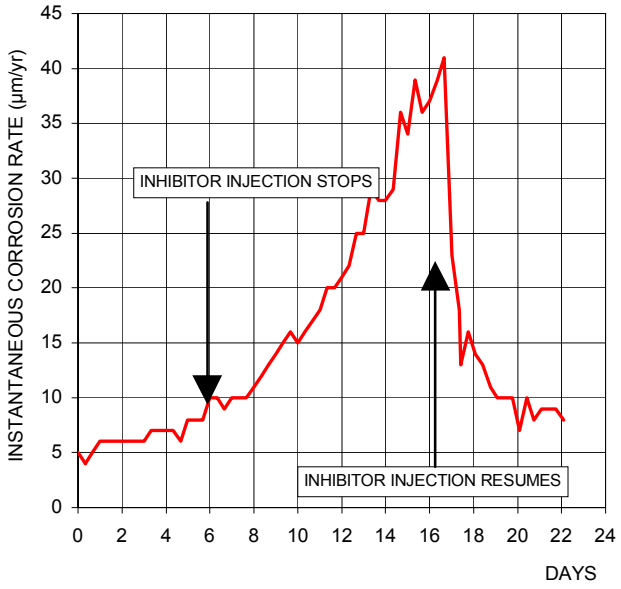

Figure 10: Defilming (desorption) experiment of submersed metal surface. Variation of instant corrosion rates

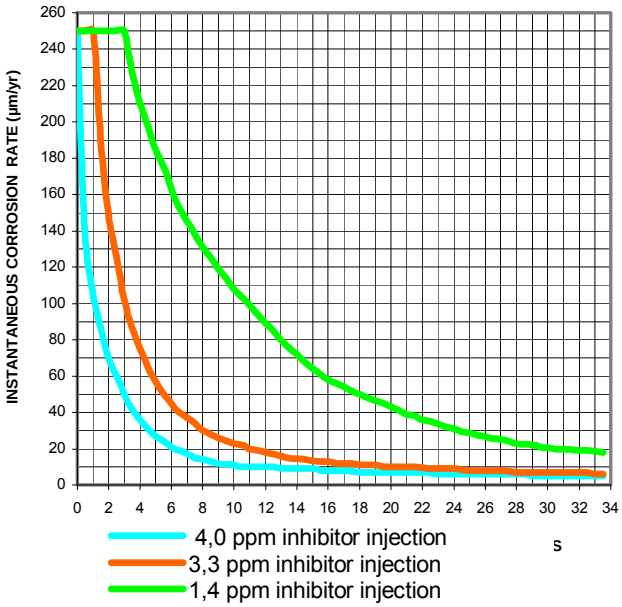

Figure 11: Corrosion inhibitor filming kinetics

Table 4: Geothermal fluid chemical profile and assessed scaling tendancies

Fluid chemical composition (mg/l)					
Cations		Anions			
Na	310	Cl^-	160	TDS	1,480
K	30	HCO_3^-	620	pH	6.42
Ca	60	$CO_3^=$	0	Temperature	105°C
Mg	12	$SO_4^=$	180		
Ba^{++}, Sr^{++}	traces				
Fe^{++}	8				

Scaling tendancies		
$CaCO_3$		Sulfates
Ionic strength	0.02	$CaSO_4$: precipitation unlikely
Saturation pH	5.53	BaSO4, SrSO4 : no precipitation
Langelier SI (pH 6.42)	0.88	
$CaCO_3$ supersaturation/precipitation potential : 130 g/m^3		

2.5 Mechanical damage removal

During a Paris Basin geothermal well life (20 years minimum), a number of heavy duty workovers are likely to occur, addressing well clean-up (casing jetting), reconditioning (lining/cementing of damaged casings) and stimulation (reservoir acidizing and casing roughness treatment). The probability level of such events is analysed in the risk and mitigation assessments section.

The conventional remedial strategy consists of cleaning the well by removing scale by either hydrojetting tools or rockbits driven by drill strings or coiled tubings (the latter being restricted by a limited flow capacity compared to drill pipe performance). In geothermal service and iron sulphide deposits (identified as corrosion products rather than native reservoir produced scale), the jetting concept described in has been successfully applied.

A typical workover rig set up in a landscaped site South of Paris is shown in fig. 12. Worth mentioning in this context is that workovers, contrary to a widely shared opinion, may prove environmentally friendly thanks in particular to the waste processing line outfit (250 m^3/hr capacity) sketched in fig. 13 which has been substituted to the past practice of digging a refuse pit. The line actually achieves a three fold function (i) fluid degassing, (ii) solid filtering (50 µcm cut), (iii) cooling (30°C) respectively, thus securing the dumping to the free brine sewage system of a cooled, gas and solid.

Another, recently tested, restoration procedure known as soft acidizing proved efficent on several damaged injector wells in the Paris area [Ventre and Ungemach, 1998]. The technique consists of injecting continuously from surface highly diluted HCl solutions mixed with an iron sequestering additive. The injected acid volume is equivalent to that normally squeezed into the reservoir via a drill string in conventional -petroleum/geothermal/ground water well- acid jobs. Only do injection times differ - 60 hrs against 1 hr - and the etching process alike which, in the conventional procedure, concerns the reservoir alone whereas soft acidizing addresses both well casing and/or formation damage.

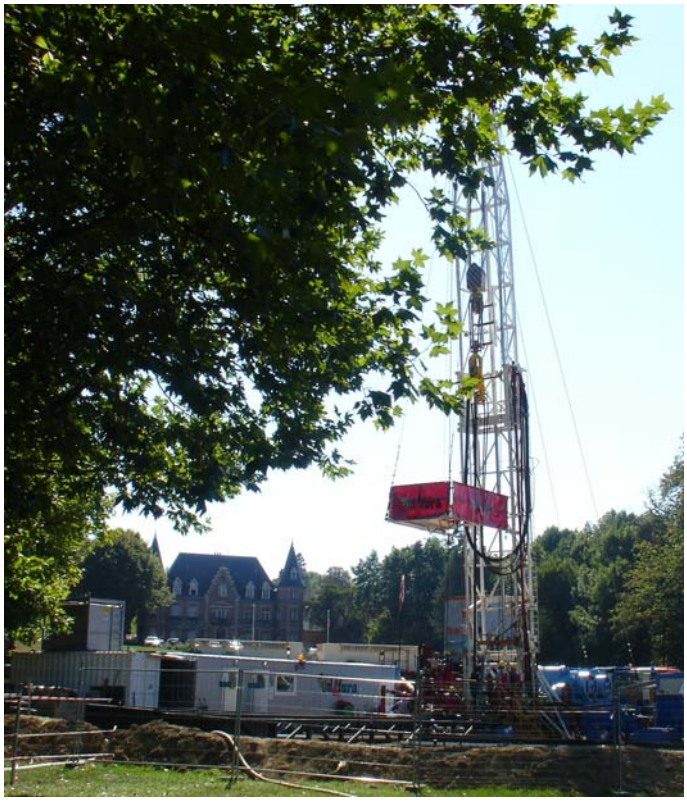

Figure 12: Workover set up

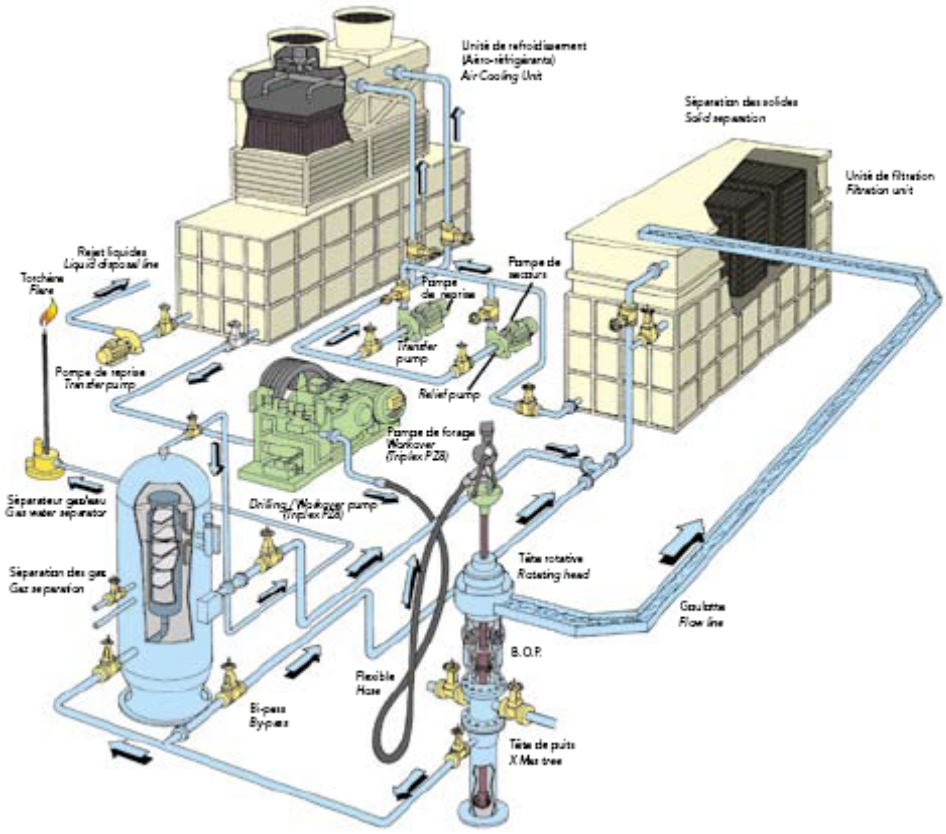

Figure 13: Workover waste fluid processing line

3 CONCLUSIONS

The following conclusions may be drawn from the presented monitoring and maintenance programs.

3.1 High enthalpy liquid dominated geopower sources

The methodology, which can be described as a large scale surface PVT facility consist of:

(i) HP and LP steam separators;

(ii) Numerous gauging (pressure, temperature, flowrates, pH) and sampling (liquid, steam condensates, non condensable gases) facilities on both steam and flashed brine lines;

(iii) Suspended particle monitoring;

(iv) Brine clarifying, and

(v) Filtering hardware.

This protocol, validated on several fields in the USA (Imperial Valley) and Italy (Phlegreaen fields), enables to optimise power plant design and production management. It is elsewhere a rapid and economic means of bridging the gap between field exploration and development. It should be substituted to field assessment strategies often limited to the sole Russel-James method, which in many respects proves inadequate in thoroughly appraising reservoir production and injection performance.

3.2 Low enthalpy geoheat sources

The monitoring protocols and maintenance/surveillance policies implemented on Paris Basin GDH systems benefited from a know how gained from a thirty year learning curve.

The technically and environmentally relevant in securing a sustainable development of the resource and well integrities in densely populated (sub)urban areas and thermochemically sensitive, if not hostile, fluid environments.

4 REFERENCES

Cioppi, D., Quercia, Tore, G., Ungemach, P. And Vetter, O. (1982). A New Approach to Geothermal Production and Testing. Recent Experiences in the USA and Italy. *International Conference on Geothermal Energy BHRA*, Florence, Italy, May 11-14, 1982, paper D3, 235-266.

Ungemach, P. (2004). Carbonate Geothermal Reservoir Management in France. *Int. Geoth. Days, IGD Poland 2004*. Low Enth. Geoth. Resources. Exploitation and Devel., Zakopane, 13-17 sept. 2004.

Ungemach, P., Ventre, A.V. and Nicolaon, S. (2002). Tracer Leak Off Tests as a Means of Checking Well Integrity. Application to Paris Basin Geothermal Production Wells. *27th Workshop on Geothermal Reservoir Engineering*, Stanford University, Stanford, CA, Jan. 28-30, 2002, paper SGP-TR-71.

Ungemach, P. (1997) Chemical treatment of Low Temperature Geofluids. *Int. Course on District Heating Schemes*, Cesme, Turkey, 19-25 Oct. 1997, Course Proc. 10/1-10/14.

Ventre, A.V. and Ungemach, P. (1998). Soft Acidizing of Damaged Injection Wells. Discussion of Results Achieved in the Paris Basin. *23rd Workshop on Geothermal Reservoir Engineering, Stanford University, Stanford*, CA, Jan. 26-28, 1998, Conf. Proc., 33-43.

Vetter, O. and Kandarpa, V. (1982). Handling of Scale in Geothermal Operations. *International Conference on Geothermal Energy, BHRA*, Florence, Italy, paper EZ, 355-372.

3. GEOTHERMAL DISTRICT HEATING AND COOLING. TYPICAL WELL DESIGNS AND DRILLING/COMPLETION PROGRAMS

Pierre Ungemach, Miklos Antics
GPC INSTRUMENTATION PROCESS, Roissy-en-France, France

INTRODUCTION

Contrary to current oil and gas practice, drilling and completion of high enthalpy, dry and flashed steam, wells address non sedimentary volcano-tectonic settings and hard and abrasive rock environments, often exhibiting massive circulation losses. Such is not the case of low to medium enthalpy geothermal wells which, in most instances, are completed in sedimentary reservoirs, therefore applying straightforwardly standard petroleum drilling technology. However, completion designs should differ; as a matter of fact geothermal completions aim at maximizing fullbore well delivery, whereas hydrocarbon production, at least one order of magnitude lower than its geothermal counterpart , is in general completed inside the wellbore via a tubing-packer-safety valve- perforated casing/cement suite.

Current low to medium enthalpy geothermal drilling/completion technology will be illustrated through selected examples focused on (i) deep district heating and cooling wells drilled in carbonate and sandstone reservoirs, (ii) design of injection wells in fine grained clastics alternating sand, clay, sandstone depositional sequences, (iii) medium depth dual completion wells exploiting tepid aquifers in conjunction with water/water heat pumps, and, last but not least, (iv) an anti-corrosion well concept combining steel casings and fiberglass liners.

1 GEOTHERMAL DISTRICT HEATING AND COOLING WELLS

1.1 Deep wells

The standard design of a geothermal district heating and cooling (GDHC) system is described in fig. 1 (geothermal loop features).

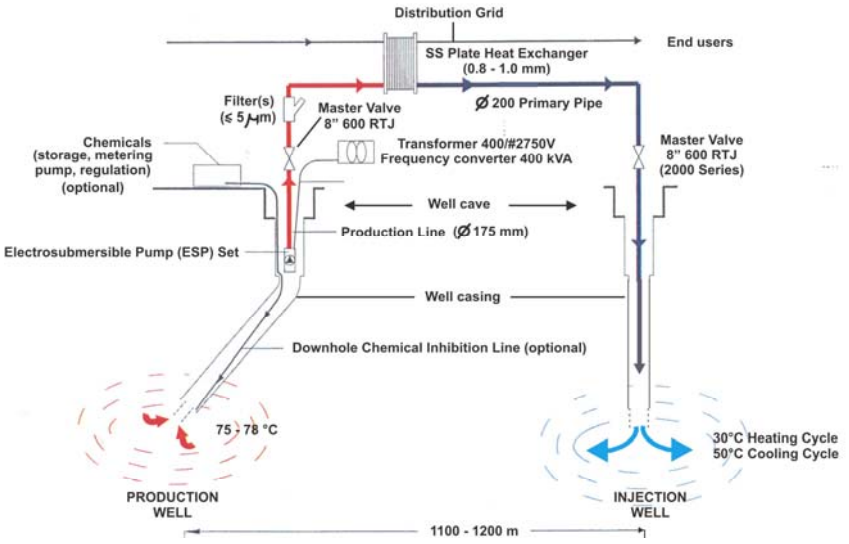

Figure 1: Geothermal District Heating & Cooling – Primary Loop Schematic

The system for waste disposal, pressure maintenance and heat recovery considerations is based on the geothermal doublet concept of heat extraction depicted in fig.2 and 3 with respect to carbonate reservoir environment and either a casual steel cased or combined steel cased/fiber glass lined well completion.

The impact of two standard GDHC production casing programs [pumping chamber x production casing] on well losses can be visualised in fig. 4.

Fig. 5 addresses the design of a well producing from a thick sandstone hot water aquifer, complying with the programme summarised in table 1 and in fig. 6 time-depth chart.

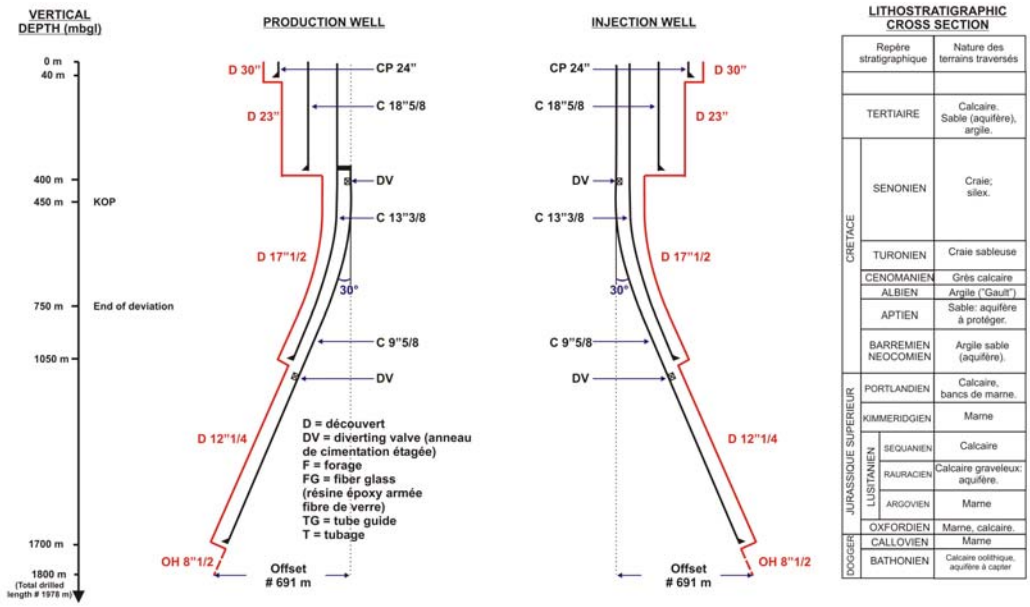

Figure 2 : Conventional (steel cased) GDH doublet design

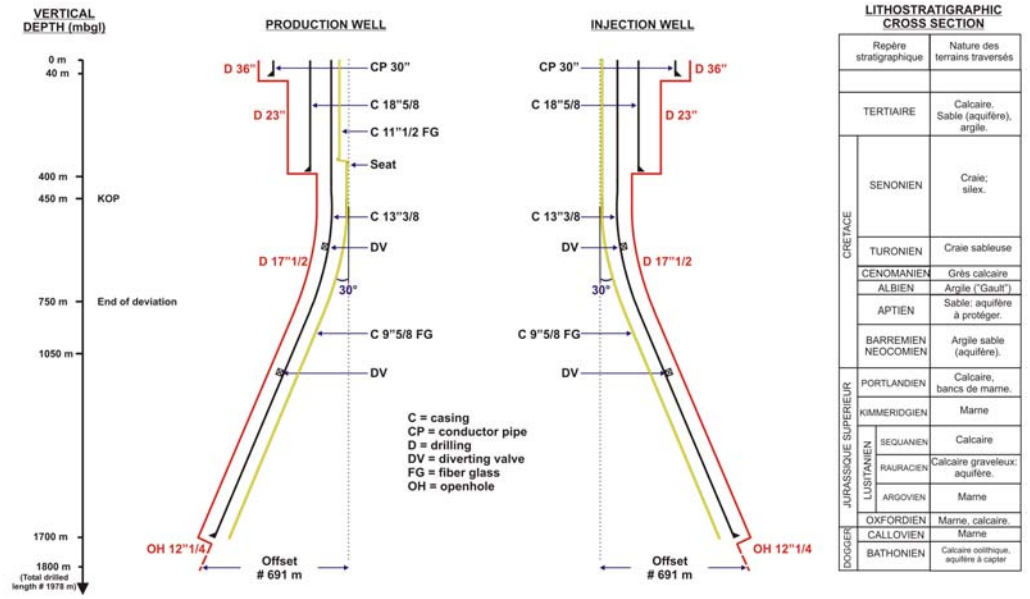

Figure 3 : GDH doublet completion combining steel casing and fiber glass liners

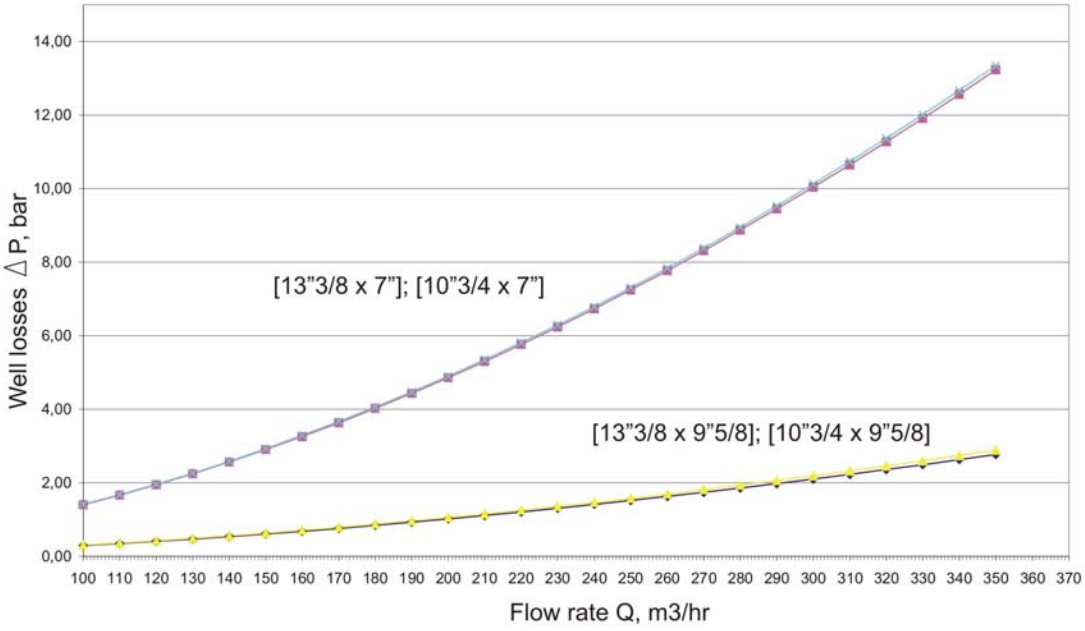

Figure 4: Friction losses as a function of production casing programmes

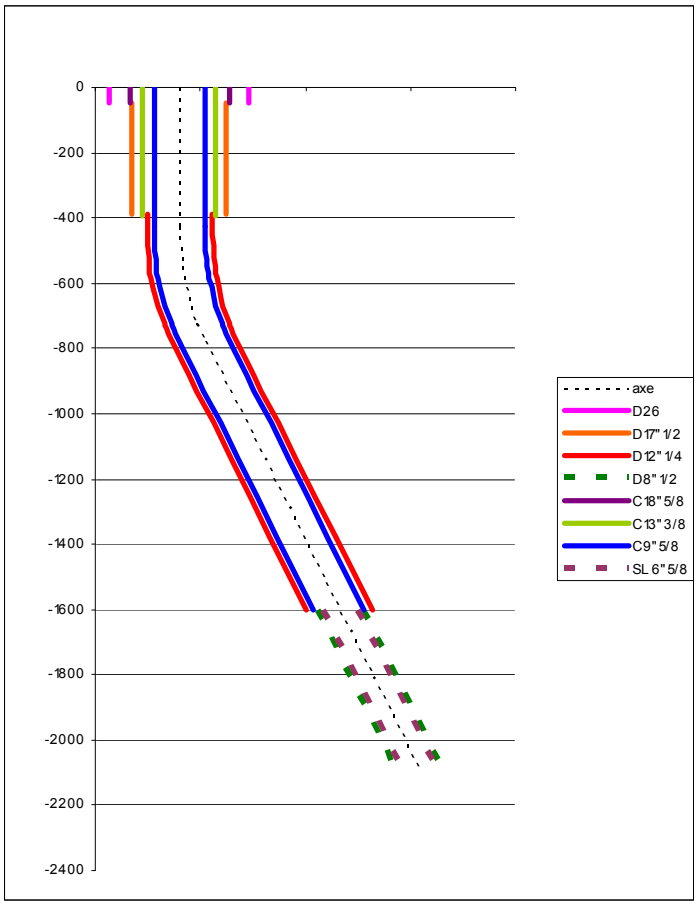

Figure 5: Production well profile. Consolidated sandstone reservoir

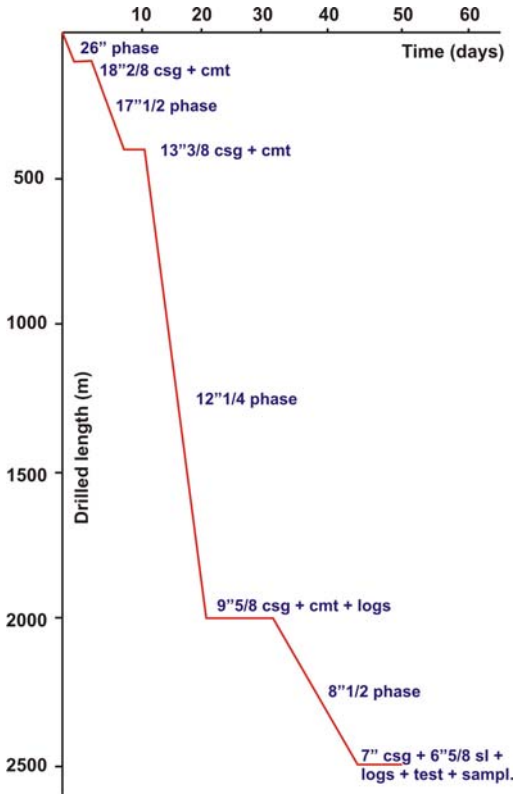

Figure 6: Projected drilling/completion/testing time vs depth diagram

1.2 Medium depth wells

Fig.7 is an illustration of a water/water heat pump assisted GDHC doublet based on a dual aquifer completion scheme in a sandy formation context, casual in petroleum production but unusual in geothermal and groundwater projects.

Note incidentally that fig. 7 design may accommodate the operation of two submersible pump sets.

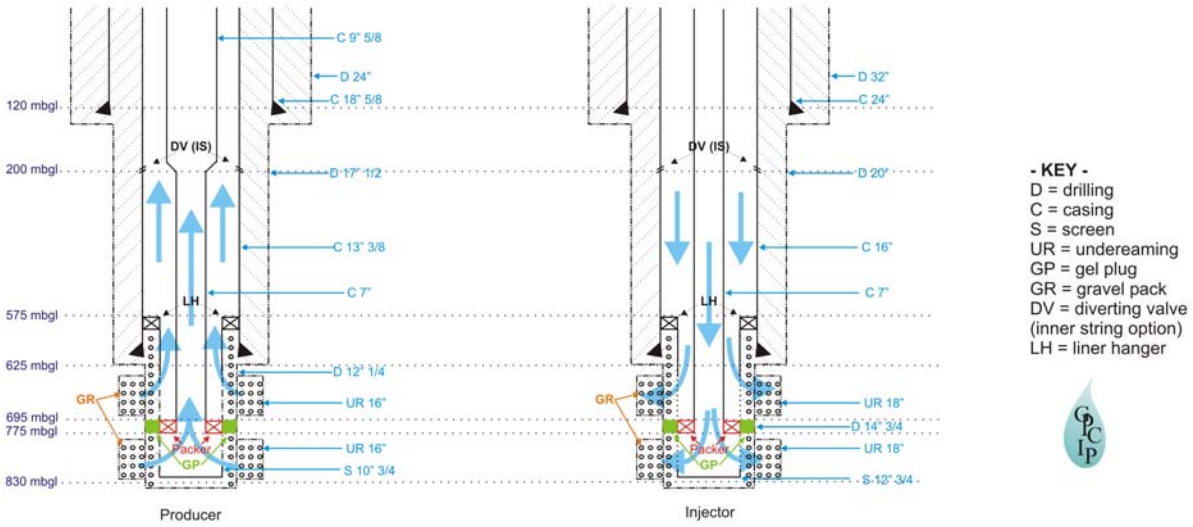

Figure 7: Dual, heat pump oriented, water well completions. Note that the producer well can be equipped with two submersible pump sets.

2 WATER INJECTION IN FINE GRAINED RESERVOIR CLASTICS

Injection wells are known to undergo severe injectivity losses further to near wellbore permeability impairment and subsequent formation damage, a topic further discussed in section 6.5.

Given the produced, heat depleted, brine is injected into the source reservoir, no water incompatibilities are to be feared. Therefore, matrix plugging by fine, preferably external, particles is the prevailing damaging mechanism. To be defeated or at least mitigated it requires, in addition to surface filtration facilities, careful completion design regarding casing diameters, undereaming and gravel pack grain size and placement, screen selection among others. Based on field experience the foregoing should lead to sandface velocities lower than the 1cm/s critical threshold.

A typical well completion designed to secure 150m3/h injection flowrates in the Great Hungarian Plain (Pannonian basin), fulfilling the aforementioned requirements, is attached in fig. 8.

Projected well/reservoir performance	
Top reservoir depth	1,500 m
Static WHP	-5 bars
Total pay	400 m
Net pay (h)	110 m
Effective porosity (ϕ_e)	0.2
Permeability (k)	100 mD
Skin factor (S)	-2
Formation temperature	90 °C
Mean injection temperature	35 °C
Fluid (eq. NaCl) salinity	2.5 g/l
Fluid dynamic viscosity (production) (μp)	0.32 cp
Fluid dynamic viscosity (injection) (μi)	0.73 cp
Total compressibility factor (c_c)	10^{-4} bars^{-1}
Fluid density (ρp) at 90 °C	965.34 kg/m^3
Fluid density (ρi) at 35 °C	994.06 kg/m^3
Target injection rate (Q)	150 m^3/hr
WHP (150 m^3/hr, 35 °C)	20.5 bars
Sandface velocity (v_{sf})	0.23 cm/s
Velocity at completion outlet (v_c)	0.61 cm/s

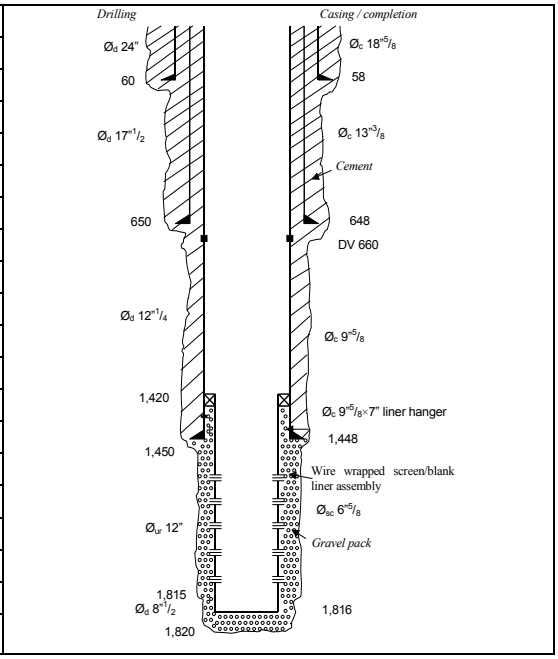

Figure 8: Water injection in a clastic sedimentary environment. Typical well completion design [Ungemach, 2003]

3 ANTI CORROSION WELL CONCEPT

The design, depicted in fig. 9, is a material response to corrosion damage. It has been successfully implemented on a Paris Basin self flowing well in early 1995 and since then the well has been operating, at a constant 200 m^3/h discharge, without any workover nor even light well head servicing recorded whatsoever, contrary to his steel cased GDHC companions which undergo at least one heavy duty workover every ten years or so.

The well combines steel propping casings, providing the required mechanical strength, with a fiberglass production/injection column, chemically inert vis-à-vis any geothermal corrosive fluid environment. The annulus is kept free in order (i) to circulate (or simply fill) corrosion inhibitors, preserving steel casing integrities, and (ii) to remove the fiberglass string whenever damaged (wheap destructuring) and replace it by a new one thus achieving long well life. Fiberglass integrity is assumed to last 25 to 30 years.

Operating temperatures are limited by the glass vitreous transition temperature, the practical limit being set at ca 90°C. Well inclination should not exceed 35°C. The production well architecture, displayed in fig.9, requires (i) a larger diameter fiberglass column, to accommodate an ESP placed in compression on a fiber glass coated seat at the (18"5/8 x 13"3/8) casing transition, and (ii) a slimmer liner, freely suspended under its own weight below the seat. Both liners are centralised via fiberglass coated centralisers so that there is no contact other than with fiberglass materials. Thermomechanical effects are compensated at well head by an *ad hoc* expansion spool.

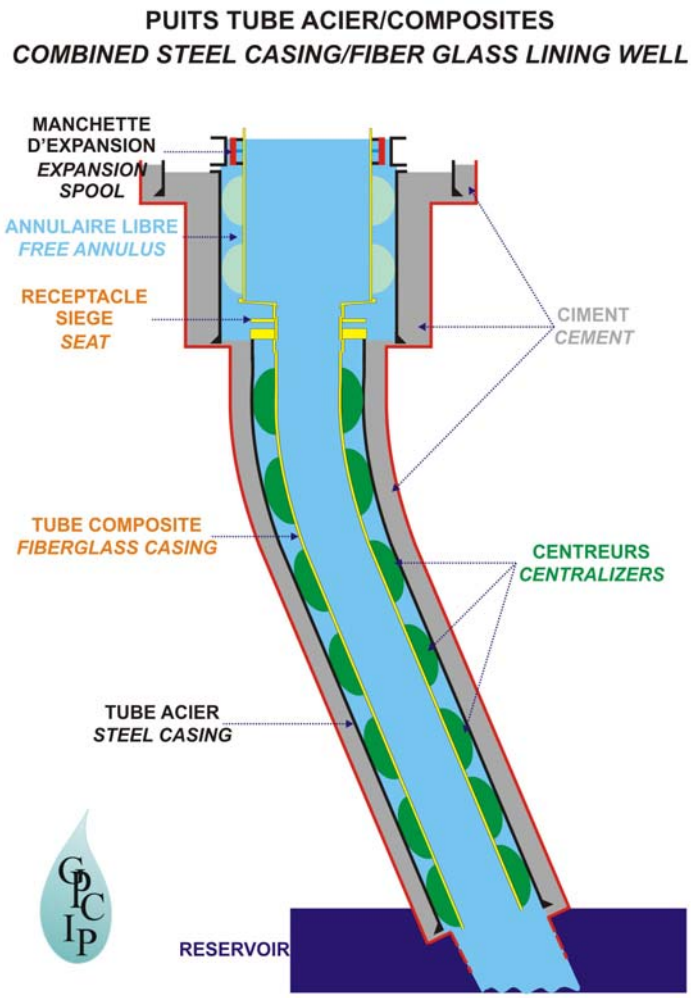

Figure 9: Combined steel casing/fiber glass lining well (GPC)

Table 1: Drilling/completion/testing programme

DRILLED DEPTH INTERVAL (mbgl)	PHASE DESCRIPTION	REMARKS
0 – 50	Drill ϕ 26", tricone roller bit, WOB # 12-25 t ; 800-200 rpm ; >3500 l/min ; penetration rate 5 m/hr. Bentonite base mud: d = 1.10 – 1.15; V # 30 – 50 M. Run 18□5/8 casing. Inner string cementing = CP55 Cement slurry, d = 1.80	Possible meterage change owing to completion of a large diameter, 0 – 20 m, foreshaft
50 – 400	Drill " 17"1/2, tricone roller bit, WOB # 15-20 t ; 80-200 rpm ; >3500 l/min; penetration rate 7-8 m/hr. Bentonite base mud: d = 1.10 – 1.15; V # 35 M. Run 13□3/8 casing. Inner string cementing = CP55 Cement slurry, d = 1.80	Designed as a future pumping chamber withstanding a 150 – 200 m water level drawdown
400 – 1850	Drill " 12"1/4, PDC bit, WOB # 12 t ; 120 rpm ; 2500-3000 l/min; penetration rate 4-5 m/hr. Bentonite/PAC, PAC+CMC/polymer base mud formulations: d = 1.10 – 1.15; V # 35 M. Start deviation @ KOP=450 m with downhole, steerable, motor, MWD, KMonel, hydraulic jar, assembly; build up gradient = 1°/10 m; slant angle # 380, azimut = __*. When reaching # mbgl drilling depth continue either with identical motorised, steerable, BHA or, with rotary assembly instead. Run 9□5/8 casing with either a liner hanger or DV + left hand connection (casing cut) to accommodate the required 13"3/8 pumping chamber space. Conventional stage cementing procedure with cementing head, shoe, float collar and DV placed @ # 1100, above the upper lost circulation horizon, POZZMIX (dry blended puzzolane/class G cement) slurry, d # 1.60. Wireline (OH/CH) logging programme = BGL/GR; SPGR; MRT; STI; CIC;	The 9"5/8 casing cutting strategy should be selected instead of the liner hanger configuration in order to meet the 13"3/8 pumping chamber space requirements. The left hand connection would enable to recover the DV and ease an eventual further 13"3/8 x 9"5/8 casing lining issue.

DRILLED DEPTH INTERVAL (mbgl)	PHASE DESCRIPTION	REMARKS
	CBL-VDL	
1850 – 2485	Drill " 8"1/4, PDC bit (rotary assembly), WOB # 8t ; 120 rpm ; 1500-2000 l/min; penetration rate 5-7 m/hr. Polymer base mud: d = 1.05; V # 35 – 40 M, 50 m full size 5" sample coring. OH/production logging programme = CNL, SGR, SpeD, BGL, HMI (optional), PLT, T, pressure build-up, BHFS (PVT). Run completion string according to flowmeter identified producing layers: 7" casing x 6"5/8 slotted liner assembly. Liner hanger set @ __** mbgl. Mud acid (HF + HCl) well stimulation (10 -20 m^3 HF 4X + HCl 14X). Bottomhole fluid sampling. Surface suspended particle monitoring. Production/injection well loop circulation test.	Mixed (casing x slotted liner) column designed and run downhole according to flow meter logging survey. Bottomhole fluid sampling aimed at liquid and gas phase analyses at reservoir conditions.

* from reservoir modelling
** from geology

REFERENCES

Ungemach, P. (1995). New Geothermal Concept. IGA News, *Newsletter of the Int. Geoth. Ass. Quaterly,* **20**, January-March, 1995.

Ungemach, P. (2003). Reinjection of Cool Geothermal Brines into Sandstone Reservoirs, *Geothermics*, **32**, 743-761.

4. CORROSION/SCALING ABATEMENT

Pierre Ungemach

GPC INSTRUMENTATION PROCESS, Roissy-en-France, France

PRELIMINARY NOTICE

Most of the material presented here is borrowed to the works of Nikos Andritsos et al [Corrosion and Scaling of Geothermal Systems, 2009] and Pierre Ungemach [Chemical Treatment of Low Temperature Geofluids, 1997].

SUMMARY

Geothermal fluid compositions will be reviewed, scaling/corrosion damage and source mechanisms described and candidate treatment measures, aimed at preventing/mitigating their impacts, discussed, bearing in mind that they ought to be regarded in most instances as ***site specific****.*

1 INTRODUCTION

Geothermal fluids often display hostile thermochemical characteristics resulting in well/formation damage and failures of surface facilities, which severely penalise exploitation economics.

Damage occurs under the form of metal corrosion and deposition on exposed material surfaces of scale species. Both phenomena may also coexist through deposition and/or entrainment of corrosion products. Most commonly encountered damages address CO_2/H_2S corrosion, alkaline carbonate/sulfate, heavy metal sulphide and silica scale. Source mechanisms are governed by pH, solution gases and related bubble point and (CO_2) partial pressures, salinity, solubility products and of thermodynamic changes induced by the production and injection processes.

Whereas scaling affects mainly high enthalpy systems, as a result of fluid flashing, steam carry over and injection of heat depleted brines, corrosion and, at a lesser extent though, corrosion is the major damage in exploitation of lowgrade geothermal heat, known as direct uses. Micro-biological activity, particularily sulfate reducing bacteria, can also be a significant corrosion contributor in such low temperature environments.

Control, abatement and more over prevention of scaling and corrosion shortcomings have evolved in the past decades from an empirical approach an *a posteriori* remedial (i.e; chemical and/or mechanical scale removal, replacement of corrosion/scaling damaged sections) practice towards a more thorough comprehension of the, often complex, mechanims involved and design of appropriate, cost effective, mitigation procedures.

2 GEOTHERMAL FLUID COMPOSITIONS

The vast majority of geothermal fluids is of meteoric origin. However, isotopic studies suggest that a small fraction (5-10 %) may emanate from other sources, magmatic, juvenile, fluids or host sediments (connate or formation waters). Note incidentally that a small amount of magmatic fluid would significantly modify the chemistry of the (originally) meteoric water inflow – Soul infiltrated meteoric waters will circulate downwards to depths up to 6-7 km, interacting with host rocks at increasingly higher temperatures and pressures causing enrichment of the source fluid in either dissolved salts and gases. As a consequence most geothermal fluids exhibit higher TDS (total dissolved solids) contents than the original, cooler, intake waters.

The amount and mature of dissolved chemical species depend on temperature, pressure, minimal-fluid equilibria and mixing with other waters. Due to their compositional variability geothermal fluid environments and structurally site specific. This specificity may apply within the same geothermal reservoir in space and also in time owing to the thermo-chemical processes occuring during well and field exploitation such as dilution/mixing with other drained fluids, sea water intrusion, boiling/condensing etc…).

One may logically infer that hotter fluids would display higher TDSs than cooler ones, an attribute however which suffers many exceptions.

The major constituants of geothermal waters are :

- Cations : Na, K, Ca, Mg, Li, Sr, Mn, Fe
- Anions : C_l^-, HCO_3^-, SO_4^{2-}, F^-, Br^-

- Non ionic : SiO_2, B, NH_3, gases

Minor constituants : As, Hg other, heavy, often toxic, metals.

A typology of geothermal waters according to their pH ranges and principal ions is given in table 1.

A compilation of water compositions from worldwide selected geothermal reservoirs is displayed in table 2.

Geothermal solution gases deserve a special comment. Many gases are present in geothermal fluids. They are released as a result of fluid flashing (high enthalpy) or pressure depletion below bubble point (low enthalpy). Liquid vs gas equilibria control partitioning of gas species between the two phases, the largest fraction being transferred to the gaseous phase. Most commonly encountered gases include CO_2, H_2S, NH_3, N_2, H_2 and CH_4, often designated as non condensable gases (NCG). They usually consist of two gases, which can be absorbed in OHNa solutions, CO_2 and H_2S respectively. CO2 is the most abundant gas in geothermal systems, often accounting for more than 90 % of total well gas discharge. Its concentration can affect, to some extent, the final liquid pH, boiling (flash) point-vs depths relationships and, last but not least, fluid scaling tendancies. It can represent a danger to humans and animals when discharged in large quantities as reported by casualties caused by uncontrolled well blow outs. Atmospheric emissions of H_2S, a well documented toxic gas, lethal at high concentrations, require thorough abatement and eradication measures.

NCGs can be divided, according to several authors, into two groups, namely.

(i) *Reactive gases* (CO_2, H_2S, NH_3, N_2, H_2, CH_4) involved in chemical equilibria, thus likely to provide relevant information on subsurface conditions.

(ii) *Inert gases* (noble gases and higher grade hydrocarbons) which participate to chemical reactions tracing occasionally gas origins.

Abatement of NCGs upstream from steam turbine inlet requires energy. Above 10 % NCG contents render condensing cycles uneconomic and reduces geopower conversion to back pressure cycles.

NCG concentrations on selected flield localities are compiled in table 3.

Table 1: Summary of water types in geothermal systems [Henley et al, 1984].

	Approximate pH range	**Principal ions**
Ground water	6 -7.5	Trace HCO3-
Chloride water	4-9	Cl, lesser HCO3-
Chloride-bicarbonate	7 -8.5	Cl, HCO3-
Steam-heated waters	4.5-7	SO42-, HCO3-, trace Cl
Acid-sulphate	1 – 3	SO42-, trace Cl
Acid-sulphate-chloride	1 – 5	Cl, SO42-
Bicarbonate	5 – 7	HCO3-
Dilute chloride	6.5 – 7.5	Cl, lesser HCO3-

Table 2: Characteristics and compositions of typical geothermal wells. Concentrations are in mg/L.

	Salton Sea, California	***Broadlands 1, N. Zealand***	***Hot Springs, Utah***	***Kilauea, Hawaii***	***Krafla, Iceland***	***Kizildere (W15), Turkey***	***Klamath Falls, Oregon***	***Dogger, Paris Basin, France***	***Nigrita, Greece***
pH	5.7	8.3	-	7.1	7.2	8.0	8.4	6.2	6.8
Temp.,°C	214	270	260	190	220	138	80	73	59
TDS (g/L)	182	3.8	7.4	15.8	1.0	2.4	0.7	7	2.5
Na	42700	1060	2320	4930	193	1192	205	3700	529
K	6500	150	461	756	20	135	4.3	60	89
Ca	18200	5	8	358	1.5	1.9	26	630	160
Mg	570	0	2	0.3	0.03	0.2	0.5	150	105
Fe	180	0.2	1	0	0.02	0	0.3	0.5	1.1
Pb	59	-	-	0	0	-		-	-
Cl	112000	1700	3860	8970	26	46	51	7980	162
SO_4^{2-}	6	40	72	24	194	631	330	775	130
HCO_3^-	220	300	232	18	328	-	35	335	2200
As	22	5	4	0.1	-	-	-	-	0.5
B	480	7	-	4.3	-	24	-	5	4.6
SiO_2	1150	600	563	750	383	356	48	14	38

Table 3. Composition of non-condensable gases from natural vents and wells [Ellis and Mahon, 1977, and other sources].

Source	**Temp. (ºC)**	**% gas in steam**	**GLR**	**CO_2**	**H_2S**	**HC**	**H_2**	**N_2+Ar+ He**	**O_2**	**NH_3**	**H_3BO_3**
Wairakei, N. Zealand (fumarole)	115	0.2		94.6	2.3	0.7	1	1.1	-	0.3	-
San Ignacio, Honduras (spring)	99	n.r.		91.3	1.8	0.1	0.1	5.0	-	1.7	-
Larderello, Italy (fumarole)	100	3		92.3	2.0	1.4	2.5	1.6	0.1	-	0.5
Larderello, Italy	200	2.0		94.1	1.6	1.2	2.3	0.8	-	0.8	0.33
The Geysers, U.S.A.	230	0.59		55.9	5.3	10.3	20.4	3.0	-	4.8	0.3
Salton Sea, U.S.A.	300	0.1-1.0		>90	>1						
Matsukawa, Japan	200	0.22		81.8	14.1	-	-	-	-	-	-
Weirakei, N. Zealand	260	0.063		91.7	4.4	0.9	0.8	1.5	-	0.6	0.05
Broadlands 1, N. Zealand	270	0.6		95.9	1.2	1.8	0.1	0.2	-	0.2	-
Reykjanes, Iceland	190	n.r.		92.0	3.8	<0.1	<0.1	3.9	-	-	-
Namafjall, Iceland	259	n.r.		33.6	48.7	-	13.2	4.4	-	-	-
Nigrita, Greece	59	-	2.4	99.2	-	-	-	0.8	-	-	-
Merksplas I, Belgium	70	-	0.7-1.1	86	-	12	-	-	-	-	-
Dogger, Paris Basin, France	78	-	10	15	<2	55	-	25	-	-	-

n.r.: not reported; GLR: gas-to-liquid ratio of non-condensible gases (Nm^3/m^3 water); HC: hydrocarbons

3 SCALING

3.1 Scale formation mechanism

A substance MnAm (ionic) crystallises according to the equilibrium reaction

$nM^{a+} + mA^{b-} \Leftrightarrow$ MnAm (solid)

The thermodynamic driving force behind the process is the change of the Gibbs free energy in the transfer from supersatured to equilibrium state i.e.

$$\Delta G = RTLn\left[\frac{(M^{a+})^n (A^{b-})^m}{Ksp}\right]^{1/n+m} = RTLn\left[\frac{IAP}{Ksp}\right]^{1/n+m} \quad (1)$$

Where :
R = gas constant
T = absolute temperature (°K)
Ksp = solubility product of the phase forming compound
IAP = ion activity product

$$S = \left[\frac{(M^{a+})^n (A^{b-})^m}{Ksp}\right]^{1/n+m} = RTLn\left[\frac{IAP}{Ksp}\right]^{1/n+m} = \text{supersaturation ratio} \qquad (2)$$

SI = Ln(S) = saturation index

If SI>0 scaling occurs

Summing up, supersaturation is the driving force in the nucleation and crystal growth processes.

Supersaturation would normally occur as a result of temperature and pH changes and also mixing of incompatible waters.

Fig. 1 represents a solubility diagramme for a sparingly soluble salt of inverse solubility [$CaCO_3$, $CaSO_4$, Ca_3 $(PO_4)_2$]. The solid line matching equilibrium conditions is the solubility curve below which the solution is stable (i.e. no precipitation). At A the solute is in equilibrium with the concerned salt species. Departing from A upwards, the various paths, either isothermal (AB), or iso concentration (AC) or both temperature and concentration varying (AD), move to another equilibrium state by precipitation of the solute in excess. For most of these salt species supersaturated solutions may stand stable for practically infinite time periods. Such solutions are called *metastable;* there is however an upper limit to this supersaturation range marked by the so-called supersolubility curve indicated by the dasked line. When reached (points B, C, D), spontaneous precipitation may occur with or without a prior induction period. Above is the *labile* domain. It should be mentioned here that the supersolubility curve is not that well defined as it depends on a number of local factors among which, alongside temperature and pH, the presence of foreign suspended particles (acting as seeds for nucleation sites), wall material (chemical affinity) or roughness (turbulences) may play an important role.

Nowadays scale speciation and supersaturation ratios of salts present in geothermal waters are calculated via computer codes and data bases accounting for all possible candidate ion pairs and most reliable values for solubility products and dissociation constants.

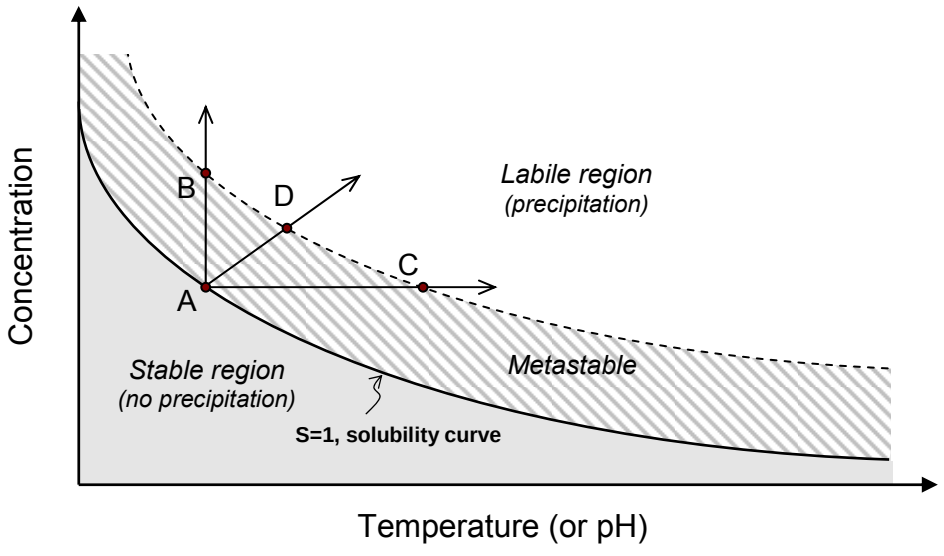

Figure 1. Solubility-supersaturation diagramme of a sparingly soluble salt with inverse solubility (e.g. $CaCO_3$).

3.2 Typical scale types

Table 4 lists a series of scale types selected in various low and high enthalpy systems worldwide. It can be seen that the dominant species address calcium carbonate, silica (and metal silicates), heavy metal sulphides and (mainly) iron oxydes.

Table 4. Scale composition in geothermal systems.

Earth Energy (Geothermal Heat Pumps)	
Component	*Examples*
Calcium carbonate	• Various sites
Iron oxides	• Various sites

Low and medium-enthalpy fluids	
Component	*Examples*
Calcium carbonate	• Oradea and Ciumeghia (Romania), Balcova (Turkey), Saidene (Tunisia) N. Kessani and Nigrita (Greece),
Iron oxides	• Nigrita (Greece)
Iron sulphide salts [in association with corrosion]	• Dogger Basin (France)

High- enthalpy fluids	
Component	*Examples*
Calcium carbonate	• Kizildere (Turkey),Miravalles (Costarika), Latera (Italy), Cerro Prieto (Mexico), East Mesa, Nevada (USA), Krafla (Iceland)
Silica (and metal-silicates) [usually associated with small or medium TDS]	• Svartsengi and Nesjavellir (Iceland), Dixie Valley (USA), Matsukawa, Otake and Onuma (Japan), Berlin (El Salvador)
Heavy metal sulphide salts (with silica and metal-silicates) [associated with high TDS]	• Salton Sea (USA), Milos Island (Greece), Asal Wells (Djibouti)
Oxides (and sulphide salts)	• Reykjanes (Iceland)

TDS: Total Dissolved Solids (mg/kg)

Calcium carbonate

It is the most frequently encountered species, especially in low and medium temperature (<150°C) settings but also in a number of high enthalpy, particularily volcano-sedimentary, environments.

Almost all geothermal fluids contain significant amounts of dissolved CO_2 in the form of aqueous CO_2 and bicarbonates (HCO_3^-). Flashing of the gaseous phase results in CO_2 release and subsequent pH increase ; supersaturation conditions are reached and $CaCO_3$ is deposited according to the equilibrium equation.

$$Ca^{2+} + CO_3^{2-} \Leftrightarrow 2CaCO_3 \text{ (solid)} \quad (3)$$

The tendancy to form calcium carbonate may be appraised via a number of indices among which ought to be cited the Langelier-Saturation-Index (LSI) and Rysnar Index both applicable to low salinity fluids and the Stiff and Davis Index for high salinity waters.

The LSI is expressed as

$$LSI = pH - pHs \quad (4)$$

Where pH is the water measured pH and pHs the saturation pH i.e. the pH at equilibrium with CaCO3. Hence the LSI represents the pH change required to bring a water to equilibrium.

In order to calculate the LSI it is necessary to know the alkalinity, the Ca hardness, the TDS, the actual pH and the following estimates.

$$pHs = (9.3 + A + B) - (C + D) \quad (5)$$

where :

$$A = [\log(TDS) - 1]/10 \quad \text{TDS in mg/L}$$
$$B = -13{,}12 \times \log \theta + 34{,}55 \quad \theta, \text{ temperature in K} \quad (6)$$
$$C = \log[Ca\ 2+] - 0{,}4 \quad Ca^{2+} \text{ as mg/L } CaCO_3$$
$$D = \log [\text{alkalinity}) \quad \text{alkalinity as mg/L } CaCO_3$$

The CaCO3 scale rating may be found in table 5.

Calcium carbonate can exist in three distinct polymorphs, calcite, aragonite and vaterite, which have been identified in scales, though vaterite is of seldom occurrence. Chemical thermodynamics predict that calcite, the least soluble polymorph, should be the phase favoured in the precipitation process.

Aragonite is also encountered in geothermal systems forming more soluble scale, sometimes as indurated as calcite. It has been shown that application of an electromagnetic field would lead to aragonite (instead of calcite scale, a property developed commercially in inhibition of low to medium temperature industrial water systems.

Table 5: Rating of waters for scaling conditions according to LSI.

LSI value	Tendency of water
+2.0	Strong scale-forming conditions, non-corrosive
+1.0	Slightly scale-forming conditions, non-corrosive
0.0	Borderline scale potential (but pitting corrosion possible)
-1.0	No potential to scale, the water will dissolve $CaCO_3$, slightly corrosive
-2.0	No potential to scale, the water will dissolve $CaCO_3$, highly corrosive

3.2.1 Heavy metal sulphides

Formation of sulphide scale (e.g. lead, iron, zinc, copper, antimony sulphides) occurs mainly in high enthalpy fluids. Here, two opposing phenomena take place as the brine flashes. For mildly acidic fluids most of the sulphide species enter the vapour phase in the form of H_2S resulting in a significant decrease of those species in the separated brine. However, the pH rise provoked by the simultaneous release of CO_2, a strong bi-acid, causes the heavy metals to precipitate as sulphides. Heavy metals at elevated brine temperatures are transported mainly as chloride complexes; additionally, precipitation of heavy metal sulphides is enhanced by two other factors (i) temperature, and (ii) enrichement in heavy metal of the separated brine as a result of flashing. The pH and temperature dependence of three heavy metal sulphide solubilities are depicted in fig 2. (Milos Island, Greece)

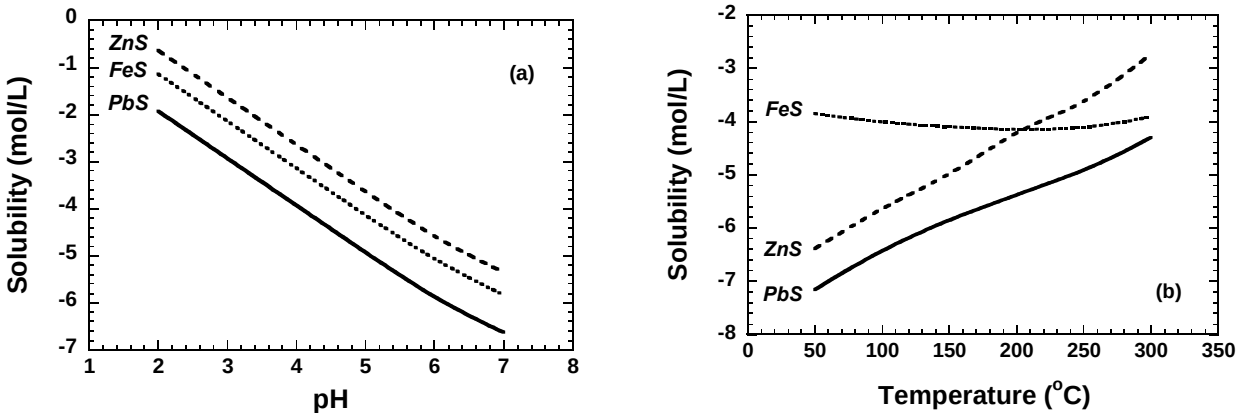

Figure 2. Solubility of heavy metal sulphides at 2 N NaCl solutions as a function of pH at a constant temperature of 250°C (a) and of temperature at pH=7 (b) [Data from Helgeson, 1969]

Iron sulphide has been shown to be a major scale species identified in Paris basin geothermal district heating wells as a consequence of steel casing corrosion damage. The scaling sequence described in fig. 3 is summarised here after.

(i) Corrosion of the (soft grade) carbon steel casing in the CO_2/H_2S aqueous system results in the presence of significant quantities of iron in the geothermal brine according to the reaction

$$\text{Fe (metal)} \rightarrow Fe^{2+} + 2e^{-} \qquad (7)$$

A minor fraction of the dissolved iron originates from the leaching of pyrite present in the carbonate reservoir rocks, but its low concentration (<1 mg/l) leads to regard corrosion of the steel casing as the major contributor.

(ii) Reaction of iron and sulphide ions, the latter resulting from bacterial reduction of sulfates abundant in the geothermal fluid causing the deposition of various iron sulphide phases, namely mackinawite, FE (i+x) S, pyrrhotite ortroilike, Fes and pyrite, FeS2, the ultimate crystallisation stag

$$(1+x)\ Fe^{2+}\ HS \Leftrightarrow Fe\ (1+x)S + H^{+}$$

$$Fe^{2+} + HS^{-} \Leftrightarrow FeS + H^{+} \qquad (8)$$

$$Fe^{2+} + 2\,HS \Leftrightarrow FeS_2 + 2H^+ + 2e^-$$
$$3Fe^{2+} + 2\,HS \Leftrightarrow Fe_3S_4 + 4H^+ + 2e^-$$

Note that the released atomic hydrogen may invade the steel lattice through preferential discontinuities ands accumulate to form molecular hydrogen, thus generating stress corrosion cracking and irreparable casing damage as recently experienced in an EGS well in the Cooper Basin (Habanero lease) of Australia.

(iii) Aging, following deposition, resulting in scale phase transformation as exemplified below

$$FeS + HS^- \rightarrow FeS_2 + H^+ + 2e^-$$
$$3FeS + HS^- \rightarrow Fe_3S_4 + H^+ + 2e \qquad (9)$$
$$2FeS + FeS_2 \rightarrow Fe_3S_4$$

Obviously, any method to mitigate iron corrosion induced scaling would imply prior corrosion prevention/control of the exposed casing material.

3.2.2 Silica and metal silicates

Amorphous silica (SiO_2) is deposited from virtually all high temperature geothermal fluids and eventually medium temperature waters. The mechanism of silica deposition is neither simple nor well understood. In contrast to $CaCO_3$ and metal sulphide species, silica deposition is controlled by the kinetics of silicic acid, $Si(OH)_4$.Owing to slow polymerisation kinetics, silica deposits build up several minutes, hours even, after meeting supersaturaation conditions. The polymerisation rate at pH < 9 depends on pH (or $[OH^-]$) according to the following equation

$$-\frac{d[Si(OH)_4]}{dt} = k\,[Si(OH)_4] - [Si(OH)_4]_e^2\,[OH^-]^{-0.7} \qquad (10)$$

Where k is a reaction constant depending upon the deposited area and subscript the silica concentration at equilibrium conditions with amorphous SiO_2. Practically, whenever pHs remain lower than 5, reaction kinetics are very slow and silica deposition quasi nil.

In several geothermal fields, such as Salton Sea (Imperial Valley, Southern California) and Kyushu, Japan, iron and aluminium are incorporated in amorphous silica in the form of type Fe-O-Si and Al-O-Si bonds, thus forming the so-called metal silicates. It may be inferred that the silica deposition rate is enhanced in the presence of aluminium an iron (as Fe^{2+} and Fe^{3+}) ions. Although the aluminium concentration in geothermal fluids barely exceeds 5 mg/kg its contribution to scale can be as high as 10 % w/w (as AlO_2);

Another distinctive attribute of silica deposits is their presence in the whole geothermal line, i.e. not confined to the vicinity of the well flashing level. As a result major shortcomings may be encountered at brine reinjection level due to reservoir pore bridging/blocking by precipitated silica colloids.

3.3 Scale handling and abatement

There exist a wide range of candidates methods to control, prevent and mitigate scaling, which are outlined below

. Avoid flashing in the wellbore by maintaining high pressures. This requires to operate submersible pump sets (either of the electric, ESP, or lineshaft, LSP, types) able to cope with temperatures up to 250°C; if not more (# 300°C) which do not exist to date. As a matter of fact 180°C seems the upper limit of commercially marketed artificial lift units. Hence, geothermal operators are bound to inhole flashing and vapour lift production and, whenever scaling develops in the well, to remove scale by means of periodic reaming workovers. Actually such mechanical reaming methods may not prove effective in removing scale from downhole slotted liners the usual completion of high enthalpy wells

. Adjustment of first stage flashing pressure at separator inlet. High inlet pressures can dramatically reduce scale formation by keeping solids saturation at low level, a reliable method in preventing silica deposition but less effective when it comes to heavy metal sulphide scaling.

. Enlarging pipe diameters, i.e. reducing flow velocities, may impact carbonate and sulphide scaling above the flashing front since the deposition process is controlled by the scale forming ions migration rate towards pipe walls.

. Avoid as much as possible undue shutdowns and changes in operational conditions while running the plant.

. Last but not least, chemical inhibitors. Chemical inhibitor agents are routinely used in preventing carbonate scale but show poor performance, if any, in defeating silica and sulphide scaling wherever the latter is not a corrosion by-product (see Paris basin case study). Acid injection aimed at reducing pHs can be contemplated as a means for mitigating silica and sulphide scale. Regarding the latter one should be aware that large quantities of acid might be mobilised owing to the buffering effect of $HC0_3^-$ ions in carbonate reservoir settings.

Whenever the foregoing fail, mechanical (well reaming and scaping) or hydraulic (hydroblast) means of removing scale remain the sole remedial issue.

3.3.1 $CaCO_3$ scale inhibition

Crystal growth inhibitors are the most widely used in controlling CaCO3 scale in geothermal installations. High pressure production and occasionally acid cleaning methods can be in certain instances, useful complements or substitutes.

Scale inhibition consists of adding moderately large molecules which are absorbed on the active growth sites of crystal surfaces, thus delaying nucleation and crystal growth, therefore distorting the crystal edifice of the scale.

Then are several classes of inhibitors, namely :

(i) T*hreshold effect* : the inhibitor acts a as salt precipitation retarder.

(ii) *Crystal distortion effect* : the inhibitor interferes with crystal growth by producing an irregular structure (most often rounded surfaces) with weak scaling potential.

(iii) *Dispersion* : the polarisation of crystal surfaces results in the repulsion between neighbouring crystal of reverse polarities

(iv) *Sequestration or chelation* : complexation with selected cations (Fe, Mg, etc…) leads to the formation of soluble complexes.

The best ways of controlling inhibitor efficiencies is to monitor Calcium concentrations at given plan localities (well heads, separator inlet/outlet, turbine, heat exchanger inlet etc…). Inhibitor concentrations range usually between 2 and 20 mg/l but doses as high as 50 mg/l have been reported. Combination of different inhibitor is often practiced which may eventually perform better than their individuel components.

The most popular in geothermal operations are the phosphorous based compounds (inorganic polyphosphates and organophosphorous compounds, mainly phosphonates) and polycarboxylates (products of polyacrilic maleic and polymethacrylic acids, polymaleic anhydrite etc…). A number of polymers are used as scale inhibitors and dispersants. A typical phosphonate complies with the following structure

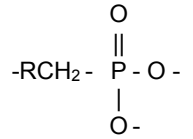

The structure of phosphonate with C-P-O bonding is more stable *vis-à-vis* hydrolysis than polyphosphates. Combined phosphate/polyacrylate formulations often demonstrate optimum efficiencies as the latter chemical adds dispersant properties to the former threshold/sequestering/chelating functions. Molecular weights (i.e. polymer chains) are kept low so as to avoid flocculating/thickening shortcomings.

The most suitable mode of using chemical additives in geothermal systems is continuous downhole injection, either upstream of the vapour flashing front (high enthalpy wells) or at bottomhole (low, medium enthalpy wells). Actually, seldomly is the injection of inhibitors carried out from surface in batch mode.

A typical downhole chemical injection outfit operated on the Latera field, Italy, is described in fig.3. In order to cope with the locally hostile reservoir environment the injection line design addressed a high grade internally coated (Hastelloy C4/teflon) continuous slim (5-10 mm as ID/OD) tubing. Such downhole alternatives need to cope with several operational obstacles, (i) formation of pseudo-scales (calcium phosphates) requiring either concentration or inhibitor formulation modifications, (ii) inhibitor stability (and corrosivity) at high temperatures, and (iii) plugging of the injection line outlet, indeed a critical issue which can be overcome by continuous (and periodically high pressure) injection.

Summing up, chemical inhibitors do not thoroughly eradicate but mitigate instead the tendancy for geothermal fluids to precipitate as a consequence of their supersaturation. The fluid remains supersaturated and it could be envisaged that long residence times might reduce inhibitor efficiencies.

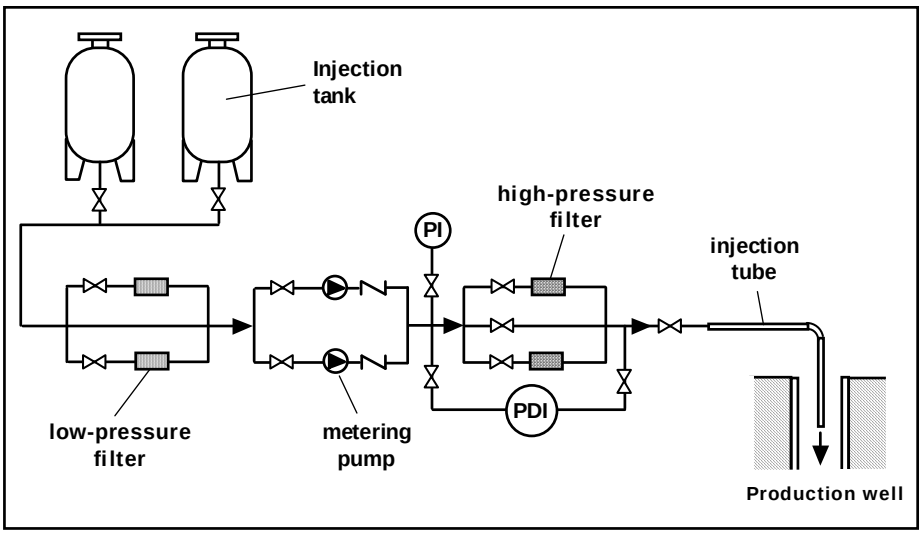

Figure 3. Simplified schematic diagramme of the inhibitor injection system [Pieri et al, 1989].

4 CORROSION

In general, corrosion may be defined as the deterioration of a material interacting with its environment. Regarding geothermal corrosion issues, the topic will address the electrolytic processes impacting the integrity of metals and alloys exposed to hostile fluid thermochemical environments.

4.1 Corrosion types

4.1.1 General(uniform) corrosion.

The most commonly encountered corrosion feature is characterised by a uniform weight loss of the exposed material. It's rate is generally low in the absence of atmospheric oxygen. Nevertheless, higher corrosion rates may be expected when exposed simultaneously to O_2 and H_2S. It does not lead, generally speaking, to severe material failures contrary to other corrosion mechanisms.

4.1.2 Pitting corrosion.

Piercing is a localised corrosion process, affecting a small fraction of the exposed material which undergoes very high corrosion rates resulting ultimately in its piercing. High localised corrosion rates may cause, unexpected before hand, casing and pipe failures. Chlorides are the major steel pitting agents and ammonium ions alike for copper based alloys. Pitting corrosion represents the major damage for plate heat exchangers owing to thin plate sections and given the fact a single hole renders the heat exchanger inoperative.

4.1.3 Crevice corrosion.

It is an enlarged version of pitting corrosion, where corrosion products grow in a crevice space, thus building up a highly localised corrosive environment. Chloride anions favour hydrolysis reactions initiating the process. Crevice corrosion is also a distinctive signature of bacterial corrosion.

4.1.4 Underdeposit corrosion.

It deals with a crevice corrosion developing below a deposit, either scale, corrosion products or a variety of other debris which generate enhanced corrosion rates. It is difficult to combat because the deposits opposite a barrier restraining the efficiency of corrosion inhibitors.

4.1.5 Galvanic corrosion.

It occurs when different metals or alloys get in contact with each other, in an electrolytic solution, the highest ranked in the galvanic suite undergoing faster corrosion. A typical galvanic corrosion case is illustrated by a steel flange in contact with a bronze valve.

4.1.6 Impingement.

It represents an accelerated corrosion mechanism related to coated metal structures. When the protective film gets damaged further to mechanical / hydraulic wear or abrasion, corrosion rates are likely to accelerate because of high local fluid velocities, turbulences and cavitation effects.

4.1.7 Stress corrosion cracking (SCC).

SCC is a type of localised corrosion which produces cracks in a specific corrosive environment subject to tensile stresses (either applied, residual O_2 by gas intrusion). It has serious consequences since SCC can occur within the design casing stress range thus causing occasionally irreparable well damage. There are various SCC classes, chloride-SCC (steel), ammonia-SCC (copper alloys) and H_2S/H_2-SCC respectively, the latter leading to catastrophic failure of high strength steel grades casings exposed to aqueous CO_2/H_2S environments.

Other types of corrosion address intergramelar corrosion, dealloying, erosion corrosion and corrosion fatigue.

4.2 Governing parameters

4.2.1 Temperature.

As a general rule, the higher the temperature, the higher the corrosion rate. This results from the temperature dependant reaction kinetics and the higher diffusion rates of wang corrosive by products at increasing temperatures. They are exceptions somehow, under given solubility conditions. For instance many gases display lower solubilities at higher temperatures in open systems, thus causing corrosion rates to diminish.

4.2.2 pH.

Almost always do corrosion rates increase with decreasing pHs (i.e. increased acidity). This is a direct consequence of increased aggressive (H^+) ion concentrations and solubilities of most potentially corrosive agents.

4.2.3 Oxygen concentration.

Oxygen is an aggressive oxidising gas and therefore a major corrosion agent. Corrosion rates increase with oxygen concentrations until diffusion rates to surface reach a maximum, a principle which applies to most other oxidising agents such as Cl_2, H+,Br_2

4.2.4 Fluid velocity.

Its relation to corrosion is complex although, as a general rule, corrosion rates increase with velocities but not linearly. At very low velocities, even static conditions diffusion takes place that is likely to induce corrosion. Corrosion rates increase until a plateau is reached, which reflects the diffusion limit at a given temperature, at somewhat moderate fluid velocities. However, when they increase to such high values that the metal surface film gets damaged, corrosion resumes, increasing with increasing velocities.

4.2.5 Suspended solids.

Increased suspended solids concentrations accelerate corrosion rates as they contain inorganic or organic contaminants (clay, sand, silt, biomass) present in geothermal waters.

4.3 Corrosion damage diagnosis, removal and prevention

4.3.1 Diagnosis

. Corrosivity classification

Ellis and Conover have developed, from a wide range of geothermal corrosion data, an empirical system aimed at classifying geothermal fluids according to their corrosivity. The core of the system is the so-called TKS (Total Key Species), an indicator similar to TDS (Total Dissolved Solids) as it cumulates the corrosion sensitive ions i.e. chloride, sulphate, carbonate, bi-carbonate, total sulphide and ammonium species. The Ellis system encompasses six classes (five related to liquid dominated sources, the sixth one addressing vapour dominated sources) depending on their TKS, amount of chloride in TKS, pH and fluid inlet temperature. For the majority of liquid dominated resources, chloride, sulphate and bi-carbonate ions compose the bulk of the TKS, where as for vapour dominated resources the TKS is replaced by the volume of non condensable gases present in the steam. This classification provides general information and guide lines useful to the production and chemical engineers at plant design stages.

. Pressure and flow monitoring

It is a simple means for characterising well impairment from losses in well deliverabilities compared to nominal productivity/injectivity figures. These measurements can be usefully complemented by well testing and relevant pressure drawdown/rise and/or build-up/fall-off analyses which will provide the bases for precise evaluation of damage impact.

. Direct damage assessment

It is performed via logging inspection based on multifinger, ultrasonic or borehole imaging tools. Casing calipers are reliable damage indicators (before and after well cleaming) which can achieve high resolution and accuracies thanks to 40 or more simultaneously acquired radic values. Two way times from ultrasonic sources can also retrieve internal acoustic diameters, longer echos corresponding to wall piercing, and well imaging. Material balances carried out on logs completed at diffluent dates after restoration workovers provides a means for appraising damaging kinetics (i.e. either corrosion or deposition rates).

. *Chemical control*
Analyses of liquid, gas and solid (suspended, deposited) enable to establish the fluid thermochemical profile and either validate or predict its corrosion (and scaling) tendencies. Important in these respects are the pressure volume temperature (PVT) data collected at bottomhole, the wet chemical (quantitative) and dry mineralogical (X-Ray diffractometer) (qualitative) of scale samples collected at selected in hole and surface localities. Thermodynamic modelling can be further applied to match actual data, predict future damaging trends and design *ad-hoc* inhibition protocols.

Worth mentioning are the coupon and corrosion meter methods based on weight losses/gains and polarisation resistance recording respectively which monitor corrosion rates (usually expressed in μm/yr) and control corrosion inhibition efficiencies.

4.3.2 Removal

The conventional remedial strategy consists of cleaning the well by removing scale by either hydrojetting tools or rockbits, driven by drill strings or coiled tubings (the latter restricted by a limited flow capacity compared to drill pipe performance). In geothermal service and iron sulphide deposits (identified as corrosion products rather than native reservoir produced scale), the jetting technique has been successfully applied.

Another restoration procedure, known as soft acidification, proved efficient on several damaged injector wells in the Paris area.The technique consists of injecting continuously from surface highly diluted HCl solutions mixed with an iron sequestering additive. The injected acid volume is equivalent to that normally squeezed into the reservoir via a drill string in conventional petroleum/geothermal/ground water well- acid jobs. Only do the injection times differ, 60 hrs as opposed to 1 hr, and the etching process alike, which, in the conventional procedure, concerns the reservoir alone whereas soft acidification addresses both well casing and/or formation damage.

4.3.3 Prevention

Material definition would seem the most appropriate means for preventing corrosion. Fiber glass/ epoxy resin composite casings or liners are valid candidates provided temperatures remain below glass transition temperature (105°C) and that well inclination does not exceed 35°. The concept, illustrated in Fig. 4 and implemented on a Paris basin geothermal district heating site, offers an additional capacity of circulating chemical inhibitors via the steel casing/fiberglass lining annulus.

Chemical inhibition, discussed in more details in the forthcoming section, is another alternative which requires suitable injection (especially downhole) technologies, adequate selection of candidate inhibitor agents and monitoring/evaluation protocols. Needless to say, the foregoing measures have to prove cost effective as regards the, often sensitive, exploitation economics of low grade geothermal heat.

4.4 Corrosion inhibition

To inhibit corrosion, small amounts of corrosion inhibitors can be added to water systems and process streams in order to reduce corrosion rates to acceptable levels. In general, corrosion inhibitors are incorporated in corrosion filming agents in such a way that they increase the film's capacity to prevent corrosion. The corrosion inhibition mechanism relate to the metal surface and surface/water processes. The polar nature of some molecules favours adsorption, but the idea that corrosion inhibitor films act as barriers is erroneous. The adsorption of these molecules is accompanied by the companion process of desorption. An inhibitor molecule is usually in constant motion, being adsorbed and desorbed between the fluid and the protective film. The rate of adsorption to the surface is a function of the nature of the molecule, as well as of inhibitor concentration. The same rationale applies to the desorption process. It is important in inhibition procedures to maintain a sufficient molecule concentration in such a way that the adsorption rate remains at least equal to the desorption rate, a process commonly referred to as passivation.

Corrosion inhibitors are either *organic* or *inorganic*. The former are characterised by high molecular weight structures, incorporating nitrogen or phosphorous groups. They are usually highly polarised

molecules and the most common groups include phosphate esters and phosphonates. Surfactant filming agents, based on fatty amines (octadecyclamins) belonging to the aromatic or aliphatic group, are most popular in the oil industry. Their objective is to isolate the metal surface from the corrosive fluid by means of a supposingly monomolecular hydrophobic film, whose forming kinetics can be studied through sorption/desorption tests. These inhibitors can include biocides and oxygen scavengers (by addition of sodium sulphite or hydrazine for instance). Several formulations associate quaternary ammonia and a sequestering function in a hydroalcoholic solution which renders it totally water soluble.

Inorganic inhibitors are salts of some metals and amphoteric elements (e.g. chromate and zinc salts, molybdate and silicate compounds, phosphates, etc.). Quite often these materials show persistent film-forming or passivation effects. In some instances, they react with the metal surface.

At elevated concentrations the inhibitor exhibits biocide and detergent effects whereas at lower doses it demonstrates filming properties. Combined, custom designed, crystal growth inhibition and filming formulations can also be used. This was the rationale followed on selected Paris basin wells sensitive to both fluid corrosivity and scaling generated by precipitation of native (i.e. formation issued) and, corrosion generated, iron sulphide suspended particles (see fig.2).

Bacterial corrosion is another matter of concern, especially on injection wells and self-flowing systems degassing at production well head. Biocides are implemented, in the framework of probative tests and protocols, in batch mode including brief and massive (shock effect) injection cycles.

Agents combining biocide/corrosion inhibition properties have been experimented in this respect and substituted in several instances to initially injected, either monofunctional corrosion or/and bifunctional, corrosion/scaling inhibitors.

Candidate agents, tested in the Paris area and other sites on low to medium temperature geothermal wells, are listed in the table 4 review sheet. It is the authors' opinion that the comprehension of inhibition mechanisms and efficient field applications remains widely experimental, if not empirical, and, by all means, site specific. Nevertheless, the impact of chemical inhibition, as practiced on Paris basin wells, was deemed positive and, actually, proved cost effective.

Table 4: List of selected candidate inhibitor agents

Name	Function				Description
	Antiscale	Dispersant	Anti-corrosion	Biocide	
SCI 1	X				Phosphonate non ionic
SCI 2		X			Low molecular weight polyacrylate anionic
SCI 3	X	X			Phosphonate/polyacrylate anionic
CORI 1			X		Cationic surfactants; non ionic in glycol solutions
CORI 2			X		Fatty amine derivatives in aqueous solutions
BIOC 1				X	Non ionic surfactants and aldehydic derivatives
BIOC 2				X	Cationic surfactants and quaternary ammonia
BIOC 3				X	Superior aldehydes in aqueous solution
SCORI 1	X		X		Sequestering agents and fatty amine derivatives
SCORI 2	X	X	X		Phosphonate, polyacrylate and fatty amine derivatives
CORBIO 1			X	X	Non ionic surfactants and aldehydic derivatives
CORBIO 2			X	X	Fatty amin derivatives and quaternary ammonia
SCB 1		X	X	X	Polyacrylates, fatty amine derivatives, quarternary ammonia

Because of the elevated pressures prevailing in many geothermal wells, appropriate technologies are required for inhibitors injection, wherever needed. A number of devices and protocols have been and are being developed.

One of the most reliable downhole chemical injection lines developed to date is the Auxiliary Injection Tubing (AIT). It has been implemented according to the following design criteria:

- line continuity as opposed to a threaded coupling tubing string,

- avoid downhole extraweight and well head hanging,
- accomodate three types of submersible, electric submersible (ESP), lineshaft (LSP) and hydraulic turbine (HTP) pump sets and subsequent annular restrictions,
- dissociation of pump and line handlings (running in hole, pulling out of hole),
- material definition and structure combining operational flexibility, stiffness and mechanical strength (burst pressure, tensile and yield strengths), chemical resistance (corrosion) and weight,
- compatibility with concentrated chemical inhibitors and formation fluids,
- permanent control of line integrity, thus avoiding costly and risky fishing operations,
- minimize induced pressure losses,
- five-year lifetime under the conditions (artificial lift, high flowrates, deep deviated wells) prevailing in geothermal service.

Summing up, the AIT structure is that of a composite, slim, cylindrical and slick line combining steel, thermoplastic and elastomer materials.

The candidate in hole assemblies are illustrated in fig. 5 according to three artificial lift configurations. These lines include (i) a central core (stainless steel injection tubing), (ii) four strengthening/integrity control wires, and (iii) two to three concentric thermoplastic/elastomer encapsulating layers selected, depending upon target service conditions, among the candidate materials whose properties are summarised in table 5.

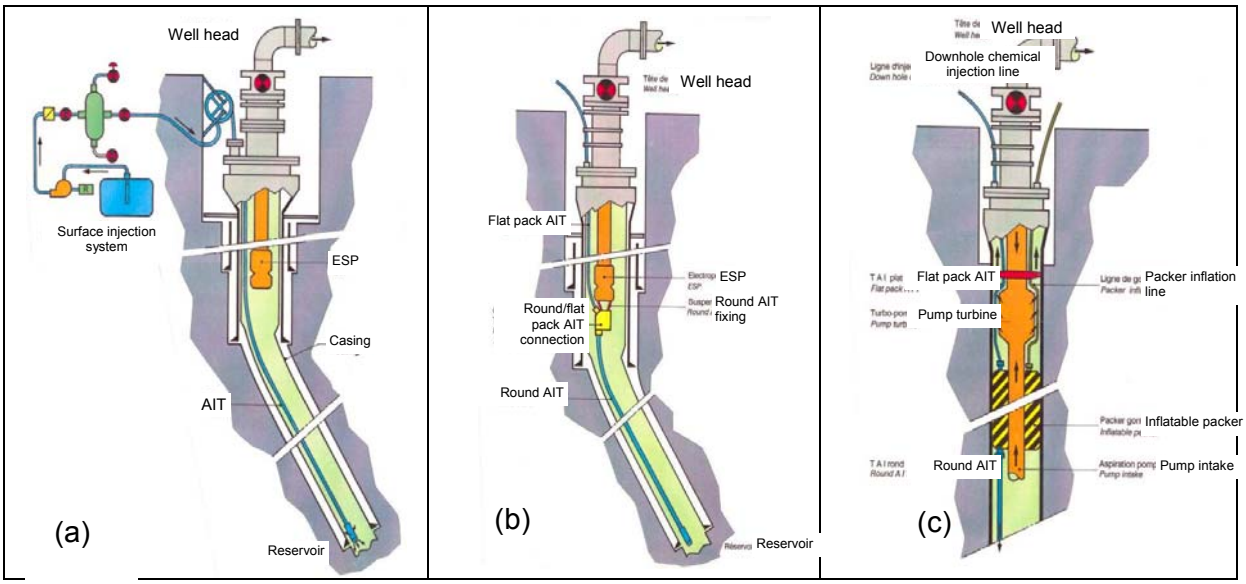

Figure 5. Downhole chemical inhibition lines. (a) Standard configuration in artificial lift wells. (b) Arrangement in an artificial lift well with restricted annulus. (c) Modification to accommodate a packer/turbopump configuration [GPC IP].

Table 5: Candidate thermoplastic and elastomer material properties

Material type (*)	PPC	PA 11	PA 6	EPDM/PP	PVDF	HALAR	PA6/PP/ EPDM	PES	TPFE	TPFA
Max. operating temp. (°C)	105	95	120	140	150	170	120	190	204	260
Tensile strength (Mpa)	25	55	35	28	46	50	43	90	22	28
Elongation (%)	300	300	240	600	80	200	300	7	300	300
Hardness	60 D	72 D	40 R	50 D	77 D	75 D	65 D	70 D	60 D	55 D
Water absorption (%)	<0,1	2,5	5	2	<0,1	<0,1	<1	2,1	0	<0,03

(*)PPC: Polypropylene Copolimer
PA 11: Polyamide 11
PA 6: Polyamide 6
EPDM: Etylene Propylene Dyene Monomer
HALAR: Chloro Tri Fluoro Ethylene
PVDF: PolyVinyle Dyene Fluoride
TPFE: PolyTetra Fluoro Ethylene (Teflon)
TPFA: PerFluoro Alkoxy (Teflon)
PES: PolyEther Sulphone

The surface injection system sketched in fig. 5a includes briefly (i) a high pressure volumetric, controlled rate, metering pump, (ii) a pulse dampening device, (iii) a back pressure, nitrogen fed, vessel preventing invasion of the AIT by the formation fluid, (iv) a no return valve, and (v) a regulation card adjusting inhibitor injected volumes to well discharge according to target concentrations.

Finally, monitoring is undoubtedly a vital segment of any chemical inhibition policy. It aims at (i) evaluating the efficiencies of selected candidate inhibiting agents, (ii) assessing optimum inhibitor concentrations, and (iii) matching the best possible cost/performance compromise.

Monitoring protocols usually involve the following headings:

- hydrodynamics: control of pressures and temperatures and subsequent well, reservoir, geothermal network and heat exchanger performances,
- fluid chemistry : general and topical (selected indicators, HS^-, S^{2-}, Fe^{3+}, Fe^{3+}, Ca^{2+}, HCO_3^-, etc.) liquid and PVT (dissolved gas phase, gas-to-liquid ratio, bubble point) analyses,
- inhibitor injection concentrations : volume metering, flow concentrations via tracing of the inhibitor active principle,
- solid particle monitoring: concentrations (staged millipore filtrations) and particle size diameters and distributions (optical counting, doppler laser velocimetry),
- microbiology: sulphate reducing bacteria numbering,
- corrosion : measurement of corrosion rates (coupons, corrosion meters),
- down hole line integrity: electrical measurements, pressurisation and/or tracer tests,
- periodic well logging inspection

5 CONCLUSIONS

The exploitation of geothermal systems often addresses thermochemically sensitive fluid environments resulting in severe well impairment and, occasionally, in irreparable damage. Such adverse fluid settings and damage have been experienced while developing large geothermal district heating systems in the Paris area as well as high-temperature systems for power production. Clearly, as in many reported case histories, these aspects, not known beforehand, had been overlooked in the early design and development stages.

Damage diagnosis and prediction of fluid corrosion and scaling tendencies have enabled to assess, *a posteriori*, adequate removal and preventing procedures. The latter led to the implementation of

relevant material definition and chemical inhibition designs based on removable fiber glass/epoxy resin well lining and downhole injection of corrosion/scaling inhibitors and biocides.

Of particular significance is the reliability demonstrated by downhole chemical inhibition and reservoir control lines. This strategy, backed by sound efficiency monitoring of candidate filming corrosion inhibitors of the fatty amin type and of combined phosphonate and polyacrylate scale inhibitors, proved rewarding so far and cost effective in safeguarding well life and restoring, close to nominal, target production ratings. Similar policies and technologies could, in spite of the site specificity of chemical inhibition, be extended, preferably at design stage, to selected geothermal development prospects and environments.

REFERENCES

Andritsos, N, Ungemach, P., Koutsoukos, P. (2009). Corrosion and Scaling in Geothermal System. In press.

Amjad, Z., and Zuhl, R.W. (2006). Particle Size and Microscopic Investigation of Iron Oxide Foulants in the Presence of Dispersants. Association of Water Technologies, Inc. 18th Annual Convention & Exposition, Charlotte, North Carolina. 13-16 September.

Andritsos, N. and Karabelas A.J. (1991). Sulfide Scale Formation and Control in Geothermal Plants. *Geothermics* **20**, 343-353.

Benoit, W.R. (1990). Development of a Carbonate Scale Inhibition Program at Dixie Valley, Nevada. *Trans. Geoth. Res. Council* **14**, 1567-1573.

Betz-Dearborn Handbook of Industrial water Conditioning, 9th ed, BETZ, 1991.

Bohlmann, E.G., Mesmer, R.E., and Berlinsji, P. (1980). Kinetics of Silica Deposition from Simulated Geothermal Brines. *J. Soc. Petr. Engineers* **20**, 239-248.

Corsi, R. (1986). Scaling and corrosion in geothermal equipment: problems and preventive measures. *Geothermics,* **15**, 839-856.

Cowan J.C. and Weintritt D.J. (1976). Water Formed Scale Deposits, Gulf Publ. Co, Houston TX.

Criaud, A. and Fouillac, C. (1989). Sulfide Scaling in Low Enthalpy Geothermal Environment: a Survey. *Geothermics*, **18**, 73-81.

D' Amore, F. & Panichi, C. (1987). Geochemistry in geothermal exploration. *Applied Geothermics*, (Ed. M. Economides & P. Ungemach). J. Wiley & Sons.

Ellis, A.J., & Majon, W.A.J. (1977). *Chemistry and Geothermal Systems*. Academic Press, London.

Ellis, P.F. (1981). A Geothermal Corrosivity Classification System. *Geoth. Res. Counsil Trans*. **5**, 463-466.

Ellis, P.F. (1991). Material Selection Guidelines. In Geothermal Direct Use Engineering and Design Handbook (ed. P.J. Lienau and B.C. Lunis), DOE, Idaho Falls, 171-189.

Ellis, P. F. and Conover, M.F. (1981). Material Selection Guideline for Geothermal Energy Systems, NTIS Code DOE/RA/27026-1. Radian Corporation, Austin, TX, January.

Epstein, N. (1983). Fouling of Heat Exchangers. In *Heat Exchangers: Theory and Practice,* Taborek, J. et al (eds), Hemisphere Publ. Co.

Fontana, M. G. (1986). *Corrosion Engineering*, McGraw-Hill, 3rd edition, New York.

Gallup, D.L. (1997). Aluminum Silicate Scale Formation and Inhibition: Scale Characterization and Laboratory Experiments. *Geothermics,* **26**, 483-499.

Gallup, D.L. (1996). Brine pH Modification Scale Control Technology. *Geothermal Resources Council Transactions,* **20**, 749-755.

Gallup, D.L. (2002). Investigations of Organic Inhibitors for Silica Scale Control in Geothermal Brines, *Geothermics,* **31**, 415-430.

Gill, S. (1996). Development of Scale Inhibitors, *Proc. Corrosion 96*, NACE Conf., paper 229, 18.

Helgeson, H.G. (1969). Thermodynamics of Hydrothermal Systems at Elevated Temperatures and Pressures. *Am. Jour. Sci,* **267**, 729-804.

Henley, R.W., Truesdell, A.H., Barton, P.B. and Whitney, J.A. (1984). *Fluid-mineral equilibria in hydrothermal systems*. *Reviews in Economic Geology*, **1**, Soc. of Economic Geologists.

Huttrer, G.W. (1997). Geothermal Heat Pumps: An Increasingly Successful Technology. *Renewable Energy*, **10**, 481-488.

Kemmer, F. N. (1988). *The NALCO Water Handbook*, McGraw-Hill, 2nd edition, New York.

Knipe E.C. and Rafferty, K.D. (1985). Corrosion in Low-Temperature Geothermal Applications. *ASHRAE Transactions*, **91**, 81-91.

Langelier, W.F. (1936). The Analytical Control Of Anti-Corrosion Water Treatment. *JAWWA*, **28**, pp 1500-1521.

Owen, L.B., and Michels, D.E. (1984). *Geochemical Engineering Reference Manual*, DOE/SF/11520-T1, Salt Lake City.

Pierri, S., Sabatelli, F. and Tarquini, B. (1989). Field Testing Results of Downhole Scale Inhibitor Injection. *Geothermics,* **18**, 249-257.

Rafferty, K. (2000). Scaling in Geothermal Heat Pump Systems. *GHC Bulletin*, March. 10-15.

Rhodes, P.R. (1976). Corrosion Mechanism of Carbon Steel in Aqueous Solutions. Paper presented at the Fall 1976 Meeting of the Electrochemical Society Inc., Las Vegas, Nevada, U.S.A.

Rothbaum, H.P., Anderton, B.H., Harrison, A.G. Rohde, and Slatter, A. (1979). Effect of Silica Polymerization and pH on Geothermal Scaling. *Geothermics,* **8**, 1-20.

Satman, A., Ugur, Z. and Onur, M. (1999). The Effect of Calcite Deposition on Geothermal Well Inflow Performance. *Geothermics,* **28**, 425-444.

Ungemach, P. and Roque, C. (1988). Corrosion and Scaling of Geothermal Wells in the Paris Basin. Damage Diagnosis. Removal and Inhibition. Paper presented at the *International Workshop on Deposition of Solids in Geothermal Systems,* Reykjavik, Iceland, 16-19 August.

Ungemach, P. (1997). Chemical Treatment of Low Temperature International Course on District Heating Schemes. Cesme, Turkey, 19-25 oct., *Course Book* 10/1-10/14.

Ungemach, P. (1995). New geothermal well concept. *IGA News*, Newsletter of the International Geothermal Association, Quarterly no 20, January-March.

Vetter, O.J. and Cambell, D.A. (1979). Carbonate scale inhibition in Republic's East Mesa Geothermal operations. *Trans. Geoth. Res. Council,* **3**, 757-760.

5. WATER INJECTION

Pierre Ungemach
GPC INSTRUMENTATION PROCESS, Roissy-en-France, France

SUMMARY

Not only is water injection an environmental prerequisite (waste disposal, land subsidence) but also, and moreover, a key issue in sustainable reservoir management. The foregoing are exemplified by the succesfull injection strategies implemented on high enthalpy, either superheated steam (Larderello, The Geysers)or liquid dominated (Imperial Valley of Southern California) systems and in the Paris Basin geothermal district heating doublet/triplet well arrays. However, injection of heat depleted brines into clastic sedimentary reservoirs alternating clay, sand and sandstone sequences has long been regarded a delicate subject among petroleum and geothermal operators. Without thorough and careful planning, injections can turn to disaster, for example when the formation and (re)injected waters prove incompatible, or there is particle entrainment, capture and release, or unsuccessfull well completion, which often lead to irreparable damage to the well and formation. The physics and chemistry of the damaging mechanisms and driving parameters are reviewed and illustrated by laboratory experiments, model runs and field trials, and application to practical well completion issues discussed.

1 INTRODUCTION

Injection of the heat depleted brine in a compressed liquid, low enthalpy, source reservoir is liquely to increase by one order of magnitude the heat recovery factor, from a single well production to a doublet production/injection well array. This can be achieved by sweeping the heat stored in the rock which is usually, in such settings, between three to four times that of the heat of the soaking fluid. For a vapour dominated field this ratio, even when considering adsorbed water, stands one order of magnitude higher.

1.1 Low enthalpy resources

Lets Ah (A area, h net thickness) be the influenced reservoir volume, Ø the porosity, $\gamma w, \gamma r, \gamma t$ the fluid, rock and total (rock+fluid) heat capacities respectively, Q the discharge rate, t* the total exploitation time and Θo, Θr,Θa the reservoir, rejection (from the heating system) and the mean outdoor ambient temperatures respectively ; the recovery factor, i.e. that fraction recovered from the heat in place, can be expressed as

$$R = \eta \frac{\theta_0 - \theta_r}{\theta_0 - \theta_a} \qquad (1)$$

with:

$\eta = \frac{Q}{Ah}\frac{\gamma_w}{\gamma_t} t^*$, the efficiency of the heat extraction system. (2)

Assuming :

A = 100 km^2 (single well), 10 km^2 (doublet array)

h = 10 m ; Q = 200m^3/hr ; t*= 30 yrs ; Ø=15 %

γw = 4.186 10^6Jm^{-3}K^{-1} ; γ r=2.143 10^6Jm^{-3}K^{-1} ; γ t= Ø γ w+(1-Ø) γ r=2.45 10^6Jm^{-3}K^{-1}

$\theta_0 = 70°C$; $\theta_r = 40°C$; $\theta_a = 10°C$

R ($\eta = 0.09 = 4.5$ % single production well

R ($\eta = 0.9) = 45$ % production/injection well doublet

High enthalpy sources

Assuming a single phase liquid (i.e. compressed water) resource at 250°C and 50 bars (reservoir conditions) and a 8 bar turbine inlet pressure, the steam to water ratio (or steam quality) *x* of the flashed water/steam two phase mixture is expressed as :

$$x = \frac{1086 - 721}{2769 - 721} \# 18\ \% \qquad (3)$$

This means that under such conditions most of the well discharge will consist of waste water which, in the case of a 50 MWe rated (P_{el}) geopower plant and a heat to power conversion efficiency η set at 22 % (dual flash condensing cycle), would amount to :

$$Qww = \frac{P_{el}}{\eta}\frac{1-x}{xh} \# 0.96 \text{ m}^3/\text{s } (3450\text{m}^3/\text{hr}) \qquad (4)$$

indeed a significant quantity whose disposal, as a consequence among others of increasingly stringent environmental regulations, would require deep water (re) injection, preferably into the source reservoir at selected localities to avoid undue premature production well cooling (i.e. thermal breakthrough).

Regarding superheated vapour (so called dry steam) reservoirs there is by definition no waste water phase apart from steam condensates. Water injection, in addition to the waste water disposal issue, exhibits several other advantages adressing :

. pressure maintenance as exemplified by the mass conservative doublet concept of heat extraction ;

. permeability enhancements of high enthalpy reservoirs further to cold water injection and thermally induced stresses (thermal stress cracking);

. *in situ* abatement of non condensable gases in vapour dominated (dry steam) fields ;

. land subsidence control

These advantages are counterbalanced by :

. faster than anticipated thermal break throughs and premature cooling of production wells, a critical issue particularily acute in fractured rock environments ;

. plugging of injector wells, in fine grained clastic sedimentary reservoirs, caused by suspended solid particles ;

. triggering of microeathquakes, known as induced seismicity, long noticed in high enthlpy fields (Geysers among others) and thoroughly analysed by Mossop & Segall [2005], which could actually be turned into an asset by releasing stresses accumulated in seismically active areas. Induced seismicity has recently shown up as a sensitive matter further to microeathquakes generated by stimulation of EGS wells in the European Upper Rhinegraben continental rift.

2 HIGH ENTHALPY SETTINGS

2.1 Vapour dominated fields

Although waste water disposal remains a primary objective of geothermal operators, the fast pressure depletion noticed in the Geysers and Larderello superheated vapour fields portrayed water injection as a key issue for sustaining steam production.

The Geysers dry steam field had long undergone anarchic over-production, resulting in sharp pressure decline and generated power losses alike, a trend illustrated in fig. 1, until water injection came into play. In a dry, superheated, steam field, injection of the steam condensate recovered downstream from the turbine outlet is of limited impact.

Therefore, an additional exogenous water source is required, which in the Geysers field consisted first of pumping seasonal inflows from nearby creeks, then, since late 1997 of processed waste water imports piped to selected peripheral wells (total 75, mostly reconverted abandoned production wells), from the distant cities of Lakeside (South East Geysers Effluent Pipeline, SEGEP, start Oct.1997) and Santa Rosa (Santa Rosa Geysers Recharge Pipeline, SRGRP, start Nov. 2003). The impact of water injection from the SEGEP system can be visualised in fig. 1. The fast depletion pressure and subsequent production decline trends have been countered and significant gains in power achieved, up to 100 MWe (@2007) respective to te base exponential decline curve. Furthermore, the present mass replacement ratio amounts, all injection sources (steam condensates, creeks, pipeline imports) included, to ca 85% of Geyser steam production. The cumulative production and injection curves displayed in fig. 2 indicate à 38 % net mass replacement of the steam produced since exploitation start

up in the late 1960s. This ratio will increase in the future but never reach 100% full replacement. Incidentally these figures may usefully contribute to the geothermal renewability vs sustainability debate. Las but not least, the non condensable gas (NCG) concentration, which had in the past dramactically increased as a result of pressure decline and extent of the vapour zone, decreased rapidly, since injection started, to its initial figures (from ca 8000 to 2000 ppm, quoted by Ali Khan, 2009). This "forced" in situ NCG abatement process, further formalised and modelled by Pruess [2006], upgrades steam quality, conversion efficiency and net power outputs. Elsewhere, microseismicity has been reported to increase with increased water injection but larger seismic events seem unrelated to injection [Ali Khan, 2009].

Similar conclusions could be drawn for the emblematic Larderello field in central Tuscany, where identical trends, depicted in fig. 3, have been noticed since similar practices were implemented [Capetti, 2004].

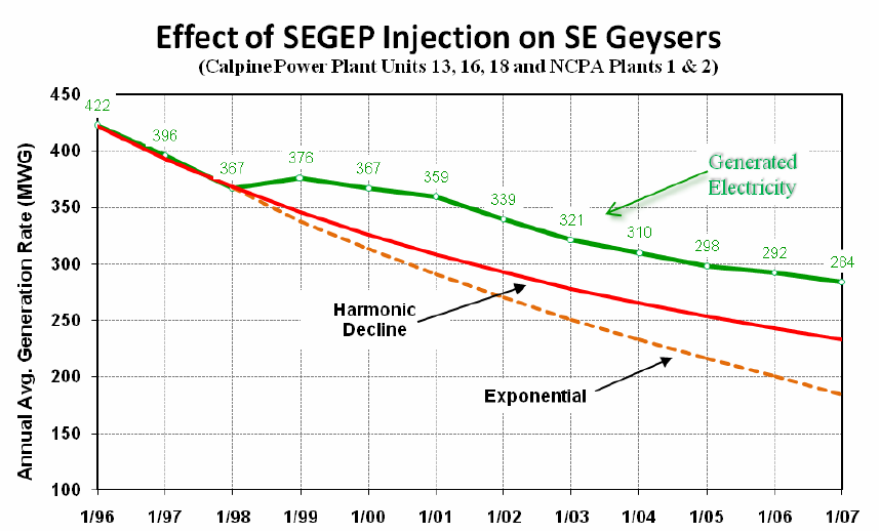

Figure 1: Effect of SEGEP Injection on SE Geysers [Calpine and NCPA].

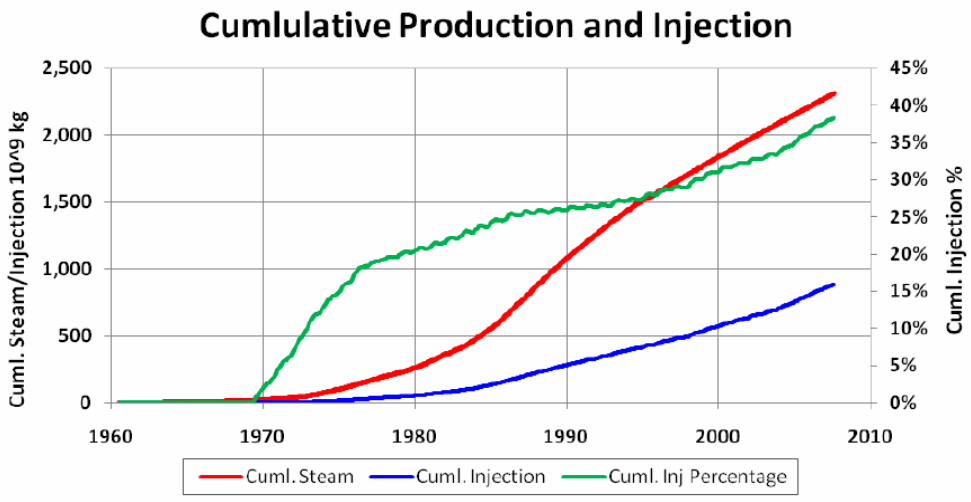

Figure 2: Cumulative Production and Injection (Division of Oil, Gas, and Geothermal Resources).

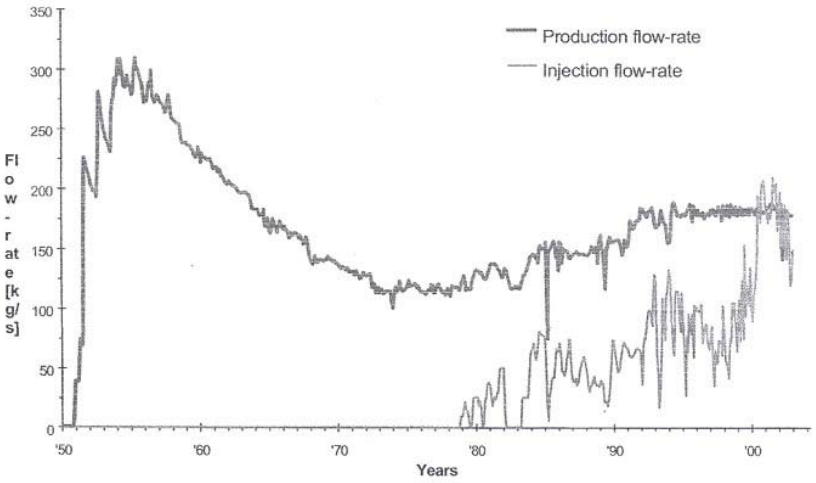

Figure 3: Influence of the reinjection on the steam flow rate of 28 wells in the Valle Secolo area, Larderello [Capetti,2004]

2.2 Liquid dominated fields

As far as flashed steam, liquid dominated, fields are concerned, water injection, although raising wider interest from operators, still remains a largely unexplored route. This attitude is likely due to well short-circuiting/premature cooling, injection well plugging, and, last but not least, to induced seismicity fears among others. It somewhat persists in spite of the positive impacts reported in the Imperial Valley of Southern California, where deep water injection succeed despite a locally hostile thermochemical environment, in defeating subsidence of an extensively irrigated farmland, and in the Kizildere and Balcova fields of Western Anatolia [Serpen and Aksoy 2005].

Liquid dominated, high enthalpy, reservoirs are often limited in size and fluid circulation is governed by prevailing fractured porosity/permeability patterns. Therefore, water injection is subject to channelling along preferential flow paths and consequent short circuiting of production wells. These distinctive features of fractured geothermal reservoirs led Bodvarsson [1969] to recommend that injection wells be drilled at least one kilometre apart and the water injected several hundred meters below the exploited reservoir. This obviously poses the problem of the injectivity of this deeper horizon which is not known beforehand.

3 MEDIUM AND LOW ENTHALPY RESERVOIR ENVIRONMENTS

The large majority of low to medium enthalpy reservoirs, eligible to direct uses, belong to sedimentary environments as opposed to high enthalpy, liquid dominated, volcano-tectonic settings.

The critical problem area deals here with the injection of cooled brines into fine grained clastic sedimentary reservoirs alternating sand, sandstone and clay sequences. If not carefully designed, injection practice may turn into a disaster caused by non-compatible, formation vs. injected, waters, external/internal particle entrainment, capture and release leading ultimately to well and formation, often irreparable, damage.

As stressed by Ungemach [2003], suspended particles of either (or both) external (carrier fluid) or (and) internal (matrix) origins represent the main permeability impairment risk to well and formation integrities.

3.1 Injector well and formation damage - an overview

Well and formation impairment caused by water injection is a consequence of one or more of the damaging factors listed below:

(i) chemical incompatibility between injected and formation (native) fluids;
(ii) microbiological effects;
(iii) water sensitivity of sandstones;

(iv) suspended solids (fines, corrosion products, scale);
(v) fines migration within the injected formation;
(vi) trapped gases;
(vii) air contamination;
(viii) incompatible chemical additives and inhibitors;
(ix) thermodynamic changes (pressures and temperatures) induced by the injection process
(x) injection flow
(xi) inadequate well completion.

The damage ensuing from the above leads to a loss of injectivity as a result of plugging of the well bore, sandface, well completion and/or formation.

Chemical incompatibilities do not affect geothermal (re)injection processes in which formation water is pumped into the source reservoir. However, the thermodynamic changes (cooling, high pressures, degassing and related pH increase) of the heat-depleted brine may trigger adverse thermochemical reactions and the consequent formation of silica and carbonate scale (Vetter and Kandarpa, 1982; Ungemach and Roque, 1988), whose solubility products and saturation indices are, generally speaking, pH-dependent, and also temperature-(silica) and pressure-dependent (carbonates).

Microbiological effects can be expected in the presence of sulfate-rich formation waters and cold temperatures, which accelerate the growth of sulfate-reducing bacteria, as reported by Rosnes et al. [1990] for North Sea injector wells. In this case the damage takes the form of extra cellular organic slime, which blocks the pore entries. The solution here is to dose with appropriate biocides.

Care has also to be taken in developing and applying the most suitable corrosion and scaling inhibitor formulations. Adverse electrolytic (anionic/cationic) and surfactant/detergent properties could trigger secondary effects that could eventually lead to the failure of an injection project. These aspects have been discussed in great detail in the specialized literature and will not be dealt with here.

Trapped gases observed in injected geothermal waters downstream from the injection pump have also been known to create damage [Boisdet et al., 1989].

Oxygen (air) contamination and subsequent oxidizing and corrosion are a major source of problems, but should not affect geothermal operations with pressurised production or injection facilities. Additional precautions against this process include oxygen scavenging, through injection of sodium sulfite or hydrazin.

The water sensitivity of sandstones is a phenomenon associated with clays welling and with the dispersion of colloidal clay particles in fresh waters [Khilar and Flogler, 1983]. Migrating clay particles in their carrier fluid can be captured in pore constrictions, thus leading to a reduction in permeability. Since this type of damage is clearly related to fresh water, it may seem less important in geothermal (re)injection, as the latter generally involves saline brines. Khilar and Flogler (1983) provide an exhaustive study of models of particle entrainment, and of capture and release mechanisms.

The damage originating from suspended solid particles is the most common in oil and geothermal engineering, and is considered a major challenge for the industry. It includes fine migration and formation invasion, particle vs pore parameters (size, shape, concentrations, tortuosity) and the various forces (hydrodynamic, retention) involved in the entrainment, settling, capture and release mechanisms.

These aspects are illustrated in fig. 4, and their implications on injection flow rates, well completion and damage prevention or removal will be discussed in some detail

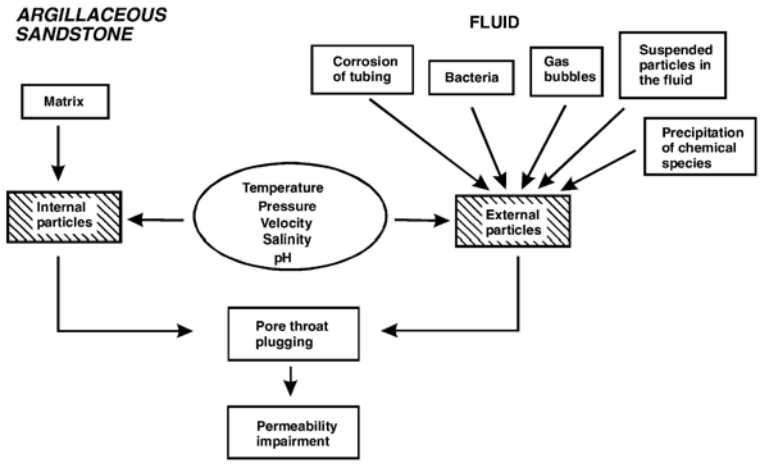

Figure 4: Permeability impairment induced by particles [European Commission, 1997].

3.2 Particle-induced damage. A review of types of damage and source mechanisms

Barkman and Davidson [1972] identified four types of damage, illustrated in fig. 5 and described below.

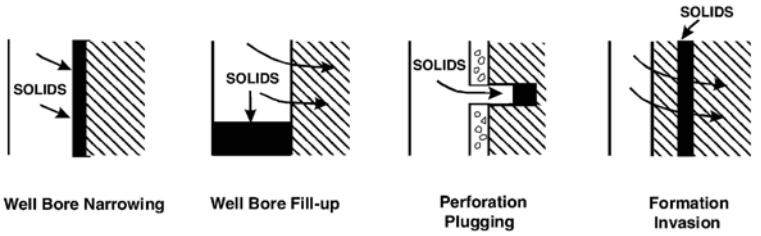

Figure 5: Well and formation impairment mechanisms caused by solid particles [Barkman and Davidson, 1972].

3.2.1 Wellbore narrowing (or sandface bridging)

The particles are fixed against the wellface, thus forming a filter cake. This damage can be removed by reversing flow from injection to production (a procedure known as backwashing) and by means of well stimulation techniques (acidizing, mud acid). Incidentally, this filter cake may prove beneficial with regard to the filtering of suspended solids, although at the expense of injectivity.

3.2.2 Wellbore fill-up

This occurs as a result of particles sedimenting downhole by gravity, thus reducing the net pay interval. The sediments can generally be removed during a successful well completion job, by circulation clean-up.

3.2.3 Perforation plugging

Solids get blocked in perforations, a situation somewhat similar to wellbore fill-up. This impairment can be removed, partially or totally, by back washing at high depletion pressures, and by acid treatment.

3.2.4 Formation damage

The fine particles entrained in the formation start bridging at a distance from the wellbore where pressure gradients and subsequent velocities can no longer sustain entrainment or avoid capture, thus forming a plugging collar. This damage is often considered irreparable.

Elementary mechanisms (particle retention sites and forces, capture and deplugging processes) have been described and classified deep filtration types with regard to particle sizes, retention sites and driving forces by Herzig et al [1970] (fig.6).

3.3 Elementary mechanisms

3.3.1 Retention sites

These can be divided into four categories:

. surface sites: the solid particles are retained on the surface of a matrix grain;

. crevice sites: the particles are wedged between the convex surfaces of two grains;

. constriction sites: the particles bridge pore entries because pore size is smaller than particle diameter;

. cavern sites: the particles settle in small pockets formed by several grains, known as pore ‘‘bellies’’ or dead-end sheltered areas.

3.3.2 Retention forces

Briefly, they consist of:

. fluid (axial) pressure, which fixes particles at constriction (bridging) sites;

. friction (tangential) forces, which are exerted on deformed particles at crevice sites;

. surface forces, which address Van der Waals, attractive forces and electric (static and kinetic) forces that are either repulsive or attractive depending on the physical–chemical nature of the suspension;

. chemical forces, which mainly involve colloidal solutions and subsequent chemical bonding.

3.3.3 Capture mechanisms

These include (fig.7) :

. sedimentation; due to the solid–liquid density contrast, gravity becomes dominant and the particle, which moves more slowly than fluid velocity, is likely to settle;

. inertia; the buoyancy entailed by particle apparent weight causes the particles to deviate from the fluid streamline, bringing them into contact with the grains;

. hydrodynamic effects; lateral migration of particles towards retention sites

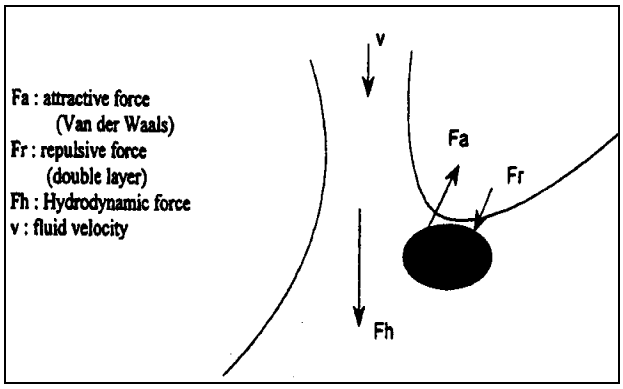

Figure 6: Forces reacting in the particle-grain-fluid system

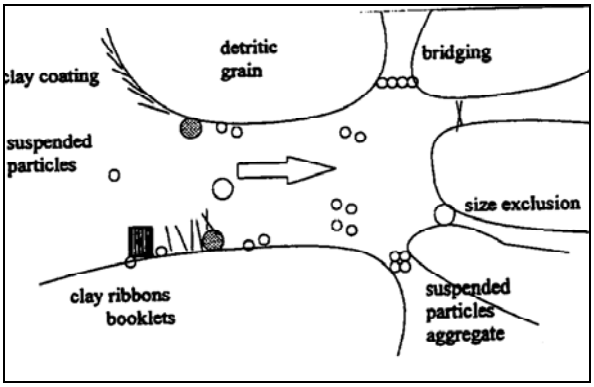

Figure 7: Mechanisms of particle capture

3.3.4 Deplugging.

This can occur either spontaneously due to the natural flow conditions or artificially as a consequence of, operator generated, hydrodynamic changes such as flow-pressure pulses or flow reversal (backwashing).

3.4 Governing parameters

The following factors affect plugging kinetics:

(i) carrier fluid (flow rate, dynamic viscosity and density),
(ii) suspended particles (concentration, shape - spherical, non spherical, size - diameter - and density),
(iii) porous matrix - porosity, permeability which have a macroscopic meaning, grain size and distribution - assumed spherical of diameter d for the sake of simplication; porosity and permeability are plugging dependant, i.e. they vary with the particle retention rate.

It would be fair to add that interactions are likely to occur between suspended particles as a result of electrokinetic effects leading to flocculation which can be enhanced by addition of coagulant and flocculant additives.

3.5 Classification of deep filtration types

They are summarized in table 1. It can be seen that, as inferred from common sense, the larger the particle size, mechanical filtration, volume retention sites, hydrodynamic forces and sedimentation/direct interception capture prevails whereas for the smaller particles, chemical and colloidal filtration, surface retention sites, Van der Waals electrokinetic and chemical bounding forces and direct interception/diffusion are dominant.

Table 1: Classification of deep filtration types [Herzig et al.]

Filtration type	mechanical	physico-chemical	colloidal
Particle size	7-30 μm	1-3 μm	<0.1 μm
Retention			
• sites	constrictions, crevices, cavernes	surface	surface
• forces	frictions fluid, pressure	Van der Waals, electrokinetic	Van der Waals, electrokinetic, chemical bounding
Capture mechanism	sedimentation, direct interception	direct interception	direct interception, difusion
Deplugging:			
• spontaneous	unlikely	possible	possible
• provoked	flow reversal	increase in flow rate	increase in flow rate

3.6 Selected modeling and laboratory works

Donaldson [1997] studied the flow of silica particles through selected sandstone core plugs with pore sizes varying from 0.5 to 40 μm in order to investigate the probability for particles, assumed spherical, to enter the pores and percolate through a filtering medium restricted to capillary tubes.

Davidson [1979] investigated the plugging phenomenology by circulating suspended particles through normalized, high porosity/permeability, porous media. He estimated the extent of the invaded area as a multiple of well bore radius and the time required for achieving a two fold injectivity decrease as a function of solid particle concentrations. In so doing the critical velocity needed to avoid particle deposition was found to be inversely proportional to particle diameter.

Gruesbeck et al [1982] carried out flowing experiments with formation (native) particles to assess the plugging mechanism by relating linear flow velocities to rates of particle entrainment and to evaluate critical velocities and damage radii. One conclusion drawn by the authors was that critical velocities vary as the reciprocal of the damage radius.

Khilar et al [1983] developed a mathematical model aimed at simulating release and capture of colloidal suspended clay particles, according to the mechanisms sketched in figure 3. Their approach is based on a material balance relating variations with time of the clay particle concentration *c* to the rates of particle release (r_r) and capture (r_c) through the expression

$$\frac{dc}{dt} = r_r - r_c$$

The release process is assumed to conform to a first order decay mechanism expressed as

$$r_r = \alpha \cdot \sigma_1$$

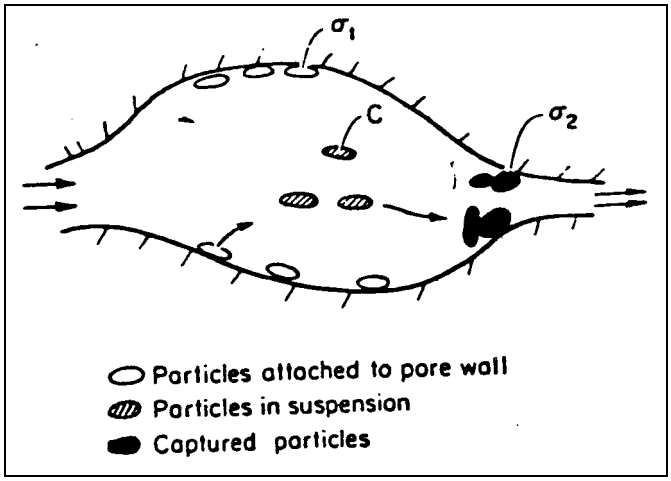

Figure 8: Particle release and capture mechanisms [Khilar and Fogler]

where α is a release coefficient, depending on salt concentration and fluid linear velocity and also on temperature through a relationship of the Arrhenius type, and (ii) σ_1 the attached particle concentration.

The capture is essentially sensitive to particle concentration *c* and pore geometry, the latter implying that capture results from direct interception (or drag forces). Therefore capture rates can be related linearly to concentration through :

$$r_c = \beta \cdot c$$

where β is the capture coefficient.

Summing up it may be concluded from these experiments and modelling works that the rate of impairment

(i) increases with increasing temperatures as a consequence of a temperature dependant release coefficient (fig. 9) ;

(ii) decreases with increasing inlet velocities and is very sensitive to changes within the low velocity range (fig. 10), and

(iii) strongly depends on the particle/pore size ratio as shown in fig. 11 which reveals the effect of both low velocities and high particle to pore ratios.

Note that all experiments were conducted on reference sandstone cores with artificial solid (mono-dispersed) suspensions and at low inflow velocities compared to the rates practiced in geothermal (re)injection.

A pragmatic approach to particle filtering requirements proposed by Harris et al (1982) is worth a mention. These authors consider that particles of diameters greater than one third of pore throats may cause intermediate bridging; diameters lower than one tenth of pore throats are entrained ; and particle sizes lower than one third of pore throats result in formation invasion and deep bridging of formation pore constrictions. Moreover, they apply a rule of thumb to an ideal porous medium made up of spherical grains in which permeability k is related to porosity Φ by the equation :

$$\Phi = \sqrt{k}$$

Hence, assuming a transmissivity kh equal to 2 Dm and a net pay h of 10 m, the afore-mentioned design parameters would lead to a critical pore size of 15 μm and a 2 μm minimum filtering criterion.

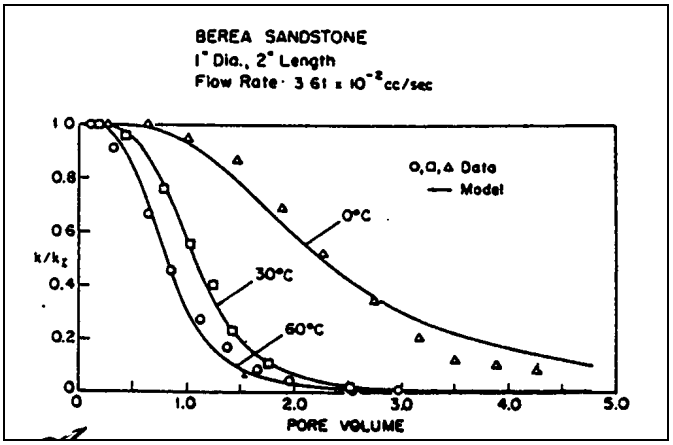

Figure 9: Effect of temperature on permeability reduction [Khilar and Fogler]

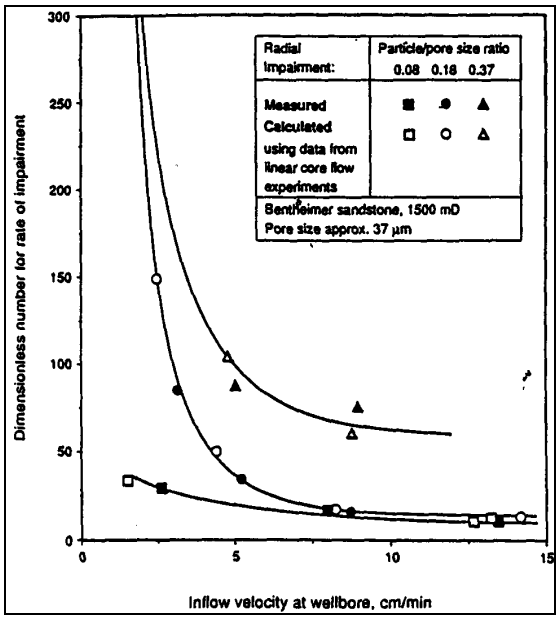

Figure 10: Rate of impairment as function of inflow velocity [Van Valzen et al]

In a comprehensive review paper on particle invasion and related injectivity problems. Vetter et al [1987] address (i) the somewhat idealised description of both the porous medium and solid suspensions, (ii) the lack of adequate particle measurement devices and/or protocols, and (iii) the frequent misconceptions on invasion and migration mechanisms.

For instance, they elaborate on the following dilemma. In a model assuming spherical particles and circular pore sections, how would a needle-shaped fine travel ? Depending on its orientation and the "equivalent" radius adopted, it would either be blocked at pore entry or pass through it, thus contradicting previous assumptions and the entrainment/bridging mechanisms. Vetter et al. (1987) also query invasion depth in relation to flow velocity. Clearly, as the distance from the wellbore increases, the pressure gradient and velocity decrease, thus favouring particle deposition and subsequent formation of a plugging collar. Most of the studies reported by these authors are, however, restricted to the near-wellbore area. Finally, they emphasize the omissions in submicron and colloidal particle characterization and the lack of precise assessments of invasion and damaging mechanisms and remedial strategies.

Recent research has shed some light on these problems by conducting core flooding experiments, and developing simulation codes at pore and core scales, extending them occasionally to the design of field test and injection protocols to accommodate the microscopic and macroscopic academic investigations and engineering problems.

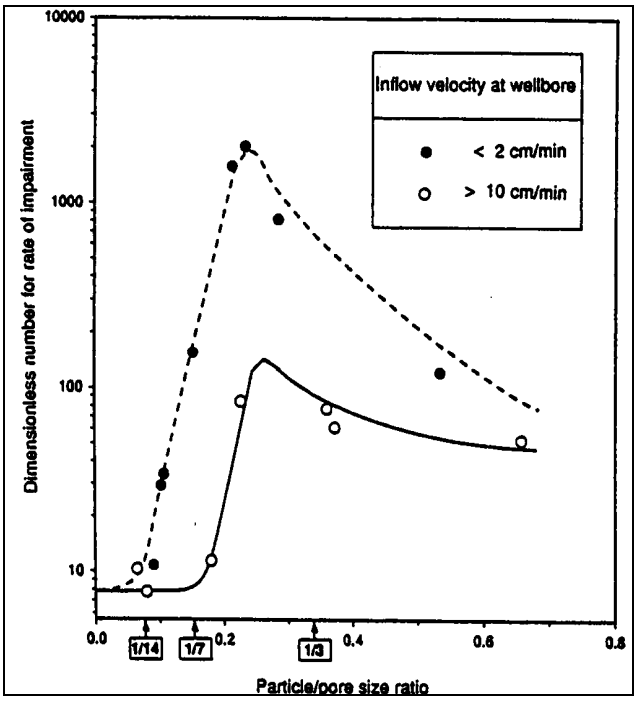

Figure 11: Rate of impairment as a function of particle/pore size ratio [Van Valzen et al]

Worth mentioning in this respect is the, EU supported, research project reported by the European Commission [1997].

The contributions of external and internal particles can be isolated by core percolating experiments using solid free and solid inseminated solutions. These in lab core tests emphasize the opposing effects of hydrodynamic forces on permeability reduction, which are less critical in the case of external particles – the formation of an outer filter cake, that can be removed by backwashing – than in the case of internal particles and associated capture mechanisms (fig. 7), acting at pore level and involving particle to grain interactions (fig.6), which require sophisticated physics and modelling to bridge the pore to core gap.

4 MODELLING AND FIELD TESTS

4.1 Particle induce damage. Pore and Core scare modelling

4.1.1 Pore scale modelling

A sound appraisal of, particle induced, formation damage and plugging kinetics implies that transport processes be modelled from microscopic (pore) to macroscopic (near and distant well bore) scales [European Commission, 2001].

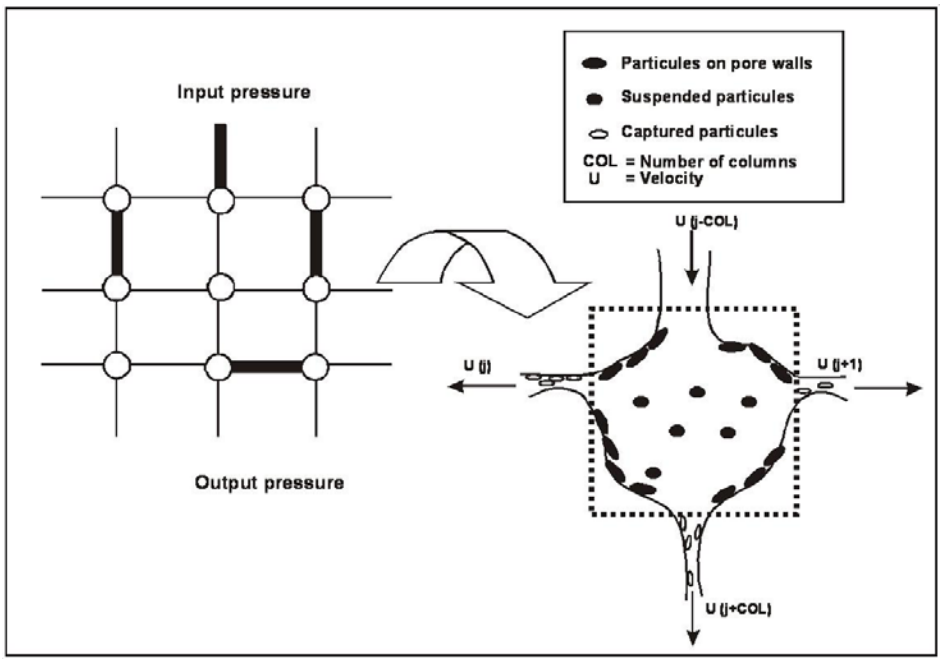

Figure 12: Pore scale modelling (internal particles) network simulation of pore geometry with nodes as pores and branches as throats [European Commission, 1977].

Accordingly, network theory is used to model the permeability decrease induced by internal particle release and capture. Microscopic hydraulic condcutances are generated and placed randomly in the porous network, assumed to conform to an assemblage of cells combining modes (pore bellies) and four connected branches (pore throats) as shown in fig. 12, with release and capture occuring in pore bellies and throats respectively.

The solution of the fluid mass conservation equation at each node allows to calculate the equivalent macroscopic hydraulic conductivities and velocities. It takes into account three entrapment mechanisms (straining, interception and diffusion) and the actual velocity field. As far as plugging kinetics are concerned a good match between simulated and core flooding results is achieved by assuming particle release in pore bellies, capture at pore throats and first order kinetic laws.

The statistical approach inherent to the network model is best suited for accomodating topological changes within the porous matrix and investigating in fair detail fluid/solid interactions. It also provides a particle concentration (σ) dependant permeability functional $k(\sigma)$ which can serve as an input to a core scale simulator.

4.1.2 Core modelling

With respect to external particles, core scale modelling can be used as a means for simulating the core floading experiments and relevant release/deposition mechanismq via the solid concentration dependant, filtration $\lambda(\sigma)$ and release $\alpha(\sigma)$ coefficients and permeability $k(\sigma)$. An optimisation procedure can ease the calibration of the aforementioned parameters and be used ultimately in a radial symmetry, well field applicable, simulation code.

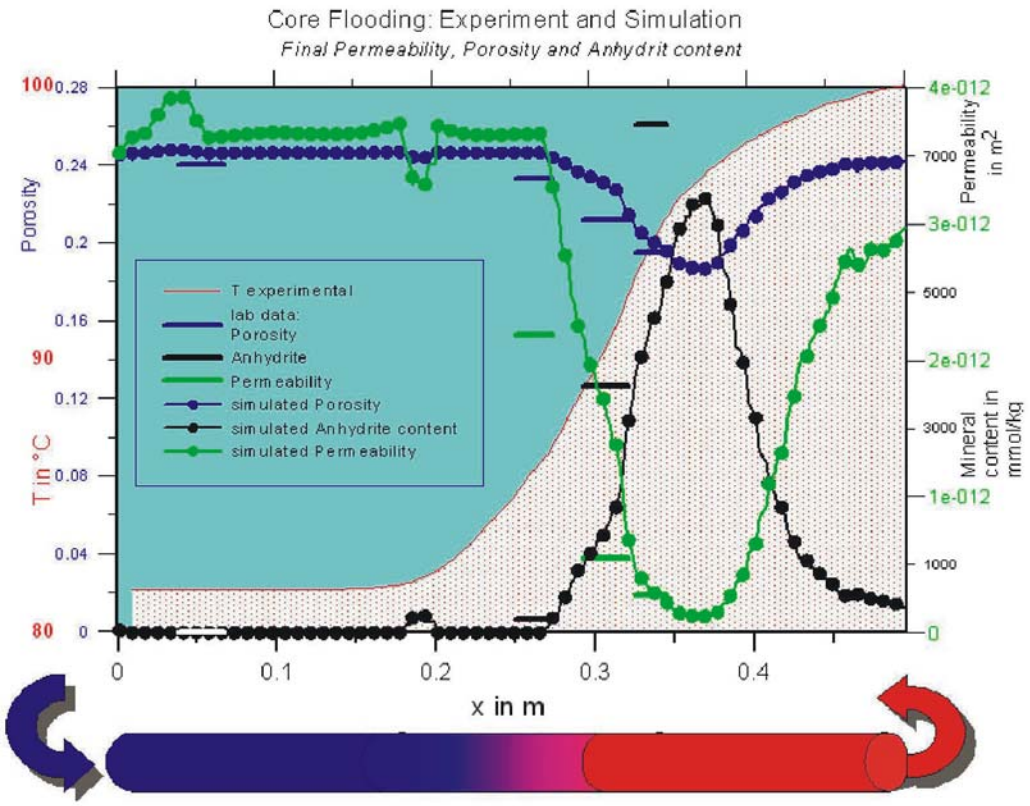

Figure 13: Core scale modelling, external particles [European Commission, 1997 and Clauser, 2003].

Fig. 13 summarises the results of a hydrothermal/thermochemical coupled simulation of a core flooding test using Shemat software [Clauser, 2003]. It shows a good match between observed and computed interacting porosity/permeability/anhydrite content patterns vs temperature and radial distance to well bore. The problem here was to investigate to which extent anhydrite supersaturation/precipitation and resulting pore space reduction would impair reservoir permeability.

4.1.3 Field test

Two vertical wells, 1200 m apart, were drilled west of Paris in the early 1980s, intersecting a roughly 50 m thick interbedded sand, clay and gravel sequence of Lower Triassic age, displaying net pays of 23 and 32 m, respectively; the wells were completed by wire wrapped screen and gravel pack assemblies. Only part of the annular space was gravel packed in well 1. Production and injection tests were carried out in both wells at constant flow rates of 130 and 120 m^3/h. The injectivity testing sequences plotted in fig. 14 demonstrate two constrated pressure transients.

An abrupt pressure drop was noted in well 1, fast stabilising to a steady state injection regime and an injectivity index twice as high as the (temperature corrected) productivity index monitored previously. This behaviour suggested the build-up, during injection, of a mechanical damage caused by the upward motion of clay particles in the partly gravel packed annulus, resulting in the formation of an external filter cake bridging the pore entries at the sandface. This diagnosis could be validated by the highly positive skin factor that was obtained from fall off test data, which was restored to its initial negative value after removal of the cake by backwashing.

Bottomhole pressures in well 2 did not stabilise at all after 21 h pumping and a dramatically decreasing injectivity trend. High injection pressures (in excess of 100 bars at well head) and invasion by micrometric size particles were identified as the major damaging factors. Indeed, particle monitoring via millipore filters showed that the concentrations in solids, in the 3 to 5 µm range, decreased by one half, whereas in the 0,2 to 1 µm (colloidal) domain they had undergone a two fold increase. Moreover, the sandface inflow velocities, close to 10 cm/s, widely exceeded the 1 cm/s empirical threshold set by the industry.

The foregoing highlight the importance of particle filtering and well completion in the design of water injection undertakings.

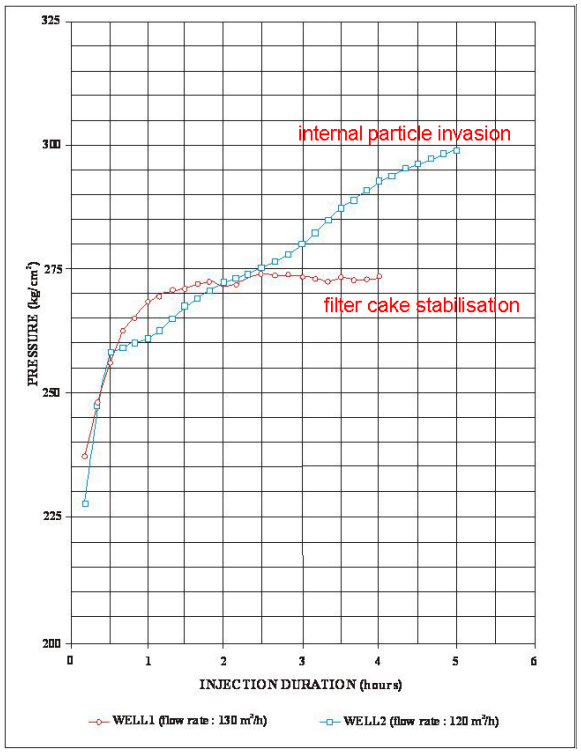

Figure 14: Particle induced damage. Field test. Paris basin Triassic sandstone [Ungemach, 2003].

4.2 Cold water injection into superheated steam reservoir

It results in a complex phase changing mechanism with a phase transition, moving from liquid, to two phase vapor states and delayed progressions of thermal fronts.

The topic has been investigated by Pruess *et al* [1987] in the idealised 1D radial flow case and further by Pruess [1987] in a more realistic fractured reservoir context, the latter evaluating the propagation of two phase plumes within a heterogeneous superheated fractured reservoir.

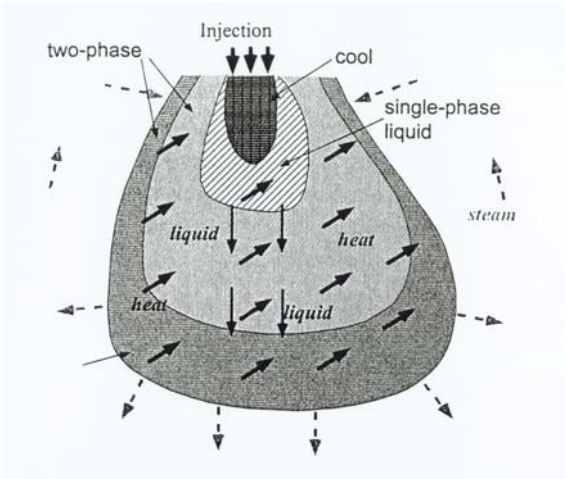

Figure 15: Schematic of cold water injection into a sub vertical fracture filled with superheated steam [Pruess, 1996].

5 CONCLUSIONS

Water injection has been shown to secure sustainable exploitation and longevity of superheated vapour reservoirs as exemplified by the successful injection of imported surface waters in the Larderello and Geysers fields. It has resulted in dilution of non condensable gases, a sort of in situ abatement process, thus upgrading turbine cycle efficiency.

With respect to single phase liquid and two phase high enthalpy reservoirs similar conclusions could be drawn bearing in mind that injection schemes should be carefully designed and monitored to avoid undue short circuiting and premature cooling production well short comings. As a result preliminary tracer tests and modelling should be the rule.

In low to medium enthalpy, fine grained sand sandstone and clayey sedimentary environments, suspended particles represent clearly the main source of damage to wells and formations. A most pertinent conclusion is that damage prognosis and design of optimum water injection strategies are in many instances empirical and site specific.

As stressed by various authors, the precise mechanisms by which a formation is plugged as a consequence of fines invasion and migration are not fully understood. This is particularly true when dealing with internal submicronic or colloidal particles and tight, fine grained, matrices. As a result, carefully designed and implemented field tests and laboratory experiments on formation cores are required to ensure reliable water injection programmes. It is recommended that investigations be carried out in compliance with the following guidelines [Ungemach, 1994].

(i) Assessment of the physical and chemical properties of the formation fluid/suspended solids/rock matrix system

- petrography/mineralogy, porosity/pore structure, permeability
- chemistry (aqueous, gaseous, solid phases), liquid rheology
- solids concentrations, size/distribution, flocculant properties

(ii) Laboratory testing on cores

- representative cores and plugs
- formation brine conditioning
- artificial particle supensions
- core flooding (solid free ands solid inseminated) tests
- model calibration at varying velocities (sandface, formation)

(iii) Design of brine handling facilities

- inhibitors (oxygen scavengers, surfactants, exotic)
- filtering and gas stripping units

(iv) Field testing

- short duration, thoroughly monitored, test
- long duration validation test simulating full scale exploitation

Last but not least a thorough well completion designs of the type displayed in fig.16 is a key issue in achieving successful water injection.

PROJECTED WELL / RESERVOIR PERFORMANCE	Top reservoir depth	1,500 m
	Static WHP	-5 bars
	Total pay	400 m
	Net pay (h)	110 m
	Effective porosity ($Ø_e$)	0.2
	Permeability (k)	100 mD
	Transmissivity (kh)	11,000 mDm
	Skin factor (S)	-2
	Formation temperature	90ºC
	Average injection temperature	35ºC
	Fluid (eq. NaCl) salinity	2.5 g/l
	Fluid dynamic viscosity (production) (μp)	0.32 cp
	Fluid dynamic viscosity (injection) (μi)	0.73 cp
	Total compressibility factor (c_t)	10^{-4} bars^{-1}
	Fluid density (ρp) at 90ºC	965.34 kg/m^3
	Fluid density (ρi) at 35ºC	994.06 kg/m^3
	Target injection rate (Q)	150 m^3/hr
	WHP (150 m^3/hr, 35ºC)	20.5 bars
	Sandface velocity (v_{sf})	0.23 cm/s
	Velocity at completion outlet (v_c)	0.61 cm/s

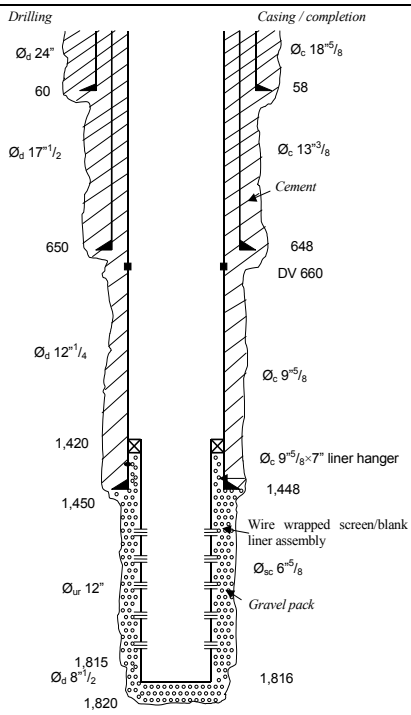

Figure 16: Projected well completion and reservoir performance. Clastic sedimentary environment

REFERENCES

Ali Khan, M., 2009. The Geysers Geothermal Field, an Injection Success Story. Paper presented at the Ground Water Protection Council Annual Meeting, San Diego, Ca.

Antics, M. 2003. Simulation of Geothermal Reinjection Processes*,* EGC 2003, Szeged, Hungary, 26-29 May 2003.

Barkman, J.H. and Davidson, D.H. (1972). Measuring Water Quality and Predicting Well Impairment. *Journal Petroleum Technology*, July 1972, 865-873.

Boisdet, A., Cautru, J.P., Czernichowski-Lauriol, I., Foucher, J.C., Fouillac, C., Honnegger, J.L. and Martin, J.C. 1989. Experiments on Reinjection of Geothermal Brines in Deep Triassic Sandstones. Paper presented at the *International Seminar European Geothermal Update, European Union Commision*, Florence, Italy, 27-30 september 1989. In : Conference proceedings, 419-428.

Capetti, G., 2004. Geothermal Energy Technologies and Strategies for sustainable Development : The Laredello Case History. Proceedings Int. Conf. Geoth. En. and Territory, Tuscany Region, Italy, 244-283.

Clauser, C., Edr, 2003. Numerical Simulation of Reactive Flow in Hot Aquifer*s*-SHEMAT and Processing SHEMAT- Springer Verlag Publ. Co., Berlin.

Davidson, D.H 1979. Invasion and Impairment of Formations by Particulates. SPE paper N° 8210 presented at the SPE 54th Annual Fall Meeting, Sept. 23-26, 1979, Las Vegas, USA.

Donaldson, E.C. et al 1977. Particle Transport in Sandstones. SPE paper N° 6905 presented at the SPE 52nd Annual Fall Meeting, Oct. 9-12, 1977, Denver, USA.

European Commission, 1997. Improvement of the Injectivity Index of Argillaceous Sandstone (BRGM, GTN, TNO, TU Delft). JOULE II Programme. Sub programme Non Nuclear Energy. Contract N° : JOU2-CT92-0183.

European Commission, 2001. Reinjection of cooled brines into sandstone reservoirs. A field application study for geothermal sites in Hungary Acronym REBRISAR (TNO, GPC, GTN, HGA). THERMIE type B action N° : STR/1475/98/NL.

Gruesbeck, C, Collins, R.E. 1982. Entrainment and Deposition of Fine Particles in Porous Media. *Soc. of Pet. Eng.* Journal of AIME, Dec. 1982, 847-856.

Harris, C. and Odom, C. (1982). Effective Filtration in Completion and Other Wellbore Operations Can Be Good Investment. Oil and Gas Journ., Sept. 20, 1982, 148-165.

Herzig, J.P., Leclerc, D.M. and Le Goff, P. (1970). Flow of Suspensions through Porous Media. Application to Deep Filtration. Am. Chem. Soc. Publ., Flow through Porous Media, 129-158.

Khilar, K.C. and Fogler, H.S. (1983). Water Sensitivity of Sandstones. *Soc. of Pet. Eng. Journal of AIME*, Feb. 1983, 55-64.

Pruess, K., 2002. Mathematical Modelling of Fluid Flow and Heat Transfer in Geothermal Systems. An Introduction in five Lectures. United NATIONS University Geothermal Training Programme, Reykjavik, Iceland, oct. 2002.

Rosnes, J.T., Graue, A. and Lien, T. (1990). Activity of Sulfate Reducing Bacteria under Simulated Reservoir Conditions. SPE paper n° 19429 presented at the SPE Int. Symp. on Formation Damage Control, Feb. 22-23, Lafayette, La, USA, 231-236.

Ungemach, P. (edt) (1983). Drilling, Production, Well Completion and Injection in Fine Grained Sedimentary Reservoirs with Special Reference to Reinjection of Heat Depleted Geothermal Brines in Clastic Deposits. *Report of an Extended Contractors Meeting held in Brussels, Belgium*, March 23, 1983. Eur. Un. Comm., Directorate General for Science, Research and Development.

Ungemach, P. and Roque, (1981) C. *Corrosion* and scaling of geothermal wells in the Paris Basin. Damage diagnosis, removal and inhibition. Int. Symp. Deposition Of Solids In Geothermal Systems, Reykjavik, Iceland, Aug. 16-19, 1988 (1988).

Ungemach, P. (1994). Geothermal Injection. A State of the Art Review, Intergeo Slovenia Geothermal School. Radenci, Slovenia, 13-19 Nov.1994.

Ungemach, P., 2003. Reinjection of Cool Geothermal Brines into Sandstone Reservoirs. *Geothermics,* **32**, 743-761.

Van Valzen, J.F.G. and Leerlooijer, K. (1992). Impairment of a Water Injection Well by Suspended Solids. Testing and Prediction. SPE paper n° 23822 presented at the SPE Int. Symp. on Formation Damage Control, Feb. 26-27, 1992, Lafayette, La, USA, 477-490.

Vetter, O.J. and Kandarpa, V. (1982). Scale Prevention and Injection Design Book. US Dept. of En. DOE/DGE Report. Washington, DC, USA.

Vetter, O.J., Kandarpa, V., Stratton, M. and Veith, E. (1987). Particle Invasion into Porous Medium and Related Injectivity Problems. SPE paper no. 16255 presented at the SPE int. Symp. on Oilfield Chemisty, Feb. 4-6, 1987, San Antonio, Tx, USA, 101-120.

Drilling, Completion and Testing of Geothermal Wells

Section 6. Risk Mitigation

6. QUANTIFYING RISK IN GEOTHERMAL DEVELOPMENT. THE HIGH ENTHALPY AND LOW ENTHALY CASES

Miklos Antics, Pierre Ungemach

GPC INSTRUMENTATION PROCESS, Roissy-en-France, France

SUMMARY

Like most resource harnessing ventures, geothermal energy shares both exploration and exploitation risks. Resource discovery and confirmation is carried out mainly by activities, among which are drilling operations, which incur high initial costs. These activities display relatively high risks and are the major barrier to accelerated development worldwide. Once the resource is proven, it mobilizes important financial resources for geothermal production infrastructure development, power plant and transmission line construction. Both the risk and high upfront capital cost make geothermal ventures less attractive to conventional financing schemes.

Quantifying the risk is therefore a key issue which is illustrated in two case studies where the exercise proved relevant so far. The first addresses the high enthalpy, power generation case, in the exploration phase where the main problems of quantifying success-failure risk of exploratory drilling are addressed and a numerical criterion to assess the well output from well testing figures proposed. The second study deals with a large geothermal district heating (GDH) scheme, where the drilling success ratio approached 100% (one recorded full and two partial failures out of around 100 wells) whereas exploitation of the low temperature deposits showed, in the early stages, severe technical and nontechnical shortcomings leading to frequent, prolonged well shutdowns and, ultimately, to their abandonment. A quantified risk prognosis was at a stage projected 15 years ahead which later proved relevant.

1 INTRODUCTION

Many of the countries enjoying geothermal resources have not fully exploited their potential because of a variety of barriers (regulatory, policy, fiscal, technical, geographical, etc.). Geothermal risk mitigation can be achieved by the following key elements: establishment of reliable geological data developed by state-of-the-art geoscientific assessment methodologies, mobilization of the latest exploration and drilling technologies, and availability of a risk insurance product on the insurance market in combination with support from government, bilateral and multilateral financial resources.

Most of the existing geological risk mitigation instruments have been supported via government funding. The commercial insurance market, except for a few recent cases in Germany (e.g. Unterhaching project by Munich Re), is not yet prepared to fit the geothermal risk insurance business into a standard product line because of the lack of adequate size of market demand or nature of the unique risk element which may not be "commercially insurable" with conventional insurance methodologies. In order to bridge this gap, the World Bank has launched the GeoFund and ARGeo programs.

While risk assessment is a complex procedure, relying on surface exploration, and shallow drilling, it is necessary to set up a series of numerical criteria which could lead to the definition of the success or failure when proceeding to the phase of resource confirmation by drilling.

Risk assessment addresses both financial issues and reservoir management strategies.

As regards financial risks incurred at exploration level, the World Bank has produced a comprehensive overview summarised in Fig. 1 risk vs. expenditure chart. It shows quite clearly that, in the compiled project areas located chiefly in East Africa and Pacific Rim countries, the exploratory drilling risk could be minimised thanks to the filtering out of the less attractive, most risky, prospects identified in the preliminary reconnaissance stages, thus leading to a 80% drilling success ratio.

After project commissioning and start-up, the first years of exploitation provide the reservoir/production engineers and management with additional clues on future development alternatives.

The latter are usually investigated by integrating all pertinent data – reservoir characteristics, surface heat/power loads, well productivities, plant performance, make-up well drilling and plant production schedules, economic parameters – into reservoir and economic models to assess ultimately well/field productivities and project economic value.

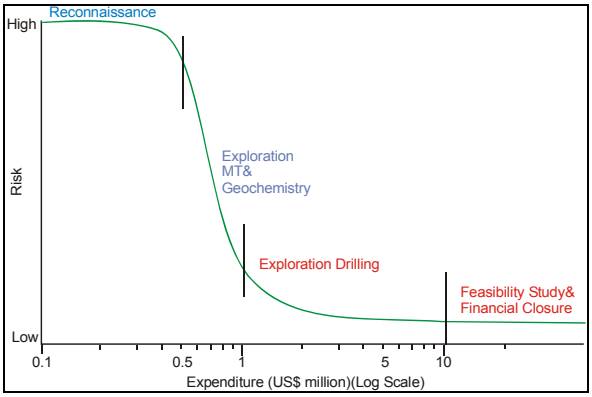

Figure 1: Expenditure and risk prior to geothermal development (source World Bank)

However, the decision making process is clouded by the many uncertainties affecting model inputs. A purely deterministic or probabilistic approach could be misleading. A thoroughly coupled deterministic-probabilistic approach could prove more relevant but by all means unrealistic in consideration of the huge numbers of model runs involved, indeed a tedious and costly exercise if manageable ever, unless kept within reasonable limits by adequate constraints.

Acuna et al. (2002) review the case of a liquid-dominated field in the Philippines where a strategic decision is to be taken as to whether a deep, poorly produced reservoir underlying the presently exploited shallow seated reservoir, should be developed or not.

In order to overcome the aforementioned limitations the authors suggest an interesting methodology outlined hereunder.

- up to ten different exploitation strategies were selected;
- the economic model calculates the project NPV (net present value) probability distribution. The uncertainty for each relevant parameter is described by the most likely (50% probability – P50); pessimistic (10% probability – P10) and optimistic (90% probability – P90) values, defining the parameter cumulative probability function;
- in order to reduce the number of reservoir simulation runs for the P10, P50, P90 uncertainties allocated to the parameters for each exploitation strategy, the model results were synthesised, after preliminary model tests, by using a polynomial approximation to key output data, and four cases reflecting changes in steam extraction rates and make up well drilling schedules constrained by existing well deliverabilities.

The polynomial approximation of reservoir performance (as well deliverability vs. cumulative produced steam) proved rewarding in that it enabled integration of this key uncertainty into the probabilistic economic model to assess the risk impact on project NPV.

2 THE HIGH ENTHALPY CASE

The resource confirmation phase is accomplished through a series of deep exploratory drill holes aiming at determining the potential of the resource which ultimately leads to the design capacity of the power plant.

After the drilling phase is completed, the wells are thoroughly tested.

2.1 Methodology

Drilling records and further downhole measurements in a shut-in well give a rough indication of the output to be expected, and therefore the method of flow measurement that is the most adequate.

The observation of the wellhead pressure over a period of time provides useful indication of any changes in either quantity or quality of flow.

The well measurement programme must comprise a full range of output testing at intervals of several days, linked together in time by wellhead pressure readings, preferably continuosly and automatically recorded.

The geothermal well output test programme should record for *several values of wellhead pressure* the following parameters:

- total mass flow rate
- temperature of single phase and/or quality of flow (enthalpy or dryness)
- phases chemical composition (constituents)

In order to provide a reliable assessment of the well performance, it is also important to keep record of:

- extreme pressure values
- description of the test, reason for selecting a particular method
- history of the well (drilling records)
- correlation to other measurements, e.g. downhole pressure measurements, interference with wells nearby

Any method is used for testing; it is governed by the well characteristics, the resources available and the accuracy. It is recommended to carry out several measurements using the same method and check the results against another method.

Available methods for flow measurements consist of:

- Orifice plate (sharp-edged orifices in combination with a cyclone separator)
  - single phase measurements – pressure drop across the plate associated with temperature measurement
  - two phase measurements – phases must be separated
- Calorimeters, not very appropriate for superheated steam and hot water, most adequate for two-phase flow mixtures

The flow results observed directly are used to calculate from the steam tables, the mass and heat flow enthalpy and dryness fraction.

The isentropic power is equal to:

$$W_{is} = q_v \Delta h_{is} \qquad (1)$$

$$\Delta h_{is} = \left(h_v - h_c\right) - T_c\left(S_v - S_c\right) \qquad (2)$$

where q_w is the steam (vapour) mass flow rate, Δh_{is} is the isentropic enthalpy drop, h is the specific enthalpy, S is the entropy, T is the temperature and v, c are subscripts referring to inlet vapour and condenser respectively.

The steam mass flow is equal to:

$$q_v = \frac{q_t\left(h_t - h_f\right)}{h_v - h_f} \qquad (3)$$

where q_t is the total flowrate at wellhead, h is the specific enthalpy and the subscripts t, v and f refer to wellhead (total flow), vapour and separated liquid respectively.

There is an optimum flash temperature. Would the latter decrease, vapour flow would increase but at the expense of the isentropic enthalpy drop, which would diminish accordingly.

The maximum useful work is given by:

$$W_{net}^{\max} = -\left(\Delta H - T_0 \Delta S\right)\Big]_{T_{gf}^{in}}^{T_{gf}^{out}} = -\Delta B \qquad (4)$$

where ΔB is commonly referred to as the change in availability [Tester, 1976]. For a given fluid and a fixed T_0 and a reinjection temperature T_{gf}^{out} which has a minimum value T_0, the maximum work (per

unit weight of geothermal fluid or per unit heat transferred) possible from an ideal reversible process is a function of only T_{gf}^{in}, the geothermal source temperature, according to the plot given in fig. 2.

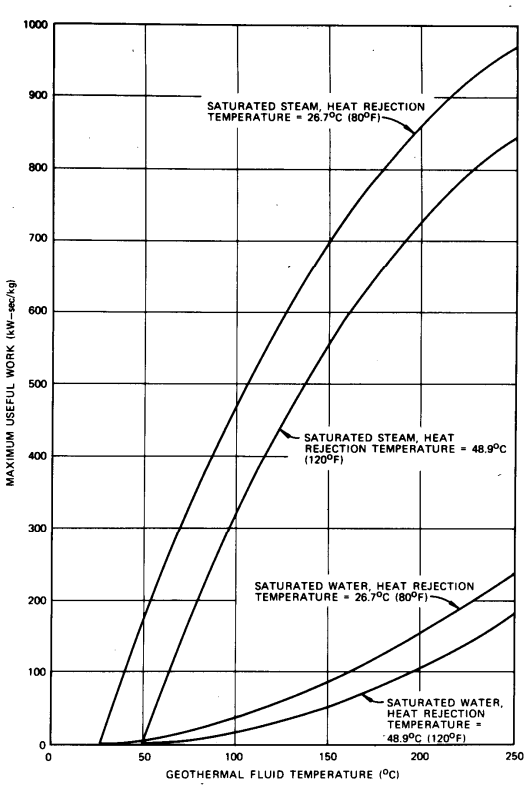

Figure 2: Maximum useful work (ΔB) plotted as a function of geothermal fluid temperature for saturated steam and saturated water sources [Tester, 1976]

2.2 Enthalpy measurements

In a paper issued in 1962 Russell James described an empirical method to measure flow rate from a discharging high-temperature well. James's experiment showed that "*the critical discharge pressure can be used to measure the mass flow or the energy flow of steam-water mixture passing through pipes*". Based on the experiment the following empirical equation describes the relationship between the various measured components:

$$\frac{M * H^{1.102}}{3600 * A * p_c^{0.96}} = 0.184 \qquad (5)$$

where M is the total flow (t/h), A the cross-section area of the discharging pipe (cm^2) , p_c the critical pressure (bar a) and H the enthalpy (kJ/kg). To use this formula to calculate the flow rate from discharging well, the enthalpy must be known. Downhole temperature measurements can yield accurate enthalpy figures should boiling take place within the wellbore.

However in many geothermal fields boiling takes place outside the well. Therefore downhole temperature measurements or geothermometers do not give correct value of the enthalpy of the steam-water mixture entering the well. In such cases a modified version of the Russell-James method has to be applied. The modification is based on measuring the flow rate of 100°C geothermal water from the silencer after separation from the steam fraction. The total flow and enthalpy from the discharging well can be extracted via an iterative procedure from the Russell-James empirical formula.

2.3 Power potential estimate

The process described here [Di Pippo, 2008] is a single flash cycle where the geothermal fluid is wet steam (mixture of water and steam) at the wellhead. The analysis presented here is based on

fundamental thermodynamic principles, namely the principle of energy conservation (i.e. First Law of thermodynamics) and the principle of mass conservation. Figure 3 shows the basic operating principles of the single flash process.

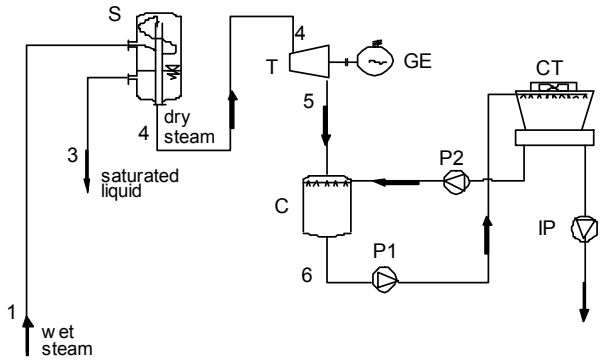

Figure 3: Single flash process schematics

The well (1) is producing wet steam which is separated via a separator (S). The saturated liquid phase is reinjected (waste heat disposal) and the dry steam flows directly to the turbine. After expansion in the turbine (T), the steam is condensed in the condenser (C) and reinjected together with the saturated liquid collected at the separator outlet.

The processes undergone by the geothermal fluid are best viewed in a thermodynamic state diagram in which the fluid temperature is plotted on the ordinate and the fluid specific entropy is plotted on the abscissa. Such a temperature-entropy diagram is presented in fig. 4.

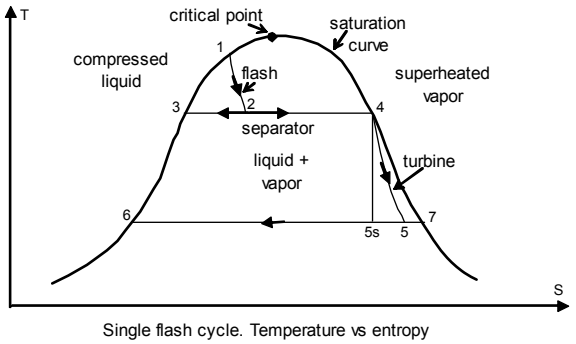

Figure 4: Temperature vs. entropy diagram of the single flash cycle [Di Pippo, 2008].

The main processes governing the geothermal fluid paths are: flashing (1-2), separation (2-3 liquid; 2-4 steam), expansion in the turbine (4-5) and, condensing (5-6).

Flashing

The cycle of thermodynamic processes [Di Pippo, 2008] begins with the geothermal fluid under pressure at state 1, close to the saturation curve. The flashing process is modelled at constant enthalpy (i.e. an isenthalpic process), because it occurs steadily, spontaneously, essentially adiabatically, and with no work involved. We also neglect any change in the kinetic or potential energy of the fluid that undergoes flash. Thus we may write:

$$h_1 = h_2$$

Separation

The separation process is modelled at constant pressure (i.e. an isobaric process), once the flash has taken place. The quality or dryness fraction, *x*, of the mixture that forms after the flash, state 2, can be found from:

$$x_2 = \frac{h_2 - h_3}{h_4 - h_3} \qquad (6)$$

by using the so-called lever rule from thermodynamics. This gives the steam mass fraction of the mixture and is the amount of steam that goes to the turbine per unit total mass flow into the separator.

Turbine expansion
The work produced by the turbine per unit mass of flowing steam is given by:

$$w_t = h_4 - h_5 \qquad (7)$$

assuming no heat loss from the turbine and neglecting the changes in kinetic and potential energy of the fluid entering and leaving the turbine. The maximum possible output would be generated when the turbine is operated adiabatically and reversibly, i.e. at constant entropy (isentropically). The process shown in fig. 4 from 4-5s is the ideal process. The isentropic turbine efficiency, η_t, is defined as the ratio of the actual work against the isentropic work, namely:

$$\eta_t = \frac{h_4 - h_5}{h_4 - h_{5s}} \qquad (8)$$

The power developed by the turbine is given by:

$$\dot{W}_t = \dot{m}_s\, w_t = x_2\, \dot{m}_{total}\, w_t \qquad (9)$$

This represents the gross mechanical power generated by the turbine. The gross electrical power will be equal to the turbine power times the generator efficiency:

$$\dot{W}_e = n_g \dot{W}_t \qquad (10)$$

All auxiliary power (parasitic load) requirements for the plant must be subtracted from this to obtain the net, marketable power. These so-called parasitic loads include all pumping power, cooling tower fan power, and station lighting.

Before eq. 8 can be used computationally, it must be recognised that the isentropic efficiency of a turbine is affected by the amount of moisture that is present during the expansion process; the higher the moisture, the lower the efficiency. This effect can be quantified by using the so-called Baumann rule which states that a 1% average moisture causes a 1% drop in turbine efficiency. Since geothermal turbines generally operate in the wet region, we must account for degradation in performance. Adopting the Baumann rule, the isentropic efficiency for a turbine operating with wet steam will be given by:

$$\eta_{tw} = \eta_{td} \times \left[\frac{x_4 + x_5}{2} \right] \qquad (11)$$

where the dry turbine efficiency, η_{td}, may be assumed constant, (at ca 85%) i.e.:

$$\eta_{td} = 0.850 \qquad (12)$$

From fig. 4, it is clear that the quality at the turbine outlet, state 5, depends on turbine efficiency. State 5 is determined by solving eq. 8 using the turbine efficiency and the fluid properties at state 5s, the ideal turbine outlet state, which are easily calculated from the known pressure and entropy values at state 5s. The ideal outlet enthalpy is found from:

$$h_{5s} = h_6 + \left[h_7 - h_6 \right] \times \left[\frac{s_4 - s_6}{s_7 - s_6} \right] \qquad (13)$$

where the entropy term, by itself, gives the fluid outlet dryness fraction for an ideal turbine. When the Baumann rule is incorporated into the calculation, the following working equation emerges for the enthalpy at the actual turbine outlet state:

$$h_5 = \frac{h_4 - A\left[1 - \frac{h_6}{h_7 - h_6}\right]}{1 + \frac{A}{h_7 - h_6}} \qquad (14)$$

where the factor A is given by:

$$A \equiv 0.425\left(h_4 - h_5\right) \qquad (15)$$

The above equations are valid provided the quality at the turbine inlet, x_4=1, i.e. the steam at the turbine inlet, is saturated steam. If x_4<1 eq. 9 becomes:

$$h_5 = \frac{h_4 - A\left[x_4 - \frac{h_6}{h_7 - h_6}\right]}{1 + \frac{A}{h_7 - h_6}} \qquad (16)$$

Based on the methodology described above, a spreadsheet was developed. In order to calculate enthalpies and entropies for the thermodynamic cycle, steam tables were implemented based on the IAPWS-IF97 code [http://www.cheresources.com/iapwsif97.shtml].

After completion of the well drilling, at least three months are needed before necessary measurements can be carried out to deem whether a well meets the predefined success criteria. Of these three months, one is reserved for thermal recovery of the well and for setting up wellhead and flow-test equipment. As soon as the well has heated up and the wellhead equipment is in place, discharge will start up to last for the remaining two months.

Well production will be constrained by the thermochemical behaviour of the geothermal fluid under varying pressure and temperatures, and related scaling (carbonate, heavy metal sulphide and silica) shortcomings which may lead the operators to modify well head pressures and outlet temperatures accordingly thus limiting the initially expected well delivery.

The predefined success criteria will be the minimum power potential of the well for which the project will be economic.

3 THE LOW ENTHALPY CASE

The Paris Basin geothermal district heating projects (GDH) and accomplishments faced five levels of risks, exploration (mining, geological), exploitation (technical, managerial), economic/financial (market, institutional, managerial), environmental (regulatory, institutional) and social acceptance (image) respectively.

3.1 Exploration risk

The mining/geological risk could be minimized thanks to two favourable factors and incentives. First, the existence of a dependable hot water aquifer (Dogger limestones) of regional extent evidenced thanks to previous hydrocarbon exploration/step out/development drilling, which enabled to reliably assess the geothermal source reservoir prior to development. This resulted later in a 95 % geothermal drilling success ratio according to the success/failure criteria set forth by the ad-hoc geothermal steering committee. Second, the coverage by the State of the geological risk amounting to 80 % of the costs incurred by the first, assumed exploratory, drilling.

As a result of the high drilling success ratio, the so-called short-term provisional fund could be allocated, at a later stage, to the so-called long-term exploitation mutual insurance budget line.

3.2 Exploitation risks

Those could not be estimated beforehand. A (long-term) fund initially financed by the State was created in the 1980s to cope with the hazards induced by the exploitation of the geothermal fluid. Later this could be supplied by operators' subscriptions.

It soon became obvious that the, initially overlooked, hostile thermochemistry of the geothermal fluid provoked severe corrosion and scaling damage to casing and equipment integrities resulting in significant production losses. A prospective survey commissioned in 1995 aimed at assessing the exploitation risks and related restoration costs projected over a 15 year well life. This exercise was applied to thirty three GDH doublets. The governing rationale, developed by Ungemach (2002), consisted of (i) listing potential and actual, technical and nontechnical, risks ranked and weighted as shown in table 4, and (ii) classifying risks according to three levels (1 : low, 2 : medium, 3 : high), each subdivided in three scenario colourings (A : pink, B : grey, C : dark) regarding projected workovers deadlines and expenditure. This analysis led to a symmetric distribution, i.e. eleven sampled sites per risk level, each split into three (A), five (B) and three (C) scenario colourings

Table 1: Summary of risk factors

Risk description	***Nature weight***	***Ranking***	***Status***	***Remarks***
Last known casing status	Technical 1	1	Fine	Residual steel thickness >75% nominal WT before treatment
		2	Fair	Residual steel thickness >50% nominal WT before treatment
		3	Bad	Residual steel thickness <50% nominal WT before treatment
Damaging kinetics	Technical 1	1	Low	Corrosion rate <150µm/an before treatment
		2	Medium	Corrosion rate >150µm/an before treatment
		3	High	Corrosion rate >300µm/an before treatment
Chemical inhibition efficiency	Technical 1	1	High	Provisional statement
		2	Low	Provisional statement
Casing lining opportunities	Technical 1	1	Full	No diameter restrictions
		2	Partial	Some diameter restrictions
		3	None	Total diameter restrictions
New well drilling expectation	Technical 1	1	Long term	> 20 yrs
		2	Medium term	> 10 yrs
		3	Short term	< 10 yrs
Other	Non technical 3	1	favorable	
		2	hostile	

The next step applied the workover/repair unit costs to the concerned wells, required to forecast the workover types and relevant schedules, thus leading to the synthetic expenditure breakdown summarized in table 5. This evaluation illustrates the paradox between competing (if not conflicting) well heavy duty maintenance strategies, i.e. repeated repair of damaged infrastructures vs. re-drilling/re-completion of new wells reflected by scenarios 2 (A, B, C) and 3 (A, B, C). Here, the optimum, in terms of investments but not necessarily cash flows, is represented by scenarios 2B and 3B, case 2C displaying definitely the worst profile.

Table 2: Recapitulation of provisions (sinking funds) required by heavy-duty well workover/repair/redrilling over 15 years (cost per well/year, 10^3 EUR)

SCENARIO	A	B	C
Risk level		1	
Yearly provision	74	99	125
Risk level		2	
Yearly provision	203 (229)	193 (221)	255 (277)
Risk level		3	
Yearly provision	222 (241)	201 (213)	206 (277)
TOTAL (Weighted average)		173 (186)	

In conclusion, an average provision (fiscally deductible) of 0.19 million euros (around 186,000 €/yr) has been recommended to cope with future exploitation hazards resulting in a 12 % increase of initially anticipated OM costs. Loose management remaining the exception, managerial risks could be reliably regarded as minimized in year 2000. Surprisingly, the risk model matched expectations as of late 2002.

3.3 Economic/financial risks

They represent a major uncertainty owing to a somewhat unpredictable, if not chaotic, energy market and pricing context in which geothermal heat must prove competitive. This is indeed a difficult challenge bearing in mind that geothermal district heating grids are structurally, especially under Paris Basin conditions, strongly capital intensive and financially exposed, in case of low equity/high debt ratios, a distinctive attribute of Paris Basin loan policies.

At the time, in the wake of the second oil shock, most geothermal district heating doublets were commissioned, oil prices, dollar exchange and inflation rates stood high and accordingly feasibility projections shaped very optimistic, in spite of their fragile financial planning. A few years later, these trends were totally reversed. This, added to the dramatic technical, financial and managerial problems undergone by most geothermal doublets, endangered grid operation to a stage the abandonment of the geothermal district heating route was envisaged. These difficulties could be overcome at the expense of the abandonment of technically irreparable/economically infeasible doublets and rationalizing exploitation technologies and management of the remaining 34 doublets operated to date.

The economic/financial risks were controlled thanks to debt renegotiation, technological/managerial improvements and stable heat selling prices agreed in long term and users subscription contracts. These contracts, passed in the mid 1980s, expired in the late 1990s/early 2000s. Negotiation of these contracts was clouded by depleted, downward trending, deregulated energy prices prevailing in years 1998 and 1999. This situation incited several operators to pass cogeneration contracts and public and private JV, a compromise deemed satisfactory to remain competitive and secure the survival of the geothermal heating grid regardless from any environmental considerations whatsoever.

In 2008, both a sharp increase of oil prices and natural gas tariffs and growing environmental concerns (global warming and related climatic disasters) modify again the energy panorama. Taxation of greenhouse gases becomes a realistic working hypothesis for the future, limiting the uncertainty margin of geothermal heating prices. In this perspective a 45 to 50 €/MWht selling price appears a reasonable threshold safeguarding the economic feasibility of most operating grids.

3.4 Environmental risks

Damages caused to the environment by casing leaks, uncontrolled well head blowouts and workover operations have been minimized. Limitation of the environmental risks is to be credited to the periodical (quarterly) doublet monitoring and casing inspection logging imposed by the competent mining/environmental authority (DRIRE) and blowout control/waste processing equipments currently operated by the industry.

3.5 Social acceptance

Geothermal energy, particularly direct uses of low-grade heat, has a structural image problem. The product and the recovery (heat exchange) process remain somewhat mysterious or esoteric to the public as opposed to obvious, visible, competing solar, wind and fuel sources. For many years indifference, at the best, was the prevailing attitude. In the early days of geothermal development (the infancy stage), it was regarded as a poorly reliable and costly, occasionally, environmentally hazardous technology. Nowadays mature engineering and management along growing environmental (clean air) concerns have gained wider acceptance by the public of the geothermal district heating alternative. Still, image building efforts need to be persued to popularize the technology.

3.6 Success/failure criteria of the SAF short term guarantee

An example of quantified risk occurrence and coverage criteria for a GDH deep drilling application, is illustrated in fig. 5. Here, the success/failure zones are delineated by two hyperbola Q(To-Ti)=C, with Q well discharge, To and Ti well head formation and grid rejection temperatures and C a constant defined by a given internal rate of return (success criteria) and zero net present value (failure threshold). The algorithm used to calculate are presented in eq. The points characteristic to the full success curve are described in eq. 17. Similarly those characterising failure are described by eq. 18.

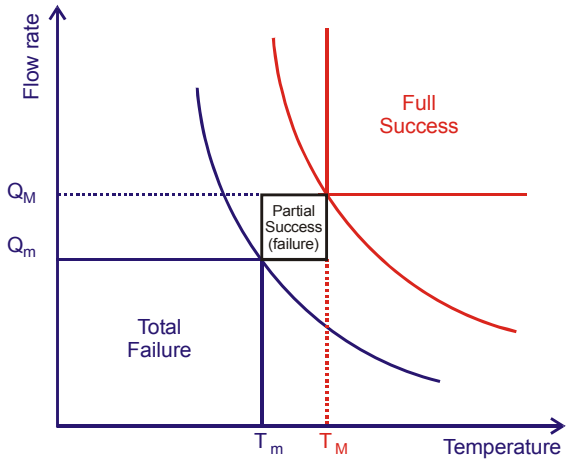

Figure 5. Success/failure curves

Full success:

$$Q\left(T_{wh} - T_i\right) = \frac{1}{1.161 \cdot nh \cdot c}\left[A \cdot INV + OMC + \frac{INV}{n}\right] \qquad (17)$$

Total failure:

$$Q'\left(T_{wh} - T_i\right) = \frac{1}{1.161 \cdot nh \cdot c}\left[A' \cdot INV + OMC + \frac{INV}{n}\right] \qquad (18)$$

Where:
Q, Q' = flowrate (yearly average) (m^3/h)
T_{wh} = production wellhead temperature (°C)
T_i = injection temperature (yearly average) (°C)

$$A = \frac{r(1+r)^n}{(1+r)^n - 1} \qquad (19)$$

$$A' = \frac{r'(1+r')^n}{(1+r')^n - 1} \qquad (20)$$

INV = capital investment (€)
OMC = operation and maintenance costs (€/yr)
c=heat selling price (€/MWh_t)
n = project lifetime (years)
nh = number of operating hours per year
r, r' = discount rates

Numerical application:
INV=12 10^6 €
OMC= 5 10^5 €
n=20 years
nh=8256 hr/yr
r=5% (total failure)
r=10% (total success)
Full equity (zero debt)
Subsidies=25% INV
c=35.45/MWt
T_i=45.4°C

Full success
Q=299 m3/h ; no subsidy, c=35 €/MWh_t
T_{wh}=70°C T_i=45°C
T_{wh}=65°C T_i=40°C
Q=200 m^3/h ; 25% subsidy, c=45 €/MWh_t
T_{wh} unchanged

Total failure
Q=246 m^3/h ; no subsidy, c=35 €/MWh_t
T_{wh}=70°C T_i=45°C
T_{wh}=65°C T_i=40°C
Q=155 m^3/h ; 25% subsidy, c=45 €/MWh_t
T_{wh} unchanged

4 CONCLUSIONS

Geothermal energy shares both exploration and exploitation risks.

Two case studies were presented. The first addressed the high enthalpy, power generation case, in the exploration phase where a numerical criterion to assess the well output from well testing figures was proposed. The second study dealt with a large geothermal district heating (GDH) scheme, where the drilling success ratio approached 100%. The success/failure curves and numerical criteria set out by the relevant mutual insurance fund were presented. Exploitation of the low temperature deposits showed, in the early stages, severe technical and non technical shortcomings. A quantified risk prognosis was at a stage projected 15 years ahead which later proved relevant.

REFERENCES

World Bank: Geothermal Energy. An Assessment. www.worldbank.org, 2003.

Acuna, J. A., Parini, M. A. and Urmeneta, N. A.: Using a Large Reservoir in the Probabilistic Assessment of Field Management Strategies. *Proceedings* of the 27th Workshop on Geothermal Reservoir Engineering, Stanford University, Stanford, CA, January 28-30, 2002.

DiPippo, R.: Geothermal Power Plants: Principles, Applications, Case Studies and Environmental Impact. Second Edition, Elsevier, pp. 91-94, 2008.

Ungemach, P. Insight into Geothermal Reservoir Management. European Summer School on Geothermal Energy Applications. *Text Book*. Oradea, Romania, April 26-May 5, 2001. Rosca, M. Edt., pp. 43-76. 2001.

Drilling, Completion and Testing of Geothermal Wells

Well Logging

7. GEOTHERMAL WELL LOGGING. AN OVERVIEW

Pierre Ungemach

GPC INSTRUMENTATION PROCESS, Roissy-en-France, France

1 OBJECTIVES

Geothermal well logging deals with three major concerns (i) reservoir exploration, (ii) reservoir development, and (iii) resource exploitation / management respectively. Hence logging requirements address the following key issues:

- Geological framework : lithostratigraphic control, structural features
- Reservoir characterisation : geometry, location of productive layers (pay zones), hydrothermal convection, pressure /temperature/flow patterns
- Fluid properties
- Design and control of well casing/completion
- Monitoring of well integrity during exploitation, which takes place downstream from former geological, hydrogeological and geophysical (mainly seismic surveys) investigations and appraisals.

It should be readily stressed that (i) well logging technology has been developed in the sedimentary environments likely to host and trap oil and gas accumulations contrary to high enthalpy geothermal volcano-tectonic settings, and (ii) temperature ratings of most logging tools stand currently below 150 °C which means they cannot be run downhole hot steam and two phase wells unless they are cooled down. As a result, standard logging tools are limited in most instaces to low to medium temperature, single phase liquid, geothermal sources and dominantly sedimentary rocks. However, (i) the performances of formation imaging and microseismic monitoring tools in identifying/mapping natural and induced fractures, along (ii) the demand of the oil and gas industry to challenge the new frontier – over 10 km depths, 400 °C and 3500 bar – encountered recently in a deep sea ultra deep drilling venture, are encounraging premises in bridging this gap.

With respect to low enthalpy geothermal deposits, whose development is fairly recent, their reconnaissance often benefited from previous hydrocarbon drilling campaigns which provided significant well control and data bases. Such was the case of the central part of the Paris Basin. Here, data collected by oil operators and made accessible to the Public thanks to the French mining law were reprocessed and complemented by heat flow measurements leading to a reliable evaluation of the resource base and related resource / reserve assessments. A similar situation was encountered in Central/Eastern Europe, particularly in Hungary.

Worth adding is that, contrary to well testing, logging information is (i) limited to the well and its immediate surroundings (with the exception of crosswell electromagnetic and seismic correlation tools), and (ii) affected by the noise induced by the drilling fluids and mud cake.

Well logging has, in the recent years, gained increased reliability from tool technology, data acquisition and interactive, computer assisted, processing software rendering interpretation a truly rewarding exercise.

2 TOOL DESCRIPTIONS

Logging tools fall usually into three categories, openhole, cased hole and production respectively. To simplify :

- Openhole tools are exploration oriented and deal with formation and reservoir evaluation.
- Cased hole tools aim at well (casing/cement/completion) integrity control.
- Production tools are measuring and sampling devices assisting well tests and fluid analyses.
- Logging while drilling (LWD) adds sensors to the drill string the signal being retrieved either in memory mode or in real time via mud pulse telemetry.
- Exploration tools deserve a special comment. As far as lithostratigraphy, porosity and permeability are concerned there is no direct in situ assessment of these petrographic and physical parameters. Instead, those are measured indirectly

through other, physically related, parameters such as spontaneous potentials, resistivities, bulk densities, transit times, natural radioactivity and rock hydrogen contents.

- Other, structural and tectonic, features can be appraised via magnetic, seismo acoustic measurements and image processing, applied to dips and fracture determination among others.
- Drilling/completion fluids, mud cake and invaded zone effects, illustrated in fig.1 for a water bearing layer, need to be corrected in order to release true (clean) formation figures.
- Tool to tool cross correlations (crossplots) are currently practiced to improve lithological identification and porosity appraisals.
- There are two parameter acquisition and transmission technologies, slick line memory gauges and real time wireline respectively.
- The basic formulae, provided by Schlumberger (1986, 1987) listed in table 1 form the driving rationale of quantitative log interpretation.
- Tool nomenclature is summarised in table 2, bearing in mind that tool acronyms are subject to changes.

2.1 Gamma Ray (GR)

The GR wirelinelog detects, by scintillation metering/photomultiplication, the rock natural radioactivity through radiations resulting from Uranium, Thorium and Potassium radioactive decay. The radiation is measured in API units expressed as multiples of a standard calibre. Owing to the clay high radioactive contents (K40 notably), the GR log is a reliable indicator of formation argillosity. It is therefore a relevant tool in assessing clean (sand, sandstones) levels and deriving accordingly sand/clay ratios. It appears also as a pertinent basic lithology tool due to its ability to identify, under the form of individualized peaks, the signature of brief organic episodes, indeed useful markers in exercising lithostratigraphic correlations from well to well.

2.2 Spontaneous (self) Potential (SP)

The SP log measures, in a well filled with a conductive mud, the electrical potential between an in hole located electrode and the surface. It therefore helps in discriminating pervious layers from clay streaks.

The SP signal originates from currents generated by the salinity contrast between the mud filtrate and the formation water. It includes an electrochemical potential and an electrofiltration potential. The first consists chiefly of a membrane potential associated to Na ion migration resulting from a gradient in concentration, particularily in the case of a clay/saline brine contact. The electrofiltration potential is a consequence of electrolyte displacement in a porous medium.

Summing up, SP is a tool measuring the resistivity of the formation water and an indicator, in most instances qualitative, of pervious/porous horizons and clays.

2.3 Induction Log (DIL), Laterolog (DLL)

The induction tool combines an emission coil (current injector) and a receiveing coil (current measuring gauge). The magnetic field created by the emission coil, excited via an oscillator, induces Foucault currents into the formation. Those further generate a magnetic field proportional to the induced current and to formation resistivity accordingly. The double tool (dual induction log-DIL) yields two induction measurements, medium depth and deep respectively. The formation resistivity Rt is derived from a set of type curves. This tool is adequate for insulated drilling fluids (oil base mud, air…) and conductive rocks (clay, marls, silstones, sandstone…) such as those encountered in cover, Molasse type, terrains.

Whenever the formation gets more resistive, as with carbonate, Cretaceous and Jurassic, rocks the dual laterolog (DLL) tool is used (see fig.2 for tool application range). The DLL achieves the penetration of a thin current disk obtained from a barrier (superior and inferior) current forcing the

measuring current laterally into the formation. The resistivity of the investigated layer is related to the electrical potential required by the measuring current penetration. Combination of measuring electrodes makes it possible to monitor deep (LLD) and shallow (LLS) currents.

The LLD signal allows a preliminary assessment of formation resitivity Rt. However a precise interpretation requires due correction of borehole, layer thickness and formation invasion effects by means of appropriate type curves.

The current focusing achieved by the DLL tool secures improved vertical resolution, wider resistivity range and better invasion appraisal (Rt/Rm contrast).

2.4 Density Log (LDL)

The tool is based on the principle of density determination utilizing the atom/photon, known also as Gamma/Gamma, interaction. It consists of bombarding the formation from a high energy gamma source and measuring the radiation (re) emittted by Compton effect which prevails, within the concerned energy level (> 1 MeV) over secondary processes such as the photoelectric effect (absorbtion of a photon by an atom and reemission of an electron) which occurs at ca 0.1 MeV level, and the production of pairs (electron/positron) at ca 2 MeV.

The electronic density of the (re) emitted radiation is straightforwadly related to actual rock density, in deed a useful property in a sedimentary rock context as the (apparent) electronic density of the rock is very close if not equal to its true density. It appears therefore as a relevant means of identifying lithologies density wise. Interpretation can be enhanced by processing the so called PEF (photo electric factor) via the photoelectric volumetric absorption index (Uma) related to lithology almost independently from porosity (Uma = PEF x ρ).

The tool is also a reliable porosity indicator (which can be correlated with other tools), owing to the density (ρ) porosity (ϕ) relationship.

$\rho = (1- \phi) \rho r + \phi \rho f$ (f = fluid, r = rock)

The LDL (lithodensity log) tool utilises two detectors (as was actually the case for the former FDC tool) equipped with highly sensitive gauges operating within different energy windows enabling to separate the Compton and photoelectric effects.

Density is measured in two detection spaces, long and short respectively, allowing to correct the measurement from the variations of the incident radiation source and borehole/formation environment.

2.5 Neutron Log (CNL)

The compensated neutron sonde (CNL) is a nuclear wireline logging tool aimed at a direct porosity measurement, often operated in tandem with the LDL tool.

It utilises the interaction between a high energy (2 MeV) neutron source and the atomic nuclei of the bombarded formation target. Incident neutrons, after successively colliding (elastic dispersion mode) with nuclei, loose their energy and are, ultimately, absorbed. This neutron capture process can be quantified by measuring the number of collisions needed to lower the energy level to 0.025 eV (thermal level).

This number (nc) is weaker, by one order of magnitude, for hydrogen than for the other elements. As a result the log will be essentially influenced by the number of hydrogen atoms i.e. by fluids (formation/conate water, liquid/gaseous hydrocarbons) and porosity.

The compensation is designed to minimize the mud noise, by addition of a short sensor, the counting ratio (NPHI) of both long and short signals being less sensitive to mud than both counting processed separately.

However neutron porosity addresses a total and not effective (i.e. that participating to flow) porosity value and needs to be corrected accordingly, in particular in argillaceous formations.

2.6 Sonic Log (BHC)

The sonic tool measures the propagation time through the formation of a sonic wave between a source (emitter) and two acoustic receivers. The system is duplicated (in opposing mode) i.e. 1 transmitter, 2 receivers vs 2 receivers, 1 transmitter in order to compensate borehole effects (inclination, excentering, caving, etc…). In a clean formation, sonic porosity ϕs is related to log transit time Δt log (μs/ft), by the following equations :

$\phi s = (\Delta tlog - \Delta tma) / (\Delta tf - \Delta tma)$ *Wyllie*

$\phi s = C (\Delta tlog - \Delta tma) / \Delta tlog$ *Raymer Hunt Gardner*

C # 0.67

Δtma and Δtr are available in tables (ma = matrix, f = fluid)

2.7 Formation Microscanner (FMS)

The FMS represents a development of the (SHDT) dipmeter tool. It releases a formation imaging in terms of electrical conductivities collected via a dense network of sensors (16 microconductivimeters per each sidewall pad) which, in the case of a 4 pad tool, covers up to 40 % of the well openhole sandface (8"1/2 drilling diameter). The tool elsewhere includes a sophisticated inclinometer (three component accelerometer and three magnetometers) outfit.

The tool delivers a developped imagery of the well face which is processed according to a fracture oriented rationale (search of fractures, microfissures and rock facies identifiable as dip angles and azimuths).

2.8 Cement Bond-Variable Density (CBL/VDL)

The casing is vibrated in longitudinal mode via an acoustic source generating compressive (P type) waves. Amplitudes of the acoustic response and transit times are recorded by means of two, one near (3 ft) and one distant (6 ft), receptors after travelling of the wave train through the casing/cement/formation sequence according to seismic paths dependant on medium acoustic impedances and casing to cement/cement to formation couplings.

The CBL item records the first arrival detected by the near receptor. The VDL item processes later arrivals from the distant receptor and displays through a standard seismic imagery, the (intensity) modulated signal.

Amplitudes and arrival times are processed in order to evaluate the cement to casing and formation bond from their acoustic coupling and typical signatures.

A badly or non cemented casing will undergo resonance, the so called free pipe behaviour. The seismic path will follow the casing and result in short transit times and high amplitudes (strong vibrating energy). Signal amplitude will stand above 10 mV and ultimately reach 50 mV (free pipe threshold).

On the contrary, a good acoustic coupling will show longer arrival times (delayed first arrival), a strong casing signal attenuation and an energetic response from the, behind cement, formation. A bad cement to formation bond would be evidenced by flatening of the amplitude spectrum caused by a week formation coupling and a high attenuation of the signal tail.

These effects can be visualised on the VDL imagery where a free pipe behaviour would be materialised by a set of parallel, black and white, bands as opposed to the herringbone structure characteristic of adequate cement bonding.

The first arrival amplitude is "captured" by an electronic gate, with a very brief opening time, in order to record maximum signal amplitude. This process may be affected by two artifacts induced on travel time monitoring by low signal amplitudes thus indicative, in most cases, of a good cement bond, stretching and cycle skipping respectively.

Cementing performance can be biased by channeling and microannulus effects. Channeling consits of fluid flow paths filled with mud, water, gas or/and drilling completion fluids, within the cement mass.

A microannulus is a consequence of the presence, between the casing and the cement, of a thin, pellicular, fluid film.

The CBL/VDL is sensitive to microannulus whereas channeling noise is better appraised by the USI tool.

2.9 Ultrasonic Inspection Tool (USI)

The USI is designed to achieve both cement evaluation and corrosion control.

It allows to vibrate the casing in both longitudinal (P waves) and transverse (S waves) modes via a rotating ultrasonic source generating pulsed trains of compressional and shear waves and to process, radially, arrival times and amplitudes.

Its resolution capacity - 72 radial measurements, vertical space increment of 0.5"- places it as a sophisticated, though sometimes ambiguous as to log interpretation, inspection logging tool.

Log outputs address essentially casing inside diameters (processing of first arrival times), thickness and filling of casing to formation or casing to casing annulus i.e. cement evalutation. The latter feature eases the detection of channeling effects.

2.9.1 Isolation Scanner (IS) [Schlumberger, 2009]

It aims at identifying low acoustic impedance bodies and water/mud contaminated cements which do not exhibit the sharp impedance contrasts required by CBL and VSI tools. The IS combines the conventional CBL/USI pulse echo technology with a higher frequency ultrasonic concept, known as flexural wave imaging. The casing exciting mode emitted and received independently from the conventional source, generates later arrivals (third interference echo) providing a circular scan of casing, annular filling, cement and near well formation status. It is recommended for lightweight cement slurries and multiple casing sections.

2.9.2 Vertical Seismic Profile (VSP)

The advanced CSI [Combined Seismic Imagery, Schlumberger, 2006] tool design includes a decoupled seismic acquisition module providing a high quality signal to noise ratio, in both frequency and time domains, of three component compressional (P) and shear (S) waves for synthetic seismograms and in depth seismic investigation purposes.

2.9.3 Cross Hole Electromagnetic

Several geophysical and logging companies operate an electromagnetic – transmitter receiver – system creating an induced EM field and formation resistivity profile reflecting fluid filling patterns and subsequent water injection flow paths.

2.9.4 Microseismic Monitoring

The system records acoustically, in one or several observation wells, the microearthquakes induced by a shock, a hydrofrac, source. It provides, a presumably reliable, fracture mapping means widely utilised in evaluating hydraulic fracturing efficiencies and EGS reservoirs.

2.9.5 Borehole Geometry (BGL)

It includes a four arm caliper whose deflections are processed vis-à-vis, thus delivering two mean diameter values.

It can be assisted by an inclinometer telemetry, useful in correlating well geometry to trajectory changes, in a cursory manner however as compared to thorough directional surveys. It displays, alongside borehole diameters, annular volumes indicative of hole caving and further cementing volume requirements.

2.9.6 Production Logging Tools (PLT)

Those consist of temperature and pressure sensors, openhole flowmetering spinners and, occasionally, openhole calipers operated either separately, by pairs or all together in a thorough combined production logging tool.

Measuring principles :

- *Temperature*. Platin thermistor
- *Pressure*. Strain gauge, Bourdon type gauges, quartz piezoelectric gauges (vibrating frequency proportional to the pressure applied to crystal faces) continuously temperature compensated, piezoresistive gauges. Whenever no multiple nor monoconductor cables are available, a simplified slick line and quartz memory gauge outfit is utilised instead. The latter has replaced the former, now obsolete, downhole clock driven Amerada/Custer gauges.
- *Flowmetering*. Borehole micro spinners are utilised to monitor, preferably counter current wise, fluid ascending speeds. Whenever low to very flow conditions prevail a so called petal like full bore high resolution tool is recommended (see fig 3).

A conventional openhole three arm caliper is often required to correct speeds from borehole irregularities (caving) and release true flowrates accordingly.

The flowmeter tool is most relevant in indentifying reservoir productive intervals, interlayer crossflow and related thief zones.

2.9.7 Casing Calipers

Casing inspection, in the sense of inside diameters (IDs), is performed via multifinger caliper tools.

Casual tools consist of 40 arm devices and retrieval of maximum/minimum casing ID.

A sophisticated 40-60 arm caliper, available for 7", 9”5/8, 10”3/4 and 13”3/8 casings, achieves the simultaneous recording of as many radii.

Such tools are extensively utilised to investigate internal casing status, assess wall roughness and evidence corrosion/scaling damage.

3 FIELD APPLICATIONS

3.1 Exploration well logging

Fig. 5 and 6 illustrate log outputs selected on a geothermal wildcat (see logging programme in table 5).

Fig. 5 is a composite production log combining an openhole 3 arm caliper, temperature and (full bore petal like) flowmeter tools on the target reservoir interval. Note the correlations between borehole caving and temperature convection on the 2100 and 2200 m depth interval. Fluid velocities need to be corrected from caving effects but indicate howewer a significant flow contribution from the afore mentioned interval.

Fig. 16 displays a fracture evaluation exercised by processing of FMS imagery in the sense of fracture and dip intensities (stereonets) and fracture aperture vs depths and azimuths.

3.2 Development well logging

The composite well log represented in fig. 5 concentrates a dense information, over the bottomhole geothermal reservoir, issued by caliper, GR, BHC, LDL, temperature and flowmeter tools. This document shows actually good agreement between the porosity (from sonic and density) peaks above the 15 % (LDL) and 12 % (BHC) cut off values and the producing (pay) zone evidenced by

flowmetering (expressed as percentages of total cumulated flowrate). The temperature log appears here as a gross indicator of the whole reservoir (total pay) traced through the strong convection hump and related temperature reversal noticed on the 1925 to 2005 m depth interval. This thick (80 m) zone was further well tested exhibiting a prolific yield (300 m3/hr self flowing capacity) and dependable characteristics (kh = 90 dm and S = -1.5). The whole logging programme is listed in table 4.

3.3 Exploitation well inspection

Fig. 6 shows a variety of damaged (and restored) casing status appraised by multifinger callipers. Fig. 6a displays typical signatures of non damaged and damaged (corrosion/scaling episodes) casings achieved by conventional 40 arm inspection tools delivering a minimum and a maximum ID. Fig.6b desmonstrates the ability of a 40, simultaneously recording, finger calliper in assessing casing roughness and wall upgrading further to jetting clean up. Fig. 6c gives a thickness and radial image of casing damage and ultimate piercing provided by a 16 simultaneously recording finger tool.

Typical logging programs are presented in table 5.

Table 1: basic formulae used in log interpretation [Schlumberger]

(1) $SP = - K \log (Rmf/Rw)$

(2) $F = Ro/Rw = a / \Phi^2$

(2') $a=1$ *Archie*

(2") $a = 0.81$ *Humble*

(3) $Sw = (Ro/Rt)^{1/2}$

(4) $$(Sw/Sxo) = \frac{(Rxo/Rt)^{1/2}}{Rmf/Rw}$$

(5) $ts = \Phi\, t_f + (1- \Phi)\, t_{ma}$

(6) $\Phi = (T_s - T_{ma}) / (T_f - T_{ma})$ *Wyllie*

(6') $\Phi = 0.67\, (T_s - T_{ma}) / T$ *Raymer-Hunt-Gardner*

(7) $pb = \Phi\, p_f + (1-\Phi)\, p_{ma}$

(8) $\Phi = (p_{ma} - p_b) / (p_{ma} - p_f)$

Parameters

F = formation factor
K = SP (temperature dependant) constant
R = resistivity
S = saturation index
SP = Spontaneous (self) potential
T = transit time

p = density
Φ = porosity

Subscripts

b = bulk rock
f = fluid
ma = matrix
mc = mud cake
mf = mud filtrate
o = (clear water saturated formation)
t = clean formation
s = sonic
w = water
xo = flushed zone

Table 2: Basic logging tool nomenclature

LOG NAME	ABBREVATION	WELL STATUS	APPLICATION
Gamma Ray	GR	OH, CH	Argillosity Lithology marker
Spontaneous (Self) potential	SP	OH	Lithology, porous/pervious layer marker
Dual Induction	DIL	OH	Lithology, formation resistivity
Dual Laterolog	DLL	OH	Lithology, formation resistivity
Litho Density	LDL	OH	Lithology, density, porosity

			Porosity/lithology crossplots
Compensated neutron	CNL	OH, CH	Porosity. Porosity/lithology crossplots
Borehole Compensated Sonic	BHC	OH	Porosity. Porosity/lithology crossplots
Formation Micro Scanner	FMS	OH	Extension of the dipmeter tool. Formation imagery. Fracture processing
Borehole Geometry, Caliper	BGL, CAL	OH	OH diameter, annular cement volumes
Cement Bond, Variable Density	CBL/VDL	CH	Cement control
Ultrasonic Inspection	USI	CH	Cement control Inside casing inspection
High Resolution Thermometery	HRT	OH, CH	Dynamic/static temperature profile
Quartz Pressure gauge	QPG	OH, CH	Dynamic/static pressure profile, well testing
Production Logging	PLT, PCT	OH	Combined (pressure, temperature, flow) tool.
Full Bore Spinner flowmeter		OH	Low speed well flowmetering (petal device)
Continuous Flowmeter		OH, CH	Flow profile
Multifinger Casing Caliper	MFCL	CH	40 to 60 arm tool Max/Min casing ID
Casing Inspection Caliper	CIC	CH	40 to 60 arm tool Max/Min casing ID
Fluid Sampler	FS	OH, CH	Bottom hole sampling (PVT analysis)
Isolation Scanner	IS	CH	Casing integrity, cement control annulus and near well status
Vertical Seismic Profile	VSP, CSI		Synthetic seismograms, wellbore seismics
Microseismic Monitoring		OH, CH	Fracture mapping, induced seismicity
Crosshole EM		OH, CH	Inter well resistivity profile, water injection

CH = Cased hole
OH = Open hole

Table 3: Exploratory well logging programme

TOOL	DEPTH INTERVAL m	WELL/LOG STATUS	REMARKS
BGL	0 – 2680	OH	Cement volume
BGL/GR		OH	OH flow section
DIL/SP/GR	0-1370	OH	Upper clastics Lithology, porosity
DLL/GR	1375 – 2680	OH	Lower carbonate lithology
BHC/GR	1375 – 2680	OH	Porosity
FMS/GR	1790 – 2680	OH	Reservoir fracturing
LDL/CNL/GR	1375 – 2680	OH	Neutron/density porosities
HRT	0 – 2680	OH/CH	Static/dynamic temperature profile
QPG	0 –2680	OH/PRO	Static/dynamic profile
PLT	1375 – 2680	OH/PRO	Full bore tool
QPG	2500	OH/PRO	Pressure buildup
BHS	2600	OH/PRO	PVT
GR/CCL	1790 - 2680	OH/CH	

OH Openhole CH Cased hole PRO Production logging

Table 4: Development well logging programme

TOOL	DEPTH INTERVAL (m)	WELL/LOG STATUS	REMARKS
BGL/GR	359 – 1905	OH	Cement volume
CBL/VDL/GR	338 – 1880	CH	Cement control
LDR/GR	1907 – 2109	OH	Reservoir only. Lithology / porosity
BGT/BHC/GR	1907 – 2109	OH	Reservoir only. Porosity and diameter
MFCT	+2 – 1895	CH	Inside casing status
USIT	10 – 1906	CH	Corrosion / cement control
PLT	1907 – 2083	OH/PRO	Producing intervals
QPG	1911	OH/PRO	Pressure draw down / build up
BHS	2060	OH/PRO	PVT

Table 5: Operating production/injection wells. Typical inspection logging/testing programmes

TOOL	APPLICATIONS
MFCT/CIC	Casing integrity control (as of IDs) and roughness analysis
CCL	Well total depth control via sinker bars and cable tension recording
CBL/VDL/GR	Standard cementing control
USIT	Additional casing integrity and cementing control
RBP	Casing pressurizing tests via packer (two single or straddle packer string) leak off tests
BGT/GR	Openhole diameter control
QPG	Well testing, single production or injection wells Combined production / injection well (loop) testing Interference test
PLT	Combined flowmeter and temperature analysis for casing leak detection or matching of openhole producing/ injecting levels
FS	PVT sampling

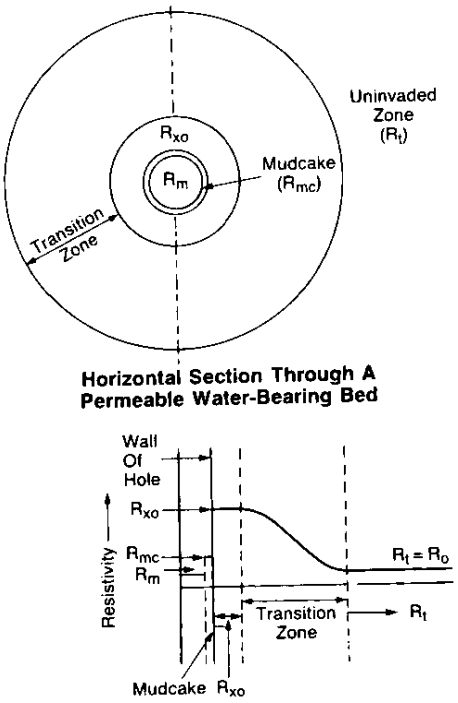

Figure 1: Radial distribution of resistivities (Rmf>>Rw, Water – Bearing Bed) [Schlumberger,1987]

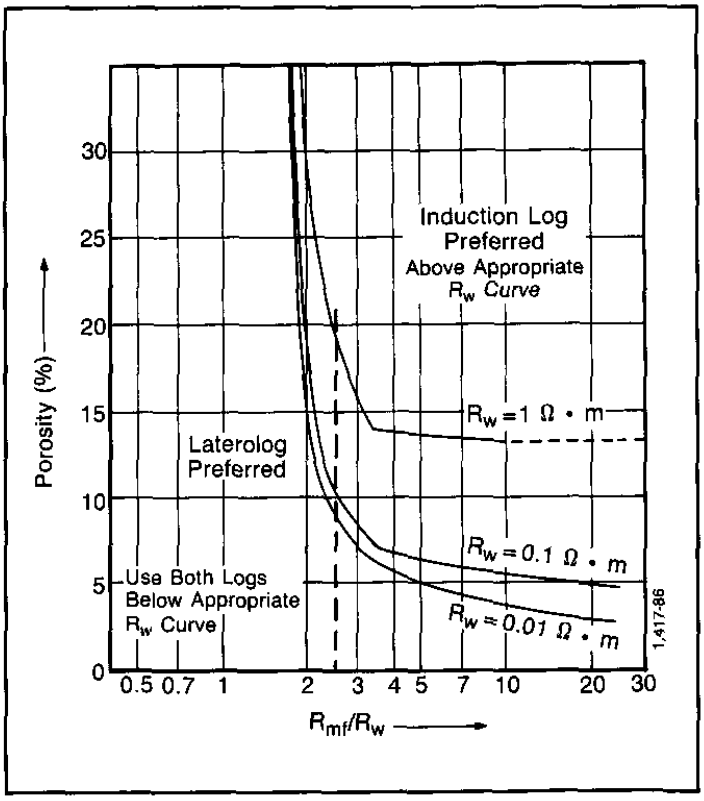

Figure 2: Preferred ranges of application of induction logs and laterologs [Schlumberger, 1987]

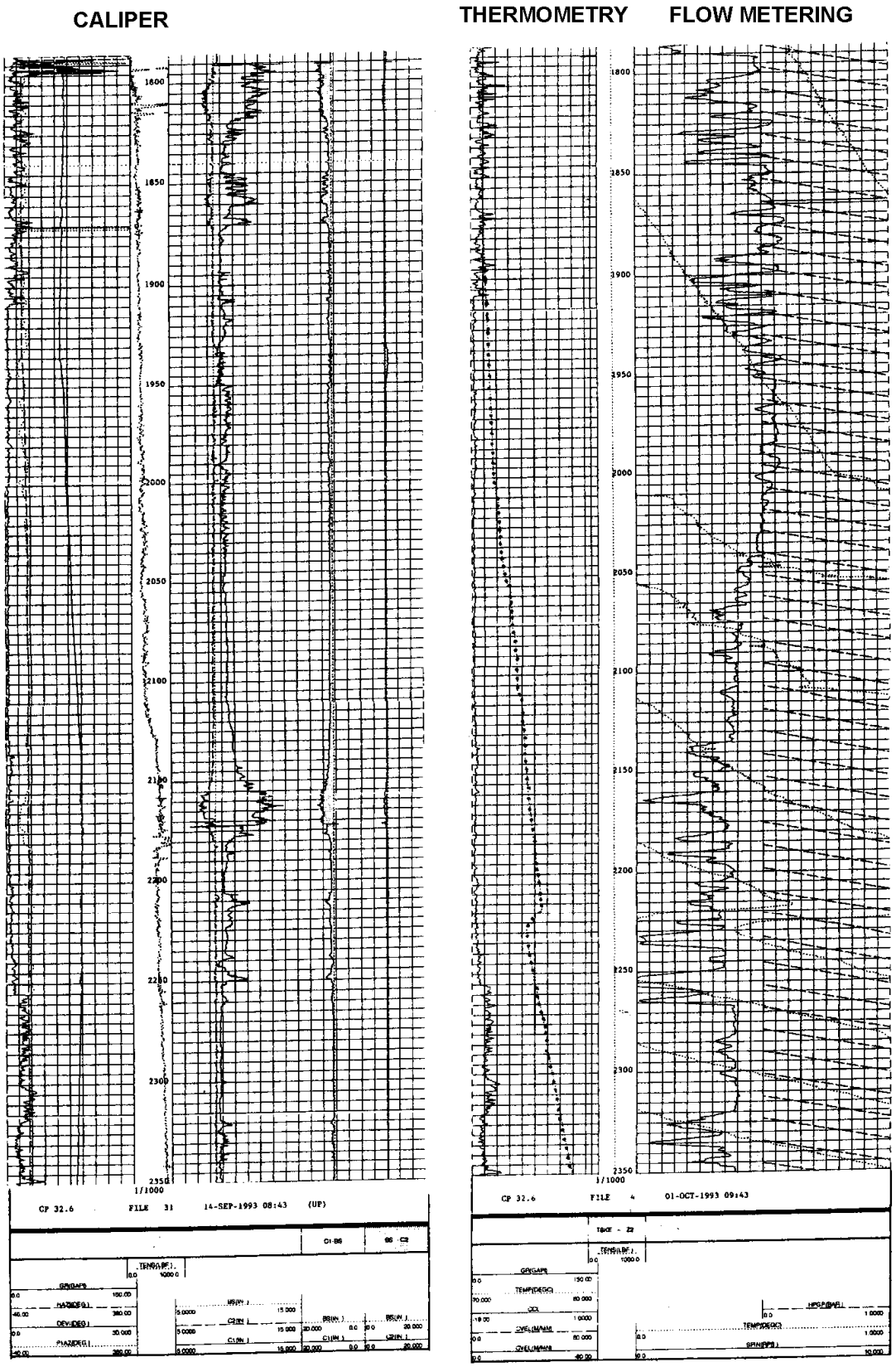

Figure 3: Well production (Caliper, thermometry, flow metering) logs [GPC and Geologie – Geophysique]

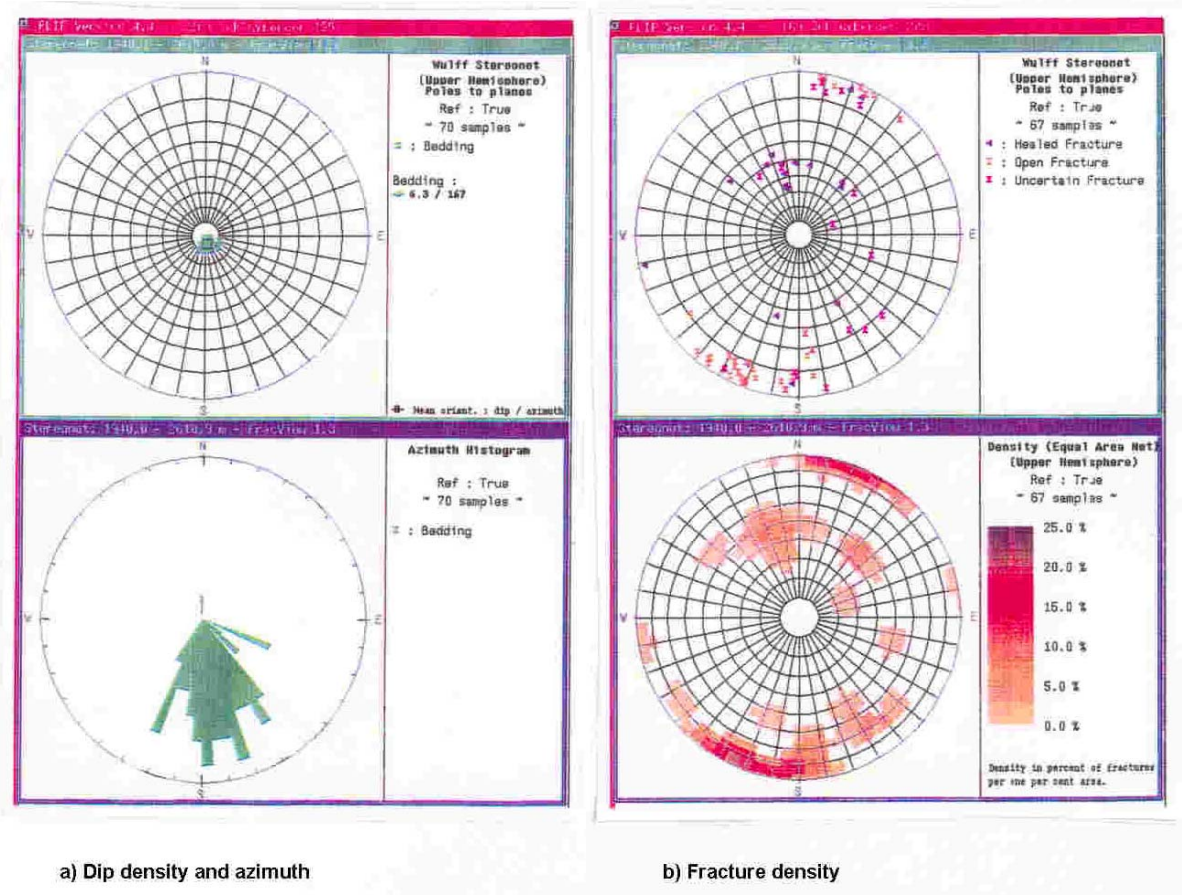

a) Dip density and azimuth

b) Fracture density

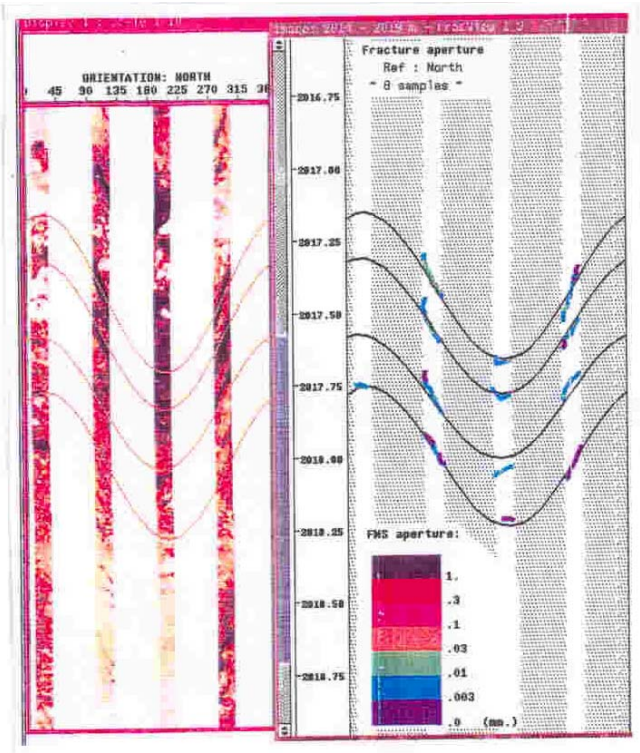

c) Fracture aperture

Figure 4: Fracture analysis. Example of FMS Image processing [GPC and Géologie – Géophysique]

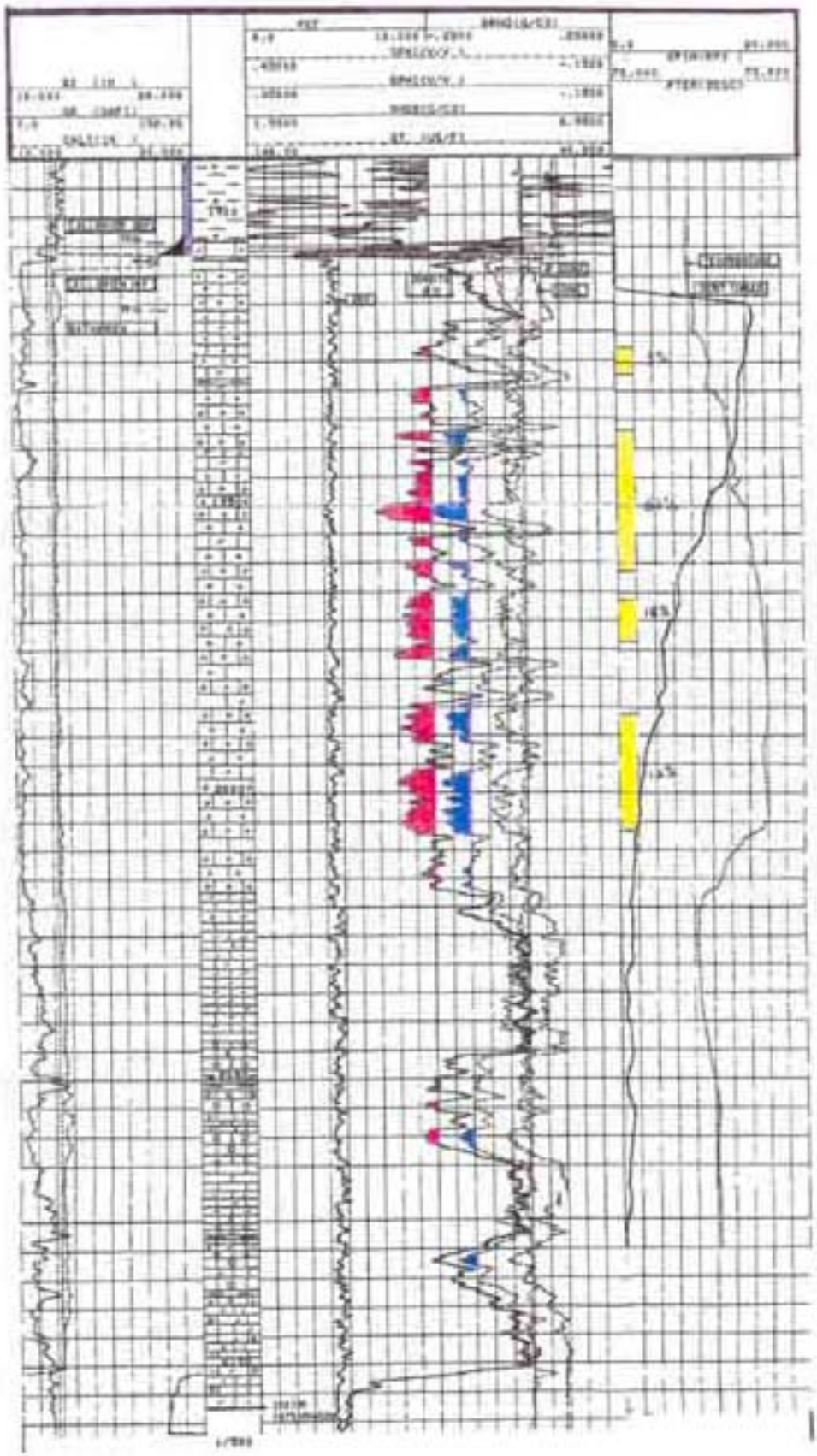

Figure 5: Composite well log – Reservoir analysis OH porosity/density (BHC, LDL, GR) and production (HRT, Flowmeter) tools [GPC]

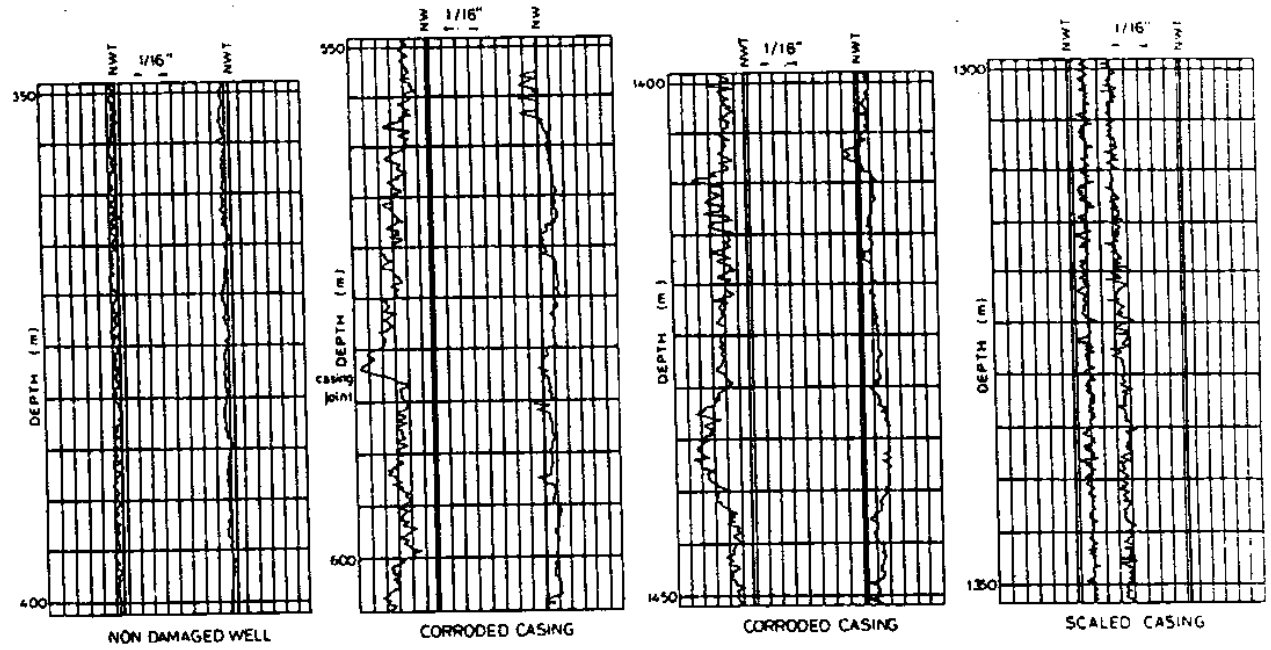

Fig. 6a: Samples of damaged geothermal wells (7" casings) logged with multifinger Calipers (NWT = Nominal Wall Thickness 7" 26 lbs/ft csg) [GPC]

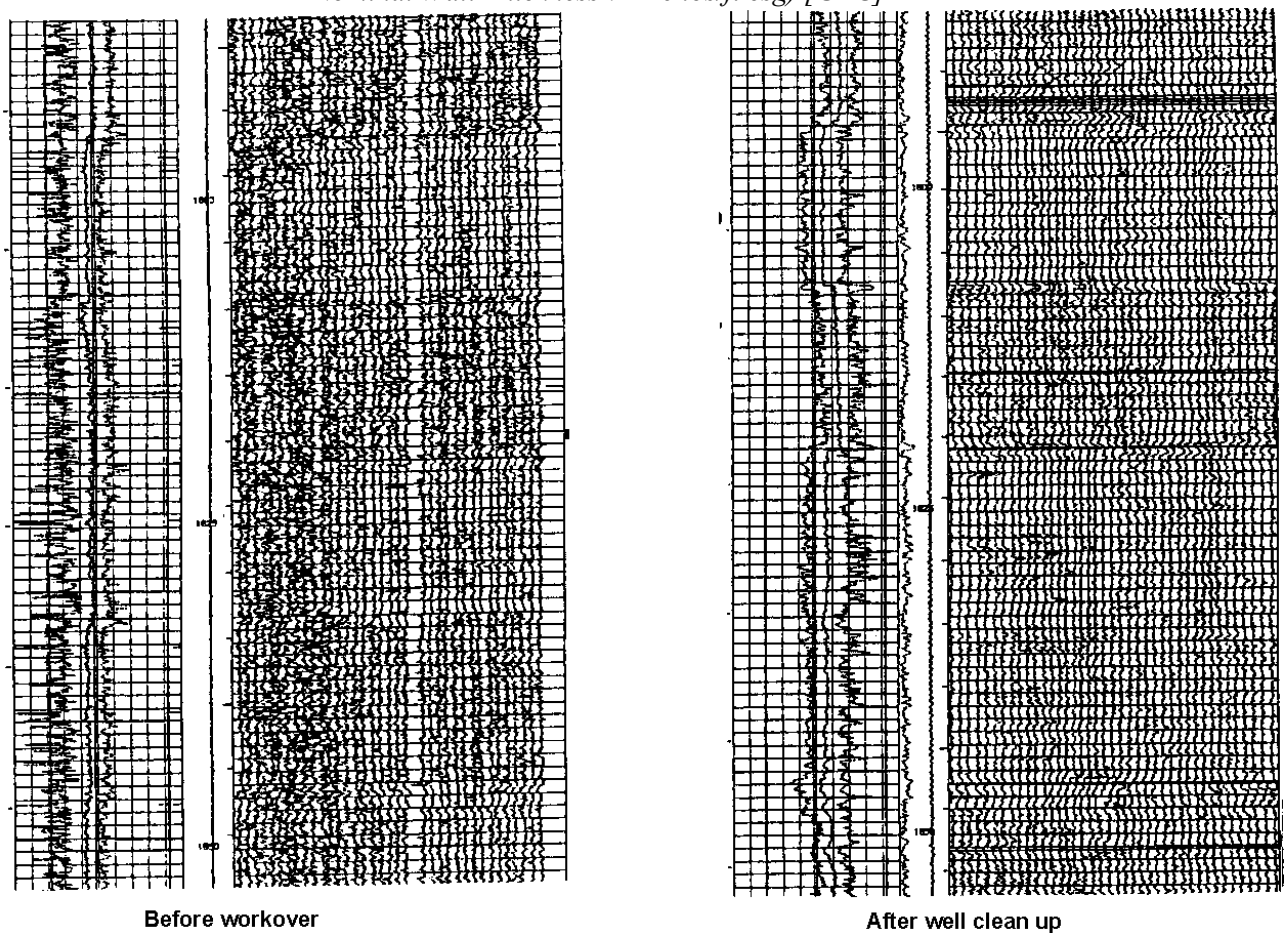

Fig. 6b: Casing Caliper tool. Forty simultaneously recording fingers. Roughness analysis [GPC]

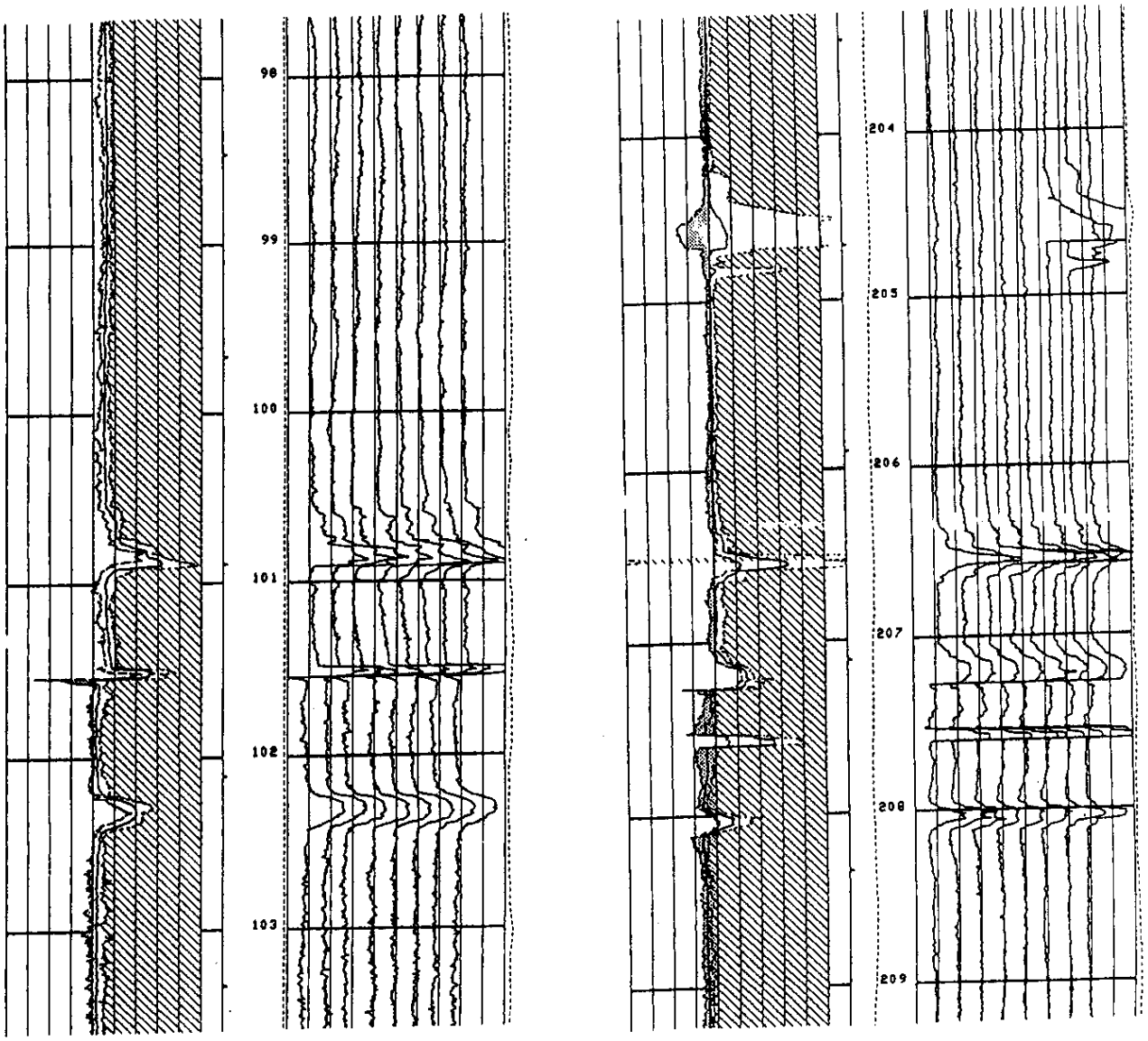

Fig. 6c: Caliper tool (16 fingers). Evidence of casing damage and piercing [GPC]
Figure 6: Examples of casing integrity control by multifinger caliper tools

REFERENCES

Hallemburg, J.K. (1998). Standard Methods of Geophysical Formation Evaluation. CRC Press LLC, Levis Publichers – New York – NY.

Schlumberger (1986). Log Interpretation Charts. Schlumberger Well Services.

Schlumberger (1987). Log Interpretation Principles/Applications. Schlumberger Educational Services

Schlumberger (2006). The CIS tool. Company brochure (available on Company's website).

Schlumberger (2009). The Isolation scanner. Company brochure (available on Company's website).

Appendix: Useful Charts

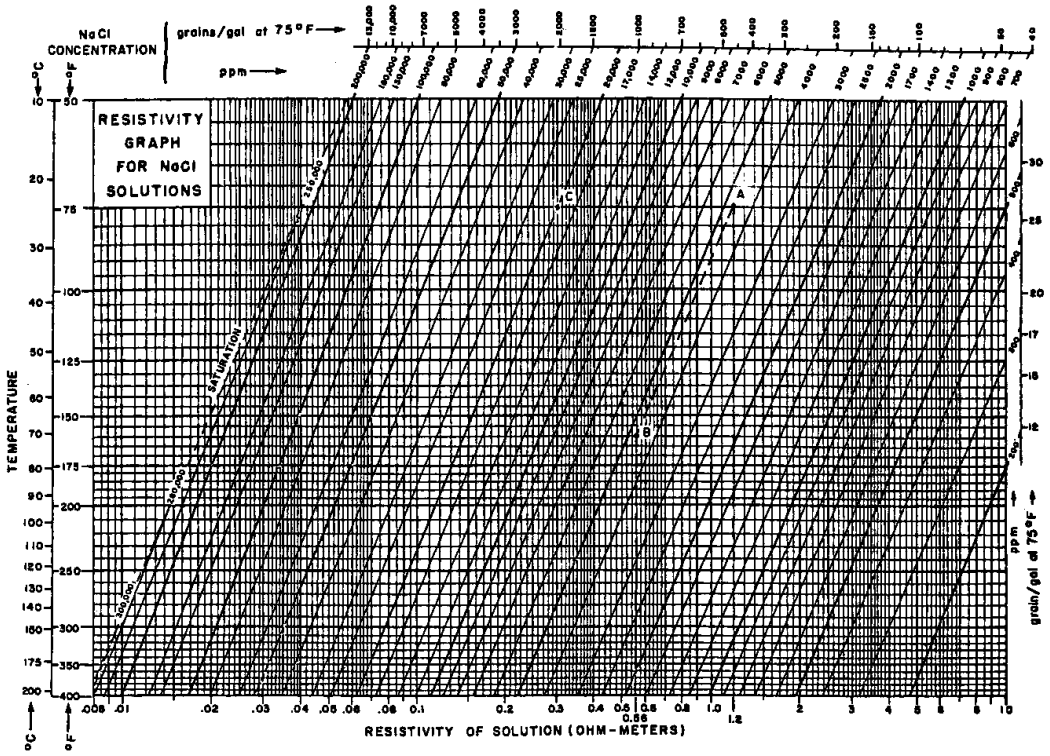

Water resistivity vs salinity and temperature
(source : Schlumberger ref. 2)

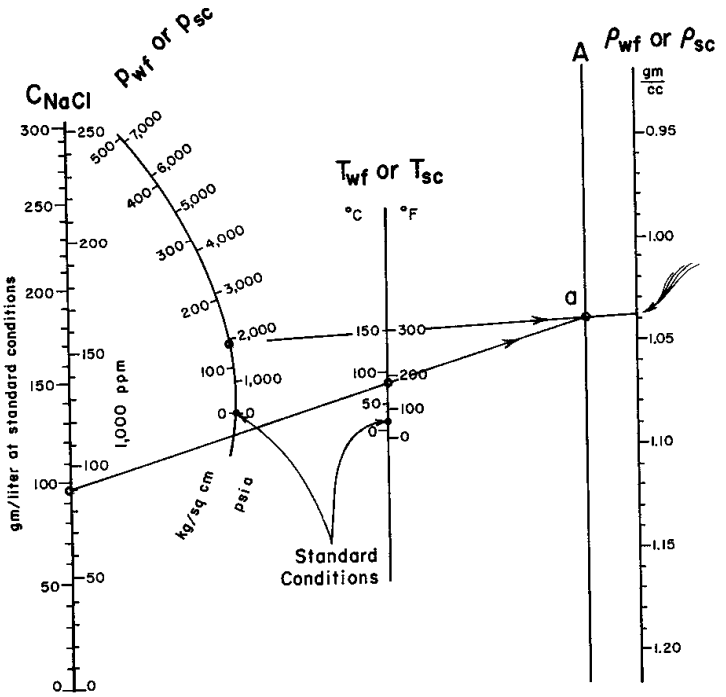

Density of NaCl solutions vs pressure and temperature
(source Schlumberger ref. 2)

Drilling, Completion and Testing of Geothermal Wells

Geothermal Well Testing.

Objectives, Technology and Safety Measures
Electronic HT Tools and Safety, Health and Environment

Peter E. Danielsen
ÍSOR, Reykjavík, Iceland

SUMMARY

In the following high temperature and pressure electronic Dewar flask tools are discussed and compared to classic mechanical tools. The high resolution, data quality and specifications of the tools is also discussed. Safety, health and environment issues are addressed and examples are given from cases where work is considered dangerous or when working with dangerous goods.

INTRODUCTION

As the geothermal industry has advanced, increasing emphasis has been placed upon accomplishing operational objectives more safely and efficiently. In pursuing these goals, operators and service companies have investigated the advances made in other technological fields, and many innovative applications have found their way into geothermal operations to accomplish these objectives.

Some of the most notable advances in technology for improving and disseminating information are accomplished by the introduction of high temperature electronic memory tools as well as more sophisticated logging and interpretation software, designed for geothermal purposes.

High accuracy and retrievability of data from high temperature and high pressure deep well logging has been the driving factor for ÍSOR to switch from mechanical tools to electronic Dewar flask tools. The electronic tools are however known to be more fragile than the classical mechanical tools, especially in deviated wells but denser, high resolution and reliable data sets obtained from the electronic tools are of high scientific value in interpretation and modeling and they are saving time and money.

Awareness on safety and health issues are awakening in general but in the case of geothermal much can still be learned from for example the oil industry, especially on areas concerning drilling and logging where the circumstances of the work itself or its surroundings are dangerous.

A safety committee working with occupational safety, health and environment issues is a necessary and important part of a company. In most countries laws have been passed stipulating that safety committees should be present within any company and legislation has been passed on how they should be composed. While focus on safety in dangerous environments is obvious, one should not forget office work and other less dangerous working areas where basic legislation is most likely covered throughout the world. A large part of a person's working life takes place in such areas and thus a healthy and stimulating work environment is of the utmost importance.

However a small part of the workforce in most companies perform their tasks under conditions where the health risks are high and where safety issues are a matter of daily scrutiny and should be of high priority of the safety committee. Rules and regulations of course differ from one country to another and in this paper the workflow of the safety committee at ÍSOR will be discussed.

1 Electronic Dewar flask tools

1.1 Pros and Cons

After working with the electronic Dewar flask tools for an extended period of time it is clear that the most appealing qualities of the tools are the high data resolution and quality. Handling and downhole deployment are also factors where the tools make an impression. At first they are seemingly costly but at closer scrutiny it is clear that the return profits are superior to the conventional mechanical tools, as is the case in Iceland.

On the downside the tools are not very sturdy but damage and breakdown can be limited to a great extend with experienced loggers controlling the slick-line. The lifespan is limited by the shear nature of aging of electronics and wear on the Dewar flask but all components can be easily replaced, updated or repaired by the manufacturer at low costs. The only real dependent is computer facility but in this day of age loggers hardly show up in the field without a laptop and the question is perhaps moreover an academic one.

1.2 Comparison

Pressure and temperature profiles as shown in Figure 1 are used to compare the mechanical Amerada (and Kuster) tools with the electronic K10 Geothermal (K10G) tools. Furthermore a weighted quality estimate of the tools is discussed based on Table 1.

The three pressure measurements shown in Figure 1 are from a flowing well (SV-09) in the Svartsengi geothermal field. The latest measurement (black stars) was carried out with a K10G tool and the two older measurements were done with mechanical tools. The well was clearly pulsating while all three measurements were performed (steam emission seen by the loggers) but only the K10G tool showed the pulsating slope in the well itself. The four temperature measurements shown in Figure 1 are from a shut in well (HE-08) in the Hellisheiði geothermal field. The two latest measurements (black stars and red rings) were performed with the electronic K10G tool, while the two older measurements were performed with mechanical tools. Several aquifers can be seen on the K10G tool profiles which do not show up on the mechanical tool profiles. Locating the aquifers, they are clearly situated at ~1100, ~1350, ~2100 and 2650m depths.

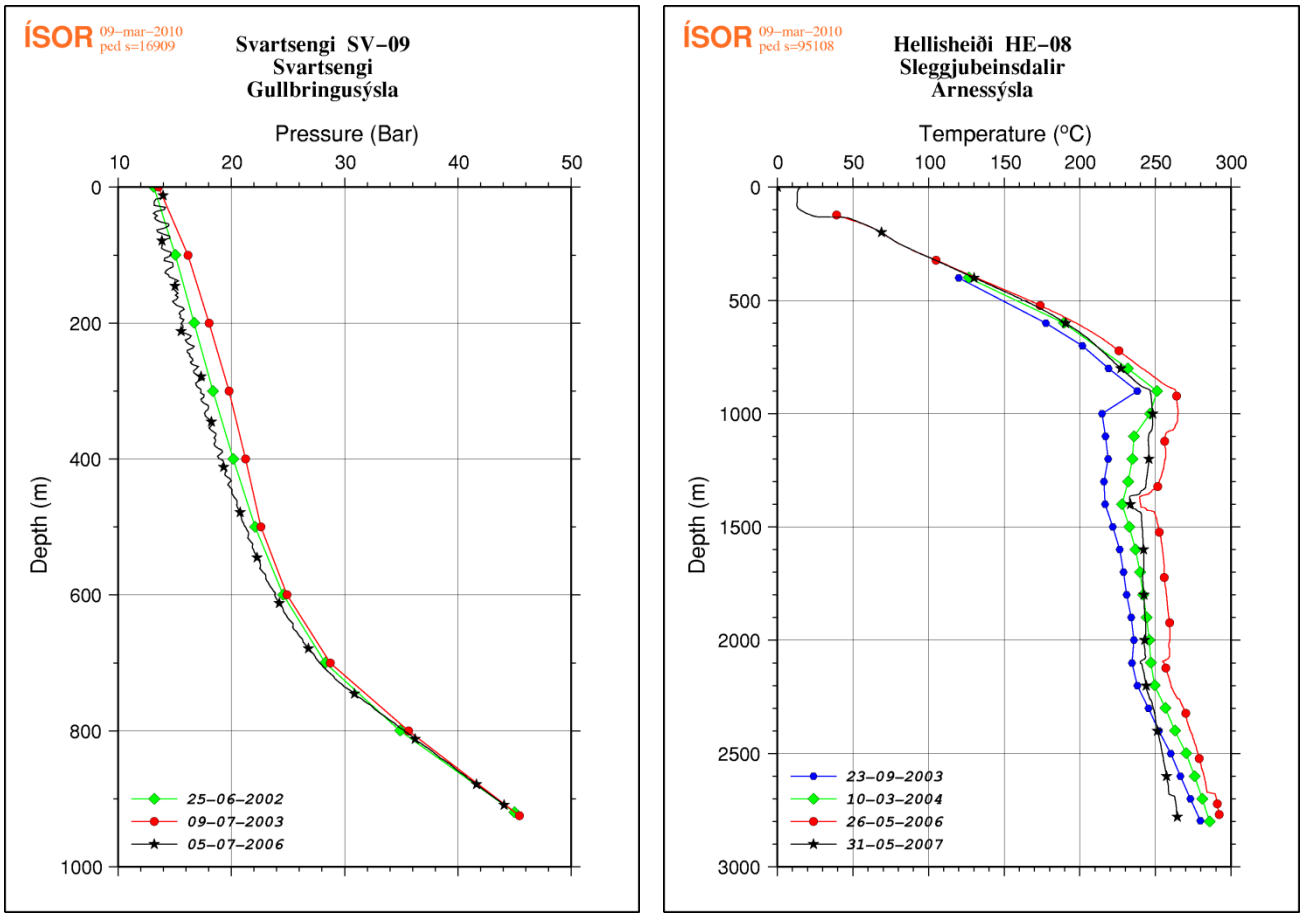

Figure 1:.Left: Pressure profiles from well SV-09, Svartsengi field, Iceland. Right: Temperature profiles from well HE-08, Hellisheiði field, Iceland.

Most operators in HT logging have firsthand experience with clock driven (Amerada or Kuster) recorders, since they have been around for well over half a century and they come relatively cheap. These tools are very sturdy and reliable, fairly easy to use (Table 1) and in fact most geothermal logging service groups are able to calibrate and repair almost any part of the tool. When preparing mechanical tools for logging which are simple per se but several procedures have to be kept in mind and there are no indicators telling you if you have forgotten an important step.

Electronic memory tools are not yet quite as widespread, since they only appeared on the marked a few decades ago and are somewhat more expensive, than the mechanical tools (Table 1). One should, though, bear in mind that the K10G log T and P simultaneously while mechanical tool log either T or P and one would need two mechanical tools to log both parameters; one could thus argue that the electronic tools are about twice the cost. The K10G (and other Dewar flask tools) are, however, much more fragile and should be handled accordingly. Normally, logging with mechanical tools would be done at a speed around 100 m/min. down and up while the K10G run no faster than 30 m/min., experience from Iceland shows that this is especially important in deviated wells. A run in a 2000 m well takes the K10G around 2 hours down and up, while it take the mechanical T tool around 3 hours and the P tool around 2 hours (Table 1). Although logging speed has decreased with the introduction of the K10G, logging time is none the less saved, meaning that it is feasible to log more wells in one day, thus limiting the cost for both manpower and equipment, cutting the budget and increasing the profit. The K10G is equipped with four memory chips and need to be programmed before a run. This of course means that more advanced equipment is needed than for the mechanical tools. Programming a K10G and consequently affirming that everything is ready for logging is pretty straightforward and it is easily noticed if the tool is not ready for logging.

Table 1: Schematic comparison of the main differences between mechanical Amerada and electronic K10G tools. Plusses indicate superior quality, weighted by number of plusses.

K10G	Properties	Mechanical
÷ ÷	***Robustness***	+++
÷	***Lifespan***	+++
+	***Computer***	÷
+++	***Data resolution***	÷ ÷
++	***Tool preparation***	+
+++	***Data handling***	+
+++	***Measuring time down and up***	÷ ÷
+	***Number of sensors***	÷
+++	***Longest measuring time***	÷
÷	***Cost per run***	+
÷	***Maximum speed (m/min.)***	+

÷	***T range (°C)***	+
÷	***Price; one tool all incl.***	**(++)**
++	***Turn a profit*** ***(based on a 2km well)***	÷

1.3 K10G

The K10G pressure transducers senses wellbore pressure through a capillary tube, while the external fast response platinum resistive temperature device (RTD) sensor remains exposed to the wellbore for accurate and fast response temperature sensing and recording [Figure 2]. The K10G can withstand pressures up to 345 bars (at 350°C) before it collapses. The internal electronics and the EXCELL battery can withstand 150°C and are only protected for a certain amount of time by the Dewar flask. The downhole logging time depends not so much on pressure as it does temperature. Kuster Co. has provided the following specifications [Kuster Co. homepage];

- 300°C for max. 9 hours
- 315°C for max. 6 hours
- 370°C for max. 4 hours (pers. comm. from Kusterco CEO, 2006)
- 400°C for max. 2 hours (pers. comm. from Kusterco CEO, 2008)

Figure 2:. External platinum temperature sensor and capillary opening (NPT plug) for pressure readings.

The accuracy of the K10G [Kuster Co. homepage] is 0,024% F.S. (Full Scale) for pressure and 0,25°C for temperature and the resolution is 0,0003% F.S. for pressure and 0,001°C for temperature with a response time of 1,5 sec/10°C. A total of 1.400.000 data points can be sampled continuously by combining the four memory chips. Another possibility is to sample onto one chip and uses the other three chips as back-up copies, the latter feature is being the standard procedure at ÍSOR.

In order to power the tool downhole an EXCELL battery is fitted after programming the tool. The idea behind the EXCELL Lithium cell is that it retains power when stored under the right conditions and will only discharge when awakened by means of a depassivator or simply by tapping it lightly onto a hard surface [Figure 3]. It is possible to program the K10G for logging at different sampling rates for any given length of time and thus setting up a logging program beforehand. This feature is used at ÍSOR when doing for instance lengthy injection tests [Table 2].

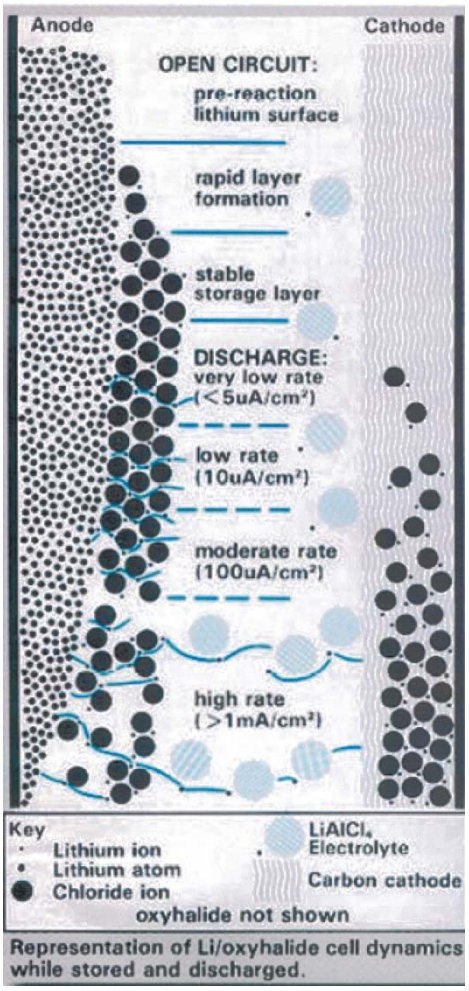

Figure 3:. EXCELL Lithium cell, storage and discharge.

Table 2: EXCELL battery lifetime expectancy.

EXCELL battery lifetime	
Sampling in sec.	**Measuring days**
5	20
10	40
15	52-64
20	59-72
30	68-84
60	81-99

1.4 Logging statistics

Logging HT wells in Iceland escalated to an all time high in year 2008 where the HT tools were run for more than a total of 1.400 km down and up hole, almost solely with the K10G [Figure 4]. As can be seen from Figure 4 no mechanical tools were deployed in all of year 2009 and this tendency has been clear since the arrival of the K10G. The K10G has been deployed more often or as much as an order of magnitude more, since it's arrival. The high in year 2008 is quite significant since the total logged distance with mechanical tools over a period of 55 years is roughly 3.600 km.

Looking at Figure 5, on the left, drilling has been ongoing in a few (2-3) geothermal fields, from 1970 and to 2000, which gives a spin-off as seen on the right in logged distance i.e. a delayed accumulated effect. From year 2000 drilling is getting more widespread in Icelandic geothermal fields and from this year drilling has been ongoing in ALL HT geothermal fields in Iceland, albeit at different intensities, but the increase in drilling is mirrored in logging, reaching an all time high in 2009 of approximately 2.750 km.

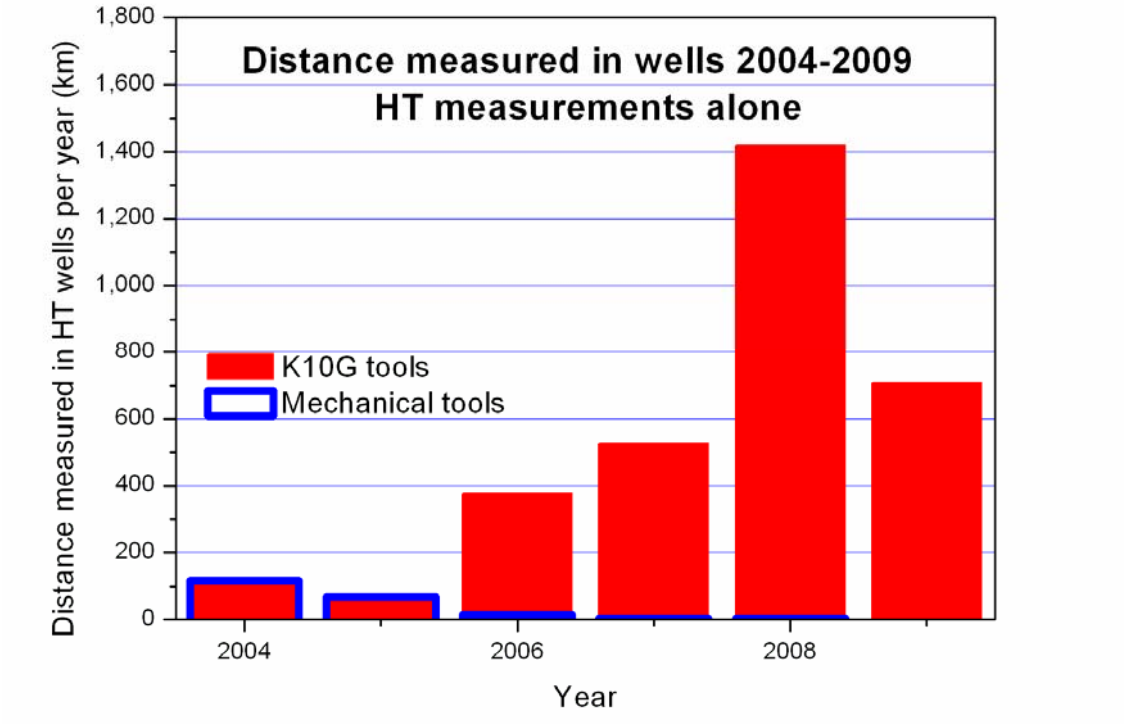

Figure 4:. Logging distances (in km) with HT tools, for a period of 6 years or since the addition of the K10G to the logging suite at ÍSOR.

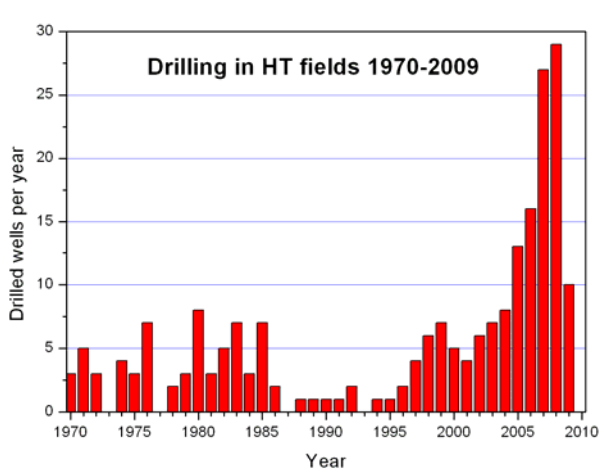

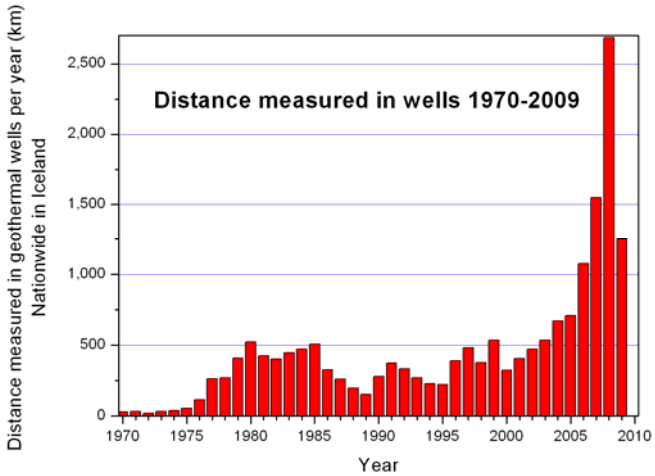

Figure 5:. Left: Distance drilled in HT fields for the period 1970-2009. Right: Distance measured in both low and high temperature wells for the period 1970-2009.

2 SAFETY, HEALTH AND ENVIRONMENT

1.5 Legislation

A safety committee in a company the size of ÍSOR should, according to Icelandic rules, consists of four members. Two of the members are appointed by the board of directors of two are elected by the employees; the chairman is then selected within the foursome. The Administration of Occupational Safety and Health is directly responsible for enforcing the legislation and answers directly to the Minister of Social Affairs.

Inside any company in Iceland the Safety Committee answers directly to the director which thus holds full responsibility with regards to any issues concerning safety, health and environment within a given company regardless of the issue or its character.

1.6 Safety Committee Workflow

The basic work of the Safety Committee is to identify and describe hazards at the workplace. This work can basically be divided into three phases; a preparation phase, a documentation phase and an implementation phase. All forms and examples are based on the instructions and guidelines on the homepage og the Icelandic Occupational Administration.

Preparation Phase

The preparation phase begins with identifying the hazards in a given area/work. In cooperation with the workforce with knowledge on a special field a Hazard Identification (HI) form is constructed, which takes into account the immediate dangers which follow working in a certain field or with dangerous material. In the following an example is used, where some of the dangers from working with radioactive sources in well logging, are shown in a HI form [Figure 6]. The HI form is not meant as instructions for work with the neutron source but only as a check list enabling internal inspection of the work procedure being followed, evaluated and changed if necessary.

One has to bear in mind that though the HI forms are necessary as evaluation check lists and important to ensure a safe working environment and thus they should cover a workflow as a whole or when needed a specific item but one should not make detailed HI forms for every little nut and bolt. The HI forms should always be considered as work in progress and thus one should not hesitate to make changes of any kind since these forms are the backbone of the safety protocol within the company.

Documentation Phase

The next step is to document work procedures by performing Risk Assessment (RA) based on the HI forms. The first part of the RA is the simple task of inspecting a given issue using the relevant HI form performing an evaluation on whether a given item on the list is ok or not ok. The items getting a NOT OK is then registered on a 5 step implementation plan [Table 3] and the results are written up in form of a short report concentrating the result on ONE single page, for better overview.

After performing RA and evaluating risks (if any) and actions to be taken, the last step in the documentation phase is to update the Risk Assessment Chart [Figure 7].

ÍSOR	**Neutron source** **Hazard Identification**	Nr. doc: Sv1 Edition nr.: 1 Date: 18.11.2009 Author: PED Liable :Department Head pp:1

Company name: **ISOR** *Department/branch:* **Technical**

Internal work: Assessment of deployment and handling of neutron sources

Topics	***Common working tasks and handling of neutron sources, with regards to safety – health of the employees –transportation –inspection – protection – training and work procedure.***	Rating: V: OK X. Not OK O: Not applicable	Laws – rules, regulations, Safety leaflets, Safety handbook and other material that applies
List of items	***Check list***		
Safety leaflet	Is Safety Leaflet (SL) for the radioactive sources available in Icelandic? Is information on radiation, pollution and protection available?	X V	*L-044/2002* *R-811/2003*
Inventory list / intensity / pollution	Are the radioactive sources and their intensity compiled in a list and does it show handling dangers and classification on the SL along with basic information needed to perform a Risk Assessment?	V	*R-811/2003*
Handling, transporting and source storage	Is handling, moving and storage facilities in order? a-Is the work procedure followed? *(M002-1)* b-Is the storage closed and locked? c-Is the storage according to ADR when sources are moved? *American Depositary Receipt*	 V V X	 *R-811/2003* *L-028/2008, 6 gr.* *Rg-810/2003* *M002-1* GR04-04
Labeling	Is the storage labeling in order? Is ADR labeling on the carrier in order?	V X	*R-553/2004* *R-236/1990* *R-984/2000* *Sbr. 5.4.1 ADR*
Radioactive Source Inst.	Are inspection of the sources and intensity measurements, at the workplace, done regularly? Is the radiation limit of individual workers monitored?	V V	*L-44/2002, 13 and 17gr.* *R-627/2003* *R-920/2006* R-491/1987 R-154/1999
Moving *Lading bill*	a. Is the storage in the carrier lockable? b. Is a lading bill present in the carrier?	X X	*L-44/2002* *R-984/2000* *Sbr. 5.4.1 ADR*

Figure 6:. Example on part of a Hazard Identification form – working with radioactive material.

Table 3:. Risk Assessment 5 step Implementation form, a few lines shown.

Danger, as noted on HI form (RA) **2**	**Possible effect on health** **3a**	**Who are at risk** **3b**	**Danger level L,M,H** **4**	**What precautions are taken now to minimize danger?** **5a**	**Suggestions / remedies** **5b**	**Cost estimate** **5c**	**Estimated finish, responsible party and confirmed finish** **5d**
Safety leaflet	Could affect health	Workforce	H	Nothing	Write safety leaflet and special instructions and information's		***Estimated finish:*** **July 2010** ***Responsible:*** ***Technical dept.*** ***Confirmed finish:***
Handling, moving and	Could affect health	Workforce	M	LB002-1	Ensure storage is according to ADR og GR		***Estimated finish:*** **July 2010** ***Responsible:***

storage							***Technical dept. Confirmed finish:***

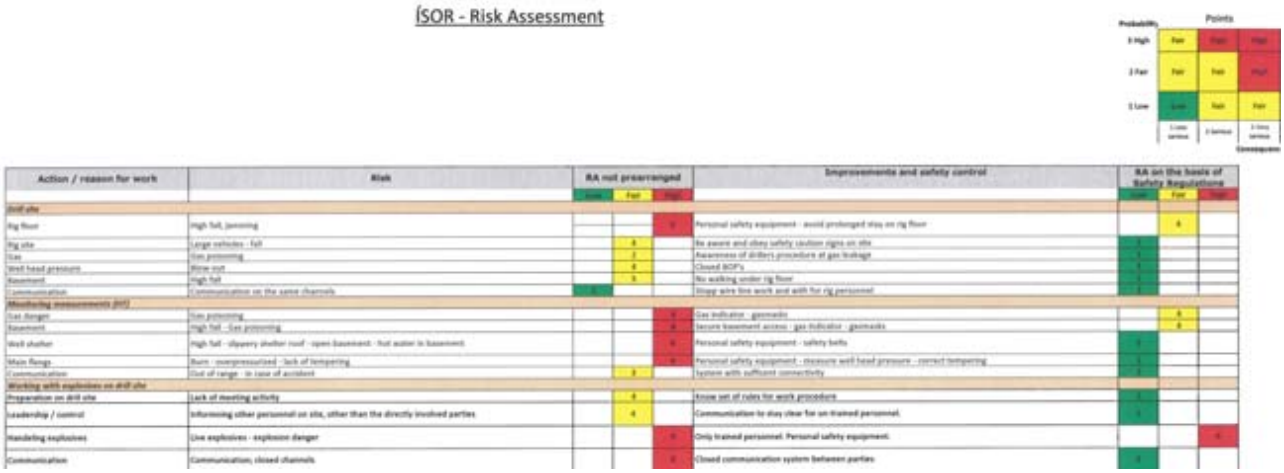

Figure 7:. Risk Assessment Chart, only partly shown.

Implementation Phase
The final phase is then to implement the workflow as a new layer on top of the entire company structure. This calls for regular unannounced inspections, in order to get a more realistic picture of the current status on safety and health issues in the company. It is however important to involve the workforce throughout the entire company, as mentioned above to identify hazards but also to communicate that this is in everybody's best interest and the wellbeing of the individual worker is more important than money and thus it is important to ensure that everybody knows that the idea behind the RA workflow is to assist workers in optimizing safety standards and ensuring them a safer working environment.

1.7 Safety Equipment

Equipping the workforce for a given task is a great responsibility and should not be left to chance. The equipment is also a good example on the aforementioned caution as not to make too detailed RA forms. Looking at for instance logging safety equipment [Table 4] one could argue that it would be reasonable to asses it as a whole but one quickly realizes that though the focus is seemingly narrow the span of the relevant equipment is wide and the equipment is already covered on separate RA forms; for instance logging truck, drilling rig, personnel and communication.

Table 4: Basic standard and personal safety equipment, example for logging purposes only.

Basic Standard	**Personal**
H2S gas indicator, gasmasks, safety belts, emergency kit, cell or satellite phone or walkie-talkie, mud jack, tow-rope, shovel, basic car repair kit.	Helmet, footwear (High Temperature), hearing protecting (class III), working suits (reflector strips), gloves (HT), goggles, neutron and gamma radiation measuring films, reflector vests (good and valid addition – but BANNED ON RIG FLOOR)

1.8 Contingency Plans

In order to perform any given task as in the example above for logging a (HT) well, contingency plans or back-up plans as a stand-alone factor is a criterion of success [Danielsen, 2008] as is safety of course. Saving time and money and at the same time ensuring a safer working environment are quite obvious assets of making contingency plans. When everybody knows what is expected in case of the need to implement the back-up plan for a given scenario it makes for smoother execution and higher efficiency from the applied workforce. At the same time it is important to keep good contact between client and contractor and contingency plans are an important step to ensure good communication flow between the two parties.

Basic rules from practical cases like tool malfunction and blow-out or similar obstacles interfering with for all parties involved logging a HT well aside, there is a need for awareness on what could be termed as "Rules of Engagement", as discussed here in the case of the experience of ÍSOR within Icelandic jurisdiction. In many geothermal HT wells logged in Iceland four safety legislation factors are in play. First of all, when the loggers are en route to the drill site they will at all times have to obey to the sets of normal legislation and rules for driving a truck on a public road. Secondly, when they enter the geothermal field they also will have to obey rules of the client but thirdly, by entering the drill site, the legislation for driving on a public road is abolished and the rules of the drilling company is in effect. Finally, on top of paying attention to what rules and legislation that is enforces from without the loggers are subject to the ÍSOR company safety, health and environment rules at all times.

3 REFERENCES

Danielsen, Peter E., 2008: High Temperature Geothermal Logging for Temperature and Pressure. ARGeo C-2 Conference, Entebbe, Uganda, p. 10

http://kusterco.com/pdfs/k10_geothermal.pdf: K10G specifications.

www.vinnueftirlit.is/vinnueftirlit/is/english/: Relevant forms, instructions and legislation. Icelandic/English.

Drilling, Completion and Testing of Geothermal Wells

Geothermal Well Testing.

Well Testing Interpretation
Injection/Production Tests, Interpretation and Monitoring

Peter E. Danielsen, Pall Jónsson and Þorsteinn Egilson
ÍSOR, Akureyri and Reykjavík, Iceland

SUMMARY

In the first part of this paper an injection, step test in well HE-29 will be discussed in order to illustrate by example how well test interpretation is done in practice. The most important modeling steps in the computer program Well Tester, designed by ÍSOR, which is currently used for interpretation of injection and production tests, will also be discussed in part I. The second part of this paper contains discussion on long-term monitoring, flow, enthalpy and discharge measurements, along with brief discussion on Horner plots and the Albright method.

INTRODUCTION

Well testing is a method commonly used to obtain initial estimates of geothermal reservoir properties. In the case of well HE-29 the production test (injection step test) was done at the end of drilling to 2502 m, on February 13, 2007. Well HE-29 is situated in the Hellisheiði geothermal field some 50 km from Reykjavík in Iceland [Figure 1]. Initial drilling in the Hellisheiði field began in 2001 and today close to 60 production and exploration wells along with some 15 injection wells has been drilled in the area and production is overseen by Reykjavik Energy. All data and results are published with the permission of Reykjavik Energy.

During a well test, the pressure response in a well, due to a change in injection or production is measured to infer a number of properties relating to the surrounding reservoir. This is commonly done by setting up a mathematical model for the pressure transient response in the well and the reservoir, due to an instantaneous step change in injection (or production). The mathematical model depends on characteristic values of the reservoir, and by tuning these values such that the modeled response fits the observed data, one can infer the characteristic properties of the reservoir.

This is an inverse modeling problem and will (as so many others in reservoir engineering) inherently yield somewhat ambiguous results. However, by carefully conducting the well test, considering the conceptual model of the reservoir and using computer aided analysis, the ambiguity in the results can be minimized. Moreover, an error estimate on the inferred parameters can be obtained through the nonlinear regression provided by the computer aided approach

The interpretation program Well Tester (current version 1.0b) was written at ÍSOR to handle data manipulation and analysis of well tests (mainly multi-step injection tests) in Icelandic geothermal fields. The goal with Well Tester was to make a user friendly program that could speed up the process of analyzing and reporting the results from a given well test. To meet this goal the process was divided into five (or in some cases six) simple steps that range from setting initial conditions to modeling to compiling all results in a final report (available in Icelandic and English).

The flow models in Well Tester are based on single phase flow through homogeneous or dual porosity reservoirs. The reservoir fluid is assumed to be slightly (and only slightly) compressible, which further limits the applicability to single phase liquid reservoirs and well tests where the fluid stays as single phase liquid throughout the test. Moreover, Well Tester is only made to handle well tests where the injection (or production) rate can be assumed to have changed in steps, i.e. Well Tester cannot use flow rate time series from an input file.

In the second part of this paper to methods to estimate formation temperature are discussed briefly. Furthermore calculations to estimate productivity from a set of measured parameters in production tests and the basic ideas and pitfalls concerning discharge tests are discussed. An example of long-term monitoring from the Svartsengi geothermal field is shown and briefly discussed.

1 PART I - WELL HE-29

1.1 Case History for HE-29

Early in the morning of February 13, 2007 the Kusterco "10" Geothermal (K10G) tool was lowered into well HE-29. The K10G tool (see paper 1 on "Electronic HT Tools and Safety, Health and Environment") was left suspended to a Measured Depth (MD) of 1600 m but since the well had been drilled in a Southerly direction with approximately 31° inclination at this depth, the True Vertical sensor Depth (TVD) was in fact 1444 m [Þórarinsson et al., 2007].

Temperature was logged continuously [Figure 2] whilst lowering and subsequently three injection steps were taken [Figure 3] where step 1 is marked with blue color. For the first step the pump rate was changed at 03:10 o'clock from 20 to 44, 5 L/s. At 06:10 o´clock the pump rate was changed from 44, 5 to 60 L/s for the second step and the final step lasted from 08:30 to 12:20 o´clock where the pump rate was changed from 60 to 25, 5 L/s. The depth to the water table was recorded as 322 m at the end of the injection test.

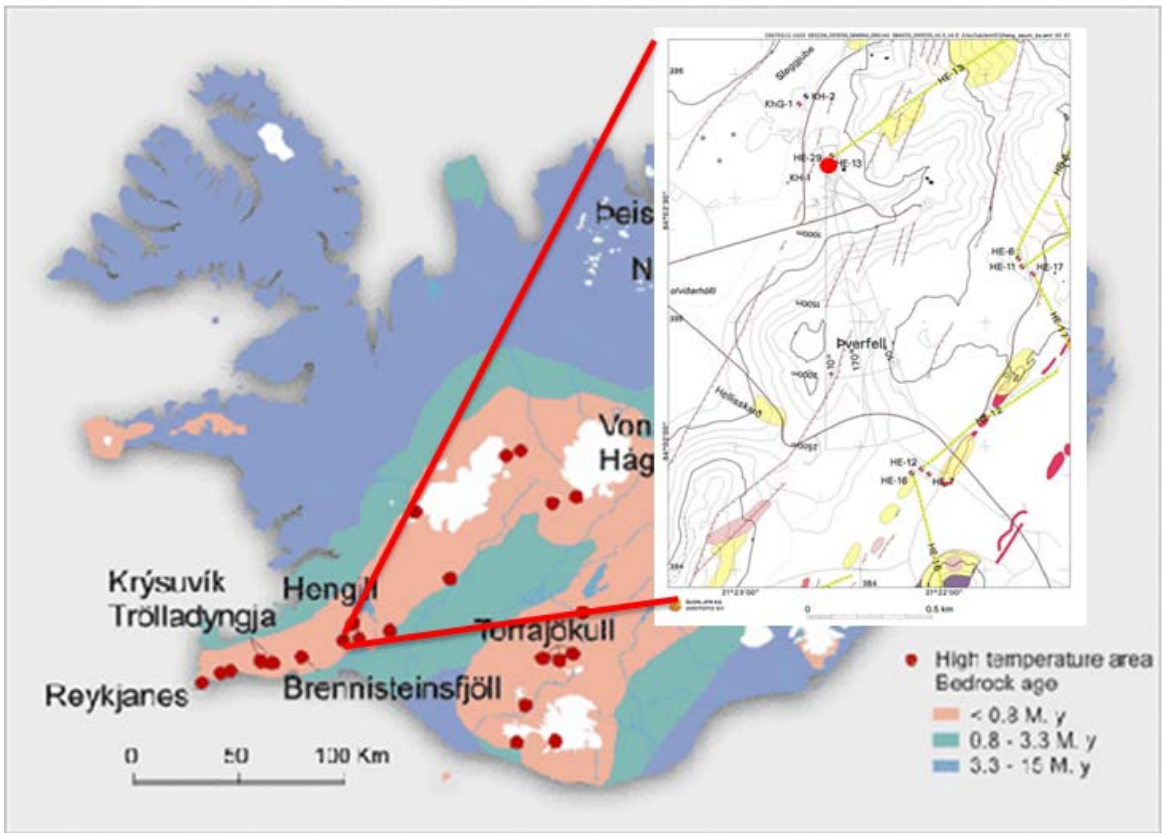

Figure 1:. Map showing location of well HE-29, Hellisheiði geothermal field.

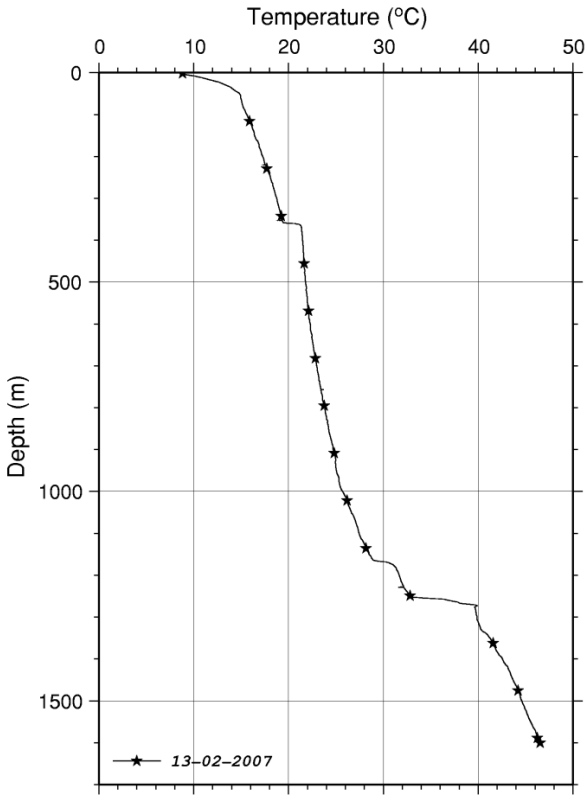

Figure 2:. Temperature measured prior to injection step test on February 13, 2007, in HE-29.

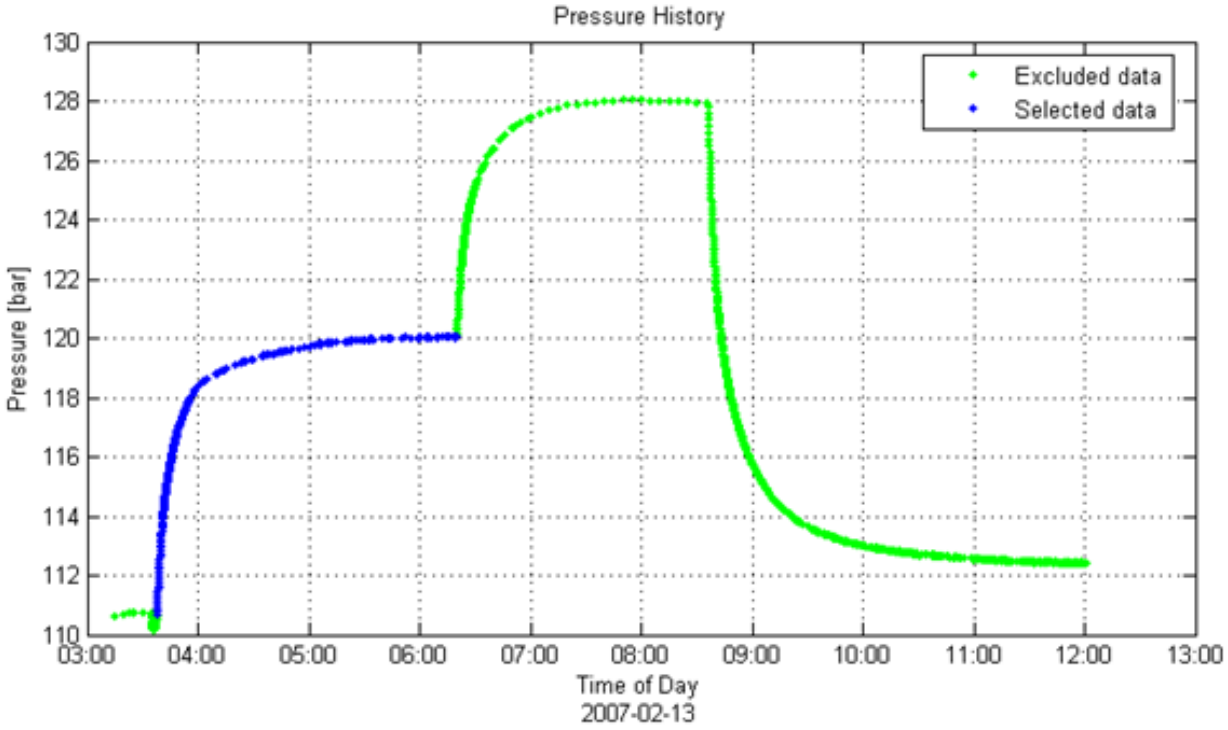

Figure 3:. Selected (blue) and excluded data (green) shown for the step test in well HE-29.

2 Modeling

2.1 Step 1

Step 1 selecting initial parameters, assumptions and modeling are shown in Table 1 and 2.

Table 1: Initial parameters chosen to model the injection step test in well HE-29.

Parameter (symbol)	Value	Units
Estimated Reservoir Temperature (T_{est})	200	[°C]
Estimated Reservoir Pressure (P_{est})	116	[Bar]
Wellbore Radius (r_w)	0.20	[m]
Porosity (φ)	0.10	[-]
Dynamic Res. Fluid Viscosity (μ)	$1.37 \cdot 10^{-4}$	[Pa·s]
Total Compressibility (c_t)	$5.32 \cdot 10^{-10}$	[1/Pa]

Table 2: Initial model assumptions for step nr. 1 in HE-29.

Well Testing Model - Step nr. 1	
Reservoir	Homogenous
Boundary	Constant Pressure
Well	Constant Skin
Wellbore	Constant Radius

On Figure 4 both time and pressure changes are plotted on logarithmic scales. On Figure 5 time is plotted on a logarithmic scale while pressure changes are shown on a linear scale.

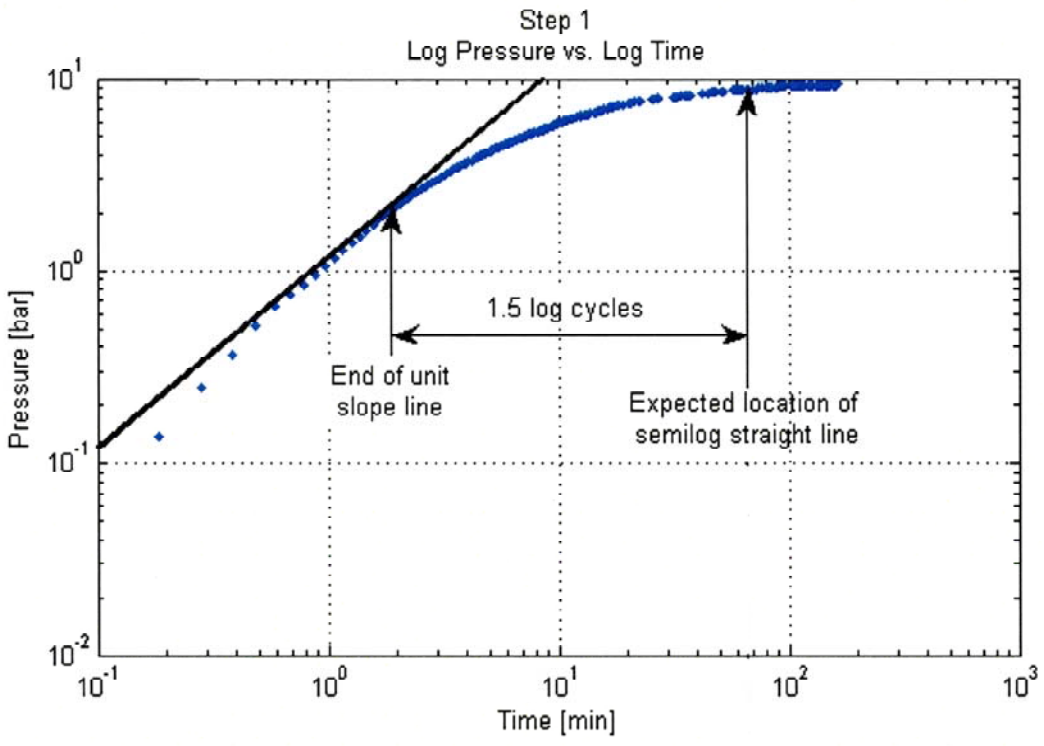

Figure 4:. Step 1: Pressure vs. Time, log-log scale.

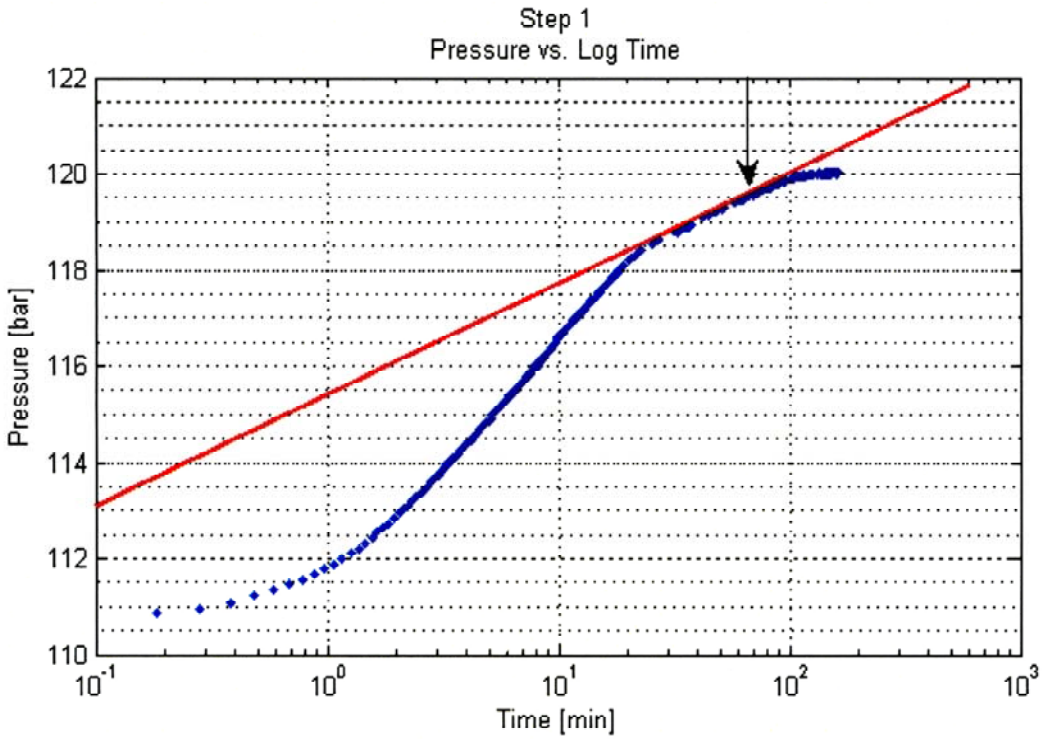

Figure 5:. Step 1: Pressure vs. Time (logarithmic scale).

2.2 Results

Step1 calculations and results are shown in Table 3 and 4.

Table 3: Calculated parameters for step nr. 1 in well HE-29.

Parameter (symbol)	Value	Lower bound 95 % C.I.	Upper bound 95 % C.I.	Accuracy [%] 95% C.I.	Units
Transmissivity (T)	$2.42 \cdot 10^{-8}$	$2.38 \cdot 10^{-8}$	$2.46 \cdot 10^{-8}$	0.9	$m^3/(Pa \cdot s)$
Storativity (S)	$4.22 \cdot 10^{-8}$	$3.81 \cdot 10^{-8}$	$4.63 \cdot 10^{-8}$	4.9	$m^3/(Pa \cdot m^2)$
Effective radius (r_e)	86.80	80.98	92.61	3.3	m
Skin Factor (s)	-0.25	-0.32	-0.18		-
Wellbore Storage (C)	$1.05 \cdot 10^{-5}$	$1.04 \cdot 10^{-5}$	$1.06 \cdot 10^{-5}$	0.5	m^3/Pa
Injectivity Index (II)	$2.62 \cdot 10^{-8}$				(L/s)/bar

Table 4: Calculated key numbers for the entire injection step test in well HE-29.

Step	Flow change ΔQ L/s	Pressure change ΔP bar	Injectivity index II (L/s)/bar
0→1	25.0	9.3	2.7
1→2	20.0	8.0	2.5
2→3	40.0	-15.5	2.6

3 PART I - WELL TESTER

3.1 General notes on Well Testing

Well testing is a method commonly used to obtain initial estimates of geothermal reservoir properties in the vicinity of a well. The method is based on observing the pressure transient caused by sudden changes in injection or production from a well. Theoretical models have been derived to predict the type of response seen. Based on the type of response, a specific model is chosen. Then the reservoir properties that this model relies on are calibrated until a good fit is seen between the actual and the theoretical pressure transient. This type of parameter estimation is often referred to as inverse modeling, since rather than calculating the reservoir properties directly; we only know the input and the output to an unknown function (our reservoir model). This unknown function and the constants that define the shape of this function is what we want to find by using the same input as was used in reality and modifying the function until the output also matches the actual observed output. Those further interested in this theory are referred to [Horne, 1995].

The main objective of an injection test is to assess the characteristics of the reservoir surrounding the well. The parameters most commonly estimated from geothermal step tests are *transmissivity* (T), *storativity* (S) and the *injectivity index* (II).

A variety of other factors can be estimated from well tests, depending on the type of well (e.g. damaged/stimulated, partially penetrating etc.) and/or reservoir (e.g. fractured, dual porosity etc.) under consideration. To be able to do this, one also needs to have the correct mathematical model for the particular type of reservoir being investigated. Well Tester has only incorporated a limited number of mathematical models but later versions might be developed, allowing a larger variety of models and reservoir parameters.

4 WELL TESTER

4.1 Parameters

The first step after data has been loaded into Well Tester is to specify values for some initial parameters that are used in the subsequent calculations. The Set Parameters menu is shown in Figure 6.

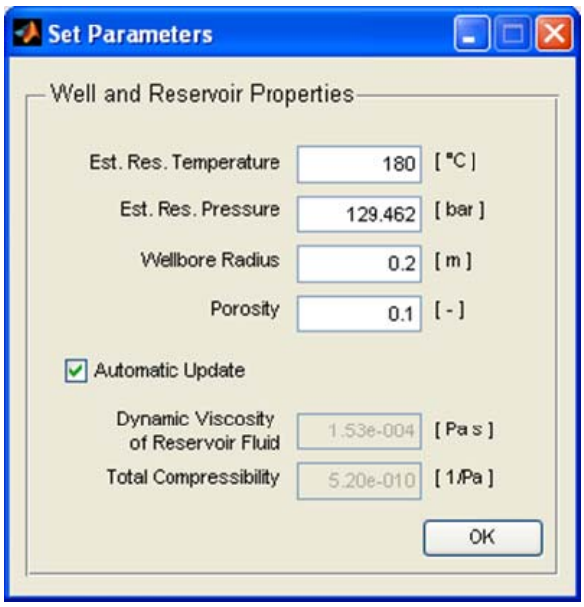

Figure 6:. Set Parameters menu [Júlíusson, Grétarsson and Jónsson, 2008].

The estimated reservoir pressure and temperature are average estimates for the part of the reservoir that is being investigated in the well test. These values are used to calculate approximate values of the dynamic viscosity of reservoir fluid and total compressibility.
An important value to be specified is the wellbore radius, since it directly affects the estimated transmissivity and storativity. The wellbore radius should be taken as the estimated radius of the wellbore at the estimated reservoir depth.
The estimated porosity of the reservoir is the required in the initial parameter menu. Porosity will vary between reservoirs but it is usually somewhere in the range of 3 to 15 percent.
The dynamic viscosity is commonly around $1.2*10^{-4}$ Pa·s with slight variations, depending on pressure and temperature. The temperature and pressure should be taken as the average estimated reservoir conditions in the influence area of the well test. The default option is to have Well Tester determine this value based on estimated reservoir temperature and pressure, using built in look-up tables.
The total compressibility is defined as the combined compressibility of the rock (c_R) and the reservoir fluid (c_w). It is often around $6*10^{-10}$ Pa^{-1}, but will vary with the temperature (T), pressure (P), estimated porosity (φ) and estimated compressibility of the rock. In many liquid-dominated reservoir applications the compressibility of the rock is the dominating factor. The total compressibility is formulated as, $c_t = \varphi c_{w@T,P} + (1-\varphi)c_R$. The default option in Well Tester is to calculate c_w from built in steam tables and then calculate c_t using the previously estimated porosity, and assuming $c_R=5*10^{-10}$ Pa^{-1} (approximate value for fissured rock).
Accurate estimates of viscosity, compressibility and porosity are not essential since these values are only used to infer bulk estimates of the reservoir thickness and permeability and other parameter estimates calculated by Well Tester are independent of these values.

4.2 Setting Steps

Well Tester will divide the data into two steps by default. The number of steps [Figure 7] can be changed by modifying the number in the corresponding dialog box and pressing the *Guess Steps* button (or just press enter). The selected guessing algorithm will then attempt to detect the first data point for each step and draw a partitioning line at that point. In many cases the algorithm will not find exactly the correct point so it is recommended to zoom in on each transition line to check this. For noisy and/or densely sampled data, increasing the number of filter points often improves the results of the step guessing algorithm, but generally it is much quicker to just modify the transition points manually, as described in following paragraph.

After the transition points have been selected, the injection rates for each step need to be specified. These values should be given in liters per second with injection defined as positive (production can be defined by using negative values). After filling in the numbers, the injection rate can be plotted along with the pressure transient by pressing *Redraw Data* [Figure 7].

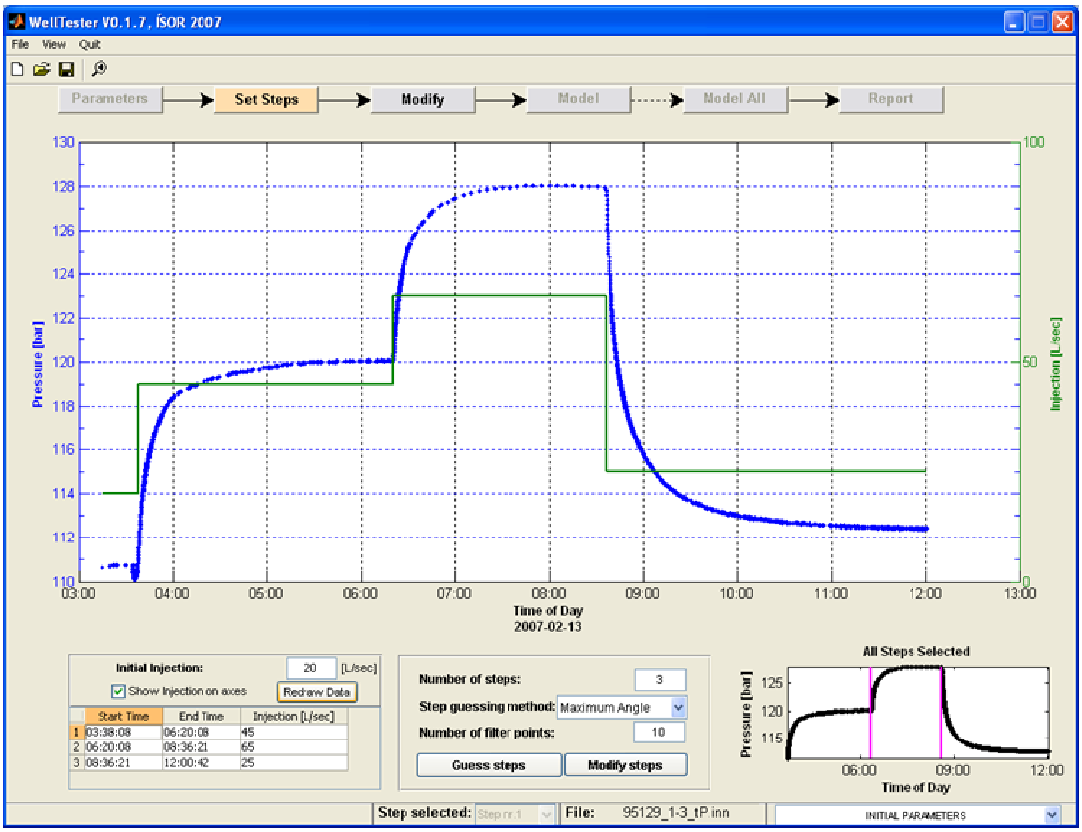

Figure 7:. Set Steps mode: After the steps have been set correctly [Júlíusson, Grétarsson and Jónsson, 2008].

4.3 Data Handling

In the modify mode [Figure 8] it is possible to clean, resample and correct the data for temperature variations within the wellbore during the course of the well test. Following is a discussion of each option and how they function. For each step it is necessary to choose either resampled or no resampling, before the Model mode can be accessed.

It is quite common to see errors in well test data that one would prefer to ignore in the subsequent analysis. Well Tester has been designed to make the task of cleaning data easy [Figure 8]. In exclude mode, one can drag a box around the points that should be excluded, and those points will be redrawn as red x's. The button *Include Points* works very similar to the *Exclude Points* button albeit enabling the user to put points back into the data set.

In cases where large amounts of data have been collected, it might be desirable to reduce the number of data points to save computational time. However, care must be taken to always retain a data set that evenly and accurately describes the trend of the pressure transient. In Well Tester the default suggestion for the number of data points is to include 300 samples in each step, although this number can be modified. The points in the resampled data set will switch to a green color [Figure 8].

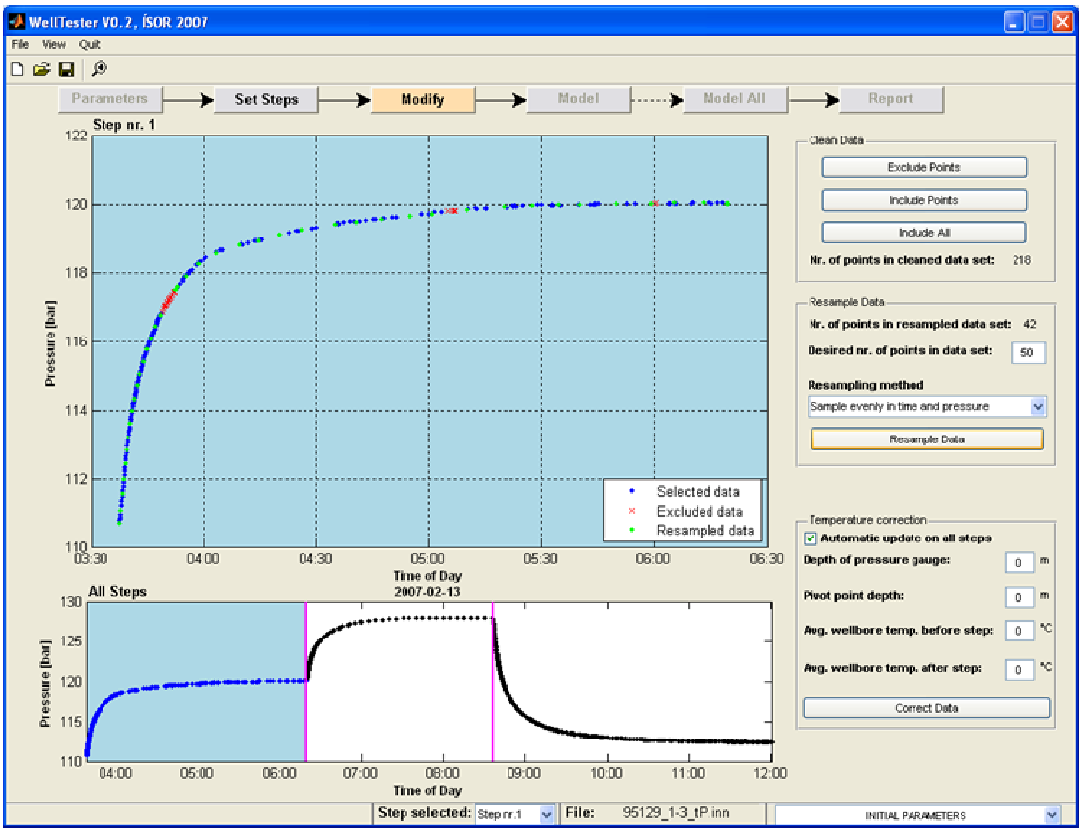

Figure 8:. Modify mode: The resampled data set is marked by green points [Júlíusson, Grétarsson and Jónsson, 2008].

4.4 Modeling

In the Model mode the user can select the most appropriate model for the reservoir being investigated. To achieve this, the so-called derivative plot is used, along with the pressure data on a log-log scale graph. The derivative plot (which is actually the derivative of pressure vs. time multiplied with the time t passed from the beginning of the step, i.e. $t\frac{dP}{dt}$) can be used as a diagnostic tool to identify the most appropriate type of model. The task of explaining exactly how to interpret the derivative plot is beyond the scope of this paper but those who are further interested should look at [Horne, 1995], which is an excellent resource on interpreting derivative plots.

The well testing model has been broken into four separate parts in the model panel. Each part defines different aspects of the reservoir and/or the well. Various models can be chosen, using the drop down lists and the corresponding model parameters will appear in the table below. Each parameter will have some default value but these can be modified and the modeled response can be plotted.

There are several options to obtain an improved initial estimate for the corresponding parameter and while working in the Model mode a tool-tip string tells the user how to choose a specific point on the graph (from which the respective parameters are calculated). Following is a brief description of how to choose each point.
The *transmissivity (T)* is calculated by choosing the intersection point [Figure 9] between a tangent to the straight horizontal part of the derivative plot and the initial unit slope. The derivative plot will not always have a very clearly defined horizontal part, so in many cases this will be a rough estimate. Note that this horizontal part usually comes after the initial

"hump" (convex) in the derivative plot; it corresponds to infinite acting radial flow in the reservoir and is usually seen more to the right on the log-log plot (i.e. at late times). The initial unit slope may in some cases not have an exact unit slope (e.g. depending on how quickly the injection was changed and what kind of fracture connectivity the well has) but by choosing a point that comes close to fitting the initial slope, a relatively good initial estimate can be made. A byproduct of calculating the transmissivity is to calculate the *wellbore storage (C),* which will also be updated in the table [Figure 9].

The skin factor can also be estimated by selecting a point on the derivative plot. This is done by selecting a point on the graph somewhere on the horizontal part of the derivative (i.e. infinite acting radial flow period, Figure 9). The algorithm that estimates the skin uses the time coordinate that is chosen and looks for the next 3 data points before and after that time. The average value of these data points is used to calculate the skin factor, using the semi-log analysis method [Horne, 1995].
When the pressure wave generated by a sudden change in injection hits a boundary in the reservoir, a boundary effect can be seen in the derivative plot. The boundary effect will be expressed towards the end of the data set as the derivative plot starts to trend towards zero or infinity. This boundary effect can be used to estimate the distance to the boundary, which is referred to as the *radius of investigation* (r_e). Whether the derivative will trend towards zero or infinity is determined by the type of boundary and whether the injection is being increased (injection) or decreased (fall-off). In production test an increase in production (drawdown) shows the same effect as a decrease in injection while a decrease in production (build-up) shows the same effect as an increase in injection. Figure 10 illustrates the decision process for determining the boundary model.

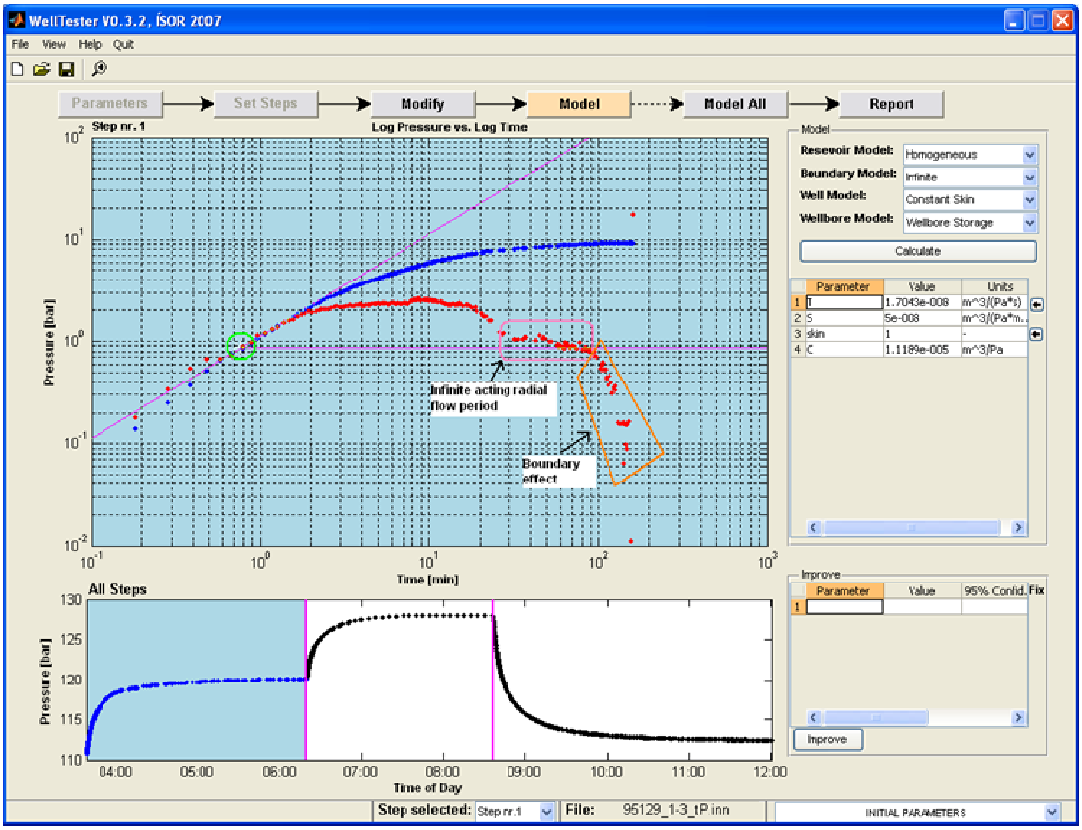

Figure 9:. Model mode: An example of how to choose a point (green circle) to calculate transmissivity and wellbore storage. The figure also illustrates the infinite acting radial flow period and a Constant Pressure boundary effect [Júlíusson, Grétarsson and Jónsson, 2008].

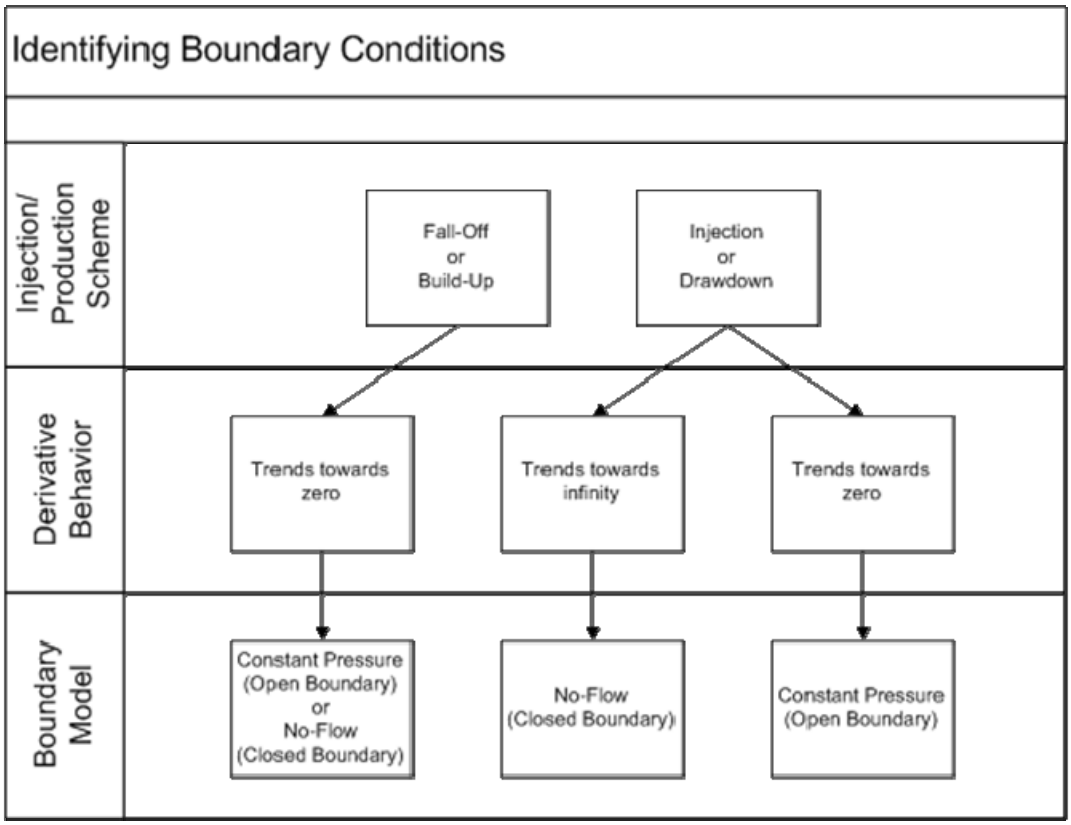

Figure 10:. Schematic diagram of how to determine boundary conditions from the derivative plot [Júlíusson, Grétarsson and Jónsson, 2008].

When the appropriate boundary model has been selected, it is possible to select the point where the derivative plot starts to trend towards zero (or infinity). An estimate of the radius of investigation should appear in the value column for r_e. This corresponds to the approximate distance to the boundary.

Some well testing programs offer the possibility of modeling boundaries of various shapes (single and double sided faults etc.). This has not been implemented in Well Tester 1.0b possibly having little applicability since many geothermal wells in Iceland already intersect the largest fractures.

A "dip" (concave) in the derivative plot can be indicative of a dual porosity reservoir (although this is not always the case). This effect is often seen around the start of the infinite acting radial flow period. When a dual porosity reservoir model is selected, two new parameters need to be determined. These are the *transmissivity ratio (λ or la)* and the *storativity ratio (ω or om)*. The meaning of these parameters is discussed by [Horne, 1995] but also in the default report from Well Tester. By selecting the point corresponding to the bottom of the dip for the storativity ratio line an initial estimate will be given for the two ratios in question [Figure 11].

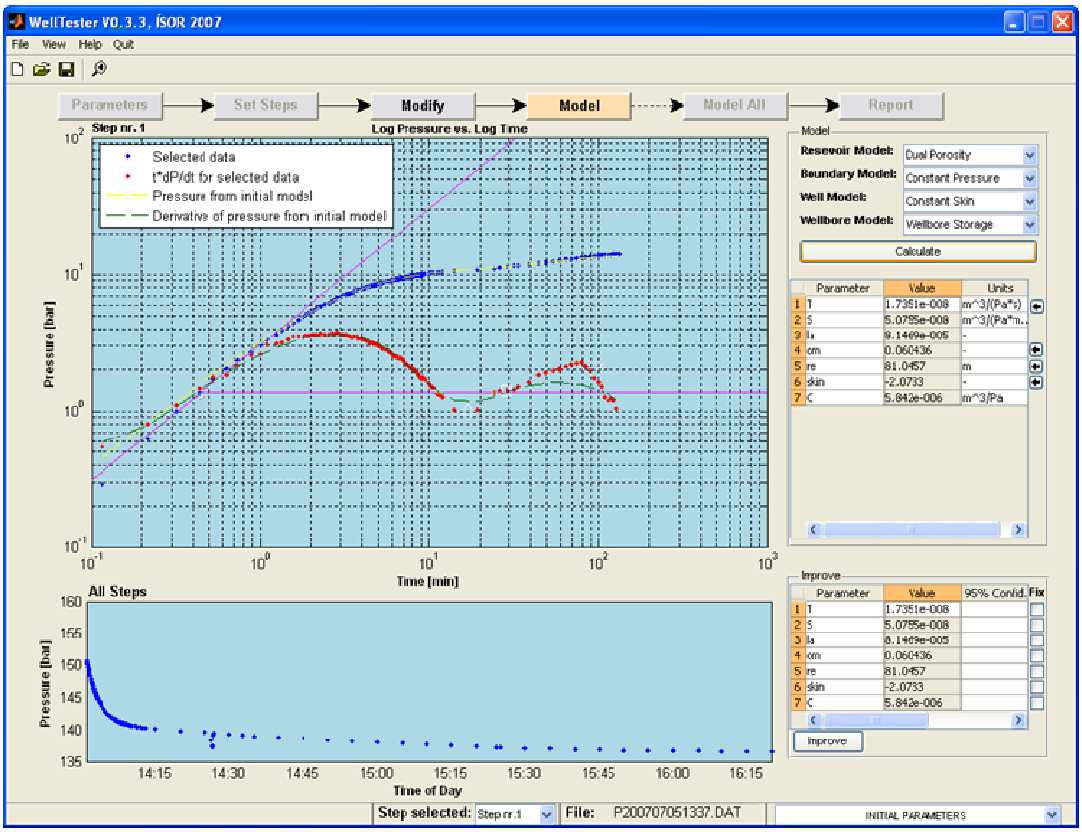

Figure 11:. A example of a data set with a dual porosity dip (between minutes 10 and 30) [Júlíusson, Grétarsson and Jónsson, 2008].

To minimize the sum of squares of the residuals, a non-linear regression algorithm (Trust-Region algorithm) is run to adjust the model parameters. An upper and lower bound can be set for each parameter by adjusting the values in the appropriate columns. Individual parameters can be fixed, i.e. excluded from the minimization procedure [Figure 12]. When the algorithm is done the adjusted parameters appear along with 95% confidence bounds.

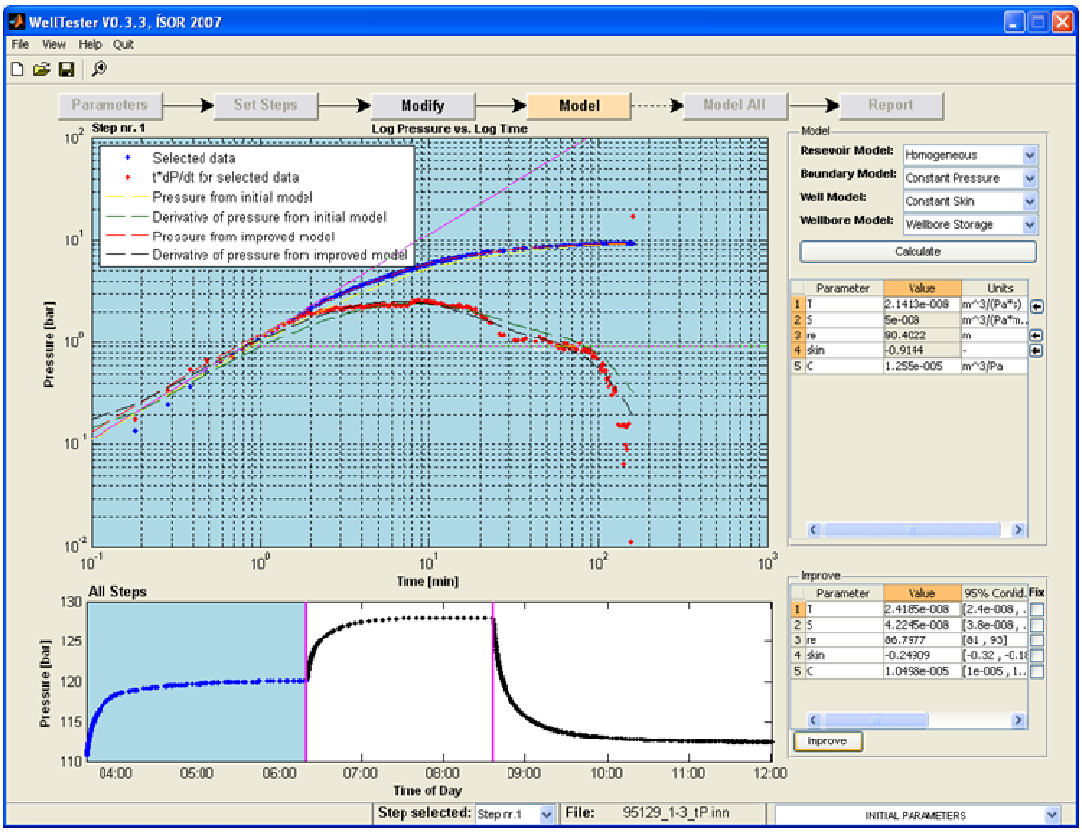

Figure 12:. An example of an improved reservoir model [Júlíusson, Grétarsson and Jónsson, 2008].

In the Model All mode the user can find those model parameters that give the best correspondence between a multi-step model and data set. In this mode it is possible to chose the previously cleaned, resampled and corrected data or use the entire data collected. It is also possible to resample the entire dataset [Figure 13].

A report including graphics, results and standard chapters on modeling theory can be generated. The amount of output desired from the well test analysis can be selected by the user i.e. either the entire report or individual figures and parameters in various formats. Well name, test technicians and test date can be filled in. Moreover, individual chapters to be written to a report can be selected. The report generated will be in Rich Text Format (*.rtf) which can be read by a number of word processors, including Microsoft Word and Open Office Writer.

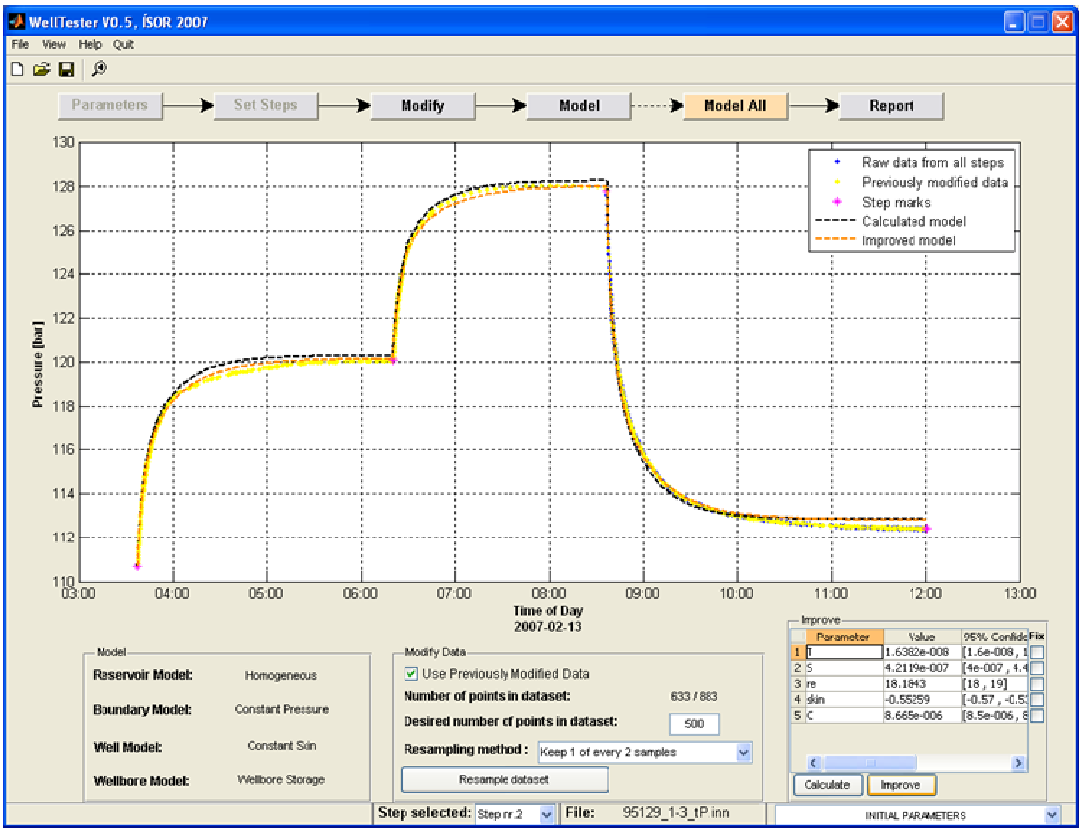

Figure 13:. The Model All tab [Júlíusson, Grétarsson and Jónsson, 2008].

5 PART I I- T/P LOGGING DURING WARM-UP AND PRODUCTION TESTING

5.1 Long-term monitoring

Long-term monitoring is an important part of exploiting and successfully running a geothermal field and consequently also the related power plant. Several parameters may be monitored over time to evaluate the sustainability and the response of the reservoir as a consequence of production.

In the early stages of the warm-up period temperature and pressure measurements will indicate at what depth equilibrium is present, by deducting the pivot point from the measurements. Regular temperature and pressure measurements will indicate how the temperature and pressure response, at depth, is to production [Figure 14 and 15]. As can be seen from Figure 15 a pressure draw down is evident over the last approximately 30 years in the Svartsengi geothermal field, where production began in 1980.

Reinjection started in 1990 thus slowing down the pressure drop in the field. Recently another injection well has been drilled and the effect of the increased injection will be for the future to show. A approximately 700 meters thick steam cap has evolved as a consequence of the draw down and it's is now used for extracting pure steam from the field, not previously an option.

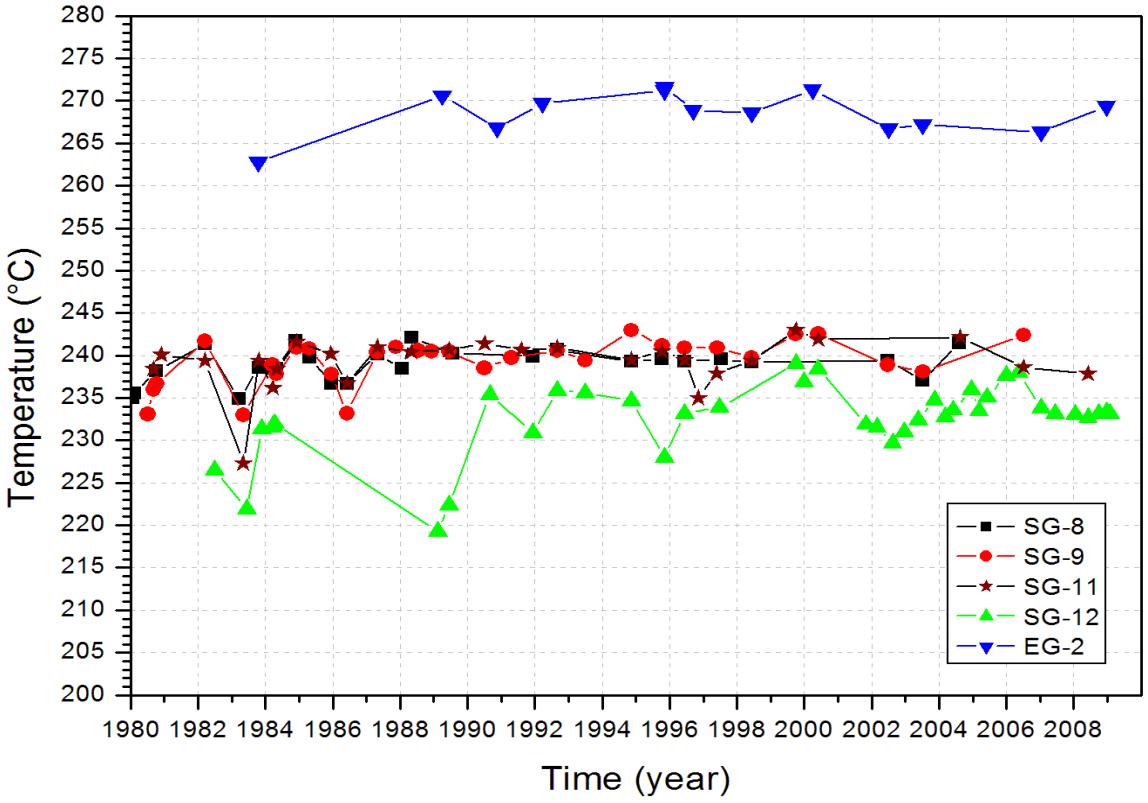

Figure 14:. Temperature history in the Svartsengi field for a period of close to 30 years.

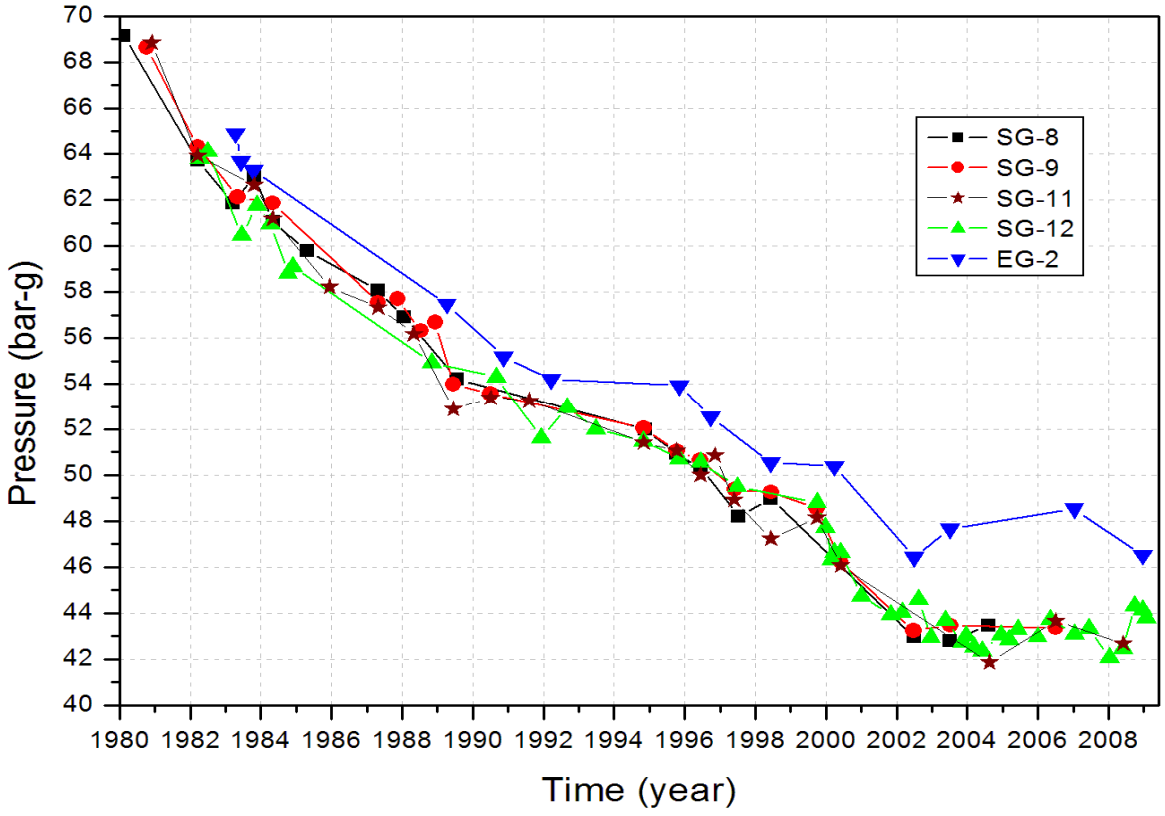

Figure 15:. Pressure history in the Svartsengi field for a period of close to 30 years.

5.2 Flow and enthalpy measurements

The purpose of step tests is to get an estimate of the flow and enthalpy but the steam flow is also interesting with respect to electricity production. In the case of two phase flow from well RN-13B (see paper III on "Case Study Examples") there are several methods to calculate these numbers, since the amount of available data is bountiful; the one chosen is discussed in the following. The Russel-James equation (2) can be used to establish the relationship between total flow and enthalpy.

The calculated production index (PI), by means of the formula below.

(1) $$PI = \left|\frac{\Delta Q_t}{\Delta P}\right|$$

The schematic standard setup of the Reykjanes separator is shown in Figure 16. The figure illustrates where the relevant parameters were measured while the production test in ongoing.

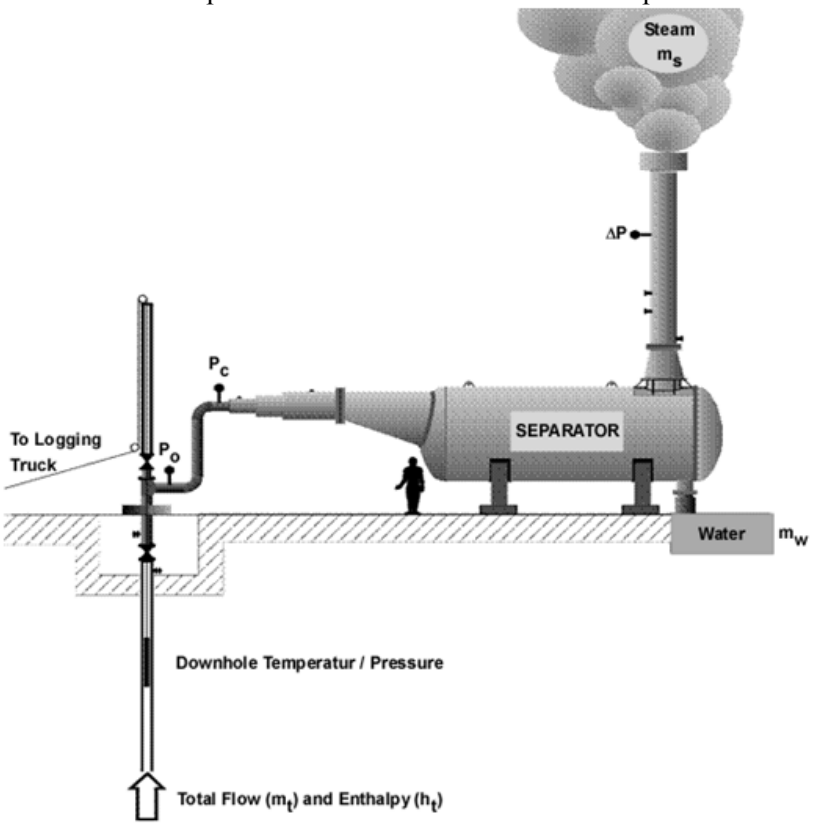

Figure 16:. Schematic setup of the Reykjanes separator illustration where the relevant parameters are measured.

(2) $$Q_t = K \cdot A \cdot \frac{P_c^{\,m}}{H^n}$$

Where Q_t is the total fluid flow measured in kg/s, $K = 1835000$ is constant, $A = \frac{\pi}{4} \cdot d^2$ is the area and $d = 0{,}160\ m$ is pipe diameter, P_c is the critical pressure in bar-a, H is the enthalpy in kJ/kg, $m = 0{,}96$ and $n = 1{,}102$ are constant. The mass ratio for the steam in the fluid is also used and it is defined by $= \frac{Q_s}{Q_t}$, where X is the steam ratio and Q_s is the steam flow in kg/s and Q_t is the total fluid flow in kg/s. Thus we obtain the total enthalpy by:

(3) $$H = X \cdot H_s + (1 - X) \cdot H_w$$

Where H_s is the steam enthalpy at a given pressure and temperature and H_w is the water enthalpy at the same pressure and temperature, both measured in kJ/kg. This formula can also be rewritten in the following manner, which can be useful in the calculations:

(4) $$Q_t = Q_w \cdot \frac{H_s - H_w}{H_s - H} = Q_s \cdot \frac{H_s - H_w}{H - H_w}$$

Where Q_w is the water flow in kg/s. At a certain air pressure Q_w is the water flow in the tub and can be calculated from the measured water height (V-notch) measured in cm according to the formula:

(5) $$Q_w = 0{,}0146 \cdot W^{2{,}47}$$

Enthalpy H is obtained by solving formula (2) and (4) for a given critical pressure P_c. Steam flow is then found by calculating the total flow from either formula (2) or (4) with the obtained enthalpy, using the total flow as the sum of water and steam flow:

(6) $$Q_t - Q_w + Q_s$$

Steam and water flow at the separator pressure $P_{sk} = 19$ bar, is the pressure required by the turbines at the Reykjanes power plant, and thus calculated from formula (4) where the total flow and total enthalpy is the same as before but the enthalpies of steam and water are now determined at a pressure of 19 bar. The results from these calculations are shown in table 2 in paper III “Case Study Examples”. For the calculations the digital readings for critical pressure were used.
The differential pressure was also measured, thereby getting an independent estimate on the quality of the calculations by comparing the total flow, as calculated from the above, together with the total flow calculated from formula (6), where the water flow is calculated from formula (5) like before but the steam flow is calculated from the differential pressure at the chimney, as it was measured by the digital manometer, with the formula:

(7) $$Q_s = 2{,}733 \cdot \sqrt{\Delta P}$$

Where ΔP is the differential pressure (annubar pressure) at the chimney measured in mbar.

When the opening of the main valve is increased the flow from the well increases giving rise to increase water inflow from the deep aquifers, increasing the amount of water in the borehole fluid, thus lowering the enthalpy and the well head pressure.
This would explain the interaction between well head pressure and enthalpy. The experience from the separator is that only a small amount a of water escapes through the chimney at a Pc below 4 bars, as is has been in this test and this corresponds with the measured results shown here, thus is it unlikely that the separator has any effect on the measurement of the enthalpy.

In the case of two phase vapor flow from well SV-23 (see paper III on “Case Study Examples”) no liquid escaped the well only gas and steam. The Russel-James equation can be used to establish the relationship between total flow and enthalpy.

Steam flow (Q_s) can also be calculated from the differential pressure in the separator chimney by using the formula (7).

Since the was no water flow from the well the flow calculated from (2) and (7) should be the same but in case of different result one would expect formula (2) to give a slightly higher result, since (2) calculates the total flow whereas (7) calculates the steam flow and if some of the steam condenses in the separator less flow will come from the chimney.
Steam and water flow at the separator pressure $P_{sk} = 5{,}5$ bar-g, is the pressure required by the turbines at the Svartsengi power plant, and thus calculated from formula (4) where the total flow and total enthalpy is the same as before but the enthalpies of steam and water are now compared to a pressure of 5,5 bar-g.

(8) $$H = X \cdot H_s + (1 - X) \cdot H_w$$

Formula (8) can also be written as:

(9) $$X = \frac{H - H_w}{H_s - H_w}$$

where $X = \frac{Q_s}{Q_t}$ is the mass ratio of steam flow, H_s is the steam enthalpy at a certain pressure and temperature and H_w is the water at the same pressure and temperature, both measured in kJ/kg.

5.3 Discharge measurements

Geothermal wells discharges either; hot liquid water, saturated/superheated steam or steam-liquid water mixtures. Traces of gas are common in the discharge.

To distinguish between the different types of wells a division into three categories is made (see also paper III on “Case Study Examples”); single phase wells (either as hot water or steam) or two phase (steam-liquid) wells. When the inflow is liquid water boiling starts in the well and when the inflow is mixed water and steam there will be boiling in both the well and the reservoir. For calculation and interpretation purposes we assume that the flow in geothermal wells is iso-enthalpic (adiabatic).

In order to determine both total flow rate and the ratio between steam and water phases, two independent observables have to be determined from the following parameters:

(for steam flow)

Water flow rate - Q_w (kg/s), Steam flow rate - Q_s (kg/s), Lip pressure - P_c (bar-a), Well head pressure - P_0 (bar-a), Water level depth; pumped wells - (m), Discharge enthalpy - H (kJ/kg), Mass ratio of steam – X, Non condensable gas content - (%), Total Dissolved Solids - TDS (ppm or mg/l), Mean inflow temperature - T_{in} (°C), which is only valid if inflow is liquid phase, Condensation (uncommon) - Water flow rate measurement, Differential pressure - $Q \propto \sqrt{\rho \Delta P}$, Chemical methods - Gas dilation, Back pressure of cones - $Q \propto \sqrt{P/V}$, Critical lip pressure - Russel-James formula

(for water flow)

Timing (common) - $Q = \rho V/t$, V-notch (common) - $Q \propto \Delta h^m$, Differential pressure - $Q \propto \sqrt{\rho \Delta P}$, Flowmeters, spinners - $Q \propto n$, Flowmeters, sonic - Travel time, Doppler shift and Chemical methods – Dilution.

It is important to be aware of the most common pitfalls in discharge measurements instrumentation and procedure. Flow metering devices should be calibrated and used according to specifications. Albeit taking the necessary precautions prior to the measurements it should be noted that pressure gauges can be poorly calibrated, one should bear in mind that orifices can be worn out. Water height measurements will not be accurate if the V-notch is not leveled. Chemical depositions or dirt could be present in either orifices, the V-notch or in the lip pipe. Fluctuations in the flow will trouble the measurements and one should bear in mind that the non condensable gasses are not accounted for

5.4 Horner plot and Albright method

Computational software for determining formation temperature has been developed at ÍSOR, for both techniques [Arason et al., 2004]. The theory behind the Horner plot and the Albright method will be discussed briefly in the following.

The Horner plot

The Horner plot is a simple analytical technique for analyzing maximum bottomhole temperatures to determine the formation temperature.

The basic criterion for the technique is the straight-line relationship between the maximum bottomhole temperature and

$$\ln(\tau)$$

$$\tau = \left(\frac{\Delta_t}{\Delta_t + t_0}\right)$$

where;

Δt = the time passed since circulation stopped,
T_0 = the circulation time.

We see that

$$\lim_{\Delta t \to \infty} \ln(\tau) = 0$$

Using this and the fact that the system must have stabilized after infinite time, the maximum bottomhole temperature can be plotted as a function of $\ln(\tau)$. A straight line is then drawn through the data and by extrapolating it to $\ln(\tau) = 0$ the formation temperature can be determined.

The Albright method

The Albright method of calculation was developed for direct determination of bottomhole formation temperatures during economically acceptable interruptions in drilling operations: 12 to 24 hours, depending on depth and rock type. This technique was developed by Mr. Kames N. Albright during the drilling of Geothermal Test Hole No. 2 (GT-2) in the Los Alamos Scientific Laboratory's (LASL) Dry Hot Rock Geothermal Energy Project.

This method assumes for an arbitrary time interval, much shorter than the total recovery time that the rate of temperature relaxation depends only on the difference between the borehole temperature and the formation temperature. If entire logging time is represented as $I = [t_1,t_N]$, where N is the number of data points in our log, then for any time interval $i \in I$, $i = [t_a,t_b]$, we find, $\forall \in \iota$,, the θ_{∞}^{i}, c^i and θ_{0}^{i} which give the best solution to the equation;

$$e^{c^i t_c} = \frac{\theta_{\infty}^{i} - \theta(t)}{\theta_{\infty}^{i} - \theta_{0}^{i}}$$

where;

$\theta(t)$ = the temperature at time t, $t \in i$,
θ_{∞}^{i} = the estimated formation temperature for the time interval i,
θ_{0}^{i} = the estimated temperature at the circulation stop,
c^i = a constant.

By assuming a linear dependence of c^i on θ_{∞}^{i} one can determine the formation temperature and doing this by plotting c^i as a function of θ_{∞}^{i}. Then a straight line can be drawn through the data and the x-axis interception (the θ_{∞} value when c equals zero) can be found. This is the value $\theta(t)$ approaches when t goes to ∞[2].

6 REFERENCES

Arason, Thordur, Björnsson, Grímur, Axelsson, Guðni, Bjarnason, Jón Ö. and Helgason, Páll, 2004: ICEBOX – Geothermal reservoir Engineering Software for Windows. A User's Manual. Prepared for the UNU-GTP, Reykjavík, Iceland, p 81

Danielsen, Peter E., 2010: Objectives, Technology and Safety Measures, Electronic HT Tools and Safety, Health and Environment. Drilling, Completion and Testing of Geothermal Wells. Short Course paper I at WGC 2010, Bali, Indonesia, p. 11

Danielsen, Peter E., Jónsson, Páll and Egilson, Þorsteinn, 2010: Case Study Examples, Wells GB-10, RN-13B and SV-23. Drilling, Completion and Testing of Geothermal Wells. Short Course paper III at WGC 2010, Bali, Indonesia, p. 15

Horne, Roland N., 1995: Modern Well Test Analysis. A Computer-Aided Approach.2nd Edition. Palo Alto Petroway Inc., p 257

Júlíusson, Egill, Grétarsson, Gísli J. and Jónsson, Páll, 2008: Well Tester 1.0b. User's Guide. Reykjavik, Iceland, ÍSOR-2008/063, p 27

Þórarinsson, Sigurjón B., Jónsson, Sigurður S., Níelsson, Steinþór, Haraldsdóttir, Svanbjörg H. and Júlíusson, Egill, 2007: Hellisheiði - Hola HE-29, 3. áfangi: borun vinnsluhluta. ÍSOR-2007/042 (in Icelandic), p. 28

Drilling, Completion and Testing of Geothermal Wells

Geothermal Well Testing.

Case Study Examples
Wells GB-10, RN-13B and SV-23

Peter E. Danielsen and Pall Jónsson
ÍSOR, Reykjavík, Iceland

SUMMARY

In this paper three case studies are described to illustrate production tests from real data sets. The first example illustrates a single phase liquid flow drawdown test on Well GB-10 in the Grábrókar lava field in Borgarfjörður just north-east of Reykjavík, Iceland. The second example is from a two phase flow production test in well RN-13B on the Reykjanes Peninsula, west of Reykjavík, Iceland. For the third example a single phase vapor flow production test in well SV-23 in Svartsengi, west of Reykjavík, Iceland, is shown.

INTRODUCTION

The RSFS company rig Trölli (Troll) completed well GB-10 with Odex equipment and cased with 14" pipes down to 36 m depth (TVD) and the casing was subsequently punctured between 22-30 m. A submersible pump was installed at 30 m depth. A speed control on the submersible pump made it easy to adjust the rate of pumping. The flow out of the well was measured with a mechanical flow meter and changes in water table due to pumping were measured with a standard water table logger. Pressure changes were also monitored in a few other wells in the vicinity.

Completion of well RN-13B was finalized with the standard injection test which was performed on February 22, 2007. Production testing of the well was performed after the warm-up period on October 11, 2007. A standard Reykjanes separator was used to evaluate the well while free flowing. Results and calculations discussed in the following indicate a very promising production well.

SV-23 was completed on May 15, 2008 after the slotted liner had been installed and the final well track had been measured by a gyroscopic survey. Production testing of the well was performed after the warm-up period, on November 13, 2008. As for RN-13B a standard Reykjanes separator was used. Again results and calculations discussed in the following indicate a very promising production well.

1 SINGLE PHASE LIQUID FLOW

1.1 Well GB-10

Drilling of well GB-10 (well ID nr. 29110) was completed on October 28, 2004 and the pumping test described in the following was conducted almost immediately thereafter. GB-10 is situated an hour and a half's drive to the north-east of Reykjavík [Figure 1], in the Grábrókar lava field [Figure 2].

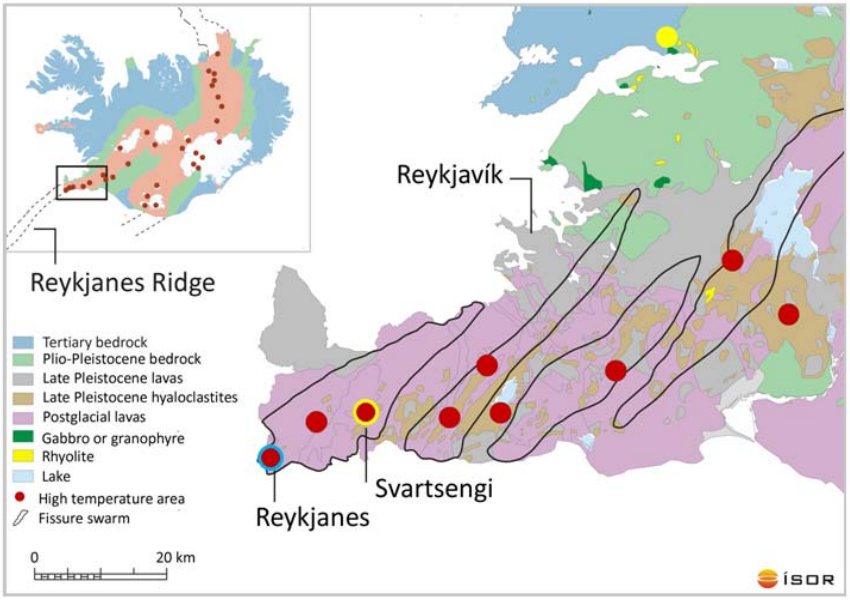

Figure 1:. Map showing well locations for GB-10 (yellow dot), RN-13B (red dot encircled by blue) and SV-23 (red dot encircled by yellow) in Iceland.

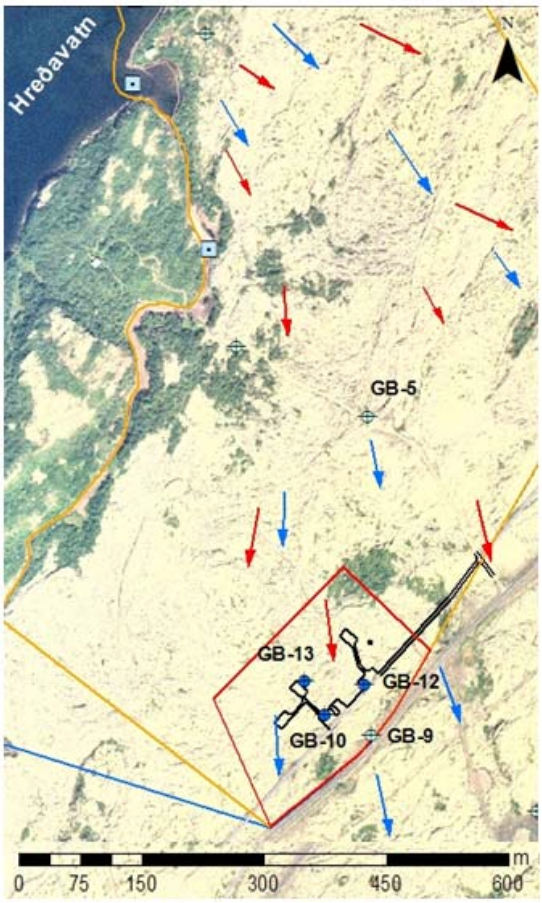

Figure 2:. Well GB-10 location in the Grábrókar lava field.

1.2 Drawdown Test

Pumping in GB-10 was increased in four steps [Figure 3]. As can be seen from Figure 3 drawdown mirrors the steps wise increase in pumping. Some drawdown was recorded in the adjacent wells in the area, indicating which wells were connected and to what extent.

The steps were fairly long but still it is clear that absolute equilibrium was not reached. Much more time would be needed in order to reach equilibrium but that is not feasible in real life. Furthermore one should correct for the general drop in water table in the entire field and a rough estimate would be that measured drawdown in GB-10 should be corrected with another half a meter or so.

The production field data was plotted versus drawdown [Figure 4] and a best fit was made using the formula $H= -7.3 – 0.305\ Q – 0.0381\ Q^2$. The water table prior to the test was -7.3 m, 0.305 describes laminar flow (Darcy's Law) and 0.0381 describes turbulent flow or well loss due to pumping. All three numbers are constants. From Figure 3 one can read that by pumping roughly 40 l/s the drawdown should be approximately 15 m. To avoid pollution from the inflow zone and well dry-up, the water table should never be forced lower than the punctured part of the casing i.e. 22-30 m.

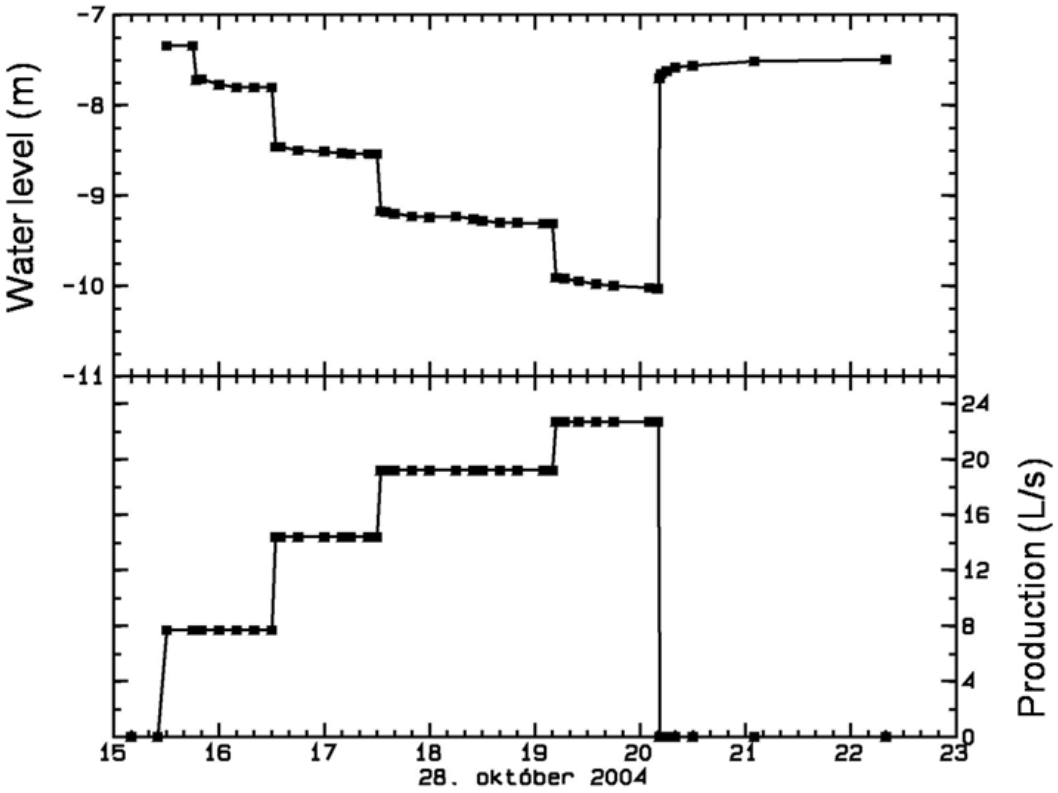

Figure 3:. Pump rates and water table drawdown shown throughout drawdown test, in well GB-10.

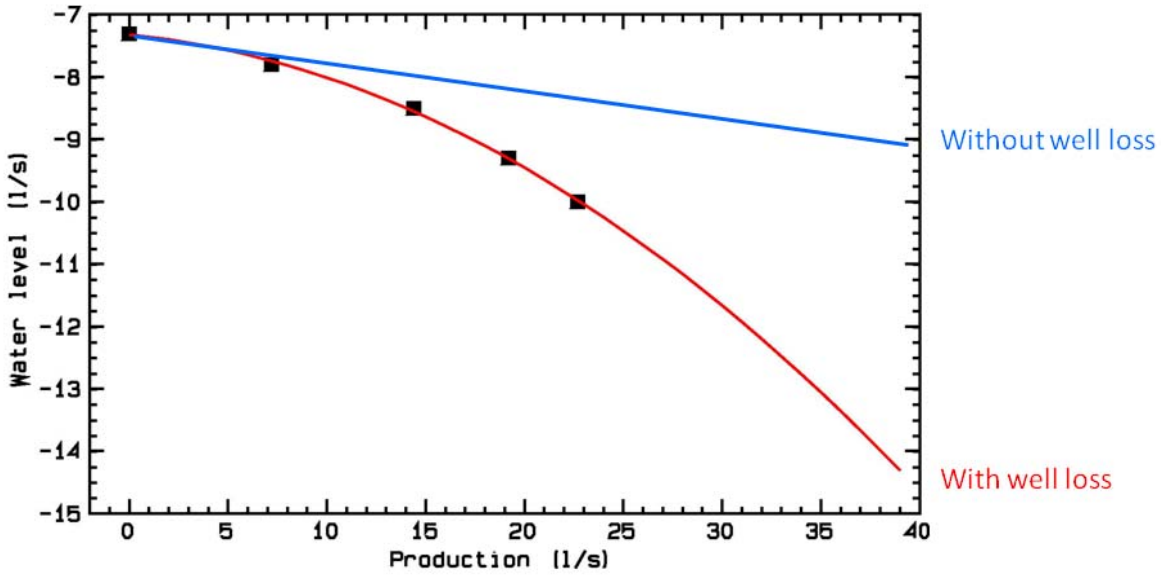

Figure 4:. Drawdown in well GB-10 while pumping out of the well.

2 TWO PHASE FLOW

2.1 Well RN-13B

Drilling of well RN-13B (well ID nr. 18963) was completed on February 22, 2007 as a 2530 m (MD) deep well, deviated at a 30° inclination in a straight southerly direction or 180° [Figure 1 and 5]. A 9-5/8" slotted liner was inserted down to 2495 m (MD) depth. The routine injection test that was performed on February 22, 2007, gave an injectivity index (II) of 8 (L/s)/bar.

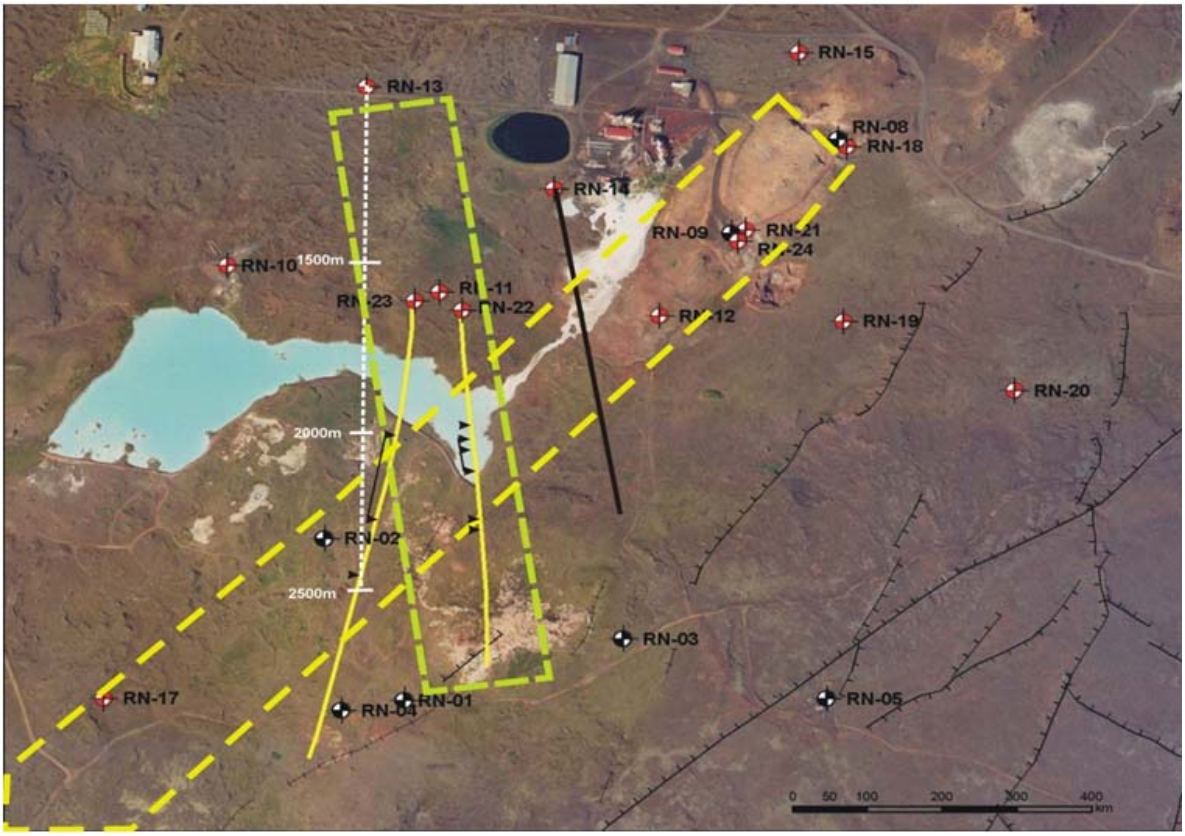

Figure 5:. Well RN-13B location on the Reykjanes Peninsula, the white dotted line indicates deviated well path.

Figure 6 shows temperature and pressure profiles measured both while drilling, during the warm-up period and also in connection with the production test.
From the temperature profiles [Figure 6, left] it is clear that several aquifers can be seen between 800 and 900 m depth. One major aquifer is visible at approximately 1150 m depth where hot fluid enters the well and flows out again at approximately 2100 m depth. The aquifer at 1700 m depth is only prominent in the measurement from October 11, 2007. In this measurement the bottomhole temperature was 302°C and lowers steadily to 280°C at 2100 m depth. Hot fluid enters at this depth and the temperature rise to 284°C and remains virtually unchanged up to 1700 m depth, where hot fluid is injected through another aquifer thus increasing the temperature to 296°C. The temperature changes very little until 1480 m depth from where it lowers steadily up to 1350 m depth which is the depth of the boiling point in the well. The temperature then lowers from 1350 m depth to 255°C at the well head.

The first pressure measurement [Figure 6, right] carried out in connection with the step injection test at the end of drilling showed a water table at approximately 470 m depth whilst injecting 40 L/s of

cold water. When the first warm-up measurement was taken, on April 2007, the well had built up 58 bar pressure on the well head and was boiling down to around 1130 m depth.
From the pressure profile made just before the production test in October 2007, it can be seen that the pressure was 3 bars lower below the boiling point depth (1150 m) which indicates a 30 m draw down in the Reykjanes field after production began in May 2006.

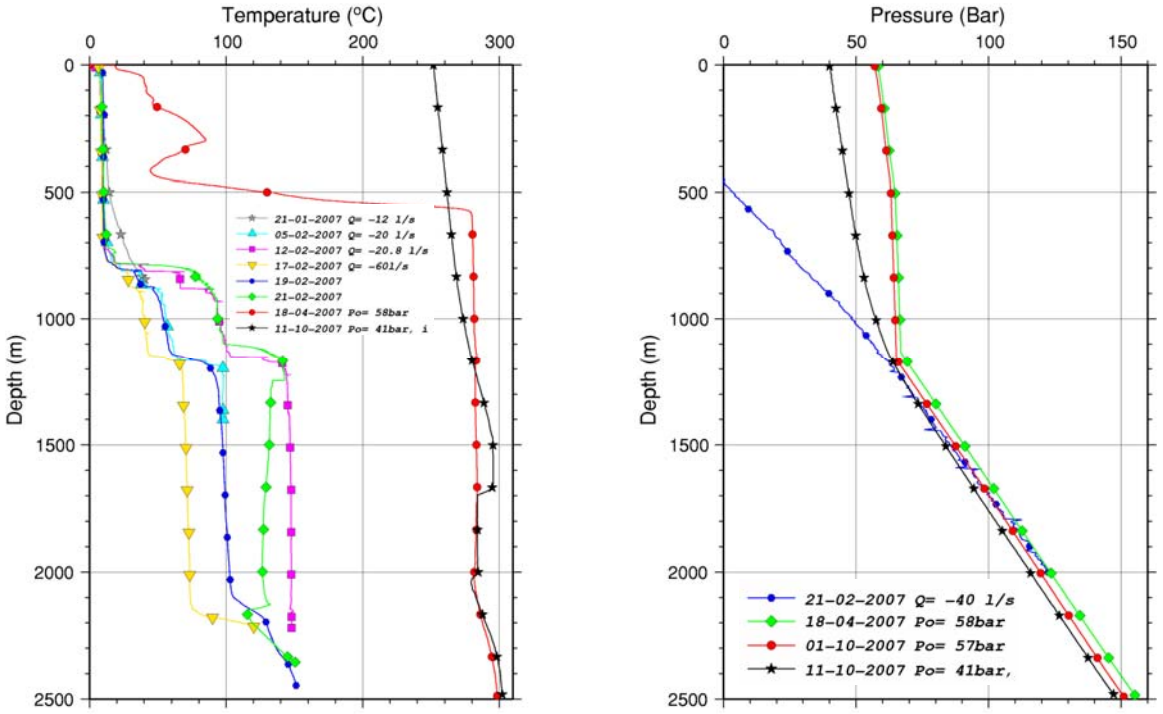

Figure 6:. Temperature and pressure measurements recorded while drilling, during warm-up and in connection with the production test in well RN-13B.

2.2 Production Test

The amount of opening of the well was variable from the time when the well was put into production and onwards to the production test as can be seen from the pressure measurements on Figure 6 and also during the productions test itself [Figure 7] on October 11, 2007.

The production test was done by monitoring P_o (bar-g), P_c (bar-g), ΔP (bar-g) and W (cm) while opening the main valve in four steps and finally returning to the original position [Figure 7 and Table 1]. The change in pressure at the bottom of the hole was also recorded by a K10G downhole tool [Figure 7 and Table 1]. The calculated results are shows in Figure 8 and Table 2 and 3. The calculated production index (PI), calculated by means of formula (1) found in paper II "Well Testing interpretation ".

The schematic standard setup of the Reykjanes separator is shown in Figure 16 in paper II on "Well Testing interpretation".

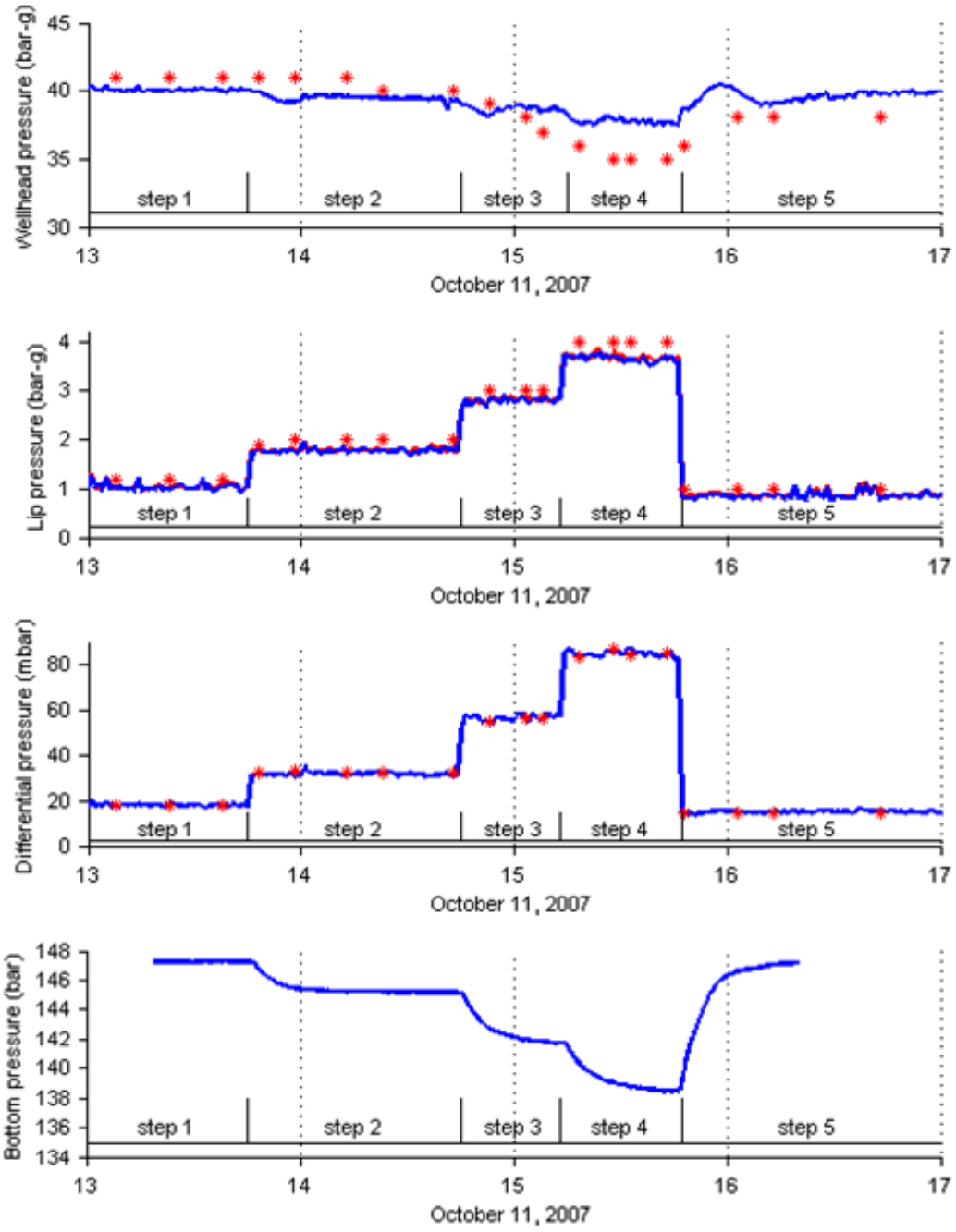

Figure 7:. Results of discharge measurements, blue line indicates digital measurements while a red star indicates analogue measurements done by hand.

Table 1: Continuous and handwritten measurements from production test in RN-13B.

Step	Opening %	P_o bar-g		ΔP mbar		P_c bar-g		P_b bar-g	W cm
		cont.	manual	cont.	manual	cont.	manual		
1	20	40.0	41.0	18.1	18.2	1.04	1.2	147.3	14.3
2	23	39.4	40.6	31.7	32.5	1.78	1.9	145.2	16.3
3	27	38.6	38.0	56.6	56.4	2.80	3.0	141.8	18.6
4	30	37.7	35.3	84.8	85.0	3.66	4.0	138.4	20.5
5	20	40.2	38.0	14.8	14.6	0.85	0.9	147.2	13.6

Table 2: Calculated results from production test in RN-13B.

Step	P_o bar-g	P_c bar-g	W cm	Separator pressure 1 bar					Separator pressure 19 bar			
				Q_w kg/s	Q_s kg/s	Q_t kg/s	X %	H kJ/kg	Q_w kg/s	Q_s kg/s	Q_t kg/s	X %
1	40.0	1.04	14.3	10.5	11.3	21.8	51.9	1590.6	13.8	8.0	21.8	36.5
2	39.4	1.78	16.3	14.5	15.2	29.7	51.1	1573.0	19.1	10.6	29.7	35.6
3	38.6	2.80	18.6	20.1	20.4	40.5	50.4	1555.8	26.4	14.1	40.5	34.7
4	37.7	3.66	20.5	25.6	24.7	50.2	49.1	1527.5	33.6	16.7	50.2	33.2
5	40.2	0.85	13.6	9.3	10.3	19.6	52.7	1609.7	12.3	7.4	19.6	37.6

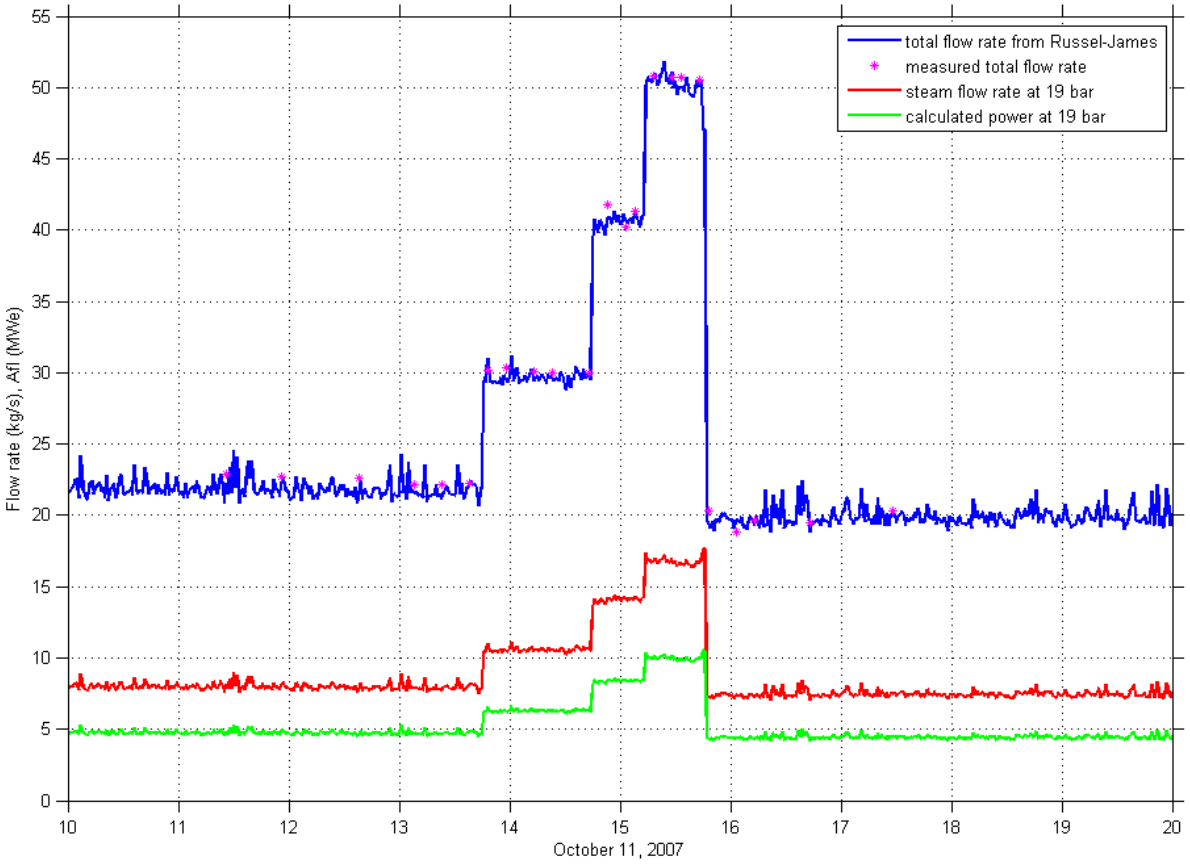

Figure 8:. Calculated total flow from Russel-james (blue line), measured total flow rate as read from manometers (red stars), calculated steam flow at 19 bar (red line) and calculated power (MWe) at 19 bar separator pressure (green line), in the step production test in well RN-13B on the Reykjanes Peninsula, October 11, 2007.

Table 3: Calculated results from production test in RN-13B.

Step change	Flow rate change ΔQ kg/s	Pressure change ΔP bar	Productivity index PI (kg/s)/bar
1 to 2	7.9	-2.1	3.7
2 to 3	10.8	-3.4	3.2
3 to 4	9.7	-3.4	2.9
4 to 5	-30.6	8.8	3.5

According to the calculations the average production index is 3.3 (kg/s)/bar [Table 3], which is not considered high for a well in the Reykjanes field [Figure 9].
The enthalpy of RN-13B is fairly high or around 1570 kJ/kg as an average and is among some of the highest measured in the Reykjanes field. The boiling point is at roughly 1350 m depth and the measured temperature just below is 290°C. Assuming that the borehole fluid consists only of water the enthalpy should (as read from steam tables) be close to 1290 kJ/kg. At this temperature the measured enthalpy is much higher and increases with increasing well head pressure indicating (as shown in the above) that boiling begins above the aquifer at 1150 m depth, increasing the steam flow into the well. By doing so the enthalpy of the wellbore fluid increases and exceeds the enthalpy of water and this increase in the amount of steam could explain the increase in enthalpy from 1290 kJ/kg t o1570 kJ/kg.
When the opening of the main valve is increased the flow from the well increases giving rise to increased water inflow from the deep aquifers, increasing the amount of water in the borehole fluid, thus lowering the enthalpy and the well head pressure.
This would explain the interaction between well head pressure and enthalpy. The experience from the separator is that only a small amount a of water escapes through the chimney at a Pc below 4 bars, as it has been seen in this test corresponding with the measured results shown here, thus it is unlikely that the separator has any effect on the measurement of the enthalpy.

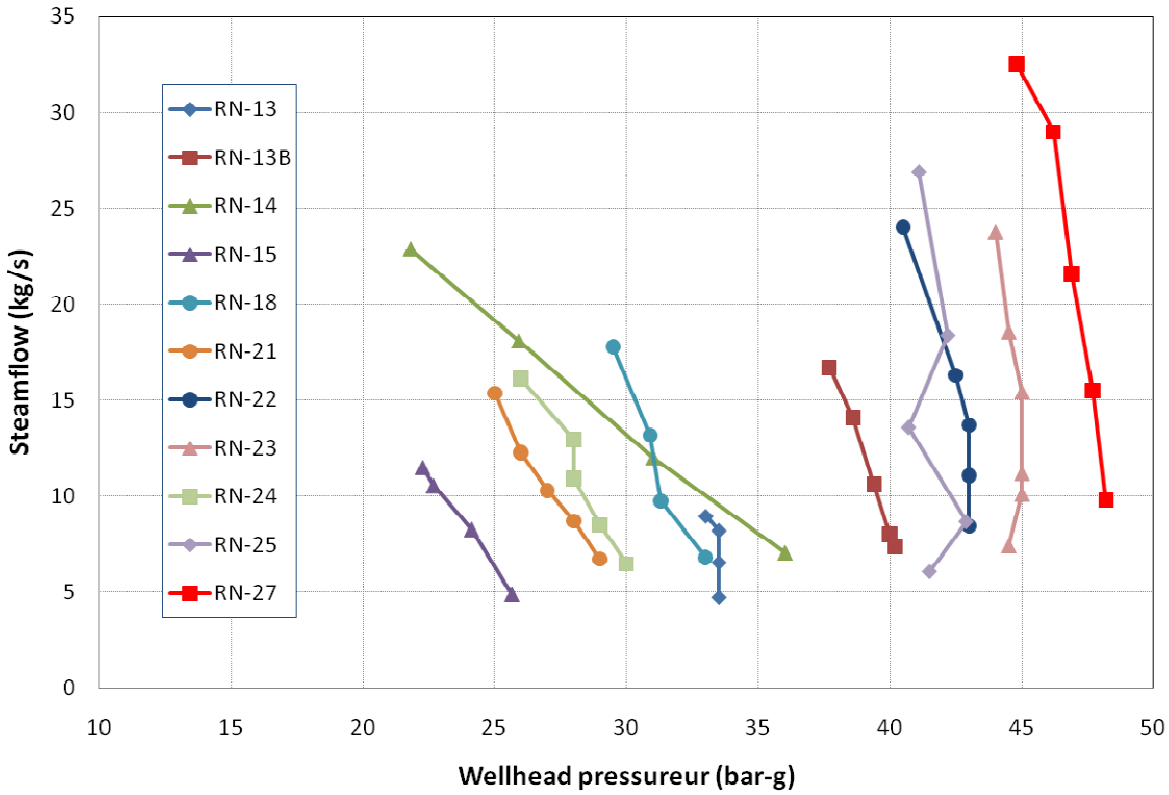

Figure 9:. Production curves for RN-13B compared to several other wells in the Reykjanes field.

3 SINGLE PHASE VAPOR FLOW

3.1 Well SV-23

Drilling of well SV-23 (well ID nr. 16923) was completed on May 15, 2008 as a 700 m (MD) deep well, deviated at a 45° inclination in a easterly direction or 85° [Figure 1 and 10]. A 9-5/8" slotted liner was inserted down to 657 m (MD) depth.

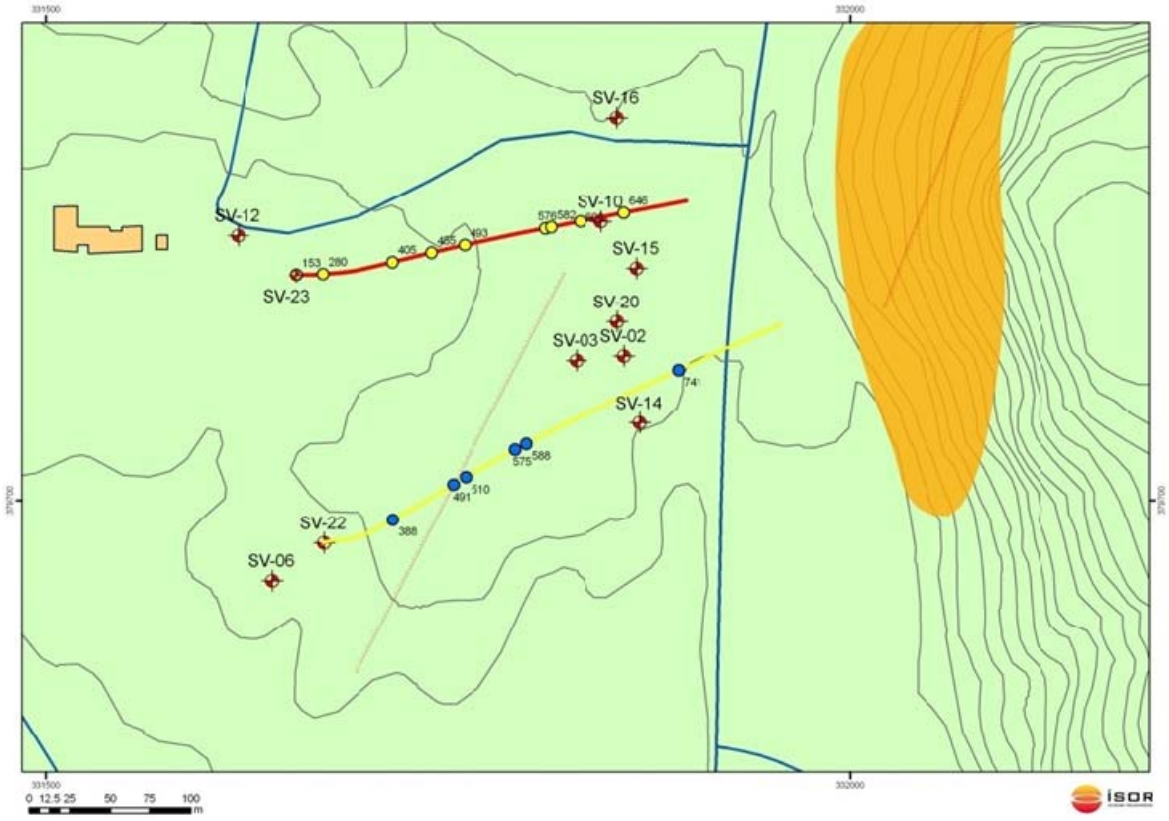

Figure 10:. Well SV-23 location in the Svartsengi field, red line indicates deviated well path.

Figure 11 shows temperature and pressure profiles measured during the warm-up period and also in connection with the production test.
From the temperature profile done in October it can be seen that the temperature was 73°C at 250 m depth and had increased to 219°C at 320 m depth. Below this depth very little change is seen. The two profiles were made in connection with the production test show very little change in temperature from the well head to the bottom of the hole around 220°C.

When the well was opened the well head pressure changed very little [Figure 11, right] or within 0.1 bar. The first pressure measurement (green line) was done on October 29, 2008, and the well head pressure then was 21.9 bars. The pressure increases fairly linearly down to 300 m depth and from there the slope changes and the pressure increases slower but still linearly. This is what would be expected from looking at the temperature profiles [Figure 11, left]. The well is clearly divided in gas above 300 m depth and steam below, probably somewhat mixed with gas from lower aquifers.

No water table is evident in the well because the boiling pressure in steam mixed with gas is higher than for clean steam. Thus one would expect that the pressure will not reach that of steam and gas mixture despite the pressure being higher than the boiling pressure for clean water at the measured temperature in the well.

When the pressure profile was measured [Figure 11] just before the production test the pressure change was largely linear down the entire well bore except for a minor change in slope just below 400 m depth. The slotted liner is hanging from 423 m depth and from this depth the well ID is smaller and this is probably the reason for the change in slope since the steam/gas mixture is compressed to a greater extent in the liner than above. This becomes more evident in the profile measured after the production test has ended, most likely because of the increase in flow.

Immediately after the well was opened it was clear that it was completely dry and thus no water flowed over the V-notch.

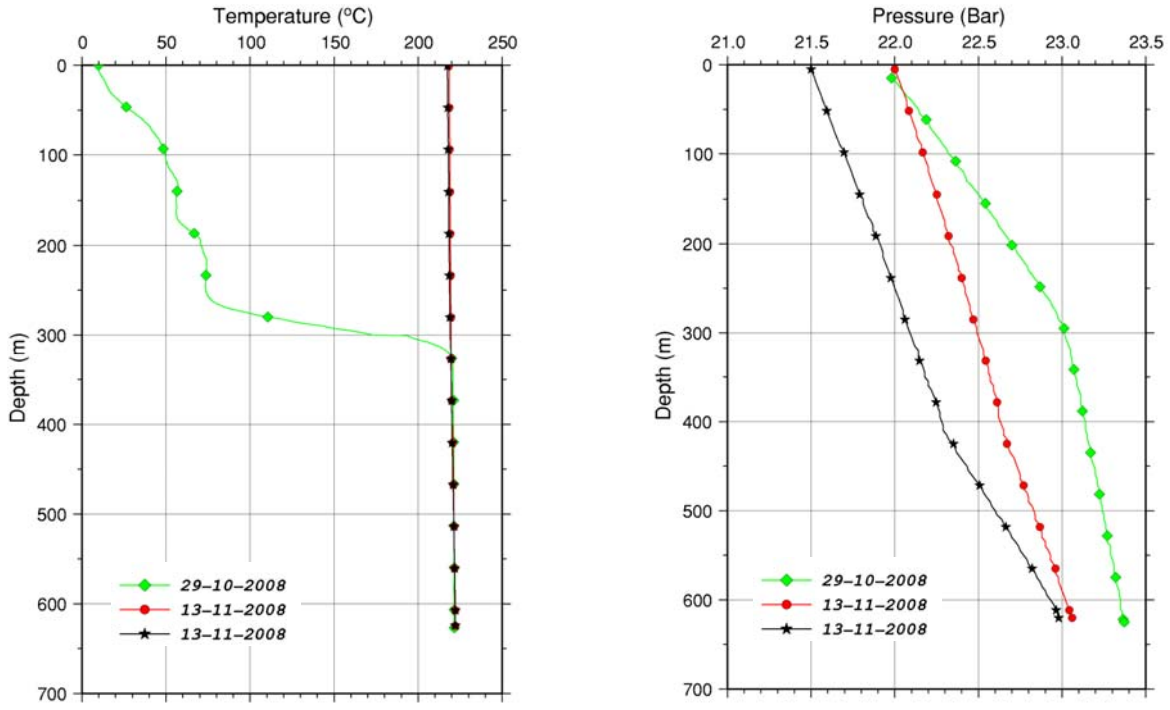

Figure 11:. Temperature and pressure measurements recorded while drilling, during warm-up and in connection with the production test in SV-23.

3.2 Production Test

The amount of opening of the well was varied for a couple of days from when the well was put into production and onwards to the production test and then again during the productions tests itself [Figure 12] on November 13, 2008.

On the day of the production test the downhole K10G tool was used to record downhole temperature and pressure. The K10G was lowered into the well at 12 o'clock measuring a profile down to the well bottom, then it was lifted 1 meter above bottom (624 m) and left suspended there for the entire production test. When the five step production test [Figure 12] ended at 16:04 o'clock a profile was measured up the well and the K10G tool was extracted at 16:40 o'clock.

Downhole temperature and pressure, P_o (bar-g), P_c (bar-g) and Δ P (bar-g) were measured while opening the main valve in five steps [Figure 12 and Table 4] and also for the duration of the test. The calculated results are shows in Figure 13 and Table 6 and 7. The calculated production index (PI), calculated by means of formula (1) given in paper II "Well Testing interpretation ".

The schematic standard setup of the Reykjanes separator is shown in Figure 16 in paper II on "Well Testing interpretation".

During the production test no water was flowing from the well and thus no measurements were recorded from the V-notch. Steam cleared the pipe to conduct water during the first two steps, for what was believed to be condensed water and from the third step and onwards only steam was emitted from the pipe.
The digital ΔP manometer on the separator chimney was out of range at 121.4 mbar but from the handwritten data a maximum ΔP of 130.5 mbar was observed.

The mechanical manometer shows 0.9 bar higher pressure for Po but since the readings from the digital Po correlates with chemical measurements the mechanical reading is assumed to be too high and was thus corrected by -0.9 bar and subsequently fit the digital data [Table 4].

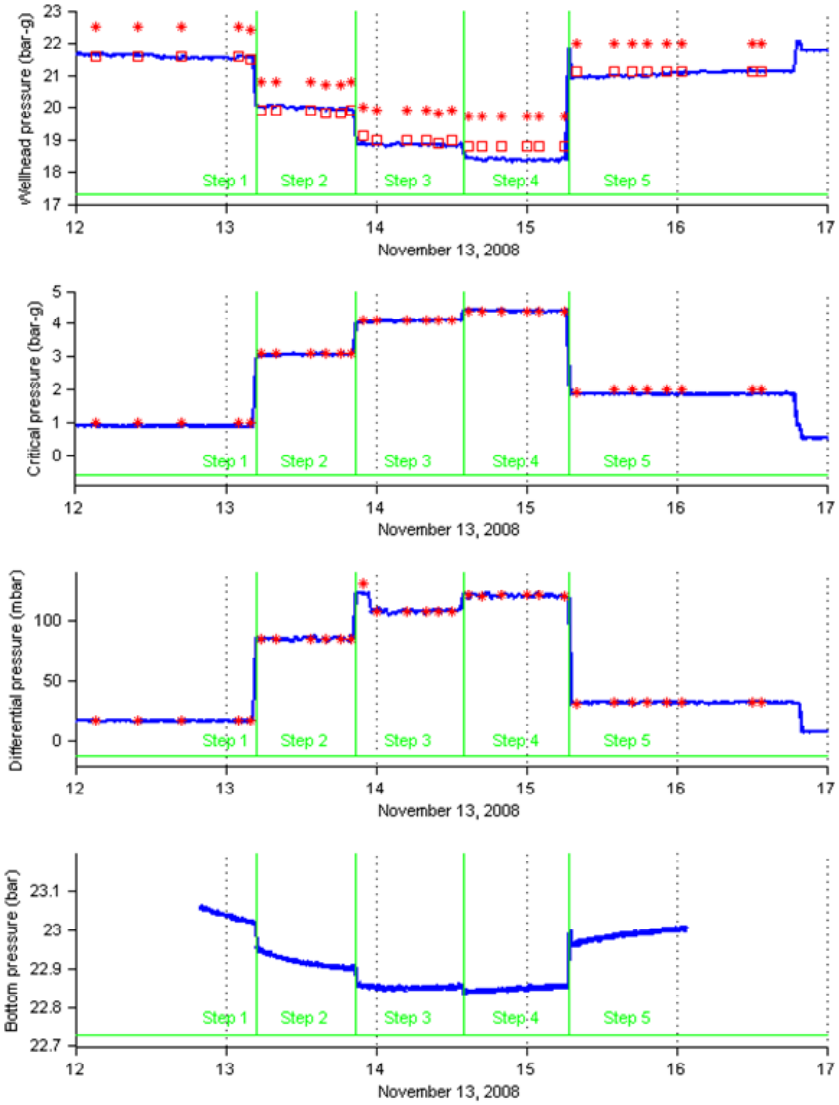

Figure 12:. Results of discharge measurements, blue line indicates digital measurements while a red star indicates analogue measurements done by hand. Red boxes indicate P_o hand measurements corrected by -0.9 bars.

Table 4: Continuous and handwritten measurements along with bottomhole pressure and temperature from the K10G tool at 624 m depth, from production test in SV-23.

Step	T_0 °C	P_o bar-g		ΔP mbar		P_c bar-g		P_b bar-g	T_b °C
		cont.	manual	cont.	manual	cont.	manual		
1	219,0	21,6	22,5	17,5	18,0	0,89	1,0	23,02	222,12
2	216,0	20,0	20,8	84,7	85,0	3,06	3,1	22,90	222,02
3	212,7	18,8	19,9	107,2	107,4	4,09	4,1	22,85	221,94
4	211,0	18,4	19,7	119,9	120,3	4,39	4,4	22,86	221,94
5	217,9	21,0	22,0	32,2	32,5	1,86	2,0	23,00	222,15

The purpose of step tests is to get an estimate of the flow and enthalpy but the steam flow alone is also interesting with respect to electricity production. In the case of well SV-23 no liquid escaped the well only gas and steam. The Russel-James equation can be used to establish the relationship between total flow and enthalpy. Steam flow (Q_s) can also be calculated from the differential pressure in the separator chimney by using the formula (7) in paper II "Well Testing interpretation ".

In the case of SV-23 no water came from the well during the test and thus only steam was measured. To determine whether the steam has been overheated or saturated at the well head it is interesting to compare the well head temperature, the well head pressure and the saturation pressure at a given temperature in all five steps. The results are shown in Table 5 where the well head pressures are taken from the digital readings. Furthermore enthalpy at the chosen temperature is shown.

Table 5: Measured well head temperature (T_0), measured well head pressure (P_0), saturation pressure (P_s) at temperature T_0 and steam enthalpy at the same temperature.

Step	T_0 °C	P_0 bar-g	P_s bar-g	H kJ/kg
1	219,0	22,58	22,75	2800,8
2	216,0	20,99	21,47	2799,8
3	212,7	19,84	20,13	2798,5
4	211,0	19,38	19,46	2797,8
5	217,9	22,01	22,28	2800,4

Table 6: Calculated results from production test in SV-23.

Step	P_c bar-g		ΔP bar-g		Q_s kg/s	Q_s kg/s	Q_s kg/s	Q_s kg/s
	digital	analogue	digital	analogue	P_c dig.	P_c ana.	ΔP dig.	ΔP ana.
1	0,89	1.0	17,5	18.0	10,9	11,5	11,4	11,6
2	3,06	3.1	84,7	83.0	22,6	22,8	25,2	25,2
3	4,09	4.1	107,2	107.4	28,0	28,1	28,3	28,3
4	4,39	4.4	119,9	120.3	29,6	29,7	29,9	30,0
5	1,86	2.0	32,2	32.5	16,2	16,9	15,5	15,6

It can be seen from these calculations that there is a reasonable comparison with an uncertainty within 4% except for the second step where it is 6%. The variability is within the uncertainty one would expect when using the Russel-James formula and thus acceptable. In the fifth step it is clear that the flow out of the chimney is less than the total flow according to the critical pressure and this is assumed to be due to the fact the some of the steam is lost from the pipe that normally conducts the water. This is not evident in steps three or four but it might well be so that the ratio of steam increases when the flow is smaller.

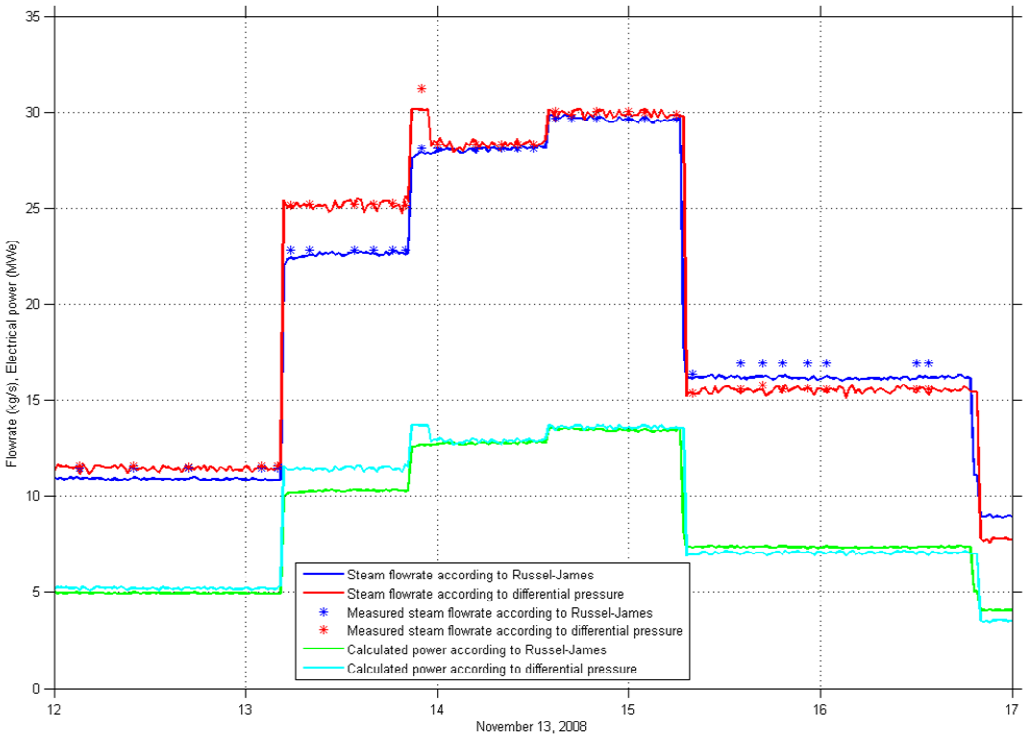

Figure 13:. Calculations from the continuous readings for the critical pressure; Steam flow in kg/s (blue line) and differential pressure (red line). Calculations from the analogue readings for the pivot point pressure; Steam flow in kg/s (blue stars) and pressure difference (red stars). Calculated power (MWe) for the steam flow (green line) and differential pressure (light blue line), in the step production test in well SV-23 in the Svartsengi field, November 13, 2008.

Table 7: Calculated results from production test in SV-23.

Step change	Flow rate change ΔQ kg/s	Pressure change ΔP bar	Productivity index PI (kg/s)/bar
1 to 2	11,7	-0,12	97,5
2 to 3	5,4	-0,05	108,0
3 to 4	1,6	0,01	160,0
4 to 5	-13,4	0,14	95,7

There is good correlation in the production index (PI) between the steps in the test except for the transition from third to fourth step, where PI is slightly higher. It is difficult to give a good estimate of PI since bottomhole pressure changes are small despite major changes in the flow rate. Still one could assume a short term PI close to 100 (kg/s)/bar but one has to expect a lower PI with time. A more realistic long term PI estimate is possibly obtained by comparing the pressure measurement from October 29, 2008, prior to the test and the profiles done in connection with the test itself. If the difference in bottomhole pressure is calculated it is 0.31 bars lower for the down measurement and 0.39 bars lower for the up measurement indicating a PI of 37 (kg/s)/bar for the down measurement and 43 (kg/s)/bar for the up measurement thus indicating a long term PI of approximately 40 (kg/s)/bar, which is considered high.

4 REFERENCES

Danielsen, Peter E., Jónsson, Páll and Egilson, Þorsteinn, 2010: Well Testing interpretation, Injection/Production Tests, Interpretation and Monitoring. Drilling, Completion and Testing of Geothermal Wells. Short Course paper II at WGC 2010, Bali, Indonesia, p. 22

Hafstað, Þórólfur H. and Kristjánsson, Bjarni R., 2006: Vatnsveitu í Borgarbyggð. Reynsludæling úr þremur vinnsluholm í Grábrókarhrauni. ÍSOR-06116 (in Icelandic), p 23

Jónsson, Páll and Friðriksson, Þráinn, 2008: Upphleyping holu RN-13B og mælingar í blæstri í október 2007. ÍSOR-08031 (in Icelandic), p 26

Jónsson, Páll and Eyjólfsdóttir, Ester I., 2009: Upphleyping holu SV-23 og mælingar í blæstri í nóvember 2008. ÍSOR-2009/010 (in Icelandic), p 33